

3825
P-286

Summary Report of Mission Acceleration Measurements for Spacehab-01, STS-57

Launched June 21, 1993

Brian Finley
Sverdrup Technology, Inc.
Lewis Research Center Group
Brook Park, Ohio

Carlos Grodsinsky and Richard DeLombard
National Aeronautics and Space Administration
Lewis Research Center
Cleveland, Ohio

(NASA-TM-106514) SUMMARY REPORT OF
MISSION ACCELERATION MEASUREMENTS
FOR SPACEHAB-01, STS-57 LAUNCHED 21
JUNE 1993 (NASA. Lewis Research
Center) 286 p

N94-29757

Unclass

March 1994

G3/18 0003825



National Aeronautics and
Space Administration

SUMMARY REPORT OF MISSION ACCELERATION MEASUREMENTS

For SPACEHAB-01, STS-57

Launched June 21, 1993

Authors:

Brian Finley,
Dr. Carlos Grodinsky,
and
Richard Delombard

NASA Lewis Research Center
Cleveland, Ohio

ABSTRACT

The maiden voyage of the commercial Spacehab laboratory module on-board the STS-57 mission was integrated with several accelerometer packages, one of which was the Space Acceleration Measurement System (SAMS). The June 21 st, 1993, launch was the seventh successful mission for the Office of Life and Microgravity Sciences and Application's (OLMSA) SAMS unit. This flight was also complemented by a second accelerometer system, The Three Dimensional Microgravity Accelerometer (3-DMA), a Code C funded acceleration measurement system, offering an on-orbit residual calibration as a reference for the units four triaxial accelerometers.

The SAMS accelerometer unit utilized three remote triaxial sensor heads mounted on the forward Spacehab module bulkhead and on one centrally located experiment locker door. These triaxial heads had filter cut-offs set to 5, 50, and 100 Hz.

The mission also included other experiment specific accelerometer packages in various locations. This summary report will not explicitly present data from these packages however, where available, data from these other packages will be given as reference.

STOKE 1000
COLOR 1000

6.3	Ergometer Exercise Period.....	23
6.4	EURECA Retrieval	27
6.5	EVA activities	30
7	Concluding Remarks	31
Appendix A:	References and Bibliography.....	A-1
Appendix B:	Spectrograph Survey Plots of Acceleration Data	B-1
Appendix C:	Average and RMS Plots	C-1
Appendix D:	Shoot Rotational Maneuver Calculations.....	D-1

List of Tables

Table 1	Get-Away-Special Bridge Experiments Summary.....	10
Table 2	STS-57 Mass Property Data.....	11
Table 3	SAMS TSH Parameters for SH-1	14
Table 4	TSH Error Budget	15
Table 5	Shuttle Maneuvers for SHOOT Experiment.....	19

1 INTRODUCTION

This report provides an assessment of the low-level acceleration environment on the first Spacehab (SH-1) mission (STS-57) as measured by the Space Acceleration Measurement System (SAMS). There were also other accelerometers on-board STS-57, a brief description of these accelerometers and their associated data acquisition systems will be covered for general information where future publications will present data set comparisons with the SAMS device.

The following will furnish interested investigators with a guide to evaluating the acceleration environment during this mission and identify areas which require further study.

The SH-1 mission was the seventh mission for SAMS with four previous missions in the Spacelab module, one in the middeck and one in the cargo bay. Reports resulting from previous SAMS missions are listed in the bibliography.

2 BACKGROUND INFORMATION

Acceleration is the rate of change of velocity and is measured in terms of meters per second per second (m/s^2). In this report, all acceleration magnitudes have been normalized to the acceleration of gravity at sea level, approximately 9.8 m/s^2 .

The acceleration environment experienced on a spacecraft is a complex combination of accelerations caused by a multiplicity of sources. Typical sources of accelerations are gravity, rotating and oscillating machinery, atmospheric drag, thruster jets, vehicle motion, crew motion, etc. The characteristics of the accelerations caused by these sources varies considerably, both in magnitude and frequency, where most time histories are non-stationary. The locations of the vehicle center of mass, the experiment(s), and the acceleration disturbance sources, along with the vehicle dynamics determine the primary acceleration disturbance at an experiment location. The magnitude of accelerations typically varies from parts of a micro-g to milli-g's. The frequency range of accelerations of concern to experiments is typically between quasi-steady accelerations to 300 Hz. Quasi-steady accelerations are characterized by very low frequencies at an orbital period, (i.e., approximately 90 minutes).

2.1 Inertial Measurements

Motion sensors can be grouped into two general categories: (1) inertial and (2) non-inertial. An inertial motion sensor provides a measurement of the motion with respect to an inertial reference frame, while a non-inertial motion sensor measures motion with respect to a non-inertial reference frame. The following sections are dedicated to the SAMS accelerometer system which measures the inertial response of the shuttle at the sensor attachment points.

tion on the curve, sensors are often calibrated by experimentally fitting a straight line through data showing the sensor voltage output as a function of the magnitude of the input. The slope of this line is also the sensitivity of the sensor, and is equivalent to the definition given previously. The units of the sensitivity are output per unit input.

It is logical that one could measure as low an amplitude excitation as desired, as long as the sensitivity of the sensor were high enough. Unfortunately, even an accelerometer with a very high sensitivity will fail to provide an accurate measurement when the excitation becomes sufficiently small due to its noise performance. In addition, the amplitude at which the measurement breaks down varies with frequency. What is needed is a plot of the amplitude at which the measurement provided by a sensor breaks down versus frequency. This function is called the incoherent power spectrum, and is obtained using signal processing techniques.

One of the problems with highly sensitive inertial sensors is that they tend to sense motions that they are not intended to sense. For example, a rotational velocity sensor will have some sensitivity to linear motion. This undesired response is called cross-axis, or parasitic sensitivity. (Ref: 1).

2.2 Sunstrand QA-2000 Accelerometers

The Sunstrand QA-2000 transducer is an inertial, linear accelerometer which functions on an electromagnetic principle. Figure 2.1 provides an illustration of the operating principle behind this proof-mass accelerometer. The inertial mass is composed of a magnetized material, and thus produces a magnetic field. An opposing magnetic field, controlled by varying the current in a coil, supports the inertial mass due to the repulsive force between the permanent and controlled magnetic fields. The current in the coil is continuously adjusted in a closed loop, such that the repulsive magnetic force restores the relative displacement to a null reading. By altering the current in the coil, the inertial mass is held fixed with respect to the sensor case (to within some tolerance). Therefore, the current required to maintain this condition, is at all times proportional to the acceleration of the case. The voltage drop across a resistor in the coil circuit is used to determine the voltage signal, which is proportional to the current by Ohm's law.

The frequency response of this sensor type was generated as defined in section 2.1.1 and is shown in Figure 2.2. The peaks at high frequencies were caused by the test apparatus, and not by the sensor itself. The phase loss however, is caused by the sensor, but is not limiting since the sensor bandwidth will be rolled-off. The noise floor of the QA-2000 was also measured as described in section 2.1.2 over a limited frequency band. The measured noise floor is presented in Figure 2.3.

The performance goal for these acceleration measurements in orbit is presented in Figure 2.3. It is desirable to employ a sensor having a noise floor that is at least an order of magnitude below the smallest disturbance to be measured. Thus, if at some frequency the performance goal is 1 micro-g, then the level of the noise floor should be at most, 0.1 micro-g. This requirement specifies a performance curve for the sensor noise. In Figure 2.3 an acceleration measurement performance goal, the sensor noise goal, and the noise floors for a variety of inertial sensor is presented on the same plot

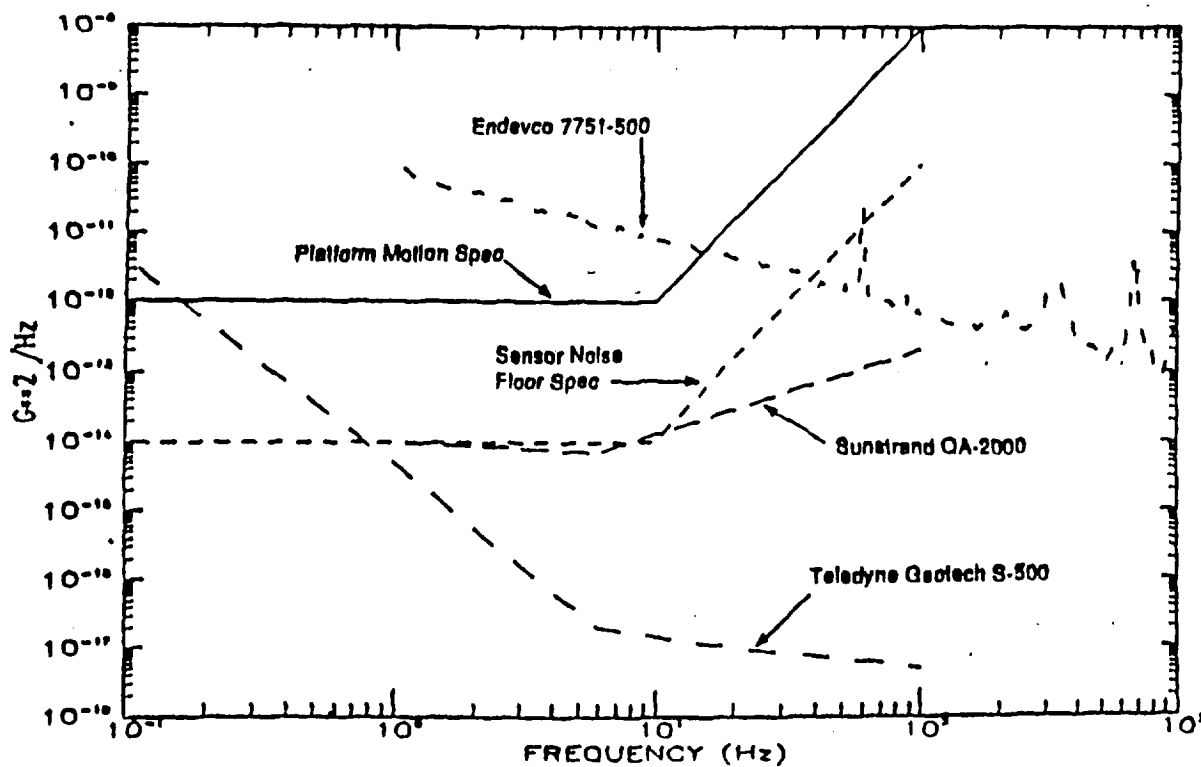


FIGURE 2.3 Comparison of Sensor Noise Floors with System Specification

2.3 Axis Coordinate Systems

The shuttle has several axis coordinate systems associated with it. One such system which is typically used for citing the location of equipment on the shuttle is the shuttle structural coordinate system, shown in Figure 2.5 (Ref: 2). The location and orientation of the SAMS triaxial sensor head (TSH) are typically cited in this axis coordinate system.

Each TSH has a fixed coordinate system associated with it in line with the sensitive axes of the three orthogonal proof-mass-accelerometers. However, for this mission the TSH's were aligned with the structural coordinate system as seen in Figure 2.5. Table 3 of section 4.1.1 gives the exact fixed axis alignment of all the TSH's. The data is measured and recorded in these fixed coordinates. The data is then translated from the TSH fixed coordinate system to the shuttle structural coordinate system. This report is published with all data converted to the shuttle structural coordinate

to the ground. After the mission, this raw flight data is converted to engineering units and Compact Disk-read Only Memory (CD-ROM) disks are produced for dissemination to users.

2.5 Time Correlation

For orbiter missions, two time systems are used. Many experiments with internal clocks have data recorded in terms of Greenwich Mean Time (GMT) based on standard time at the zero meridian. Experiments also use time synchronization signals from the shuttle to reference Mission Elapsed Time (MET), where MET begins at zero, at shuttle lift off and has the format of 000/00:00:00 (day/hour:minute:second).

The internal SAMS clock is initialized when power is applied to the SAMS unit. Depending on the shuttle resources available for a particular mission, SAMS time may or may not be synchronized with MET and another external time reference would have to be utilized to correlate the sams data in time.

If the SAMS time is not synchronized with MET, then a post-mission synchronization is applied based on the MET time at which power was applied to the SAMS unit.

On STS-57, SAMS was synchronized with MET and stored on the mission CD-ROMS accordingly.

3 STS-57 MISSION OVERVIEW

On June 21, 1993 at 9:07 a.m. EST, STS-57 was launched from the NASA Kennedy Space Center (KSC). The touchdown at KSC was on July 1, 1993 at 8:51 a.m. EST. The planned duration was for a nominal seven days with one contingency day. Bad weather conditions at the landing site forced two delays for the re-entry and landing. The Orbiter Endeavour was utilized for this mission.

A primary objective of STS-57 was the retrieval of the European Space Agency's free-flying platform named the European Retrievable Carrier (EURECA).

Also on STS-57, Endeavour carried into orbit the commercial laboratory facility called SPACEHAB, a small pressurized module situated in the forward section of Endeavour's payload bay. It was designed and constructed by the privately financed corporation, SPACEHAB, Inc.

In addition there were several other experiments including the Superfluid Helium On Orbit Transfer (SHOOT) demonstration experiment and ten Get-Away Special (GAS) experiments in the payload bay. Another of Endeavour's mission objectives was to allow two of the astronauts to perform a spacewalk for training and practice of deploy and retrieval techniques which will support Space Station assembly and the Hubble telescope servicing mission (Ref. 3).

- a) Commercial Refrigerator/Incubator Module-Vapor Diffusion Apparatus (CR/IM-VDA), two refrigerator/incubator modules which produced protein crystals.
- b) Bioserve Pilot Lab (BPL), R/IM module and multiple syringe "kits" used to conduct biomedical and fluid studies.
- c) Physiological Systems Experiment (PSE-03), two animal enclosure modules which contained rats to study microgravity's effect on organ systems.
- d) Solution Crystal Growth (SCG), room temperature growth of same crystals as SCG. The SCG experiment included a furnace in the Spacehab.
- e) Application Specific Preprogrammed Experimental Culture System (ASPECS), bioreactor which grew human cells and tissue cultures.
- f) Thermal Enclosure System-Crystal Observation System (TES-COS), observed equilibrium rates of the crystal growth process.

3.2.2 Get-Away-Special Payloads

The STS-57 mission included a GAS bridge assembly with ten GAS payloads from the U.S., Canada, Japan and Europe. Also on the bridge was one secondary commercialization payload and one GAS Can with a ballast payload. Table 1 presents a summary of the GAS payloads for STS-57.

The ballast payload contained a small accelerometer package furnished by NASA Goddard Space Flight Center (GSFC) recording accelerations during the mission for these specific GAS can carriers (Ref. 3).

maneuvers were utilized to force the liquid helium in a certain direction and as disturbances during the SHOOT operations. The impact of these acceleration disturbances on the microgravity environment are presented in section 6.2.

3.2.4 STS-57 Extravehicular Activity: Detailed Test Objective 1210

STS-57 crew members David Low and Jeff Wisoff performed a 4-hour extravehicular activity (EVA) on the fourth day of the flight as a continuation of a series of spacewalks NASA plans to conduct preparing for the construction of the space station. The impact of these acceleration disturbances on the microgravity environment is presented in section 6.5.

3.3 STS-57 Mass Property Data

Pertinent mass property data for this mission are given in table 2. The data is given in the orbiter structural coordinate system. The center of gravity varies no more than two inches in the X and Z axes and no more than one inch in the Y axis for the various payload configurations listed in the following Table 2.

Table 2 *STS-57 Mass Property Data*

Condition	Parameter	Value
Payload Bay Doors Open @ MET 0/01:28		
	Weight	239338 lbs.
	Xcg	1097.82 in.
	Ycg	0.0 in.
	Zcg	377.85 in.
Post EURECA Retrieval @ MET 3/01:47		
	Weight	243584 lbs.
	Xcg	1096.74 in.
	Ycg	0.38 in.
	Zcg	377.40 in.
Pre-Payload Bay Doors Closed @ MET 9/08:17		
	Weight	237143 lbs.
	Xcg	1096.07 in.
	Ycg	0.04 in.
	Zcg	376.54 in.

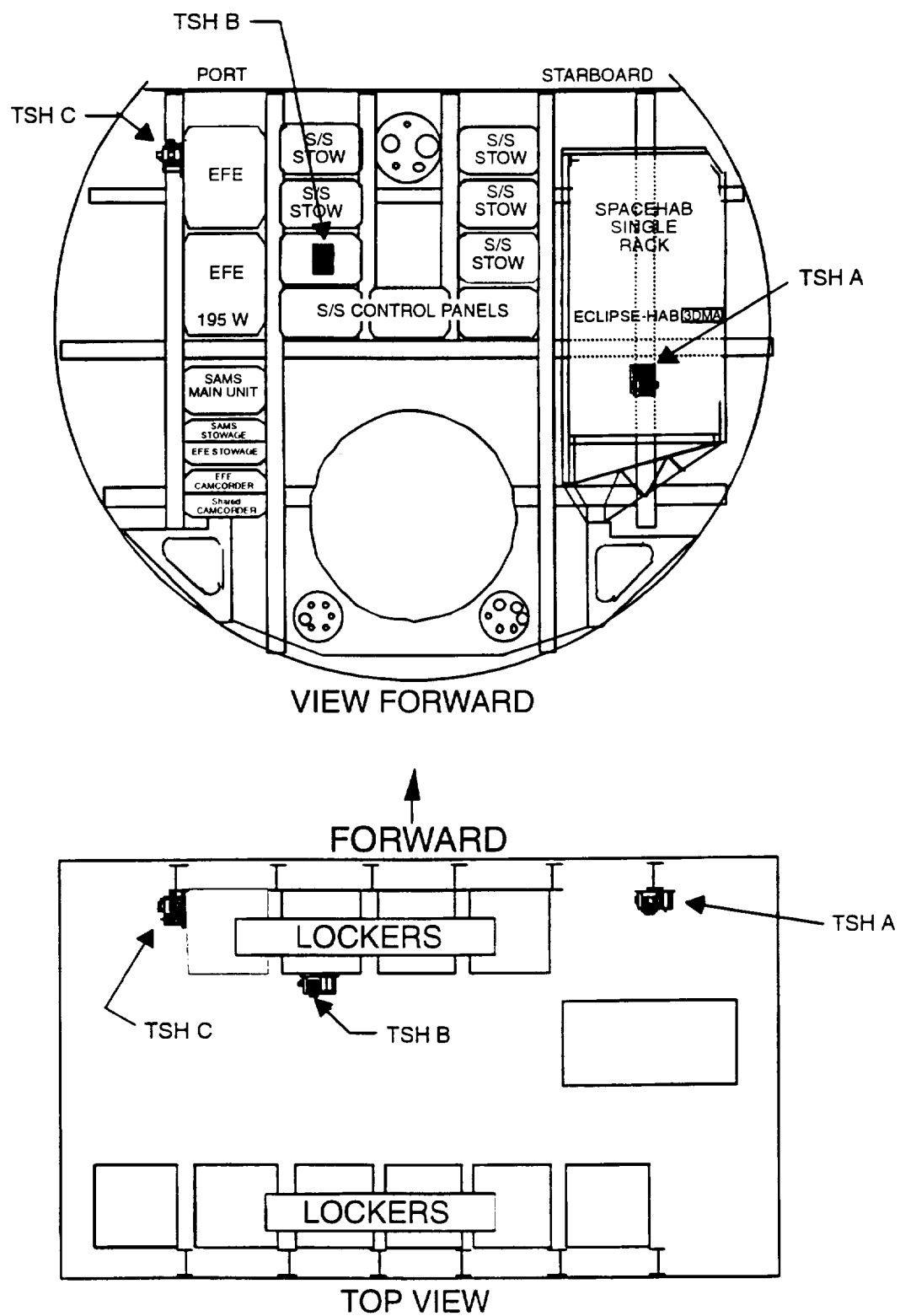


FIGURE 4.1

Spacehab Module Forward and Aft Bulkheads

strand QA-2000 accelerometer, mainly bias and scale factor errors. A third error source is the axis misalignment which is negligible in comparison to the other accumulated errors.

At a gain of 1 the 0.03 percent scale factor error (150 micro-g's) is the major contributor to the total full-scale error. At gains of 10, 100, and 1000 the major error contribution is a result of the +/- 98.6 micro-g bias error. The maximum full scale error for a gain of 10, 100, and 1000, is 15, 2.5, and 2.1 micro-g for the associated 0.03, 0.05, and 0.42 percent maximum error of full scale.

Table 4 TSH Error Budget

Gain	Accuracy percent +/- 98.6μg
1	0.03
10	0.03
100	0.05
1000	0.42

4.1.3 SAMS Operations

All TSH data was recorded on optical disks which were stored in lockers and removed after the mission.

The SAMS unit operated a total of 162 hours 13 minutes during the SH-1 mission. Recording began at MET 000/06:57:20 and ended at MET 007/15:07:02. One anomaly occurred on day 4 of the mission, when a disk drive began to record data intermittently. A malfunction procedure was followed for the remainder of the mission minimizing the loss of data. A total of 13 hours 31 minutes of data was lost, the majority between MET 004/07:17:00 and 004/20:48:00.

4.1.3.1 Gain changes

An autoranging algorithm is used in the SAMS unit along with a hardware peak detect to ensure the optimal gain range is selected. The system worked well with the exception of the X axis of head A. The gain on this axis continually changed between a gain of 10 and 100 during the mission. Post flight analysis revealed that this was caused by a hardware problem in the peak detect circuit of the X axis. A capacitor had been added to the X axis circuit to suppress a noisy clock signal which caused the circuit to operate improperly. The problem was successfully diagnosed by an analysis of the data, and corrective action has been taken.

These constant gain changes, exhibited as step functions in the data, caused an order of magnitude increase in the broadband energy. As a result, the x axis and vector magnitude spectrographs show this increase in broadband energy. (See Appendix B).

5.1.1 Spectrographs

The color spectrographs in appendix B were produced using the Sensor A data from the SAMS SPACEHAB-01 mission. The data was taken in 2 hour periods and an amplitude spectrum was performed in 10 second intervals. The spectrum data was then scaled by taking the log of each data point and assigning a color to the integer result. Eight colors were used for eight intervals between 0.1 micro-g and 1 milli-g. In using this method a range of values are assigned the same color. For example 0.1-0.3 micro-g values are assigned the color black, 0.3-1 micro-g values are assigned the color purple. Apparent resolution can be adjusted by using more or less colors.

5.1.2 AVERAGE

The average plots, in appendix C, were also produced using the Sensor A data from the SAMS SPACHEAB-01 mission. The plots were produced by taking the average of each 10 second interval of data. The average produces 1 data point for every 10 seconds (N=5000 points) of data for this 100 Hz head. The following equation was used to calculate the 10 second moving window average.

$$\text{Average} = \frac{1}{N} \sum_{j=1}^N X_j$$

Where X is the vector magnitude of the x, y, and z axis data, respectively.

5.1.3 Root Mean Square(RMS)

The RMS plots, in appendix C, were also produced using the Sensor A data from the SAMS SPACHEAB-01 mission. The plots were produced by taking the Root Mean Square(RMS) of 10 second intervals for the two hour period. The root mean square of a discrete time series for over 10 seconds was calculated as follows:

$$RMS = \sqrt{\left(\frac{1}{N} \sum_{j=1}^N X_j^2 \right)}$$

Where X is the vector magnitude of the x, y, and z axis data, respectively.

6 MICROGRAVITY PERSPECTIVE OF THE STS-57 MISSION

Various activities from this mission were characterized so that the effects may be considered for planning of future missions and experiments.

6.1 Crew Sleep Period

The crew work schedule was based on all crew members working during the same twelve hour work shift. The other twelve hours of each day were occupied with pre-sleep, sleep, and post-sleep activities.

During these sleep periods, non-essential pieces of equipment were turned off and attitude maneuver changes were minimized or eliminated. This results in a quiet microgravity environment on-board the shuttle. Figure 6.1 illustrates 2 hours of a typical sleep period during SH-1. The plots show a very quiet microgravity environment in the lower frequency ranges of .1 to 15 Hz with the levels gradually increasing with increasing frequency.

The two vertical lines spaced an hour apart in the plot are caused by the SAMS unit resetting its gain at 1 hour intervals.

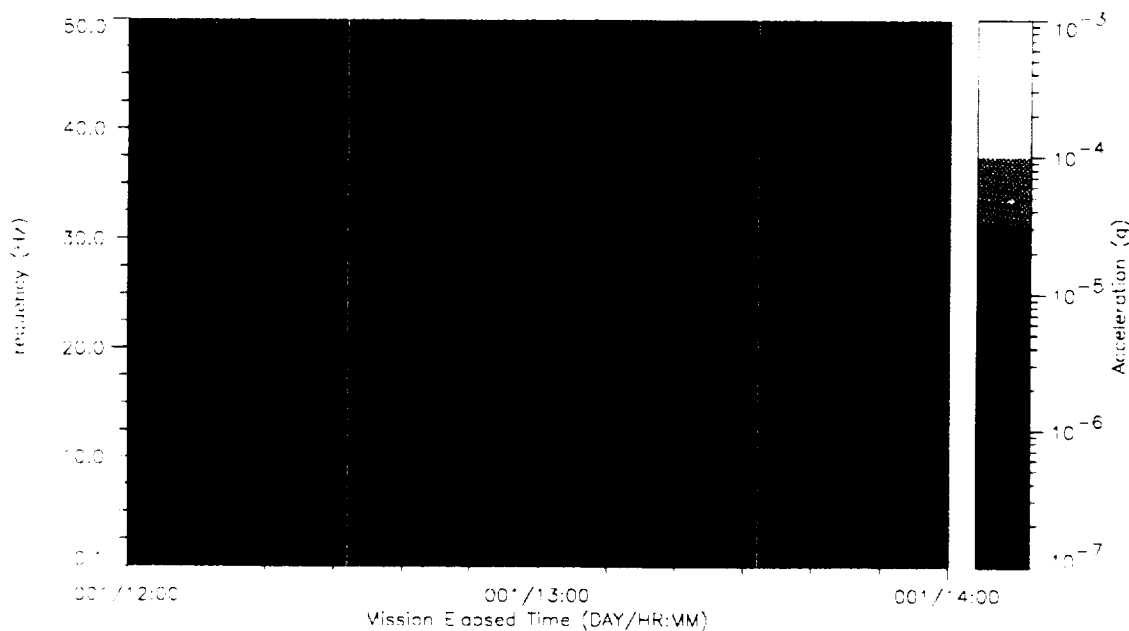


FIGURE 6.1

TSH B Spectrograph of SH-1 Crew Sleep Period Microgravity Environment

6.2 SHOOT operations

The SHOOT experiment requested four inertial maneuvers of the shuttle in order to force the experiments liquid contents to each end of the Dewars during the course of the experiment. These four maneuvers consisted of a pitch rotation at 3 deg/sec.

and three \times translational accelerations of the orbiter. These maneuvers are described in Table 5.

Table 5

Shuttle Maneuvers for SHOOT Experiment

Name	Time (approx.) (MET)	Description
pitch rotation	000/21:40 - 21:55	Pitch rotation with the right wing toward earth.
+x translation #1	000/22:28	Translation along the velocity vector induced by a primary thruster fired at the aft end of the shuttle. The burn duration was about 20 seconds.
-x translation #2	001/21:07	Translation along the velocity vector induced by a primary thruster fired at the forward end of the shuttle. The burn duration was about 20 seconds. First one thruster was fired, then two were fired.
-x translation #3	001/23:22	Translation along the velocity vector induced by a primary thruster fired at the forward end of the shuttle. The burn duration was about 20 seconds. First one thruster was fired, then two were fired.

The pitch rotation of the orbiter was initiated at MET 000/21:40:53 with two intermediate rotational rates where the nominal 3 deg/sec. rotation was achieved at MET 000/21:42:39. The 3 deg/sec. pitch rotational rate lasted for 13 minutes and 57 seconds until the rotation of the orbiter was slowed down and eventually stopped to the rotational deadband of the orbiter. Figure 6.2 gives the moving average of the x, y, and z acceleration of the 5 Hz accelerometer head during the rotational maneuver. Appendix D contains some calculations confirming the acceleration levels during this maneuver.

As shown by the three curves the y axis acceleration of the orbiter which was perpendicular to the rotational plane was not stable in that the rotation of the orbiter about the y axis must have caused an oscillatory disturbance out of the rotational plane and therefore the control thrusters must have been activated to keep the rotational plane perpendicular to the orbital flight path. As seen in this figure thrusters were fired in the y axis direction about every 200 seconds to stabilize the pitch rotational maneuver of the shuttle. The impact of these intermittent thruster firings can be seen in the acceleration histories of the other two axes with a significantly reduced magnitude.

~~PRECEDING PAGE BLANK NOT FILMED~~

cleaner than the second and third exercises. The second and third primary thruster burns from the forward end of the shuttle seem to have a 3 second disturbance. Figure 6.4 shows the non-filtered maneuvers giving the stable aft thruster firing and the 3 second pulsed forward primary thruster responses for the three \times inertial motions. As can be seen by this plot the second and third \times acceleration maneuver are almost identical as they should be, since the same thrusters were used in both maneuvers. To demonstrate this the mirror image of the second translational SHOOT exercise was taken and plotted with the third acceleration maneuver giving a comparison of the orbiters response at different times to the same input forcing function as seen in Figure 6.5.

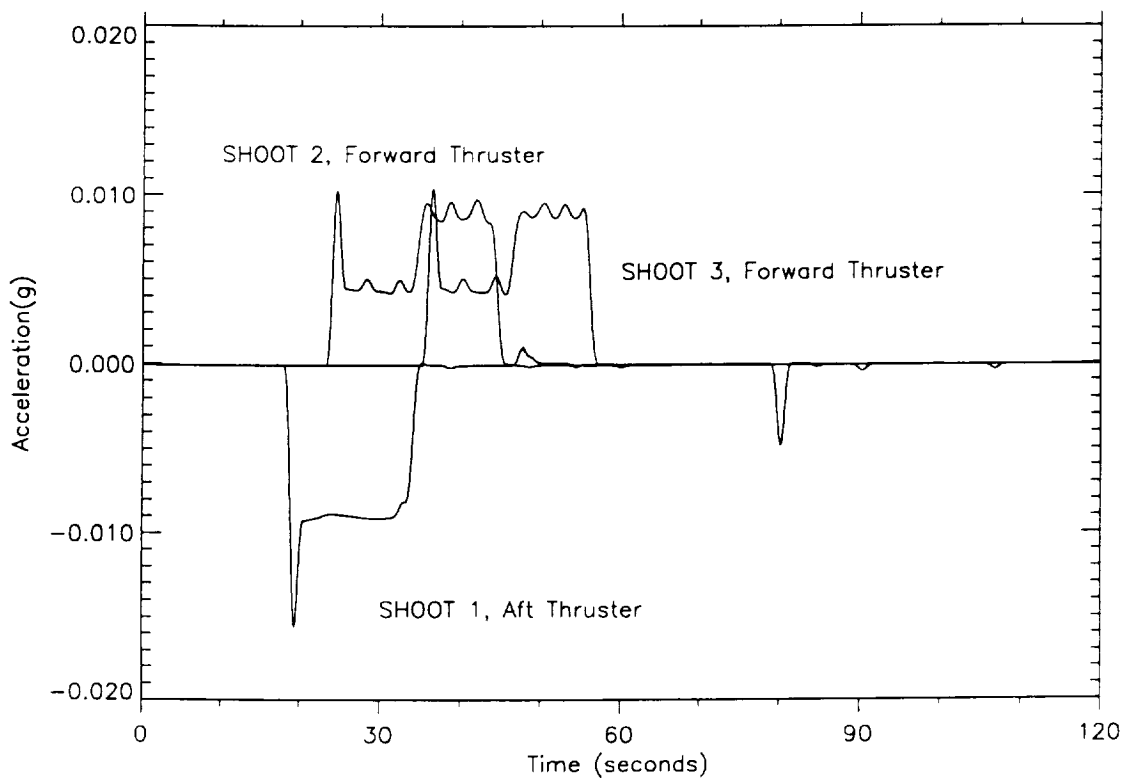


FIGURE 6.3

SHOOT Translation Maneuvers

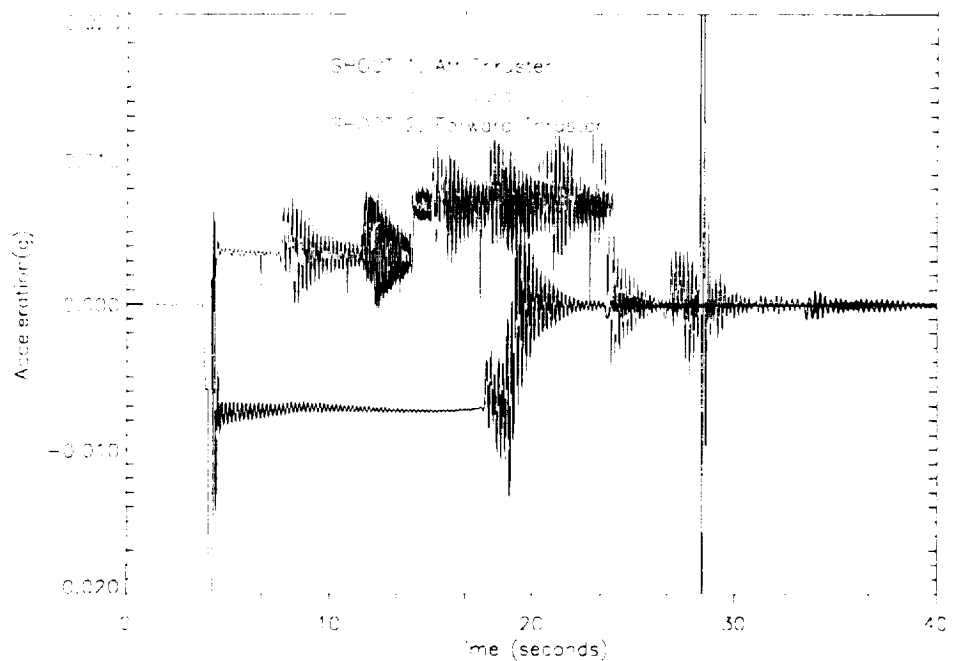


FIGURE 6.4

SHOOT Non-Filtered X-Axis Maneuvers

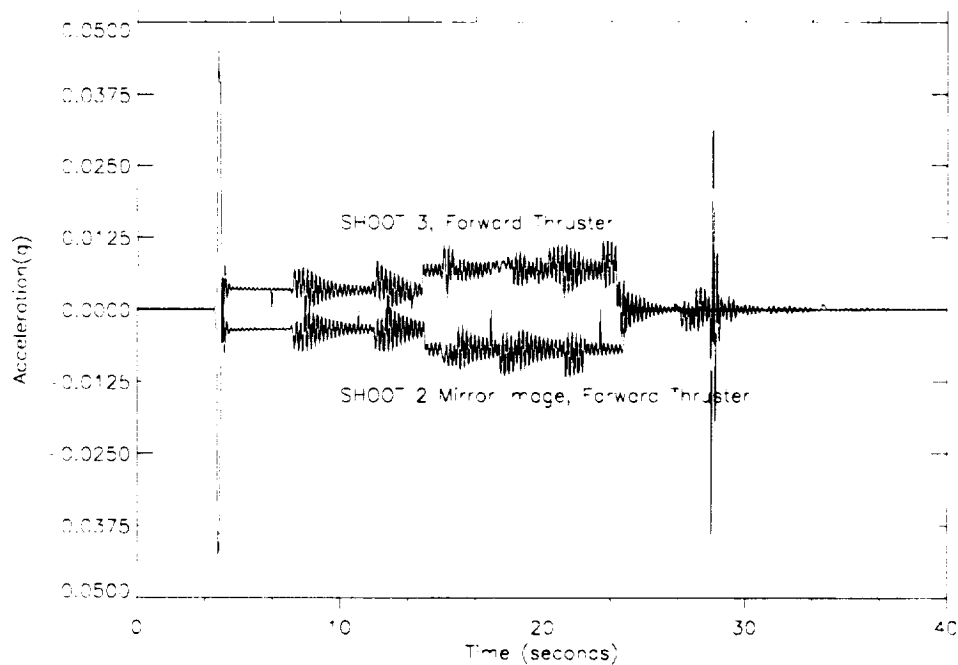


FIGURE 6.5

SHOOT 2 and 3 Non-Filtered X Maneuvers

6.3 Ergometer Exercise Period

The Spacehab-1 mission exercise equipment aboard the orbiter was a ergometer device which was attached to the middeck floor. The ergometer faces the y dimension thus, the astronauts are facing the side wall of the middeck when exercising. The pedaling rate is set by the astronaut and was not recorded. However, from the spectral content of the acceleration disturbances during an exercise period, the pedaling rate was approximately 1.25 Hz. In addition, a 1.25 Hz rocking motion of the ergometer was detected caused by the side-to-side motion of the astronaut at the pedal rate and the disturbance caused by the pedaling was at 2x the pedaling rate or 2.5 Hz. This specific crew exercise period began at MET 001/22:14:17 and lasted for approximately 20 minutes. Figure 6.6 through 6.8 gives an average of four spectrums for the x, y, and z axis showing the 2x pedal rate disturbances at 2.5 Hz in the y and z directions and the pedal rate of 1.25 Hz in the x axis, respectively.

In order to establish an average disturbance environment amplification spectrum for exercise periods, specific to this mission and with reference to the Spacehab-1 module, a non-exercise period was analyzed and a spectral ratio of these two curves were calculated for the x, y, and z directions giving Figures 6.9 through 6.11, respectively. These figures give a measure of the amplified environment as a function of frequency where the acceleration environment of the Spacehab-1 module is not significantly affected except at the discrete ergometer operating frequencies of 1.25 and 2.5 Hz. As seen in these curves the x, and z dimensions are the least affected, as expected, while the y dimension has the most amplification from nominal crew activity.

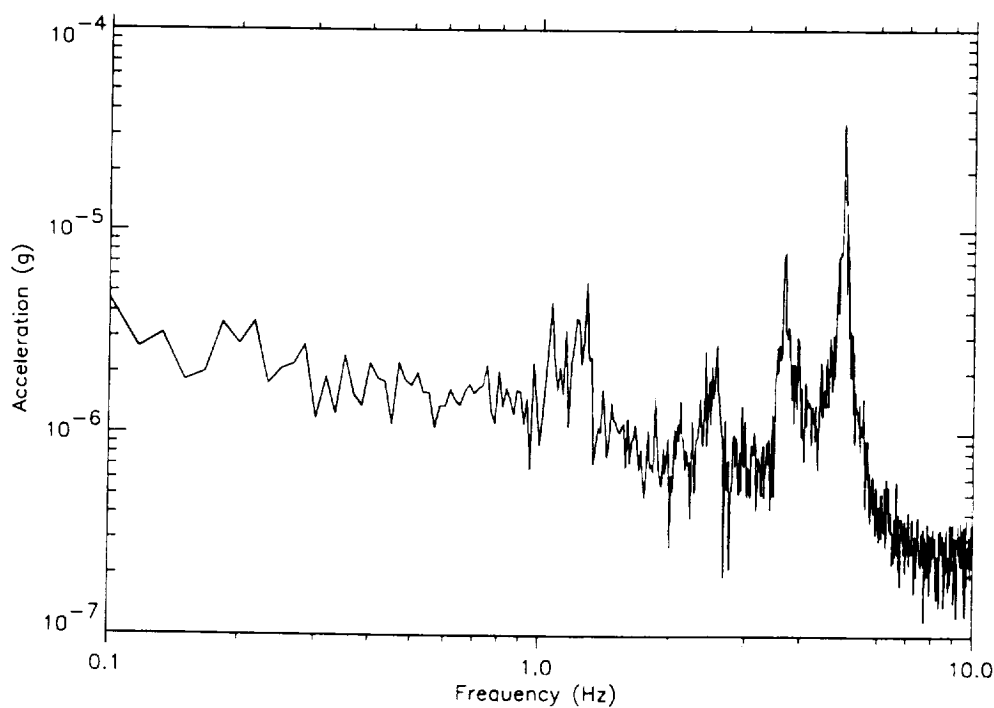
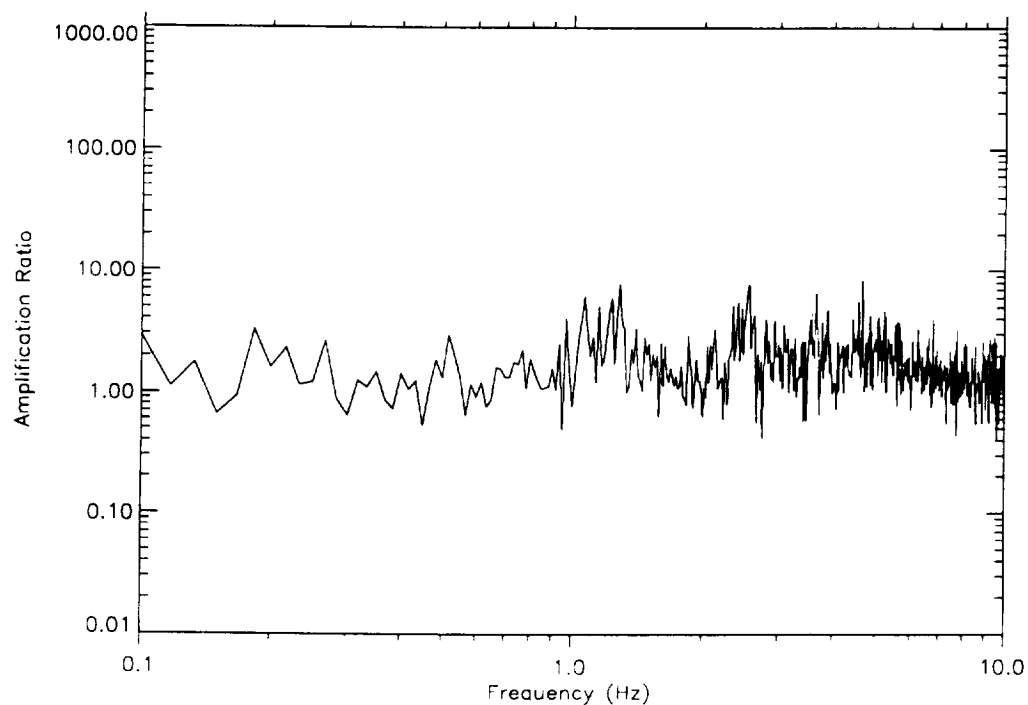


FIGURE 6.6

X-Axis Spectrum of Four Averages for Exercise Period

**FIGURE 6.9**

X-Axis Disturbance Environment Amplification Spectrum for Exercise Period

6.4 EURECA Retrieval

A major mission activity during the Spacehab-1 mission was the retrieval of the European free-flyer EURECA. This activity entailed significant maneuvering of the shuttle causing inertial motion of the orbiter. The EURECA capture will be organized into four distinct orbiter acceleration disturbance profiles, before, during and after retrieval of the EURECA satellite. These four phases of the retrieval are the target track, grapple, pre-berthing, and berthing of the satellite. The target tracking profile of the disturbance environment was predominantly driven by a target track mode of navigation by the shuttle to rendezvous with EURECA where at MET 002/23:34:00 the shuttle was taken over by the commander and flown under manual controls. Figure 6.12 shows a number of these manual maneuvers consisting of numerous pitch rotations and altitude changes causing most of the accelerations in the x, and z dimensions where the shuttle x axis was being flown into the velocity vector. The figure begins at MET 002/23:33:19, showing the x, y, and z axes with a 10 sec moving average giving a filtered response of the data at 0.1 Hz.

The grapple of EURECA was accomplished at MET 003/00:45:00. The grapple phase of the EURECA retrieval began after the shuttle was positioned above the satellite. There was no noticeable shock input to the shuttle, detected by the SAMS sensors, during the EURECA capture.

A four hour period including the capture and latching of the EURECA satellite is presented in Figure 6.13. The high acceleration levels during the chase maneuvers by the shuttle may be seen in the first 45 minutes of the data.

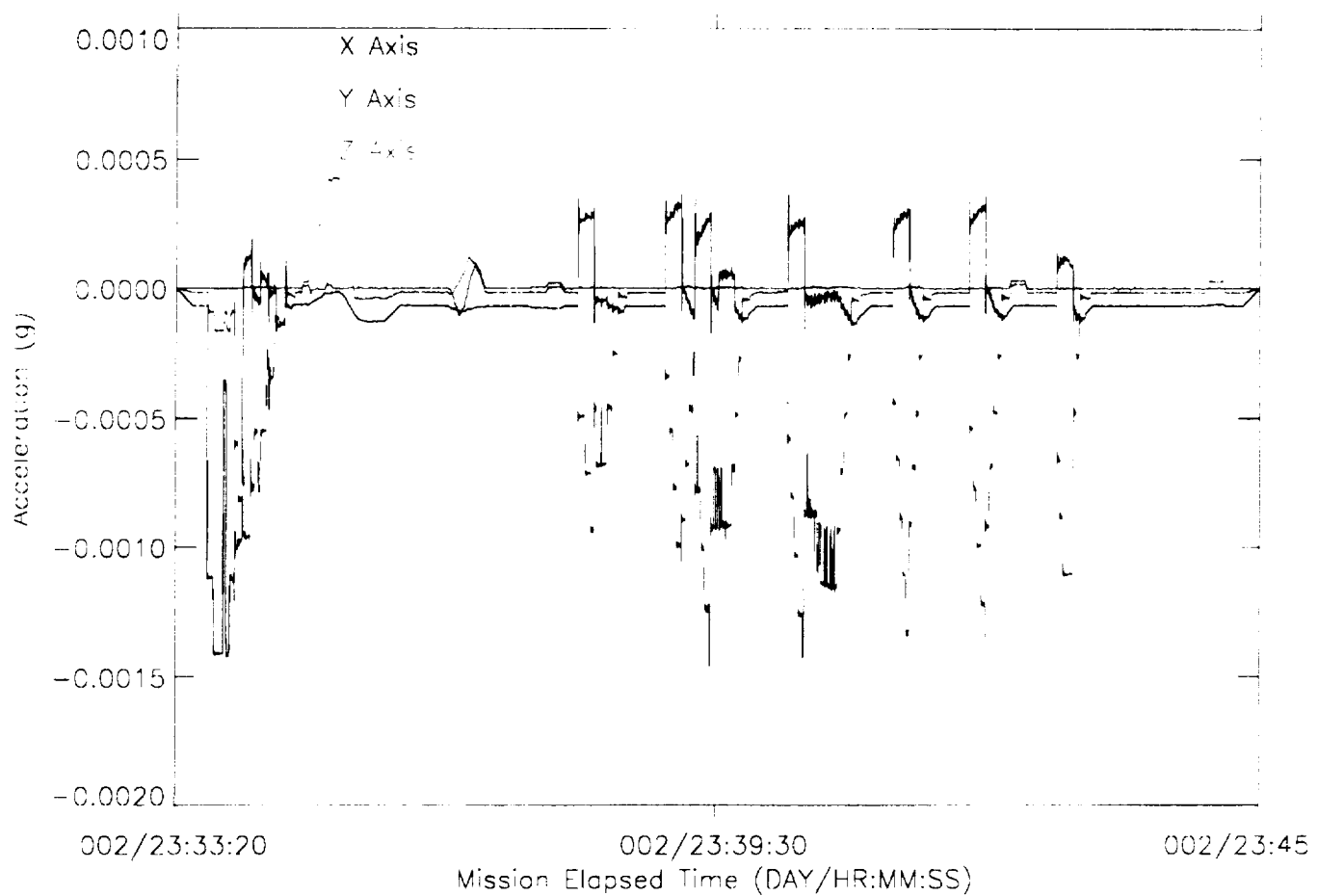
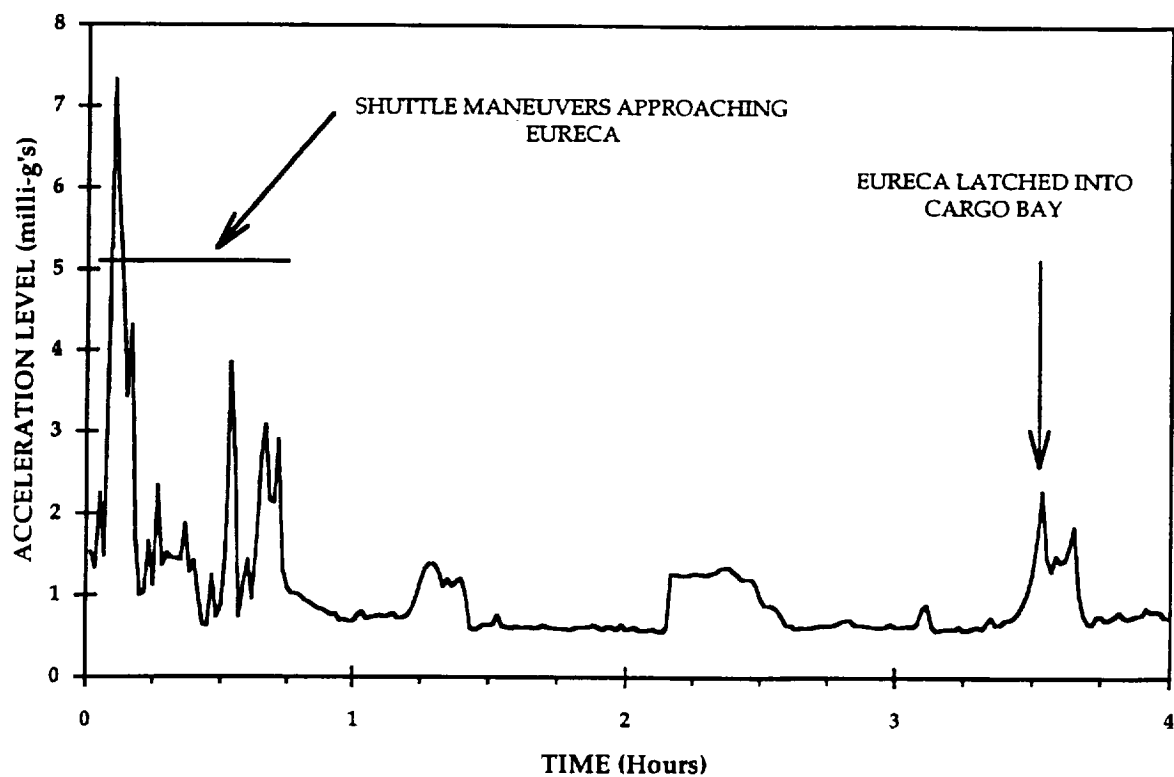


FIGURE 6.12

X, Y, and Z 10 Second Moving Average of EURECA Target Track

PRECEDING PAGE BLANK NOT FILMED

EURECA RETRIEVAL ON STS-57

**FIGURE 6.13**

Vector Magnitude of Four Hour Time History During EURECA Retrieval

PRECEDING PAGE BLANK NOT FILMED

6.5 EVA activities

EVA operations were analyzed from MET 004/02:00:00 to MET 004/03:00:00, for two astronauts tethered to the remote manipulator arm. The arm was maneuvered during this period. Figure 6.14 shows a moving 10 second average of the 5 Hz accelerometer head for the structural x, y, and z coordinates during the first 24 minutes of day four, hour two. There was a verbal reference from the astronauts that the arm was cleared to reposition itself back to antenna one position at MET 004/02:14:00 and that the arm was in-position at MET 004/02:18:00. This reference to an inertial event was from a SAMS mission log book and therefore, the actual time of the event is suspect by a few minutes. However, from the acceleration data plot one can plainly see a shift in the x axis quasi-steady level from MET 004/02:11:00 to MET 004/02:18:30. The significant deviations from the constant rigid body motion of the shuttle, due to the mass motion of the arm, are most likely from arm corrections during the end effectors path from point A to B.

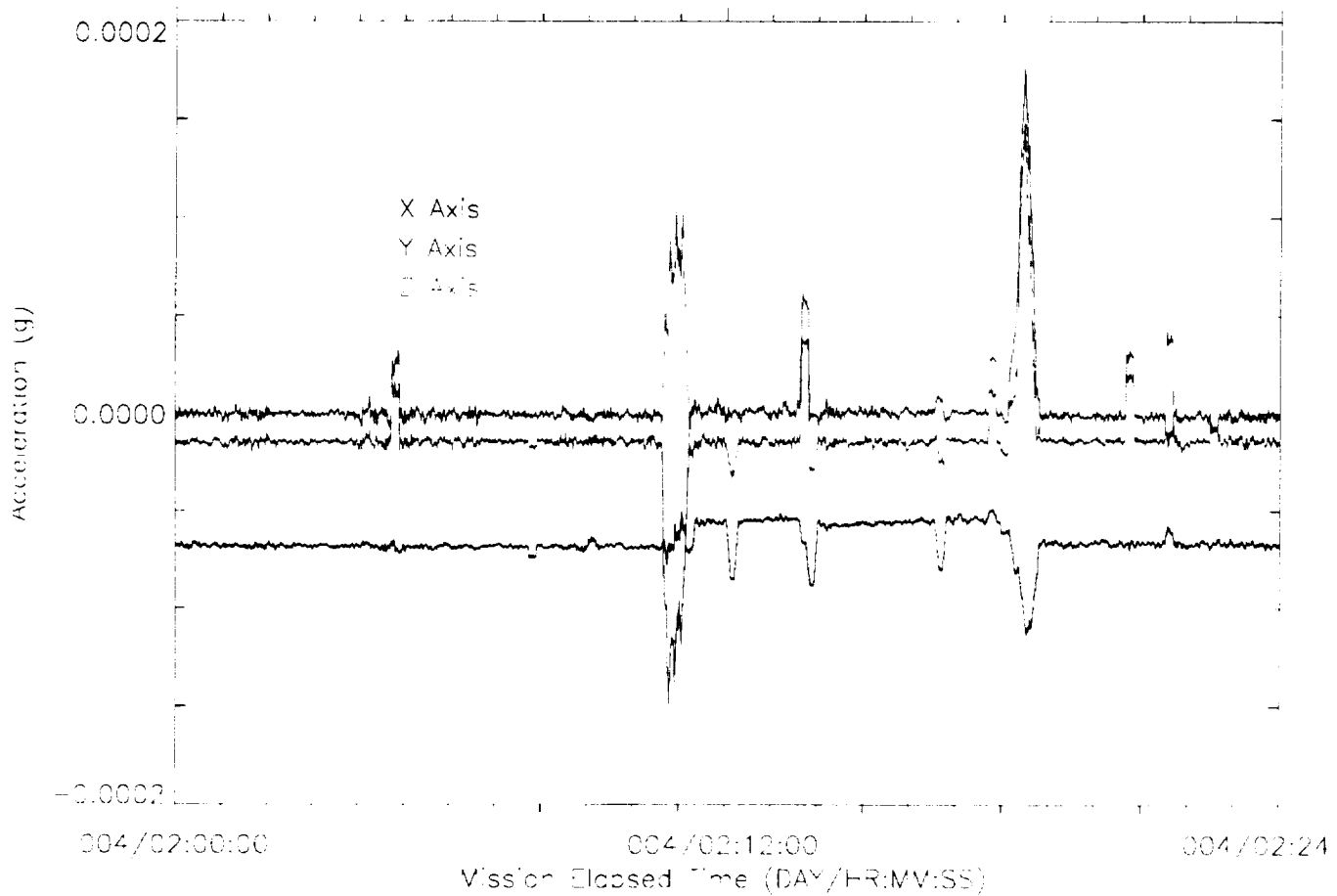


FIGURE 6.14

X, Y, and Z Acceleration Time Histories of Crew Extravehicular Activity

7 Concluding Remarks

This report serves as a road map to the SAMS data acquired during the STS-57 mission. Further analysis of specific events and comparisons with other missions will be performed and published under future documents.

There were two primary payloads for the STS-57 mission, the retrieval of the EURECA free-flyer and the operation of the first SPACEHAB module. SAMS was onboard STS-57 to support the SPACEHAB-1 payloads where three triaxial sensor heads were mounted to the forward bulkhead of the pressurized enclosure. These triaxial sensor heads were configured with a 5, 50, and 100 Hz low pass filter, respectively.

A mission summary of the vector magnitude rms, and average accelerations for the entire mission was produced for the 100 Hz head. Spectrographs were also produced on head A to give a spectral time history for the entire mission. Significant events were chosen to give a more detailed look at the acceleration disturbances at the sensor head locations in the SPACEHAB module. These events were typical sleep periods, numerous scheduled astronaut activities such as exercise, EVA's and the EURECA retrieval. In addition, a secondary payload named SHOOT required significant quasi-steady acceleration disturbances which were analyzed for the resulting SPACEHAB accelerations. These disturbances were on the order of a milli-g with significant duration. The middeck exercise period was fairly benign in its disturbance of the SPACEHAB environment. The EVA and EURECA phases of the mission were characterized by certain "DC" shifts of the acceleration levels pertaining to mass maneuvers or orbiter attitude changes, respectively.

To produce the spectral and acceleration time histories, approximately 3.5 gigabytes of data were processed. The rms and average time histories were processed for only the 100 Hz head, while the spectral time histories were processed for the vector magnitude and the associated x, y, and z axes.

Appendix A: References and Bibliography**References**

1. Grodsinsky, Carlos: Microgravity Vibration Isolation Technology: Development to Demonstration. NASA TM-106320, September 9, 1993
2. NSTS Interface Control Document, ICD-2-19001
3. STS-57 Press Kit Package, Release 93-78, NASA Headquarters, Washington DC, June 1993
4. DeLombard, R.; Finley, B. D.; and Baugher, C. R.: Development of and Flight Results From the Space Acceleration Measurement System (SAMS). NASA TM-105652, (Also, AIAA Paper 92-0354, 1992).
5. Thomas, J. E.; Peters, R. B.; and Finley, B. D.: Space Acceleration Measurement System Triaxial Sensor Head Error Budget. NASA TM-105300, 1992.

Bibliography

1. DeLombard, R.; and Finley, B. D.: Space Acceleration Measurement System Description and Operations on the First Spacelab Life Sciences Mission. NASA TM-105301, 1991.
2. Rogers, M. J. B.; et. al.; Low Gravity Environment On-board Columbia During STS-40. AIAA Paper 93-0833, 1993.
3. DeLombard, R.; Finley, B. D.; and Baugher, C. R.: Development of and Flight Results From the Space Acceleration Measurement System (SAMS). NASA TM-105652, (Also, AIAA Paper 92-0354, 1992).
4. Baugher, C. R.; Martin, G. L.; and DeLombard, R.: Low-Frequency Vibration Environment for Five Shuttle Missions. NASA TM-106059, 1993.
5. Baugher, C. R.; and Henderson, F. H.: Summary Report of the Mission Acceleration Measurements - STS-43. ACAP project report, 1992.
6. Baugher, C. R.; and Henderson, F. H.: Summary Report of the Mission Acceleration Measurements - STS-42. ACAP project report, 1992.
7. Baugher, C. R.; and Henderson, F. H.: Summary Report of the Mission Acceleration Measurements - STS-52. ACAP project report, 1992.

Appendix B: Spectrograph Survey Plots of Acceleration Data

This appendix contains the color spectrograph from SAMS head A. The sensor head was located on a forward structural T-beam of the SPACEHAB module. The sensor frequency cut off was set to 100 Hz and was sampled at 500 samples per second. The spectrograms cover the majority of the time that the SAMS unit operated beginning at MET 000/08:00 and ending at 007/15:07.

Missing data is shown within the spectrographs as large bands of white. Data between MET 004/06 and 004/20 is missing due to a on orbit problem with a disk drive. Data is also missing from MET 005/18 to 005/20 because the data was not able to be read from the disk during post mission processing.

Due to the gain change anomaly on the x-axis, which was successfully diagnosed as a hardware integrator problem, the x-axis spectrographs exhibit a broadband order of magnitude increase as compared to the y and z axes. The constant gain changes, exhibited as step functions in the data, caused this order of magnitude increase in the broadband energy. As a result, the x axis is the major contributor to the vector magnitude calculation which can be seen in the spectrographs.

STS-57, Head A, Vector Magnitude

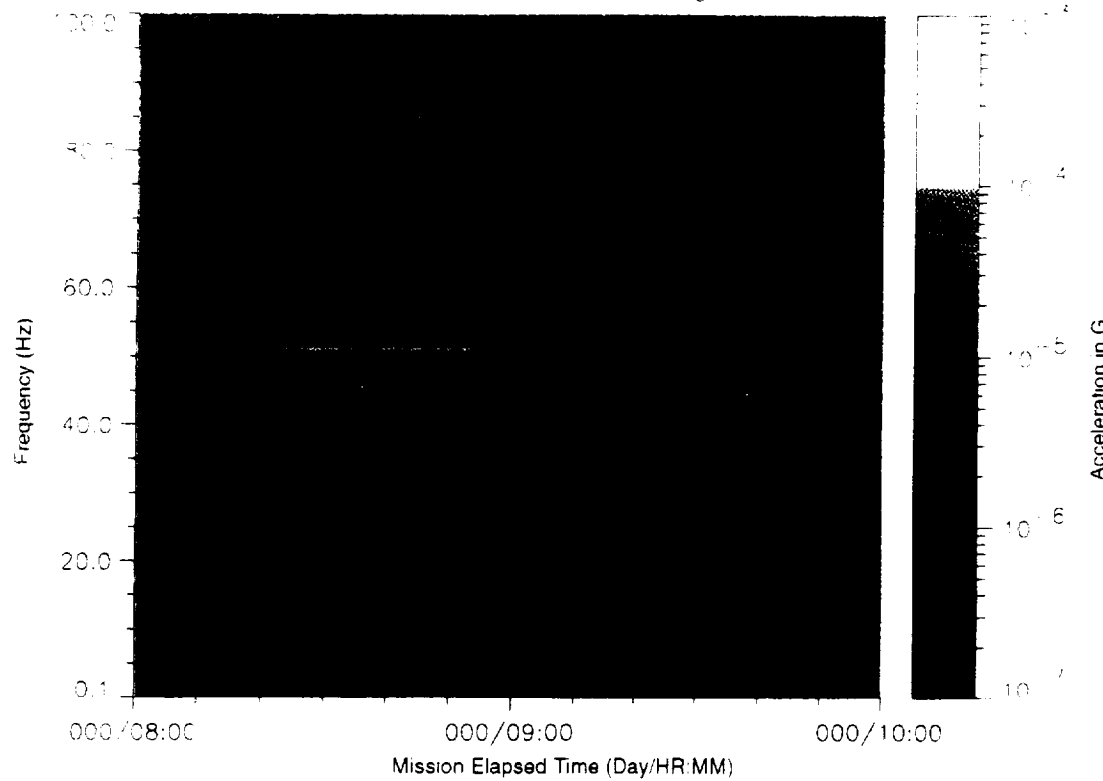


Figure B-1: SPACEHAB-1, Forward Bulkhead T-Beam

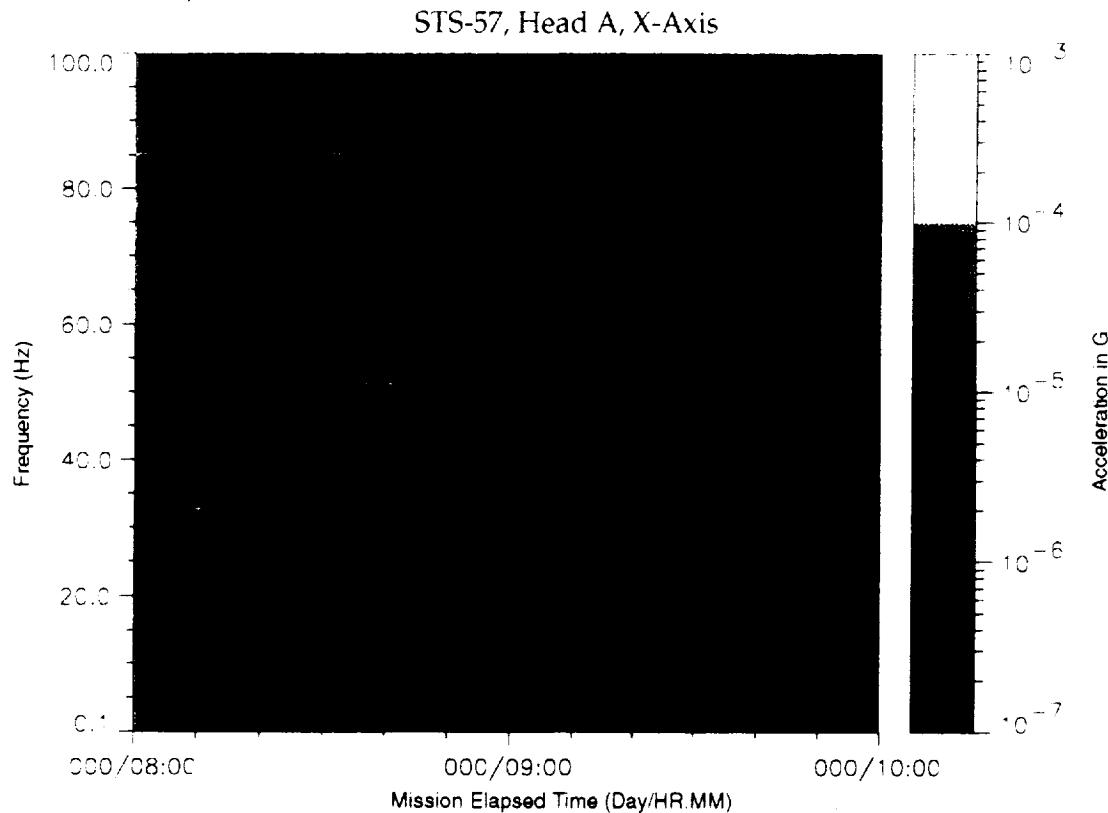


Figure B-2: SPACEHAB-1, Forward Bulkhead T-Beam

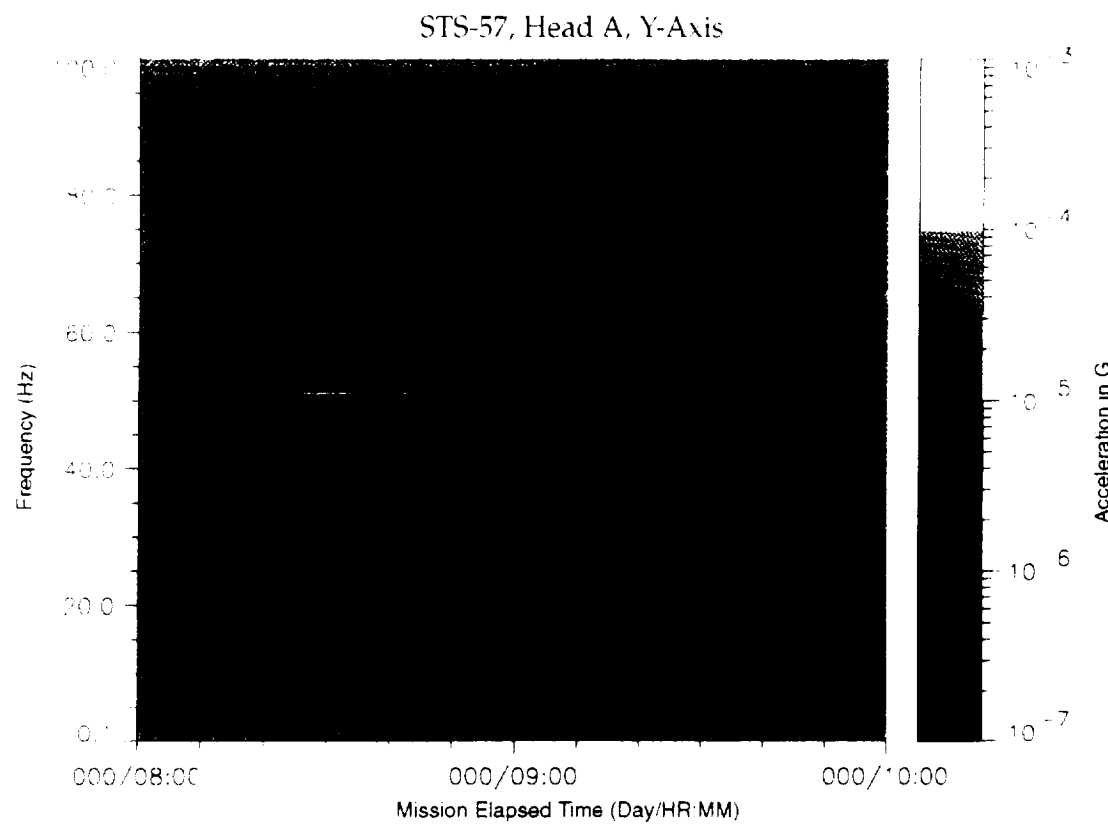


Figure B-3: SPACEHAB-1, Forward Bulkhead T-Beam

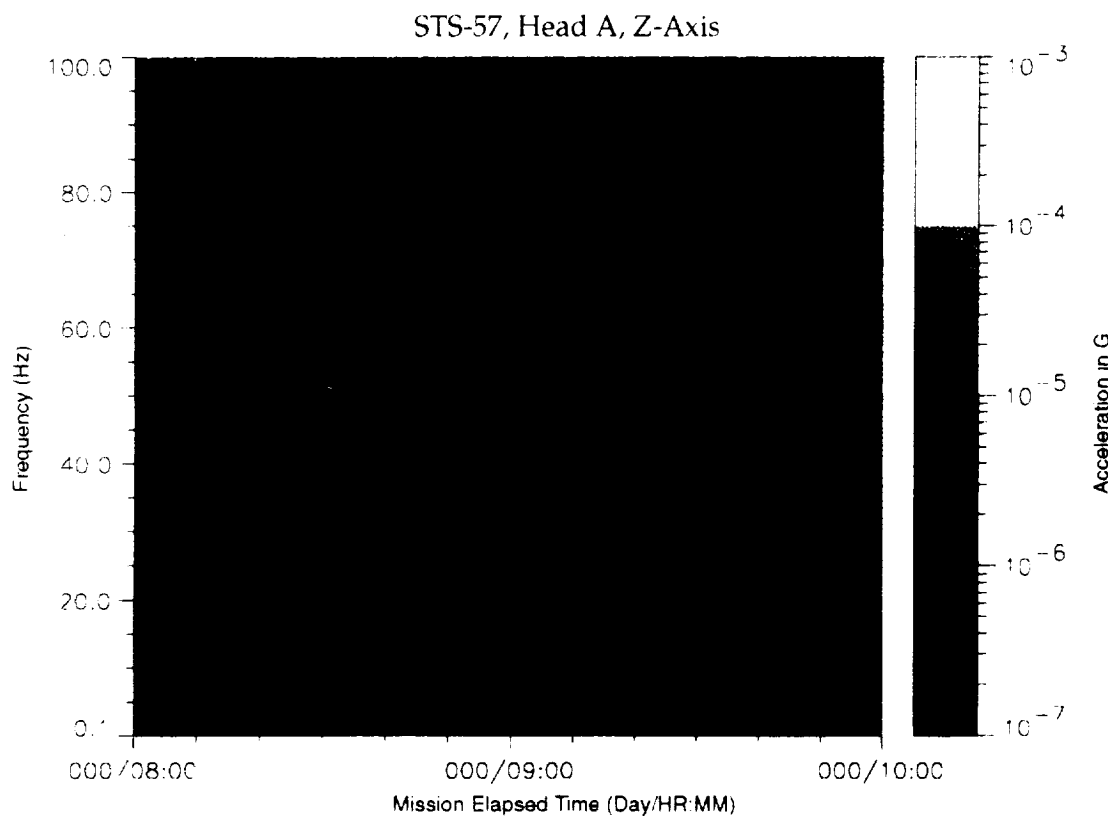


Figure B-4: SPACEHAB-1, Forward Bulkhead T-Beam

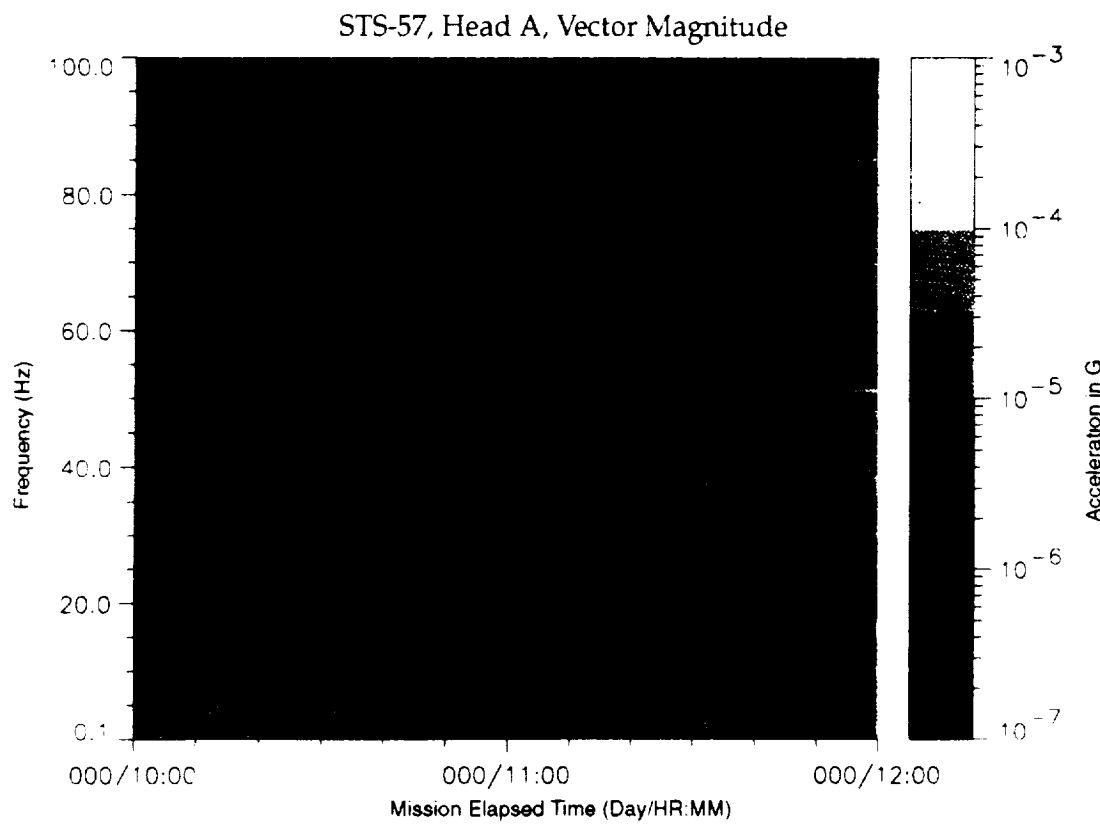


Figure B-5: SPACEHAB-1, Forward Bulkhead T-Beam

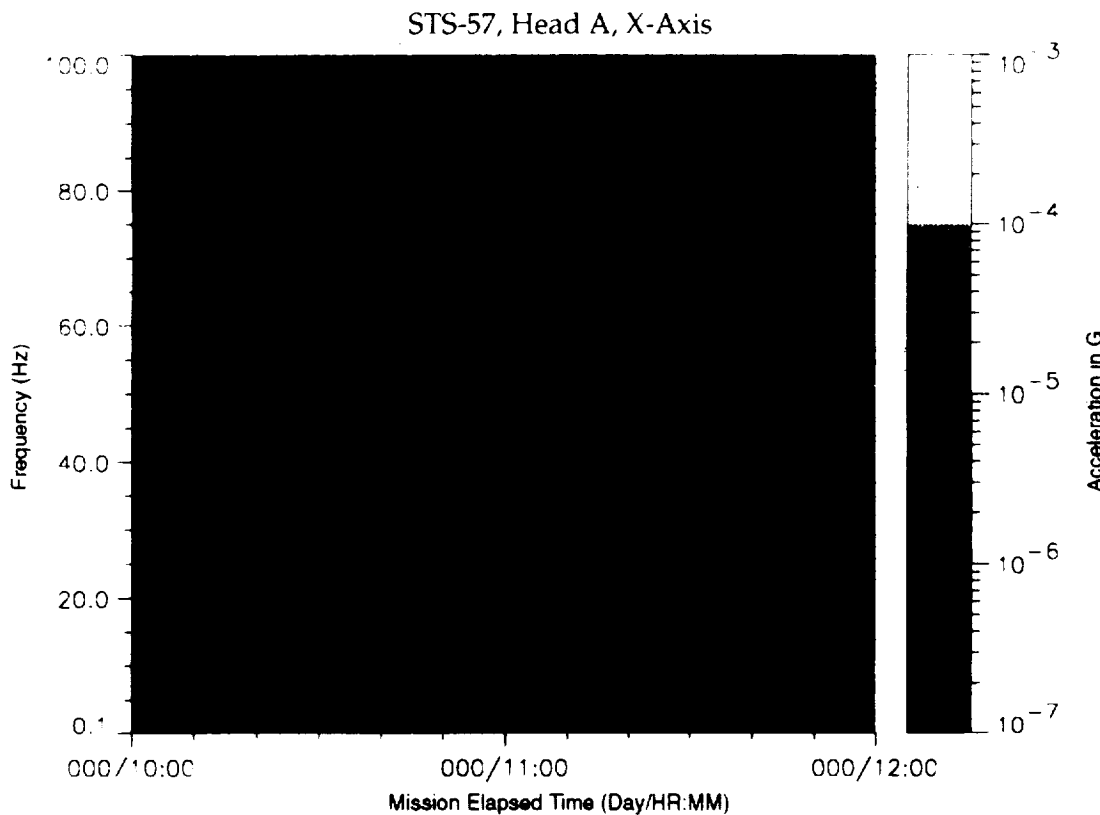


Figure B-6: SPACEHAB-1, Forward Bulkhead T-Beam

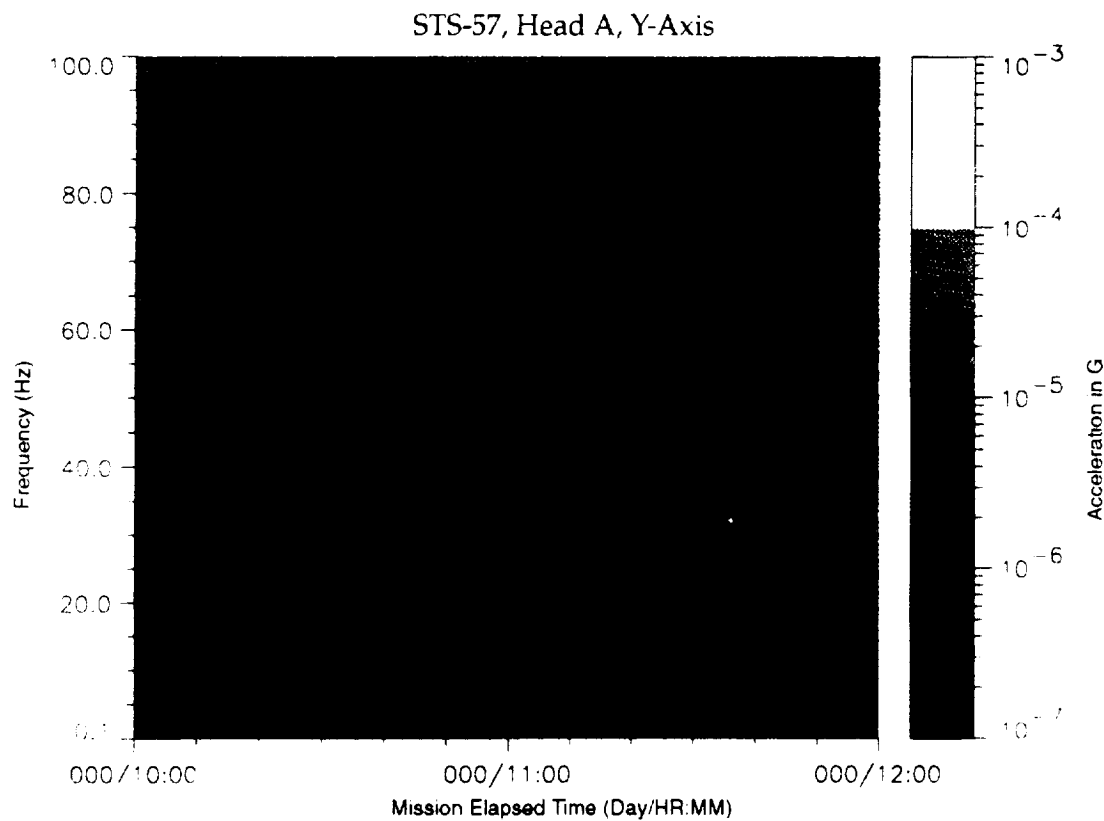


Figure B-7: SPACEHAB-1, Forward Bulkhead T-Beam

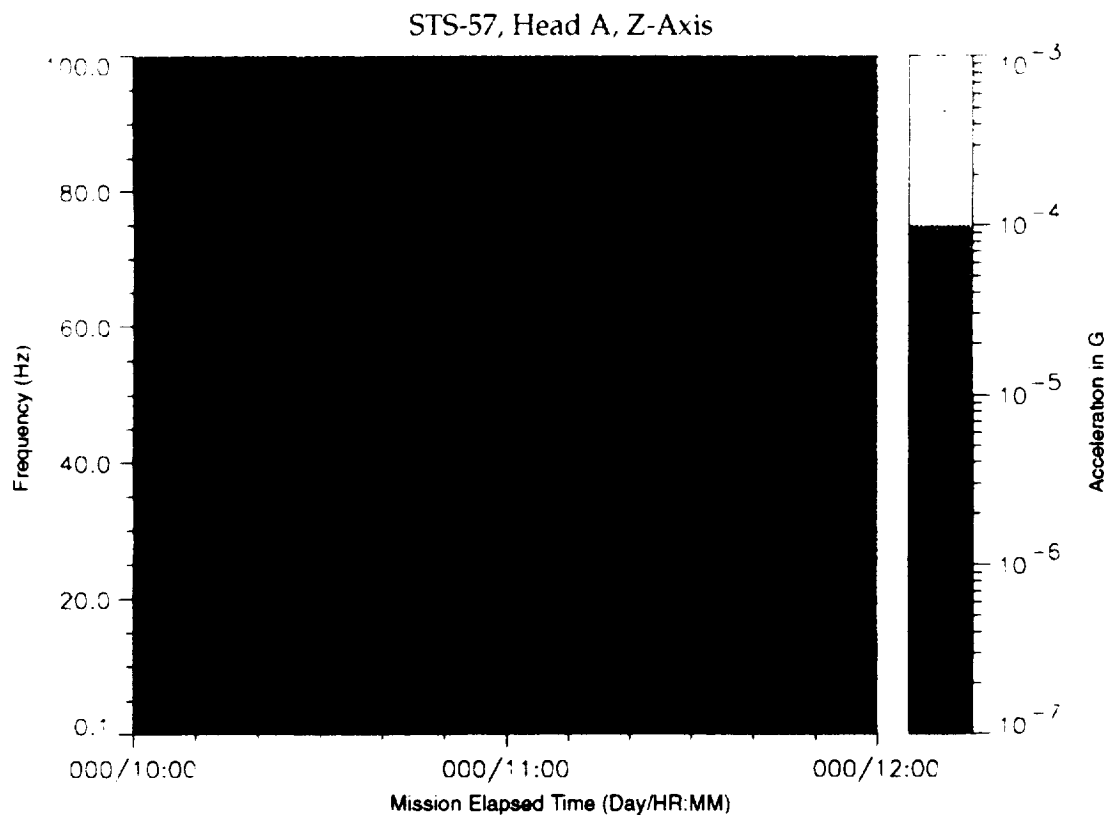


Figure B-8: SPACEHAB-1, Forward Bulkhead T-Beam

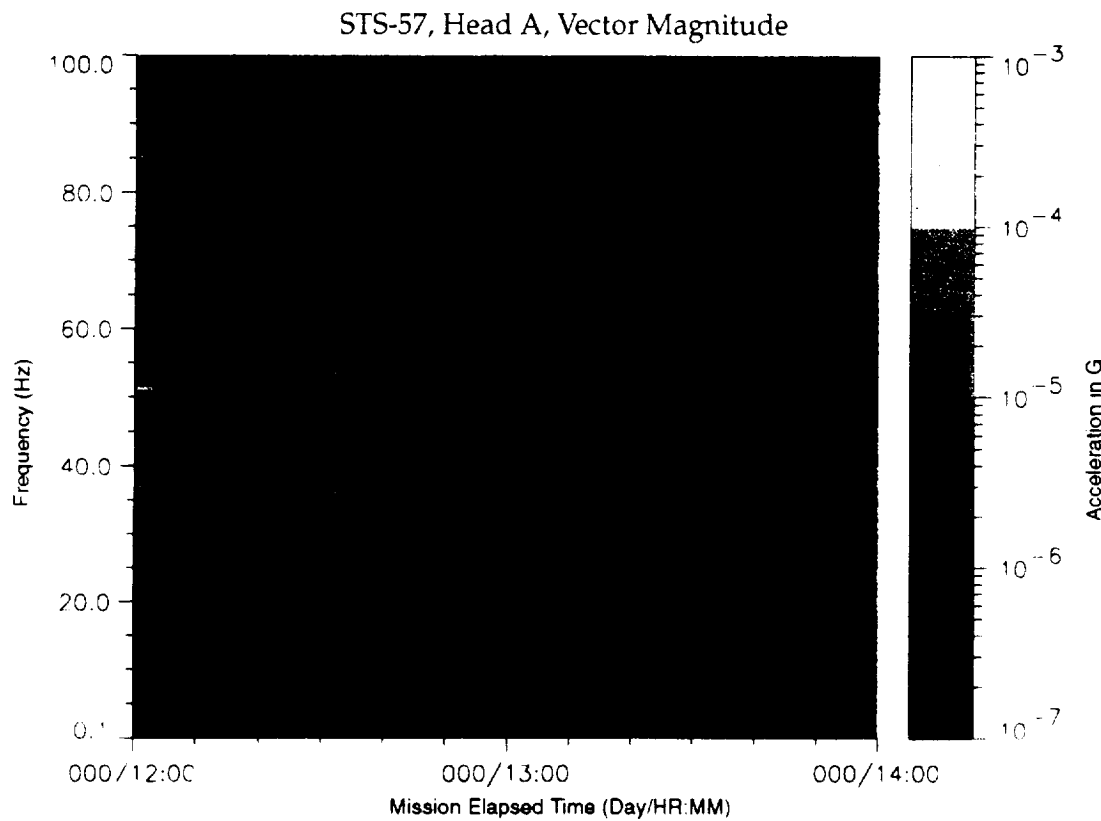


Figure B-9: SPACEHAB-1, Forward Bulkhead T-Beam

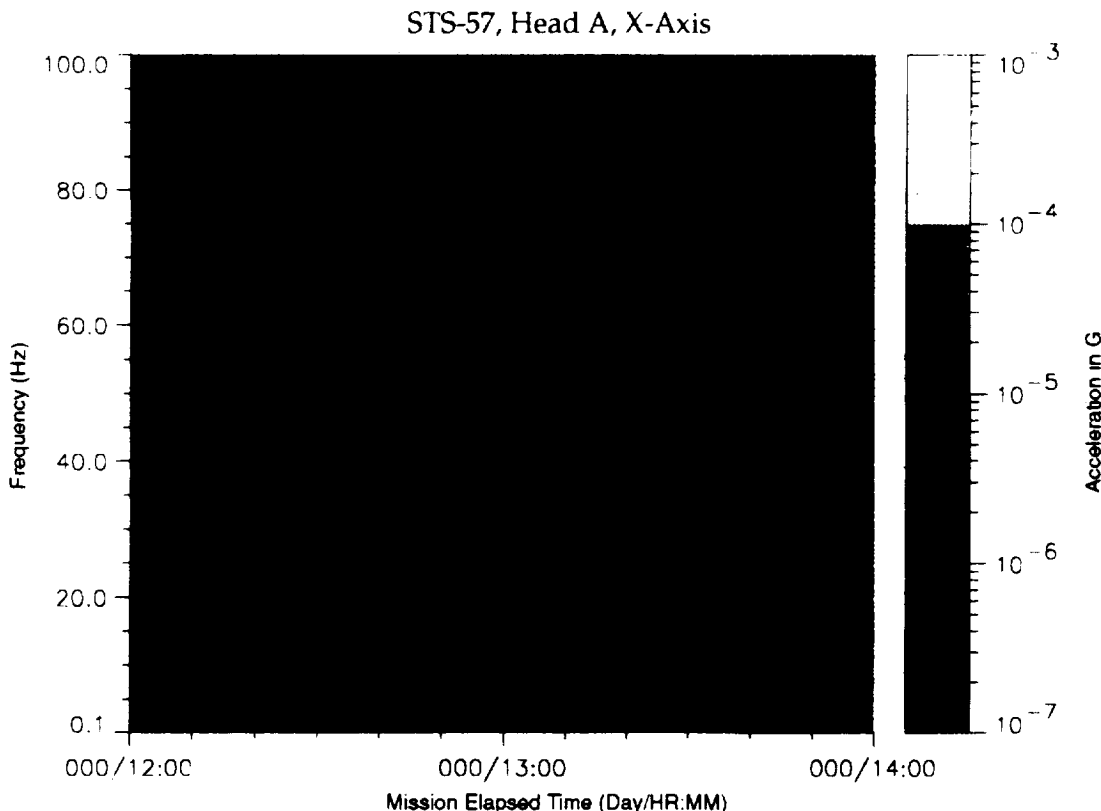


Figure B-10: SPACEHAB-1, Forward Bulkhead T-Beam

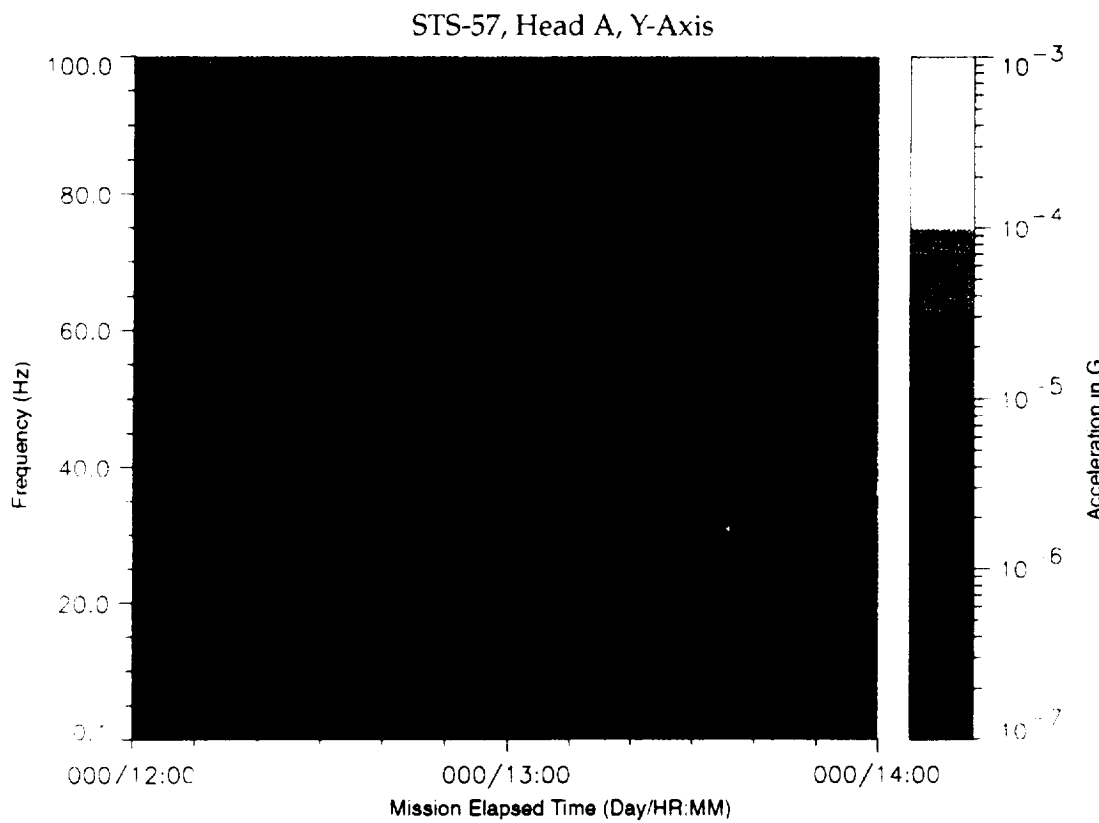


Figure B-11: SPACEHAB-1, Forward Bulkhead T-Beam

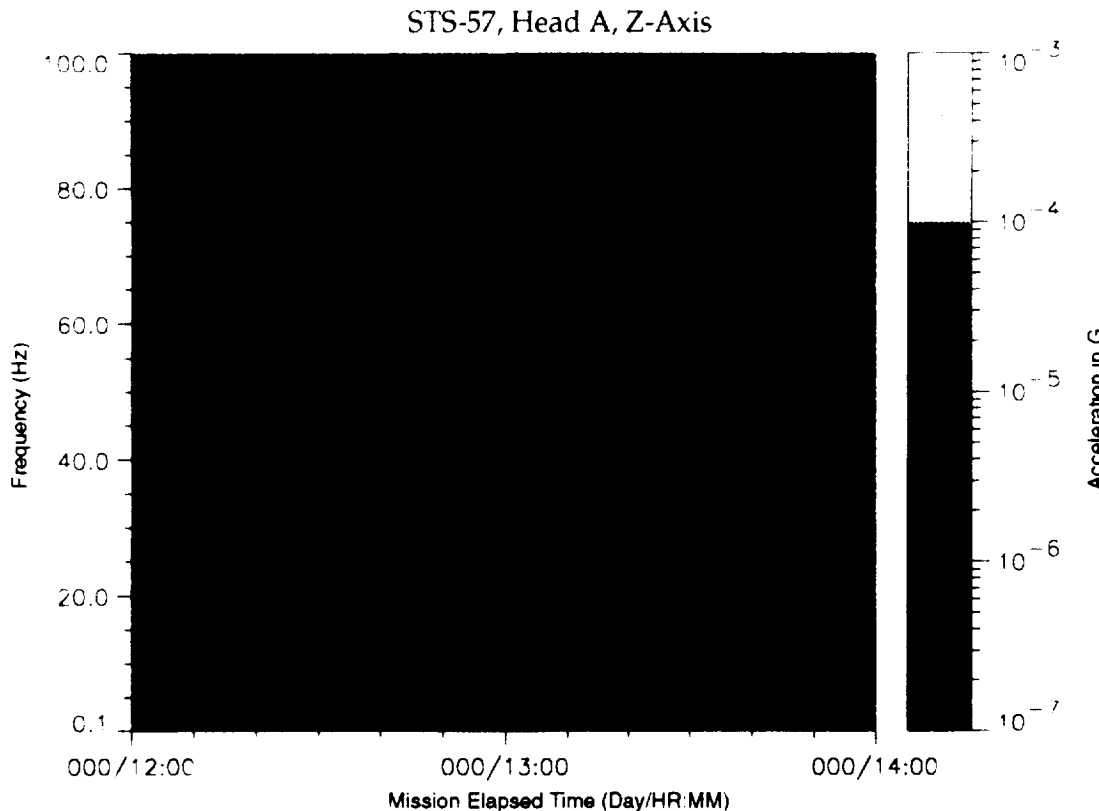


Figure B-12: SPACEHAB-1, Forward Bulkhead T-Beam

STS-57, Head A, Vector Magnitude

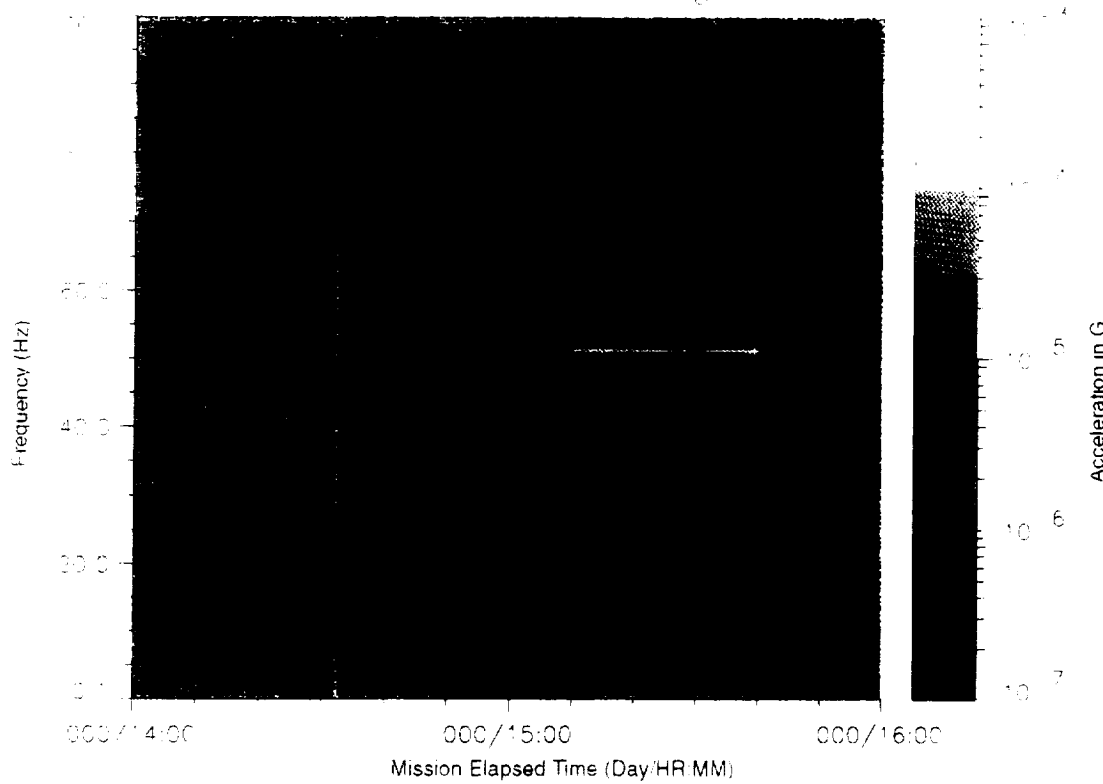


Figure B-13: SPACEHAB-1, Forward Bulkhead T-Beam

STS-57, Head A, X-Axis

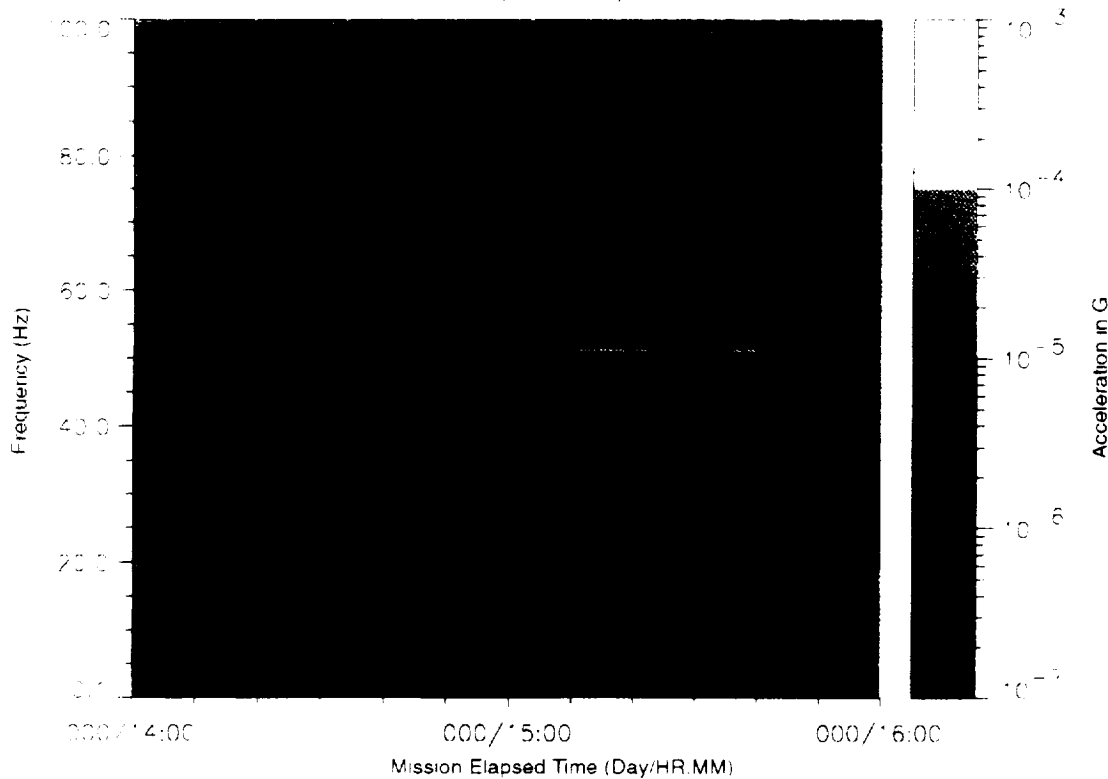


Figure B-14. SPACEHAB-1, Forward Bulkhead T-Beam

STS-57, Head A, Y-Axis

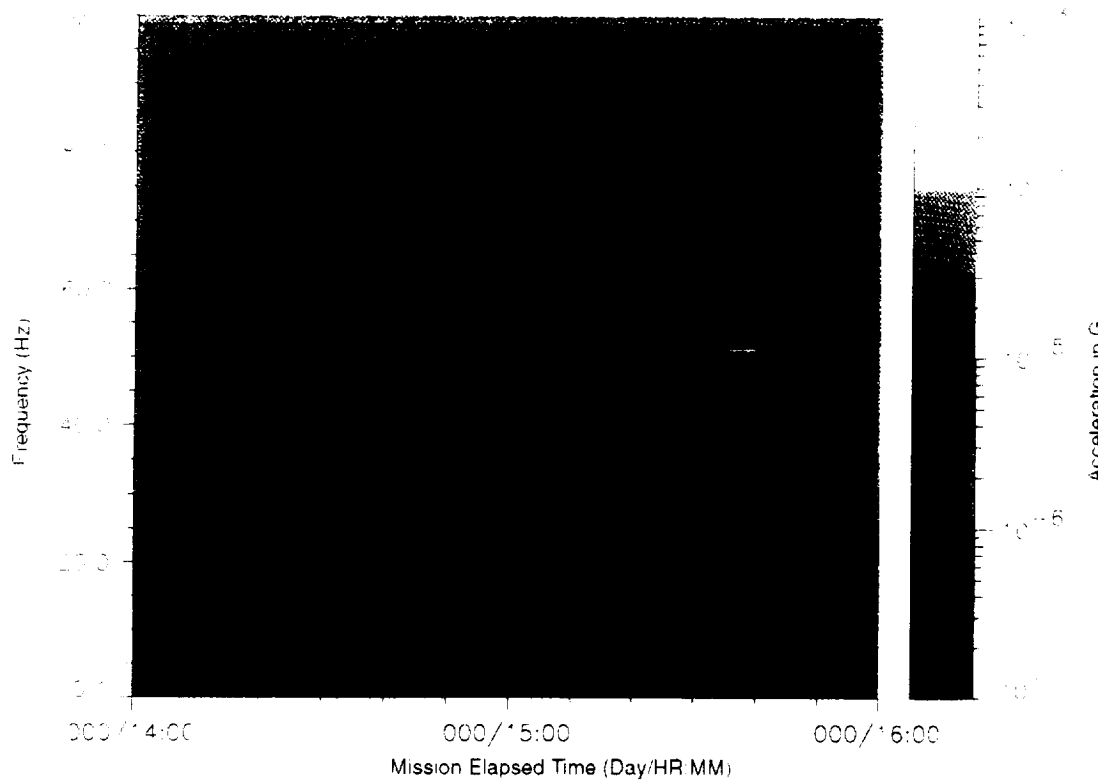


Figure B-15: SPACEHAB-1, Forward Bulkhead T-Beam

STS-57, Head A, Z-Axis

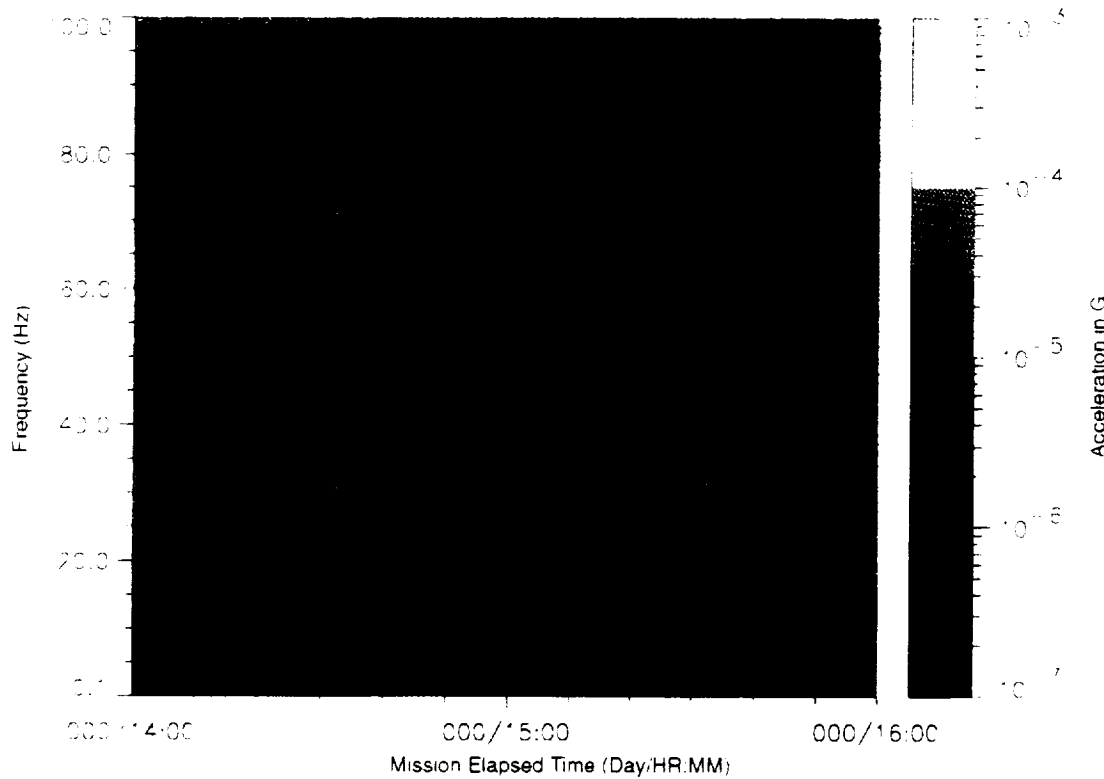


Figure B-16: SPACEHAB-1, Forward Bulkhead T-Beam

SIS-57, Head A, Vector Magnitude

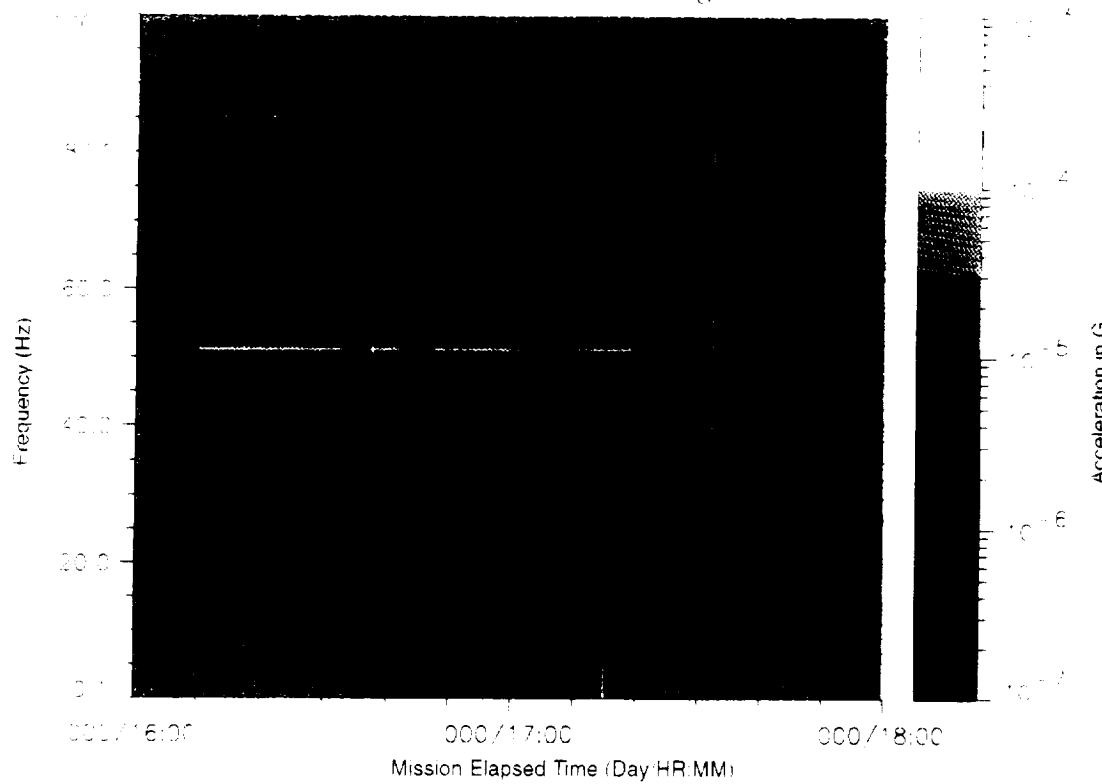


Figure B-17: SPACEHAB-1, Forward Bulkhead T-Beam

STS-57, Head A, X-Axis

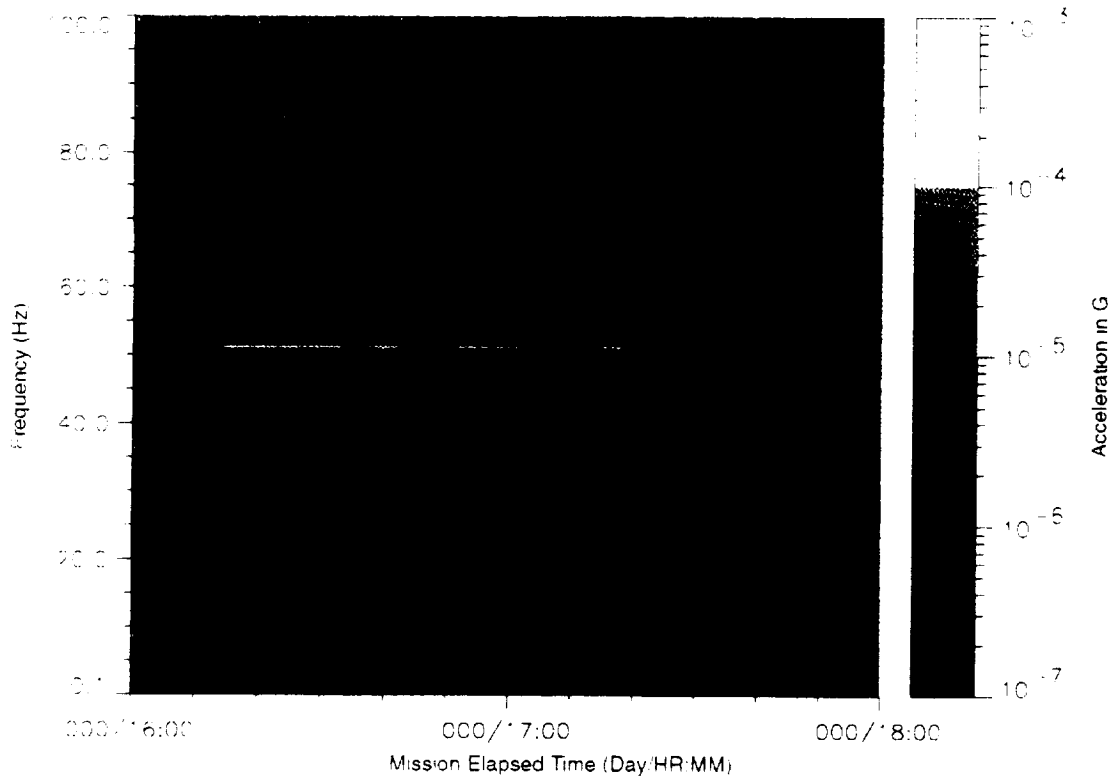


Figure B-18: SPACEHAB-1, Forward Bulkhead T-Beam

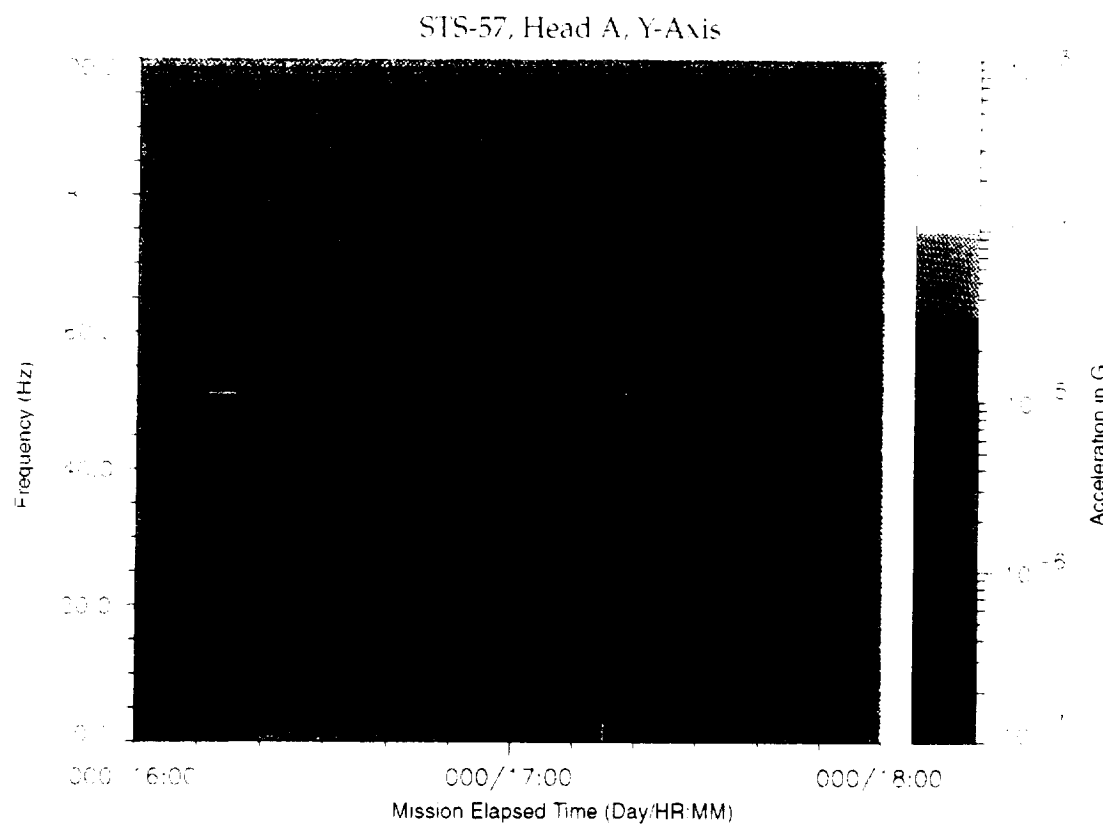


Figure B-19: SPACEHAB-1, Forward Bulkhead T-Beam

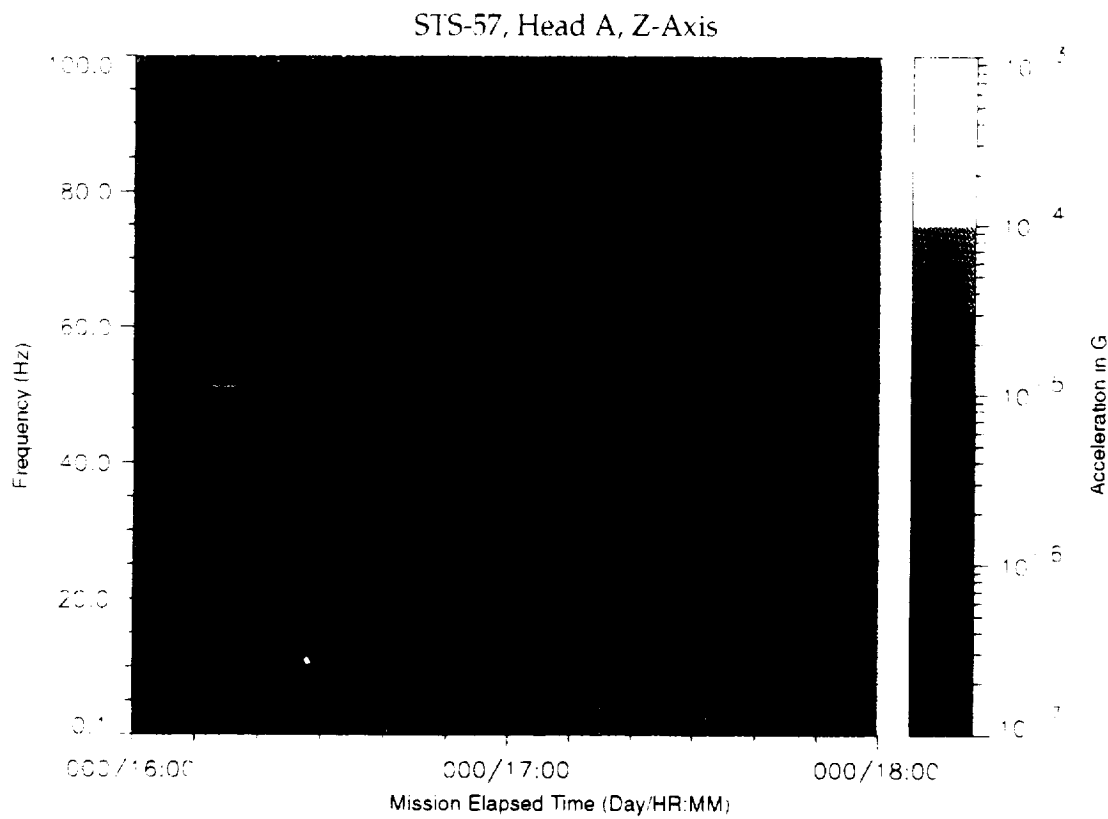


Figure B-20: SPACEHAB-1, Forward Bulkhead T-Beam

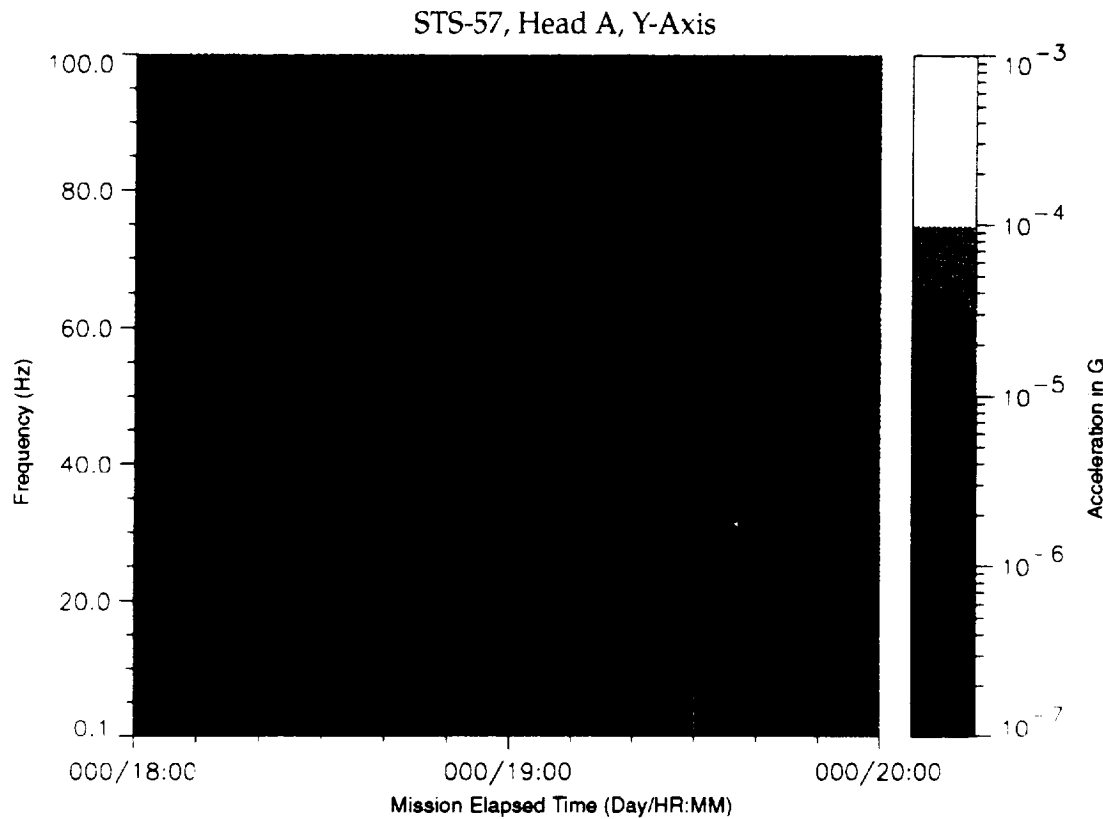


Figure B-23: SPACEHAB-1, Forward Bulkhead T-Beam

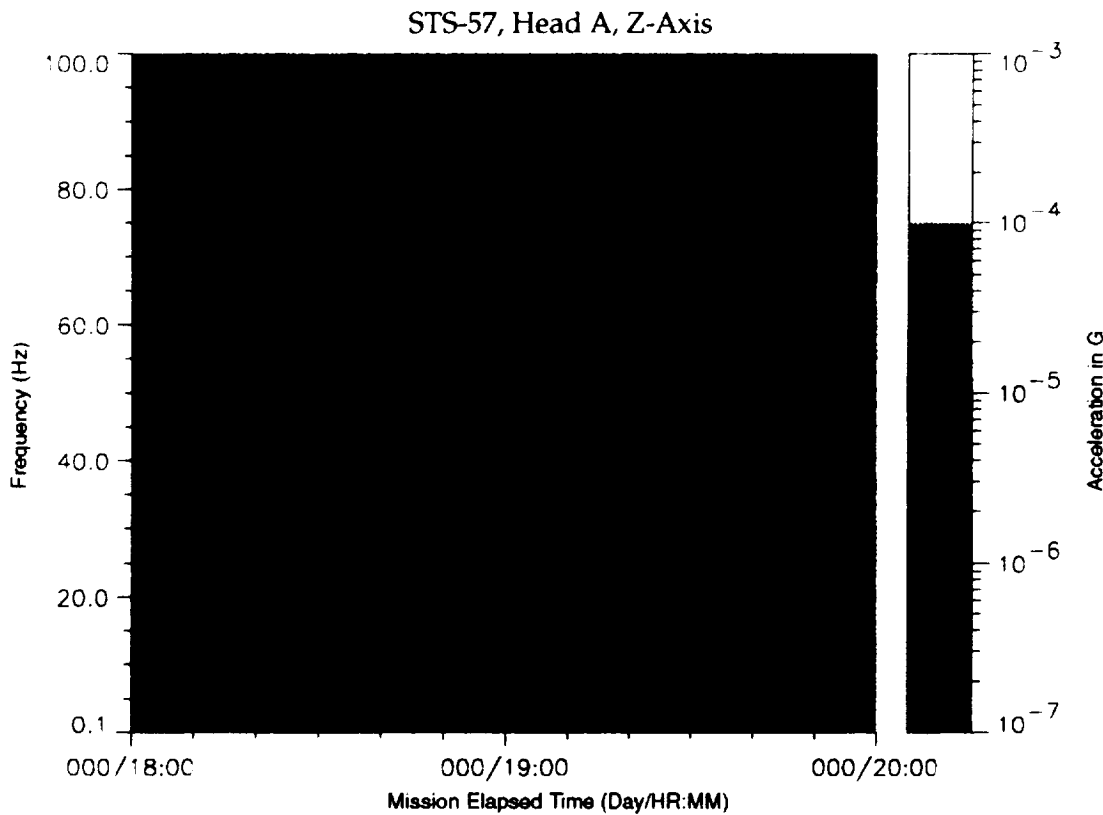


Figure B-24: SPACEHAB-1, Forward Bulkhead T-Beam

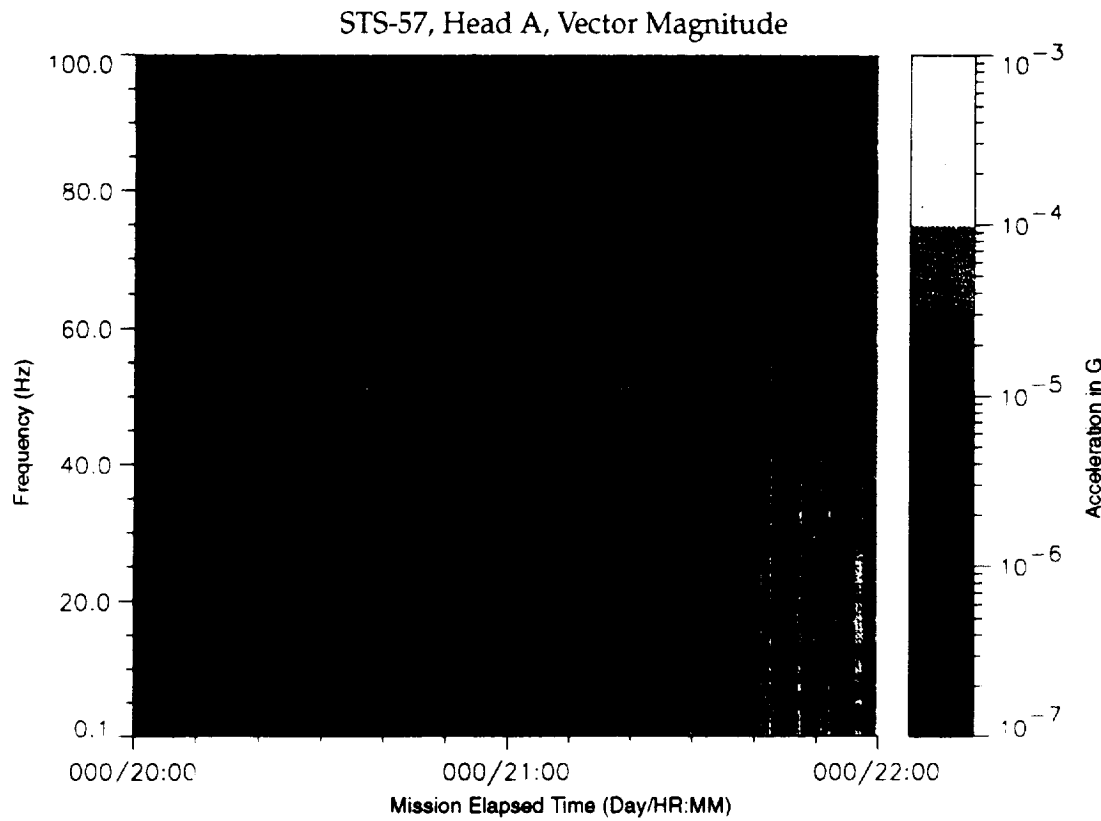


Figure B-25: SPACEHAB-1, Forward Bulkhead T-Beam

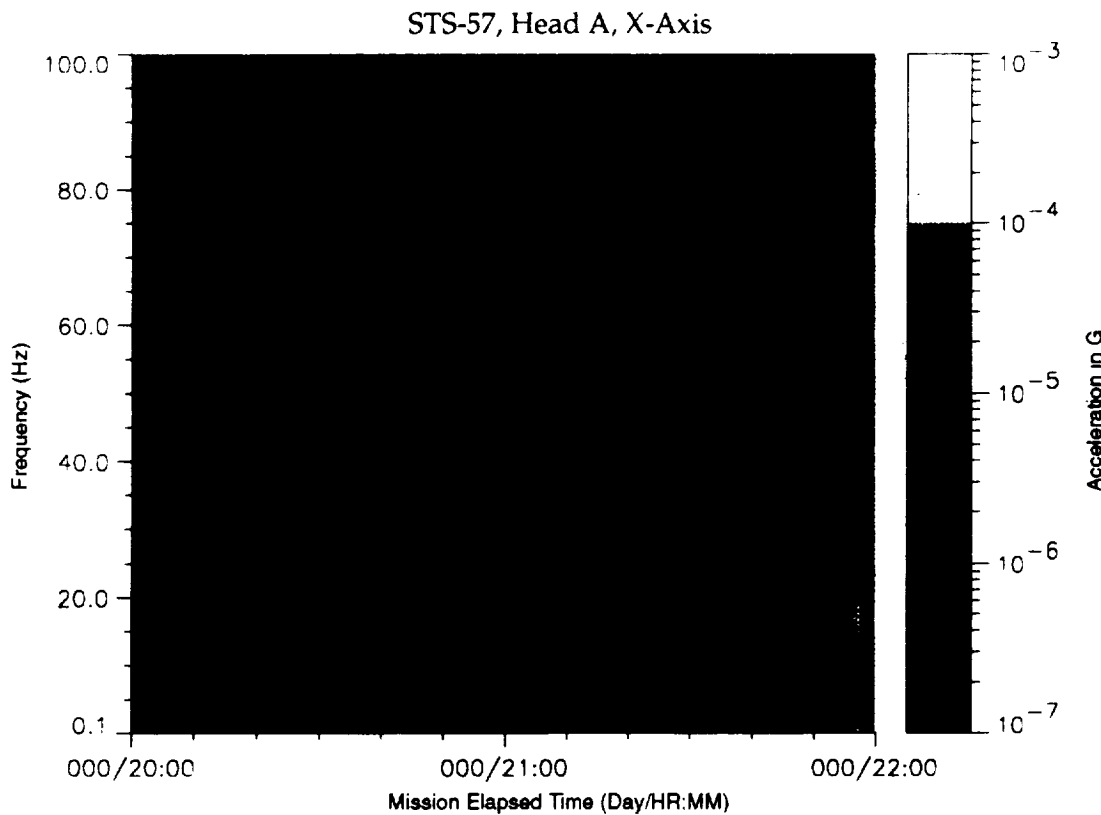


Figure B-26: SPACEHAB-1, Forward Bulkhead T-Beam

STS-57, Head A, Y-Axis

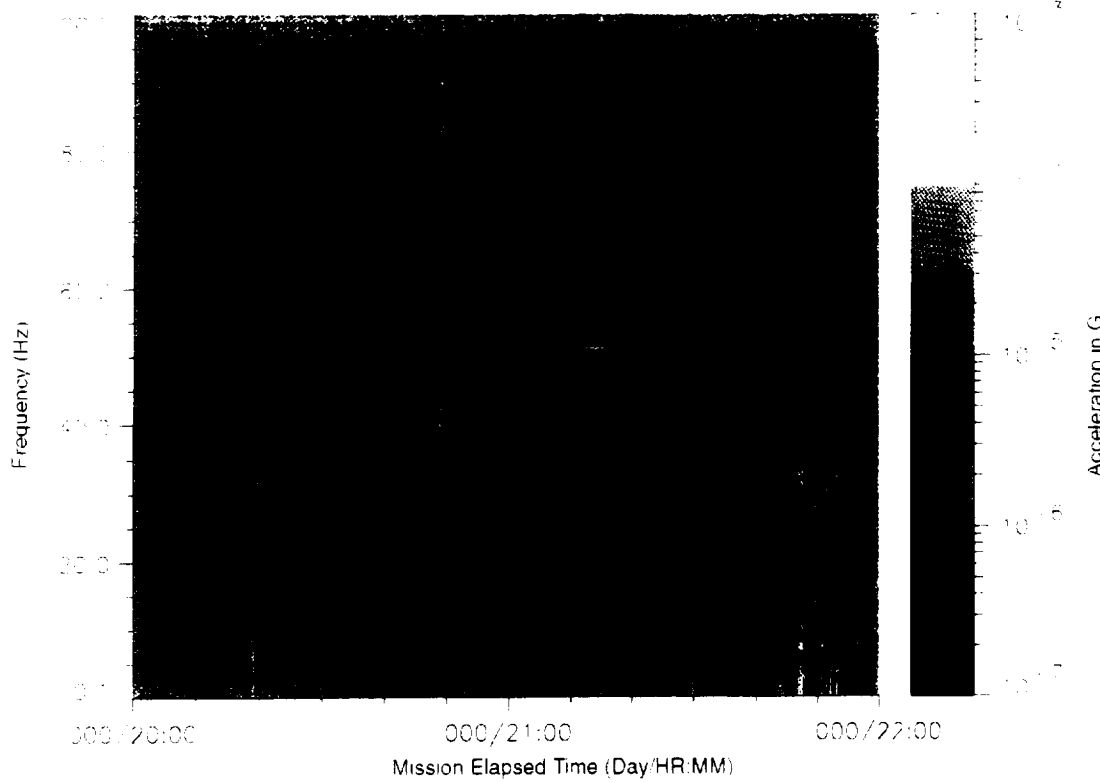


Figure B-27: SPACEHAB-1, Forward Bulkhead T-Beam

STS-57, Head A, Z-Axis

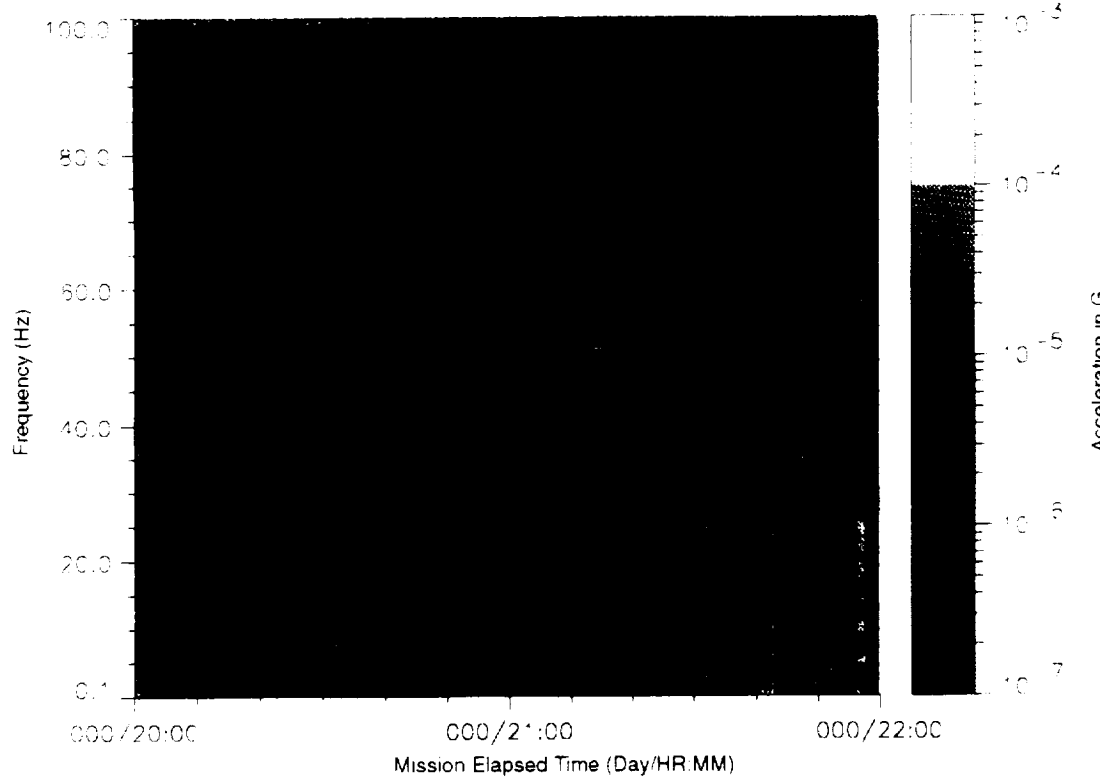


Figure B-28: SPACEHAB-1, Forward Bulkhead T-Beam

SIS-57, Head A, Vector Magnitude

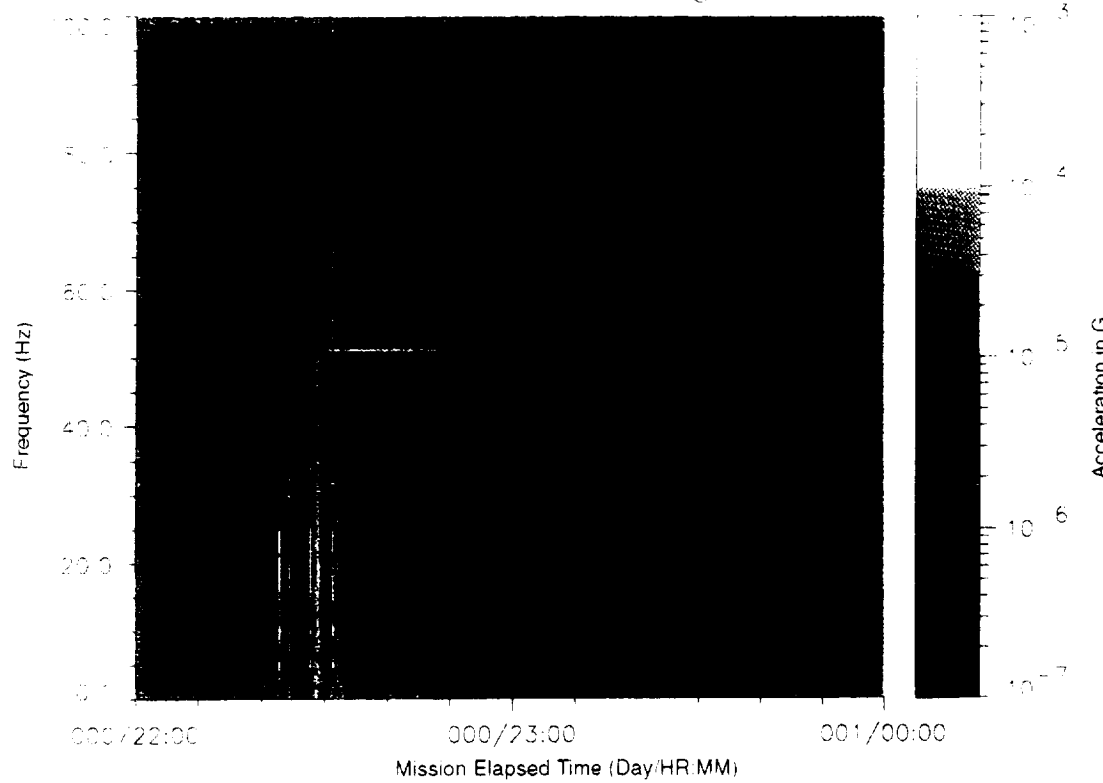


Figure B-29: SPACEHAB-1, Forward Bulkhead T-Beam

STS-57, Head A, X-Axis

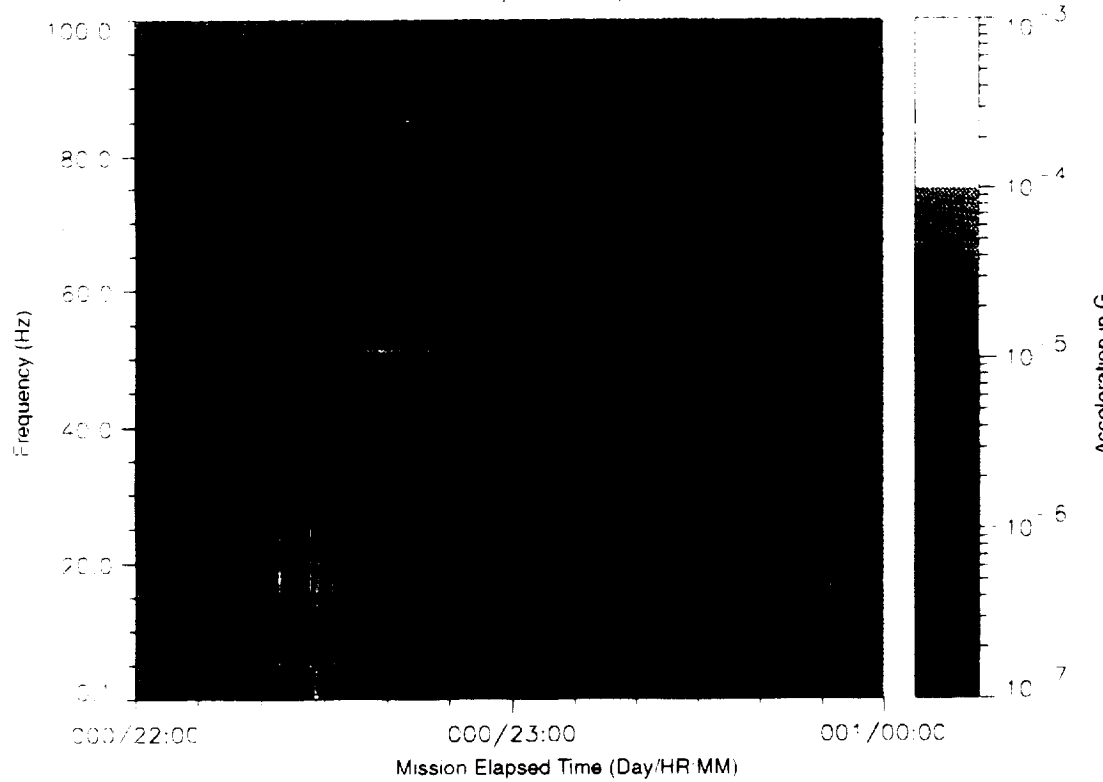


Figure B-30: SPACEHAB-1, Forward Bulkhead T-Beam

~~PHOTOGRAPHIC FILM NOT FILMED~~

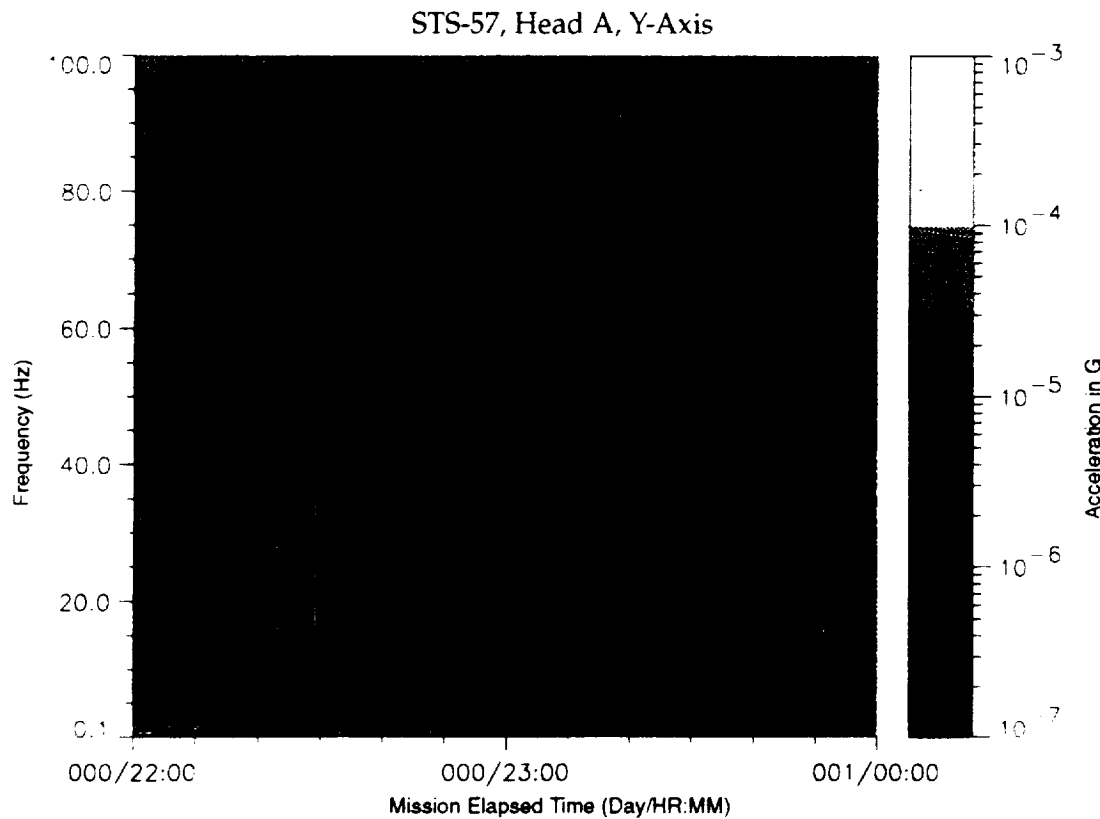


Figure B-31: SPACEHAB-1, Forward Bulkhead T-Beam

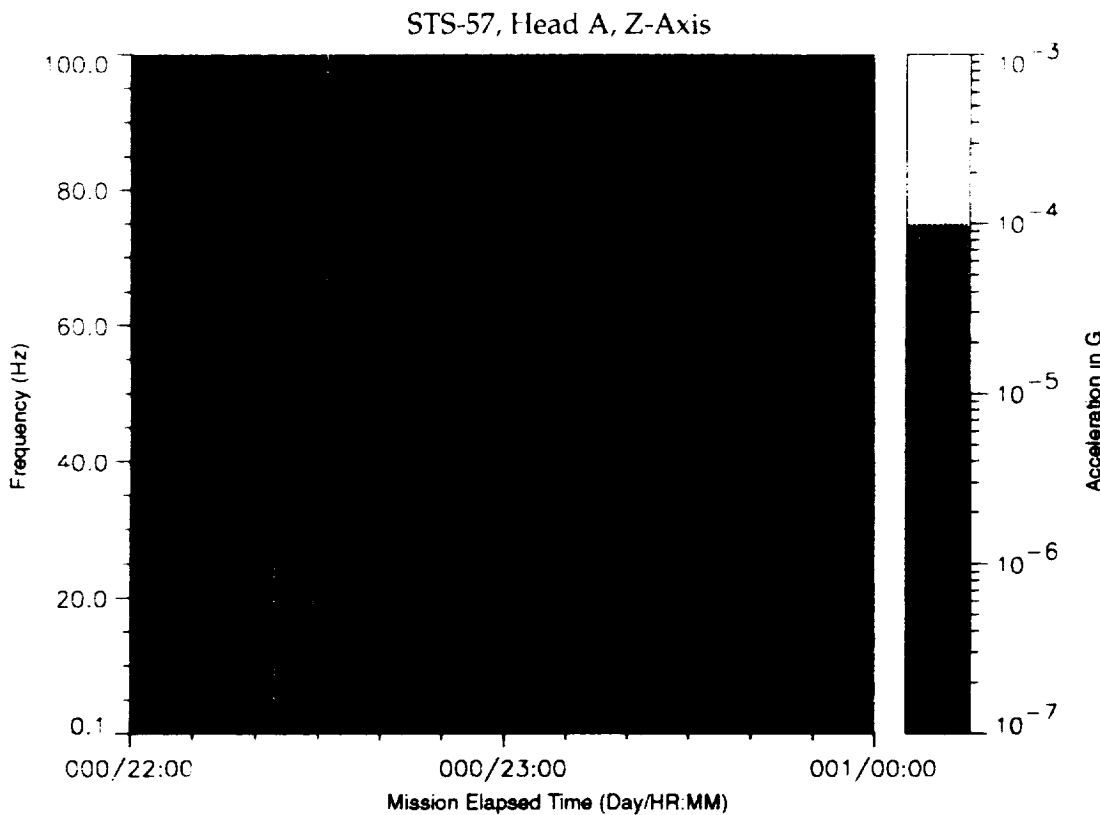


Figure B-32: SPACEHAB-1, Forward Bulkhead T-Beam

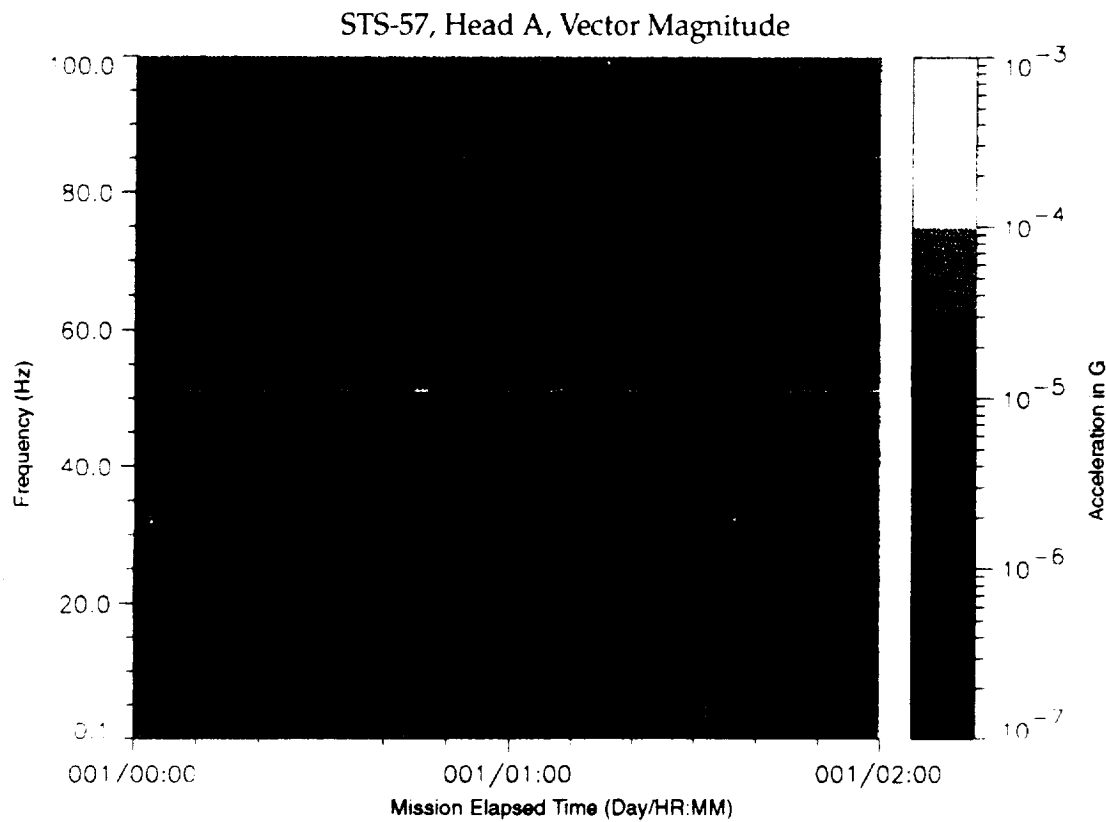


Figure B-33: SPACEHAB-1, Forward Bulkhead T-Beam

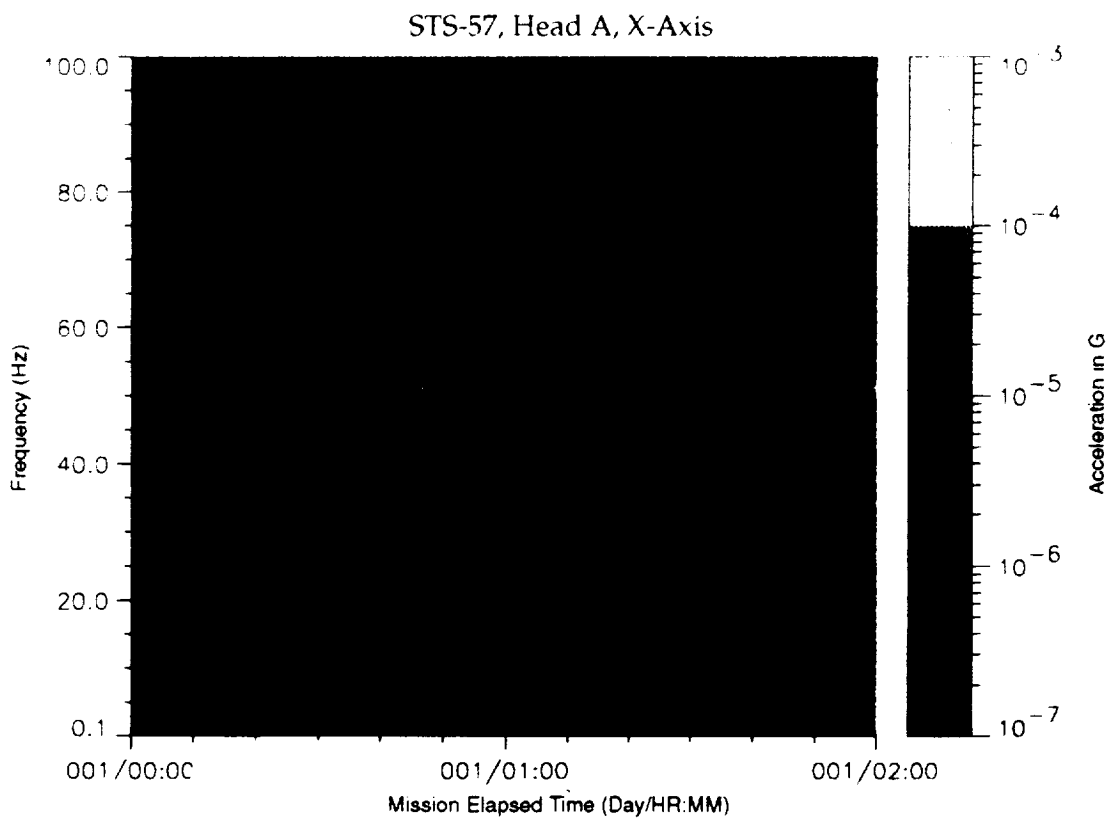


Figure B-34: SPACEHAB-1, Forward Bulkhead T-Beam

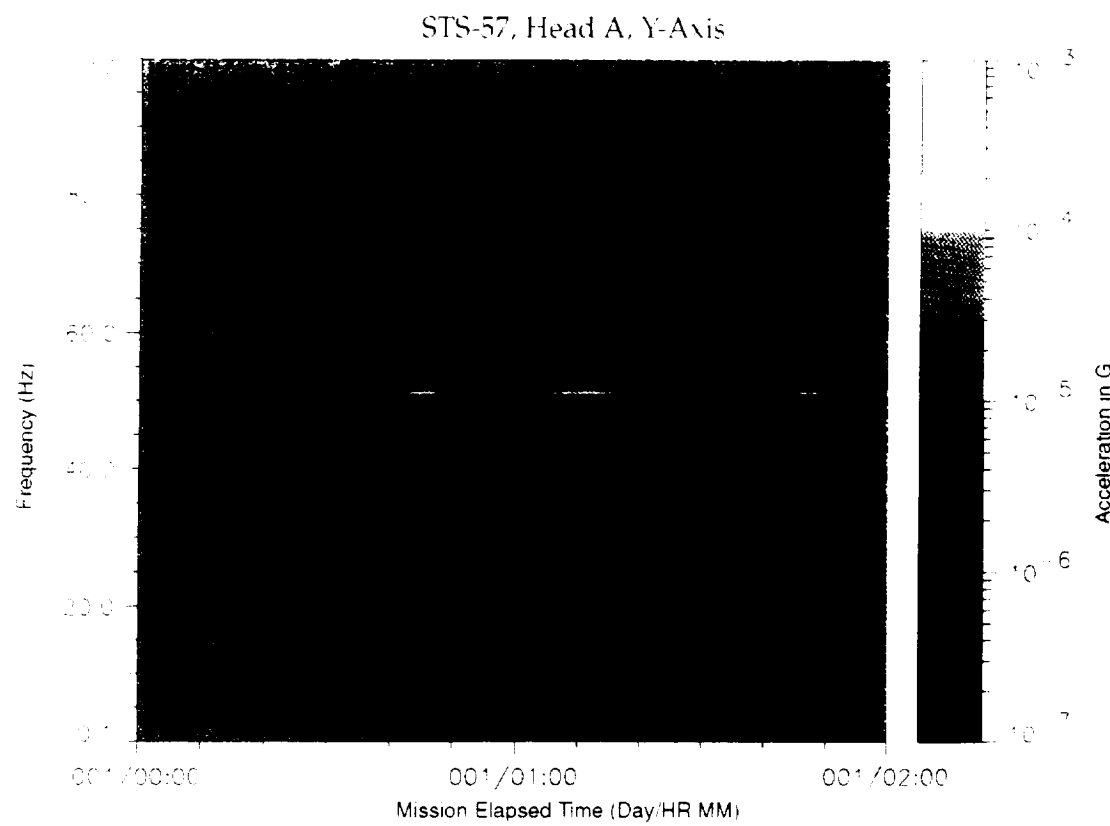


Figure B-35: SPACEHAB-1, Forward Bulkhead T-Beam

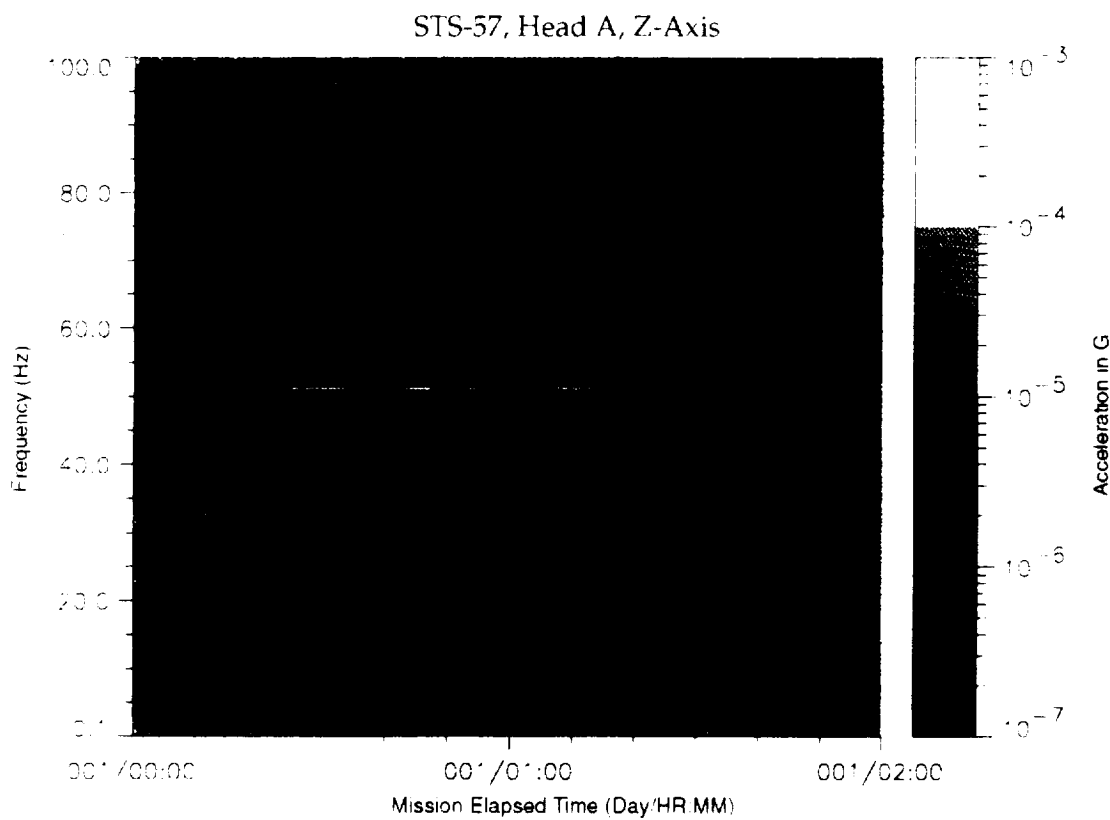


Figure B-36: SPACEHAB-1, Forward Bulkhead T-Beam

STS-57, Head A, Vector Magnitude

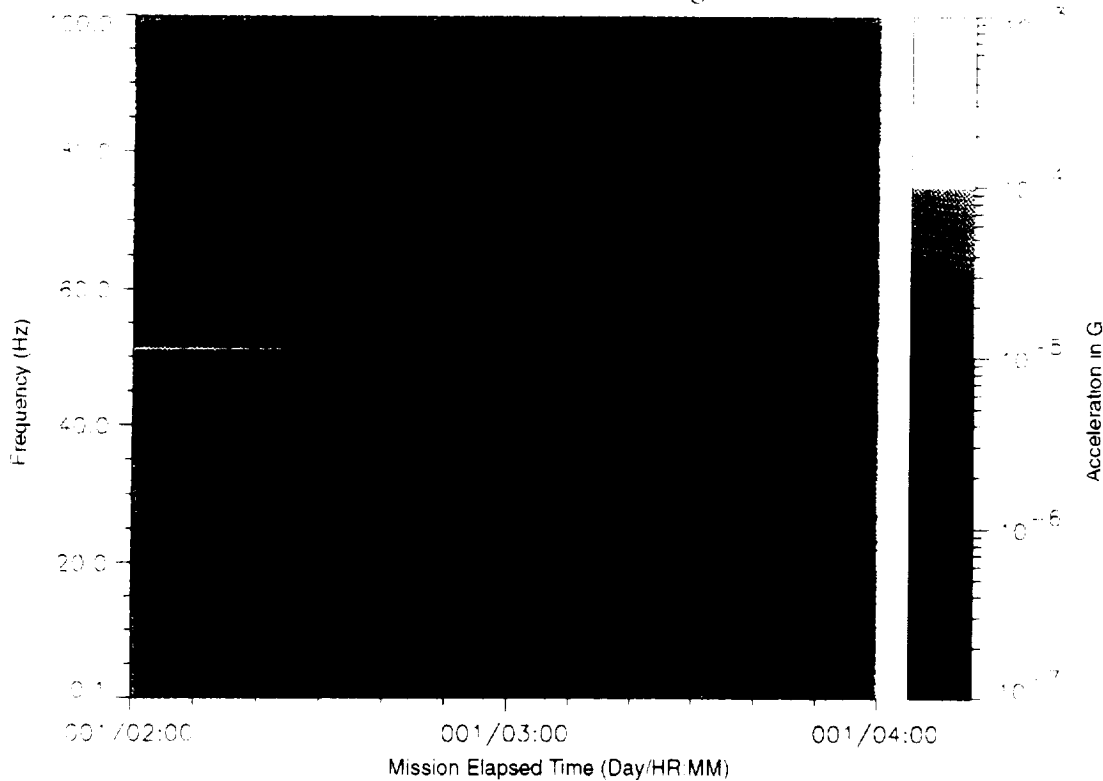


Figure B-37: SPACEHAB-1, Forward Bulkhead T-Beam

STS-57, Head A, X-Axis

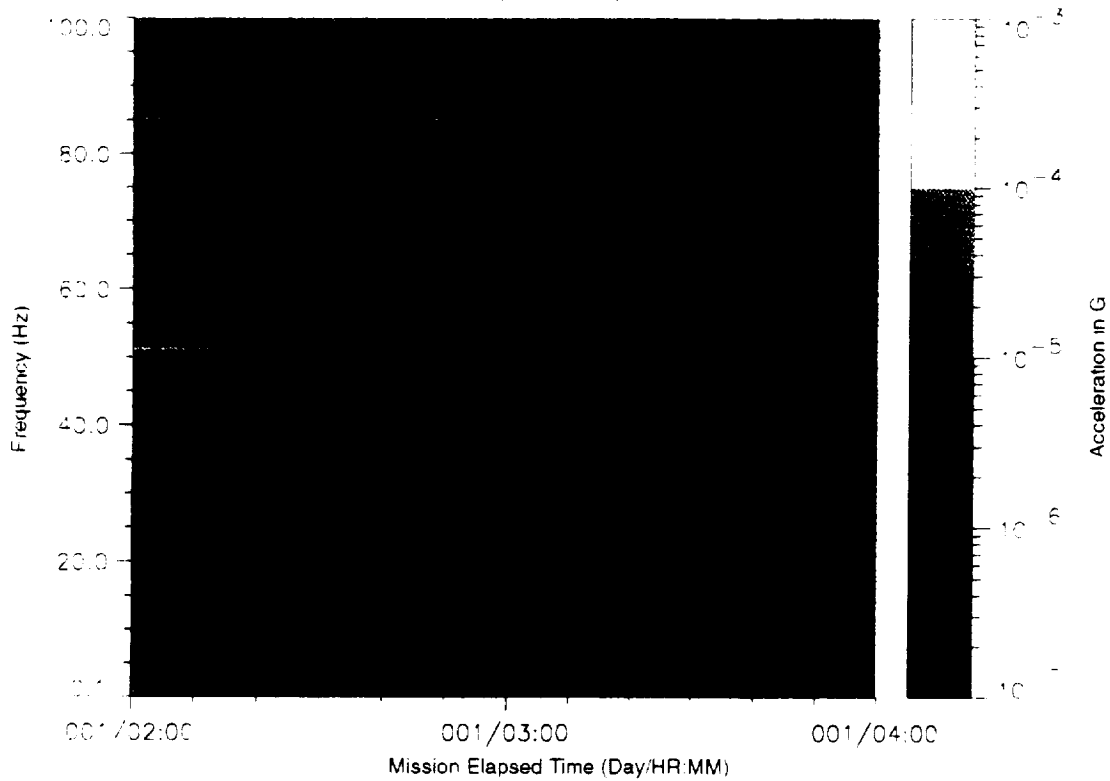


Figure B-38: SPACEHAB-1, Forward Bulkhead T-Beam

PRECEDING PAGE BLANK NOT FILMED

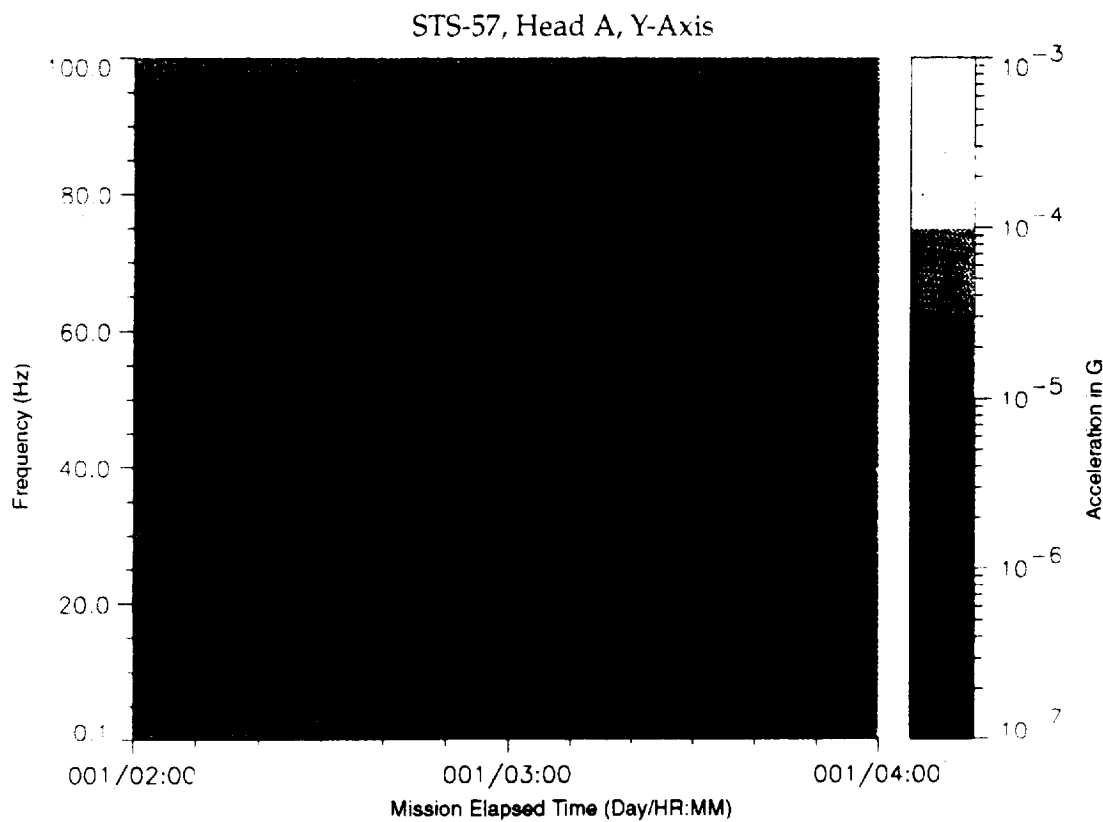


Figure B-39: SPACEHAB-1, Forward Bulkhead T-Beam

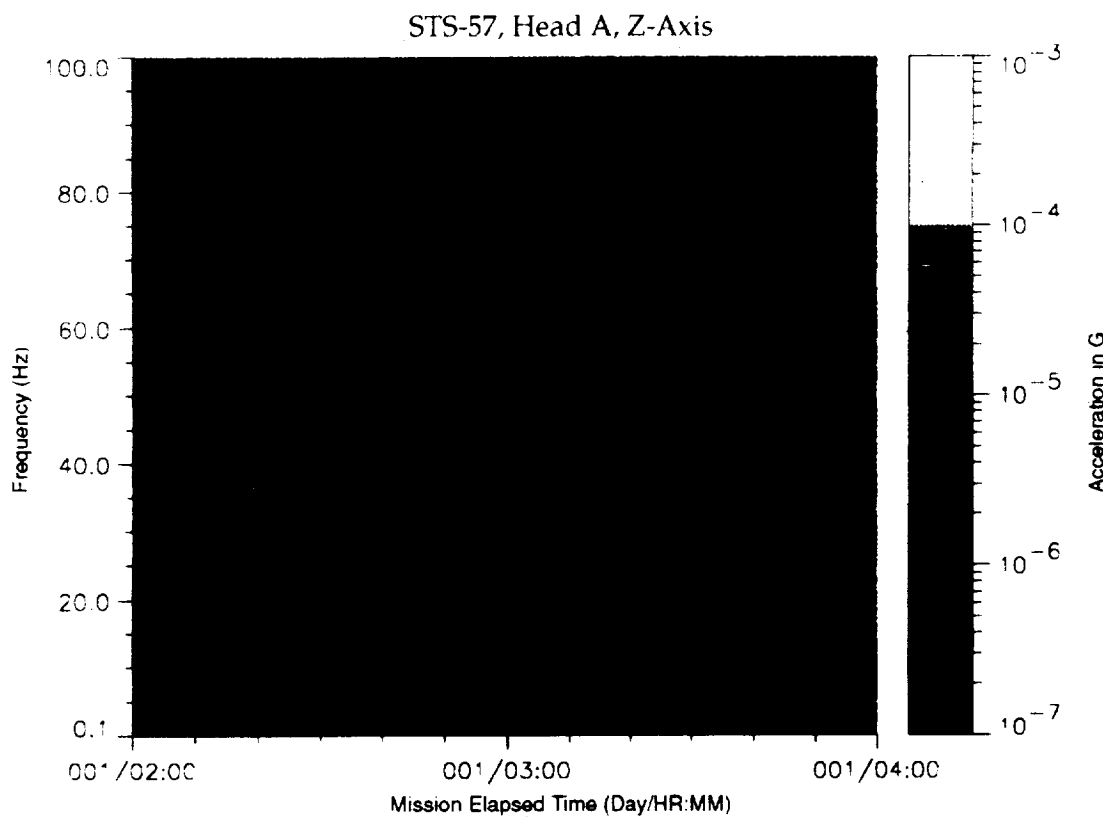


Figure B-40: SPACEHAB-1, Forward Bulkhead T-Beam

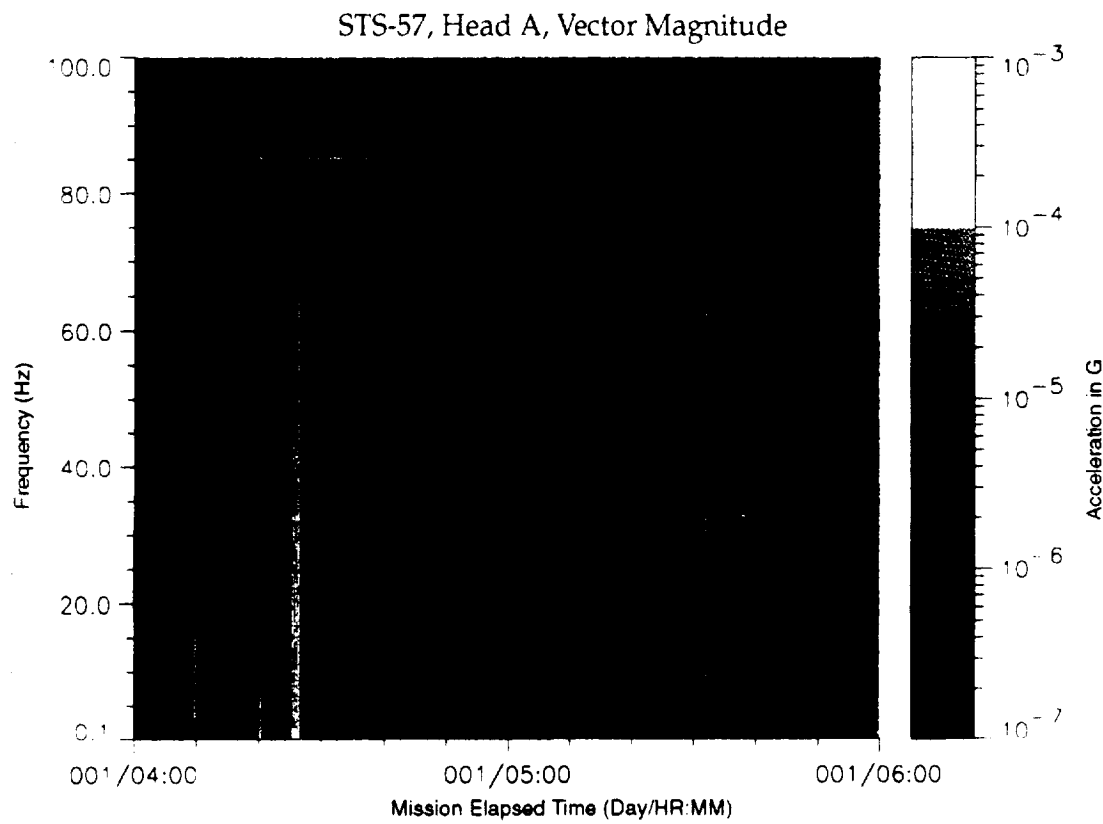


Figure B-41: SPACEHAB-1, Forward Bulkhead T-Beam

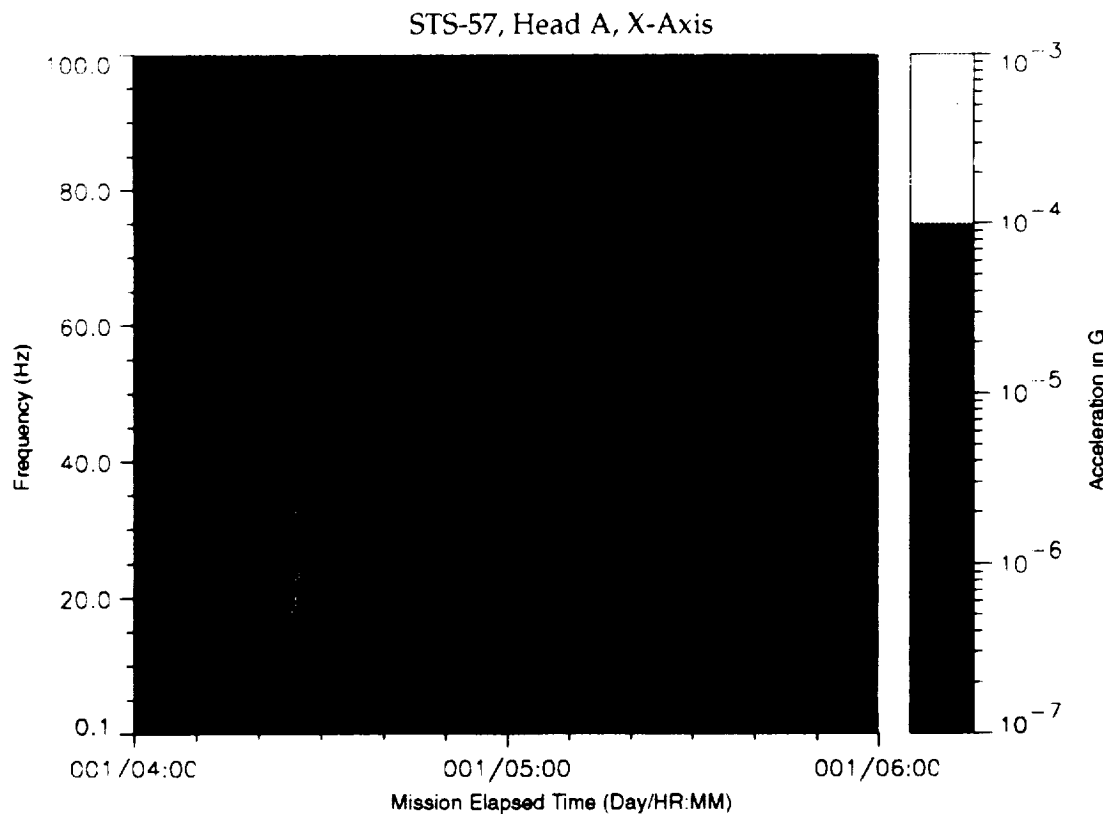


Figure B-42: SPACEHAB-1, Forward Bulkhead T-Beam

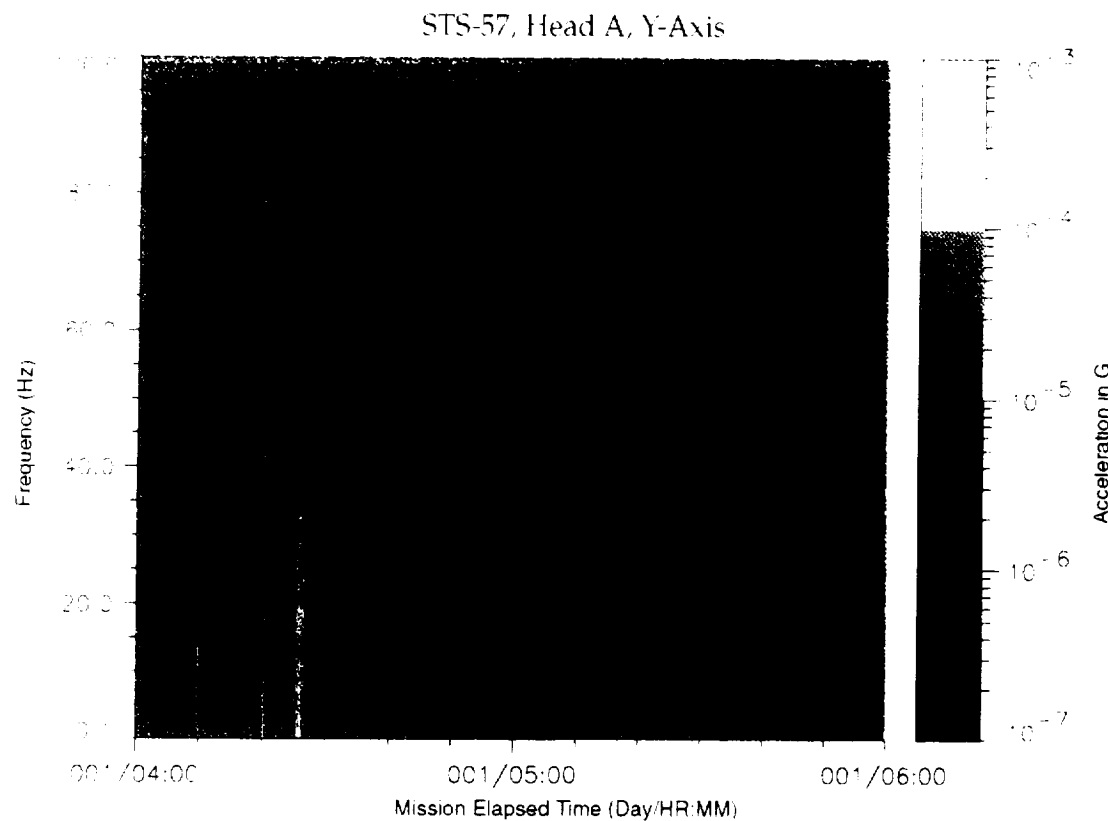


Figure B-43: SPACEHAB-1, Forward Bulkhead T-Beam

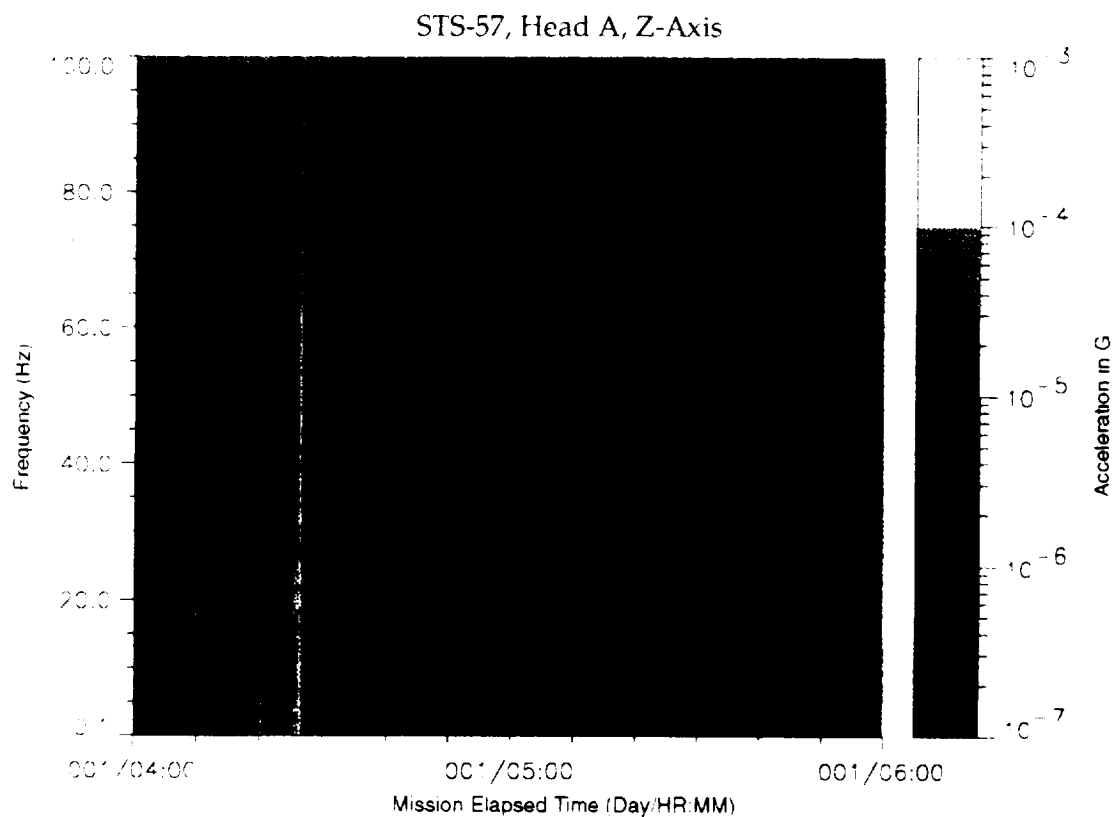


Figure B-44: SPACEHAB-1, Forward Bulkhead T-Beam

STS-57, Head A, Vector Magnitude

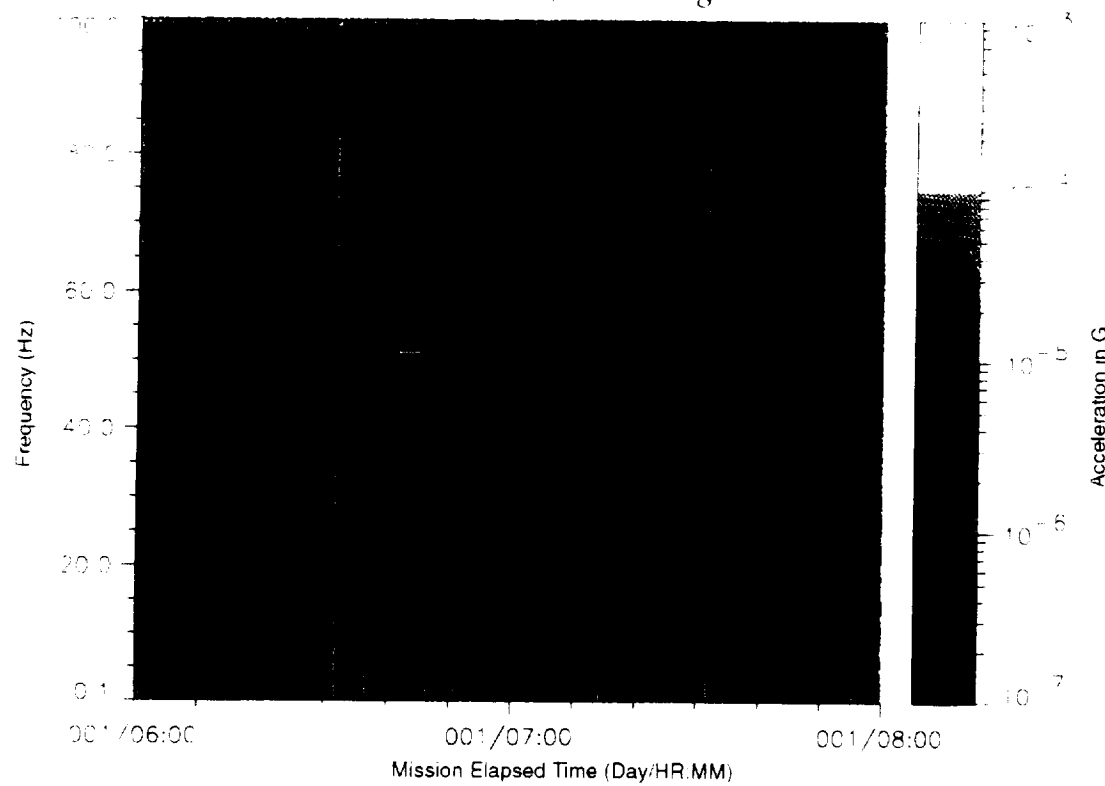


Figure B-45: SPACEHAB-1, Forward Bulkhead T-Beam

STS-57, Head A, X-Axis

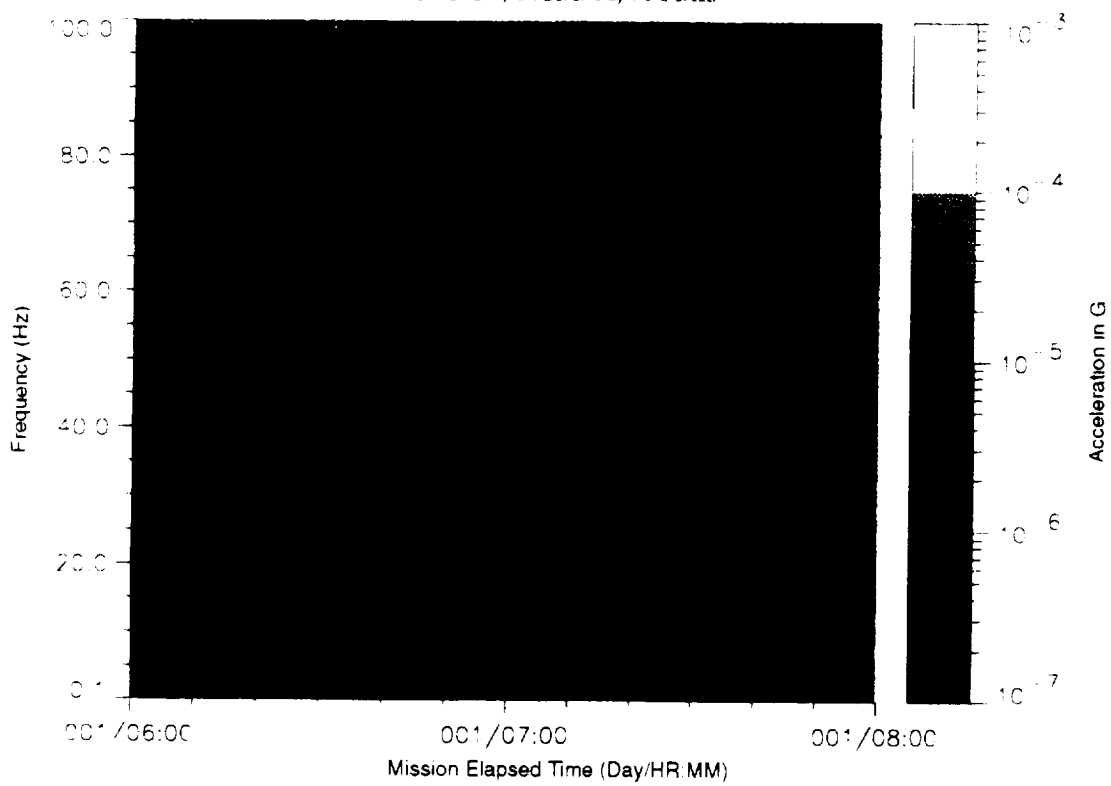


Figure B-46: SPACEHAB-1, Forward Bulkhead T-Beam

PRECEDING PAGE BLANK NOT FILMED

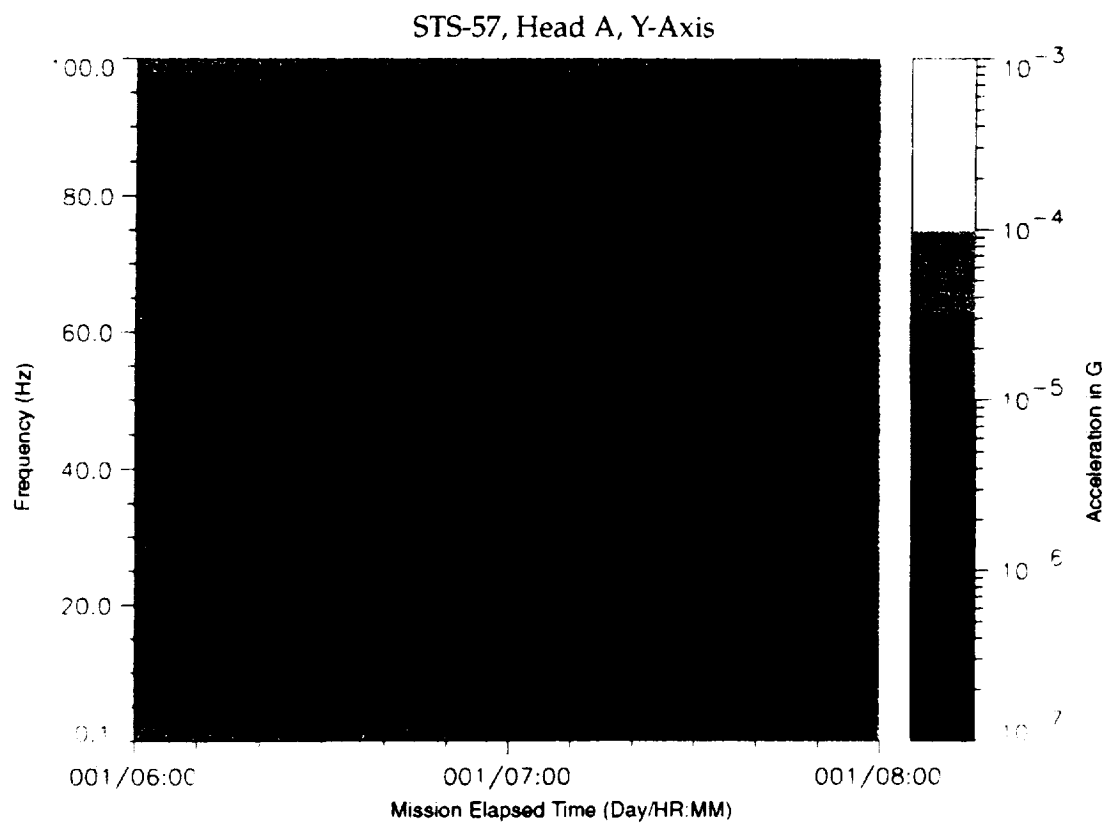


Figure B-47: SPACEHAB-1, Forward Bulkhead T-Beam

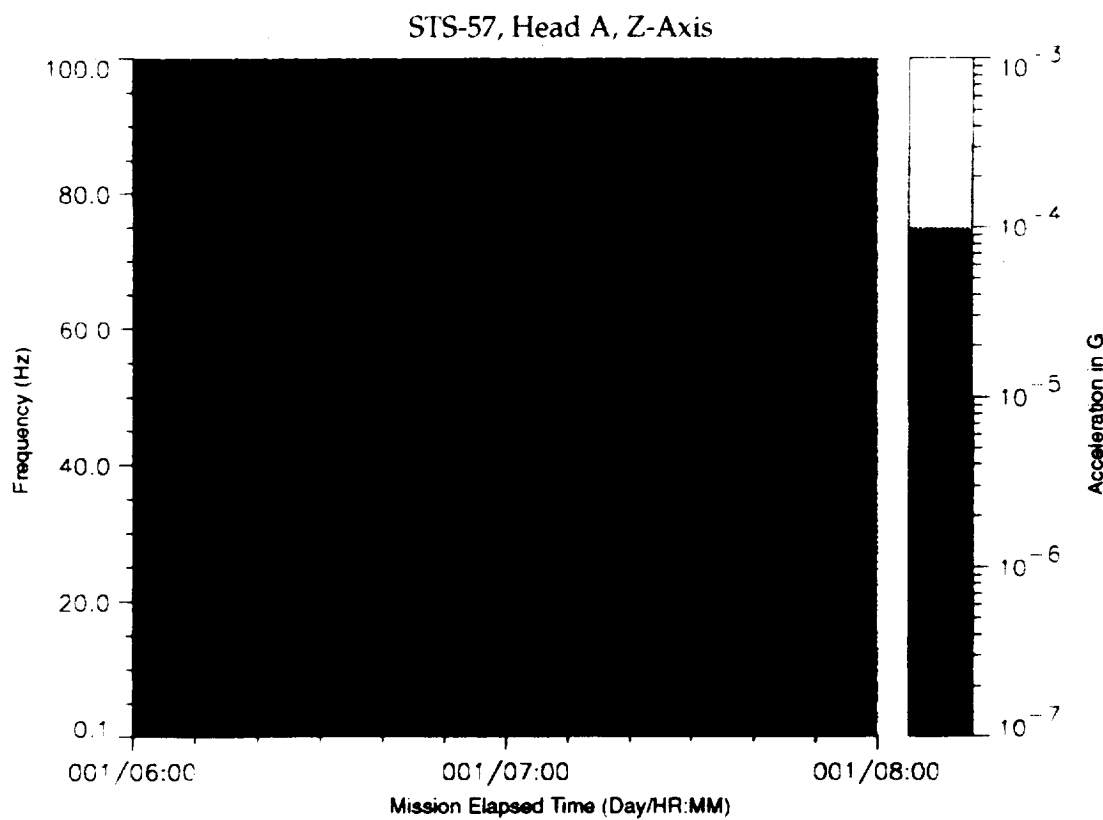


Figure B-48: SPACEHAB-1, Forward Bulkhead T-Beam

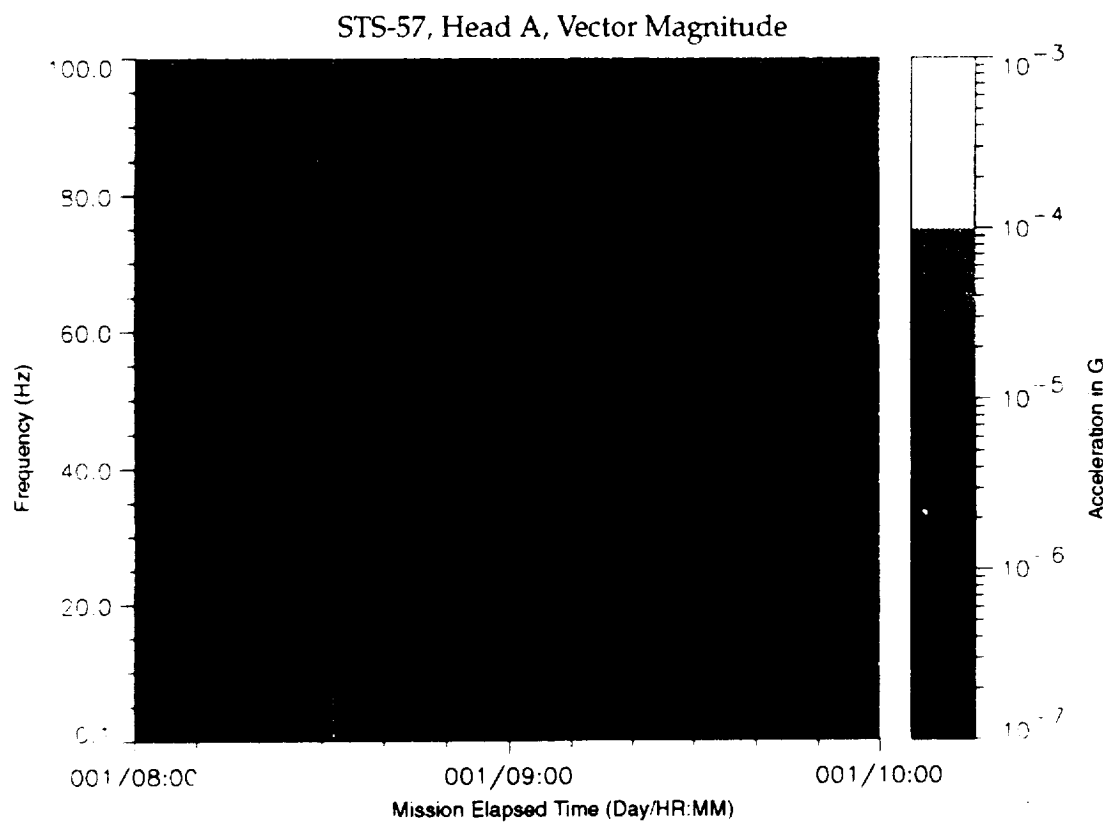


Figure B-49: SPACEHAB-1, Forward Bulkhead T-Beam

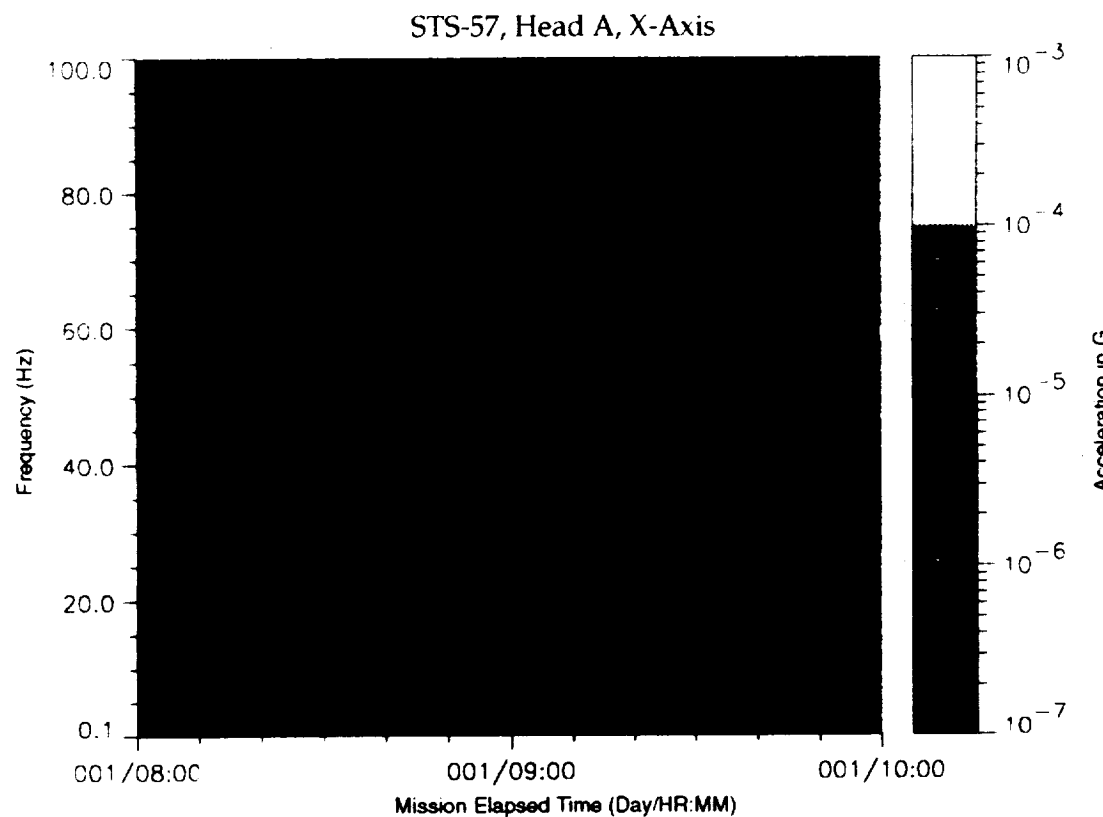


Figure B-50: SPACEHAB-1, Forward Bulkhead T-Beam

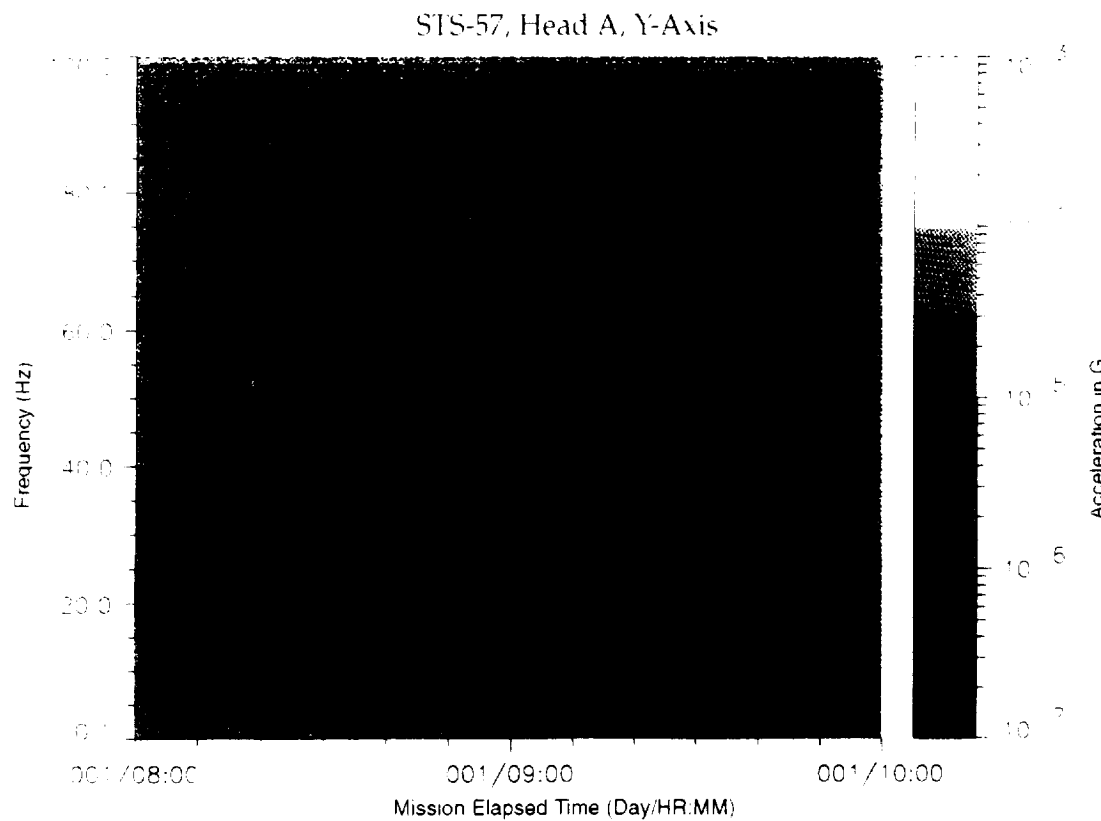


Figure B-51: SPACEHAB-1, Forward Bulkhead T-Beam

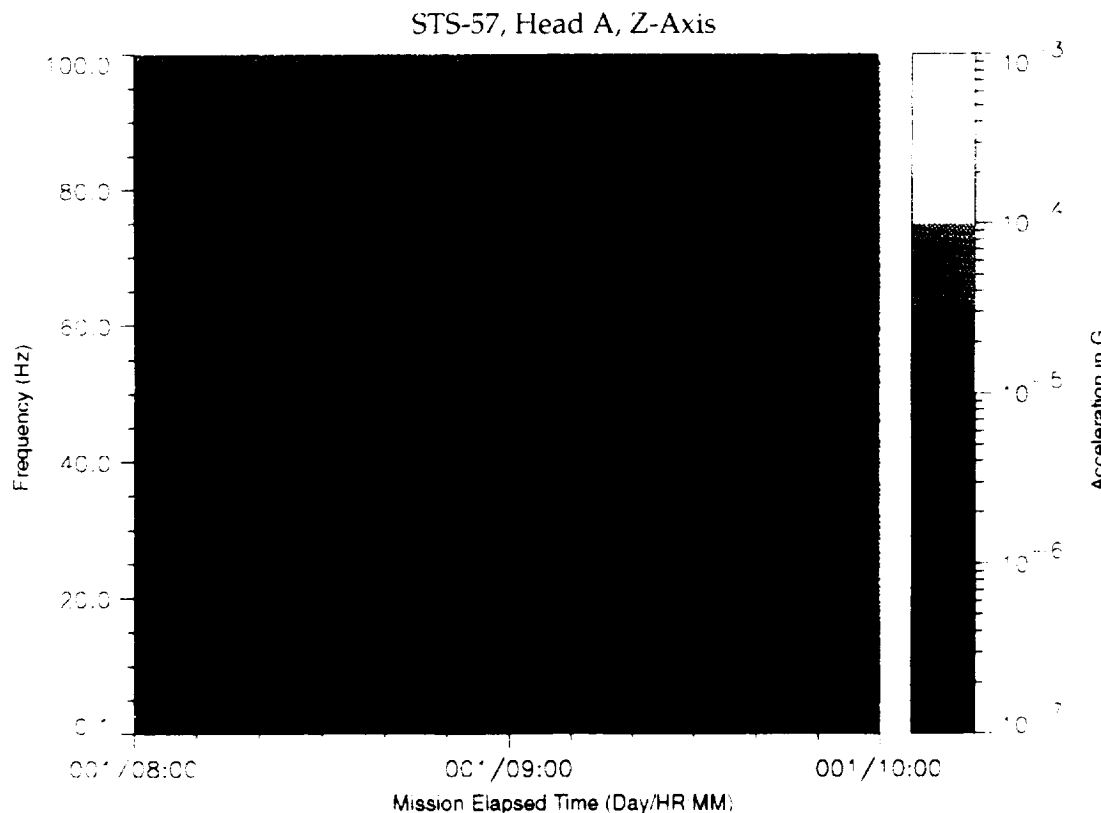


Figure B-52: SPACEHAB-1, Forward Bulkhead T-Beam

STS-57, Head A, Vector Magnitude

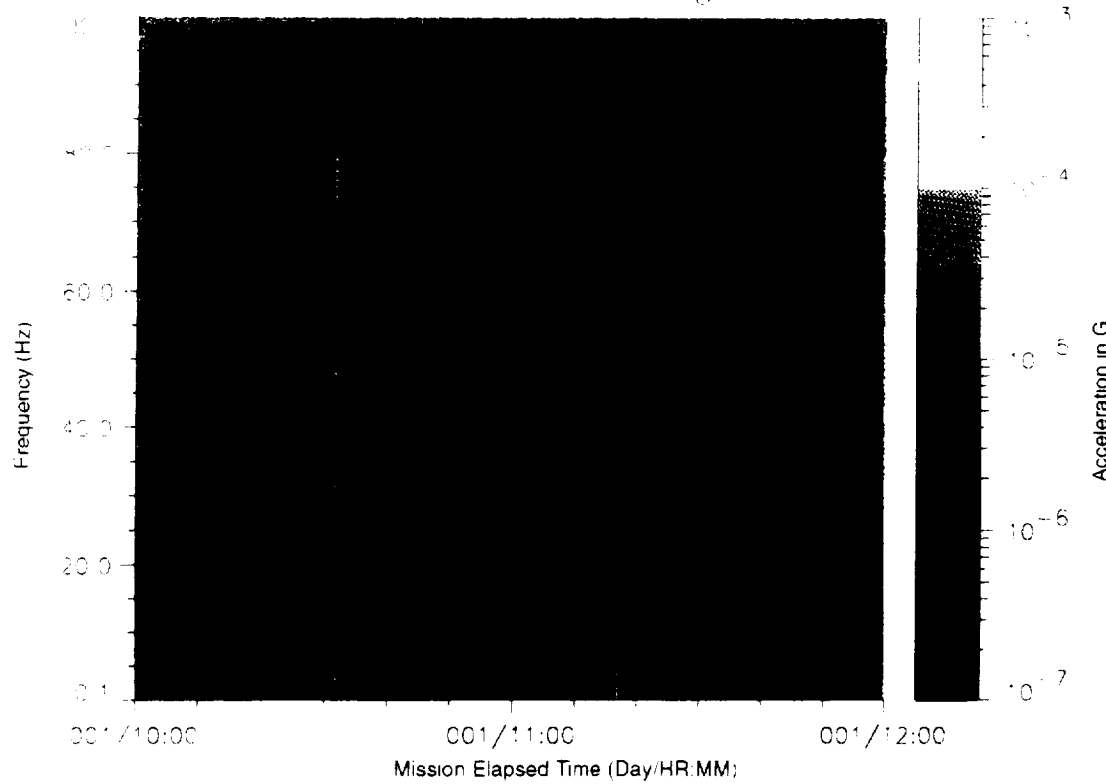


Figure B-53: SPACEHAB-1, Forward Bulkhead T-Beam

STS-57, Head A, X-Axis

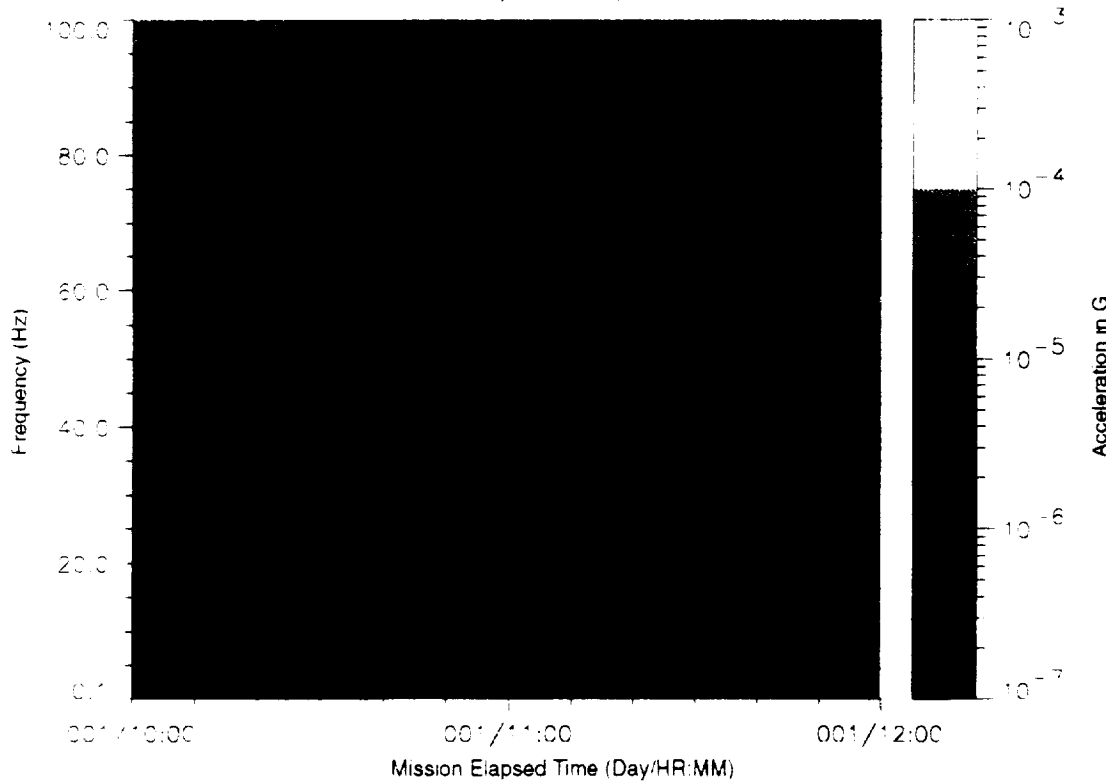


Figure B-54: SPACEHAB-1, Forward Bulkhead T-Beam

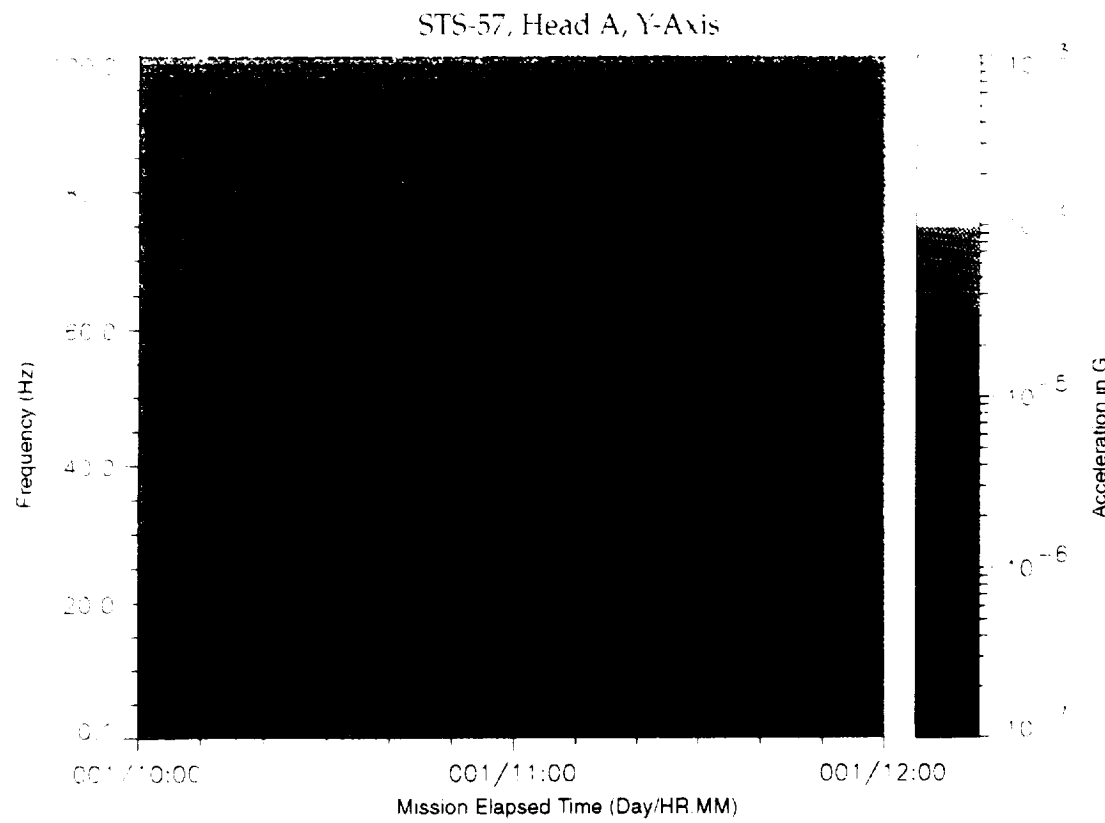


Figure B-55: SPACFHAB-1, Forward Bulkhead T-Beam

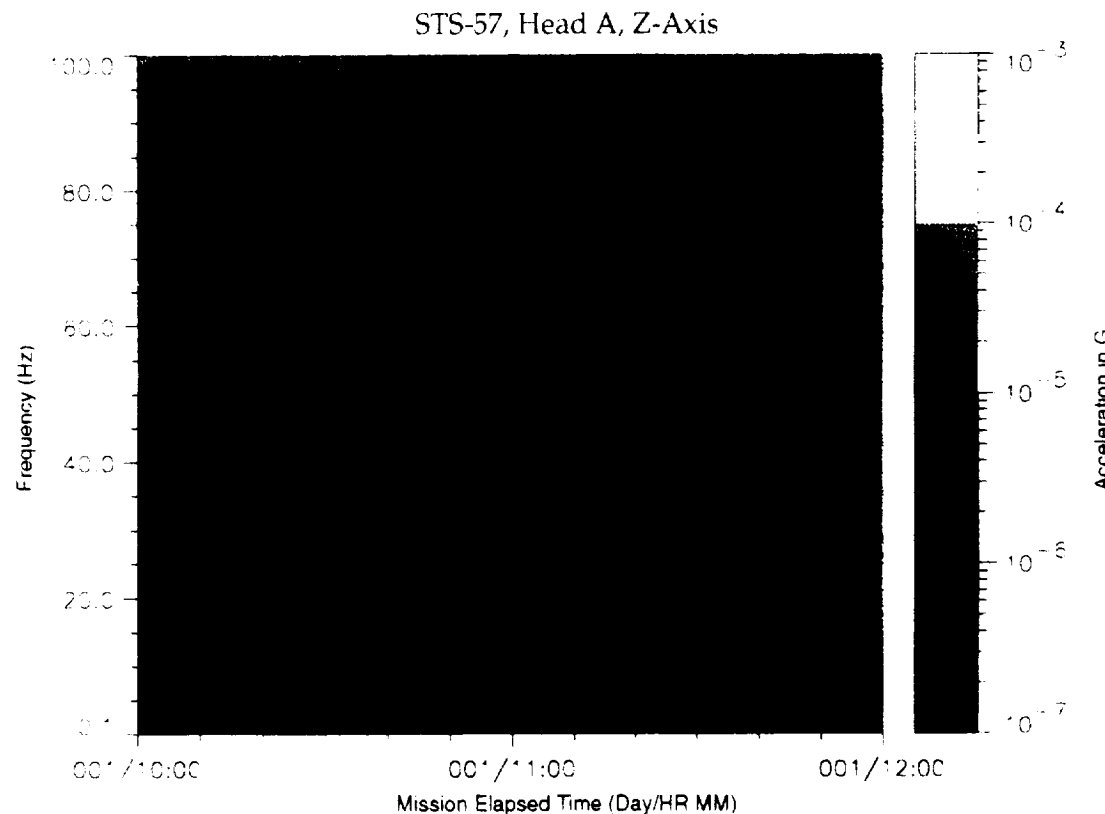


Figure B-56: SPACEHAB-1, Forward Bulkhead T-Beam

STS-57, Head A, Vector Magnitude

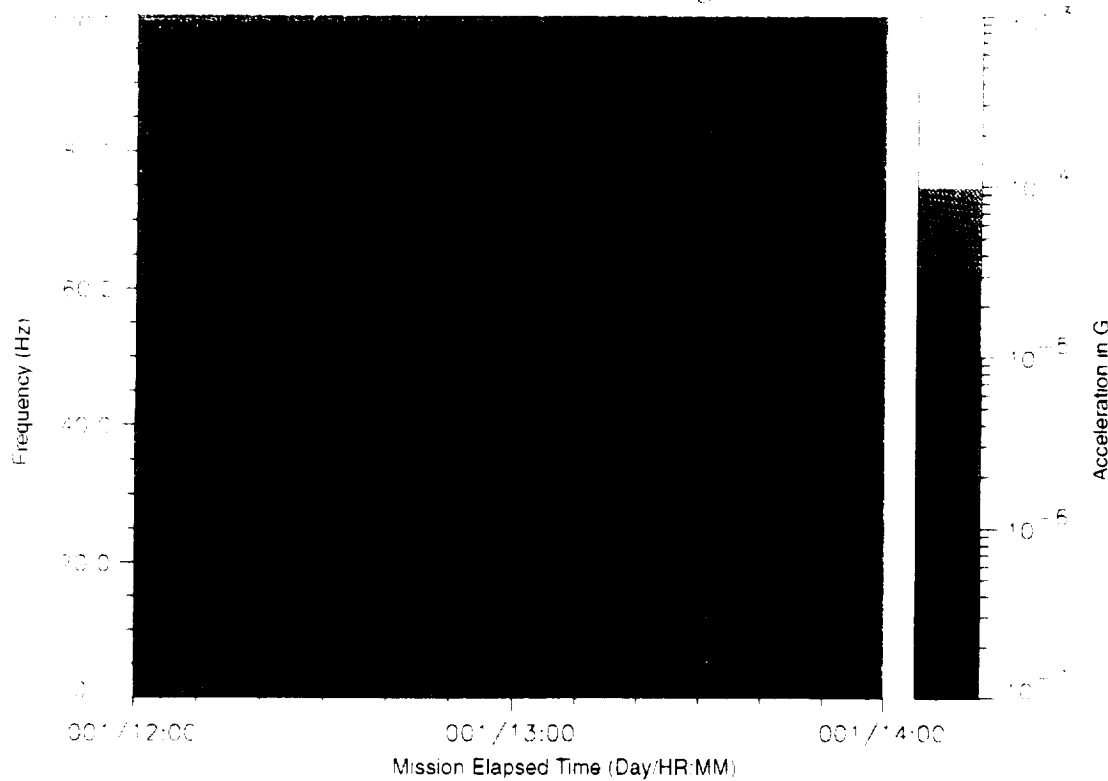


Figure B-57: SPACEHAB-1, Forward Bulkhead T-Beam

STS-57, Head A, X-Axis

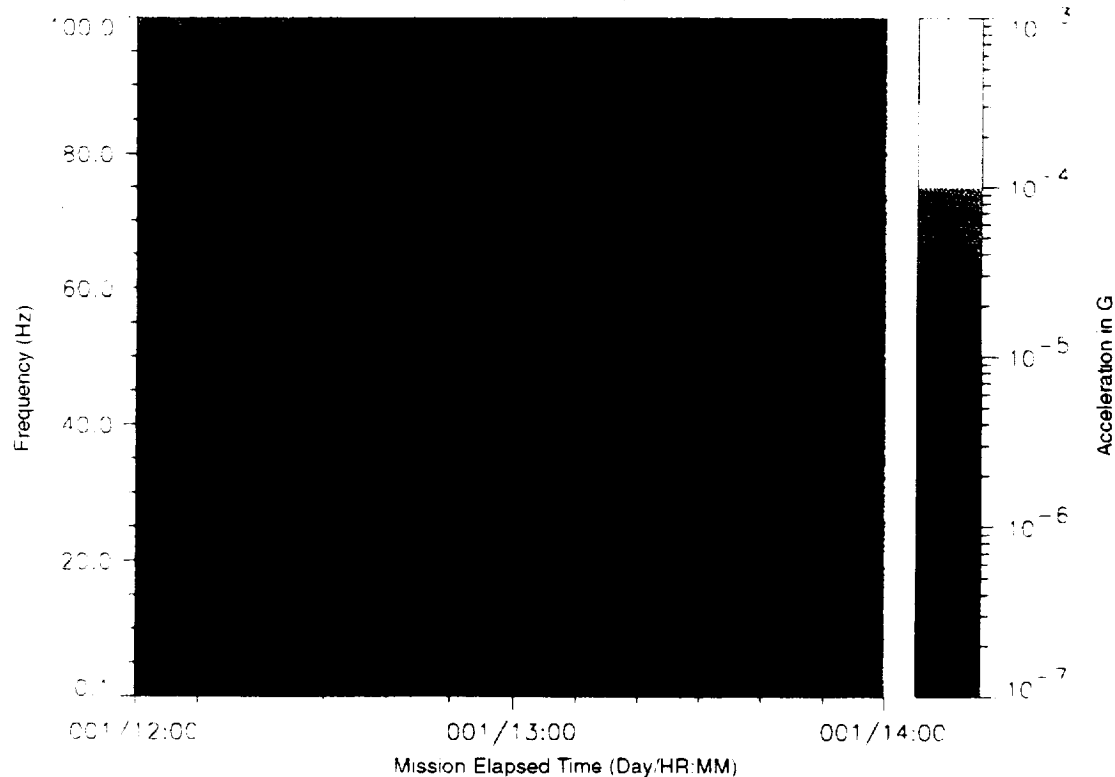


Figure B-58: SPACEHAB-1, Forward Bulkhead T-Beam

PRESENTATION MADE UNDER EARTHTIME FLIGHT

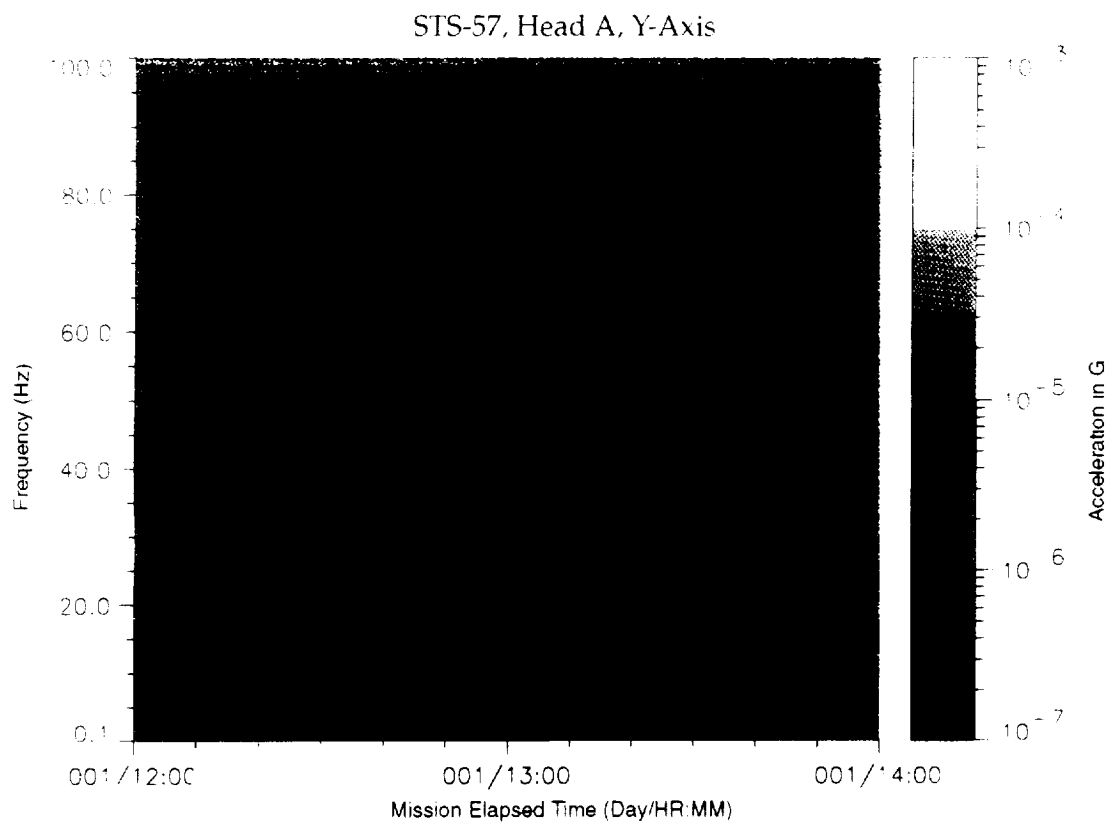


Figure B-59: SPACEHAB-1, Forward Bulkhead T-Beam

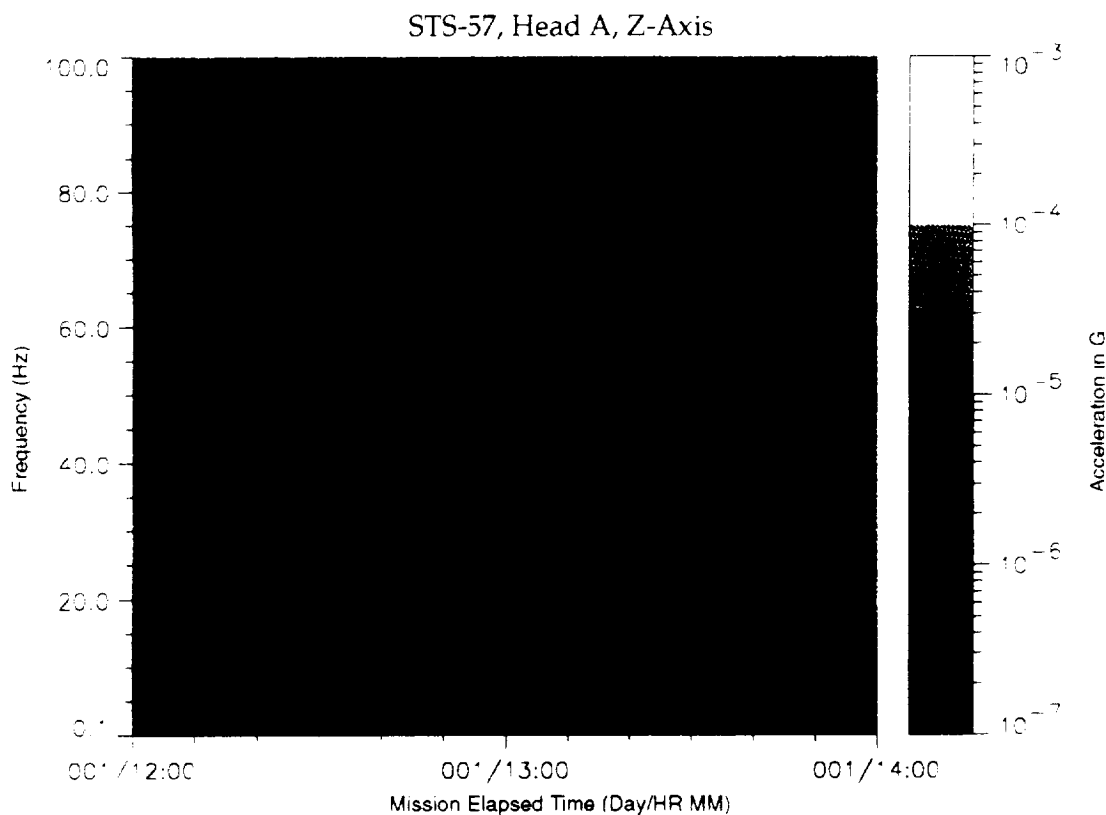


Figure B-60: SPACEHAB-1, Forward Bulkhead T-Beam

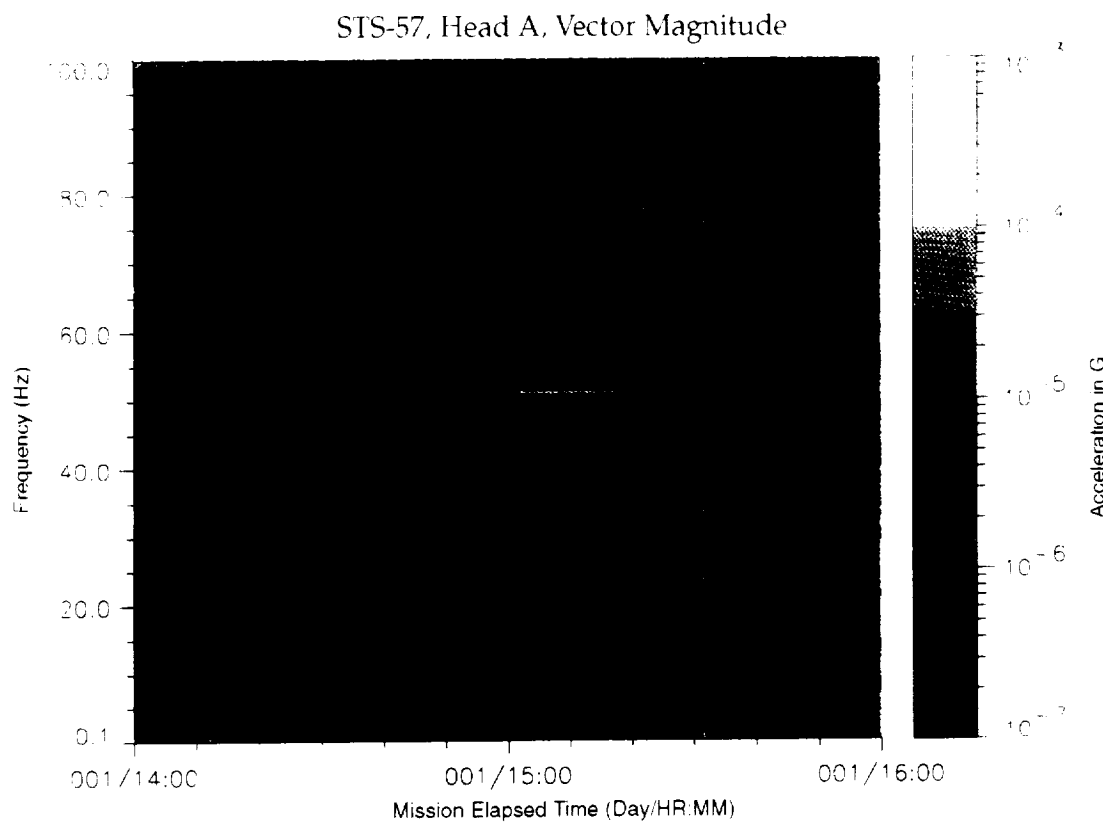


Figure B-61: SPACEHAB-1, Forward Bulkhead T-Beam

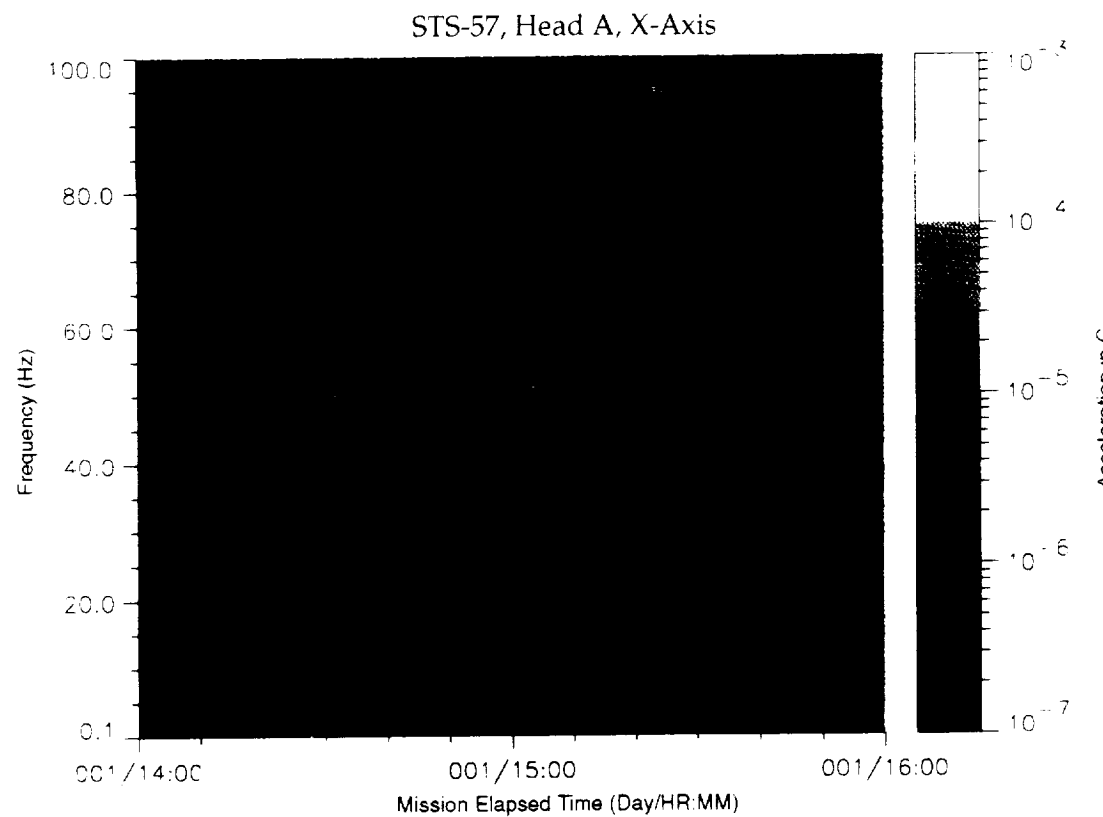


Figure B-62: SPACEHAB-1, Forward Bulkhead T-Beam

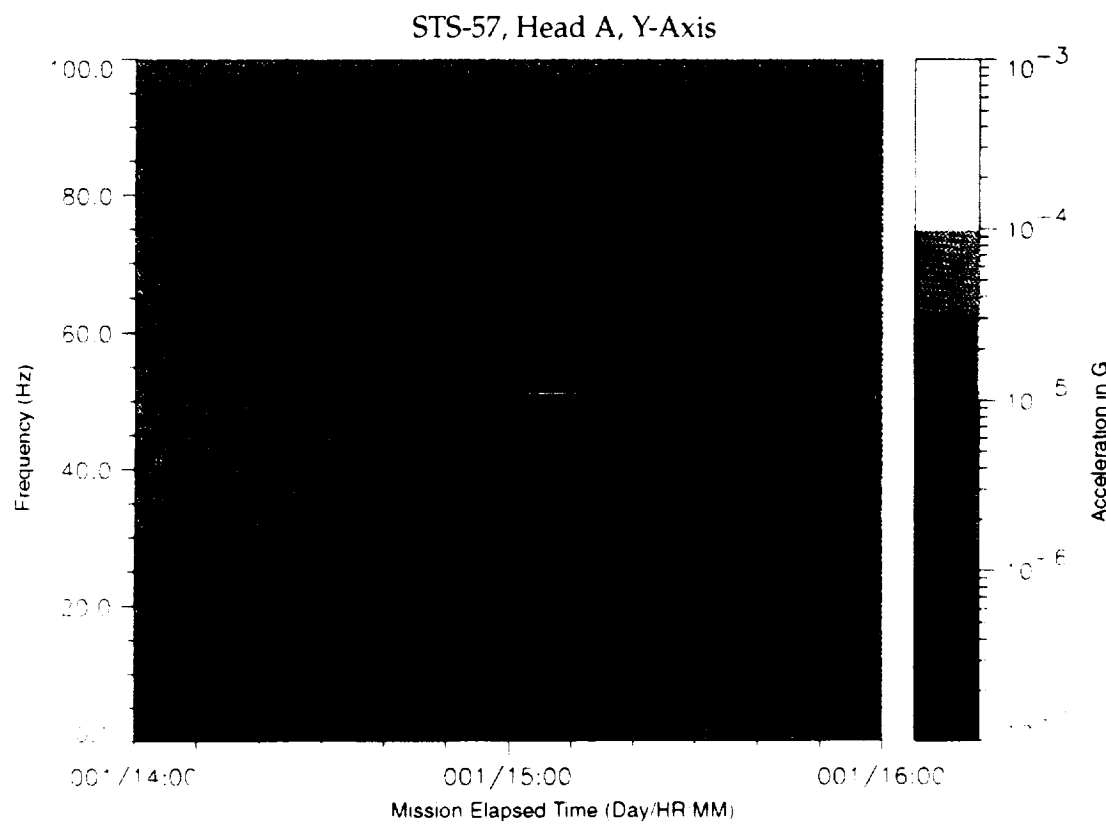


Figure B-63: SPACEHAB-1, Forward Bulkhead T-Beam

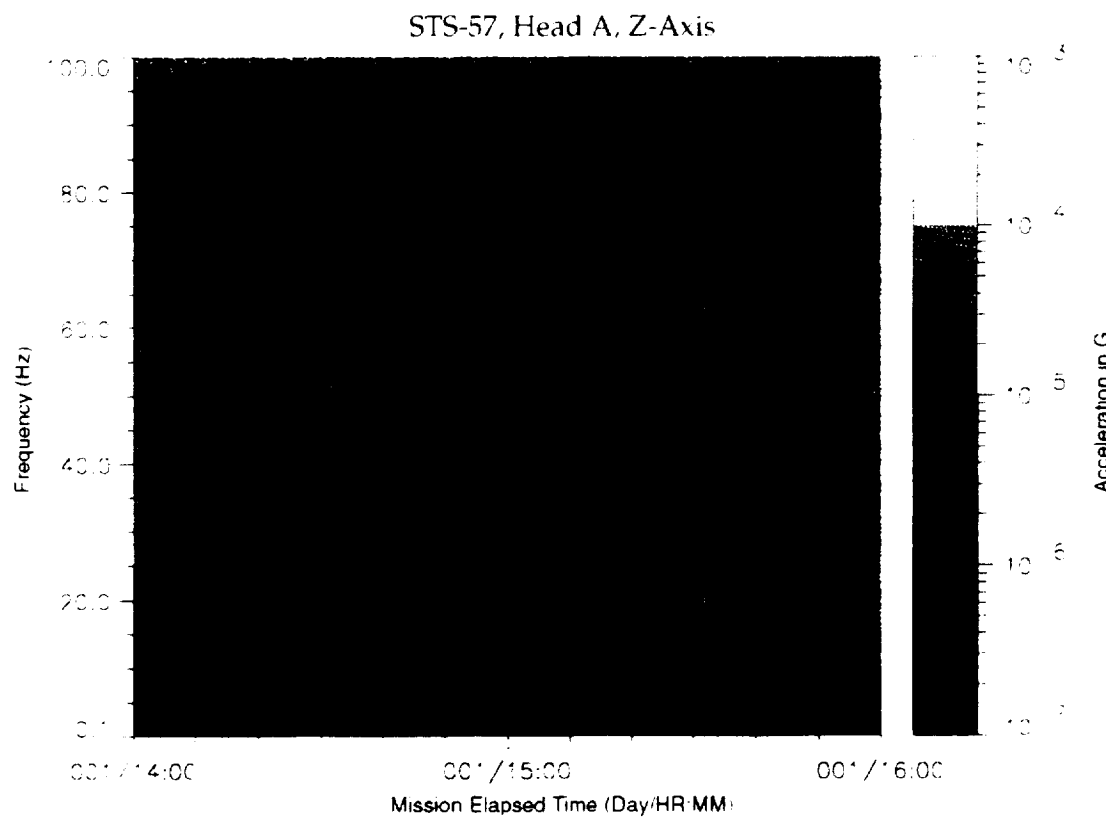


Figure B-64: SPACEHAB-1, Forward Bulkhead T-Beam

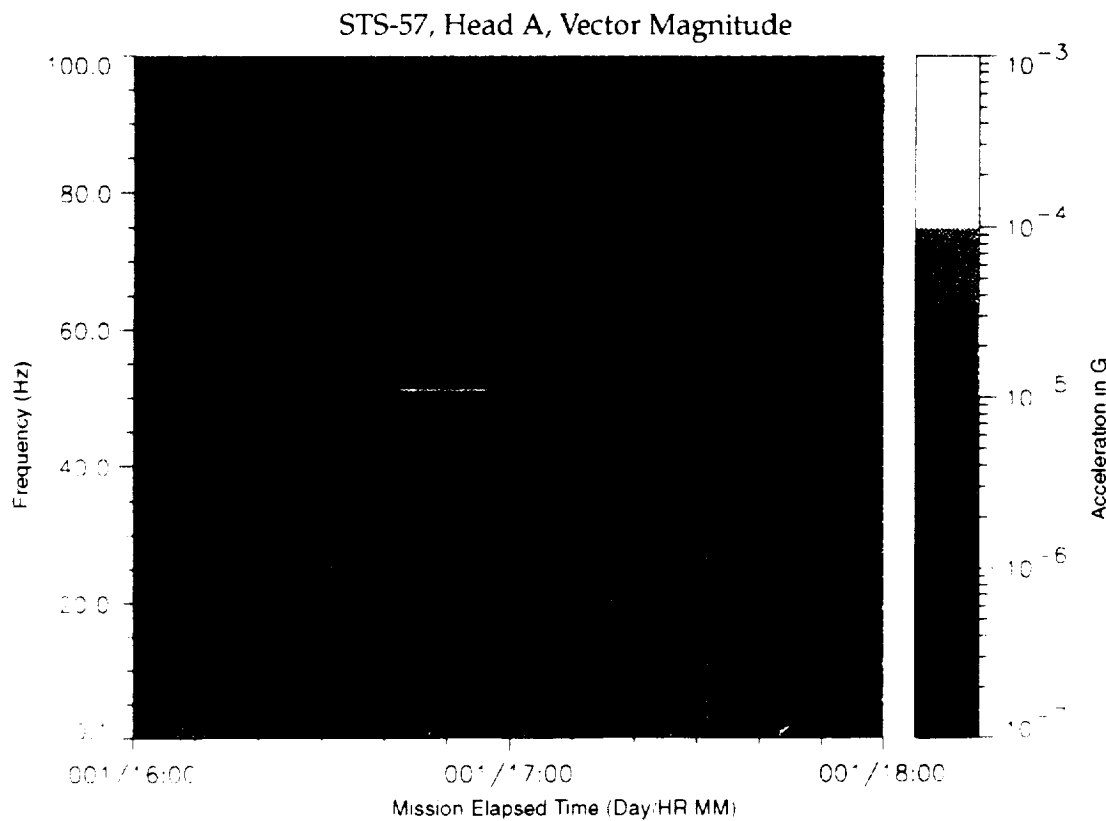


Figure B-65: SPACEHAB-1, Forward Bulkhead T-Beam

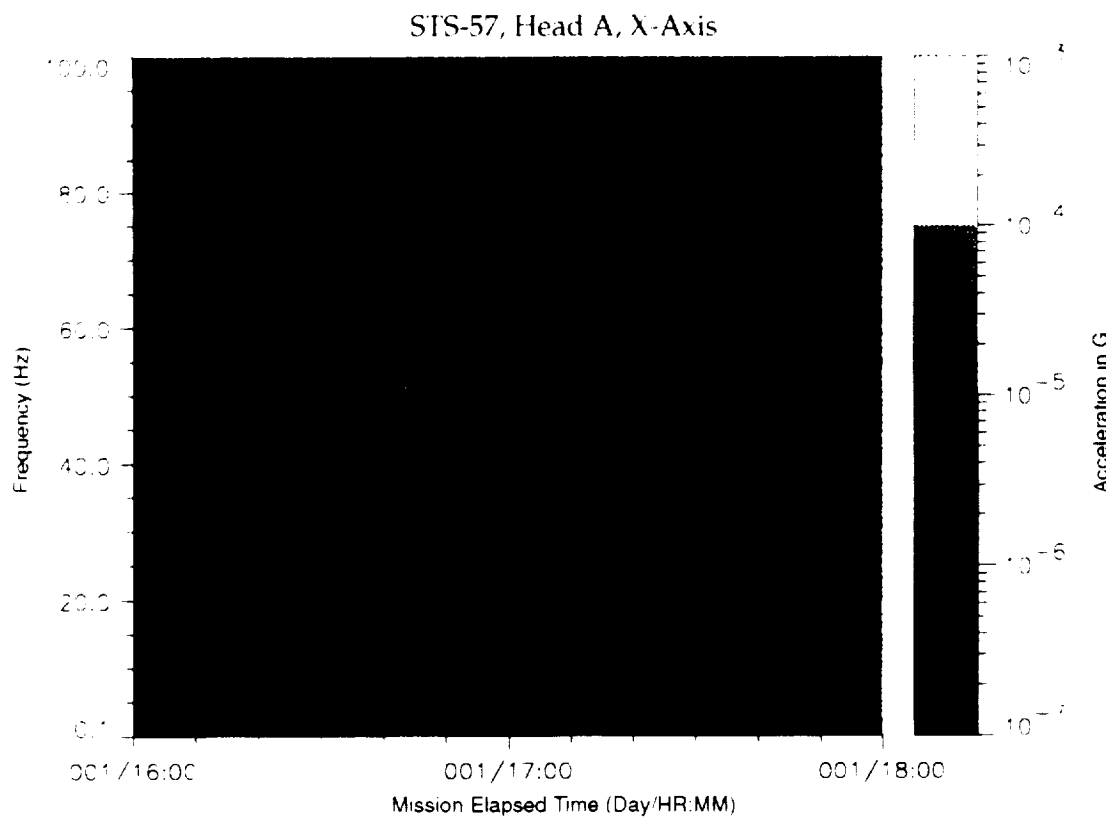


Figure B-66: SPACEHAB-1, Forward Bulkhead T-Beam

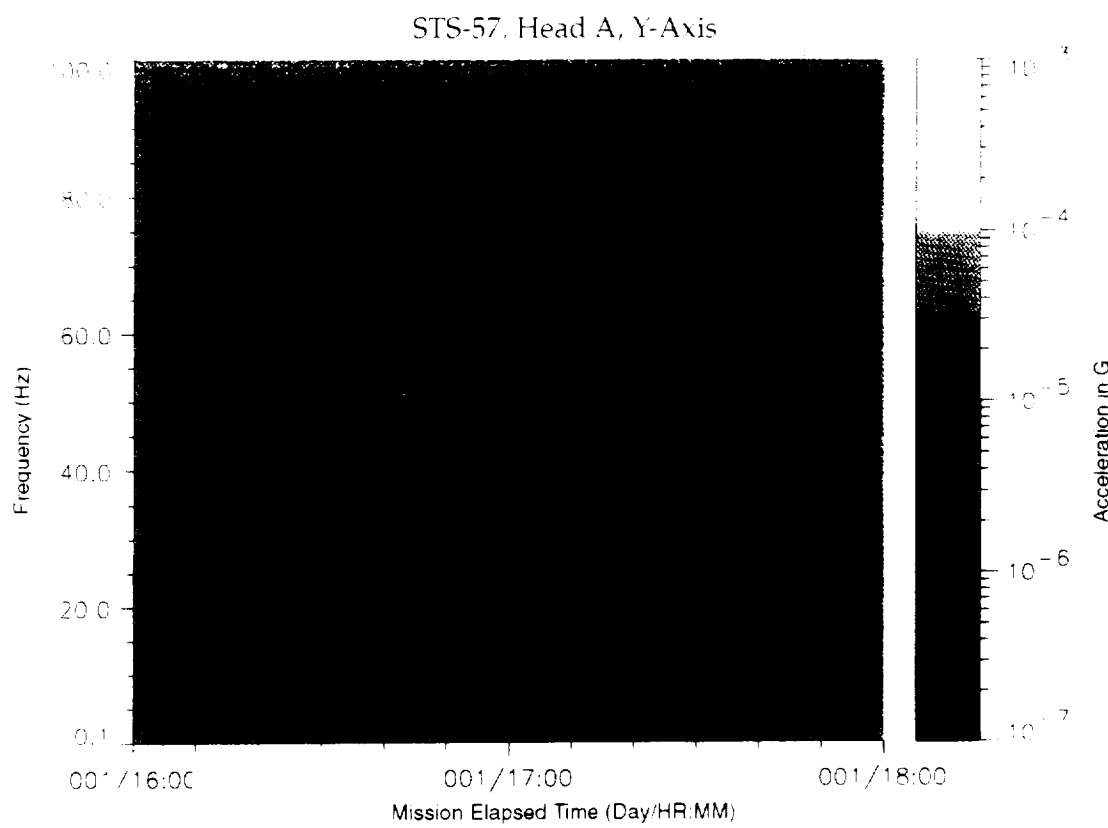


Figure B-67: SPACEHAB-1, Forward Bulkhead T-Beam

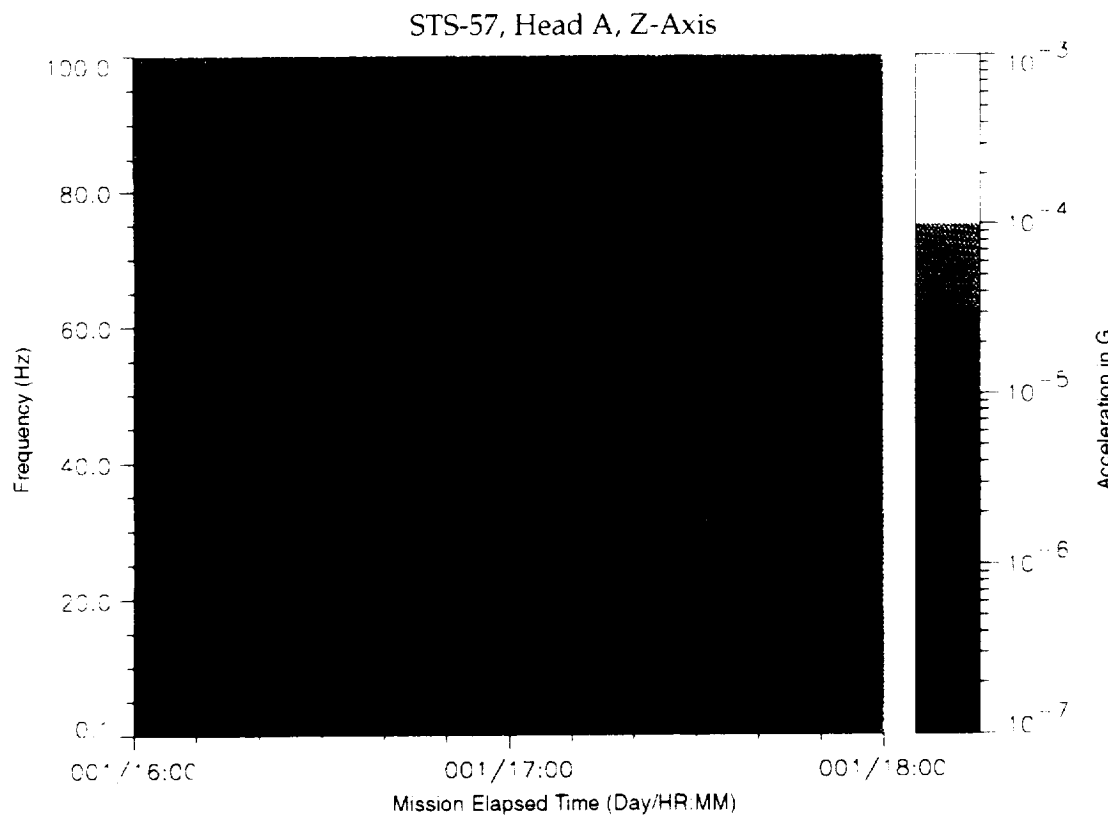


Figure B-68: SPACEHAB-1, Forward Bulkhead T-Beam

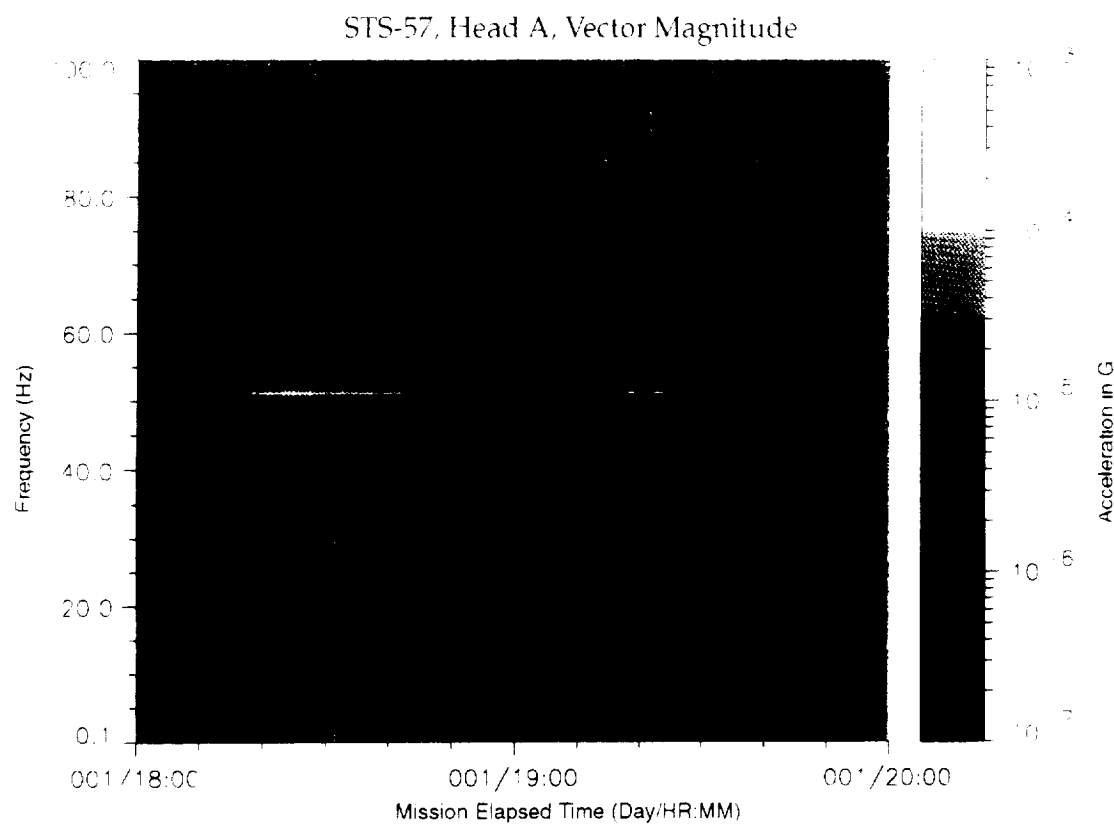


Figure B-69: SPACEHAB-1, Forward Bulkhead T-Beam

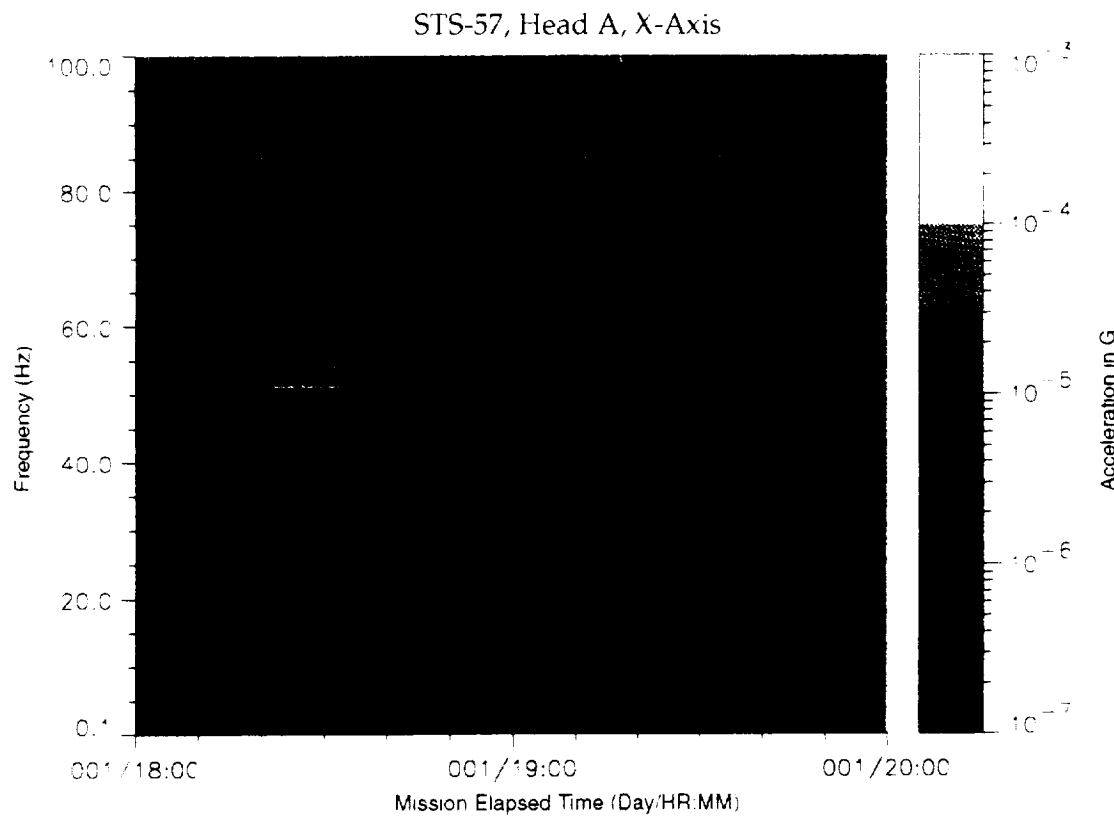


Figure B-70: SPACEHAB-1, Forward Bulkhead T-Beam

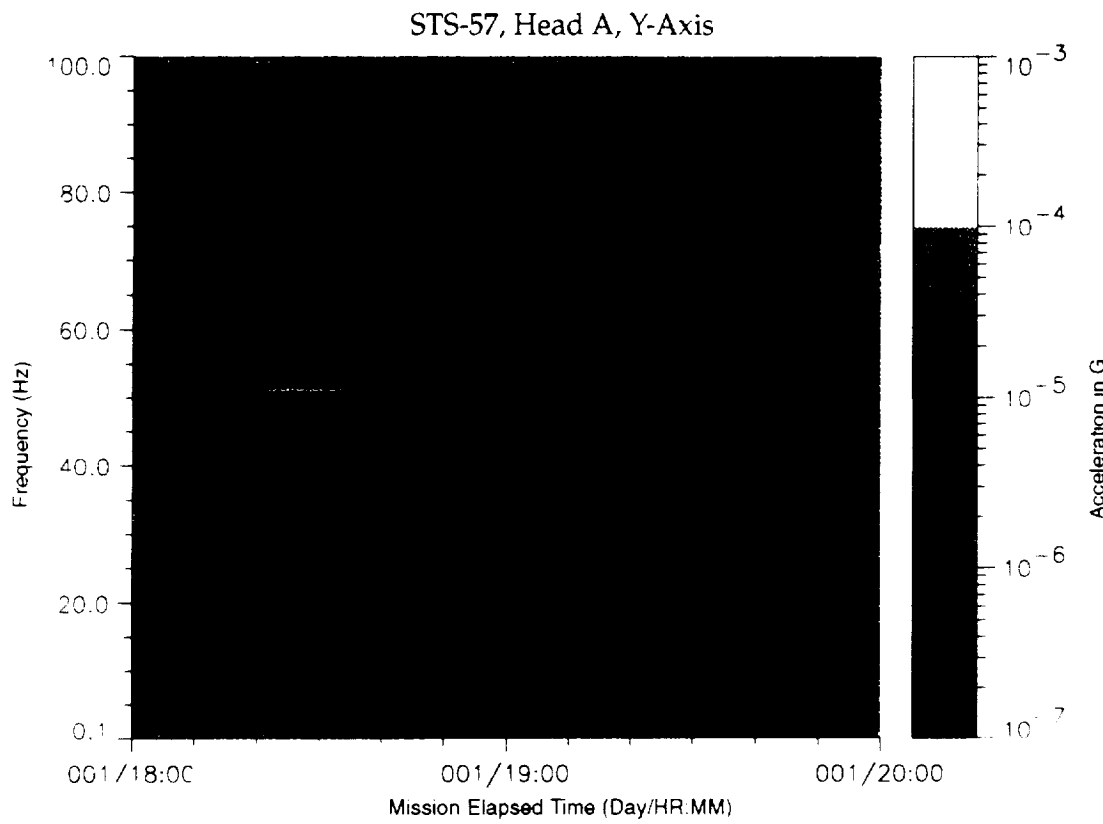


Figure B-71: SPACEHAB-1, Forward Bulkhead T-Beam

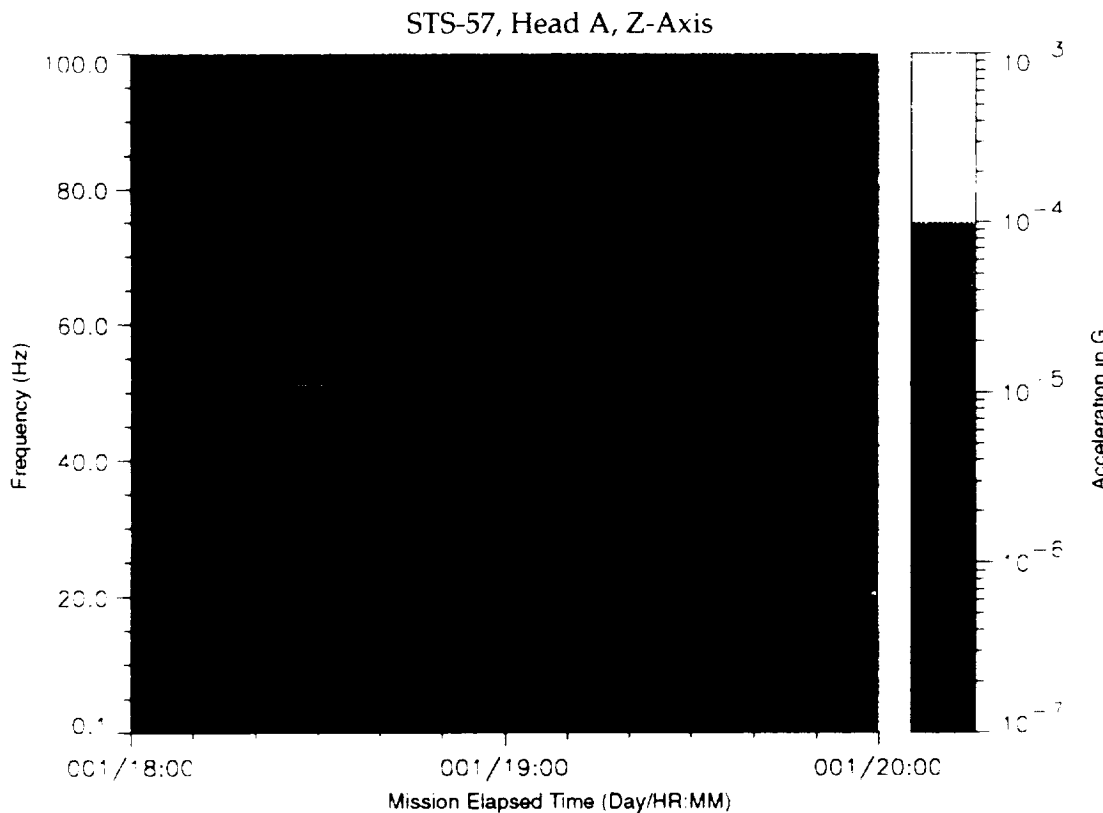


Figure B-72: SPACEHAB-1, Forward Bulkhead T-Beam

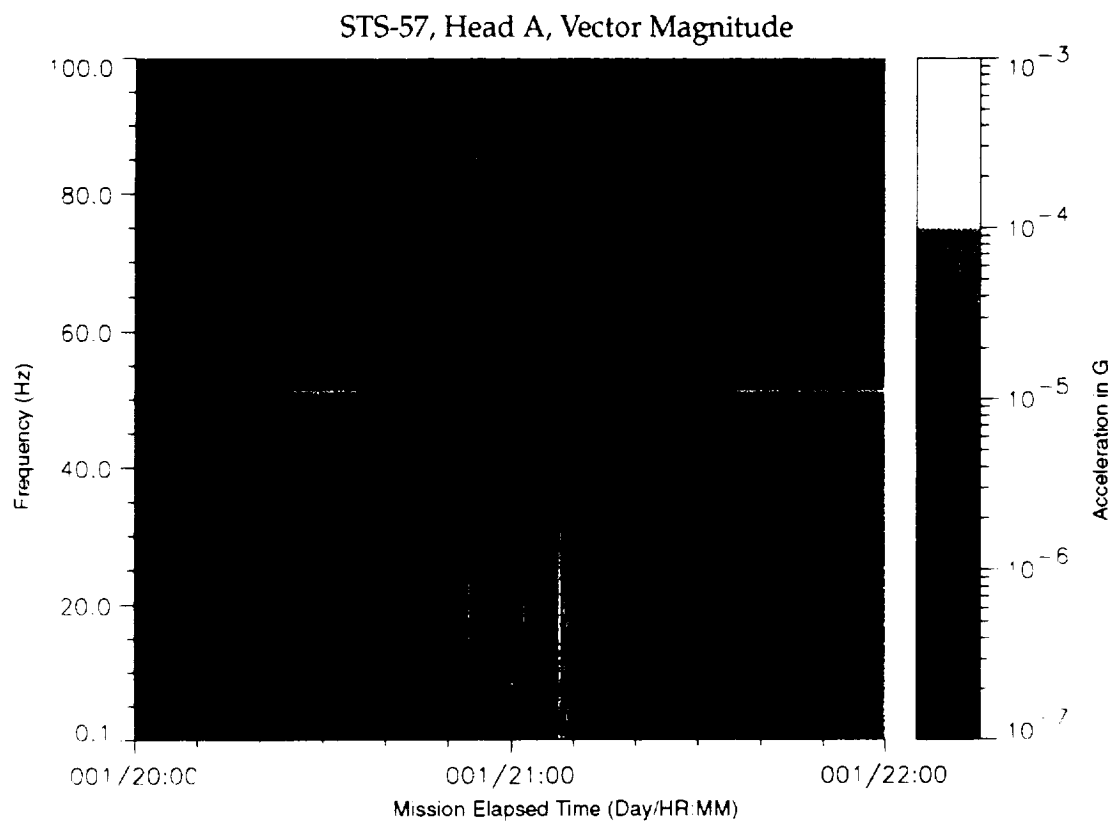


Figure B-73: SPACEHAB-1, Forward Bulkhead T-Beam

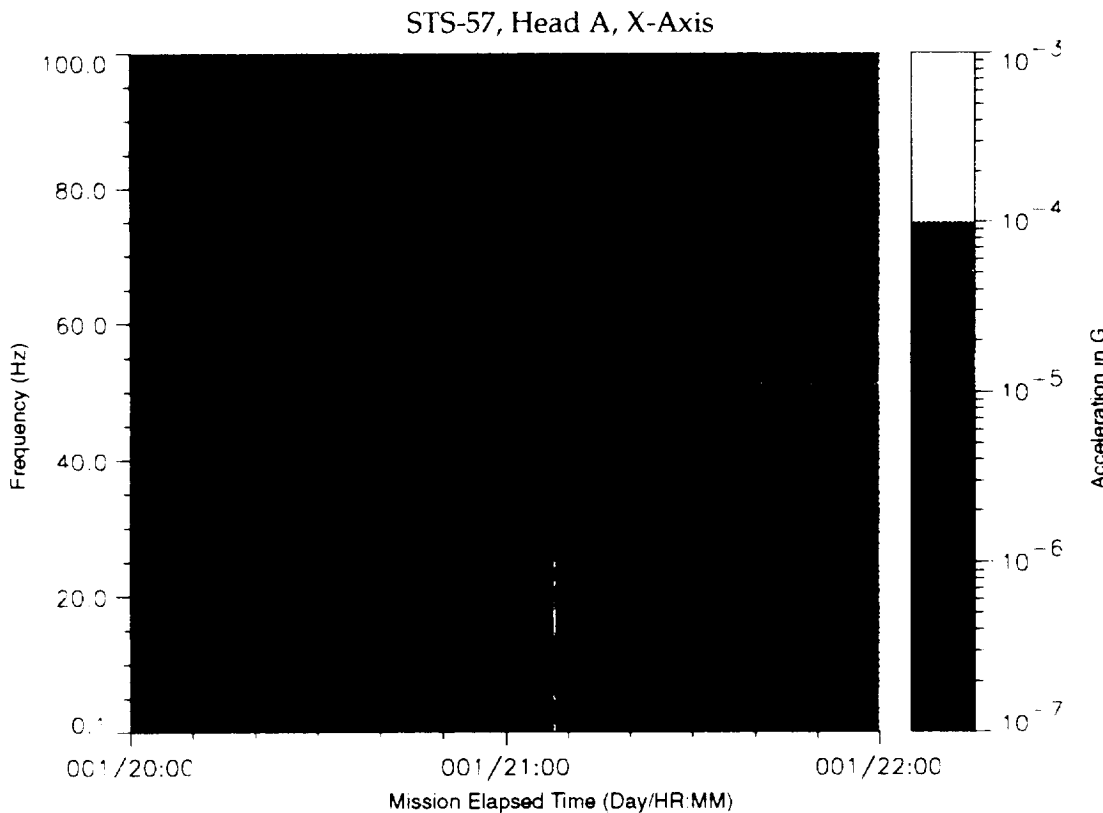


Figure B-74: SPACEHAB-1, Forward Bulkhead T-Beam

STS-57, Head A, Vector Magnitude

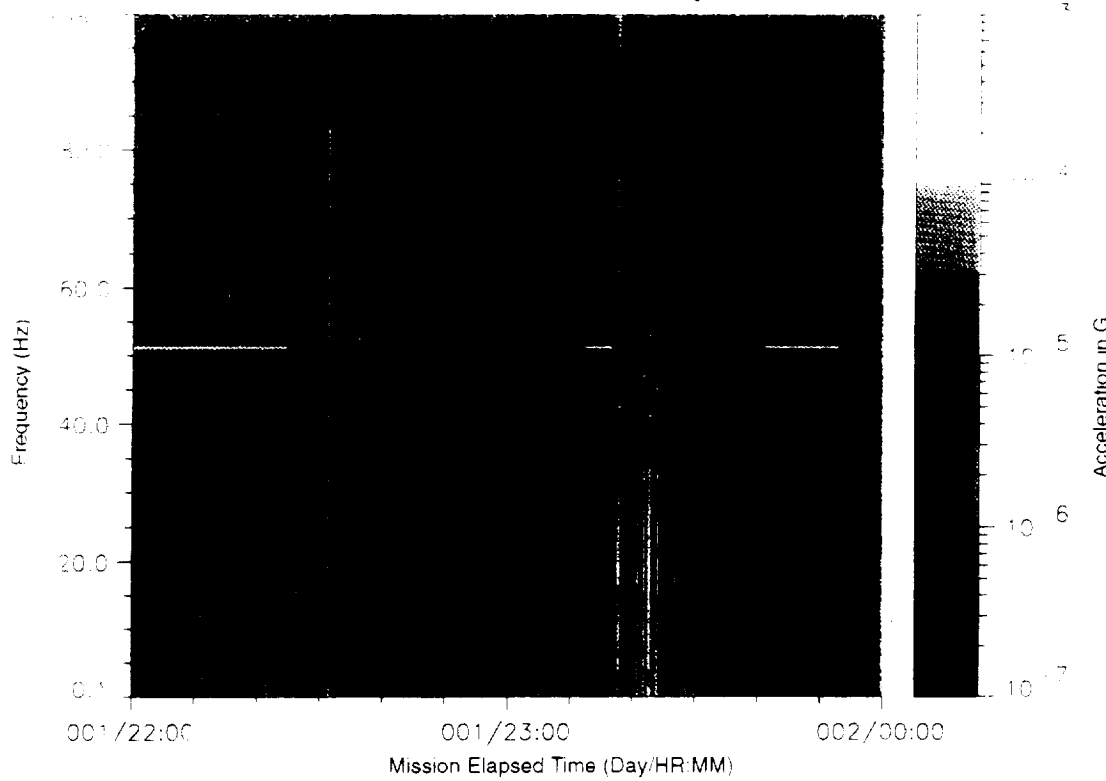


Figure B-77: SPACEHAB-1, Forward Bulkhead T-Beam

STS-57, Head A, X-Axis

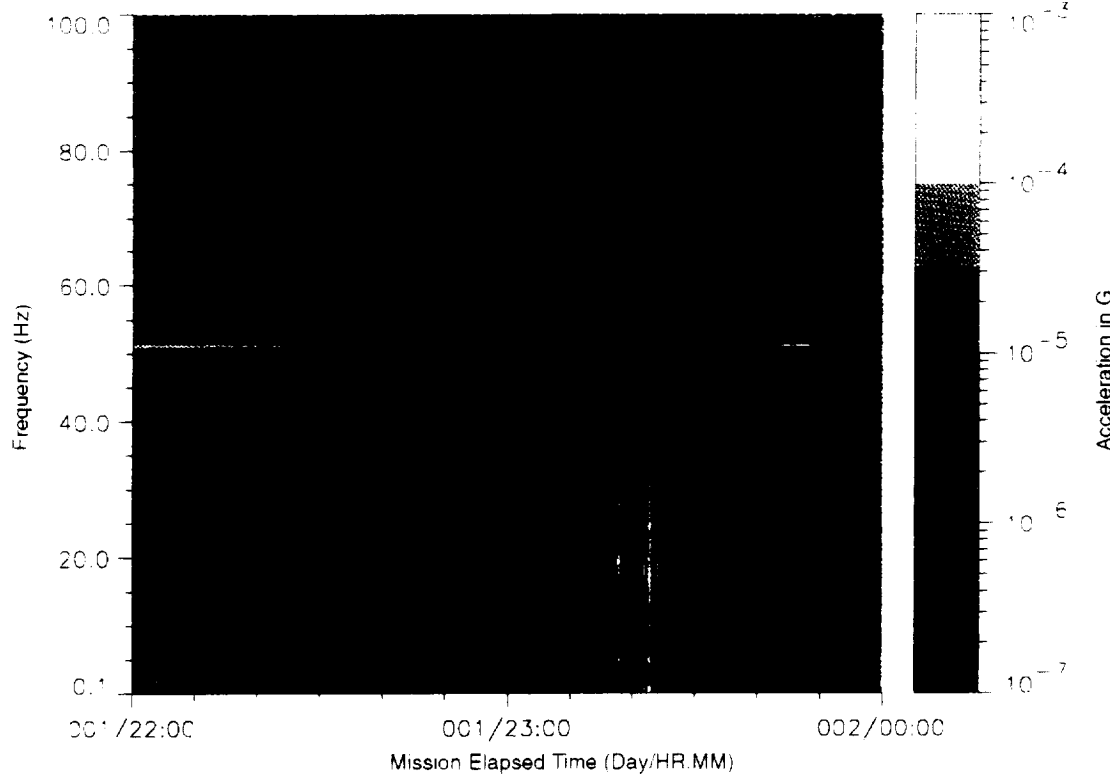


Figure B-78: SPACEHAB-1, Forward Bulkhead T-Beam

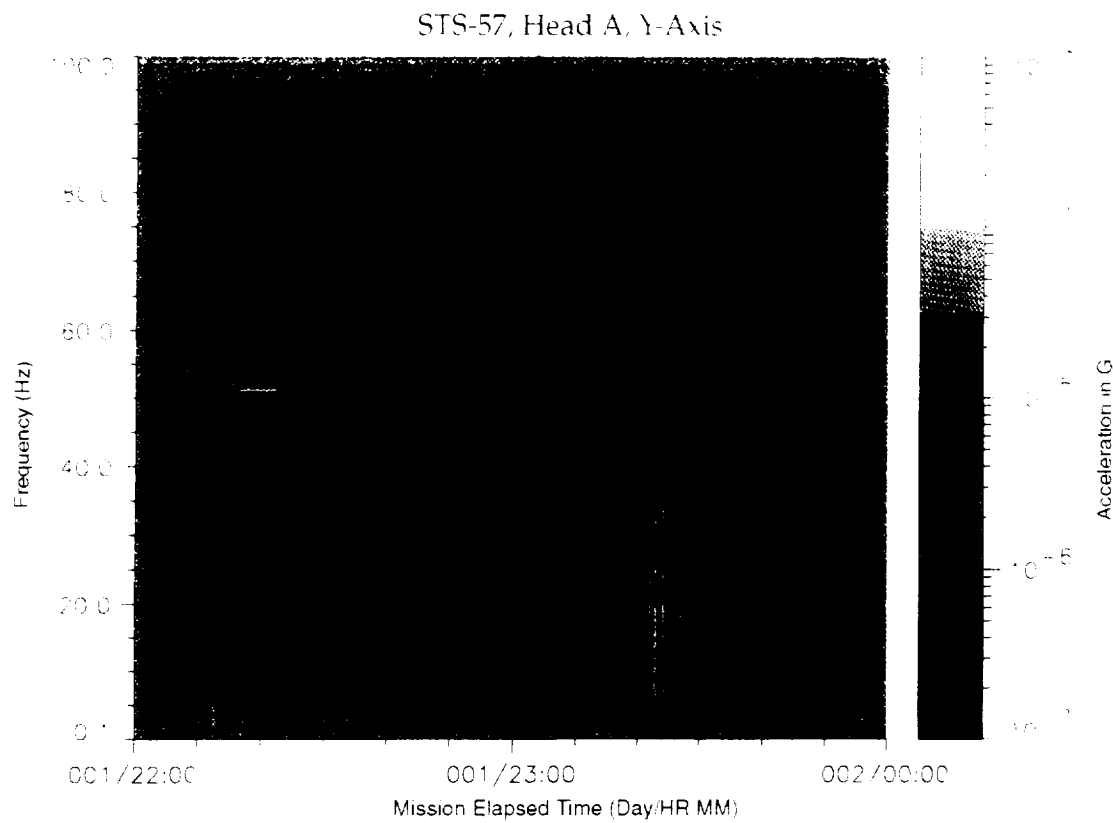


Figure B-79: SPACEHAB-1, Forward Bulkhead T-Beam

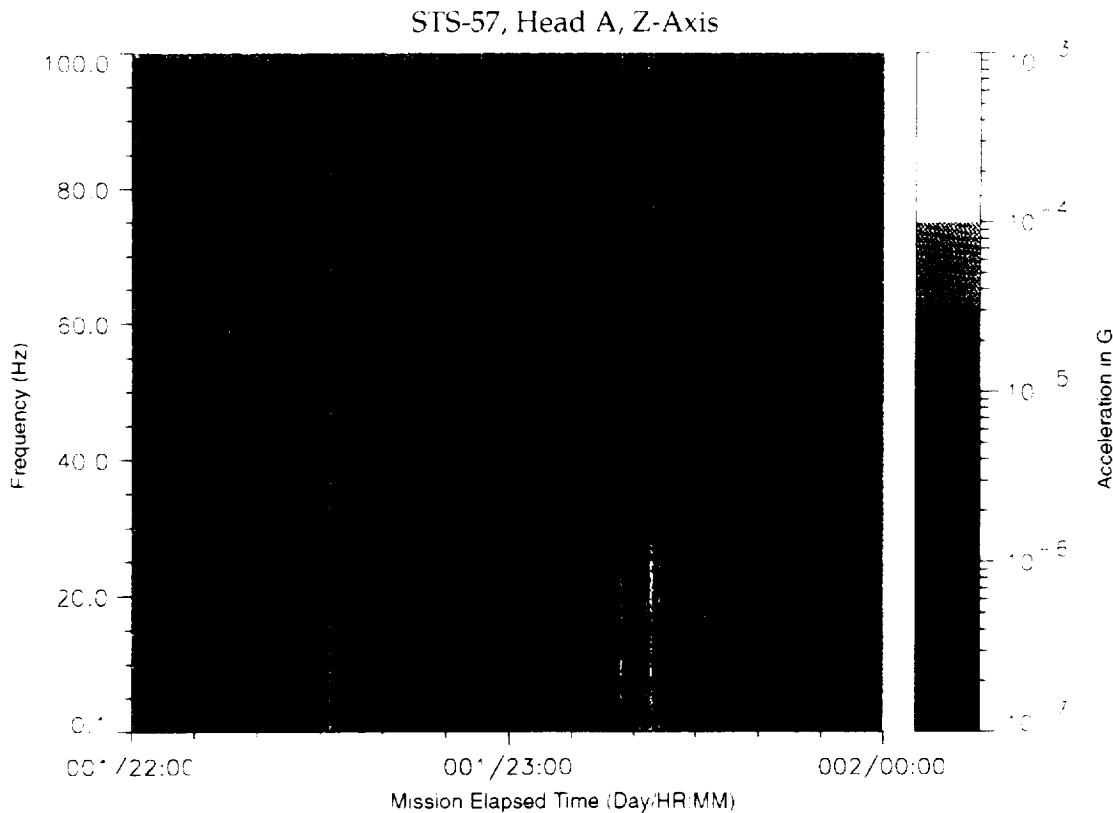


Figure B-80: SPACEHAB-1, Forward Bulkhead T-Beam

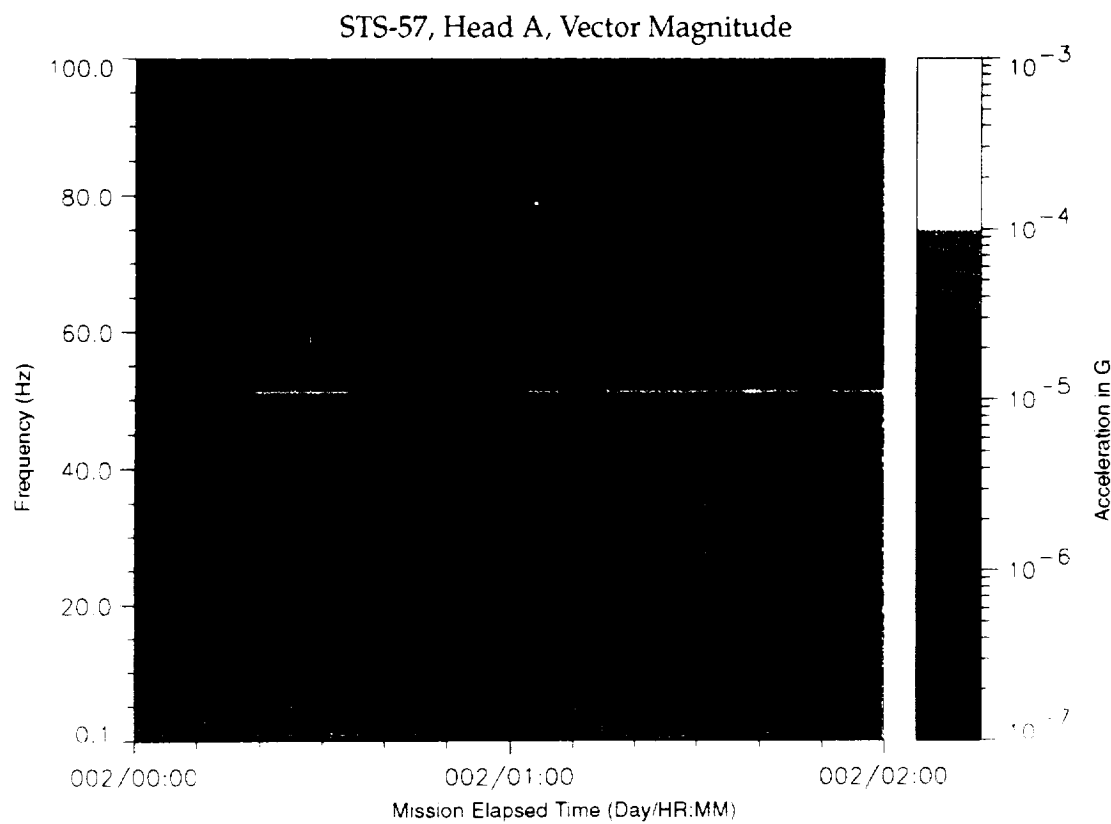


Figure B-81: SPACEHAB-1, Forward Bulkhead T-Beam

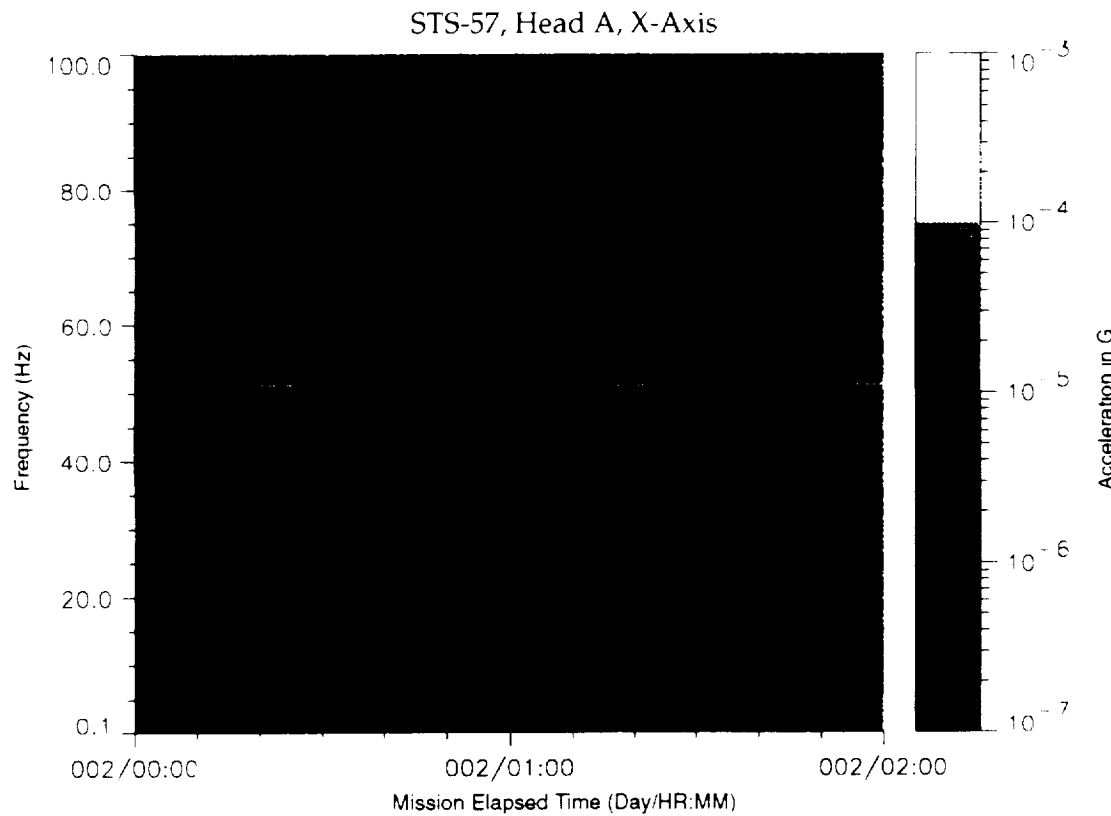


Figure B-82: SPACEHAB-1, Forward Bulkhead T-Beam

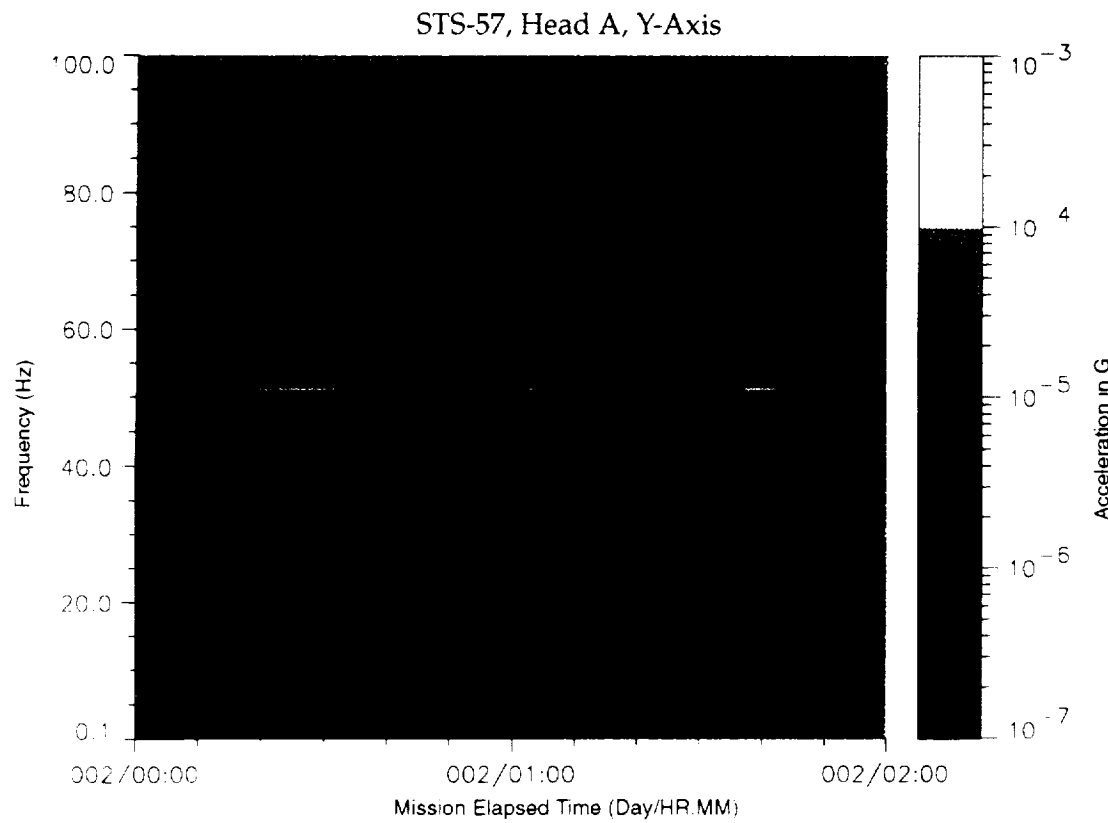


Figure B-83: SPACEHAB-1, Forward Bulkhead T-Beam

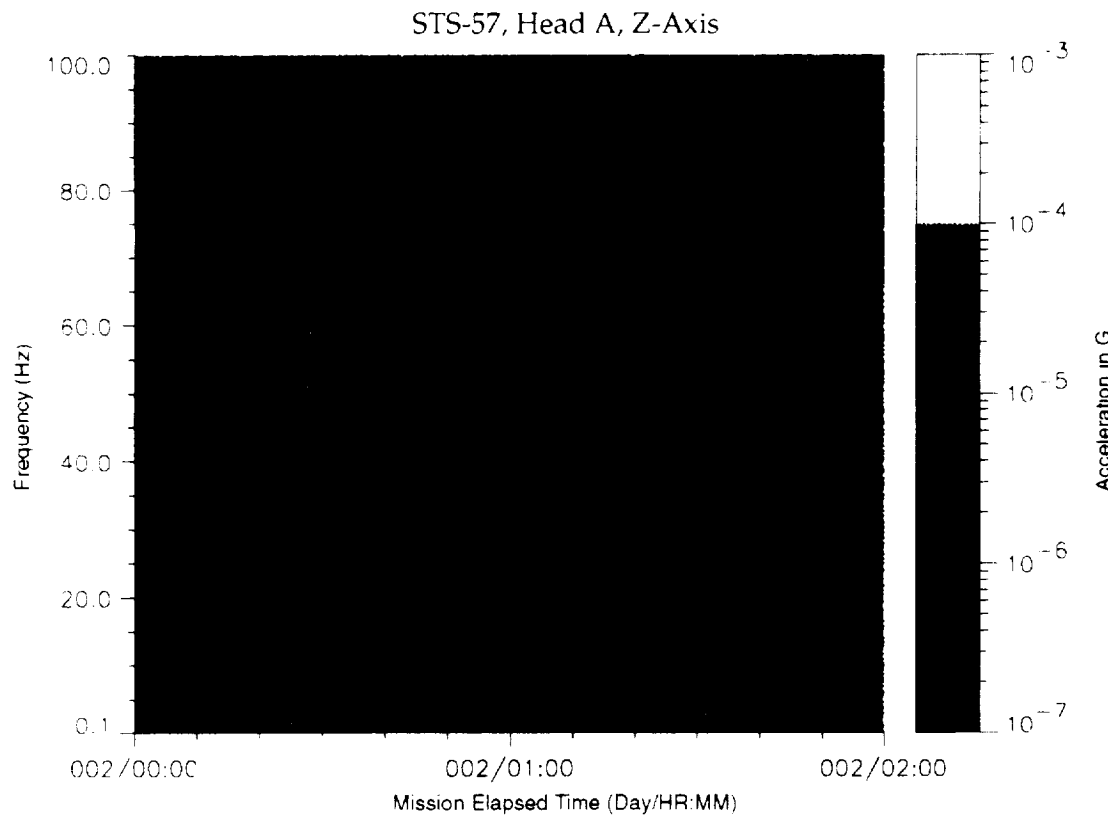


Figure B-84: SPACEHAB-1, Forward Bulkhead T-Beam

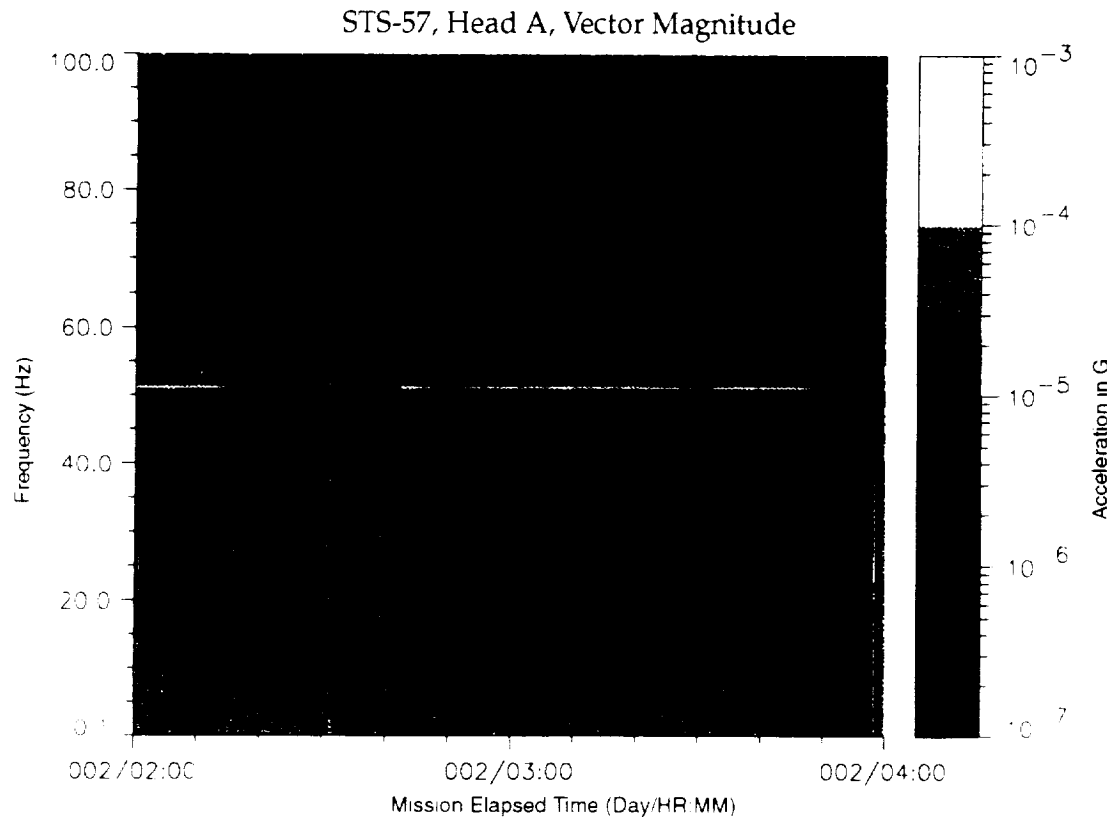


Figure B-85: SPACEHAB-1, Forward Bulkhead T-Beam

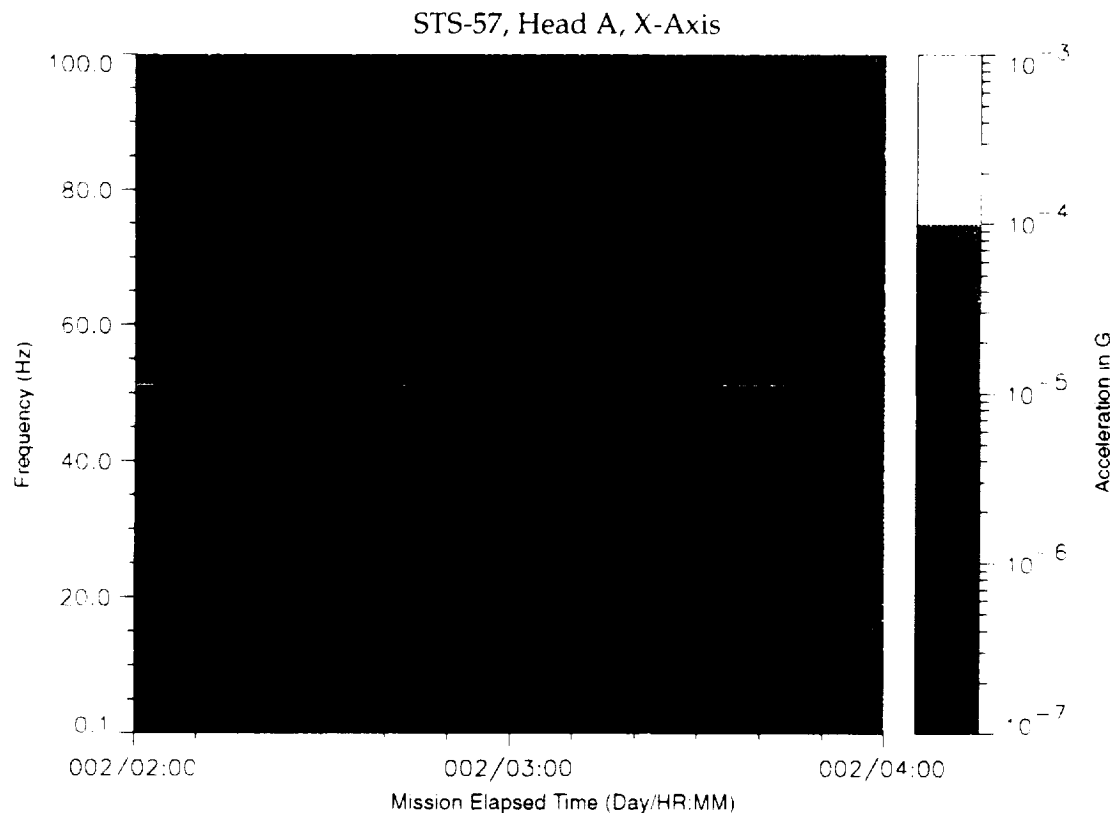


Figure B-86: SPACEHAB-1, Forward Bulkhead T-Beam

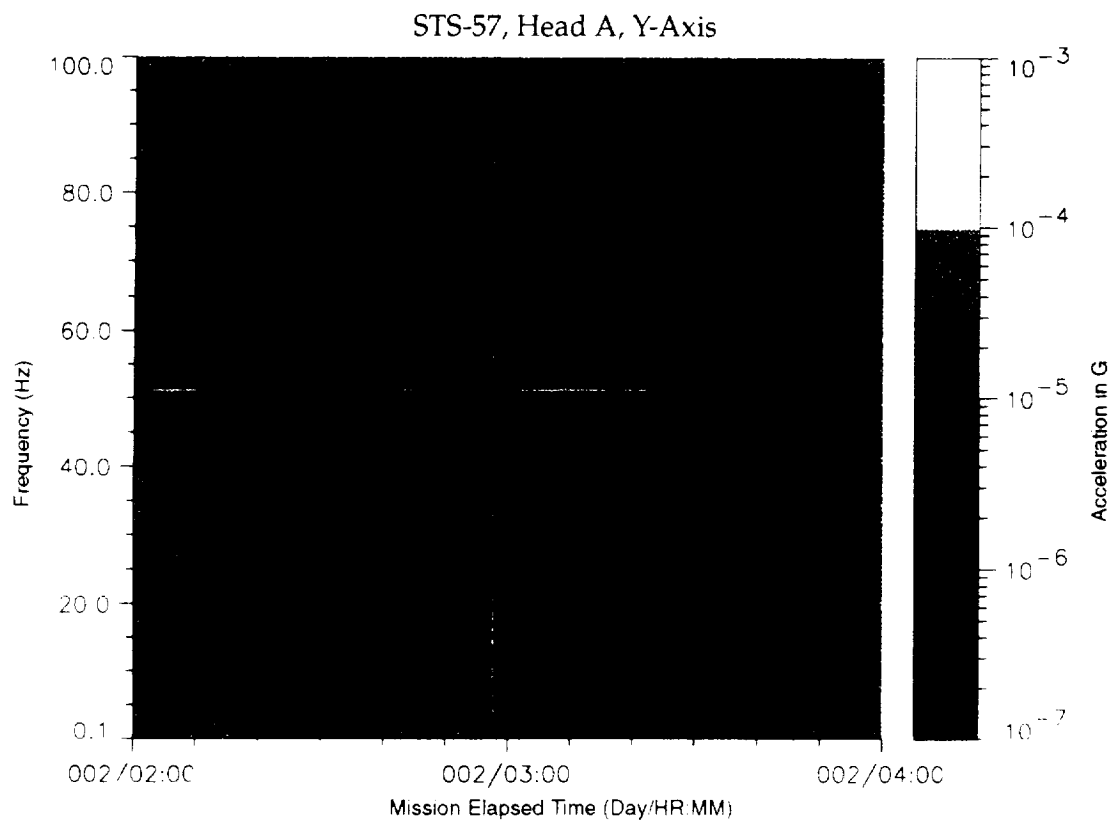


Figure B-87: SPACEHAB-1, Forward Bulkhead T-Beam

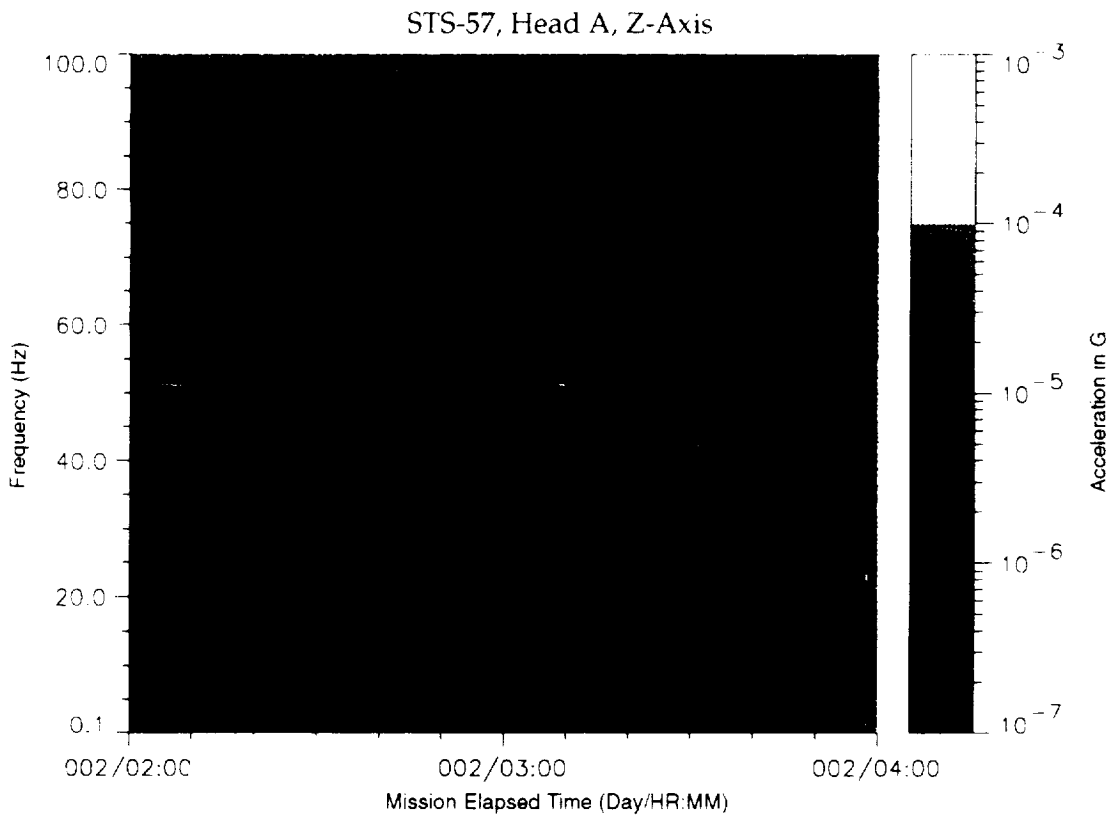


Figure B-88: SPACEHAB-1, Forward Bulkhead T-Beam

STS-57, Head A, Vector Magnitude

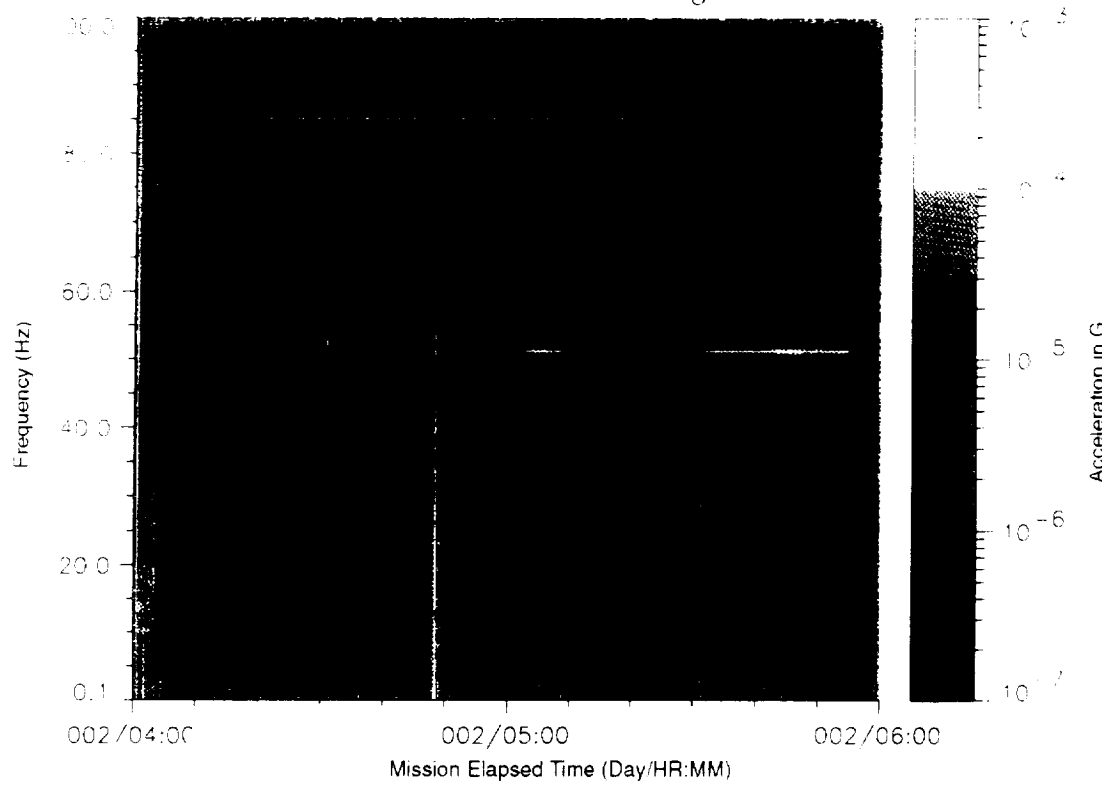


Figure B-89: SPACEHAB-1, Forward Bulkhead T-Beam

STS-57, Head A, X-Axis

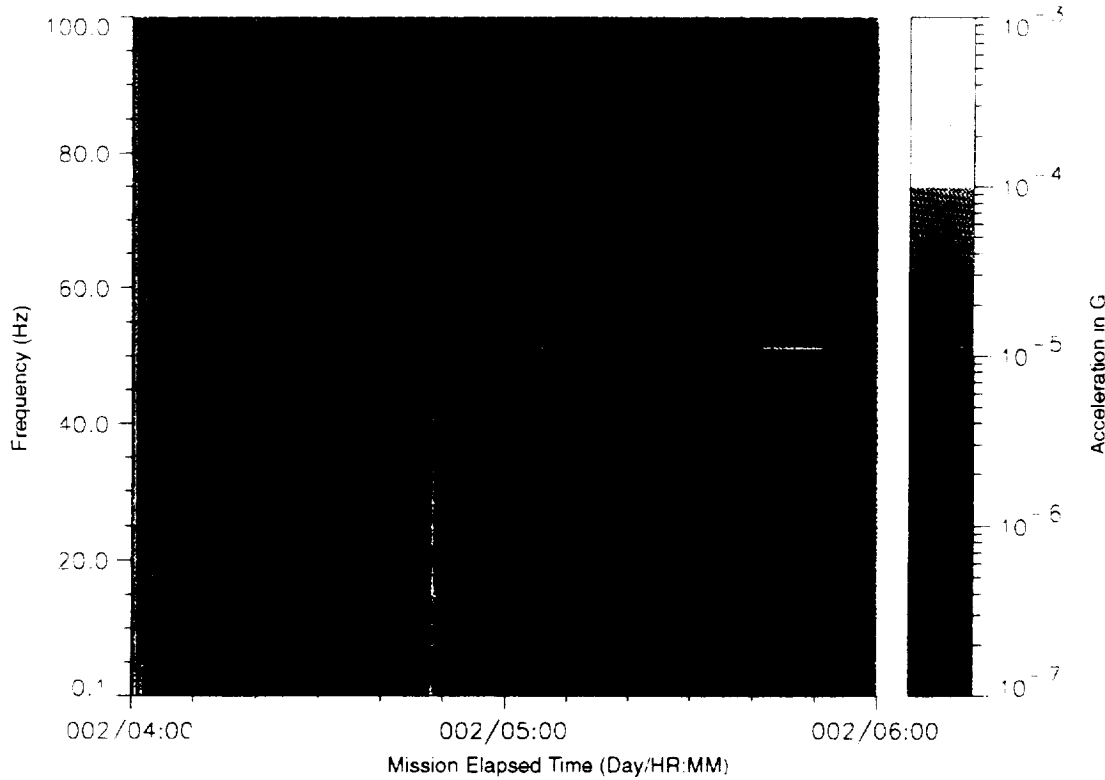


Figure B-90: SPACEHAB-1, Forward Bulkhead T-Beam

STS-57, Head A, Y-Axis

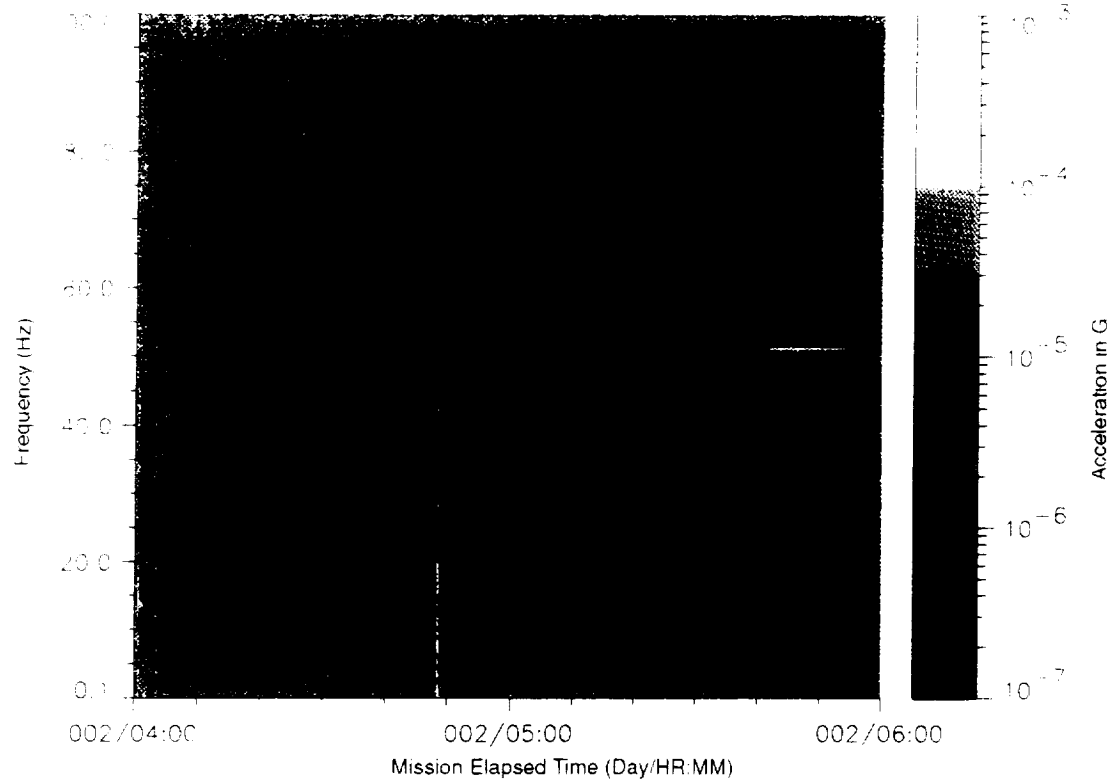


Figure B-91: SPACEHAB-1, Forward Bulkhead T-Beam

STS-57, Head A, Z-Axis

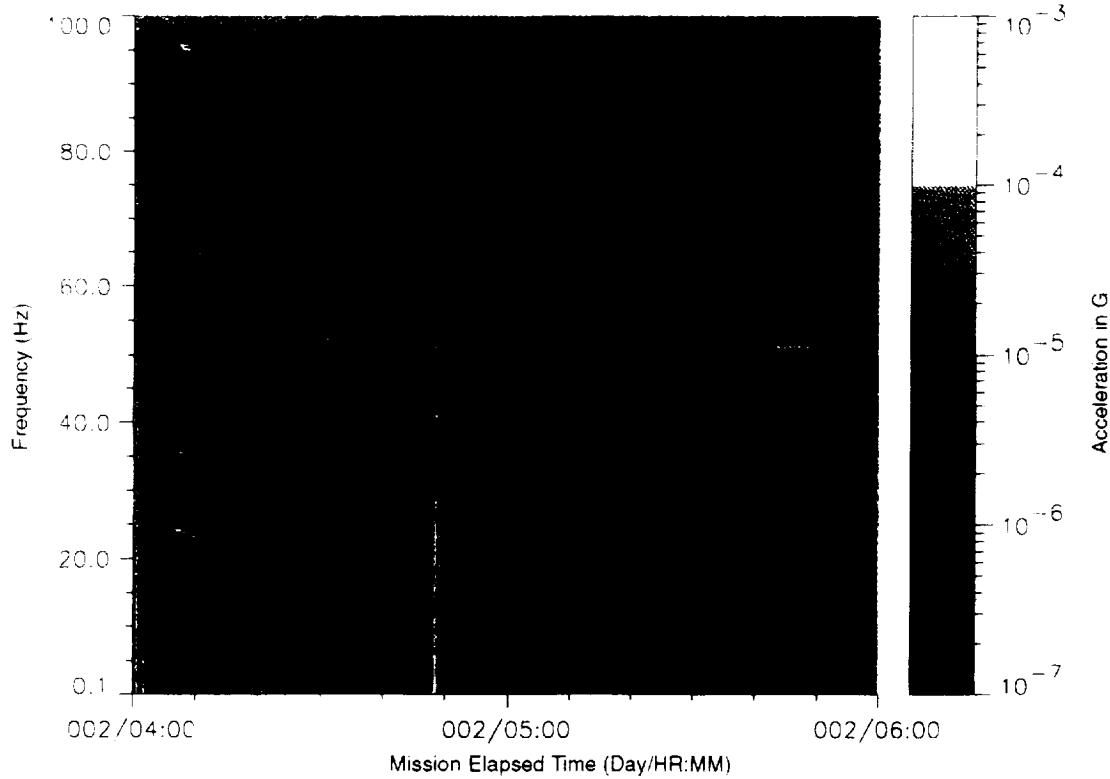


Figure B-92: SPACEHAB-1, Forward Bulkhead T-Beam

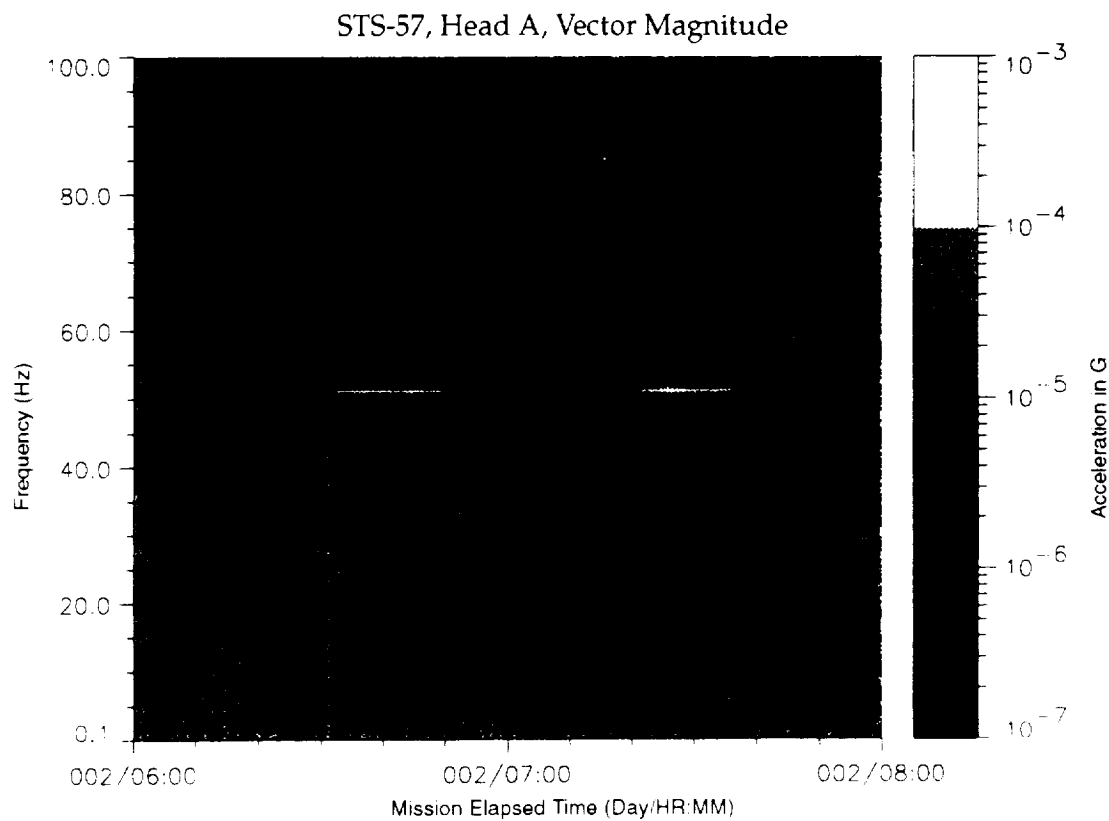


Figure B-93: SPACEHAB-1, Forward Bulkhead T-Beam

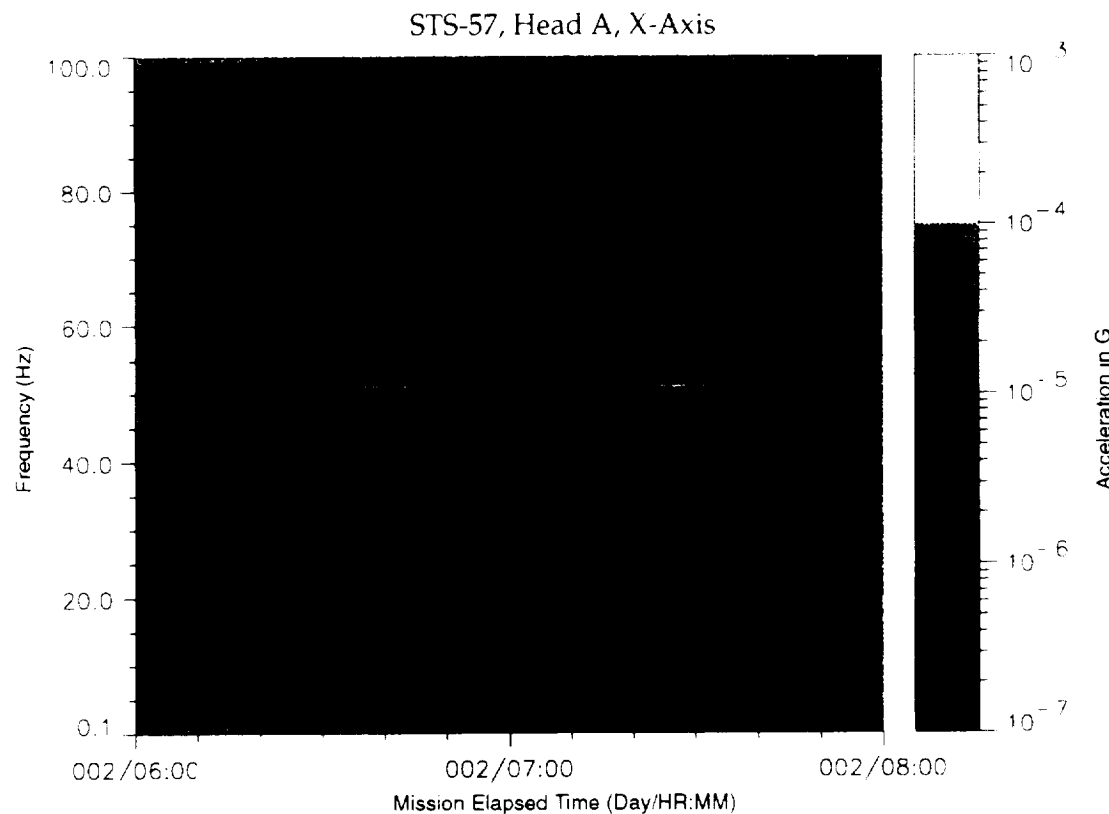


Figure B-94: SPACEHAB-1, Forward Bulkhead T-Beam

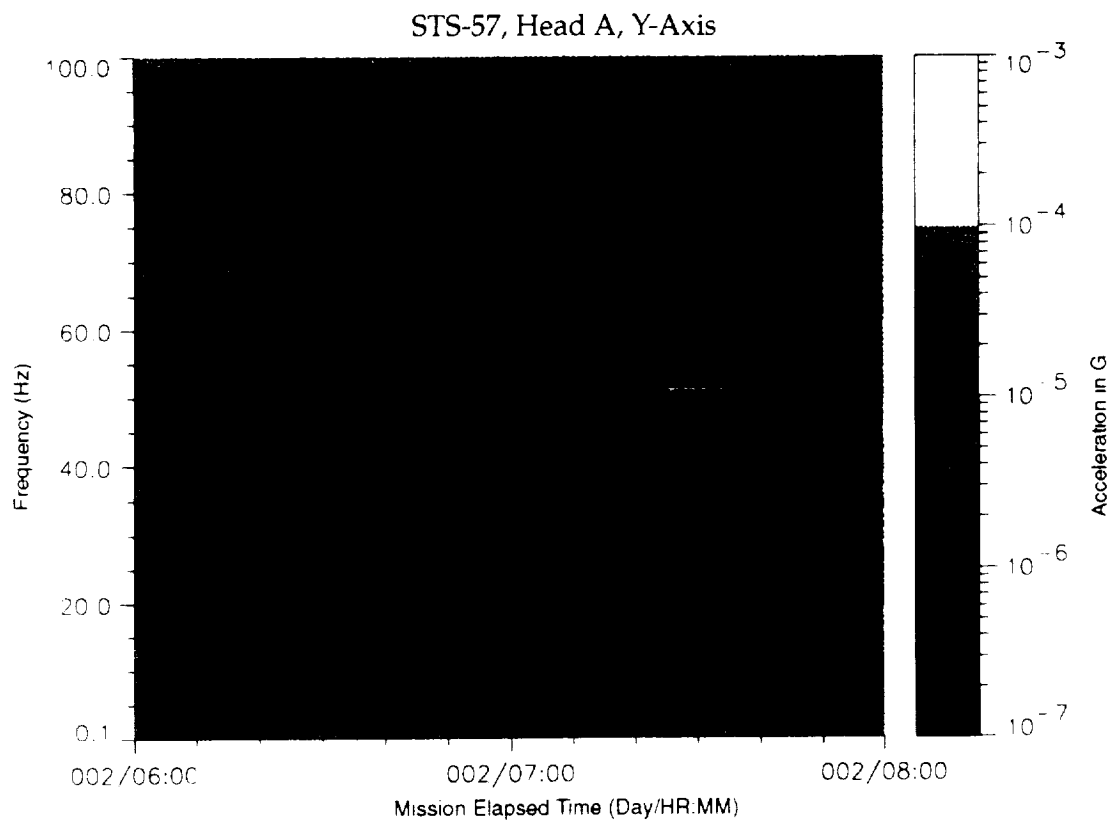


Figure B-95: SPACEHAB-1, Forward Bulkhead T-Beam

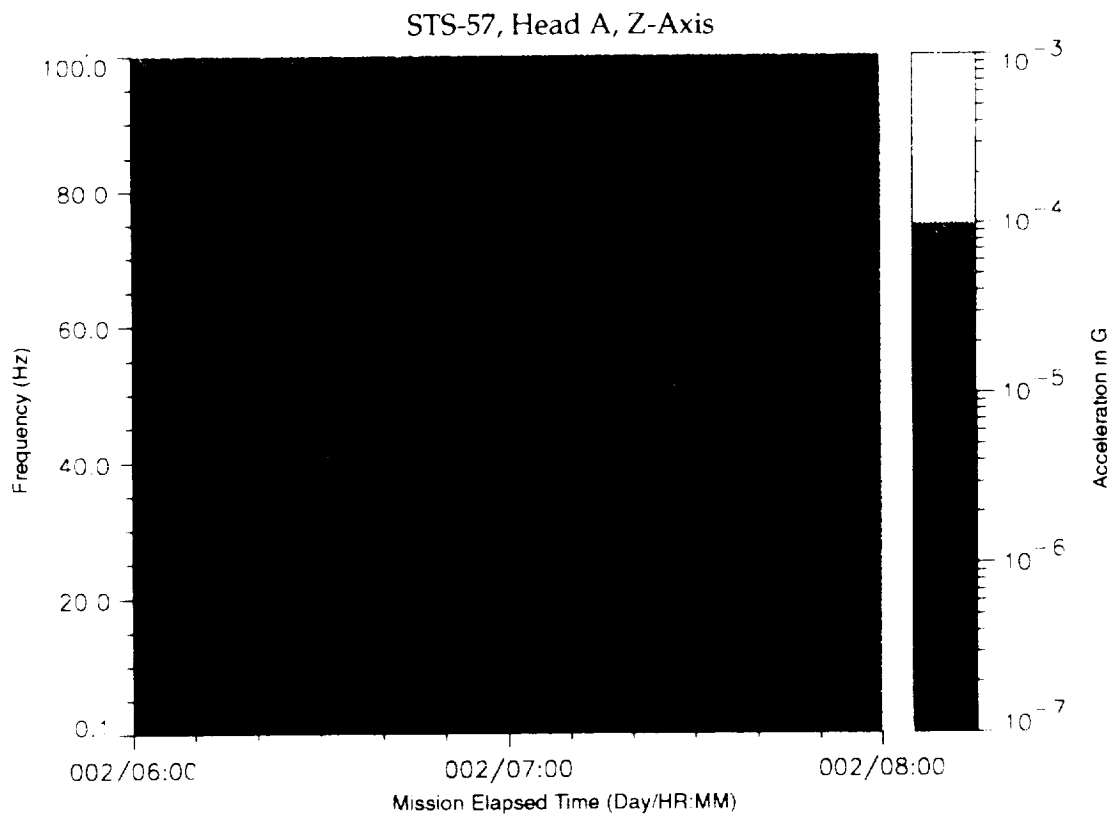


Figure B-96: SPACEHAB-1, Forward Bulkhead T-Beam

~~PRECEDING PAGE PLANK NOT FILMED~~

STS-57, Head A, Vector Magnitude

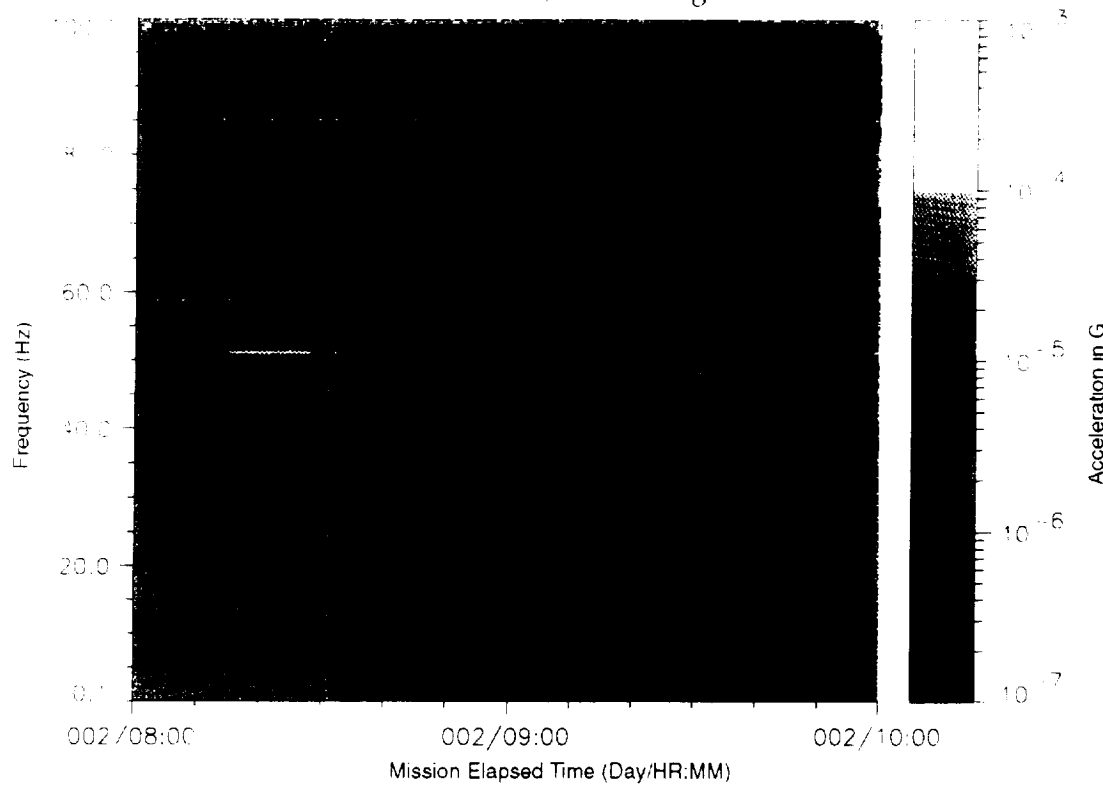


Figure B-97: SPACEHAB-1, Forward Bulkhead T-Beam

STS-57, Head A, X-Axis

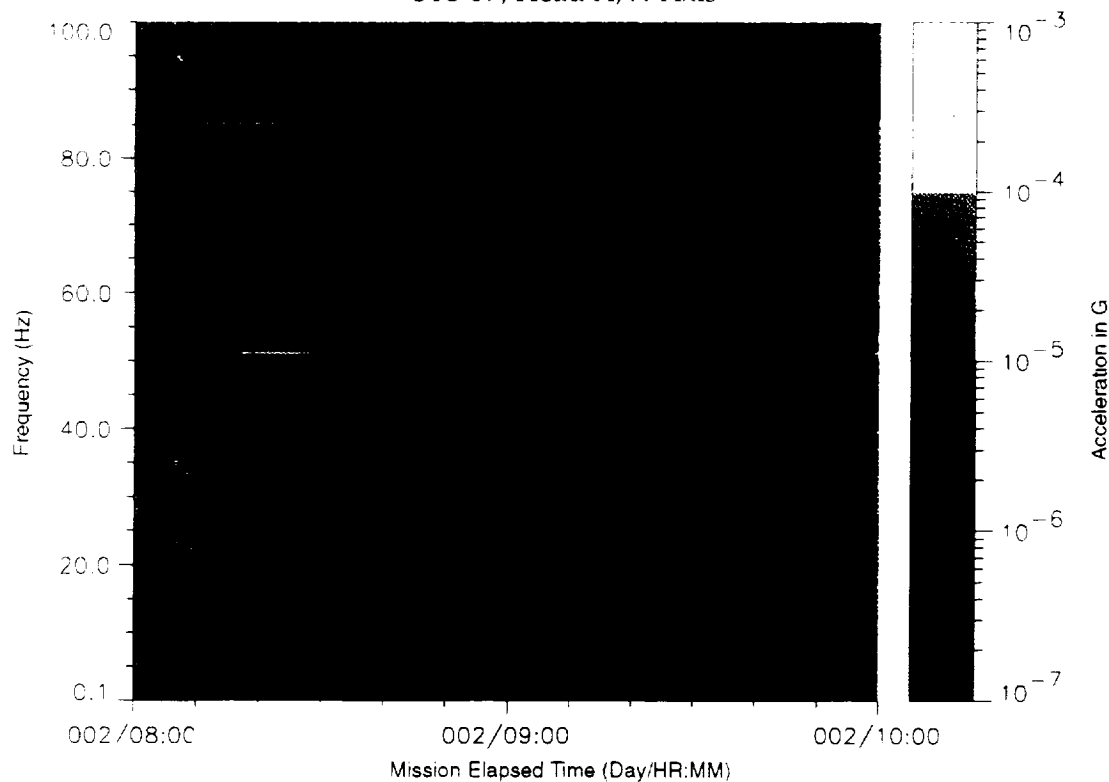


Figure B-98: SPACEHAB-1, Forward Bulkhead T-Beam

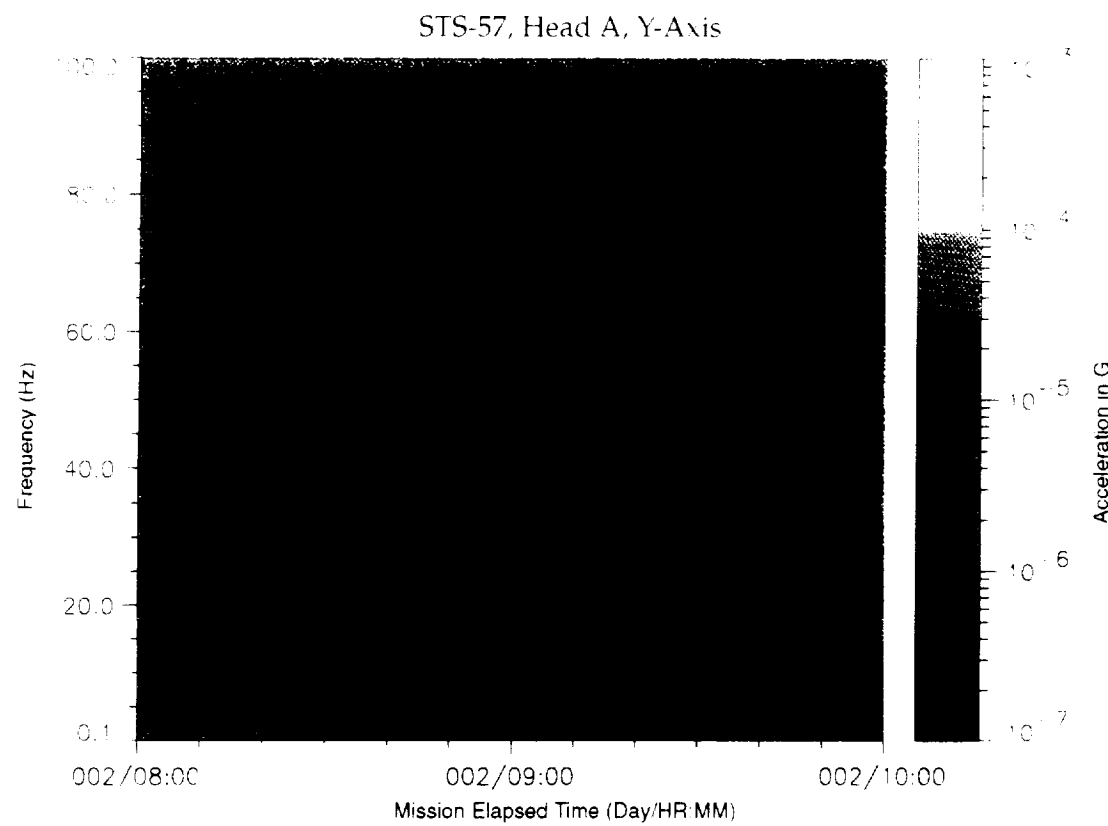


Figure B-99: SPACEHAB-1, Forward Bulkhead T-Beam

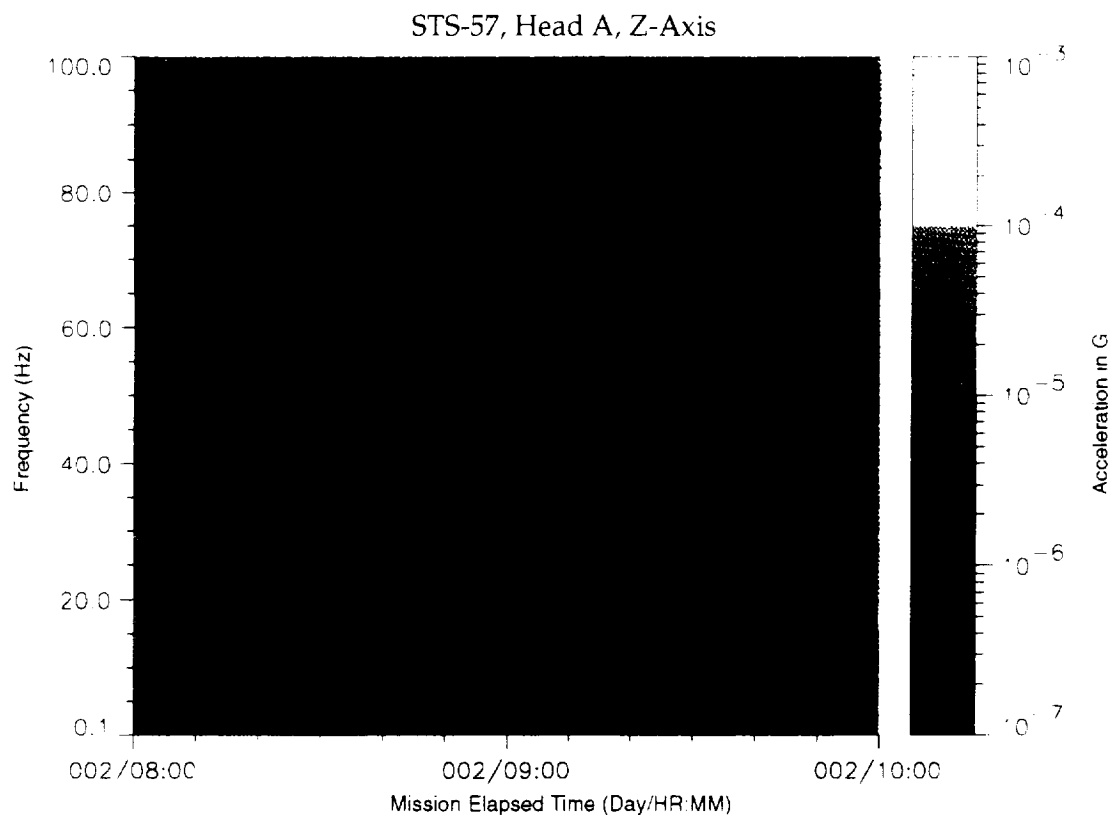


Figure B-100: SPACEHAB-1, Forward Bulkhead T-Beam

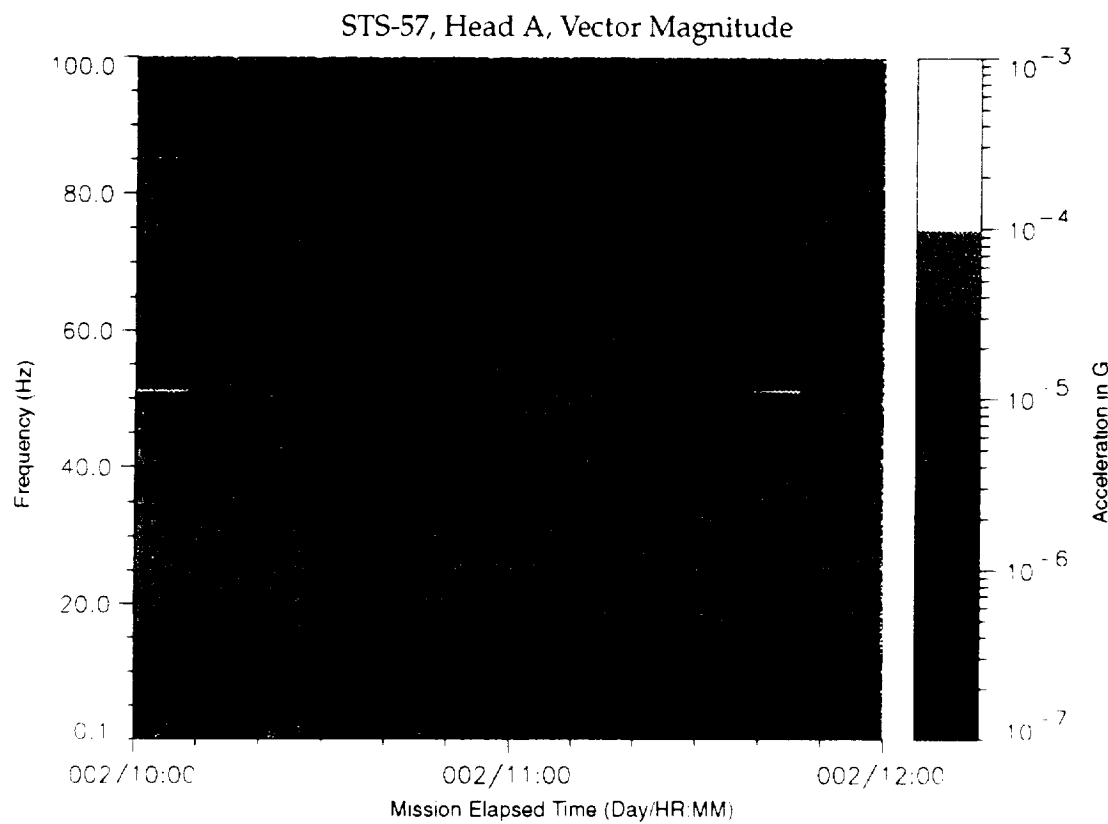


Figure B-101: SPACEHAB-1, Forward Bulkhead T-Beam

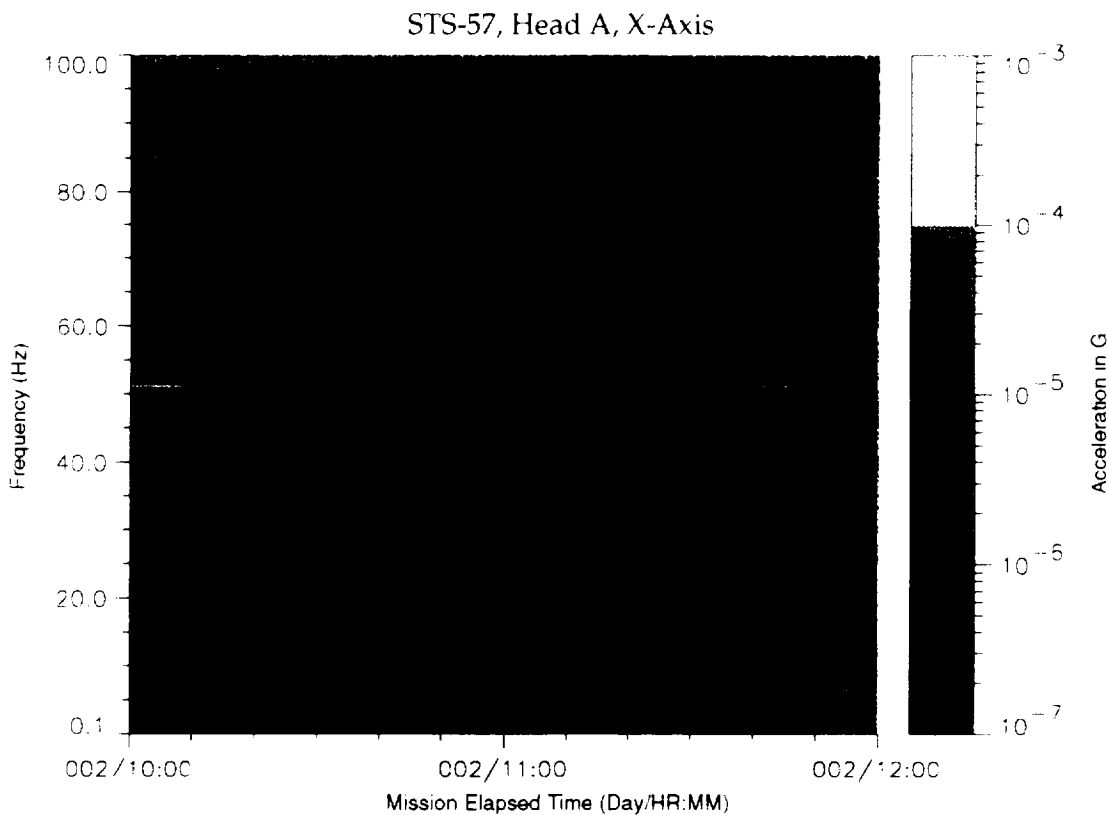


Figure B-102: SPACEHAB-1, Forward Bulkhead T-Beam

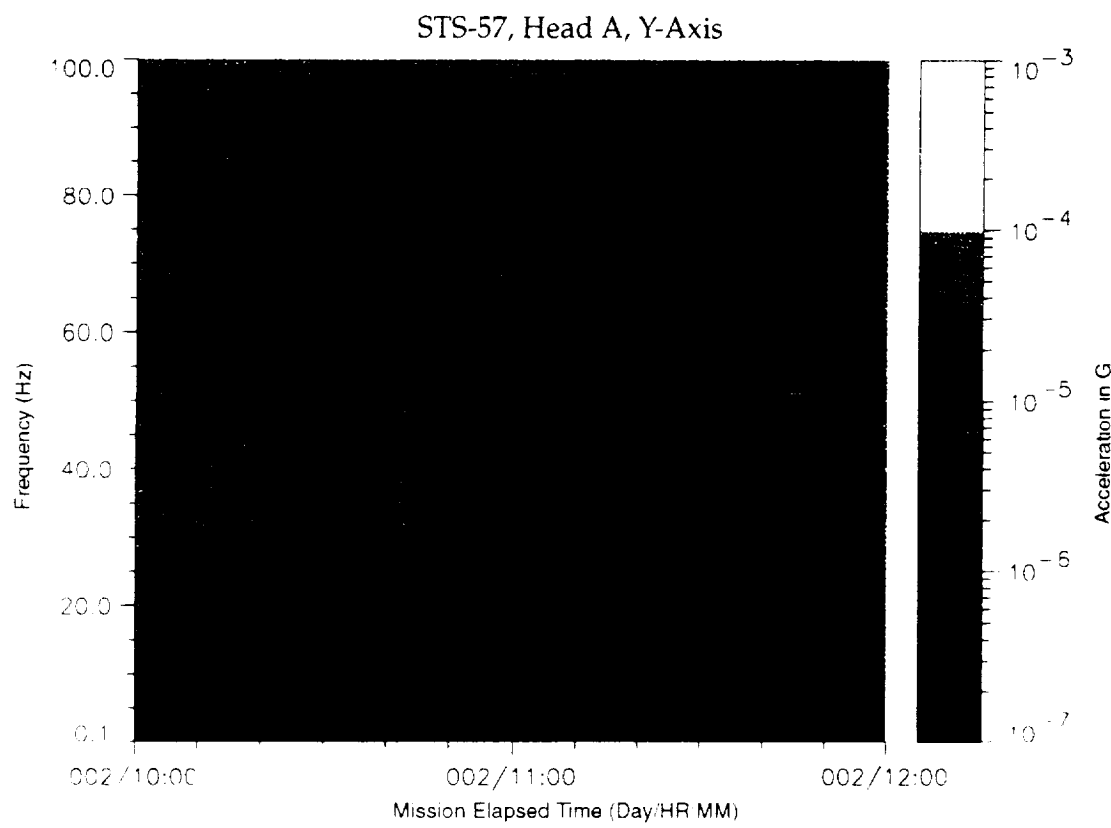


Figure B-103: SPACEHAB-1, Forward Bulkhead T-Beam

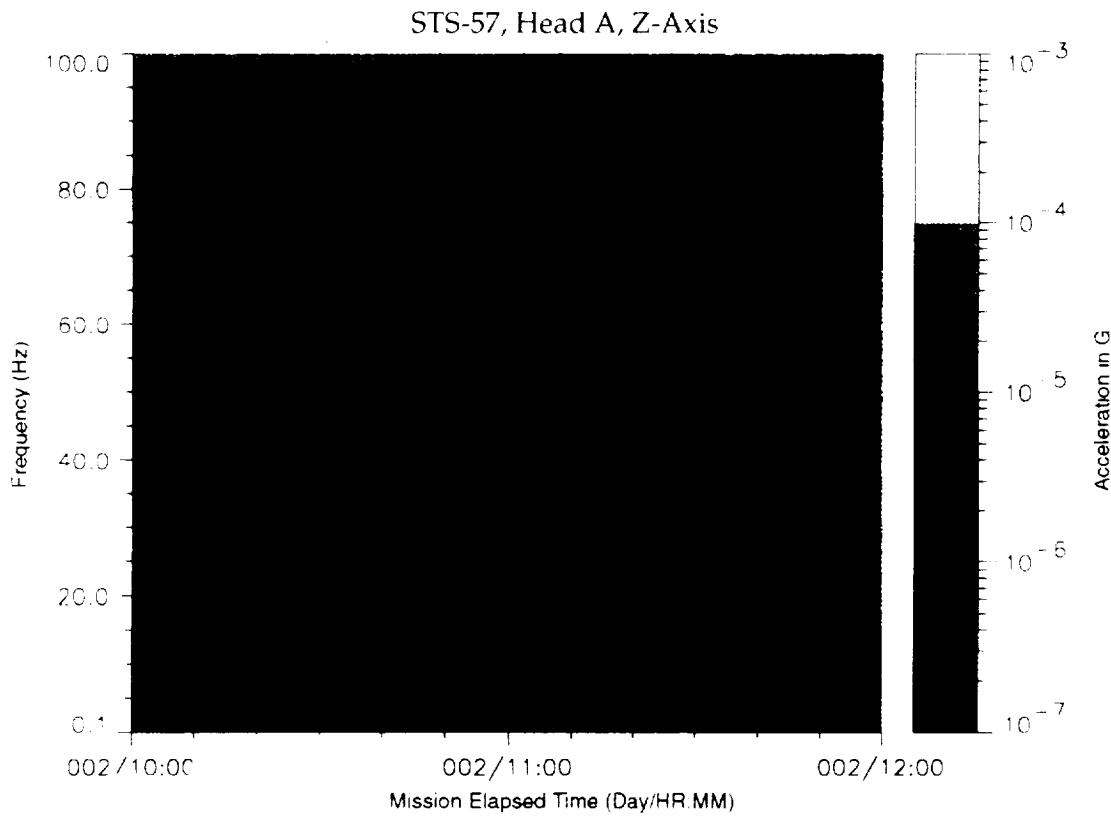


Figure B-104: SPACEHAB-1, Forward Bulkhead T-Beam

STS-57, Head A, Vector Magnitude

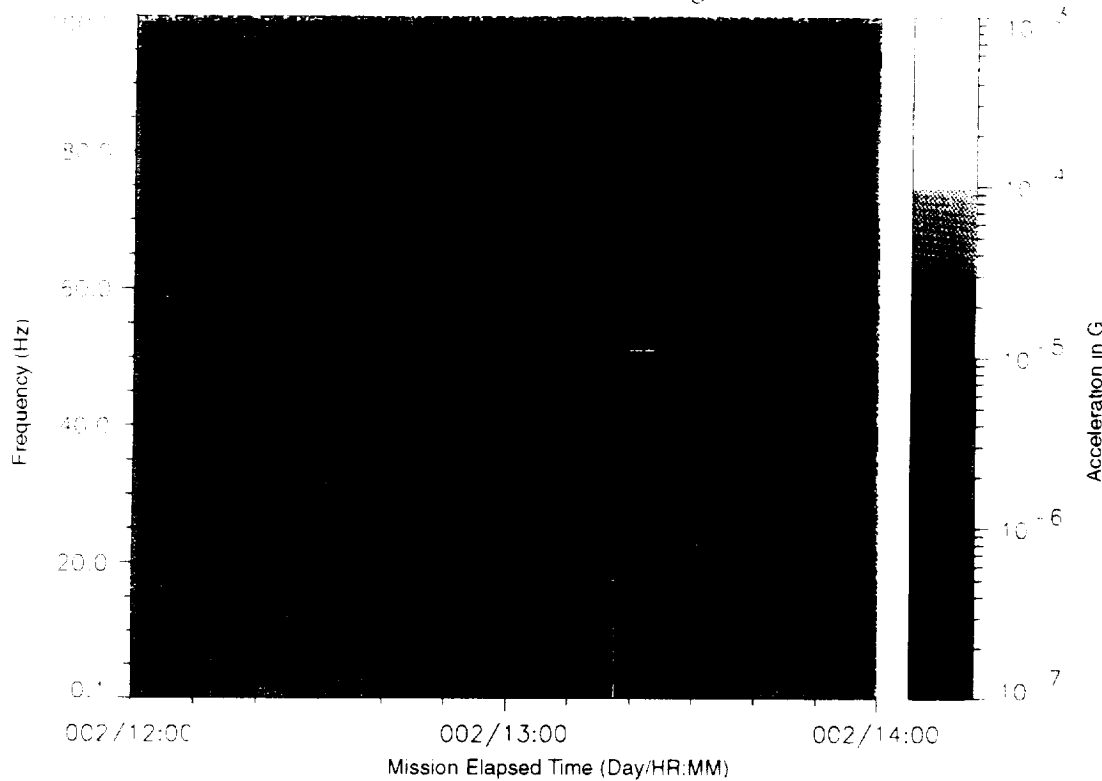


Figure B-105: SPACEHAB-1, Forward Bulkhead T-Beam

STS-57, Head A, X-Axis

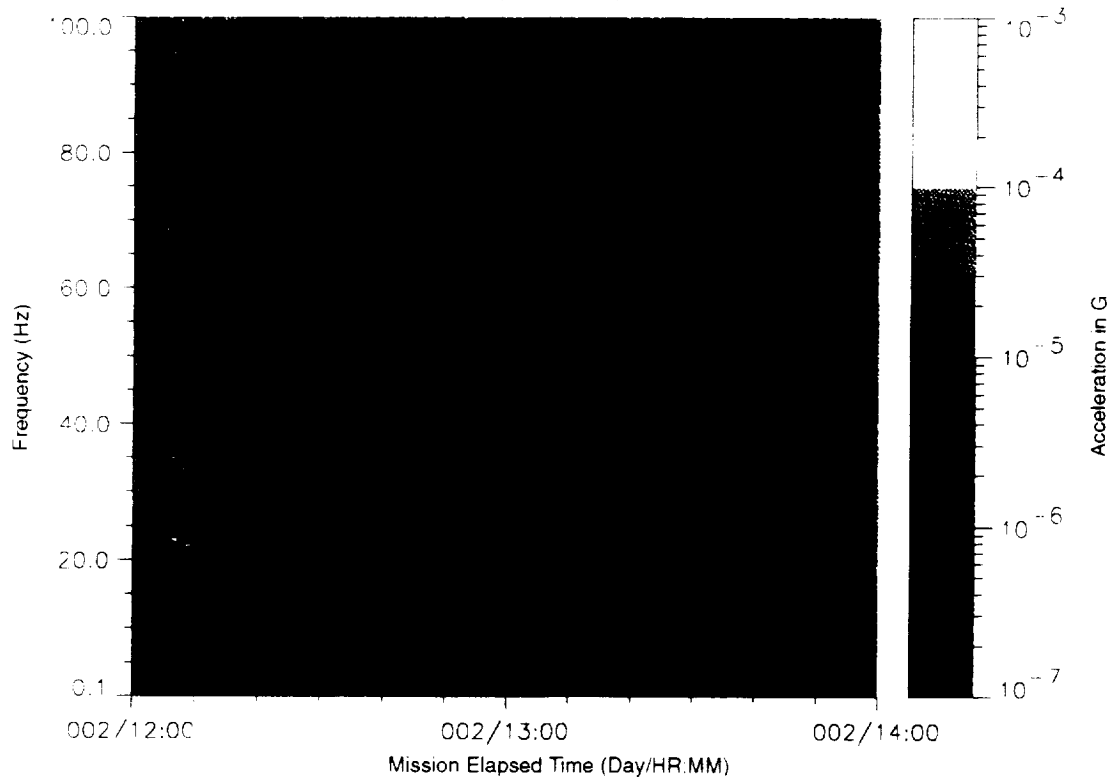


Figure B-106: SPACEHAB-1, Forward Bulkhead T-Beam

STS-57, Head A, Y-Axis

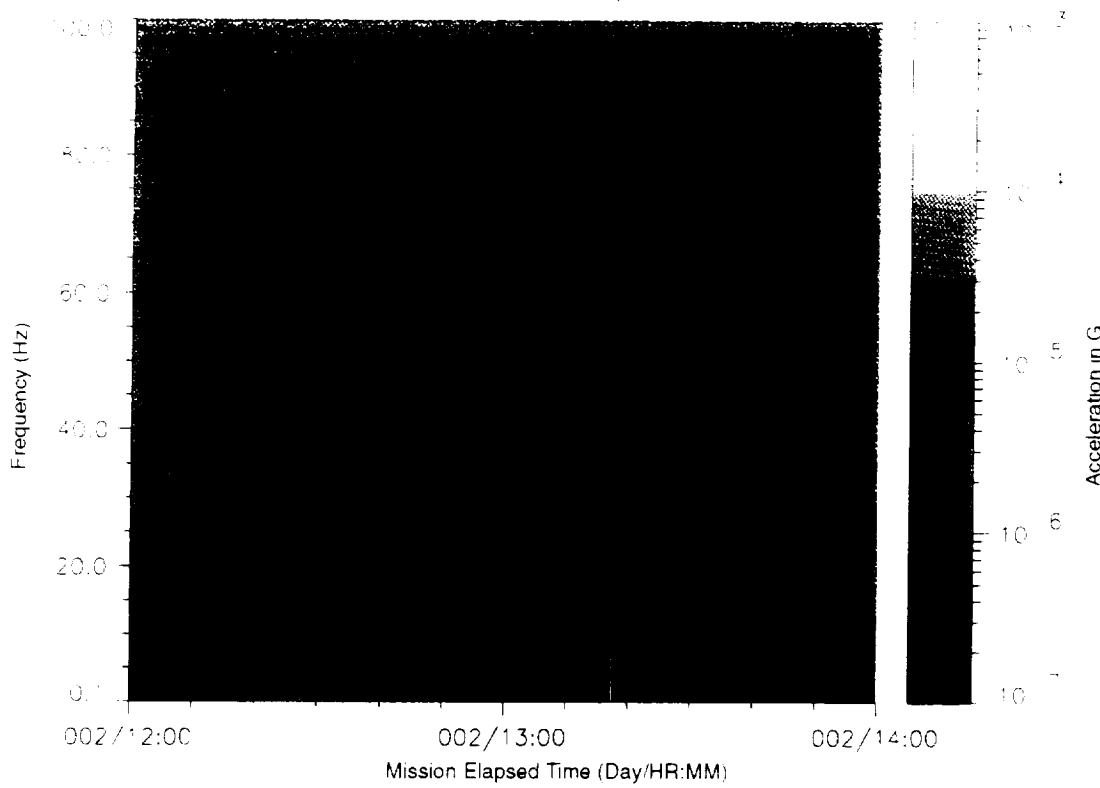


Figure B-107: SPACEHAB-1, Forward Bulkhead T-Beam

STS-57, Head A, Z-Axis

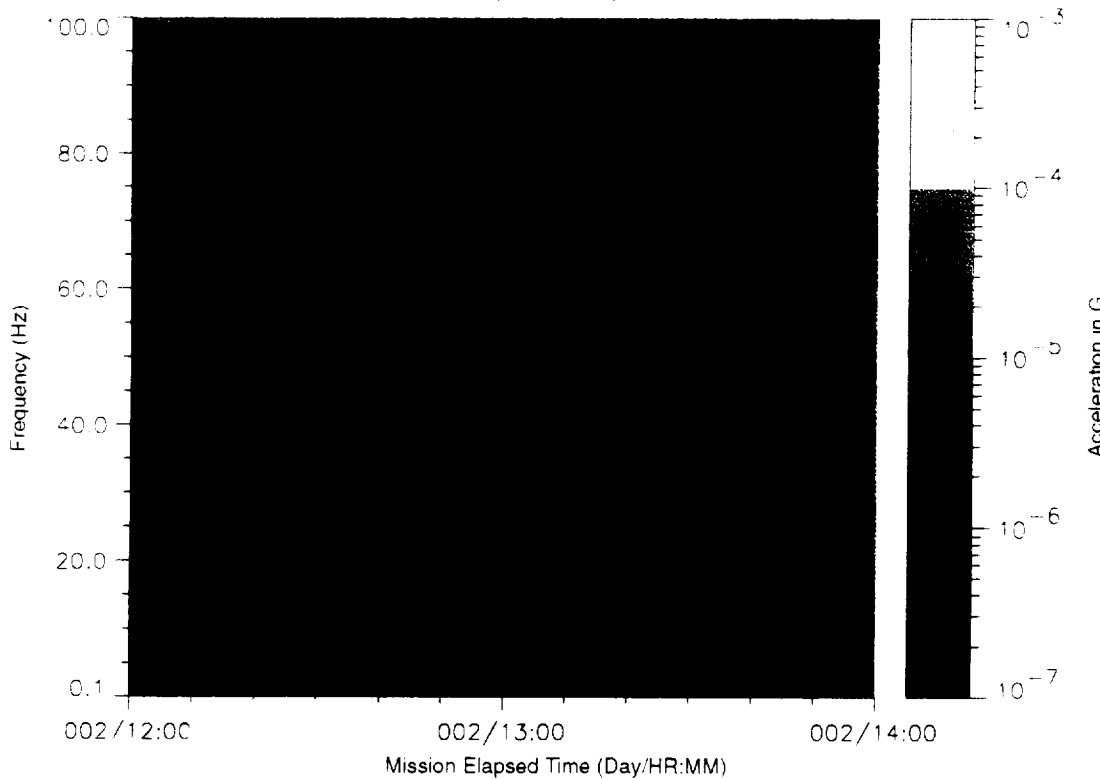


Figure B-108: SPACEHAB-1, Forward Bulkhead T-Beam

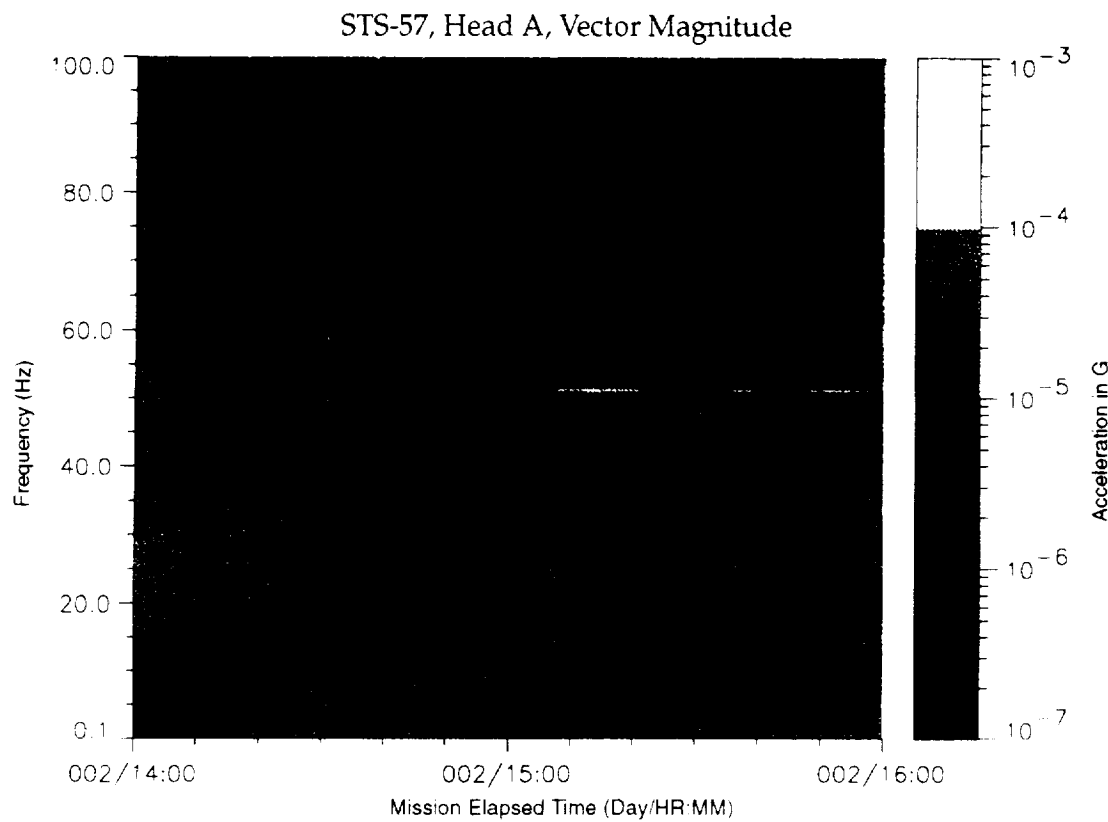


Figure B-109: SPACEHAB-1, Forward Bulkhead T-Beam

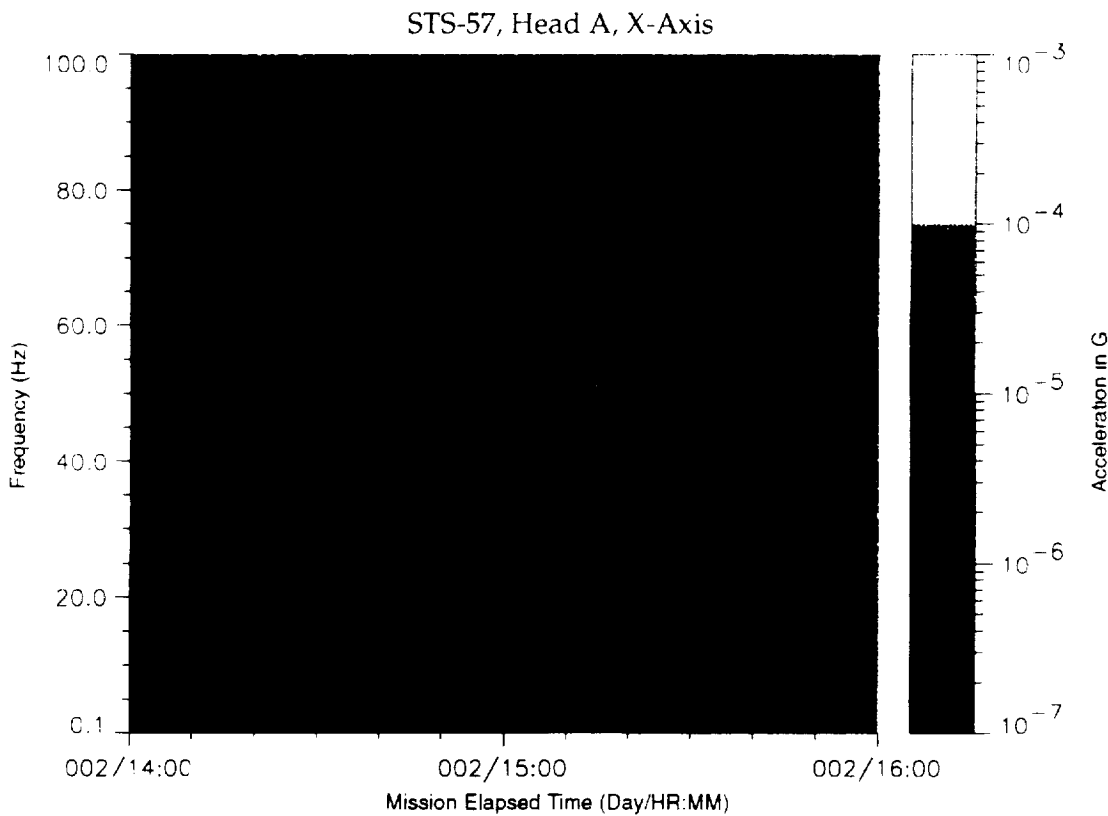


Figure B-110: SPACEHAB-1, Forward Bulkhead T-Beam

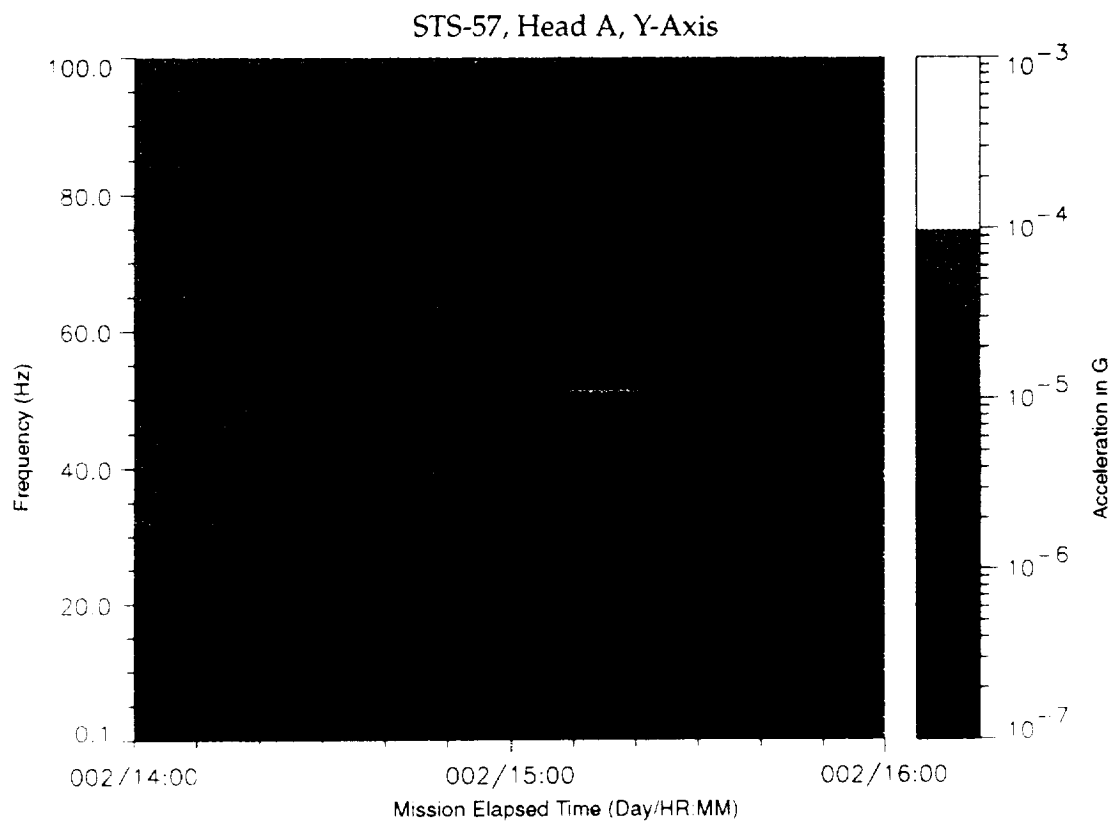


Figure B-111: SPACEHAB-1, Forward Bulkhead T-Beam

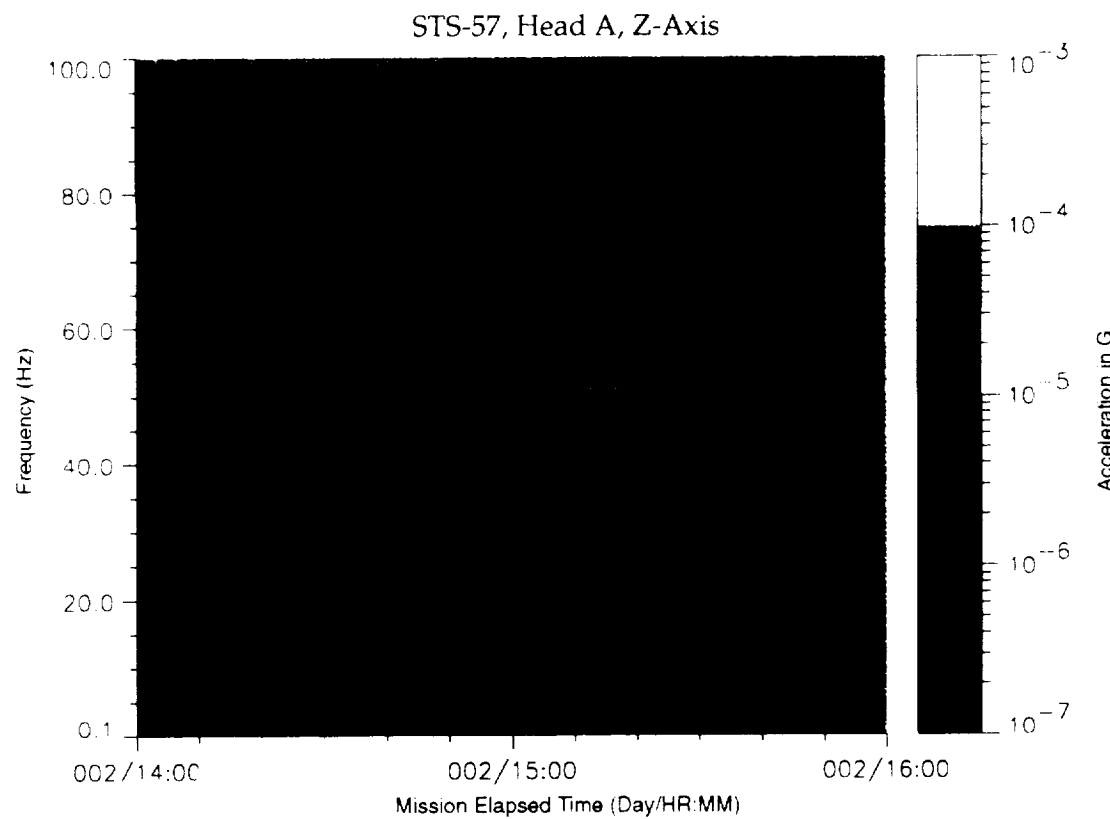


Figure B-112: SPACEHAB-1, Forward Bulkhead T-Beam

PREVIOUS PAGE BLANK NOT FILMED

STS-57, Head A, Vector Magnitude

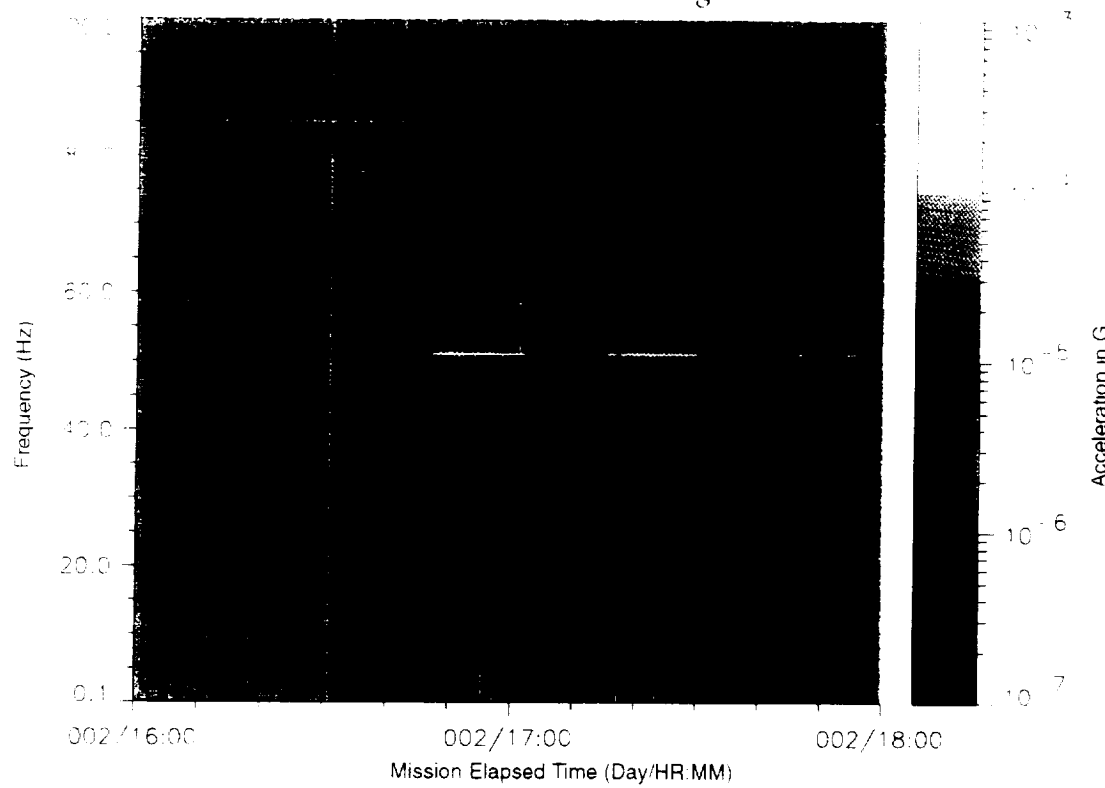


Figure B-113: SPACEHAB-1, Forward Bulkhead T-Beam

STS-57, Head A, X-Axis

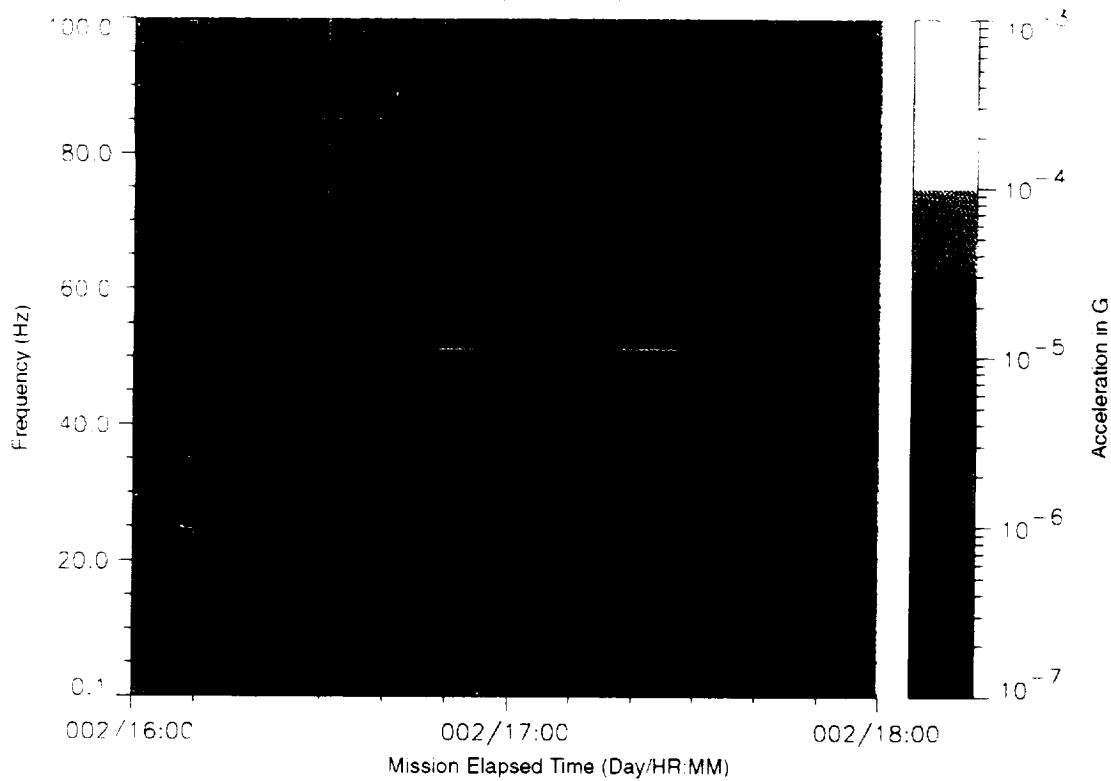


Figure B-114: SPACEHAB-1, Forward Bulkhead T-Beam

~~DATA NOT FILMED~~

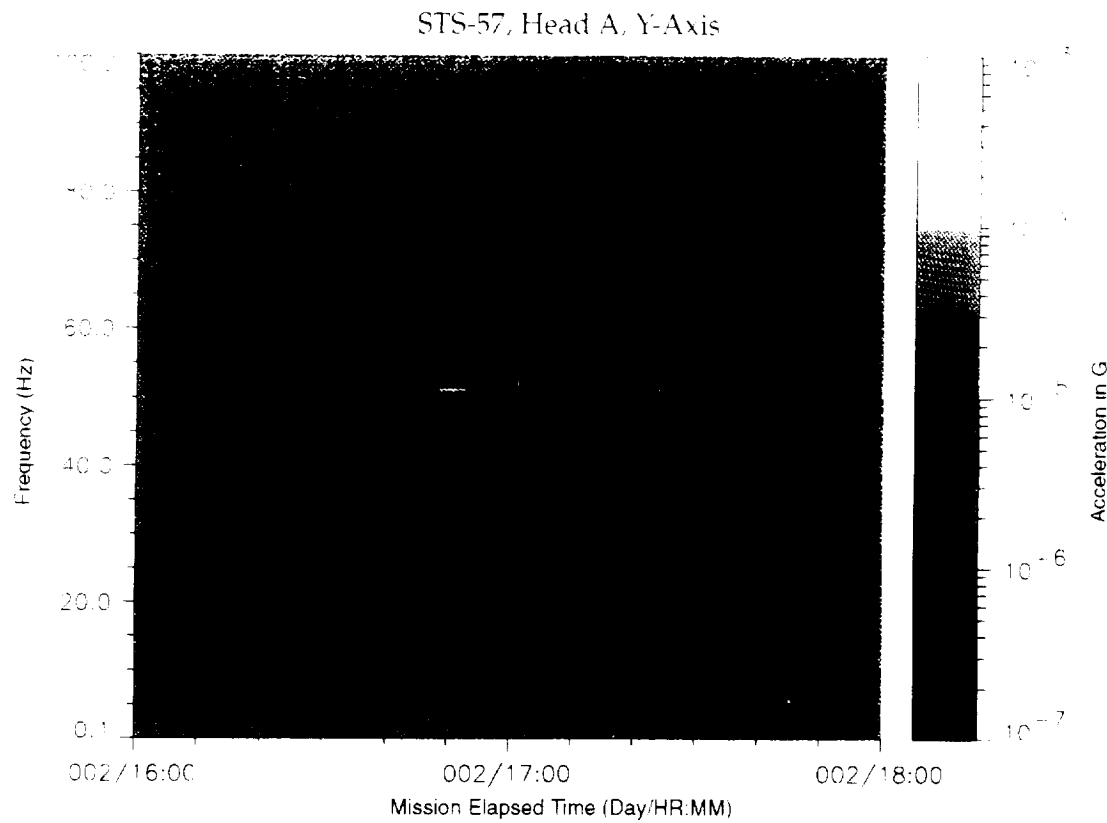


Figure B-115: SPACEHAB-1, Forward Bulkhead T-Beam

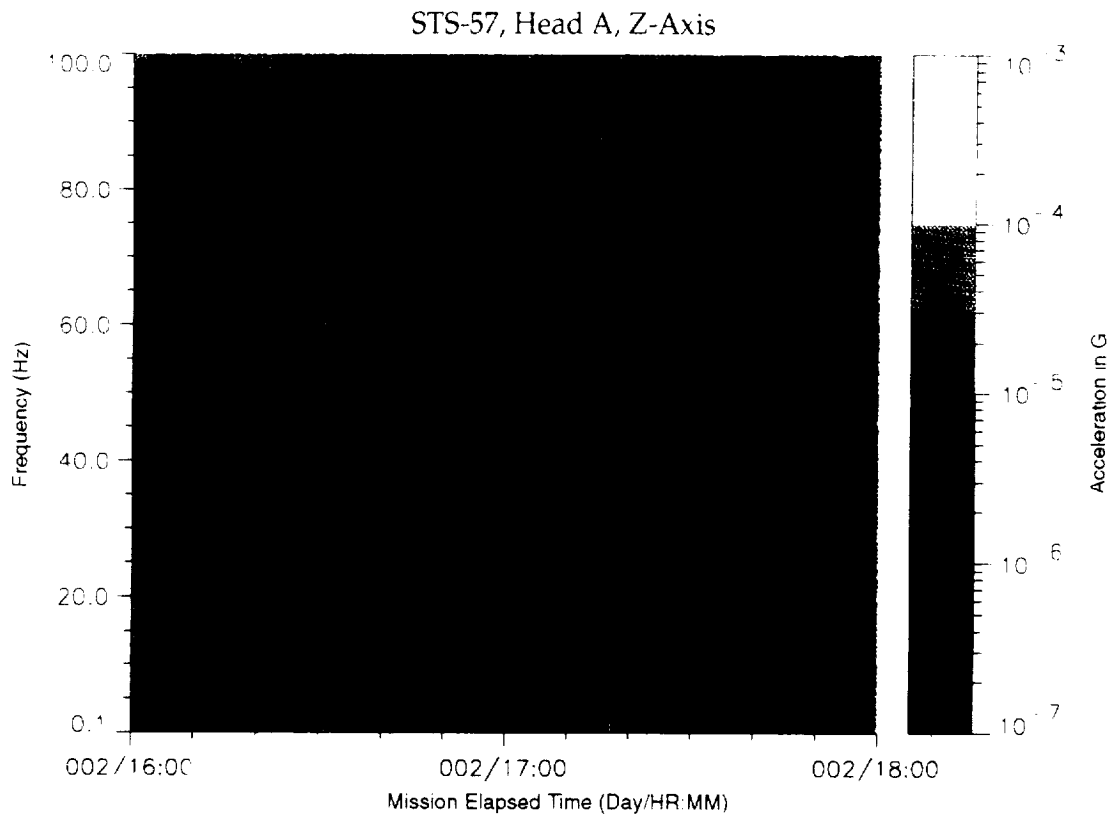


Figure B-116: SPACEHAB-1, Forward Bulkhead T-Beam

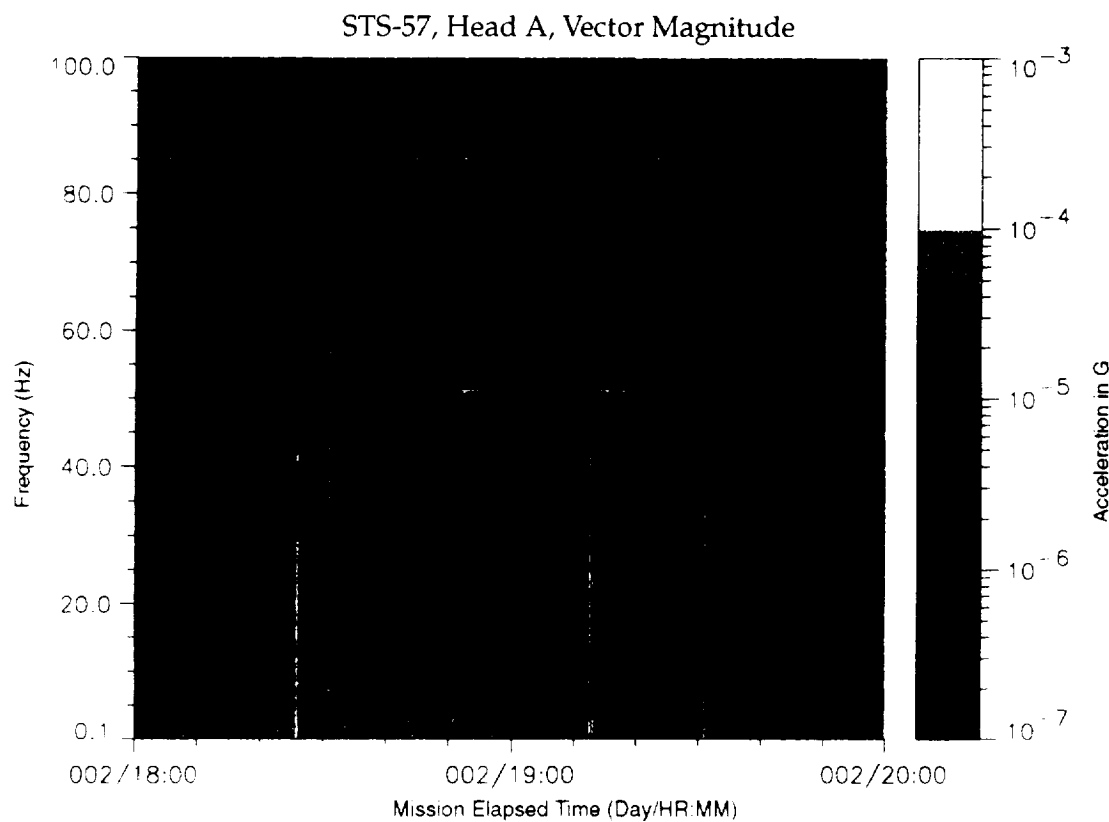


Figure B-117: SPACEHAB-1, Forward Bulkhead T-Beam

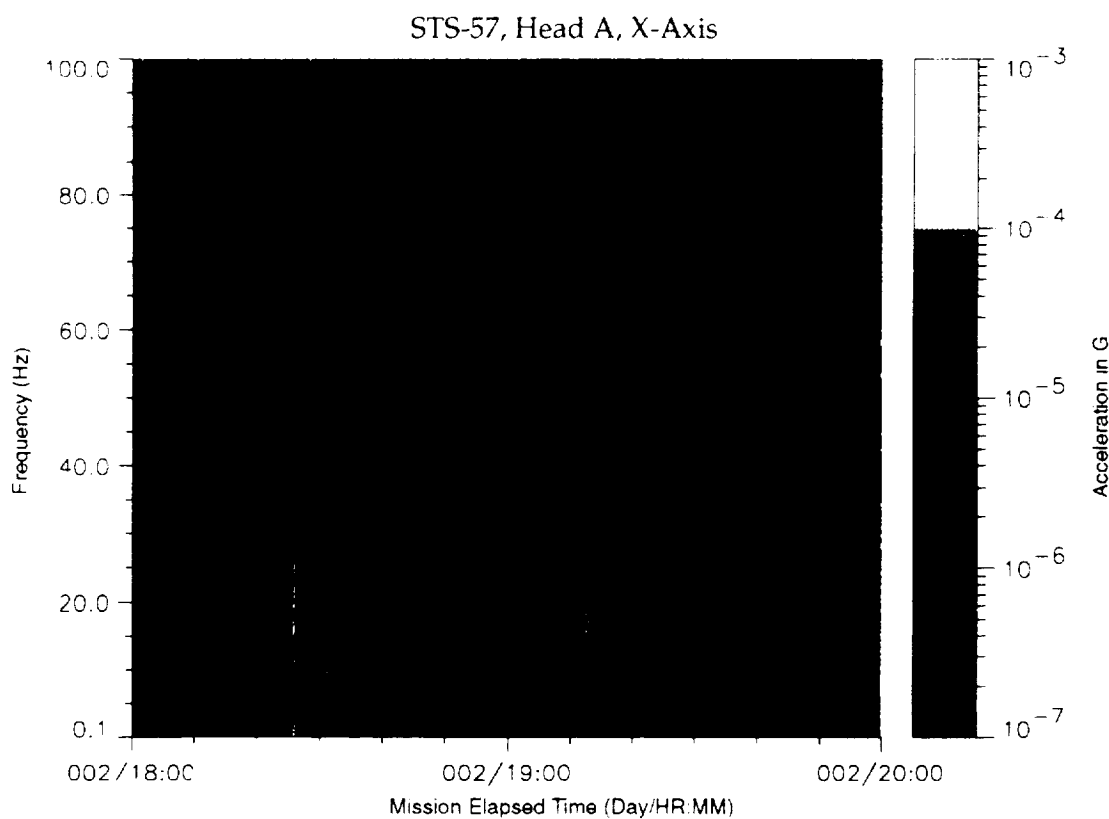


Figure B-118: SPACEHAB-1, Forward Bulkhead T-Beam

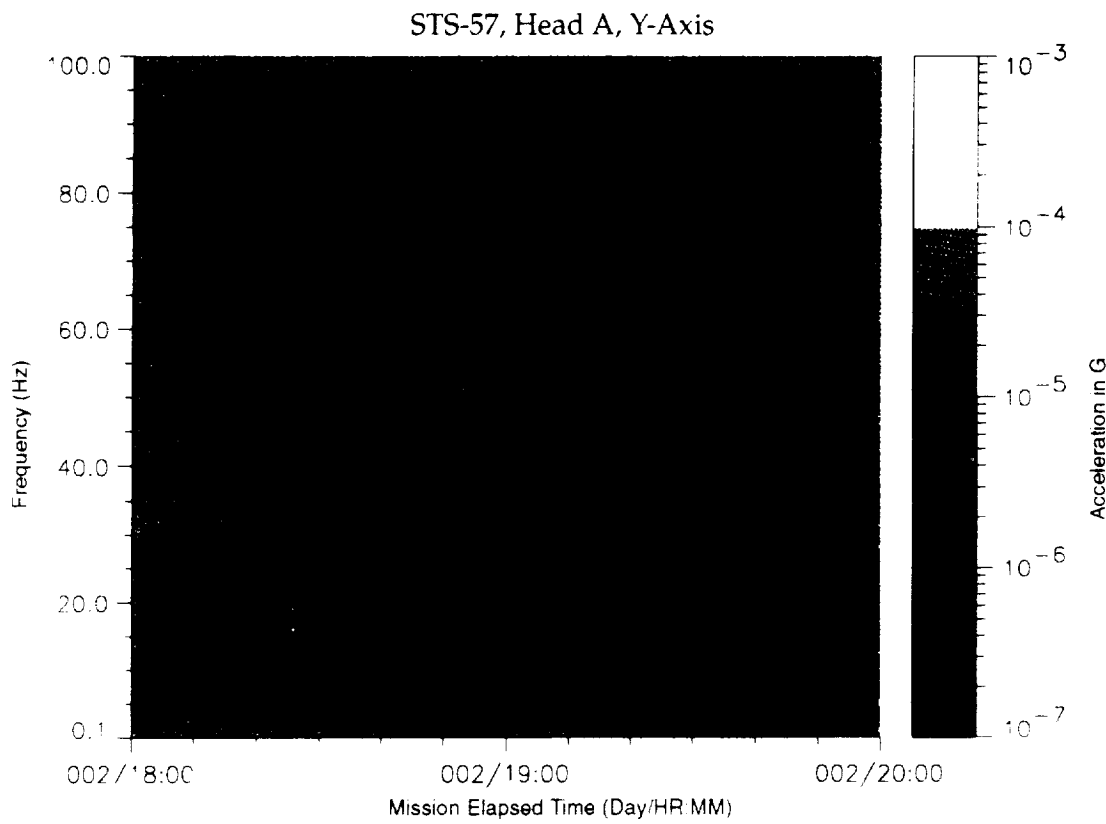


Figure B-119: SPACEHAB-1, Forward Bulkhead T-Beam

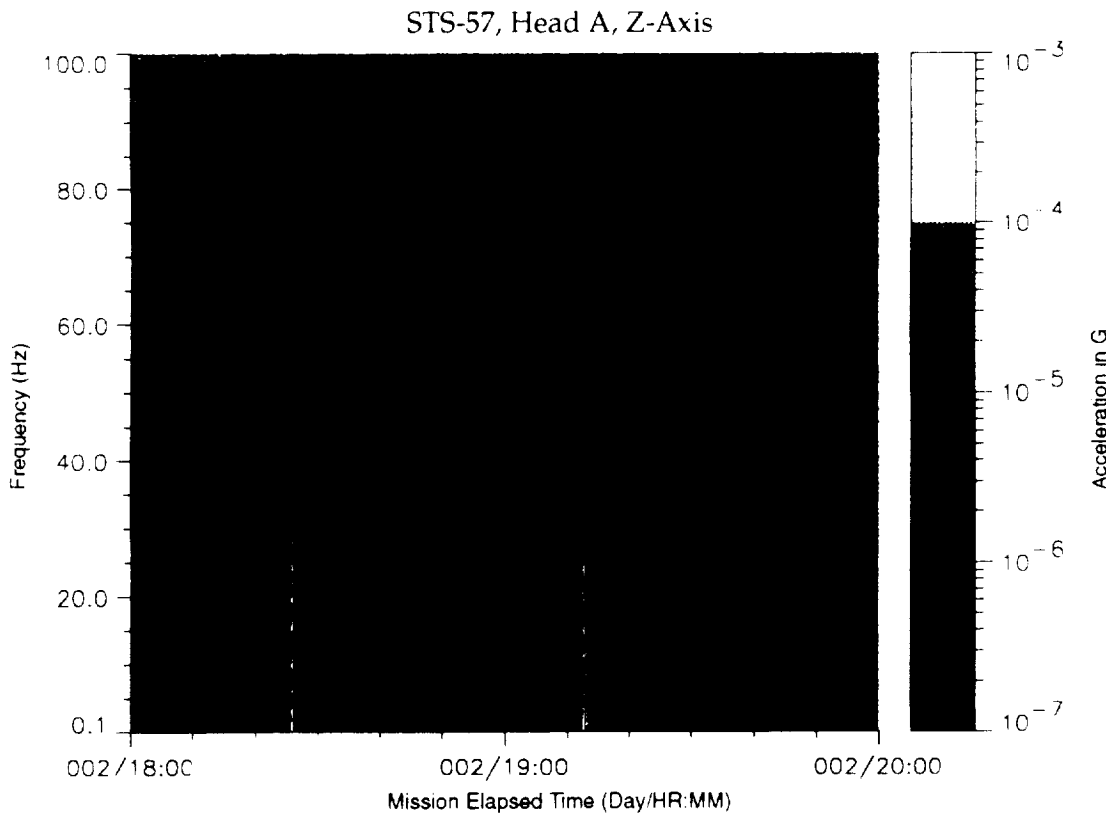


Figure B-120: SPACEHAB-1, Forward Bulkhead T-Beam

STS-57, Head A, Vector Magnitude

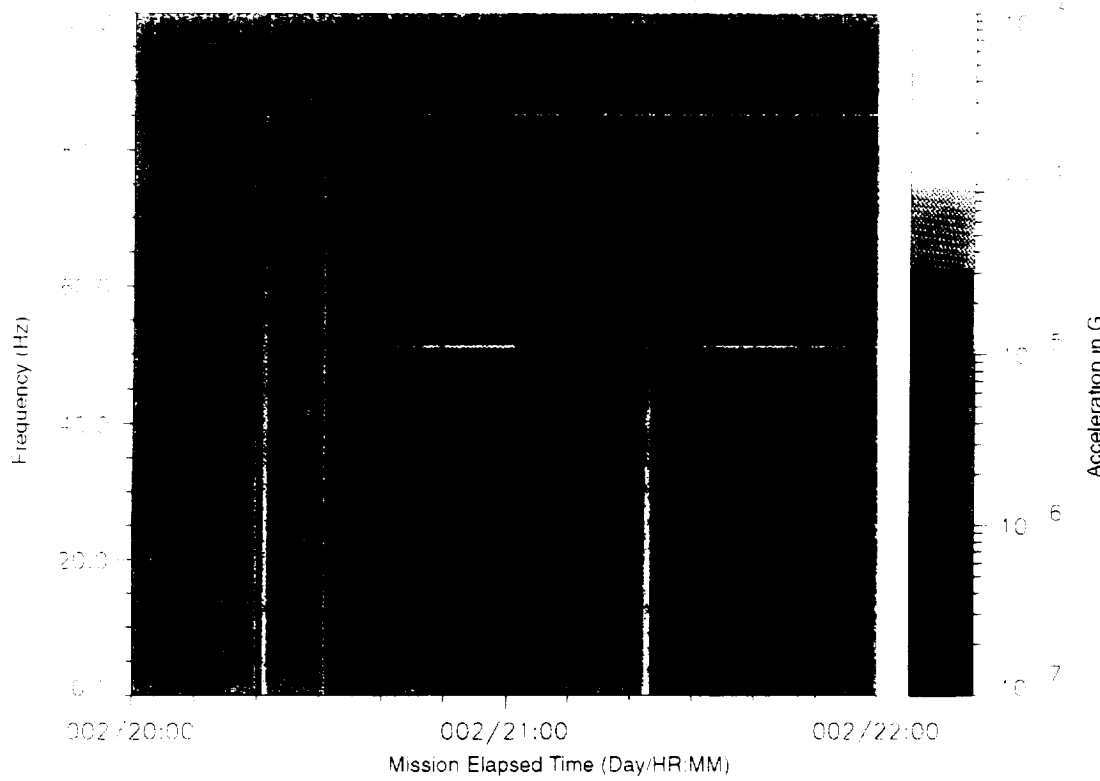


Figure B-121: SPACEHAB-1, Forward Bulkhead T-Beam

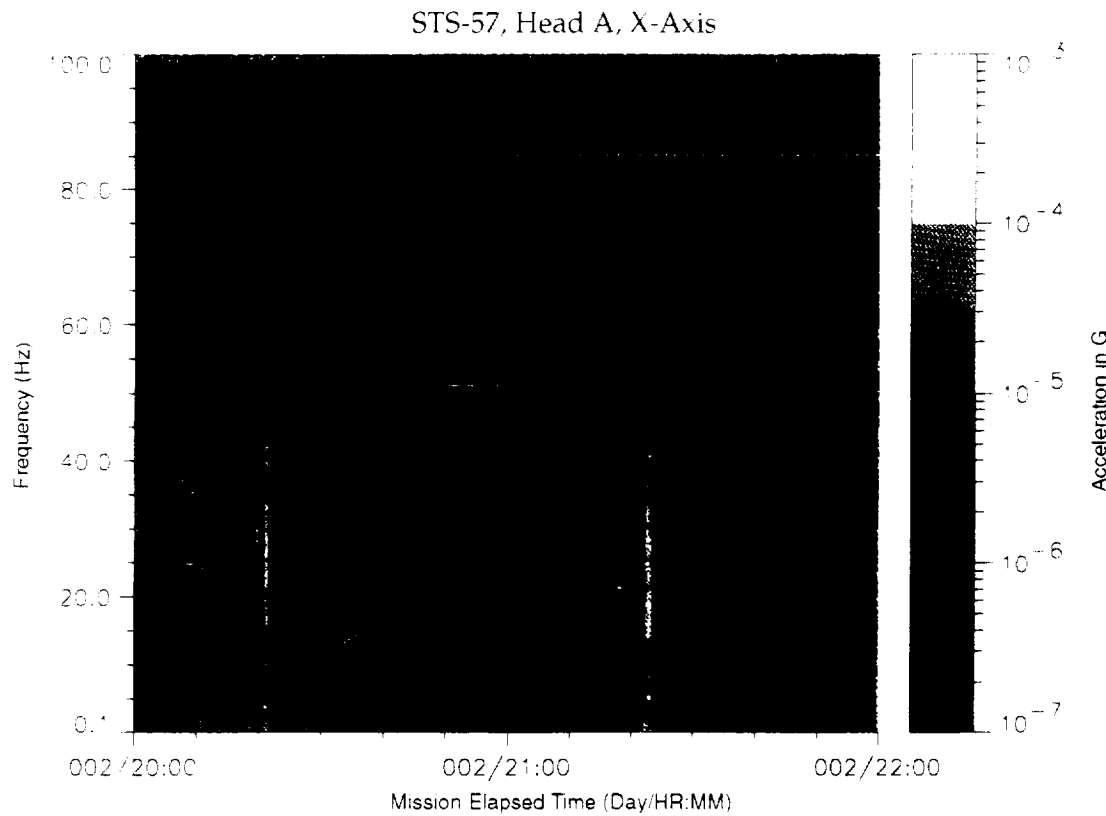


Figure B-122: SPACEHAB-1, Forward Bulkhead T-Beam

~~PRECEDING PAGE BLANK NOT FILMED~~

STS-57, Head A, Y-Axis

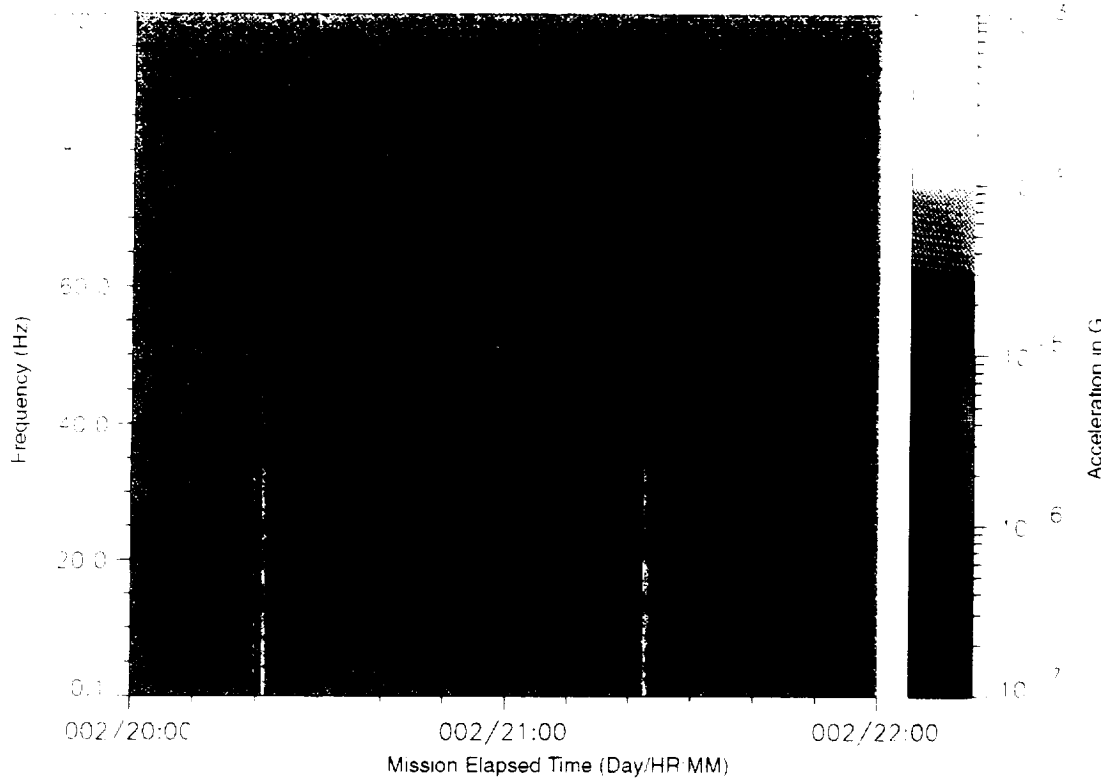


Figure B-123: SPACEHAB-1, Forward Bulkhead T-Beam

STS-57, Head A, Z-Axis

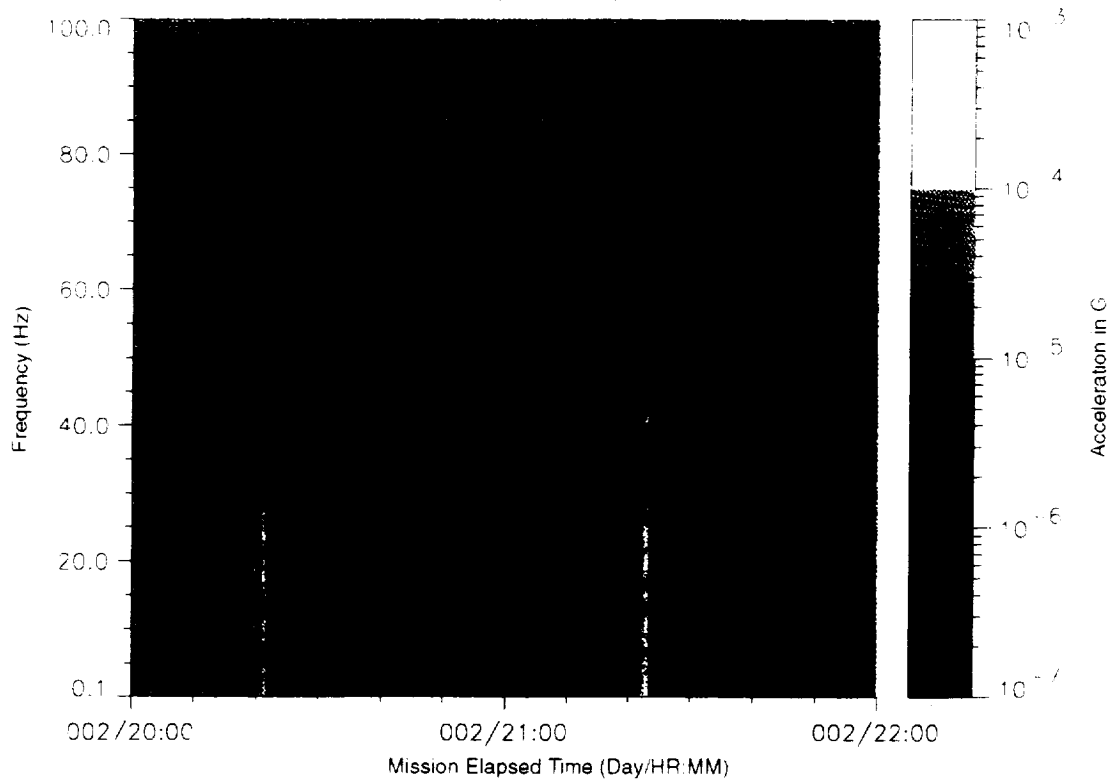


Figure B-124: SPACEHAB-1, Forward Bulkhead T-Beam

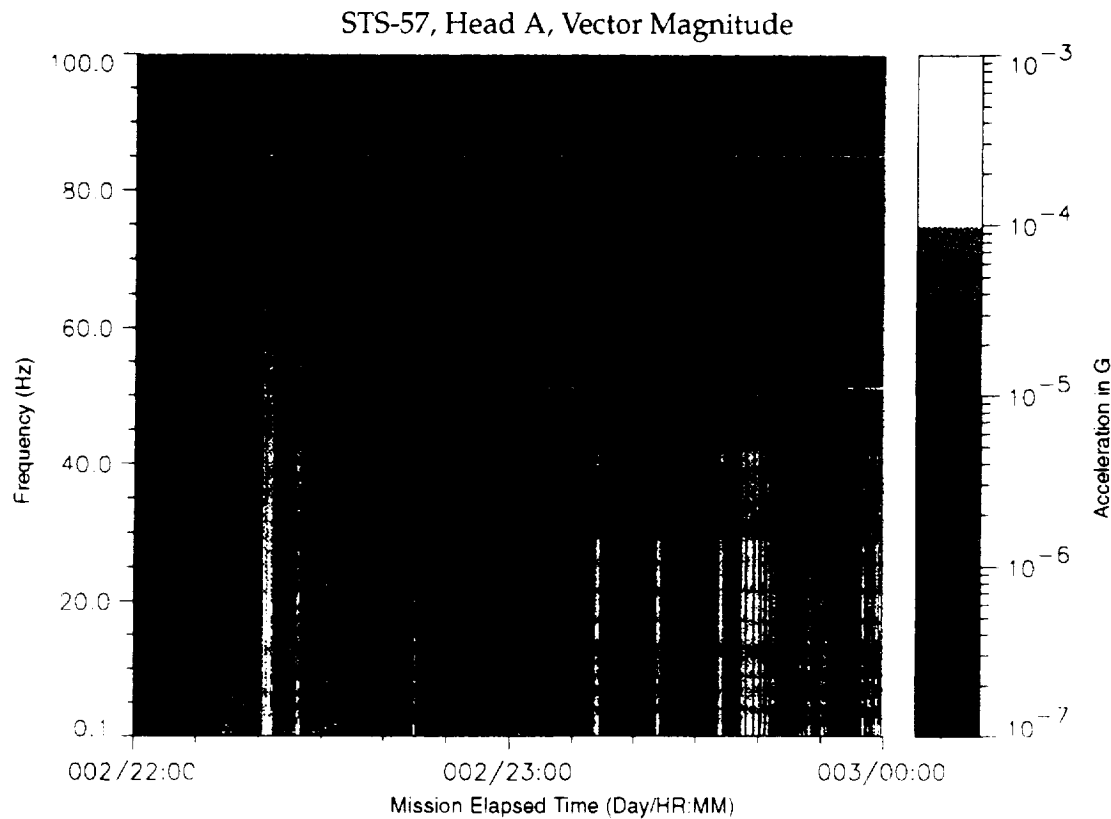


Figure B-125: SPACEHAB-1, Forward Bulkhead T-Beam

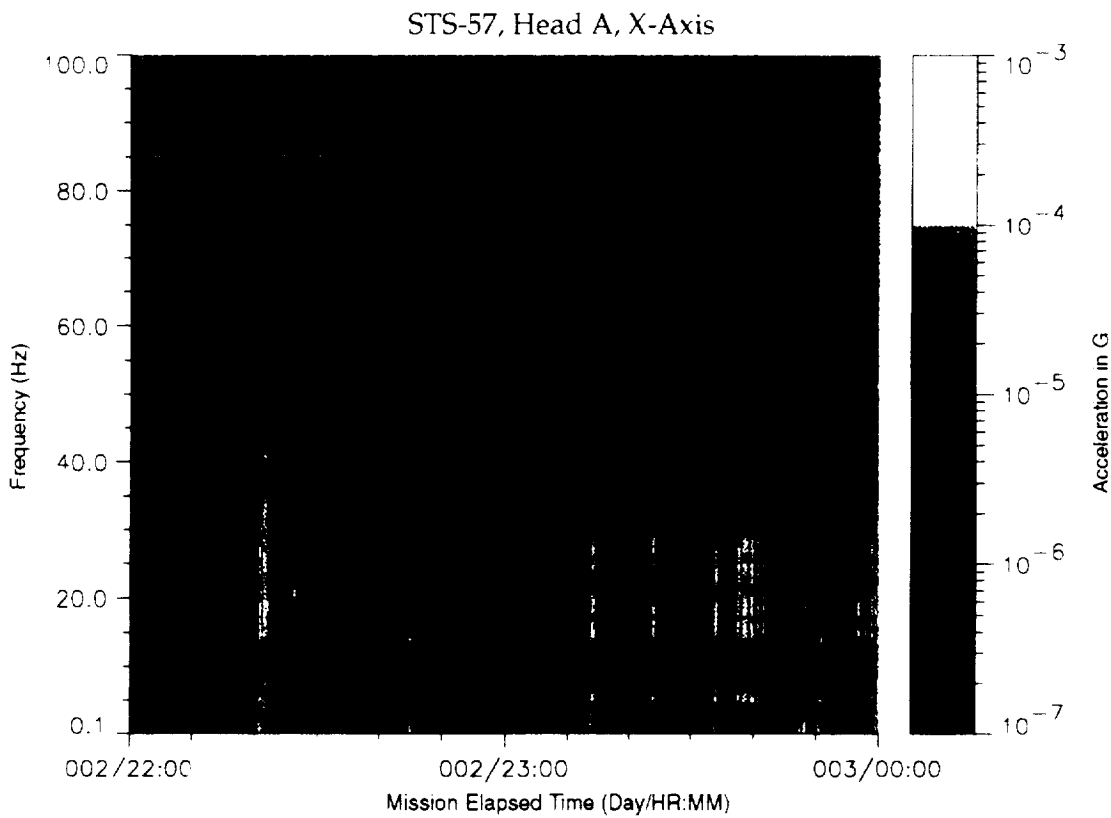


Figure B-126: SPACEHAB-1, Forward Bulkhead T-Beam

PRECEDING PAGE BLANK NOT FILMED

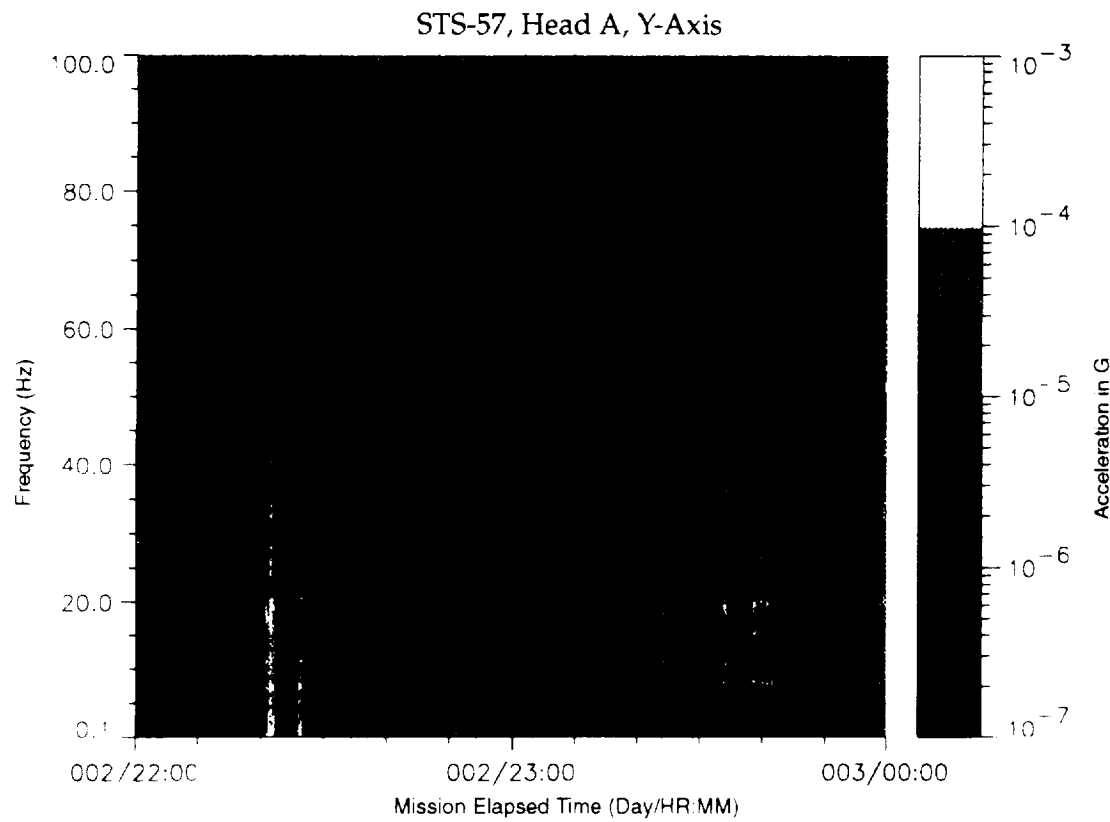


Figure B-127: SPACEHAB-1, Forward Bulkhead T-Beam

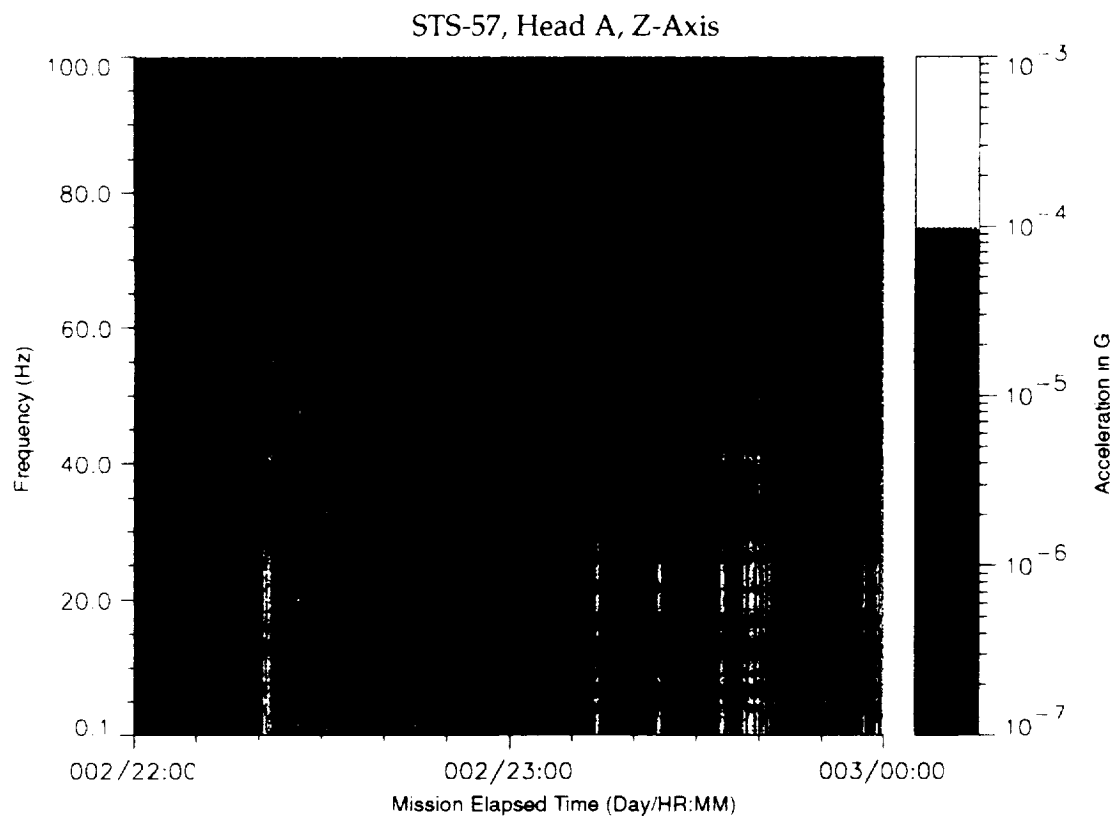


Figure B-128: SPACEHAB-1, Forward Bulkhead T-Beam

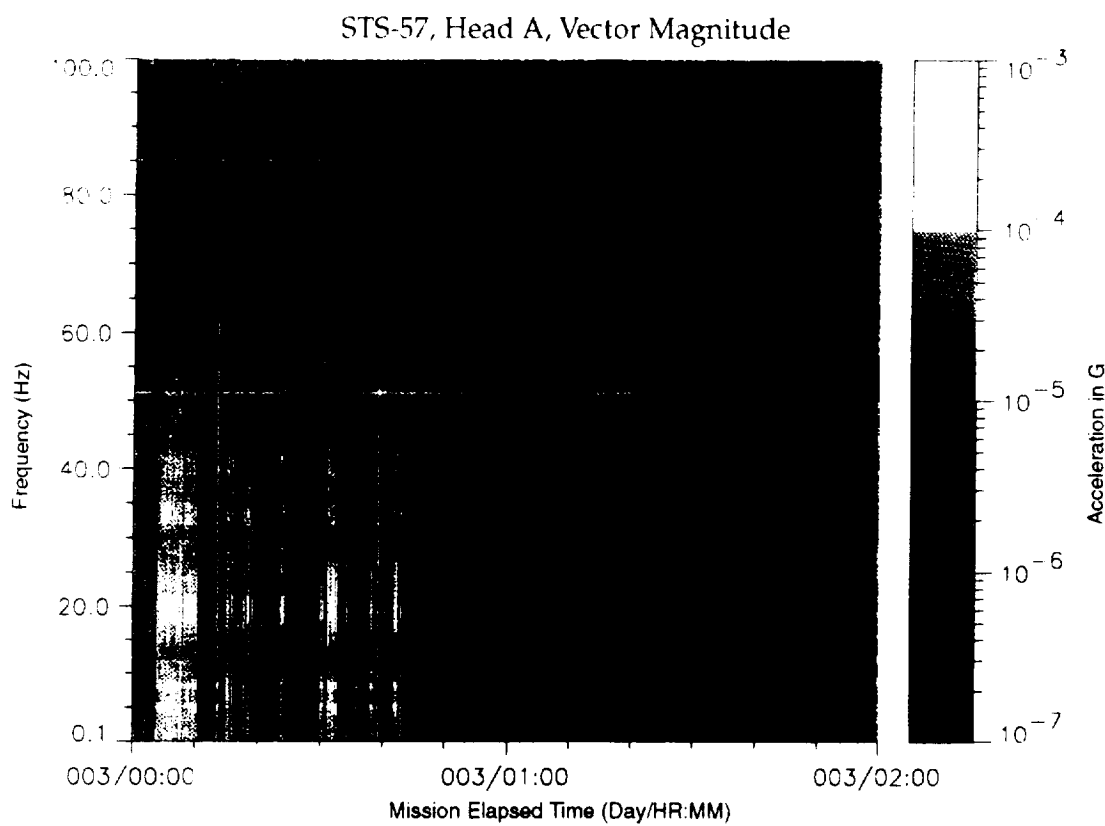


Figure B-129: SPACEHAB-1, Forward Bulkhead T-Beam

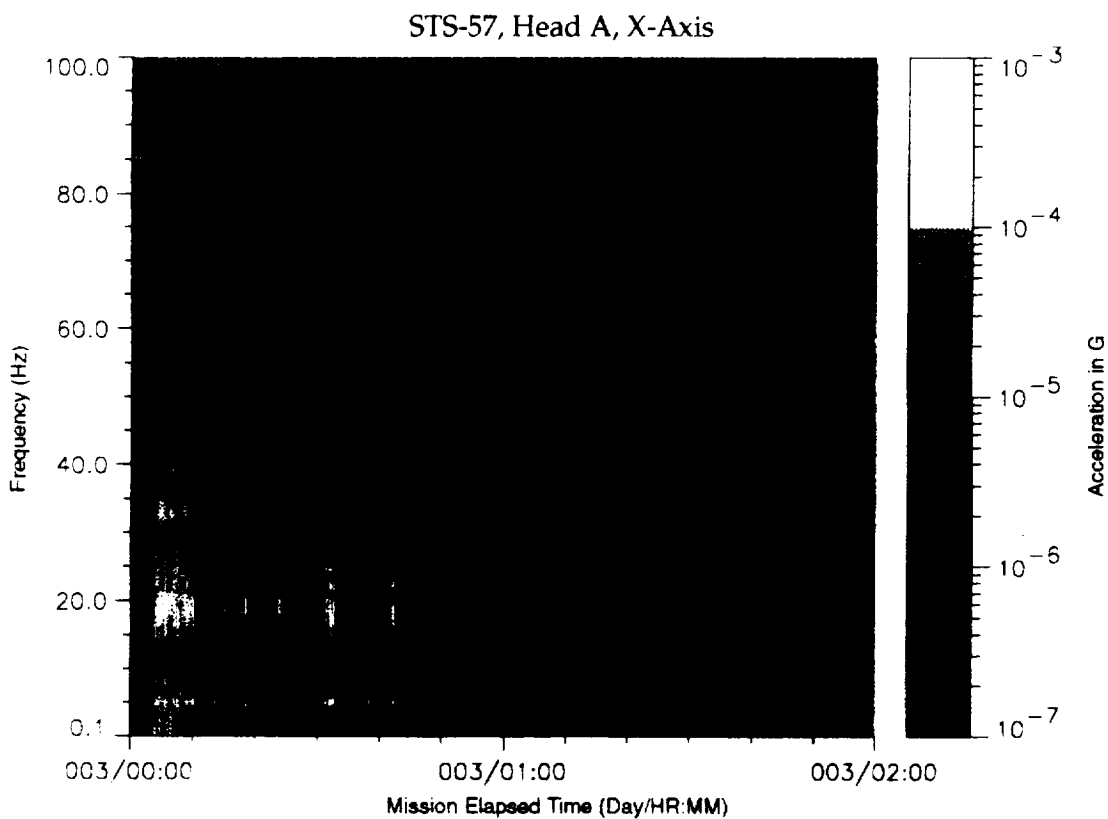


Figure B-130: SPACEHAB-1, Forward Bulkhead T-Beam

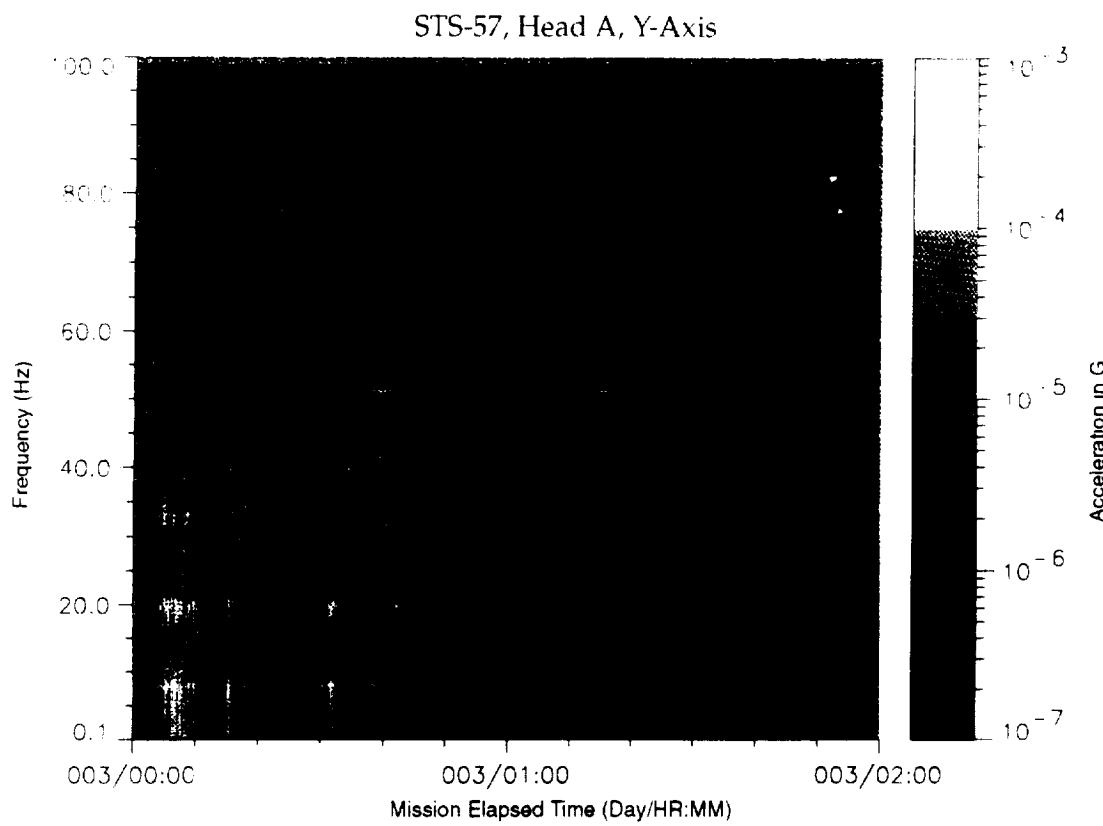


Figure B-131: SPACEHAB-1, Forward Bulkhead T-Beam

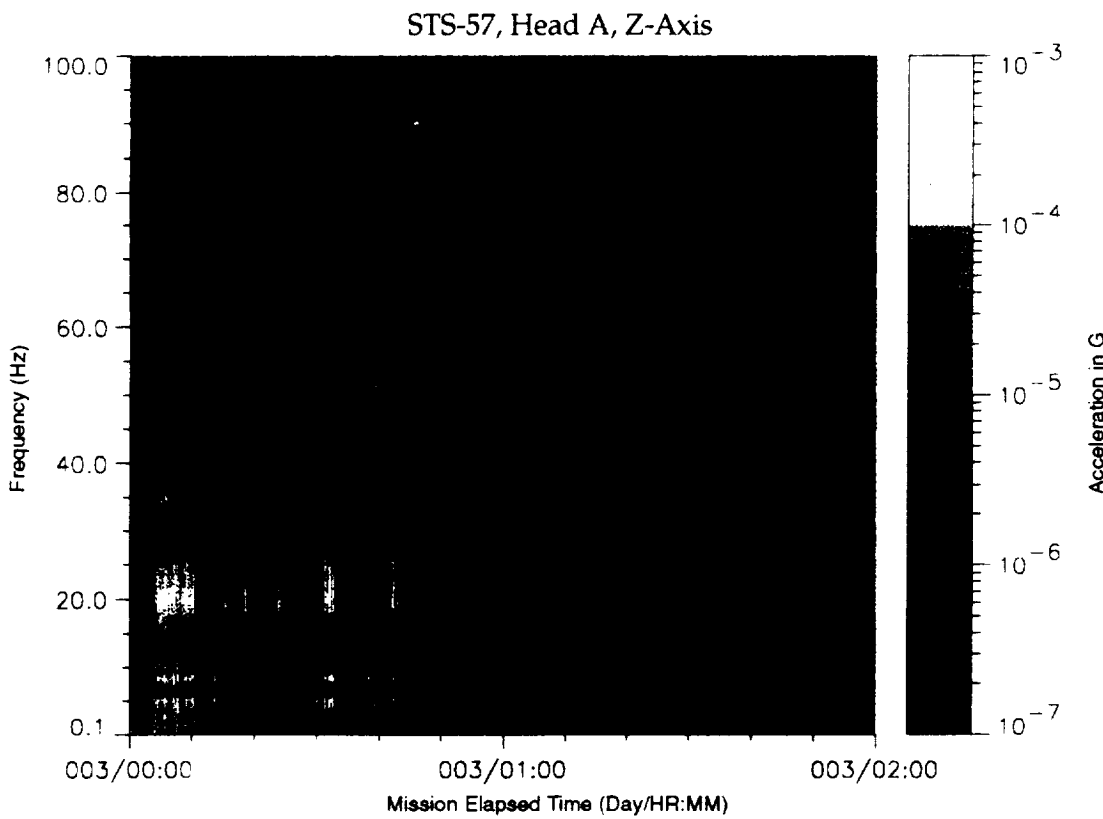


Figure B-132: SPACEHAB-1, Forward Bulkhead T-Beam

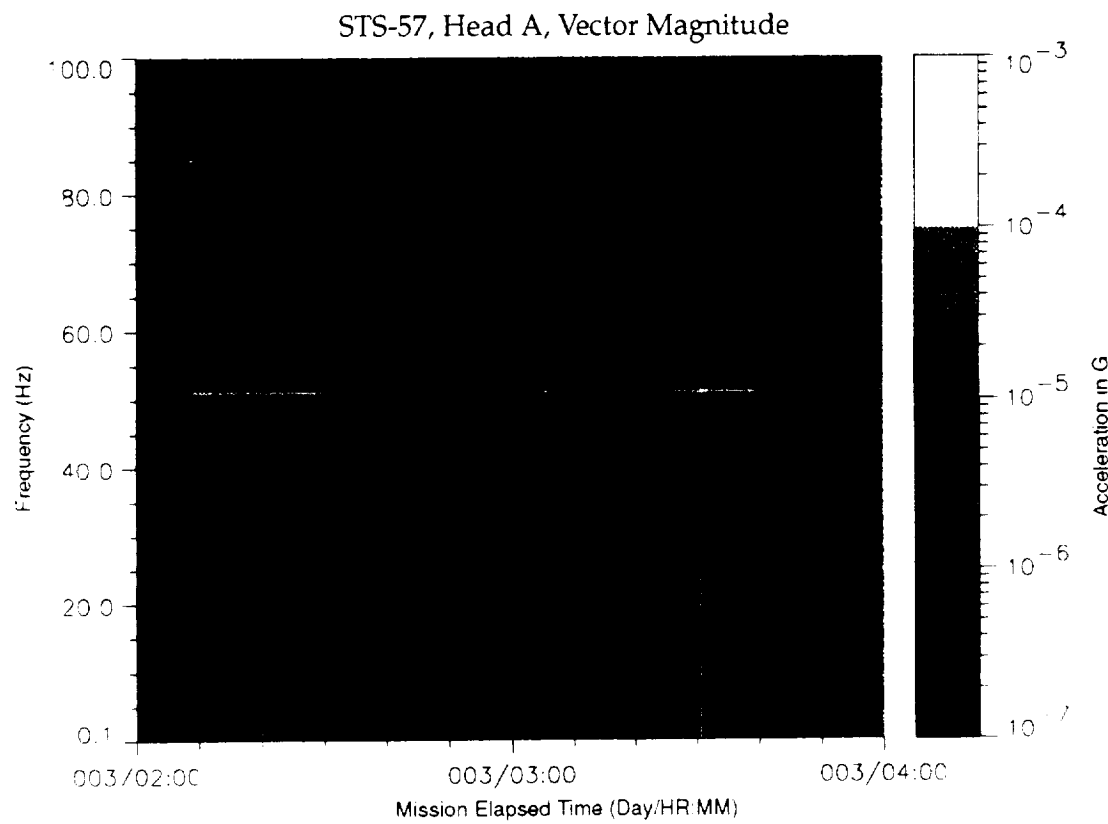


Figure B-133: SPACEHAB-1, Forward Bulkhead T-Beam

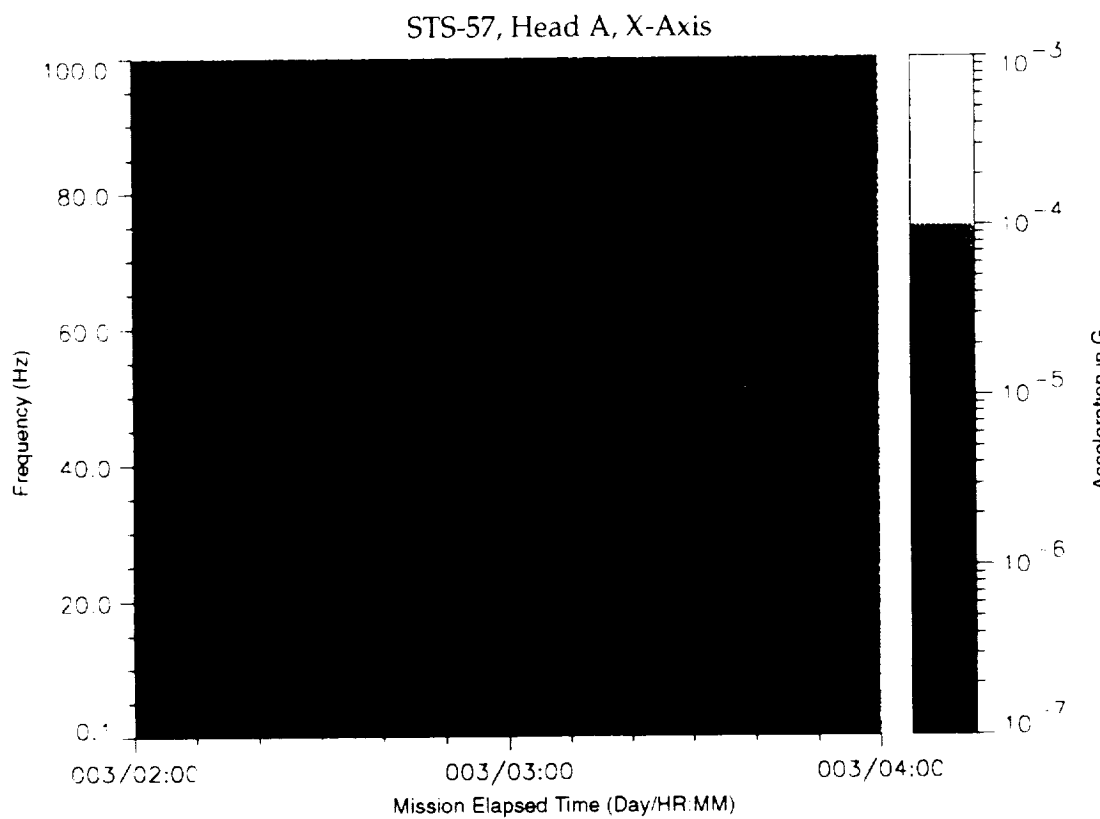


Figure B-134: SPACEHAB-1, Forward Bulkhead T-Beam

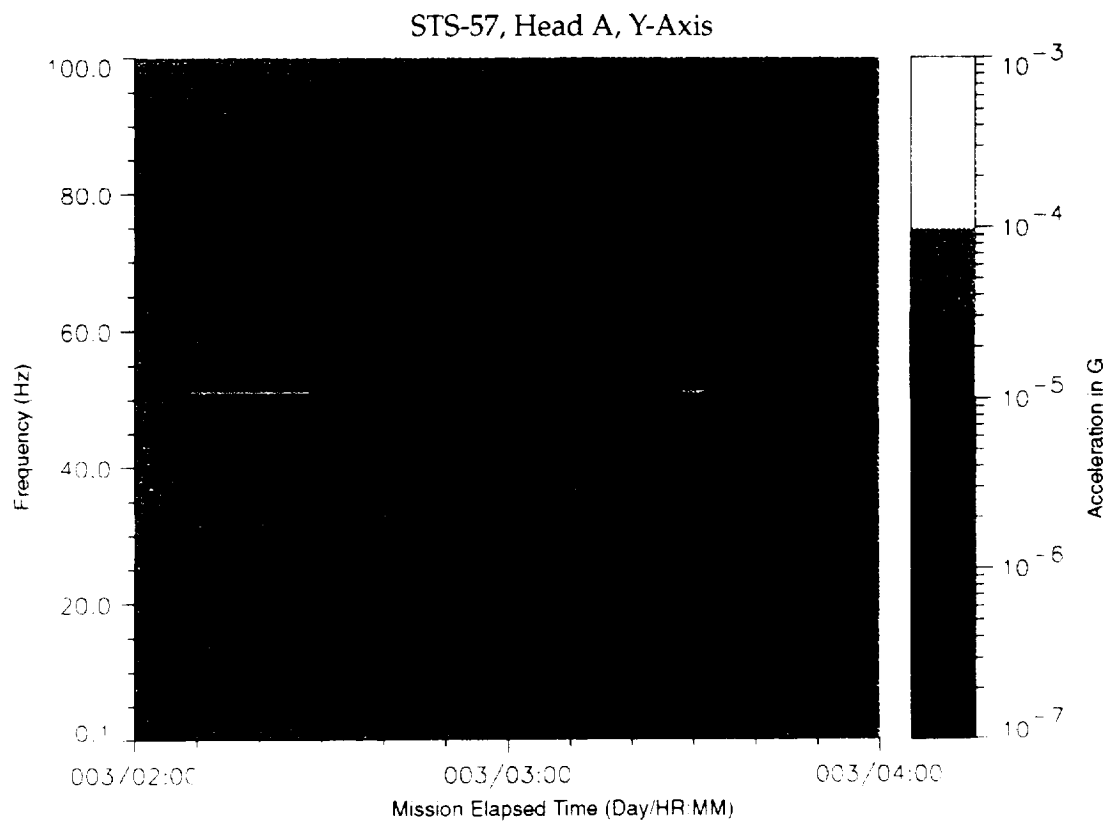


Figure B-135: SPACEHAB-1, Forward Bulkhead T-Beam

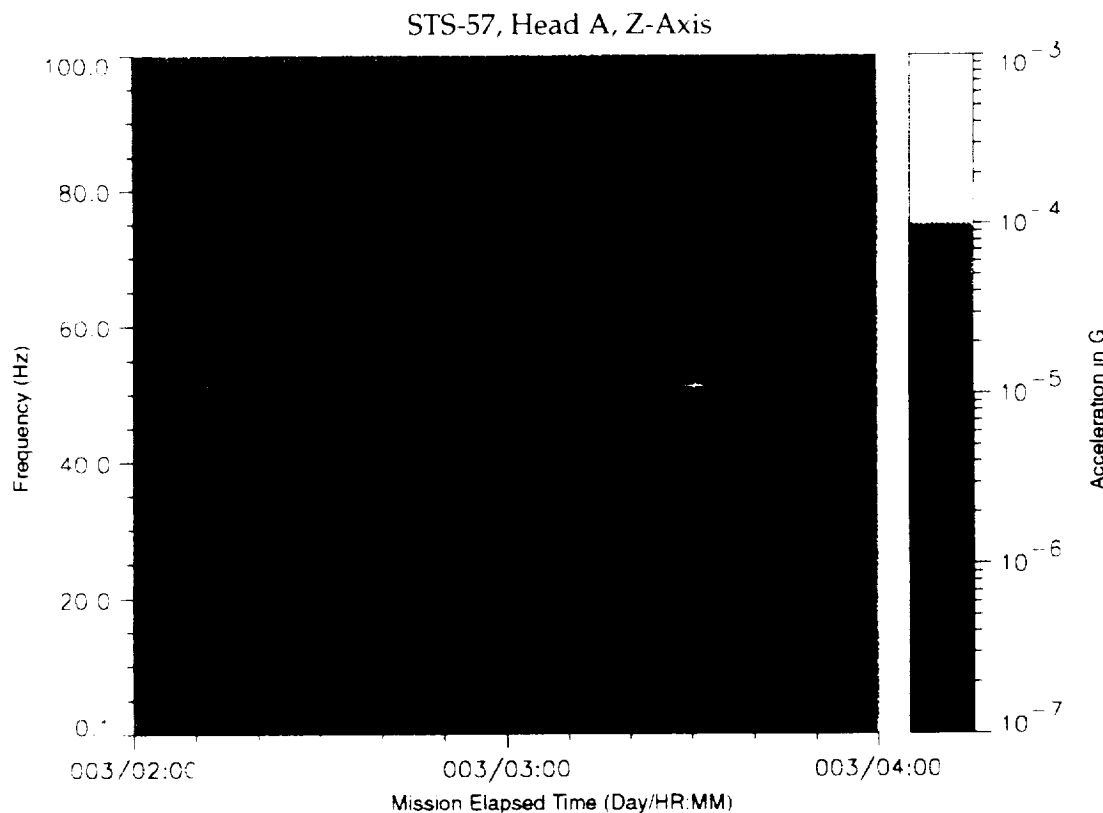


Figure B-136: SPACEHAB-1, Forward Bulkhead T-Beam

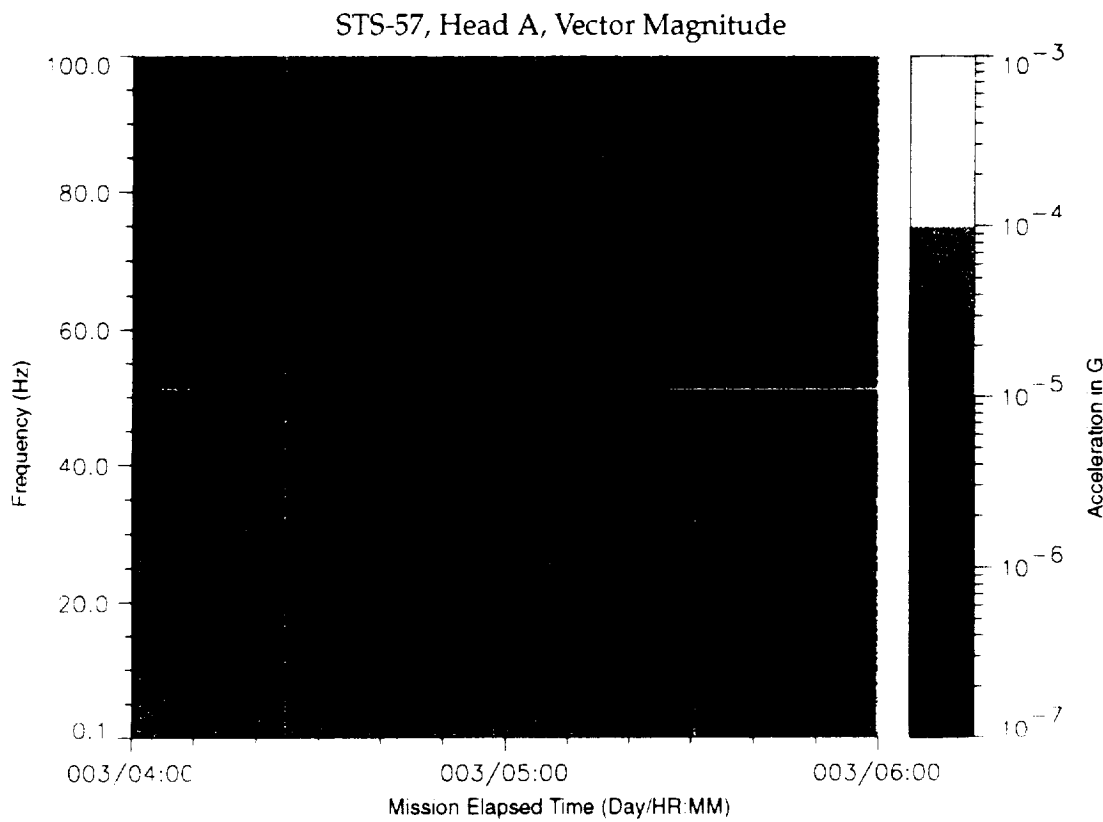


Figure B-137: SPACEHAB-1, Forward Bulkhead T-Beam

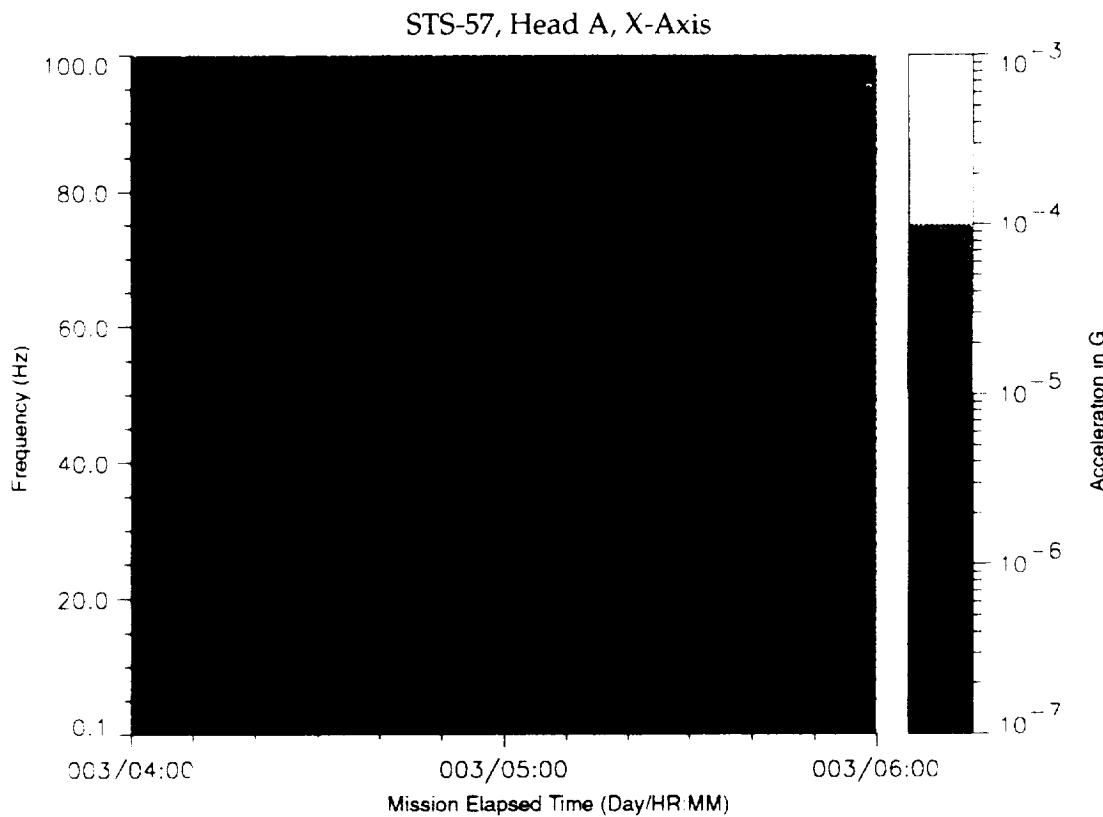


Figure B-138: SPACEHAB-1, Forward Bulkhead T-Beam

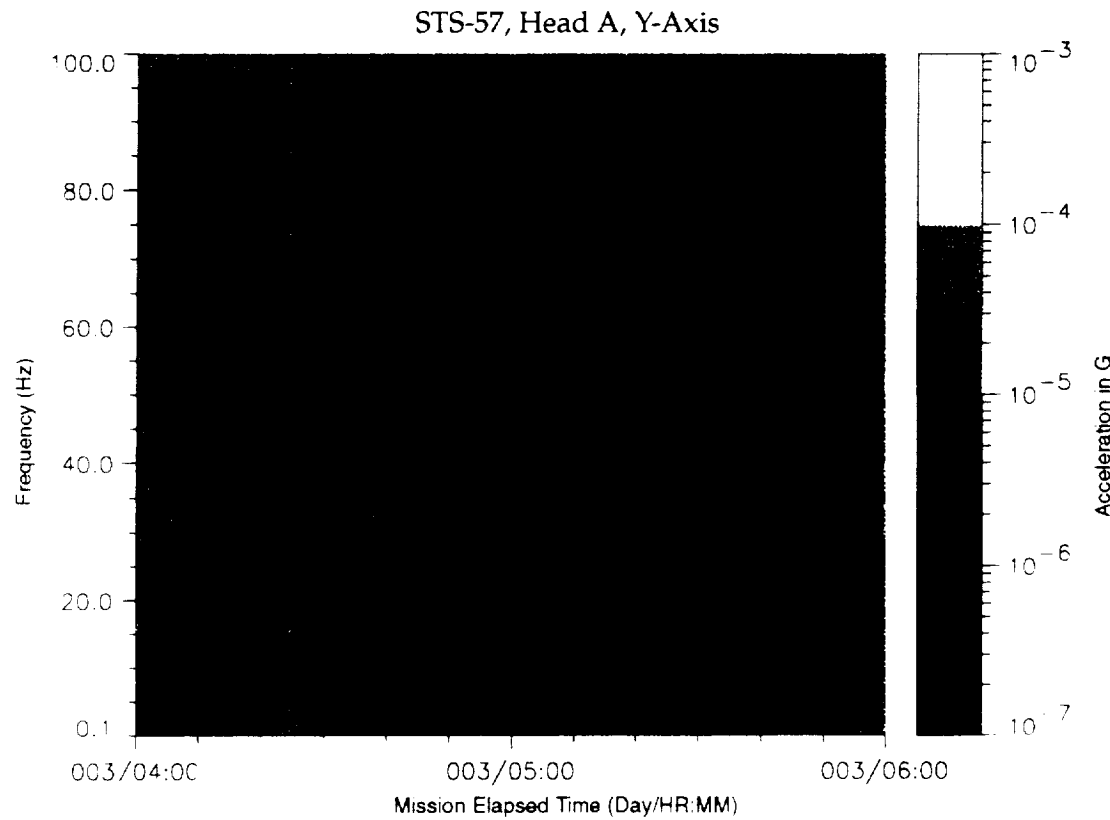


Figure B-139: SPACEHAB-1, Forward Bulkhead T-Beam

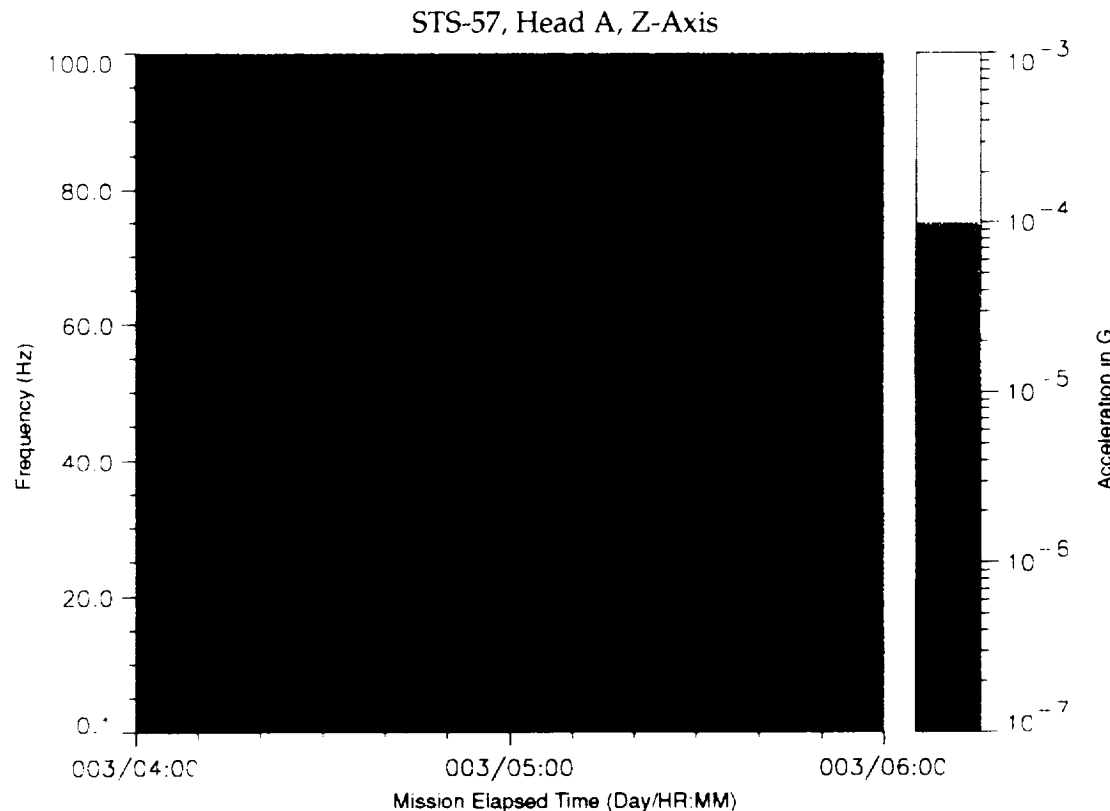


Figure B-140: SPACEHAB-1, Forward Bulkhead T-Beam

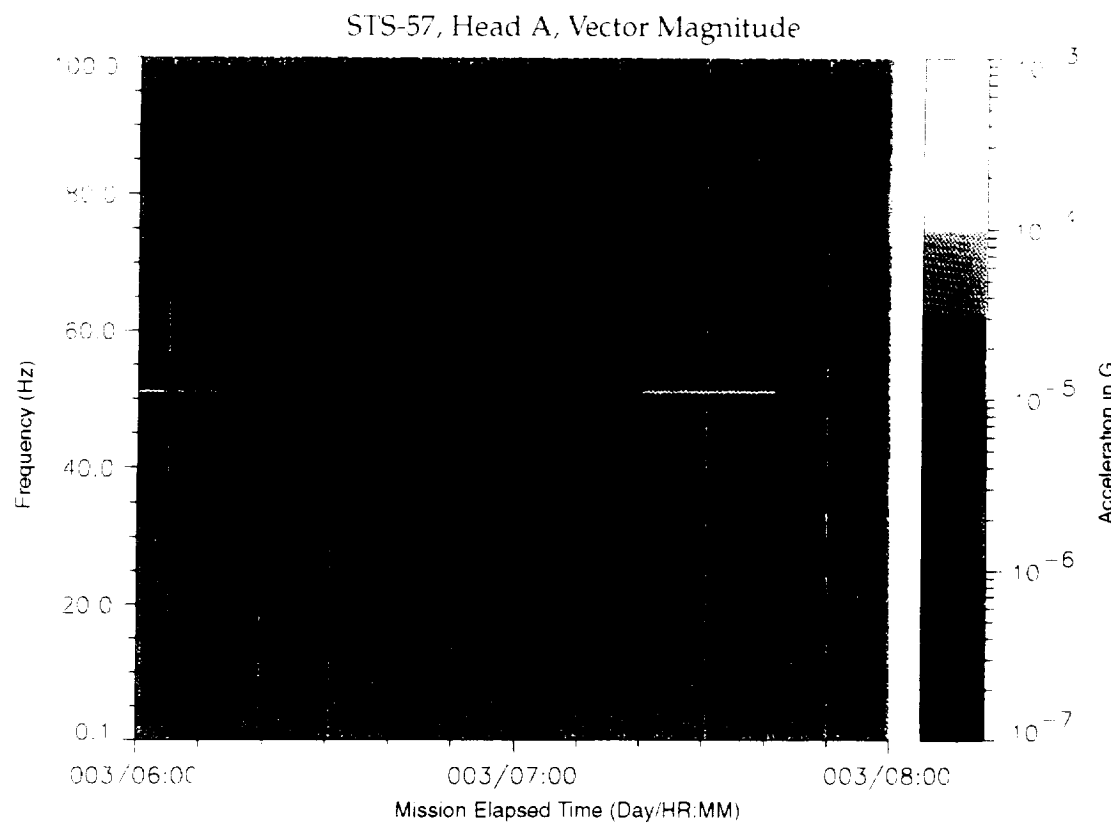


Figure B-141: SPACEHAB-1, Forward Bulkhead T-Beam

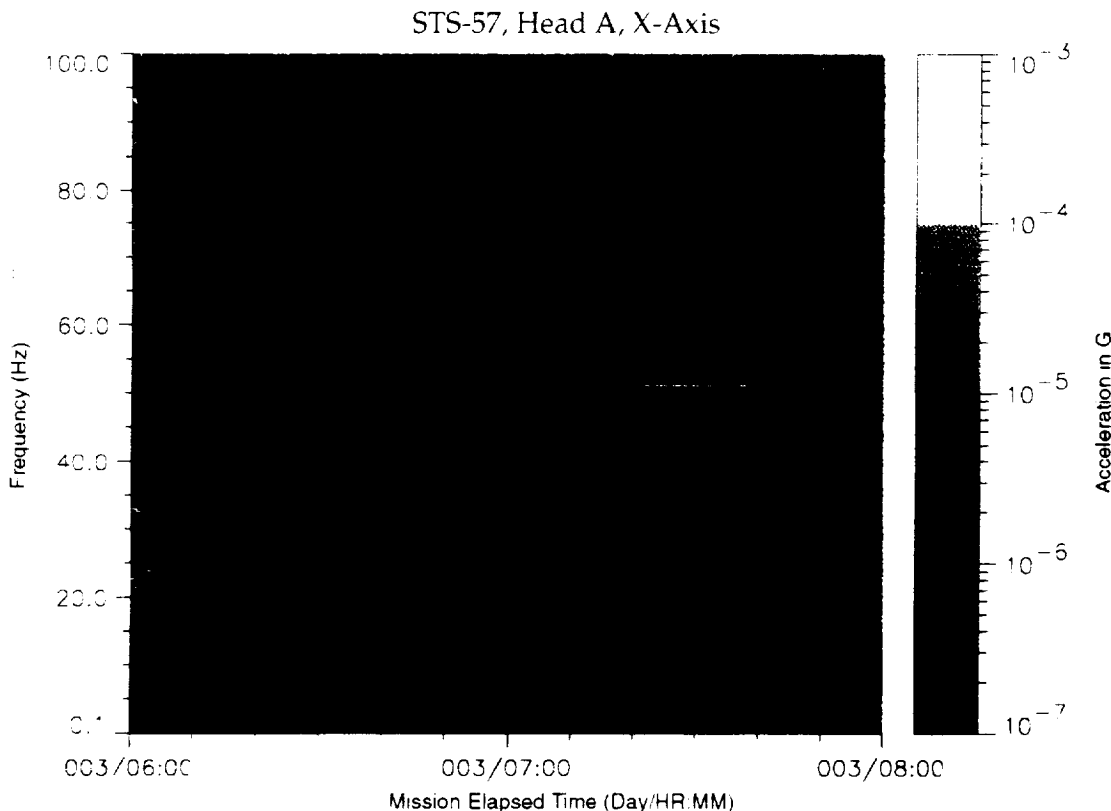


Figure B-142: SPACEHAB-1, Forward Bulkhead T-Beam

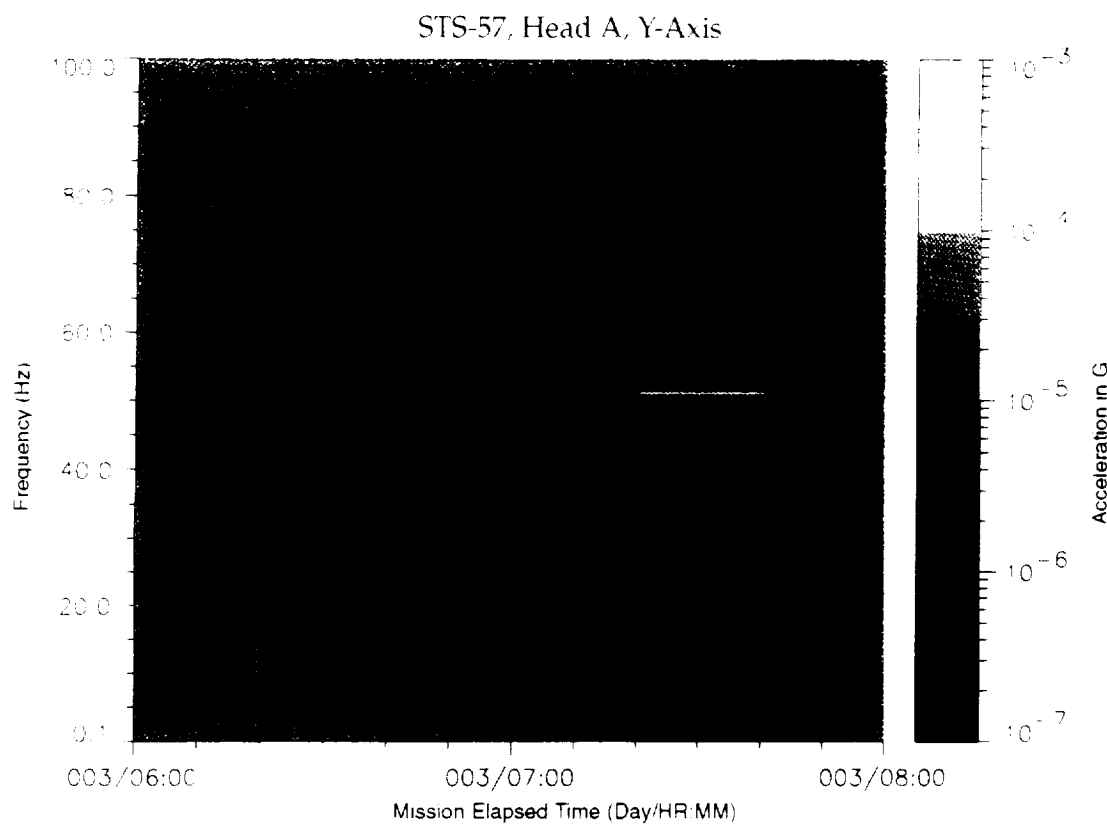


Figure B-143: SPACEHAB-1, Forward Bulkhead T-Beam

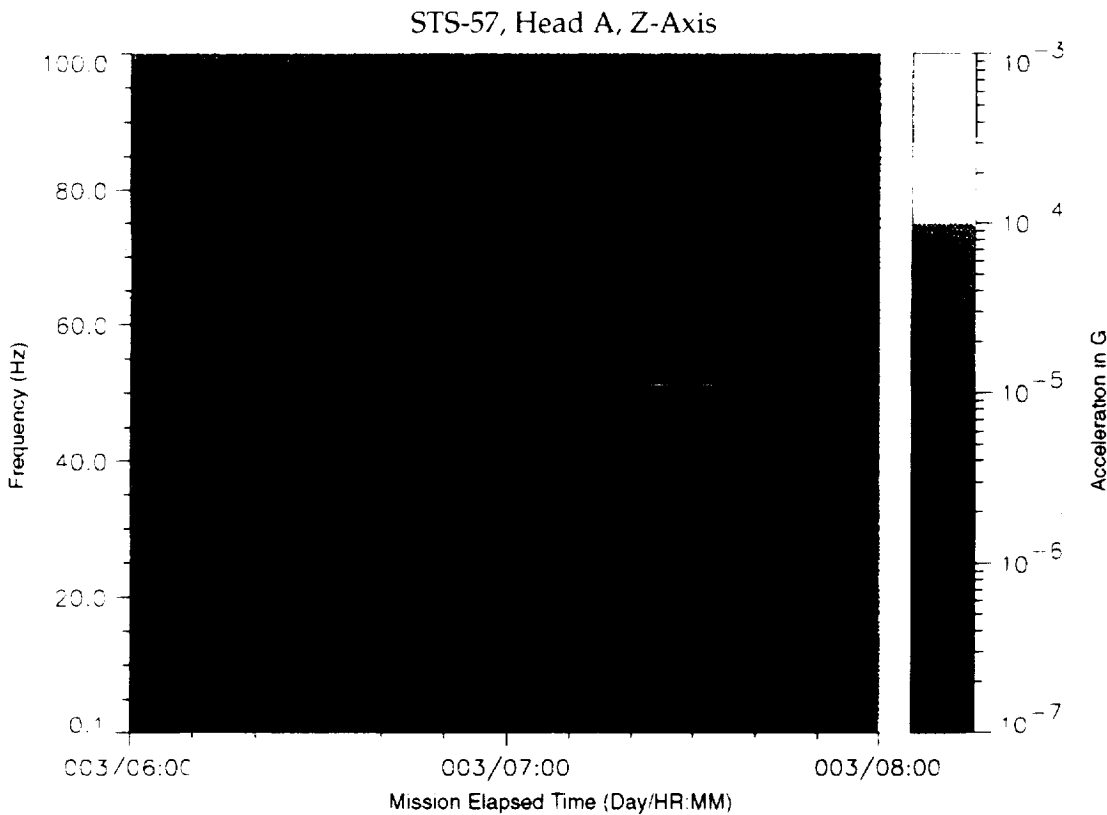


Figure B-144: SPACEHAB-1, Forward Bulkhead T-Beam

PRECEDING PAGE BLANK NOT FILMED

STS-57, Head A, Vector Magnitude

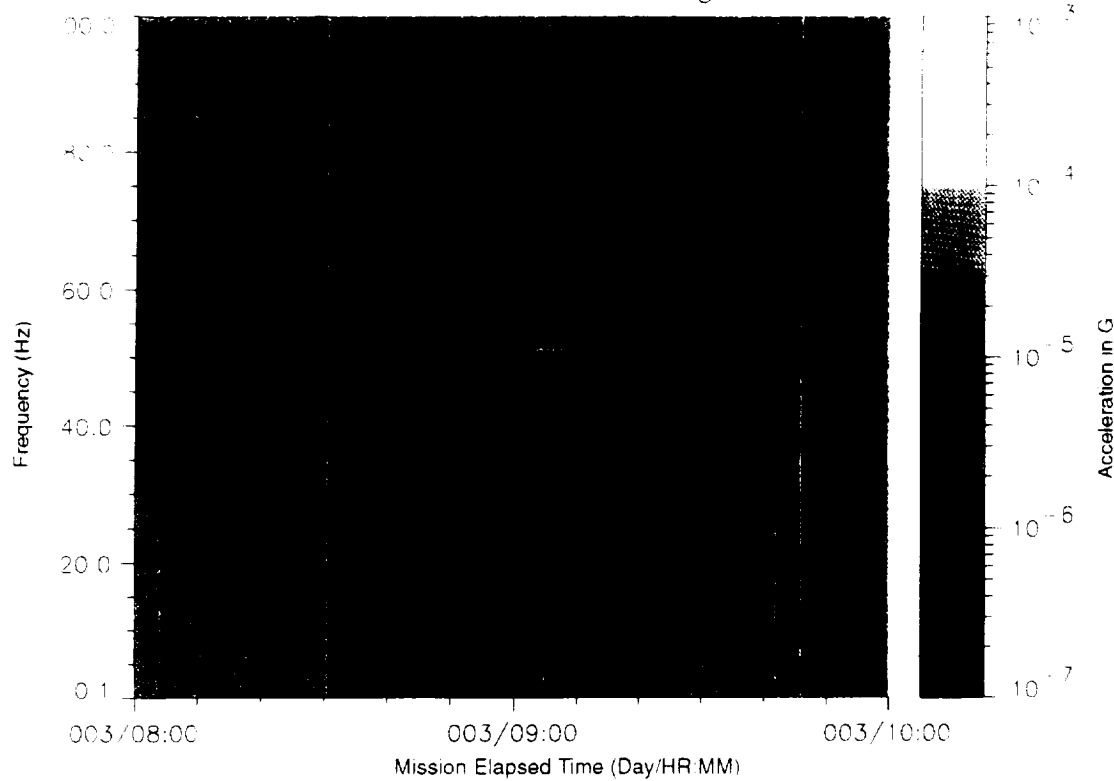


Figure B-145: SPACEHAB-1, Forward Bulkhead T-Beam

STS-57, Head A, X-Axis

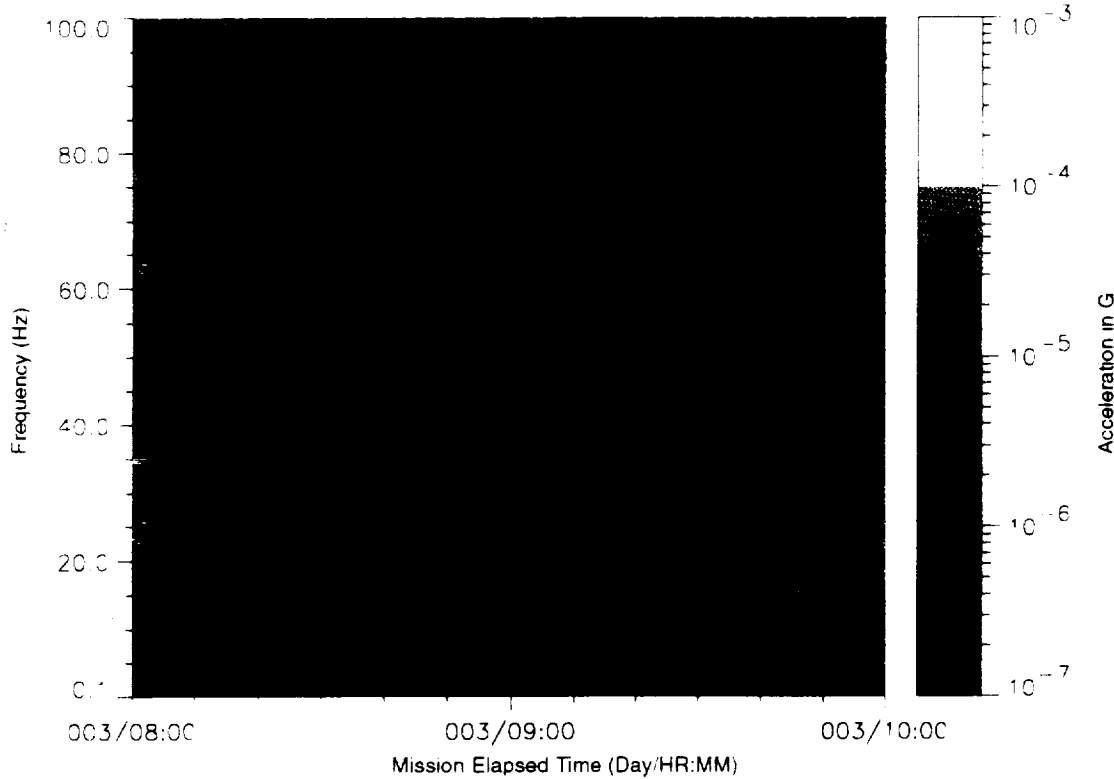


Figure B-146: SPACEHAB-1, Forward Bulkhead T-Beam

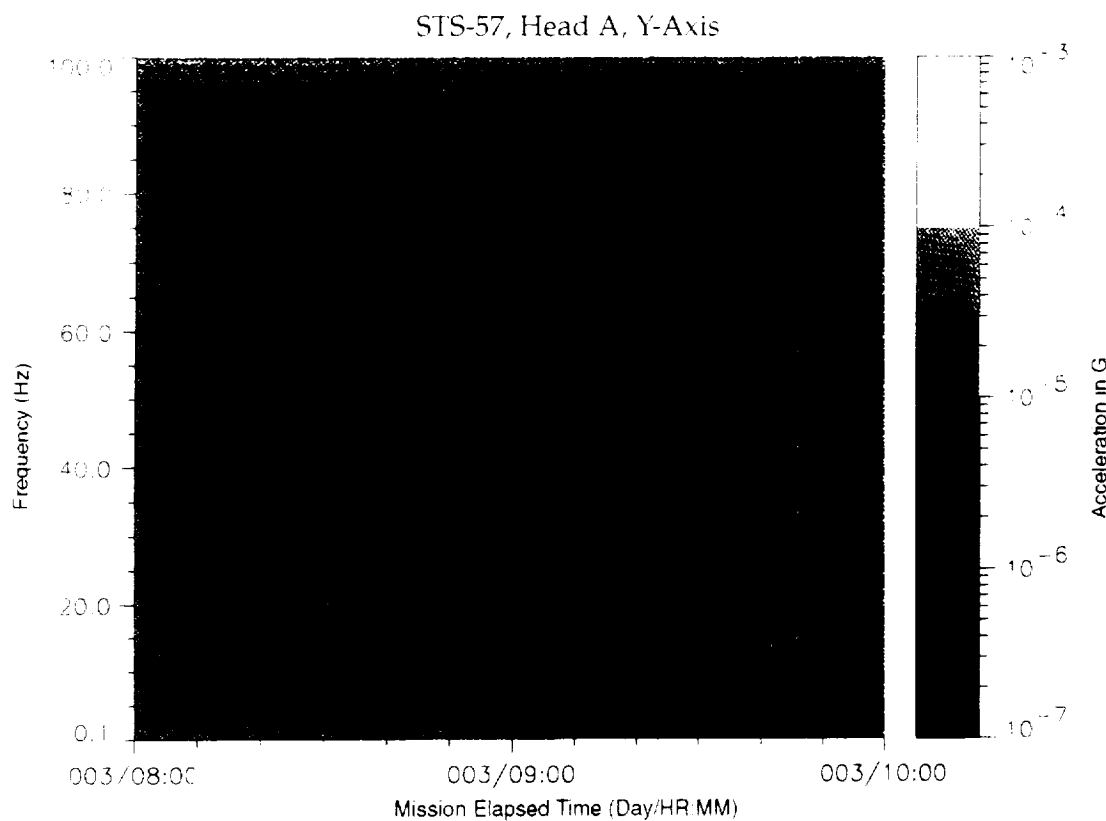


Figure B-147: SPACEHAB-1, Forward Bulkhead T-Beam

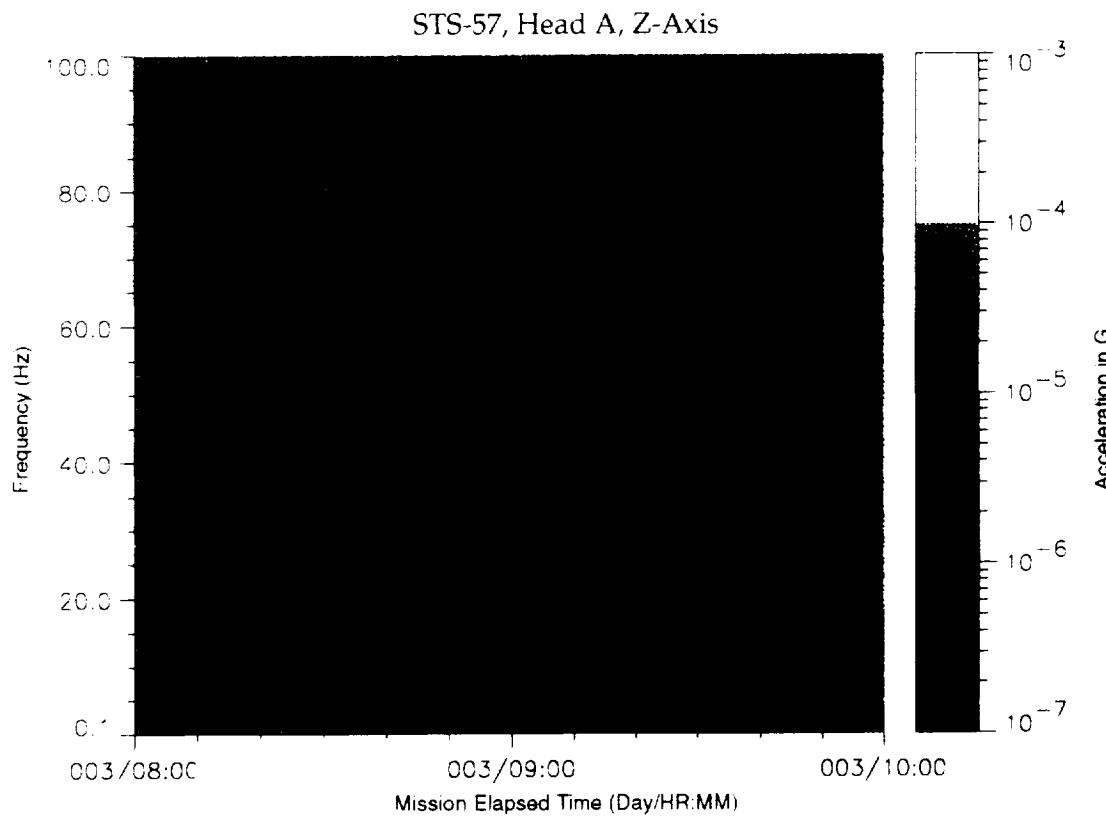


Figure B-148: SPACEHAB-1, Forward Bulkhead T-Beam

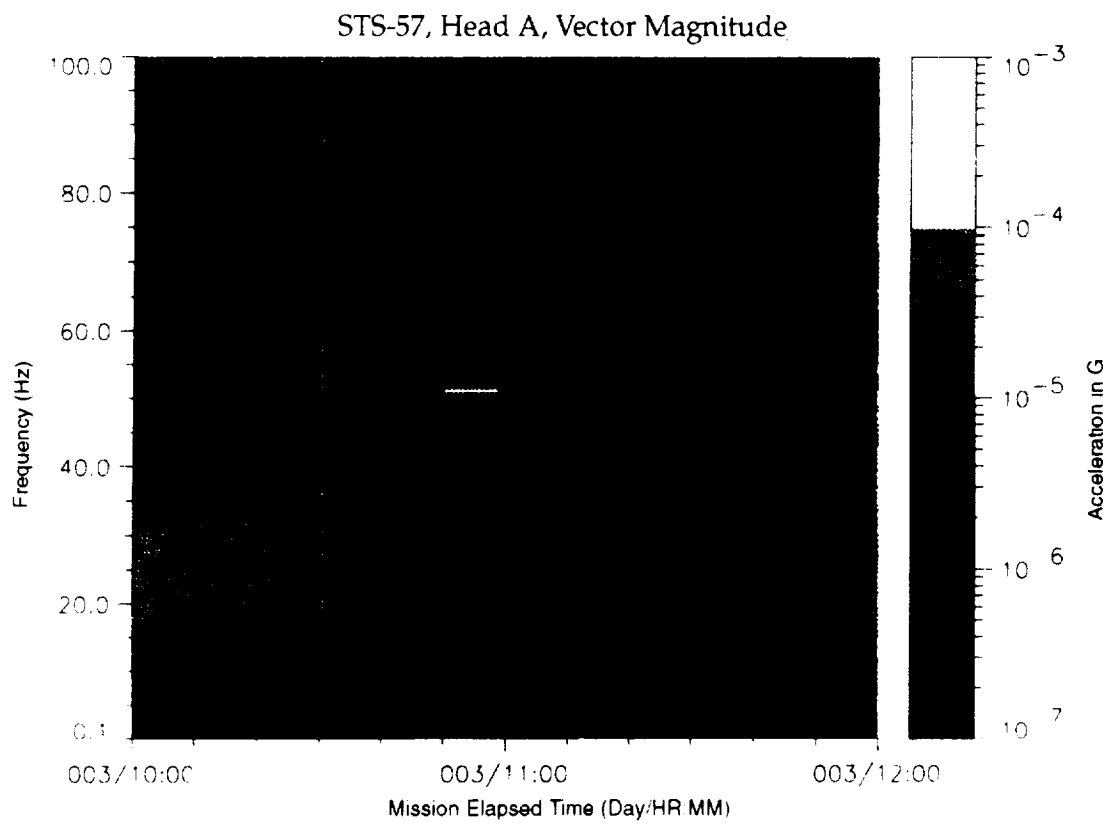


Figure B-149: SPACEHAB-1, Forward Bulkhead T-Beam

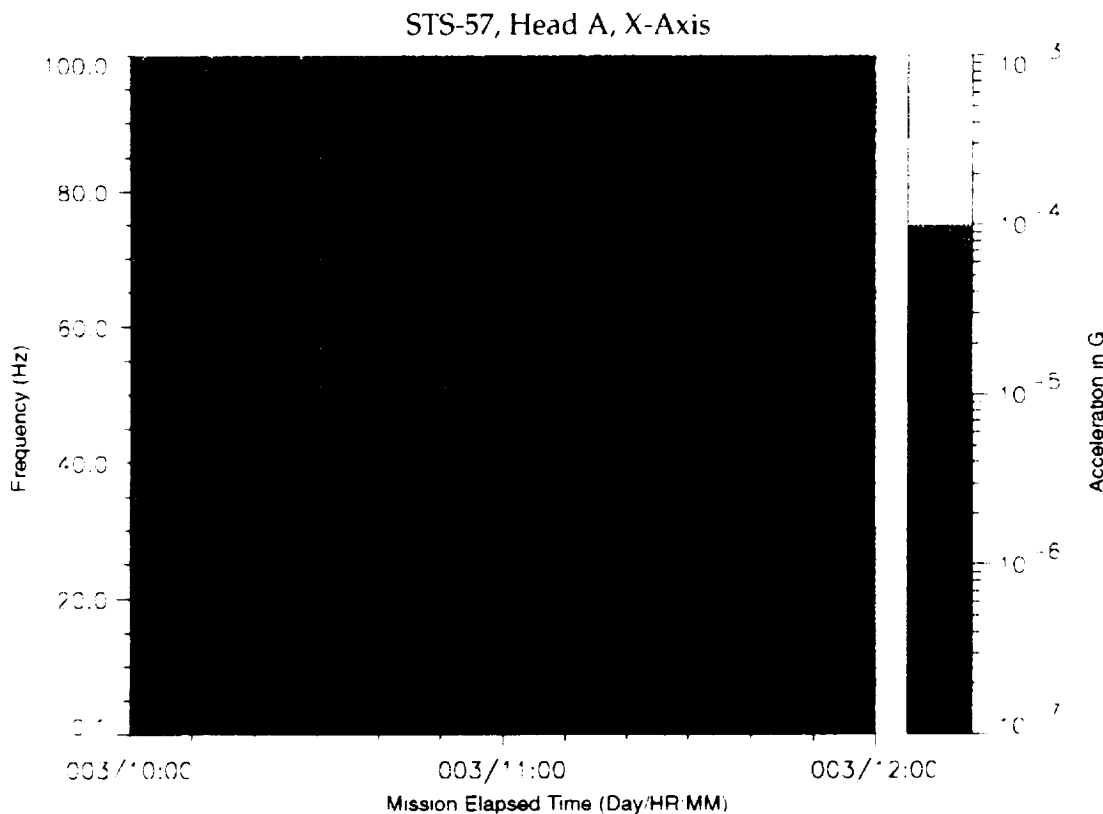


Figure B-150: SPACEHAB-1, Forward Bulkhead T-Beam

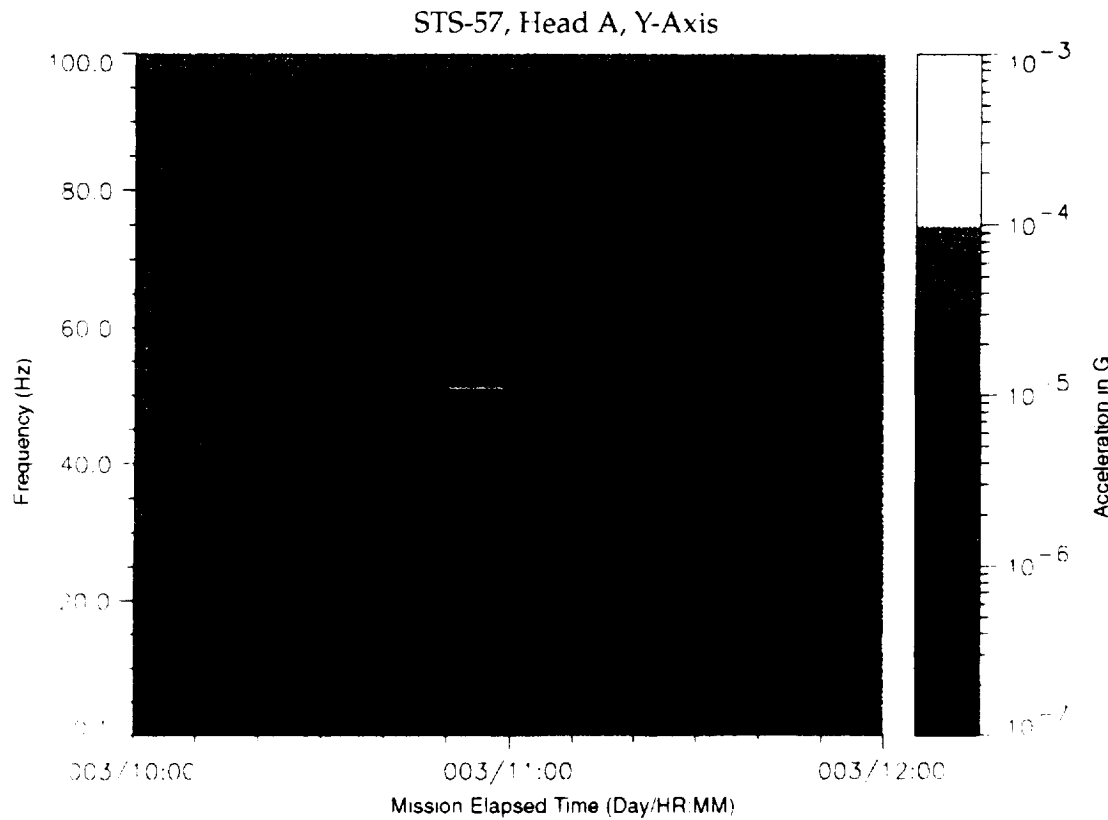


Figure B-151: SPACEHAB-1, Forward Bulkhead T-Beam

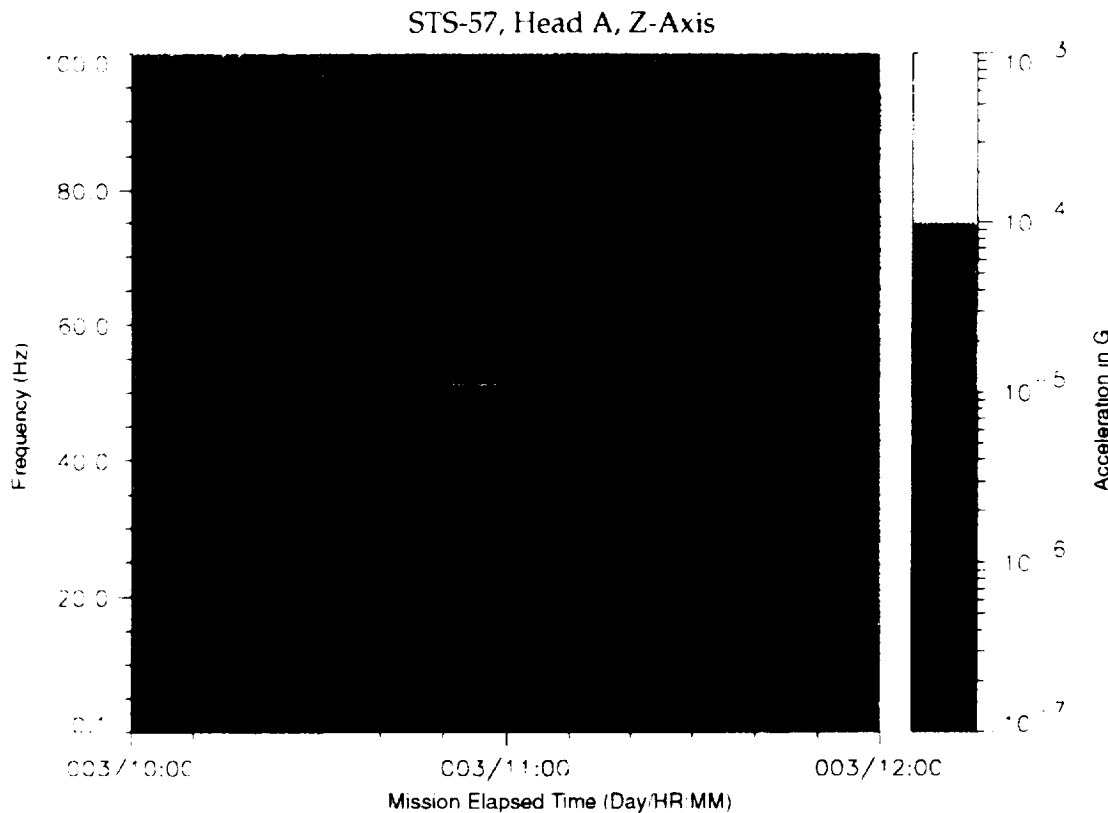


Figure B-152: SPACEHAB-1, Forward Bulkhead T-Beam

~~PRECEDING PAGE BLANK NOT FILMED~~

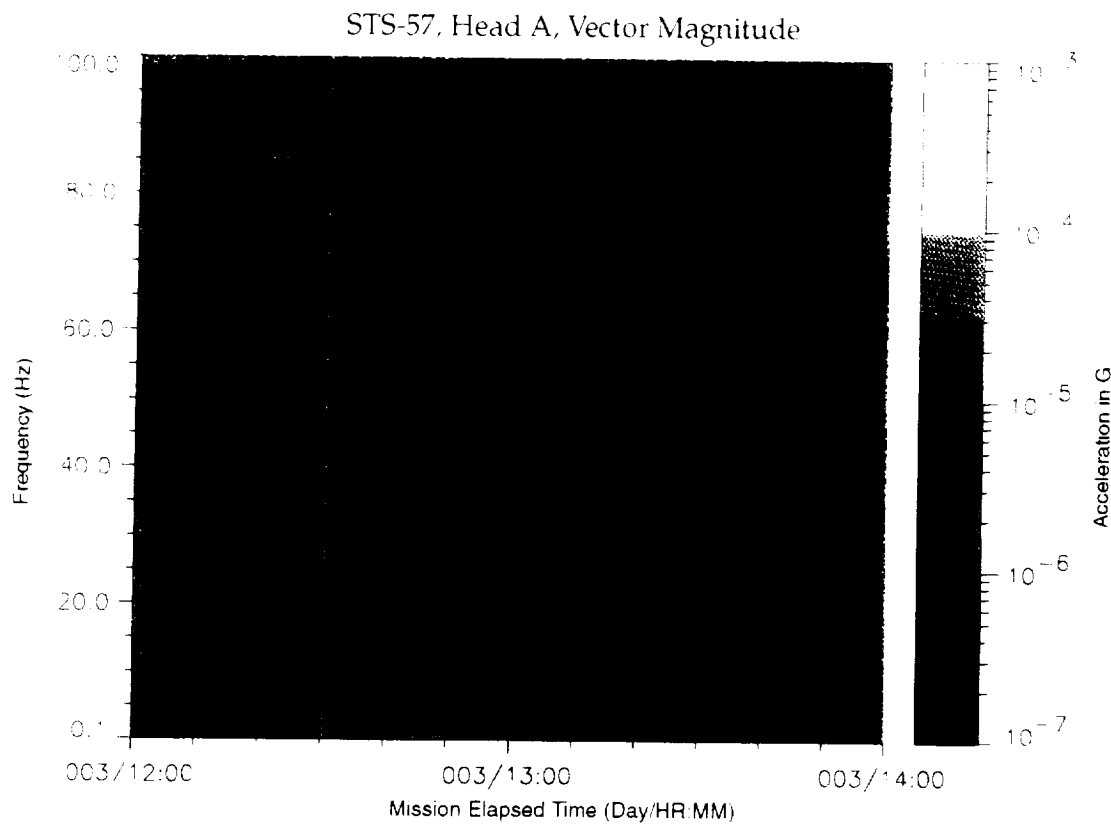


Figure B-153: SPACEHAB-1, Forward Bulkhead T-Beam

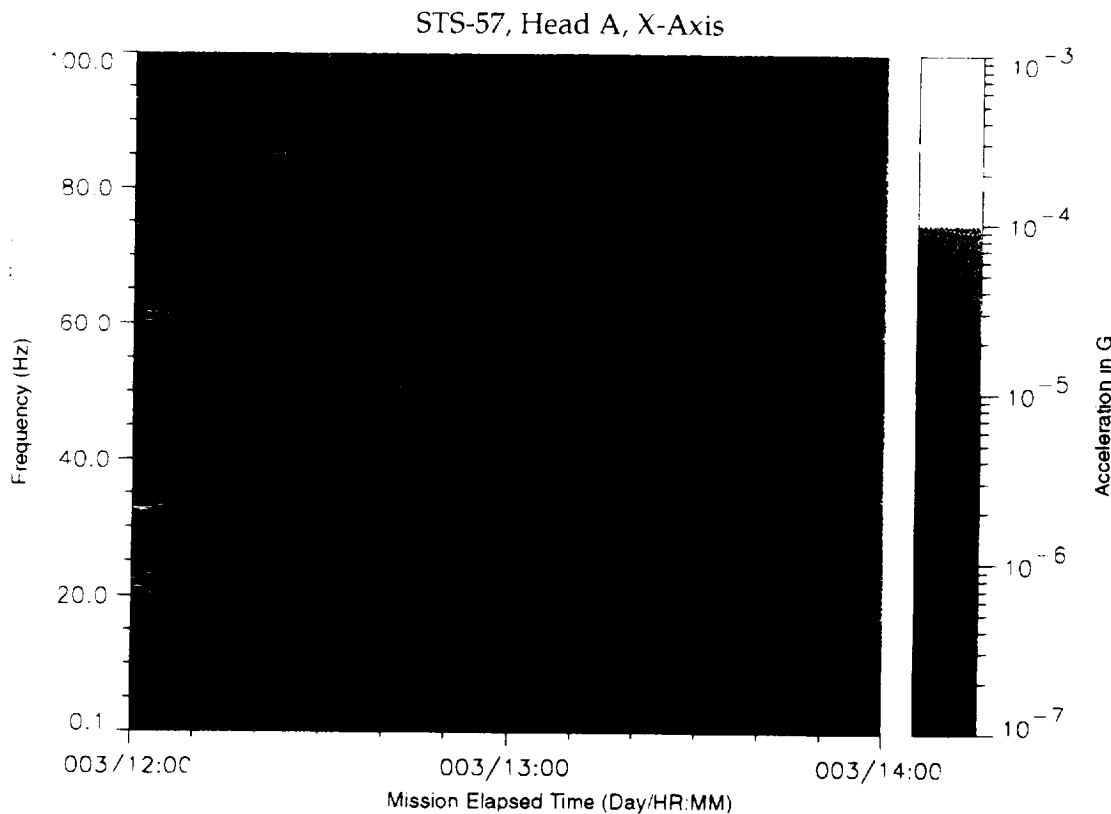


Figure B-154: SPACEHAB-1, Forward Bulkhead T-Beam

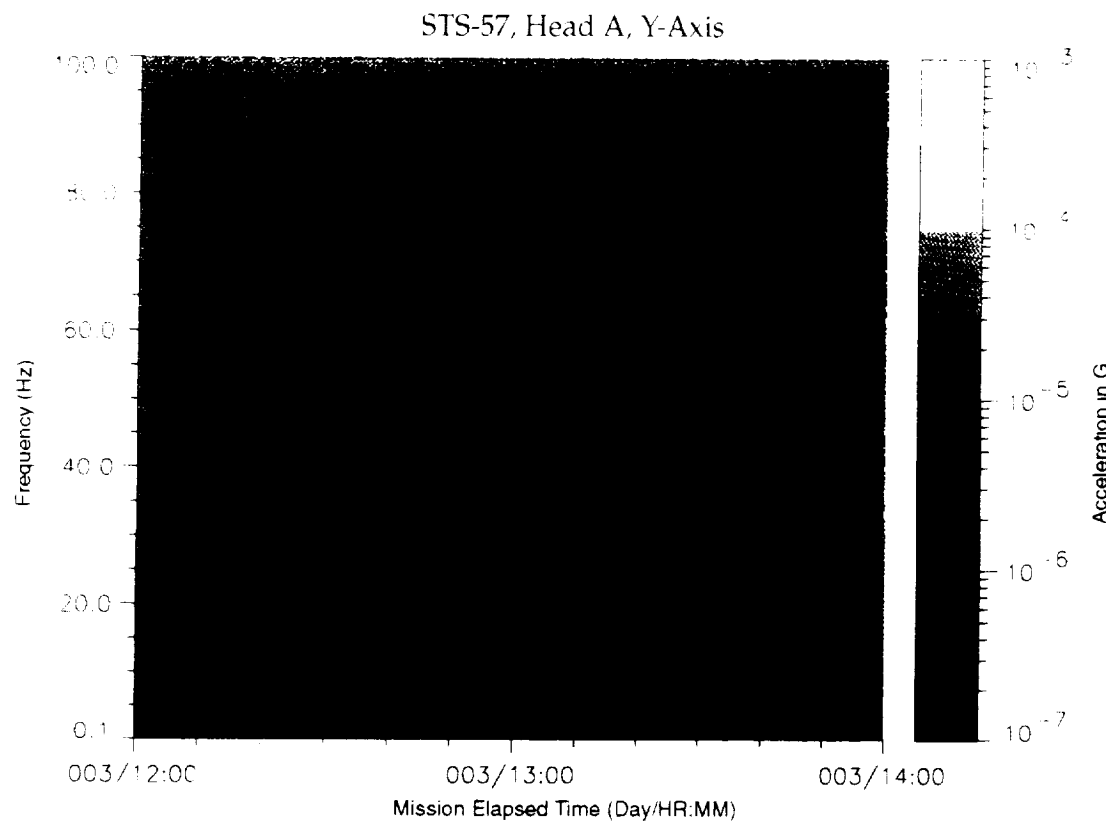


Figure B-155: SPACEHAB-1, Forward Bulkhead T-Beam

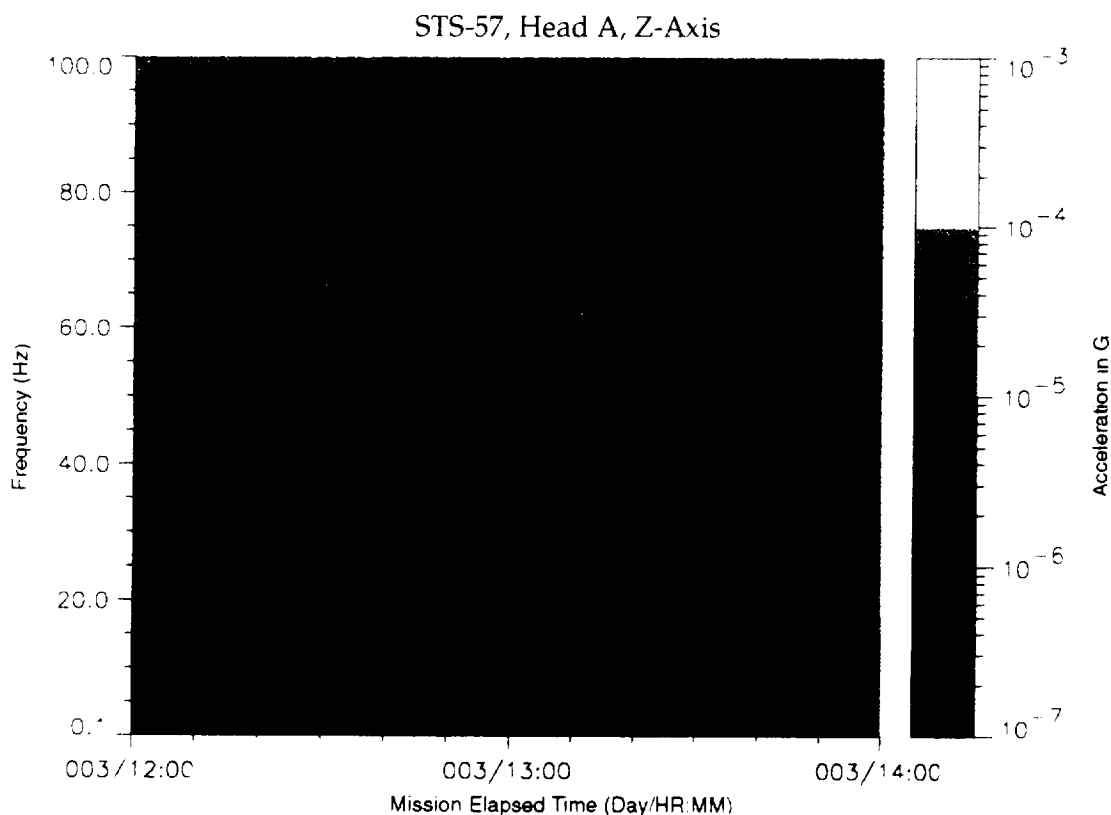


Figure B-156: SPACEHAB-1, Forward Bulkhead T-Beam

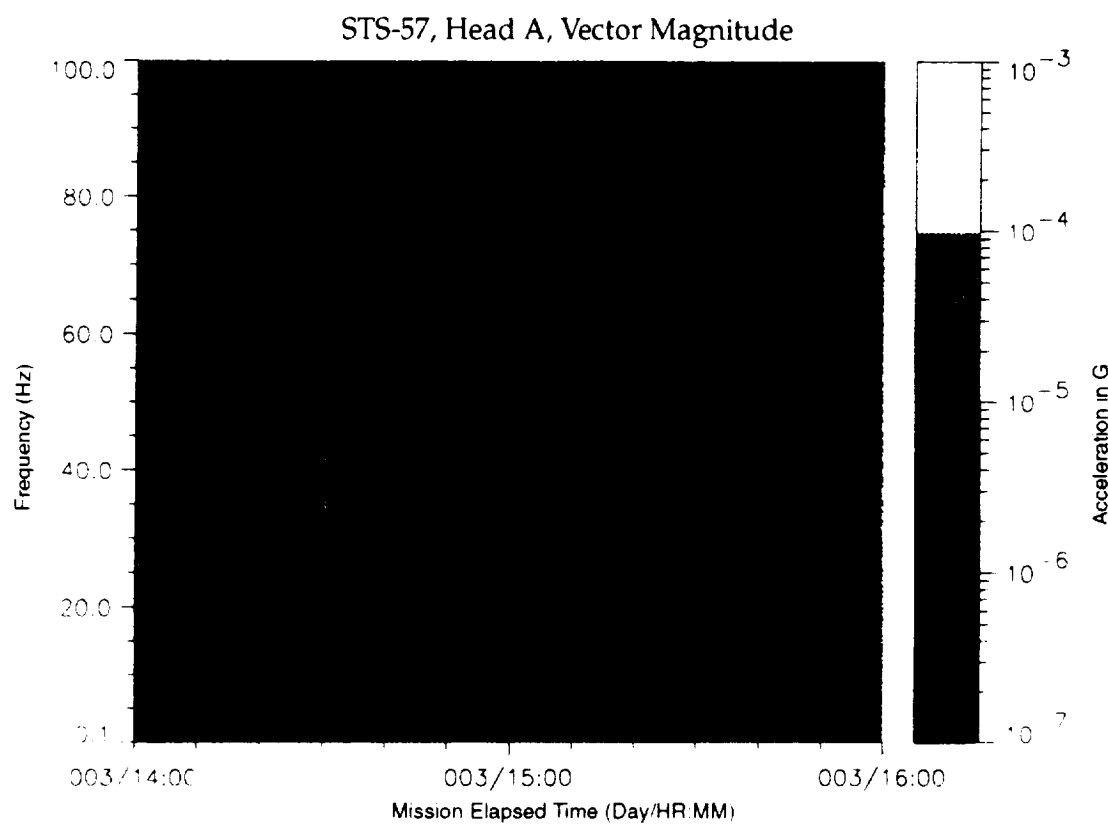


Figure B-157: SPACEHAB-1, Forward Bulkhead T-Beam

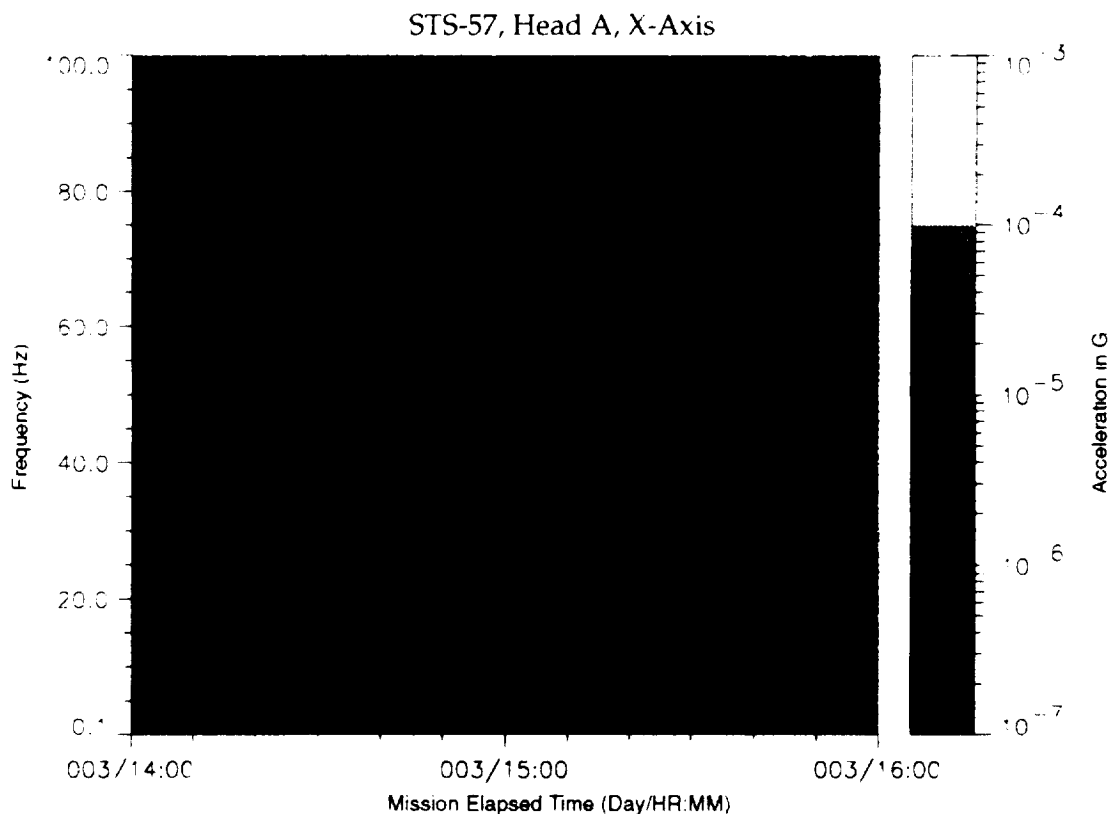


Figure B-158: SPACEHAB-1, Forward Bulkhead T-Beam

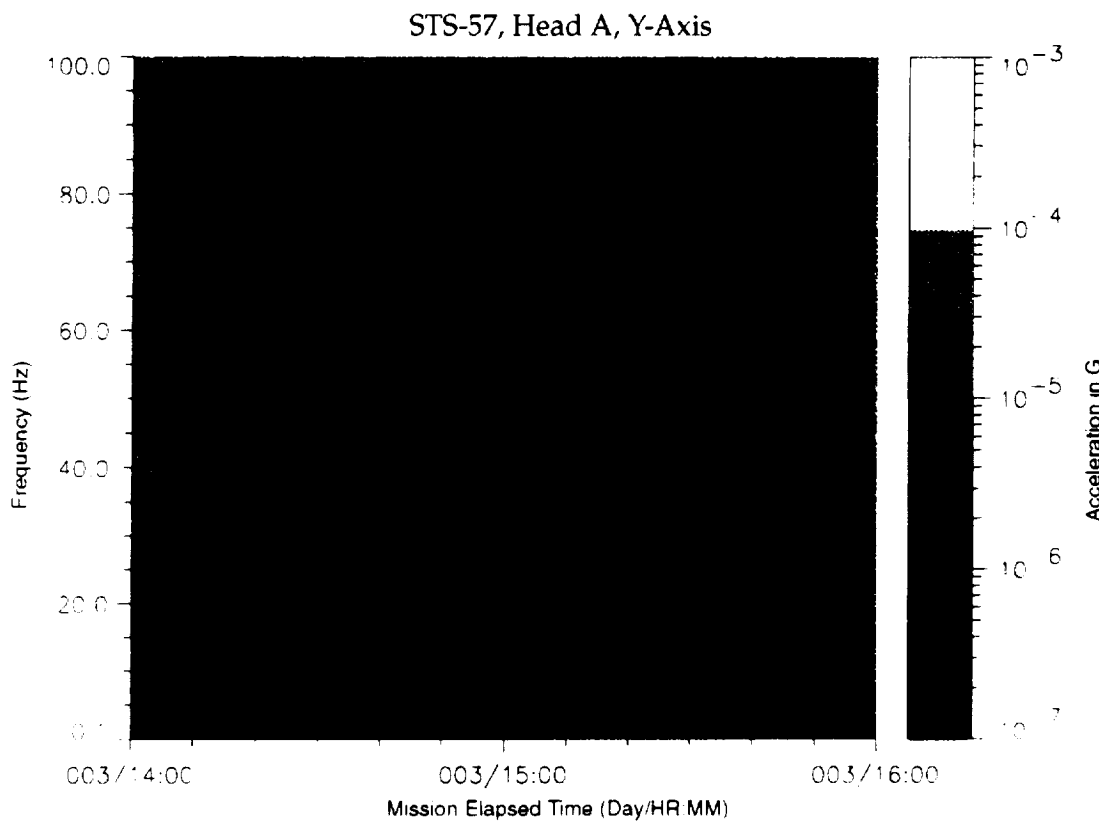


Figure B-159: SPACEHAB-1, Forward Bulkhead T-Beam

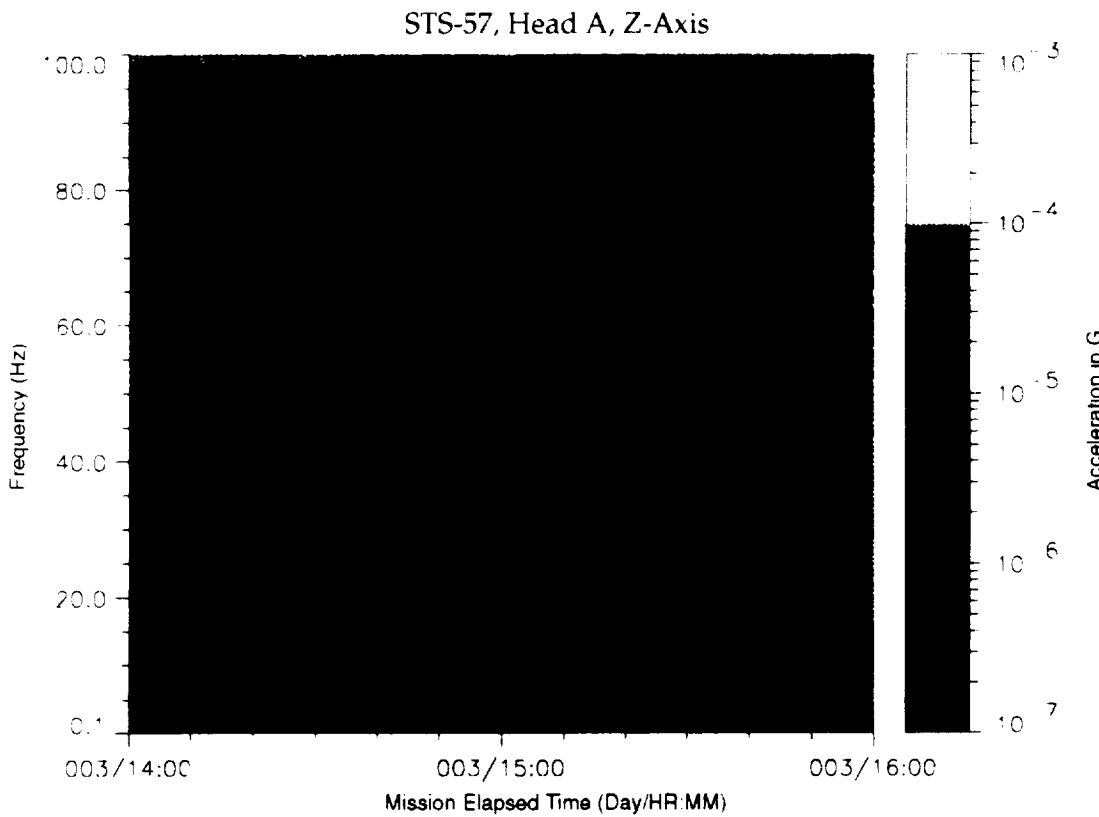


Figure B-160: SPACEHAB-1, Forward Bulkhead T-Beam

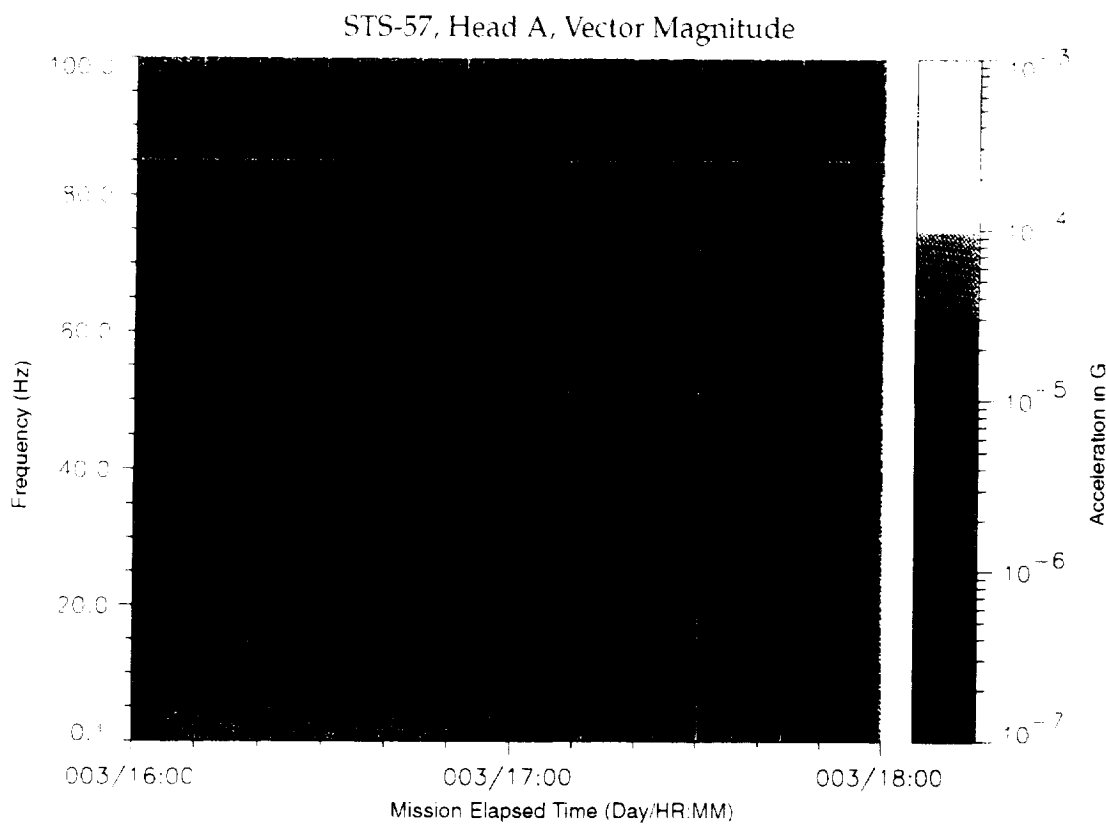


Figure B-161: SPACEHAB-1, Forward Bulkhead T-Beam

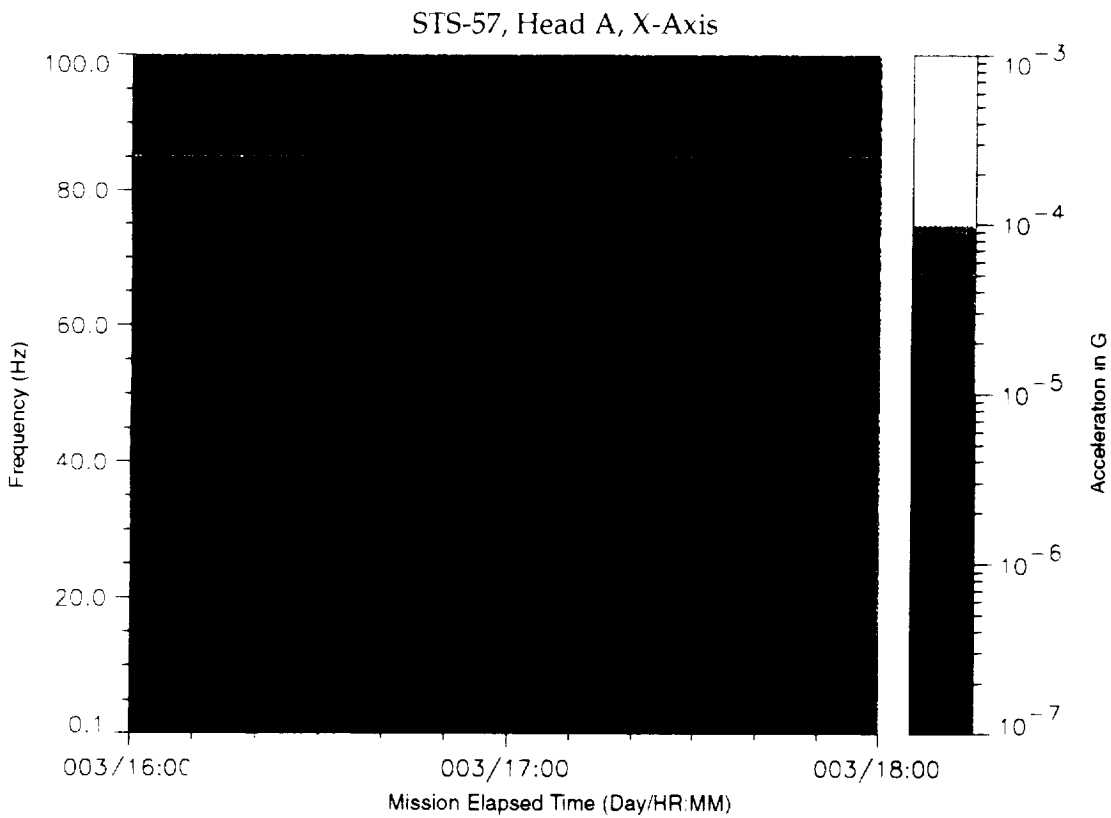


Figure B-162: SPACEHAB-1, Forward Bulkhead T-Beam

STS-57, Head A, Y-Axis

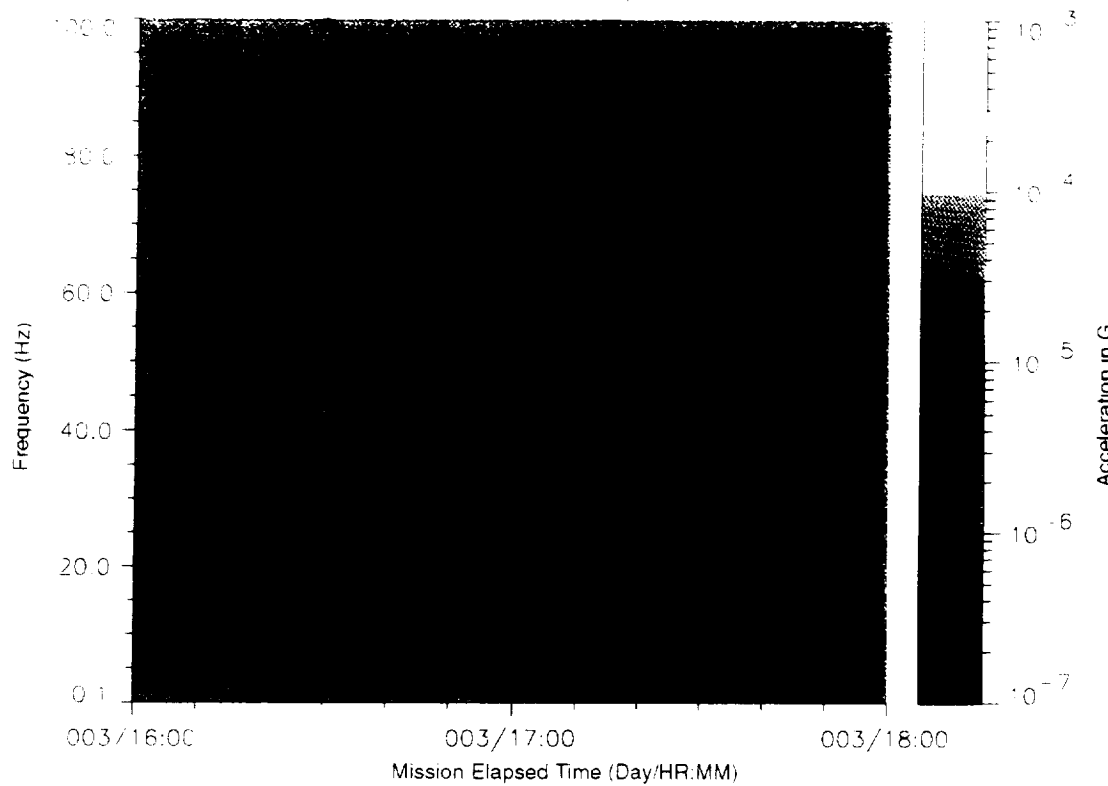


Figure B-163: SPACEHAB-1, Forward Bulkhead T-Beam

STS-57, Head A, Z-Axis

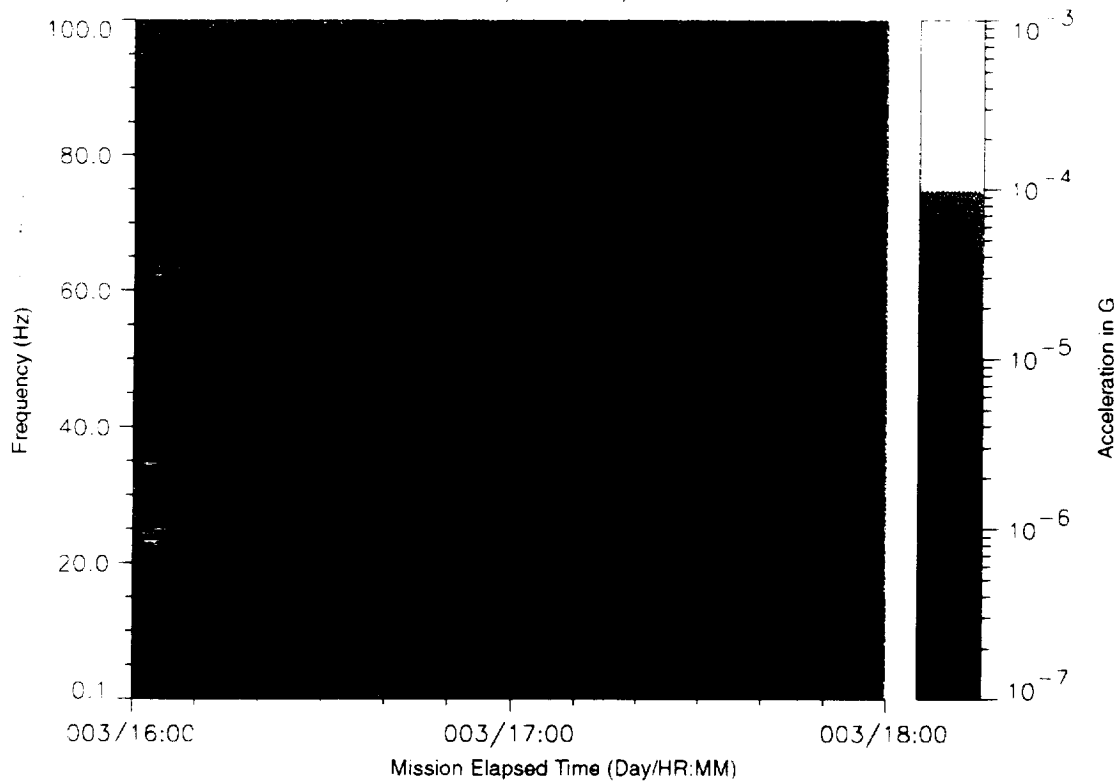


Figure B-164: SPACEHAB-1, Forward Bulkhead T-Beam

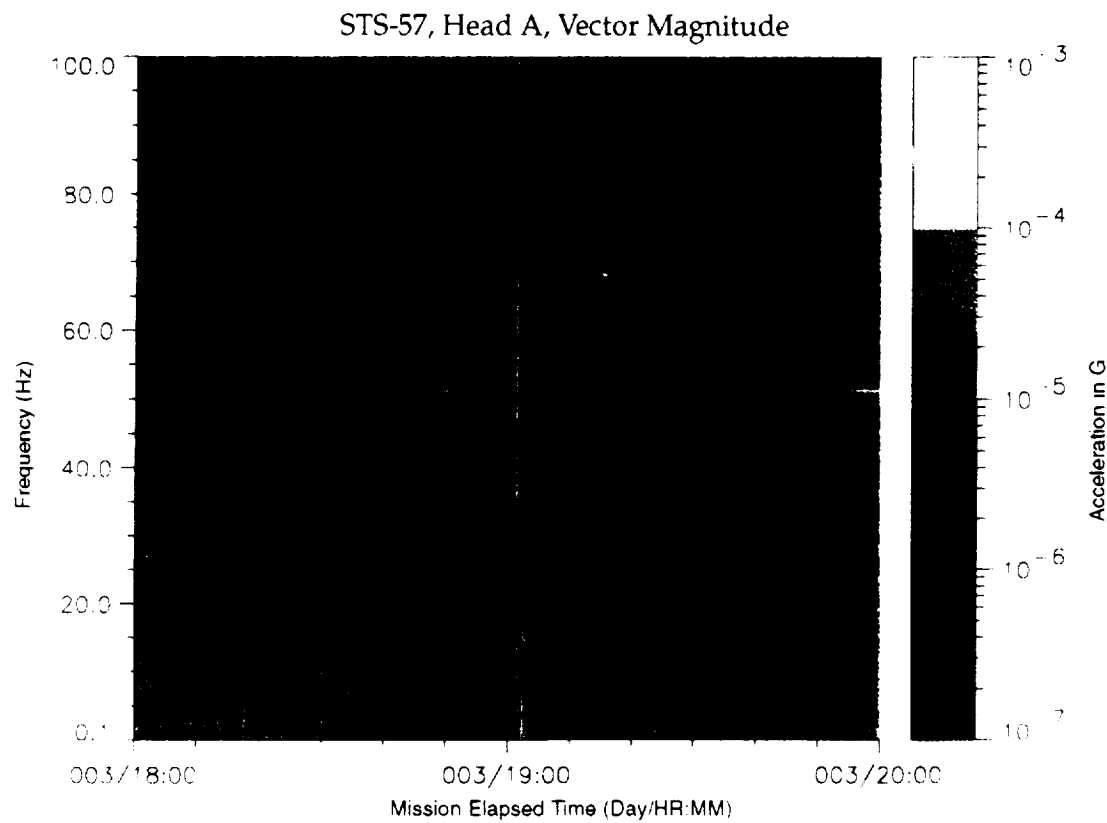


Figure B-165: SPACEHAB-1, Forward Bulkhead T-Beam

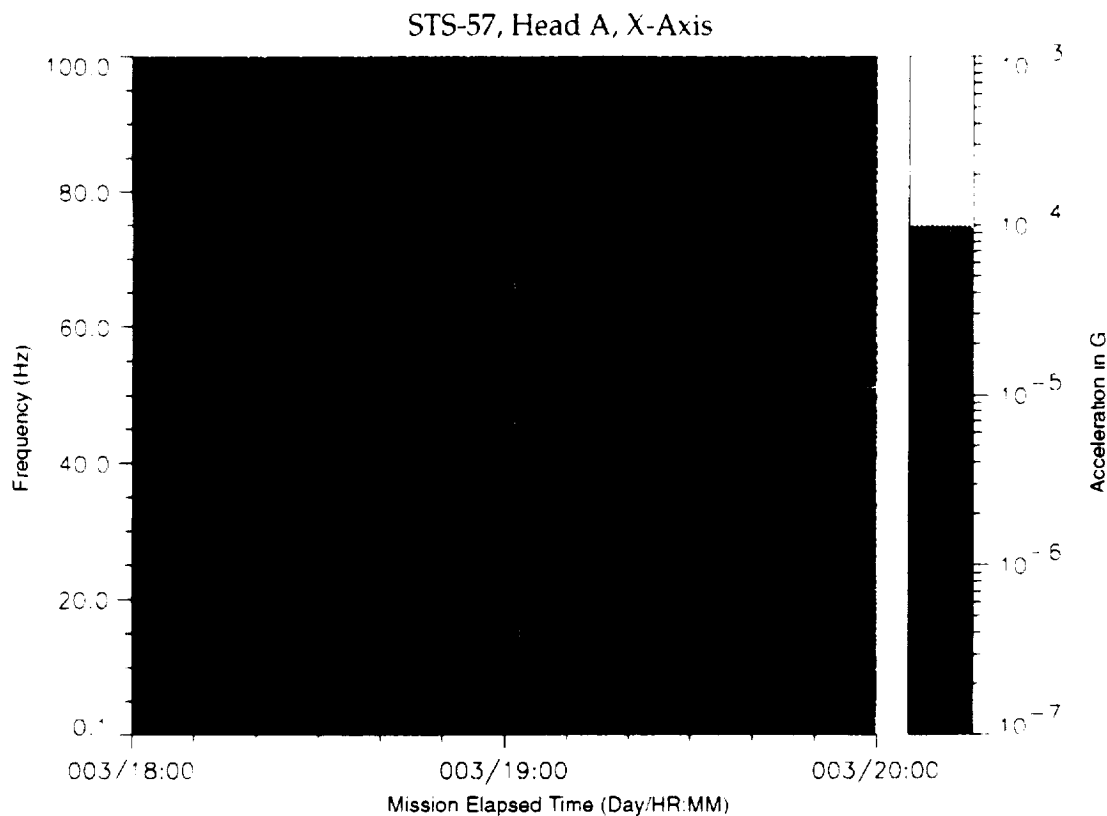


Figure B-166: SPACEHAB-1, Forward Bulkhead T-Beam

PRECEDING PAGE BLANK NOT FILMED

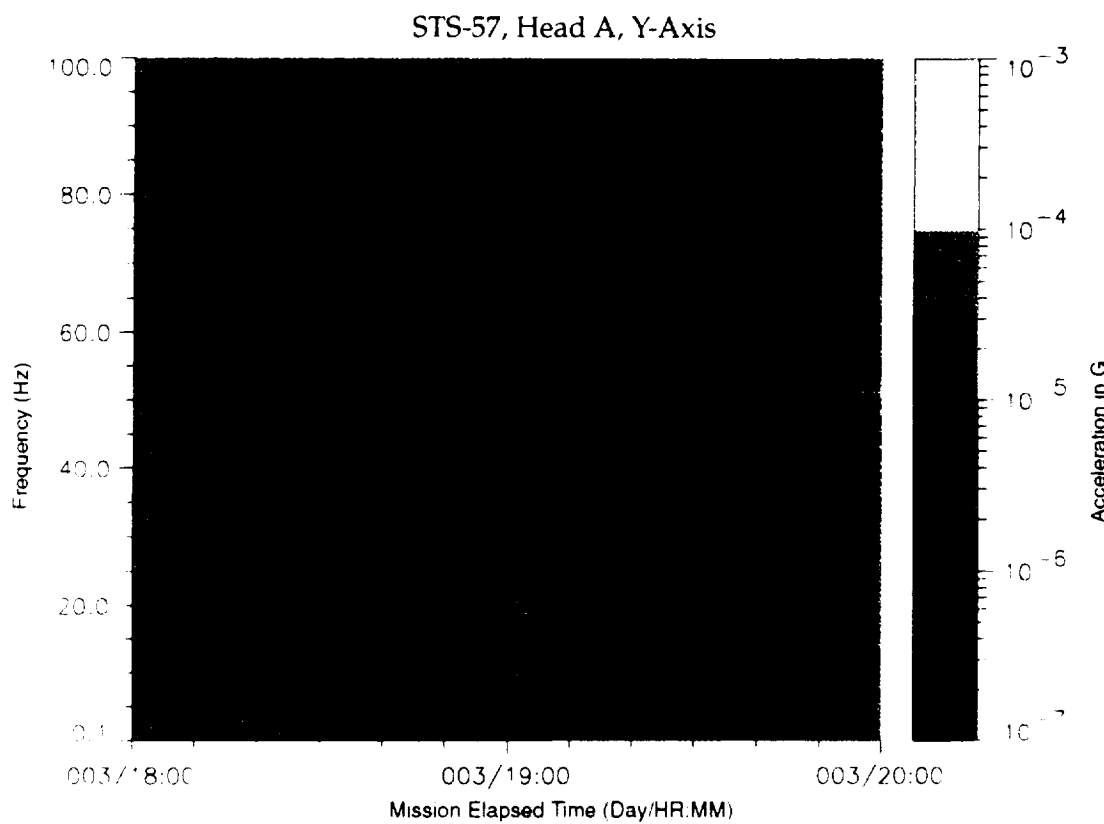


Figure B-167: SPACEHAB-1, Forward Bulkhead T-Beam

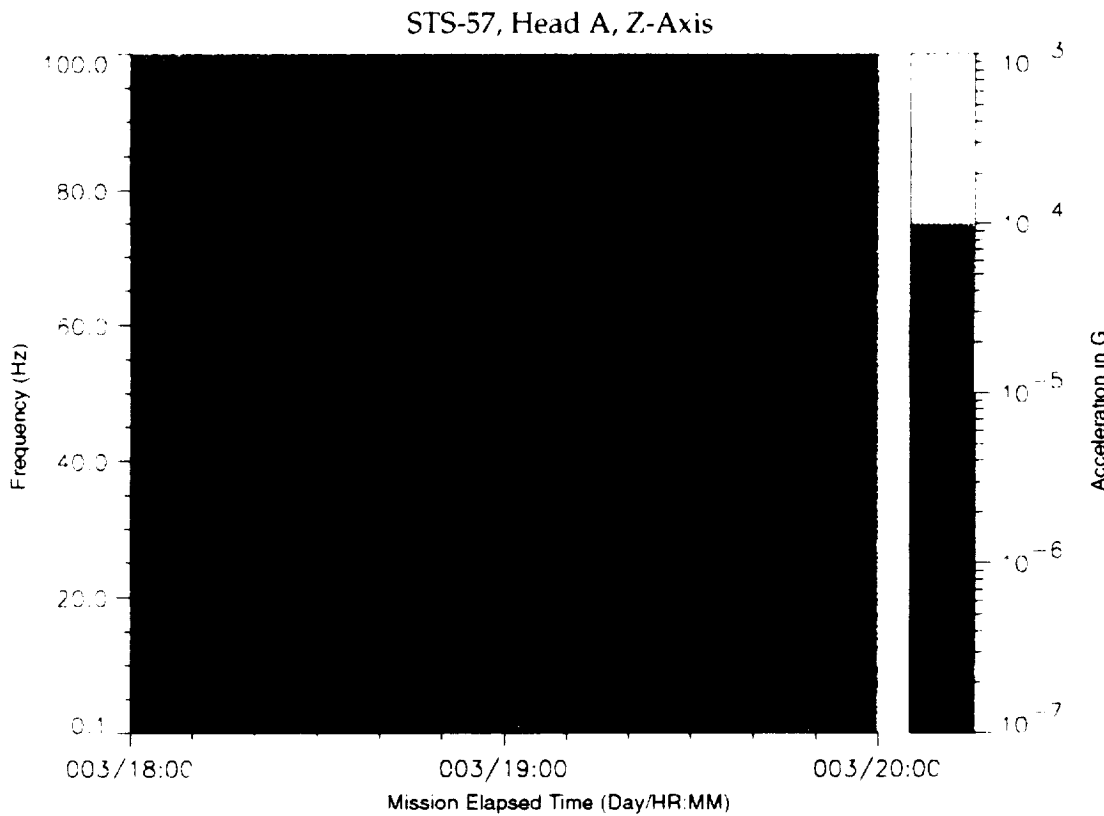


Figure B-168: SPACEHAB-1, Forward Bulkhead T-Beam

~~PRECEDING PAGE BLANK NOT FILMED~~

SIS-57, Head A, Vector Magnitude

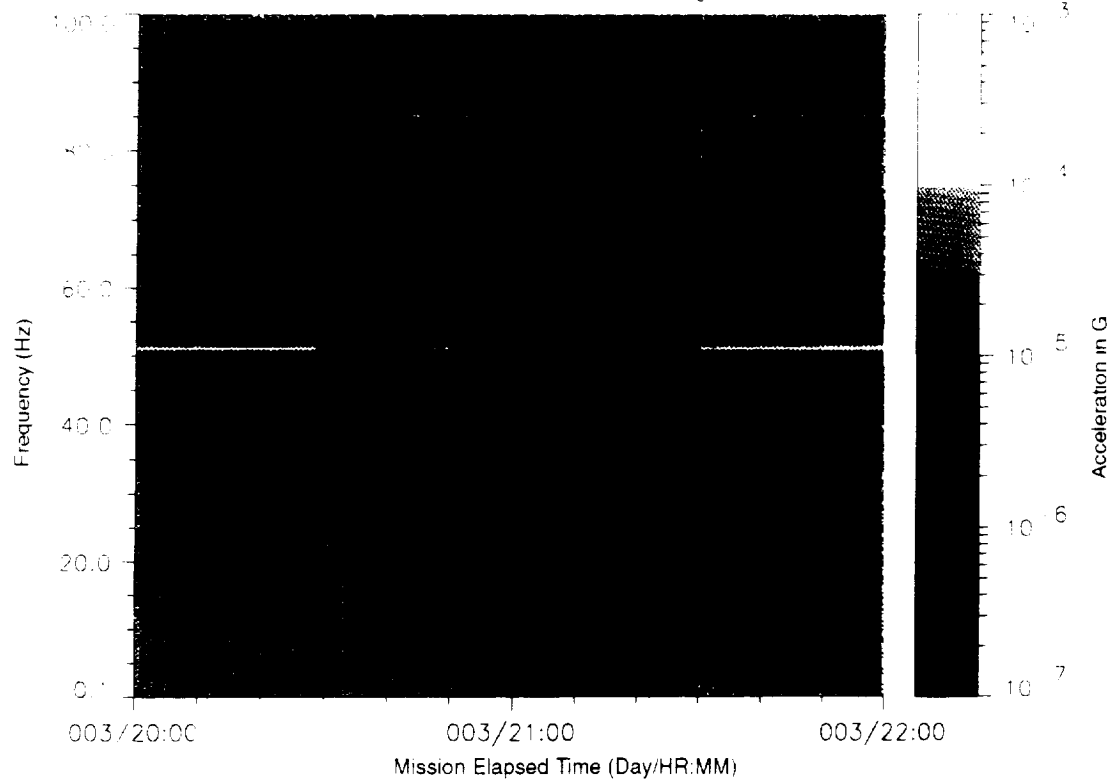


Figure B-169: SPACEHAB-1, Forward Bulkhead T-Beam

STS-57, Head A, X-Axis

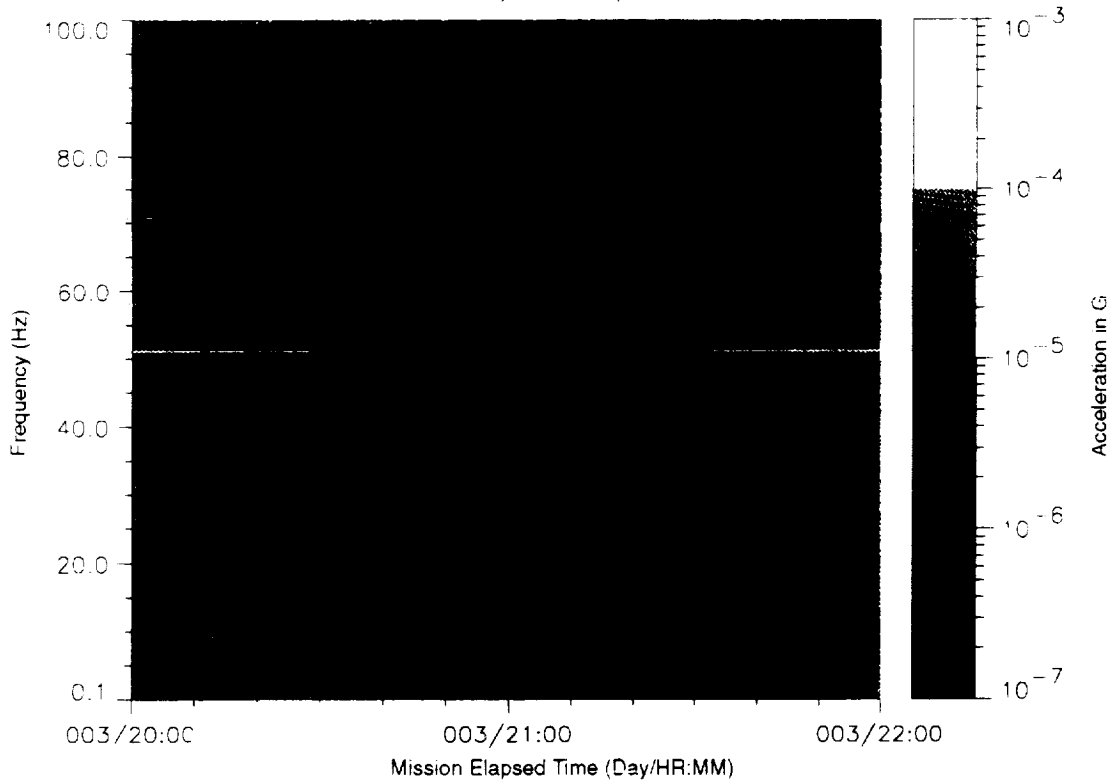


Figure B-170: SPACEHAB-1, Forward Bulkhead T-Beam

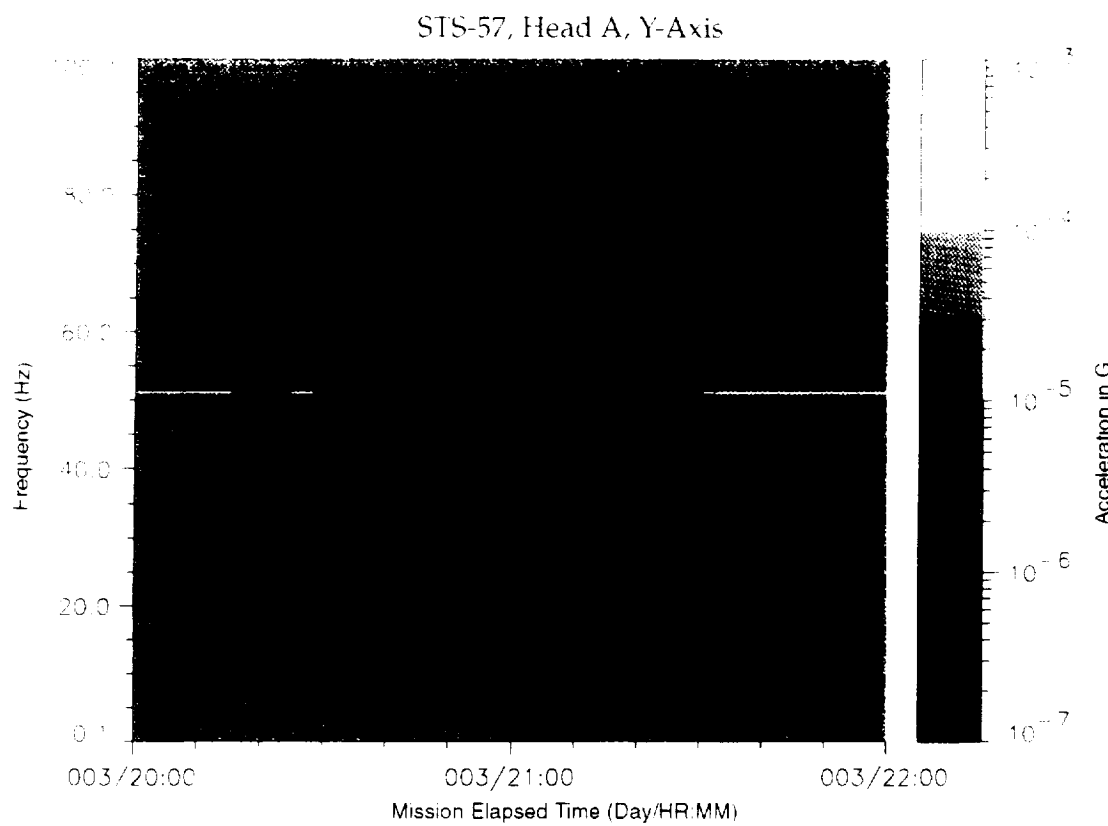


Figure B-171: SPACEHAB-1, Forward Bulkhead T-Beam

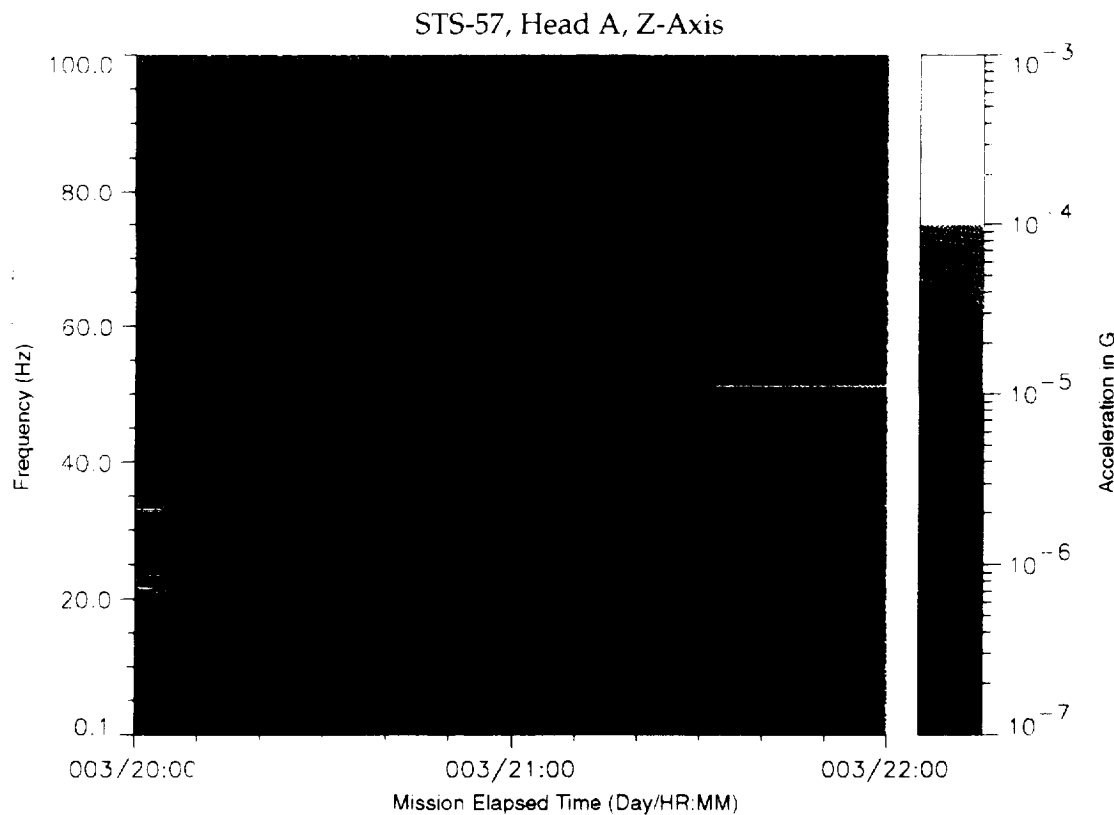


Figure B-172: SPACEHAB-1, Forward Bulkhead T-Beam

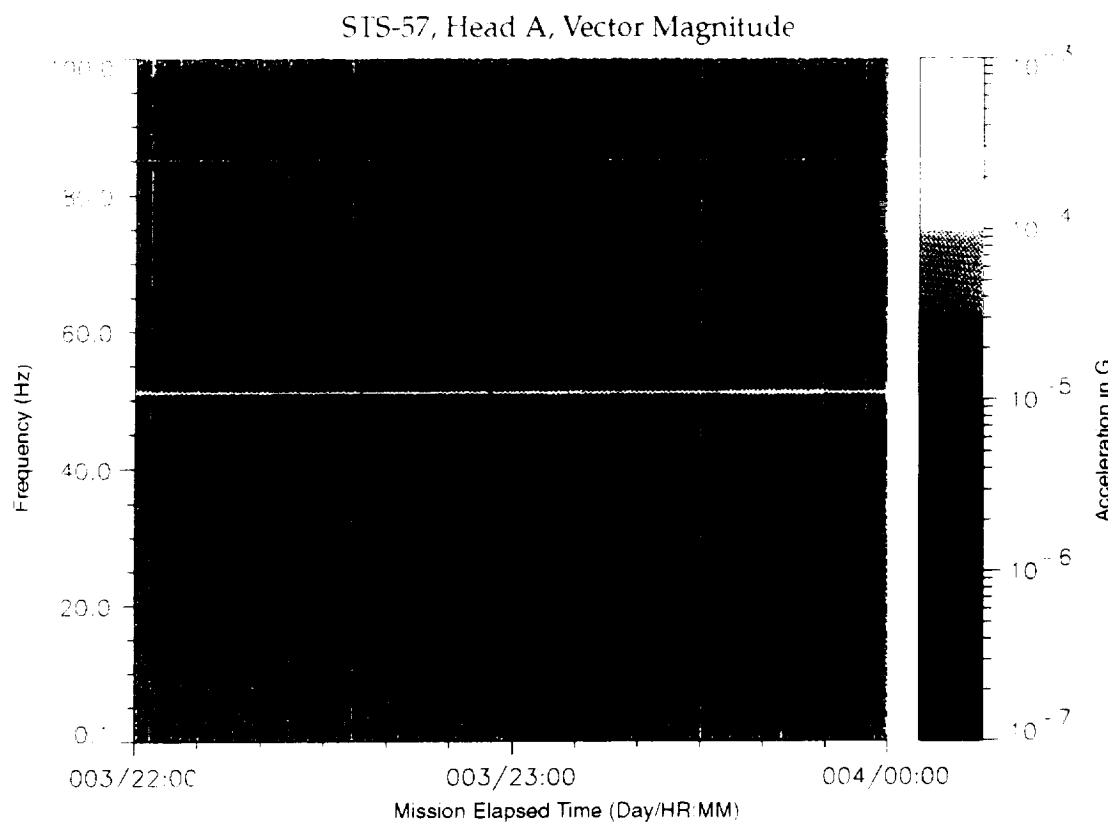


Figure B-173: SPACEHAB-1, Forward Bulkhead T-Beam

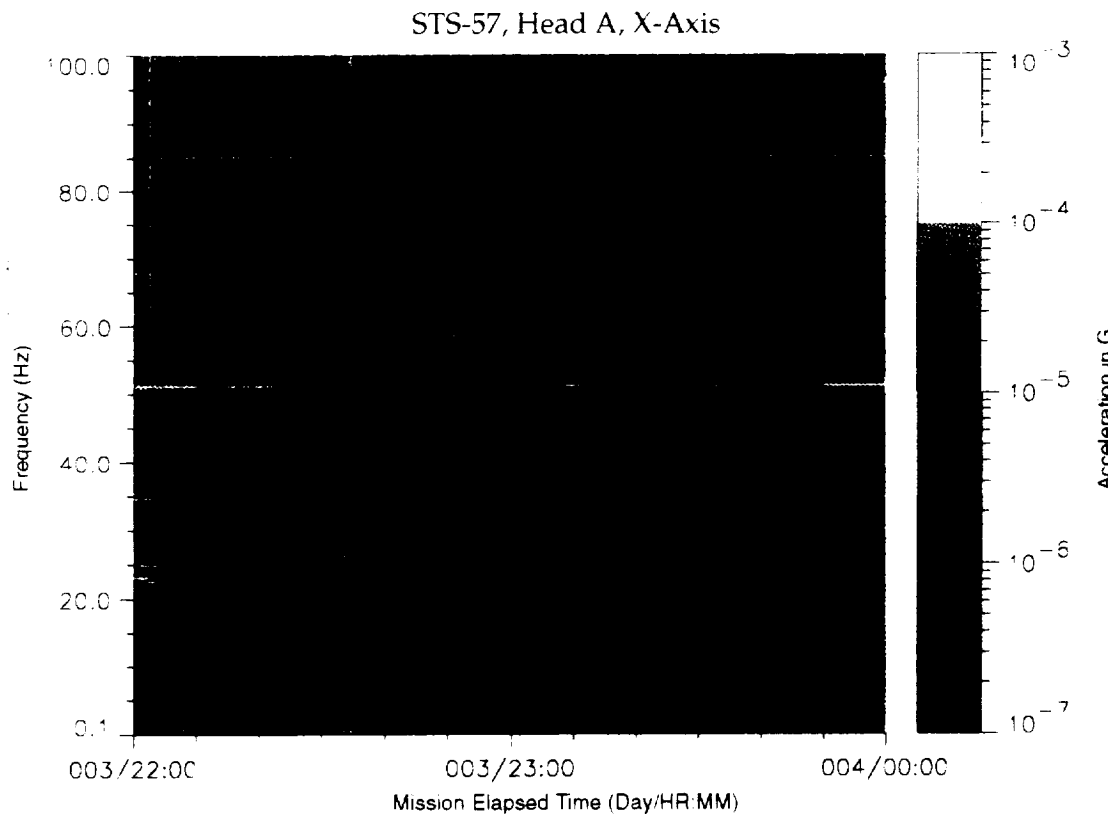


Figure B-174: SPACEHAB-1, Forward Bulkhead T-Beam

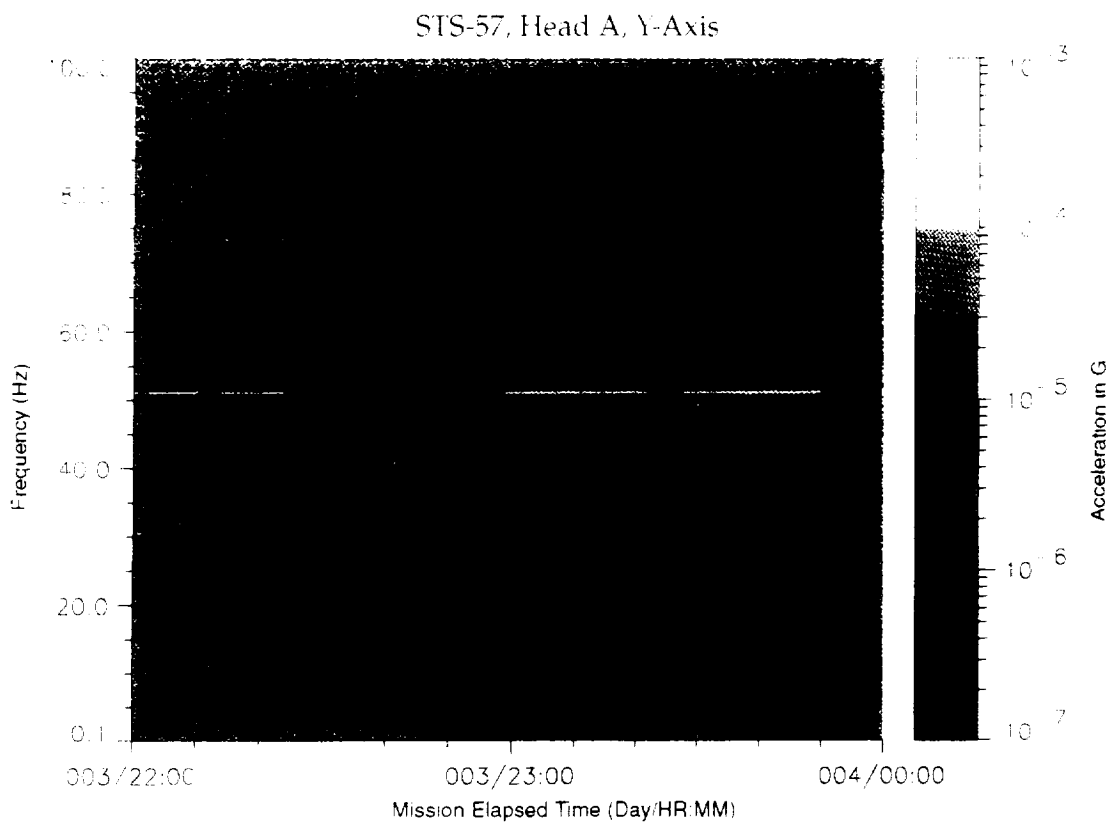


Figure B-175: SPACEHAB-1, Forward Bulkhead T-Beam

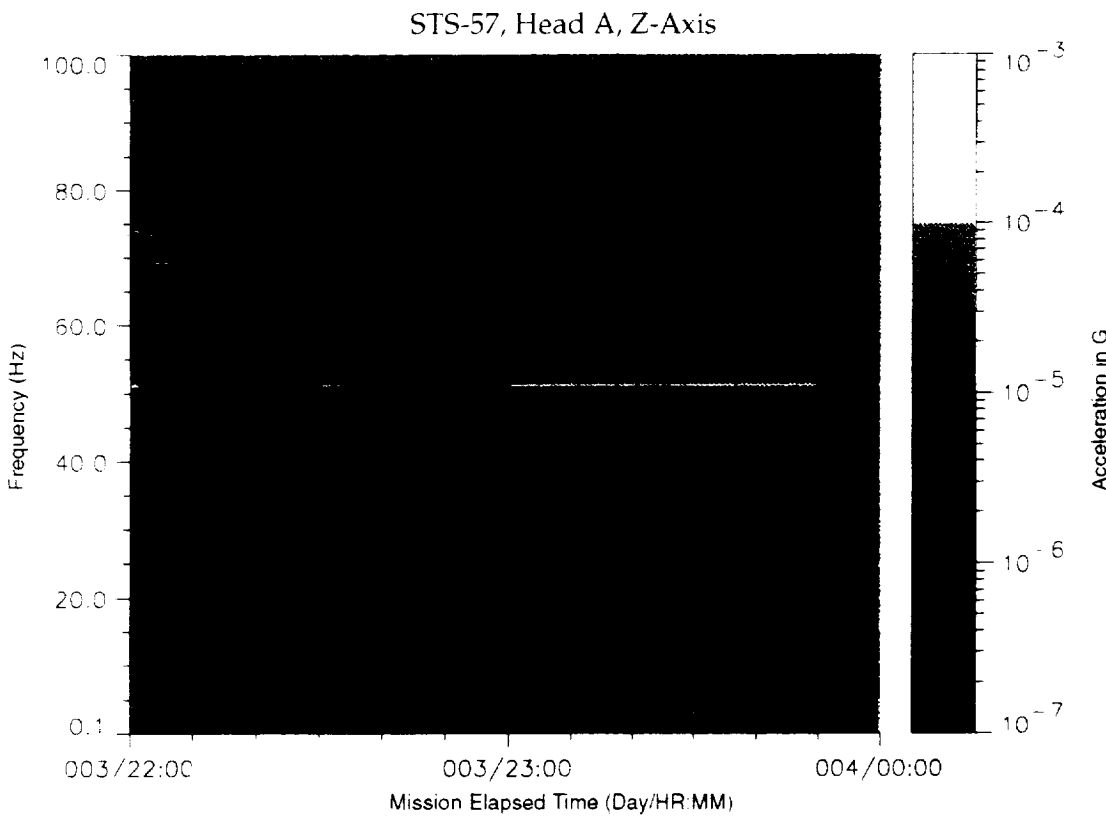


Figure B-176: SPACEHAB-1, Forward Bulkhead T-Beam

~~PRECEDING PAGE BLANK NOT FILMED~~

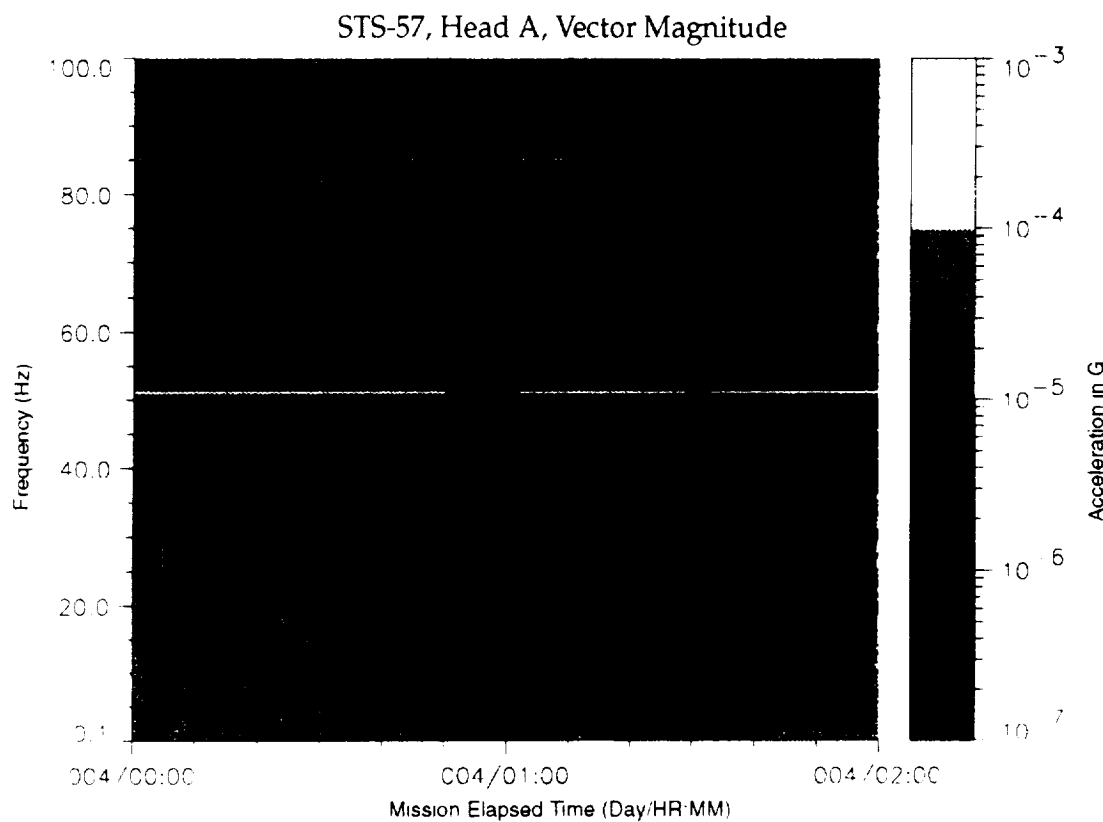


Figure B-177: SPACEHAB-1, Forward Bulkhead T-Beam

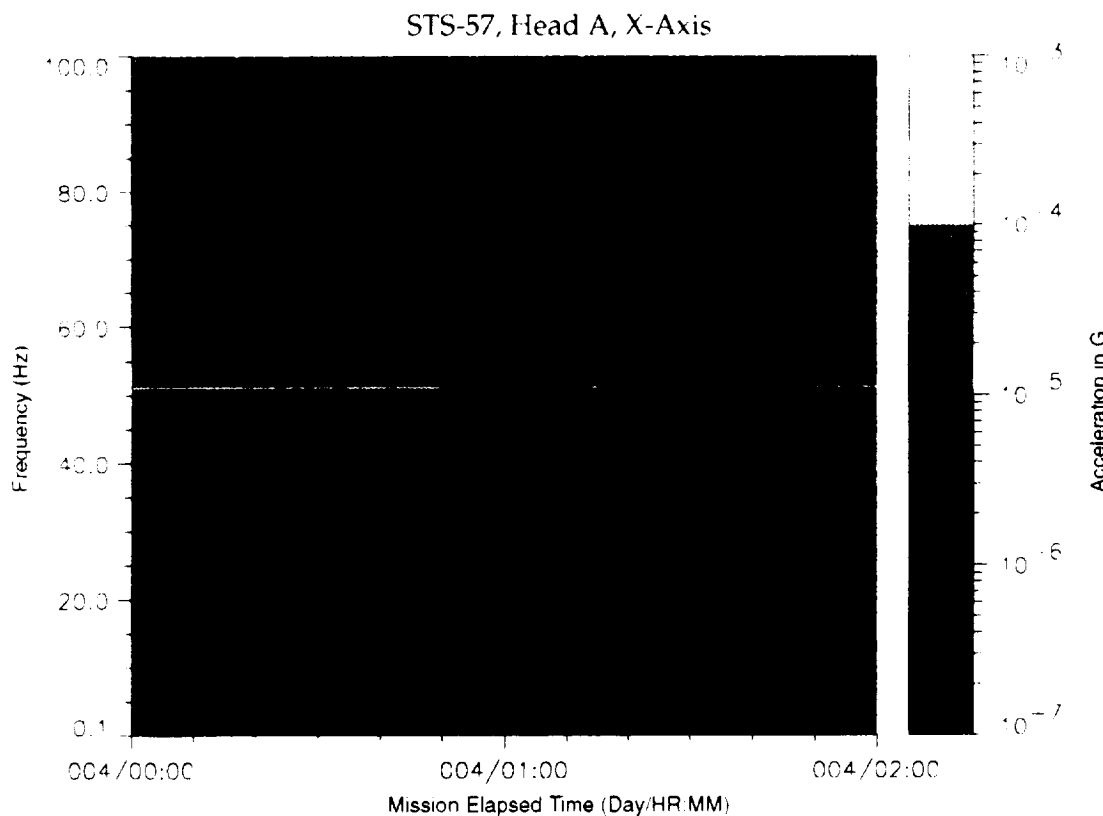


Figure B-178: SPACEHAB-1, Forward Bulkhead T-Beam

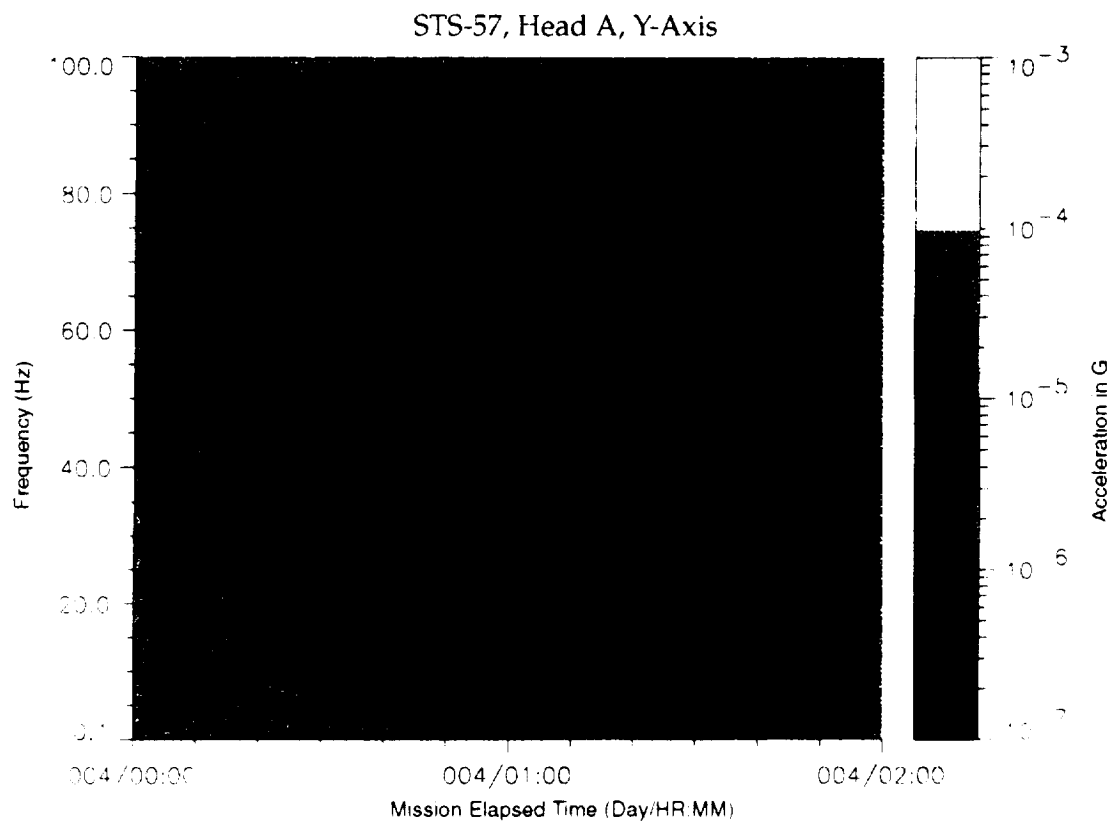


Figure B-179: SPACEHAB-1, Forward Bulkhead T-Beam

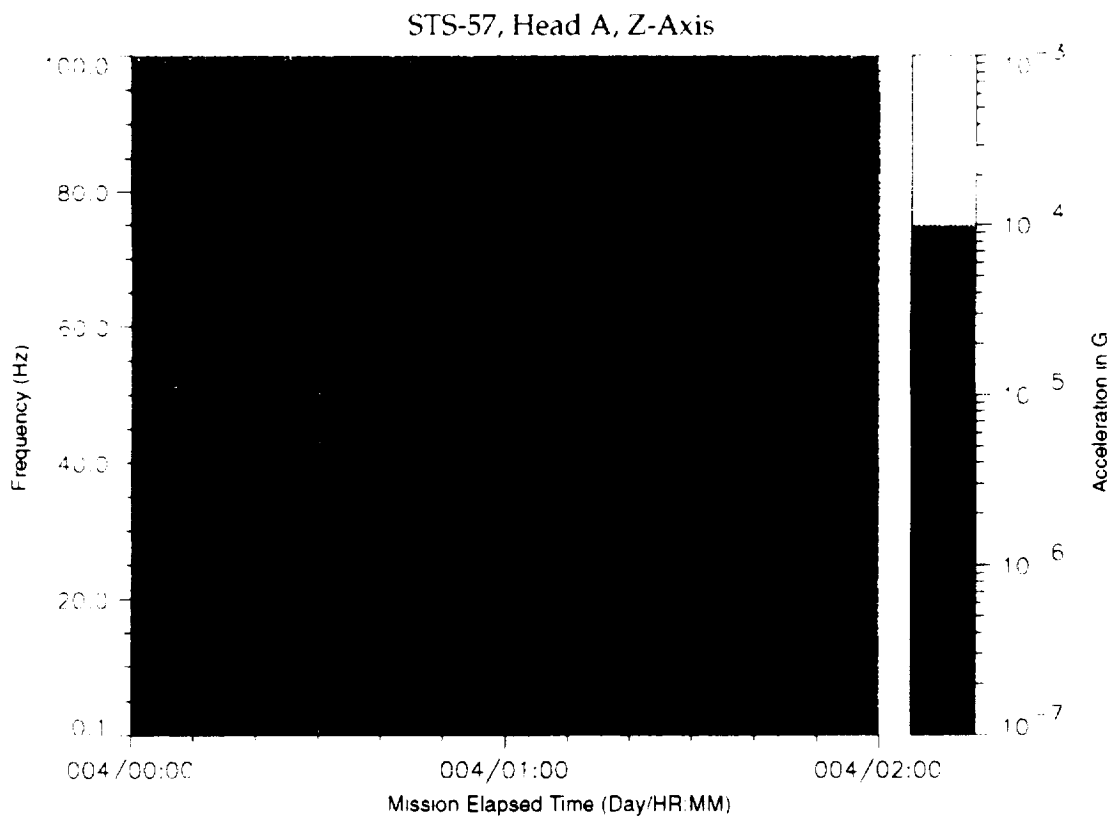


Figure B-180: SPACEHAB-1, Forward Bulkhead T-Beam

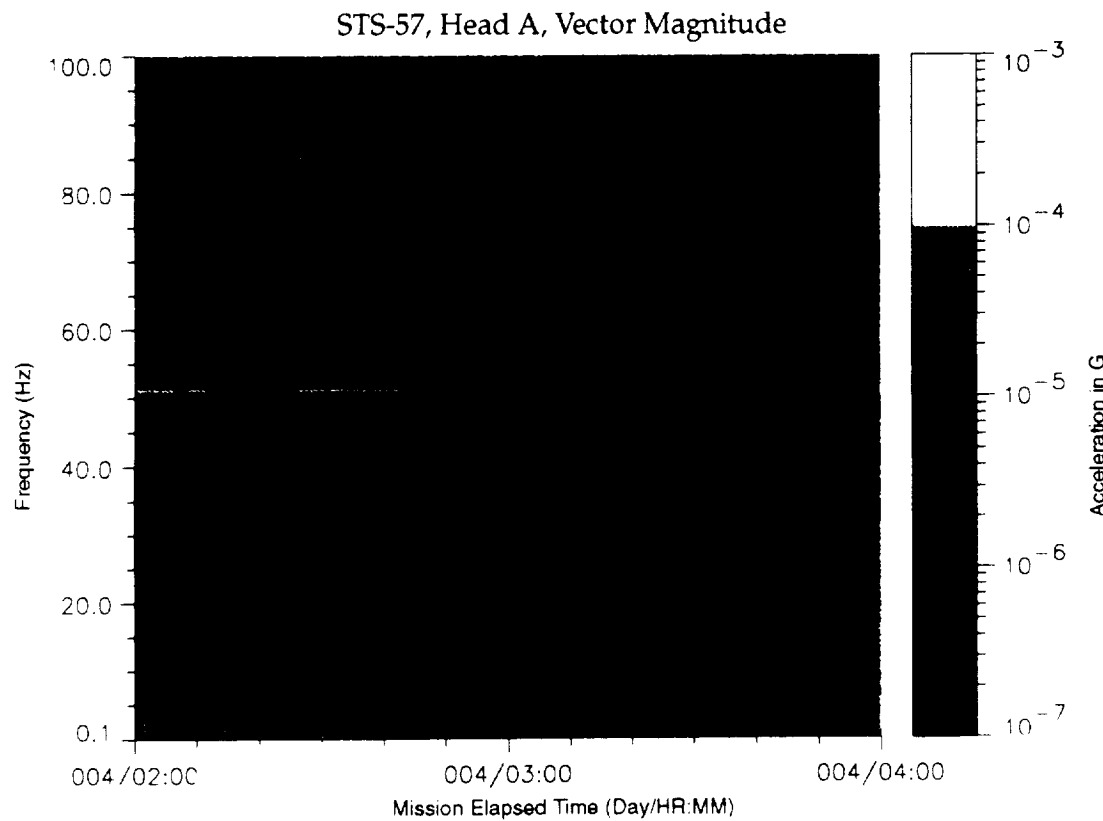


Figure B-181: SPACEHAB-1, Forward Bulkhead T-Beam

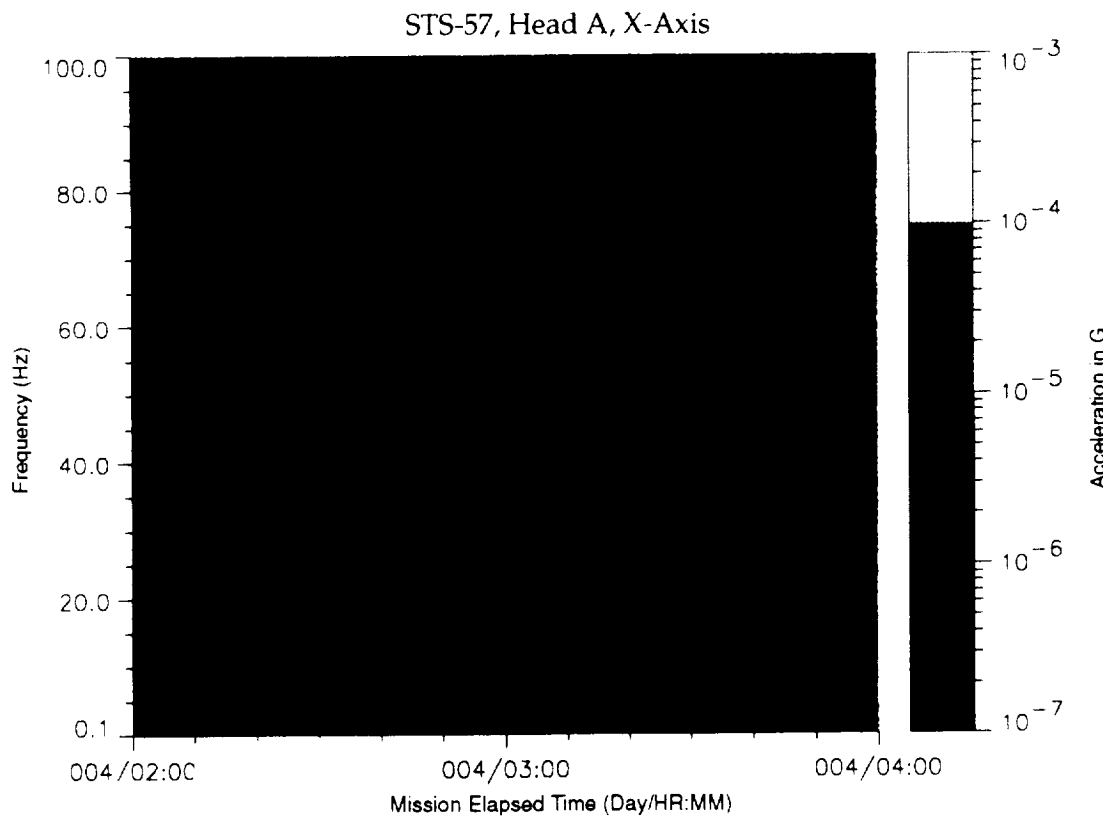


Figure B-182: SPACEHAB-1, Forward Bulkhead T-Beam

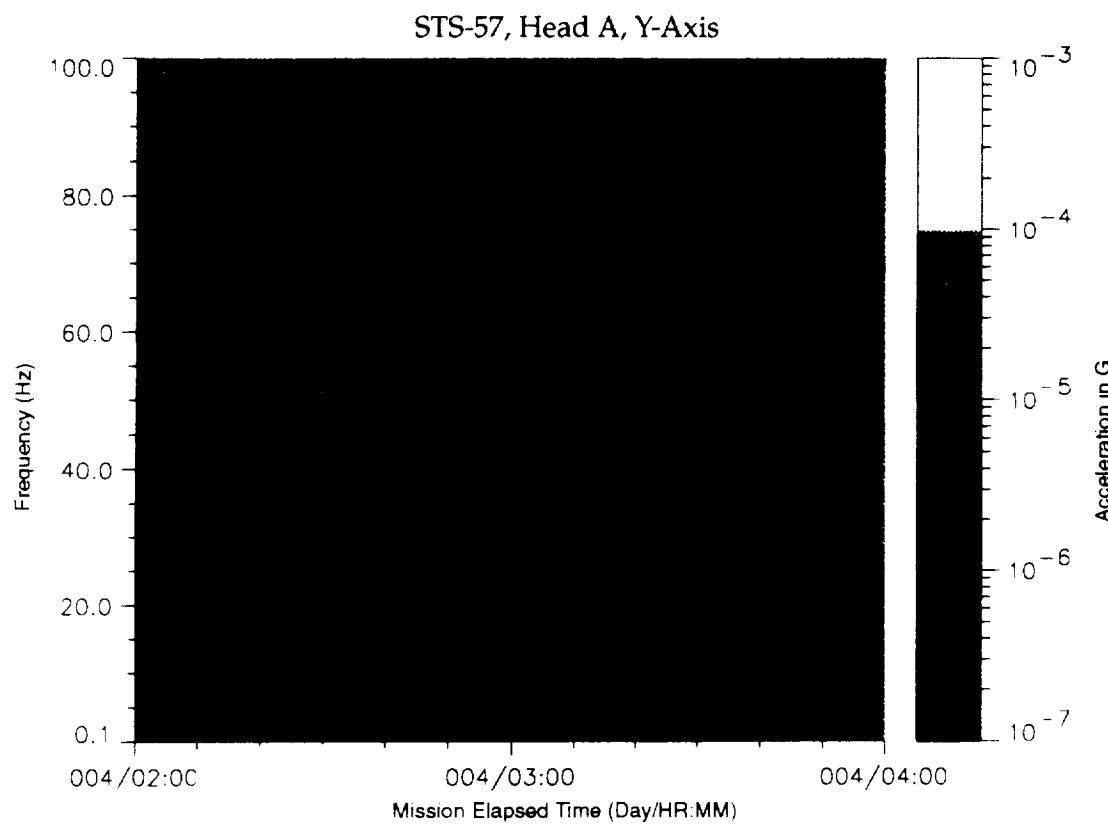


Figure B-183: SPACEHAB-1, Forward Bulkhead T-Beam

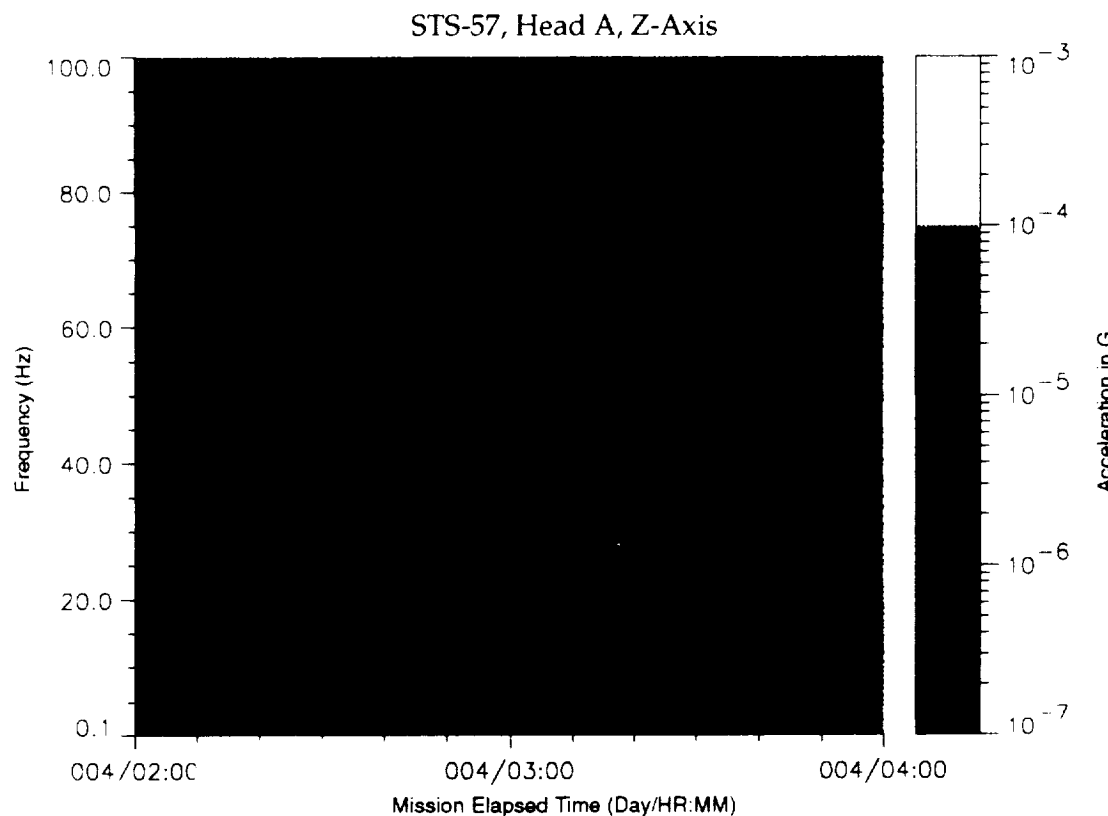


Figure B-184: SPACEHAB-1, Forward Bulkhead T-Beam

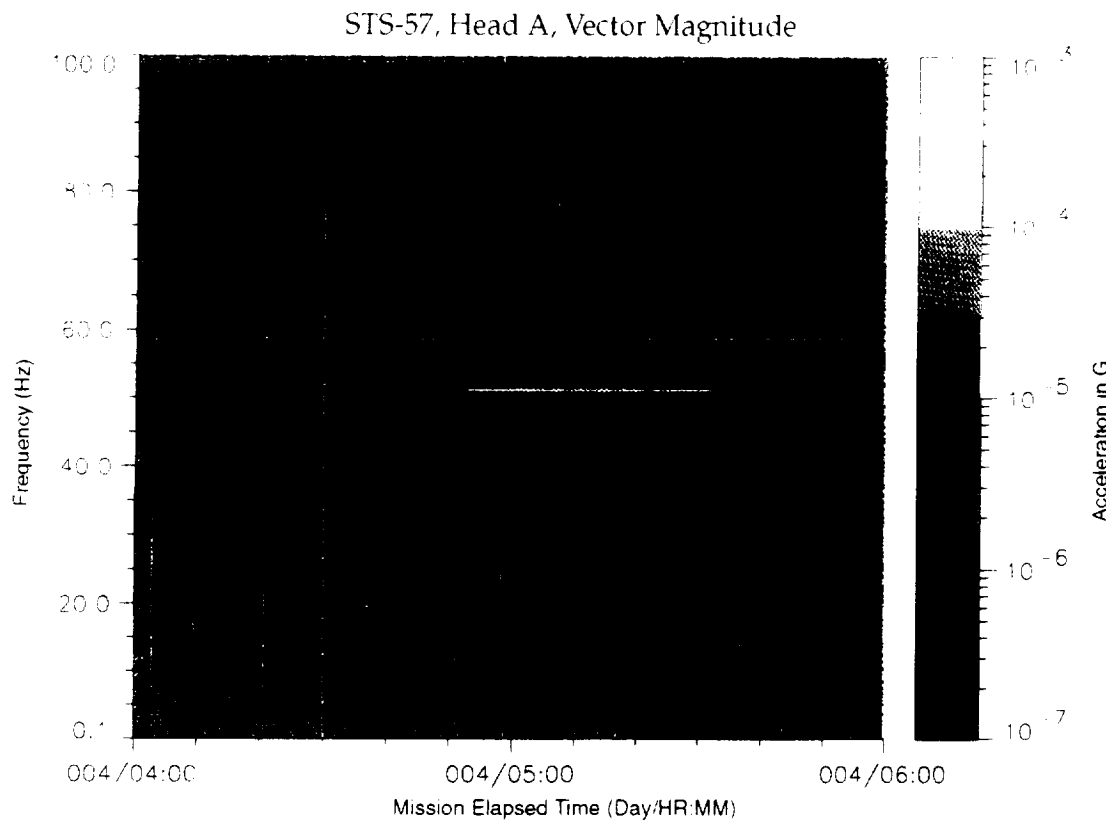


Figure B-185: SPACEHAB-1, Forward Bulkhead T-Beam

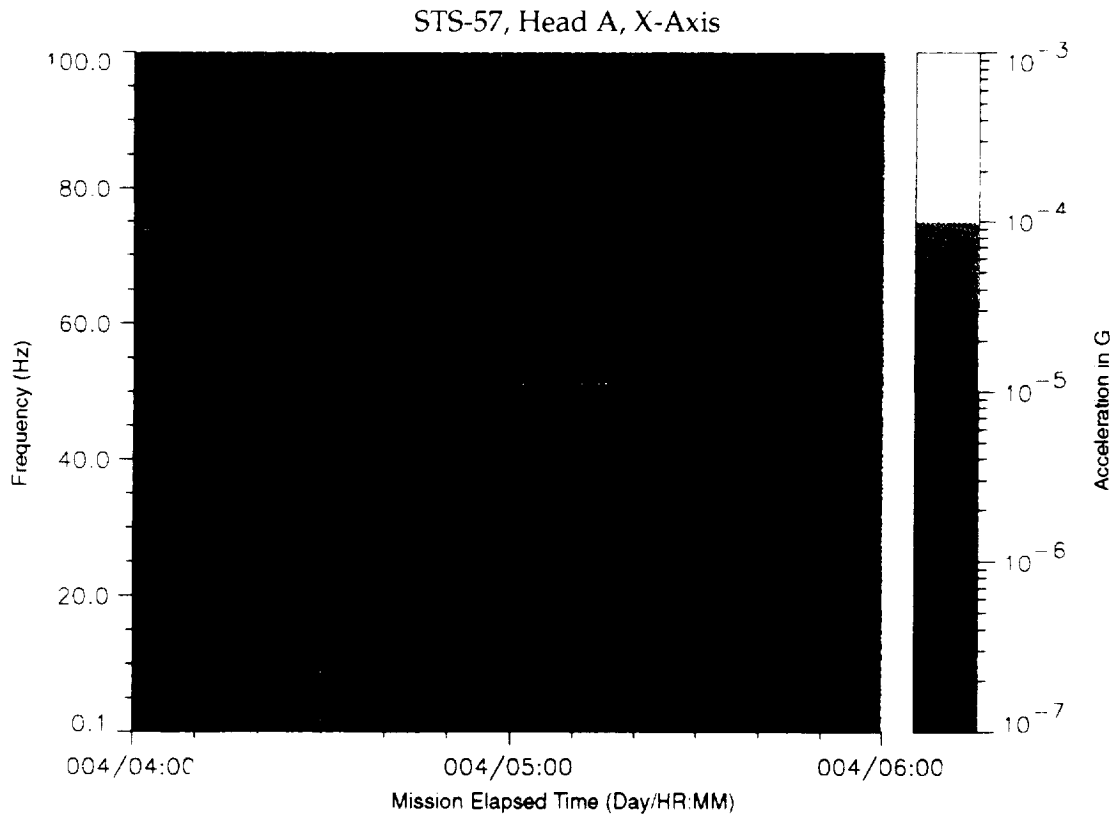


Figure B-186: SPACEHAB-1, Forward Bulkhead T-Beam

~~PREVIOUS PAGE BLANK NOT FILMED~~

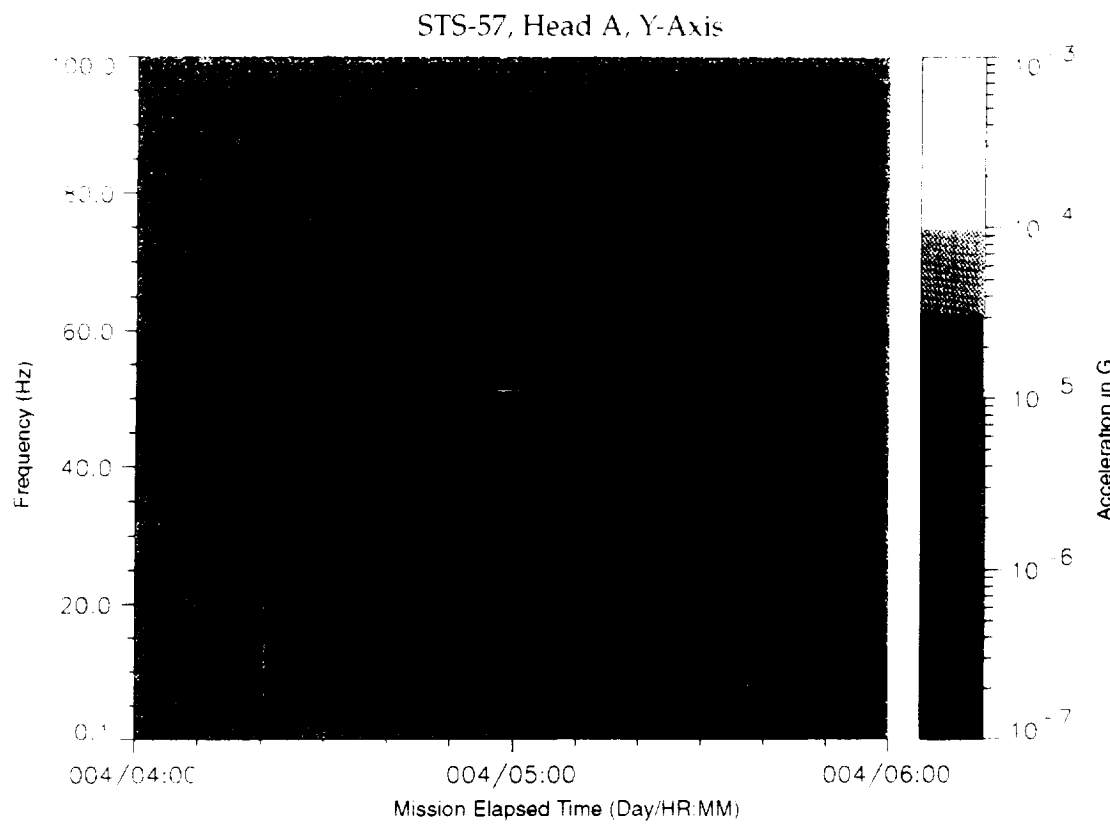


Figure B-187: SPACEHAB-1, Forward Bulkhead T-Beam

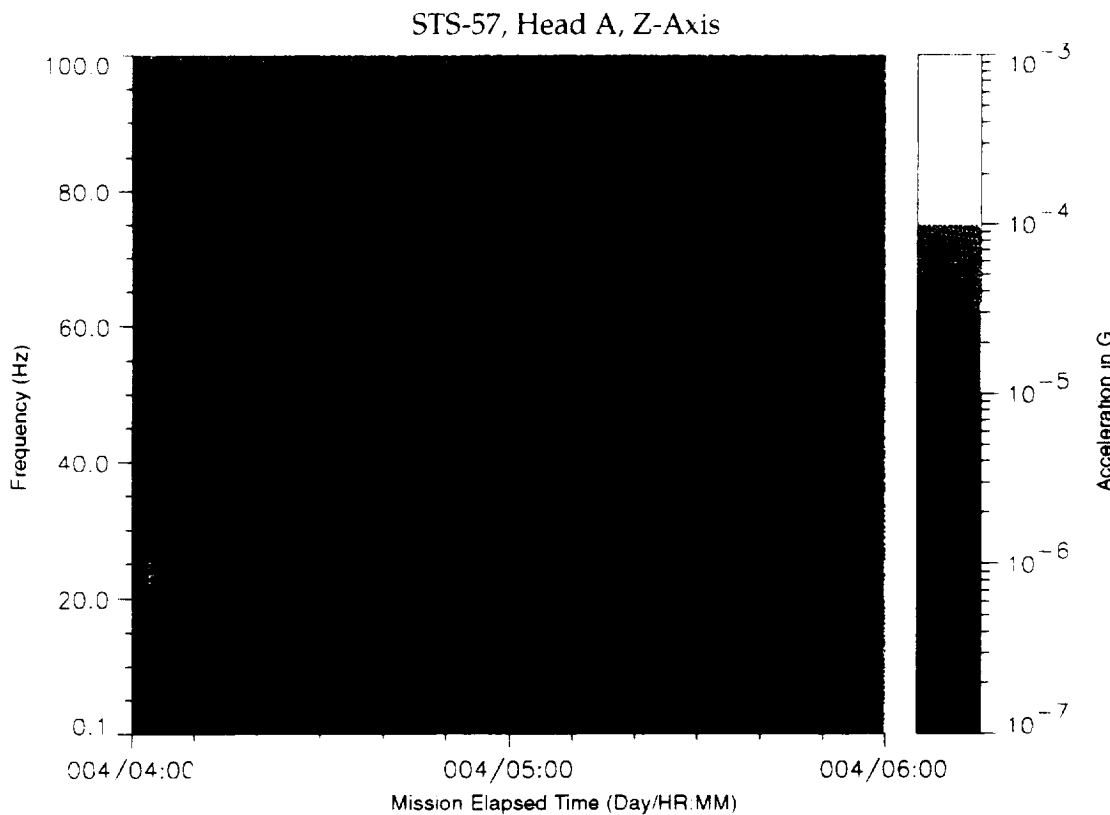


Figure B-188: SPACEHAB-1, Forward Bulkhead T-Beam

~~PRECEDING PAGE BLANK NOT FILMED~~

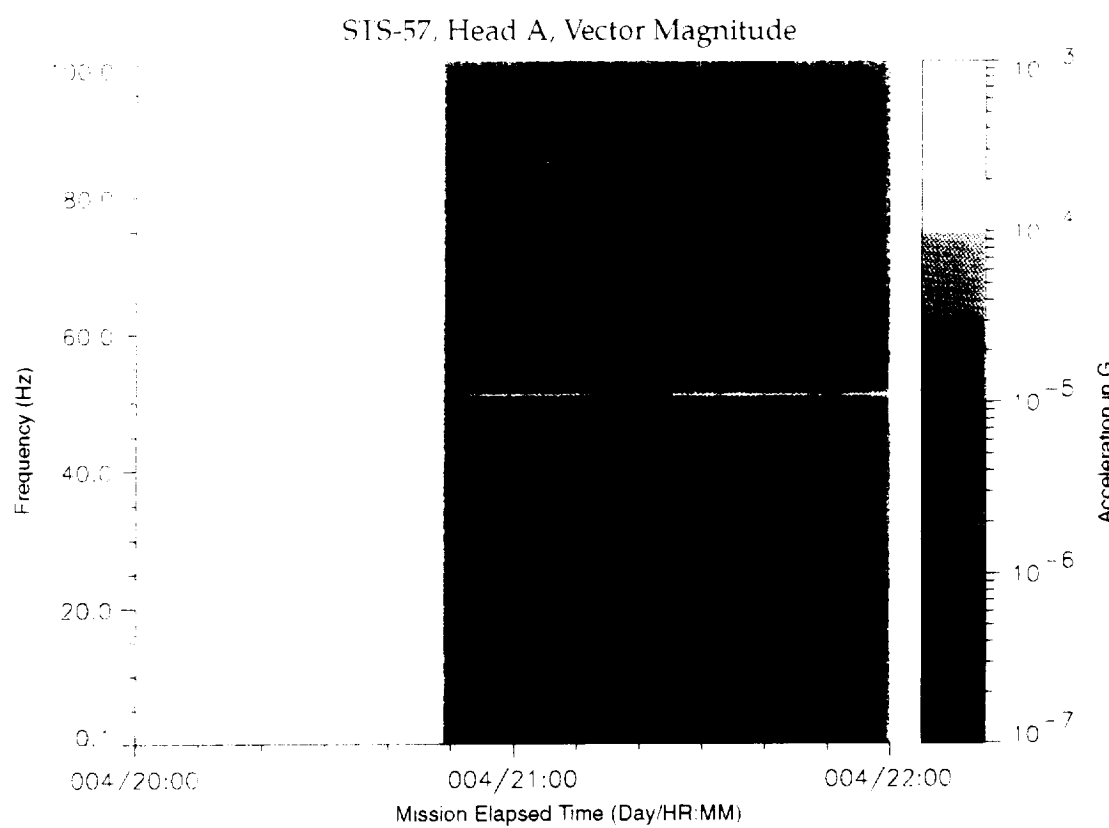


Figure B-189: SPACEHAB-1, Forward Bulkhead T-Beam

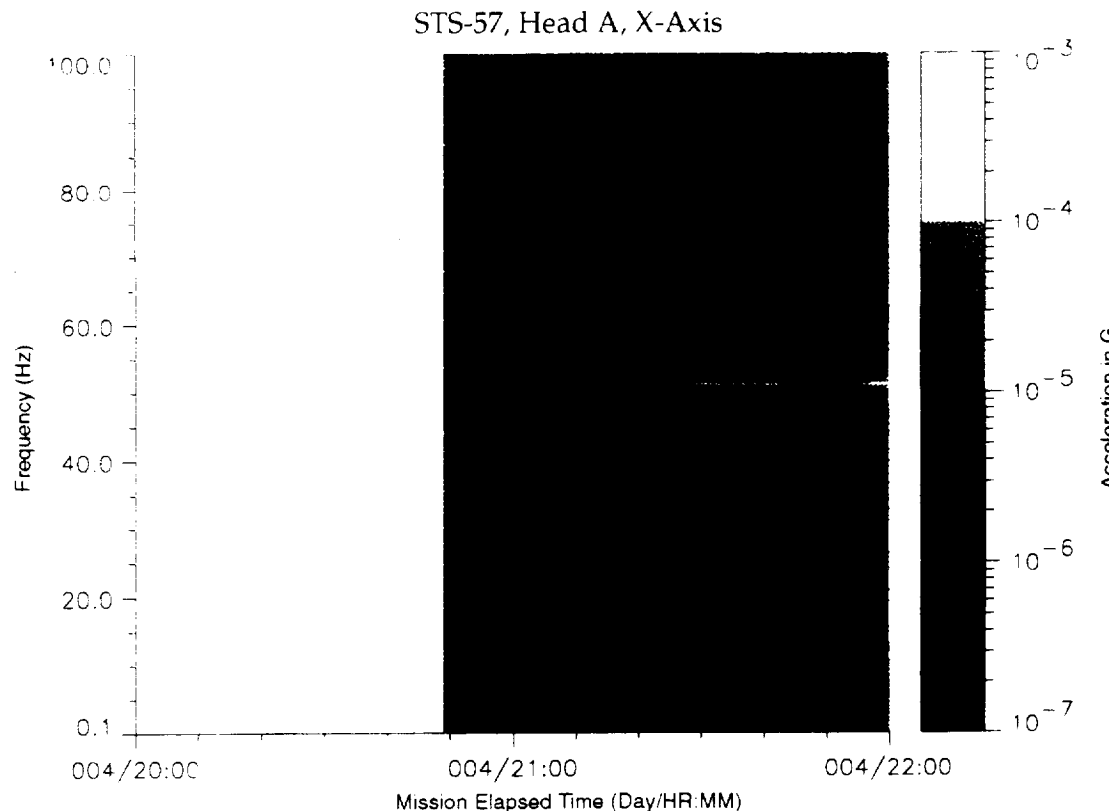


Figure B-190: SPACEHAB-1, Forward Bulkhead T-Beam

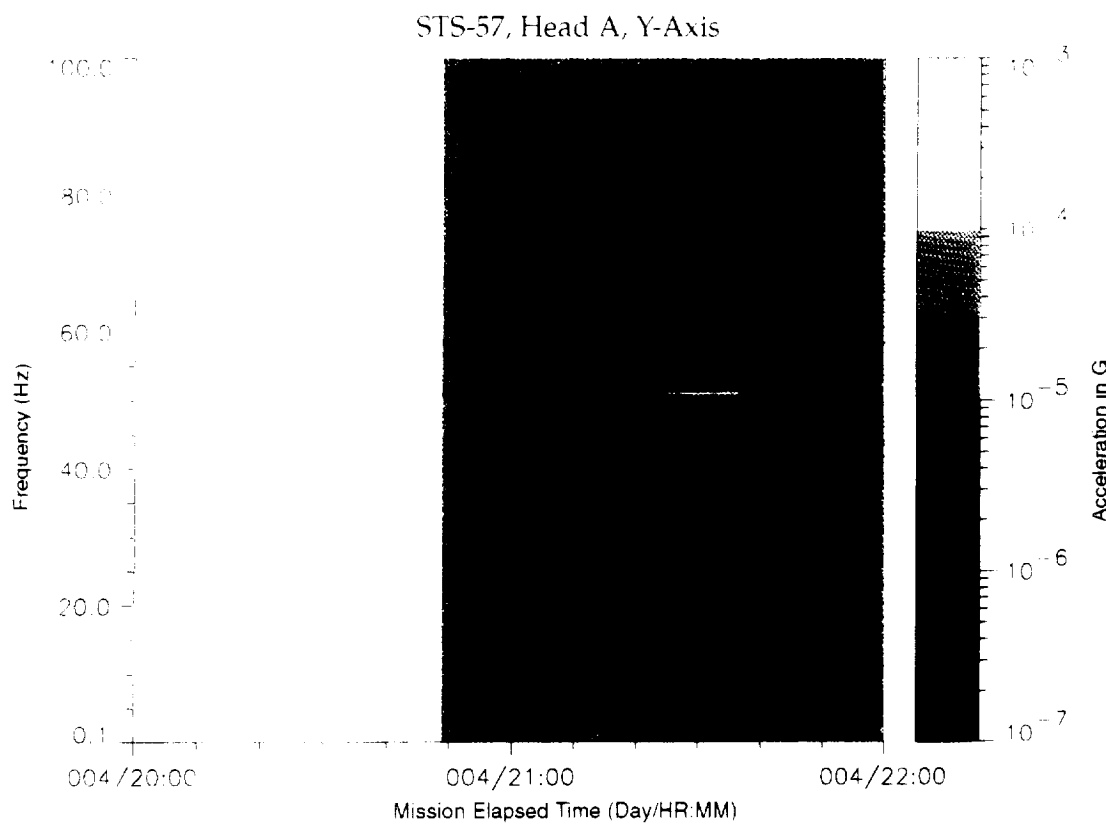


Figure B-191: SPACEHAB-1, Forward Bulkhead T-Beam

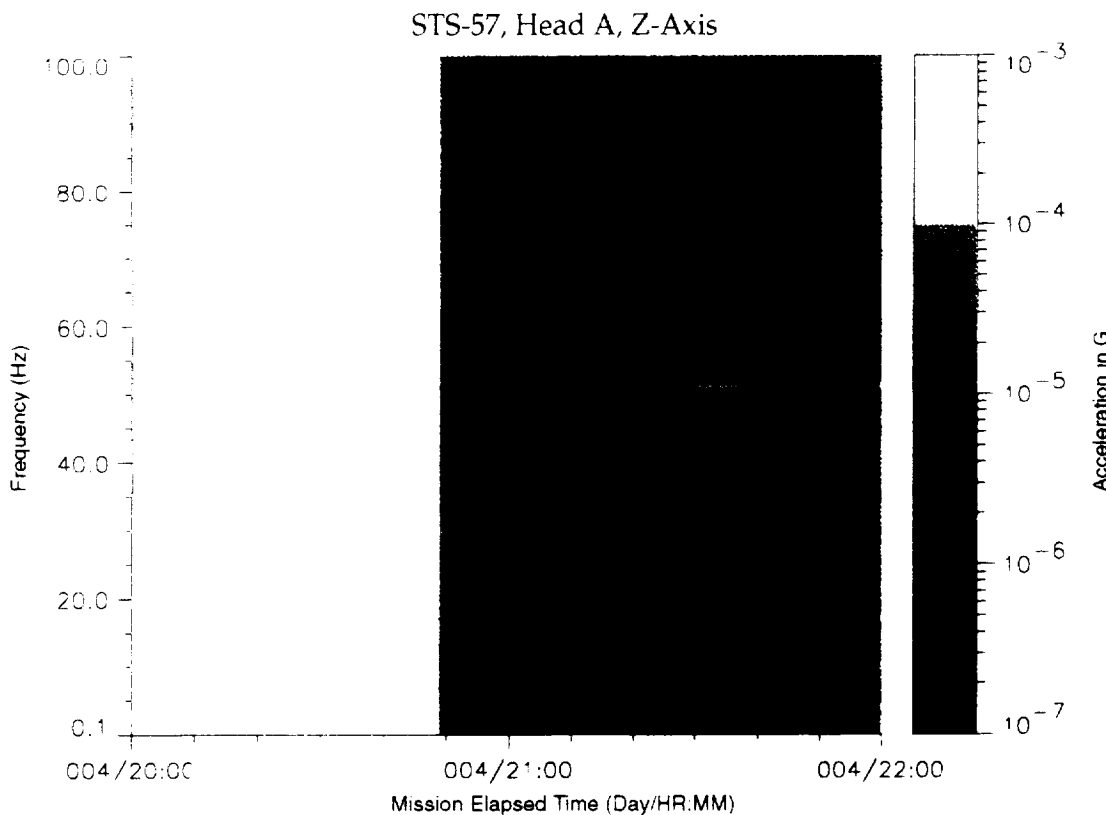


Figure B-192: SPACEHAB-1, Forward Bulkhead T-Beam

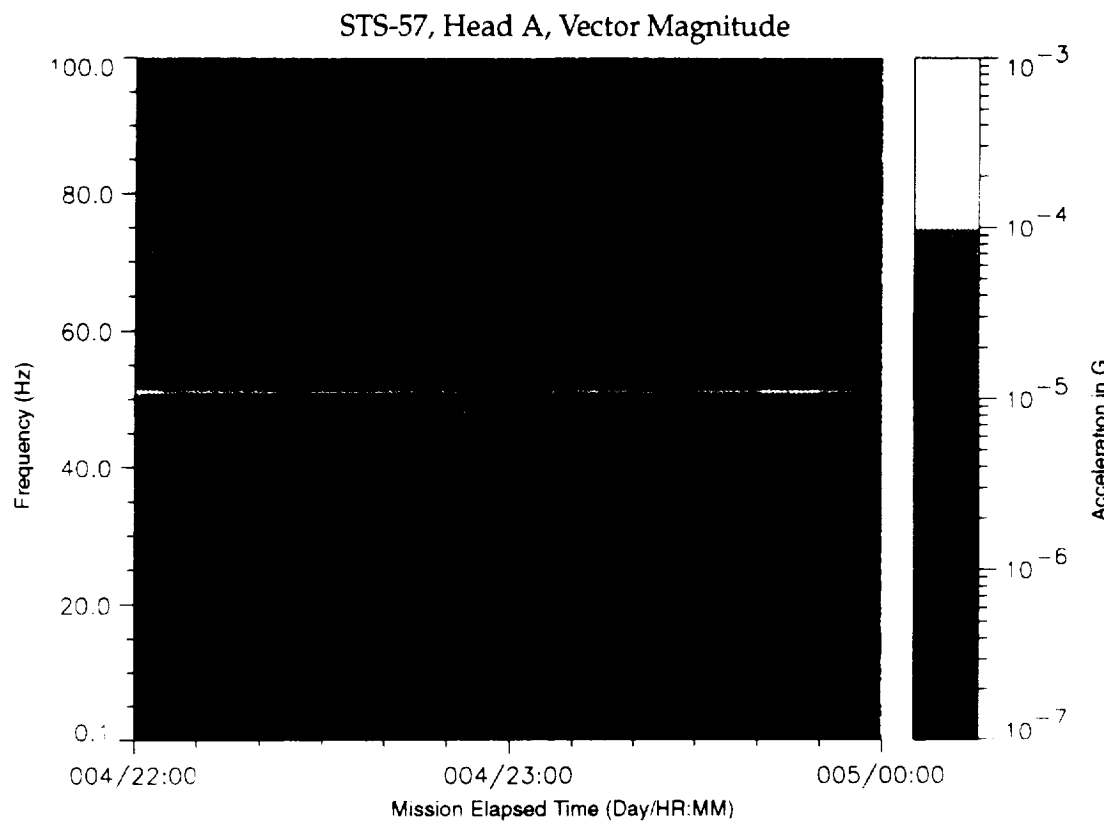


Figure B-193: SPACEHAB-1, Forward Bulkhead T-Beam

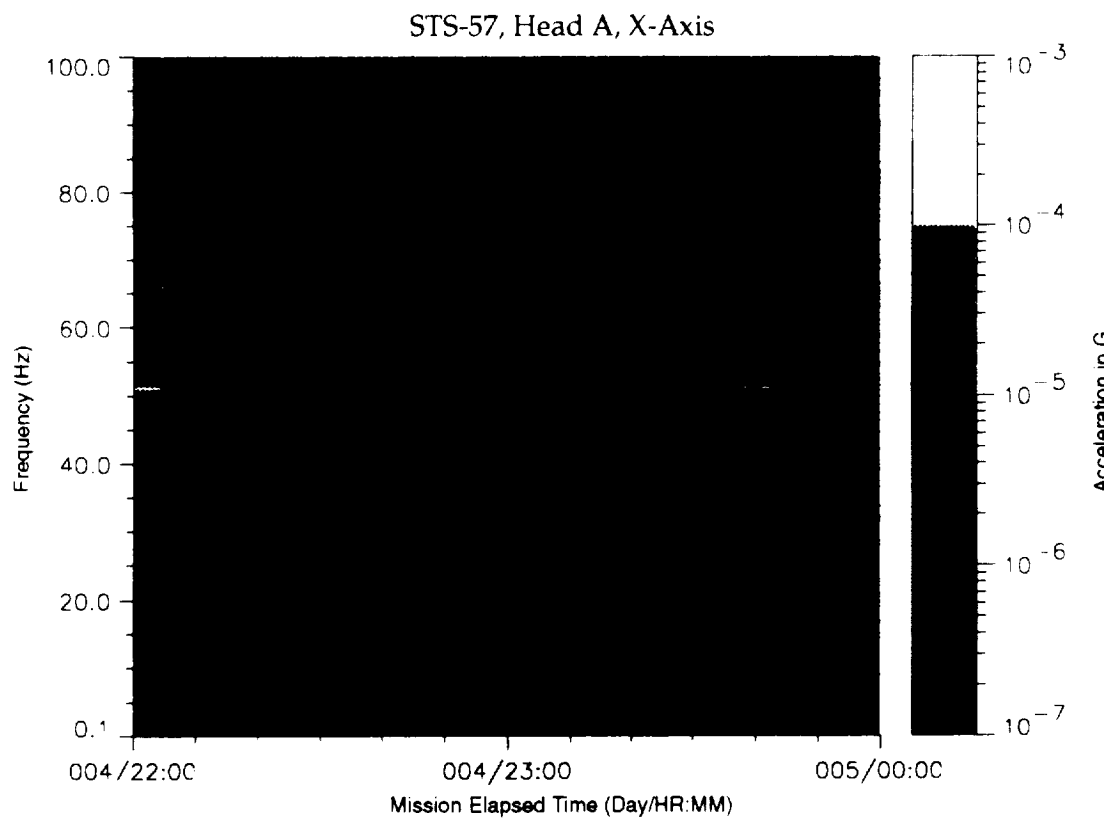


Figure B-194: SPACEHAB-1, Forward Bulkhead T-Beam

PRECEDING PAGE BLANK NOT FILMED

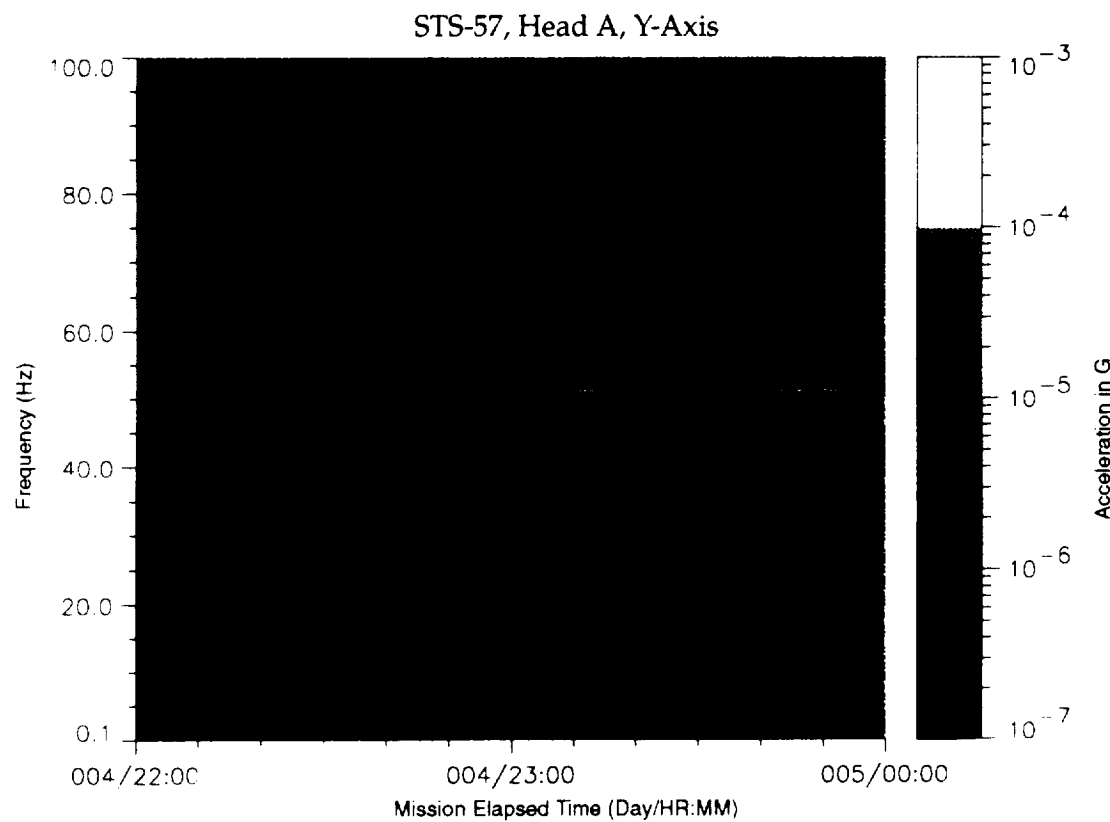


Figure B-195: SPACEHAB-1, Forward Bulkhead T-Beam

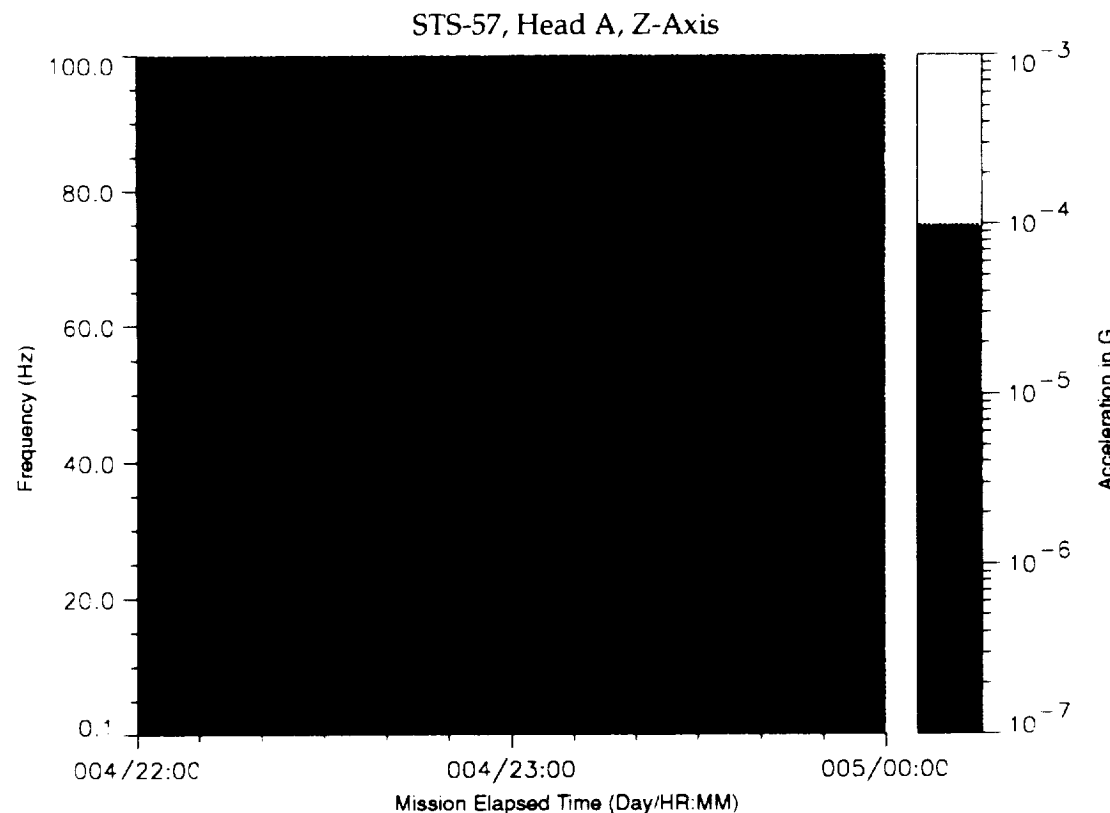


Figure B-196: SPACEHAB-1, Forward Bulkhead T-Beam

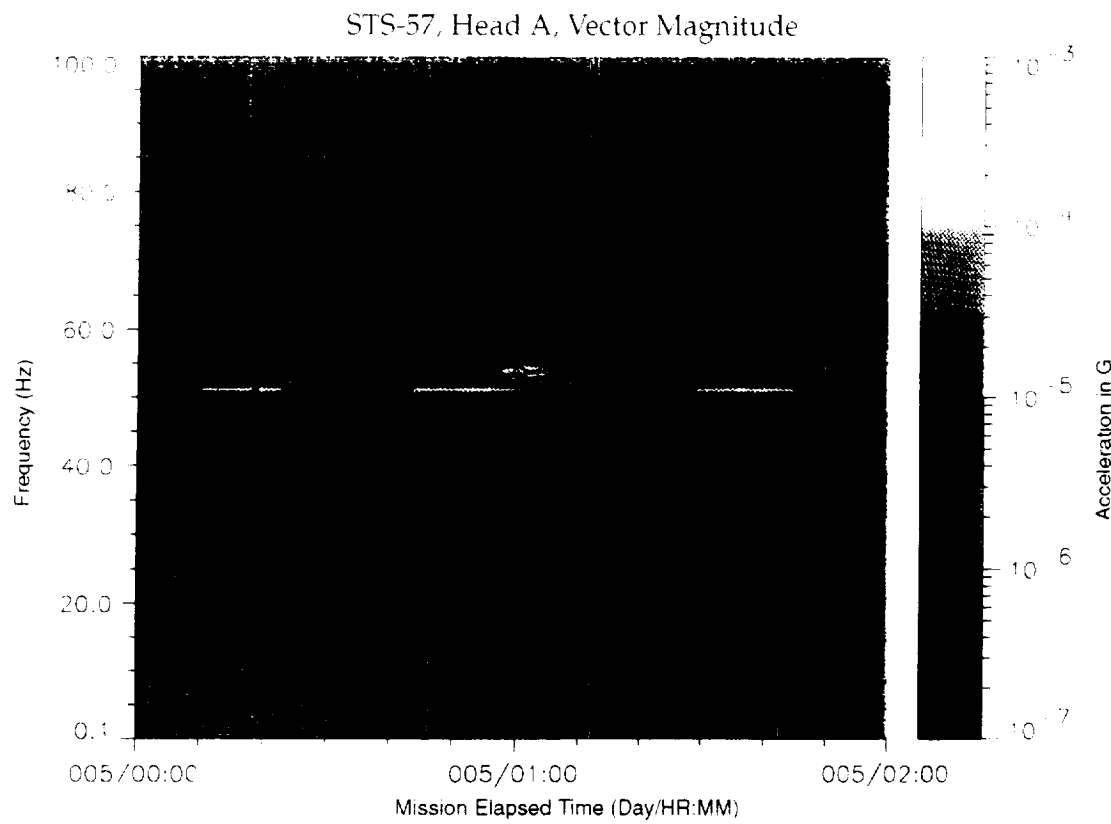


Figure B-197: SPACEHAB-1, Forward Bulkhead T-Beam

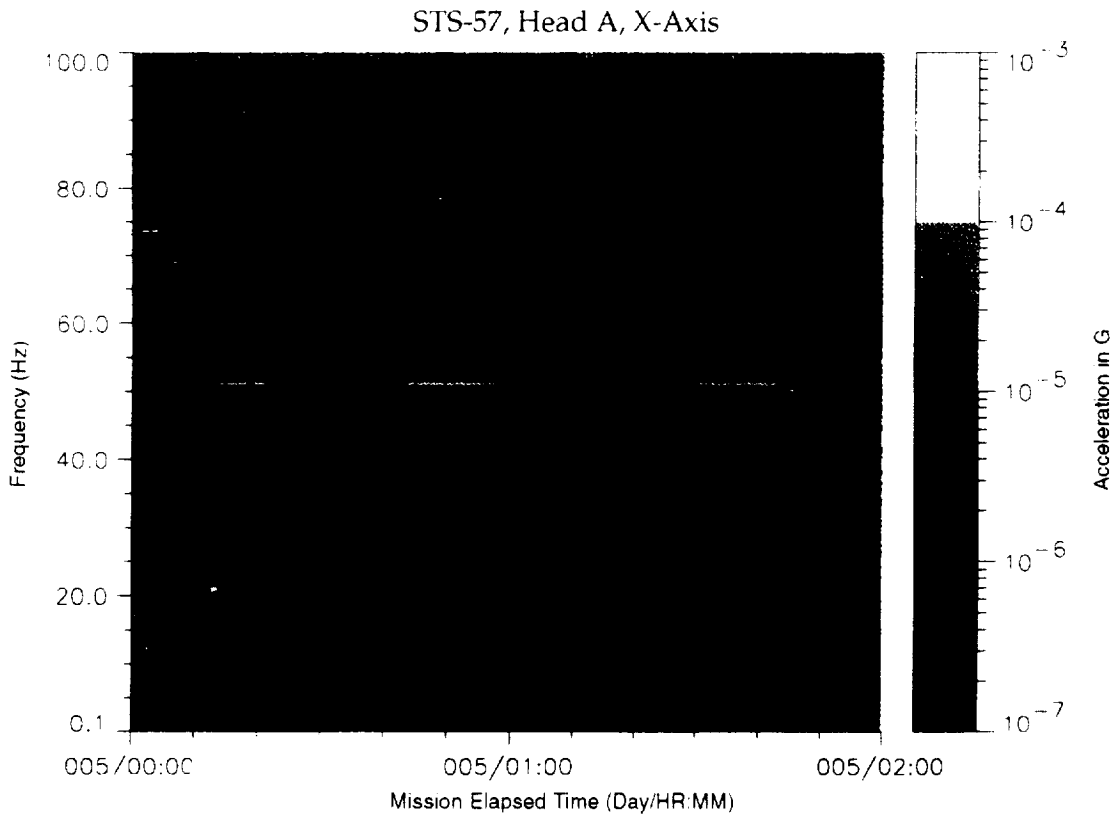


Figure B-198: SPACEHAB-1, Forward Bulkhead T-Beam

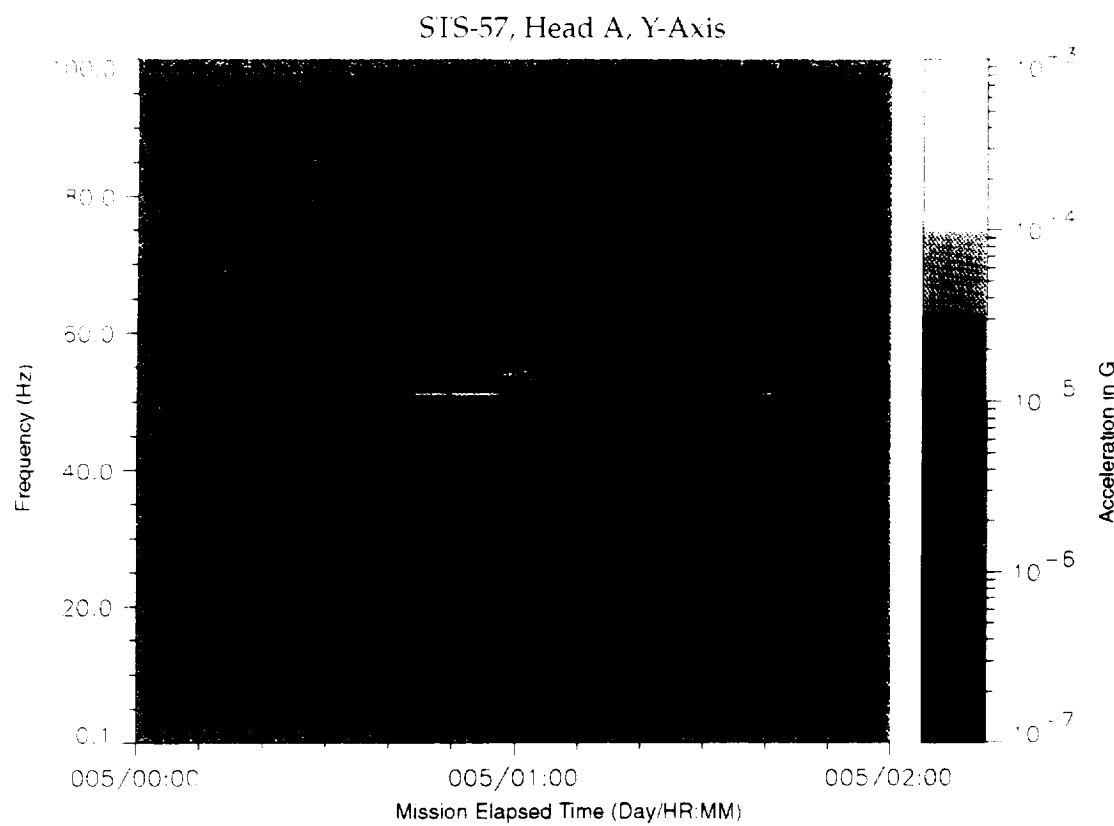


Figure B-199: SPACEHAB-1, Forward Bulkhead T-Beam

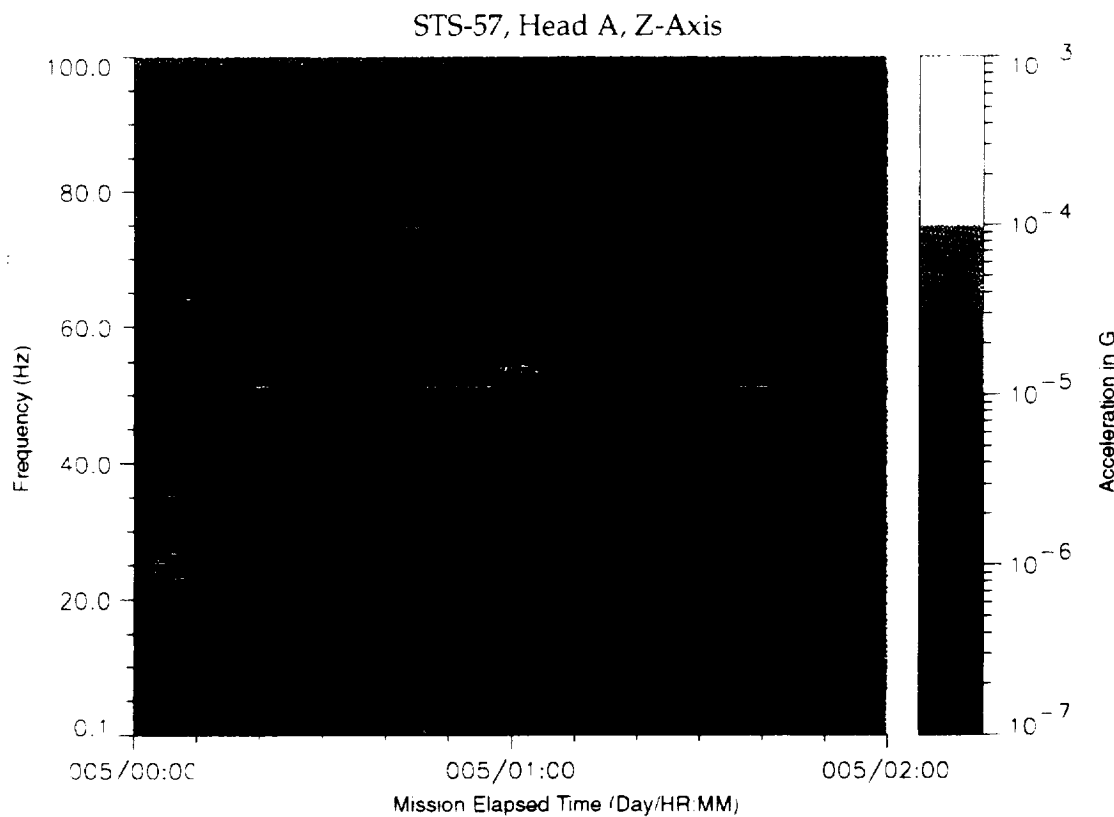


Figure B-200: SPACEHAB-1, Forward Bulkhead T-Beam

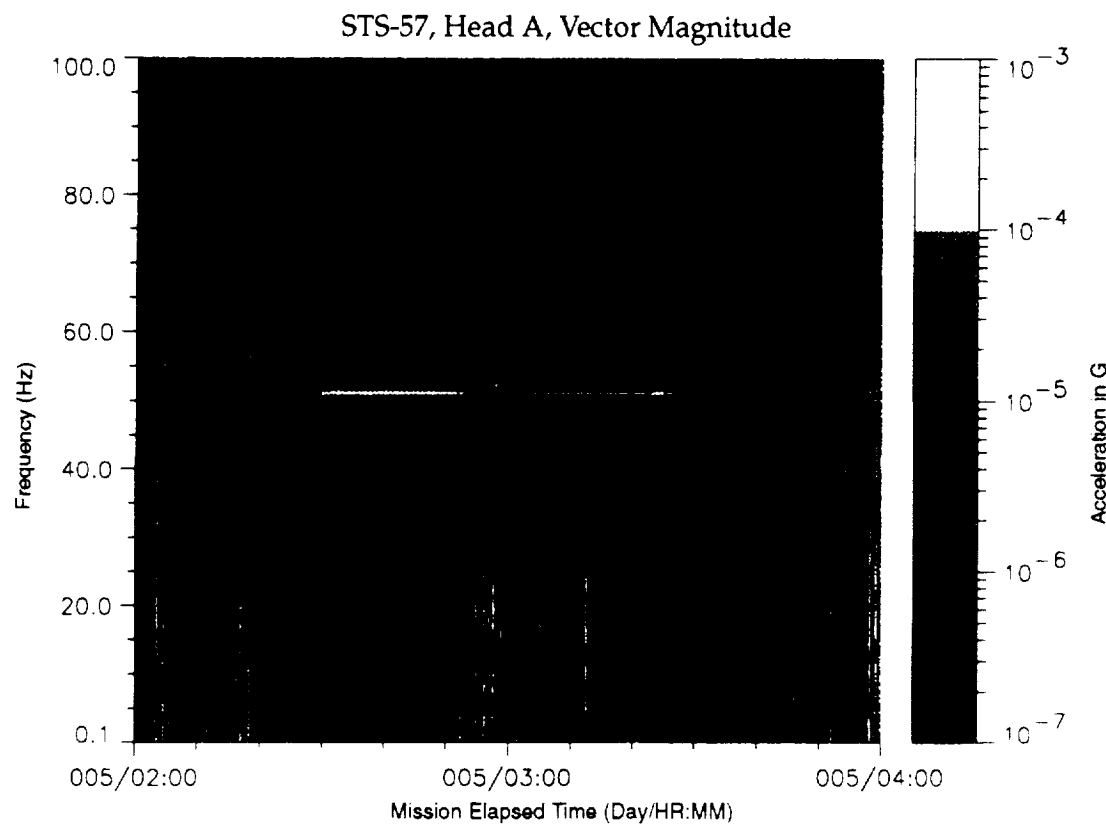


Figure B-201: SPACEHAB-1, Forward Bulkhead T-Beam

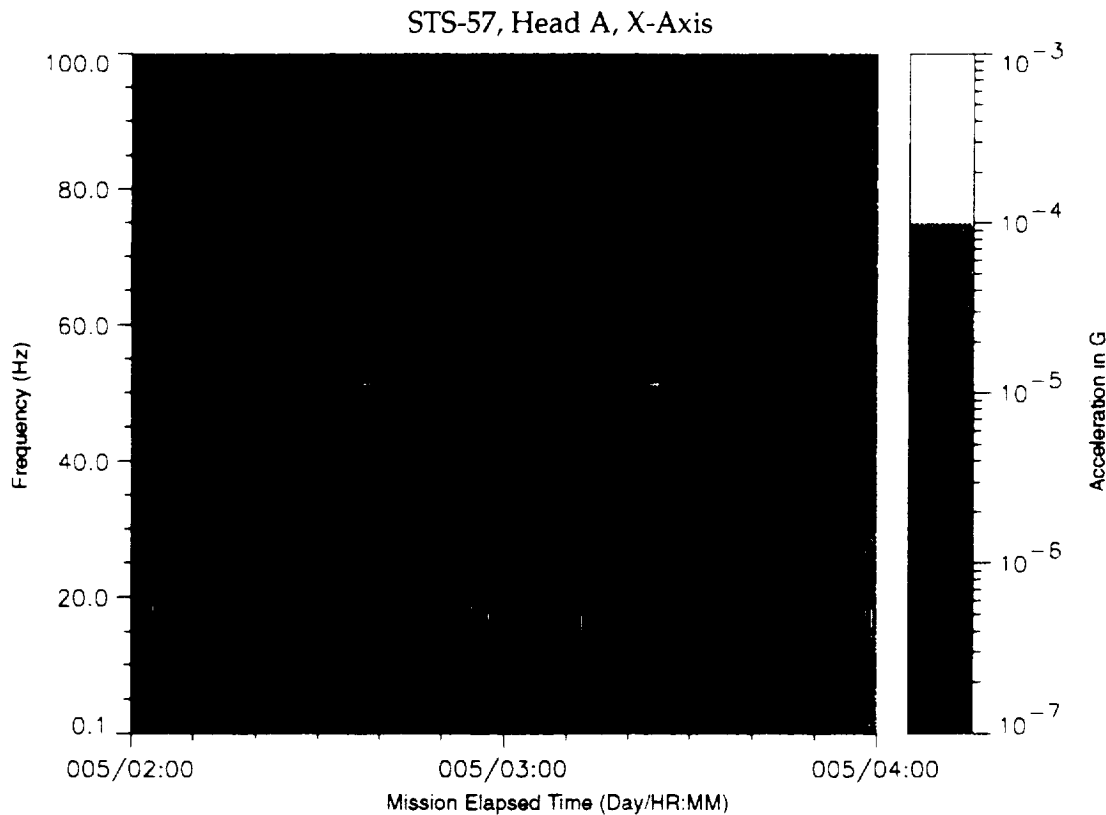


Figure B-202: SPACEHAB-1, Forward Bulkhead T-Beam

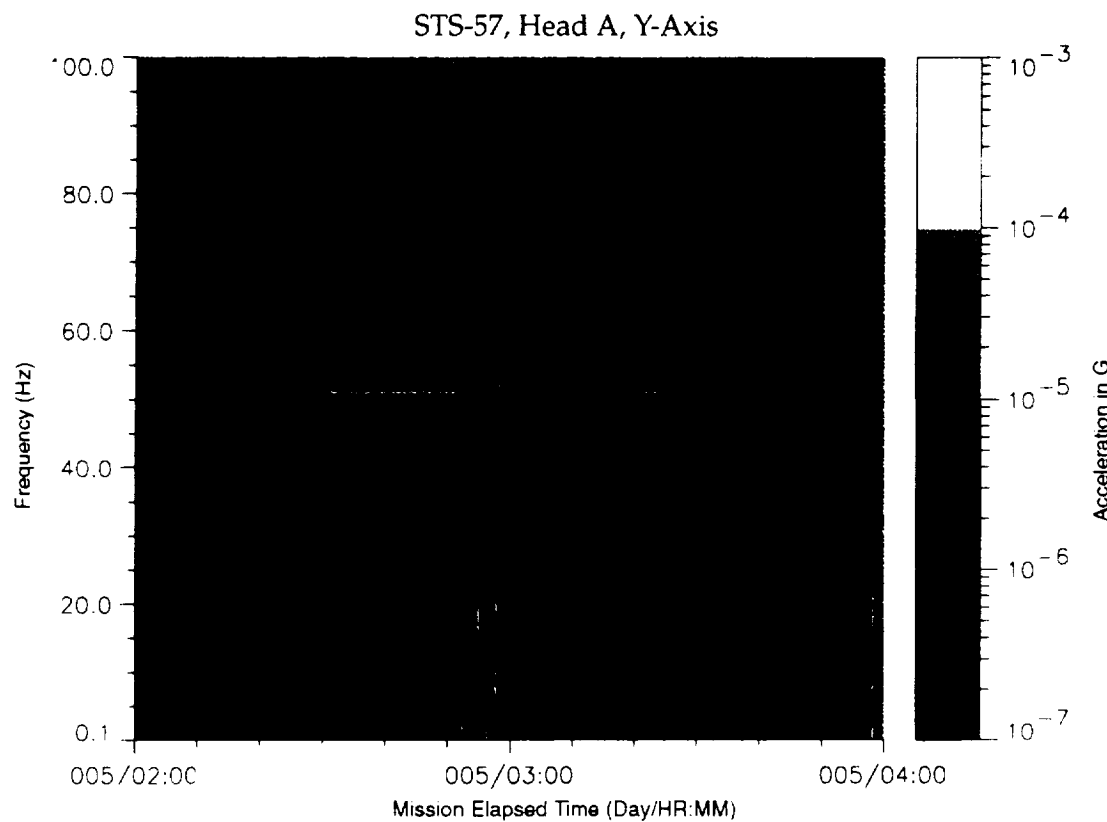


Figure B-203: SPACEHAB-1, Forward Bulkhead T-Beam

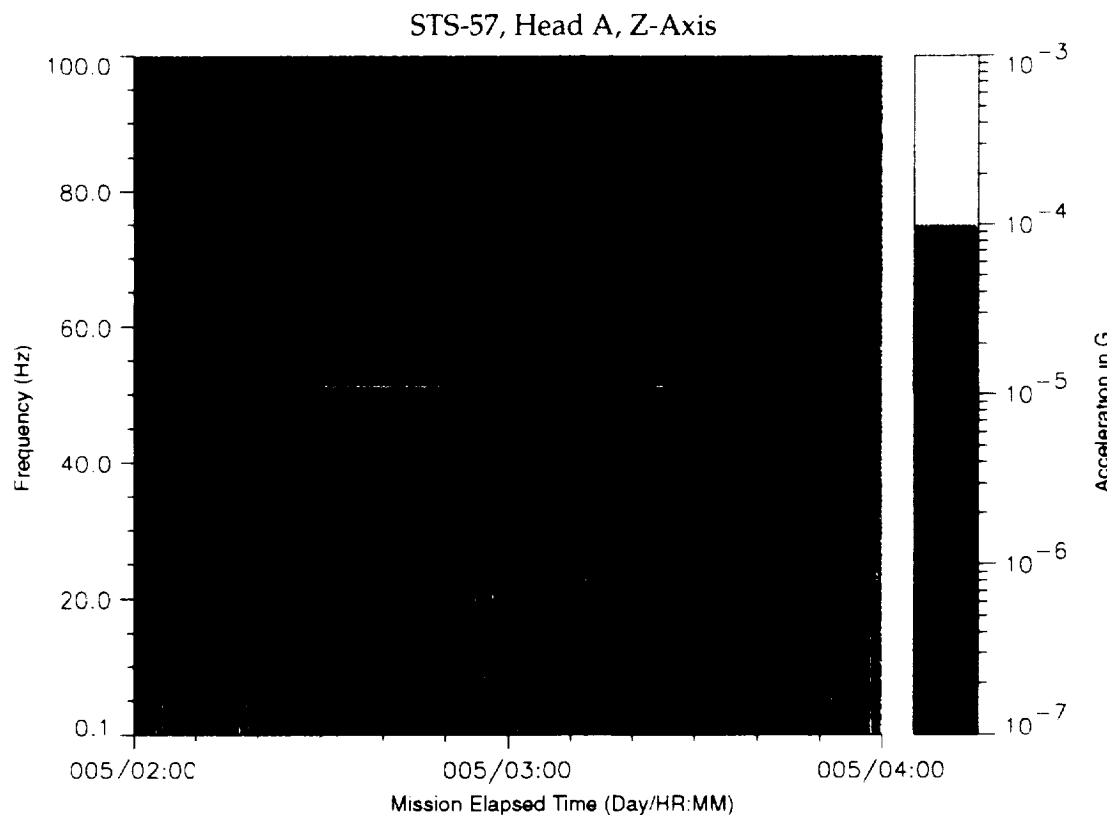


Figure B-204: SPACEHAB-1, Forward Bulkhead T-Beam

STS-57, Head A, Vector Magnitude

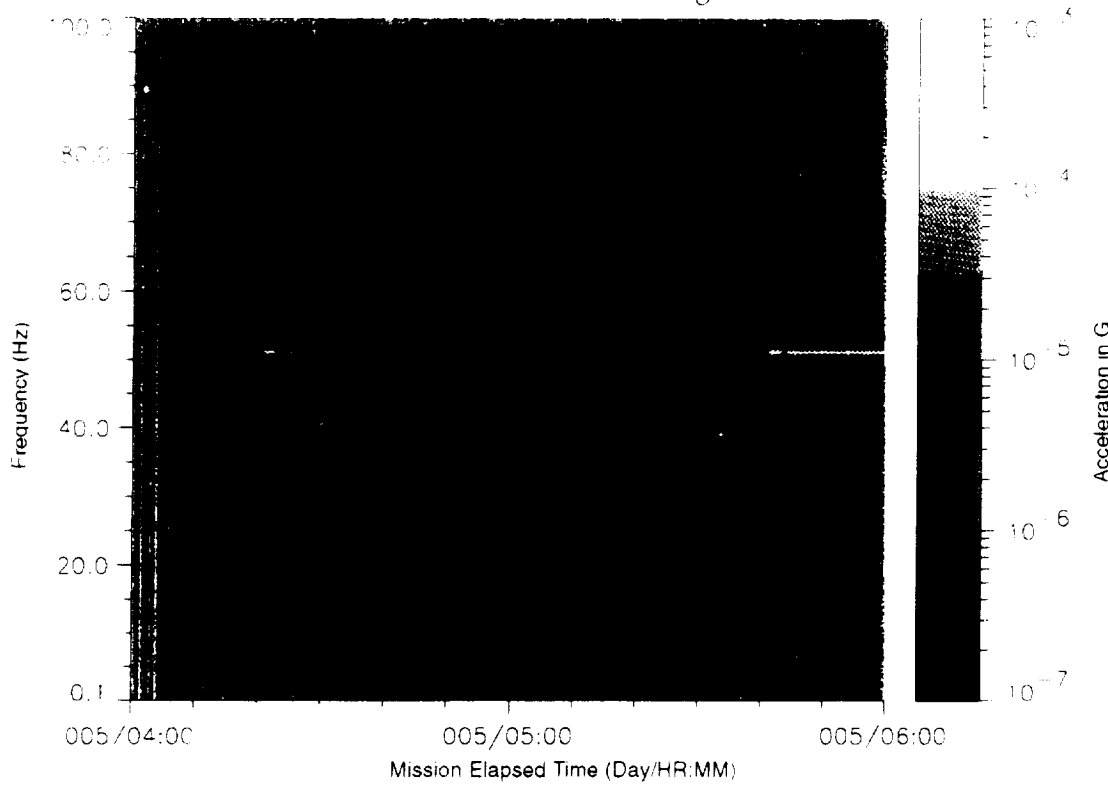


Figure B-205: SPACEHAB-1, Forward Bulkhead T-Beam

STS-57, Head A, X-Axis

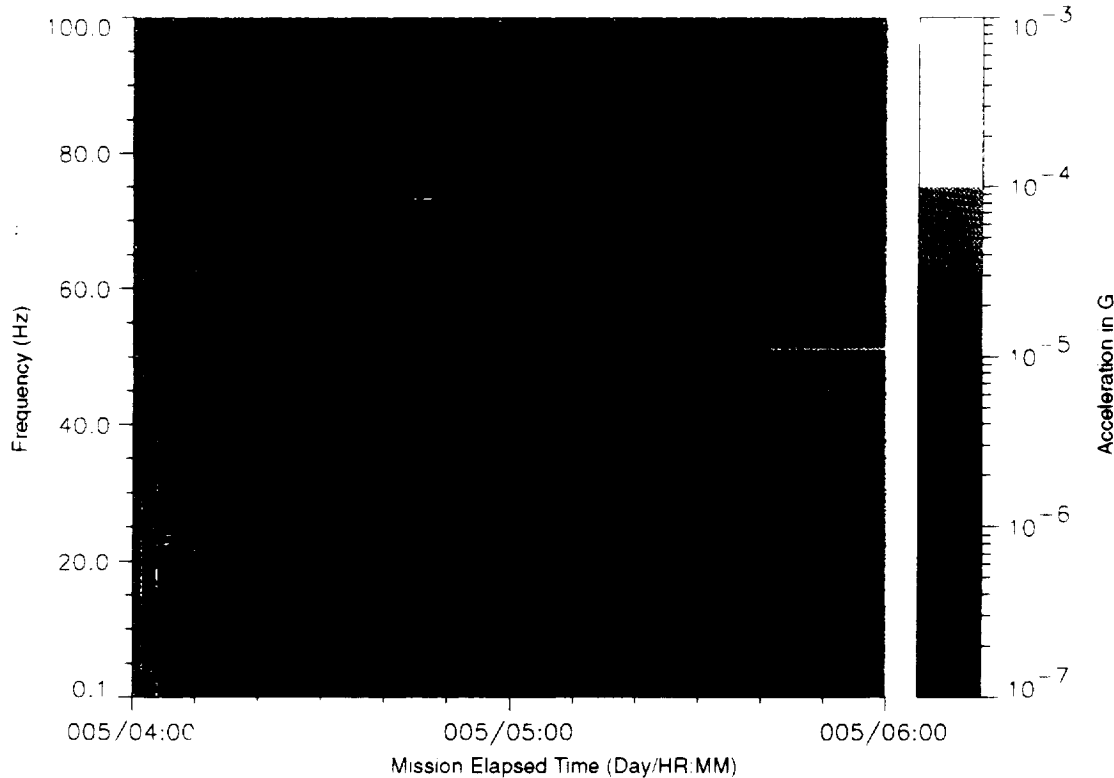


Figure B-206: SPACEHAB-1, Forward Bulkhead T-Beam

~~PROGRESSIVE PAGE BLANK NOT FILMED~~

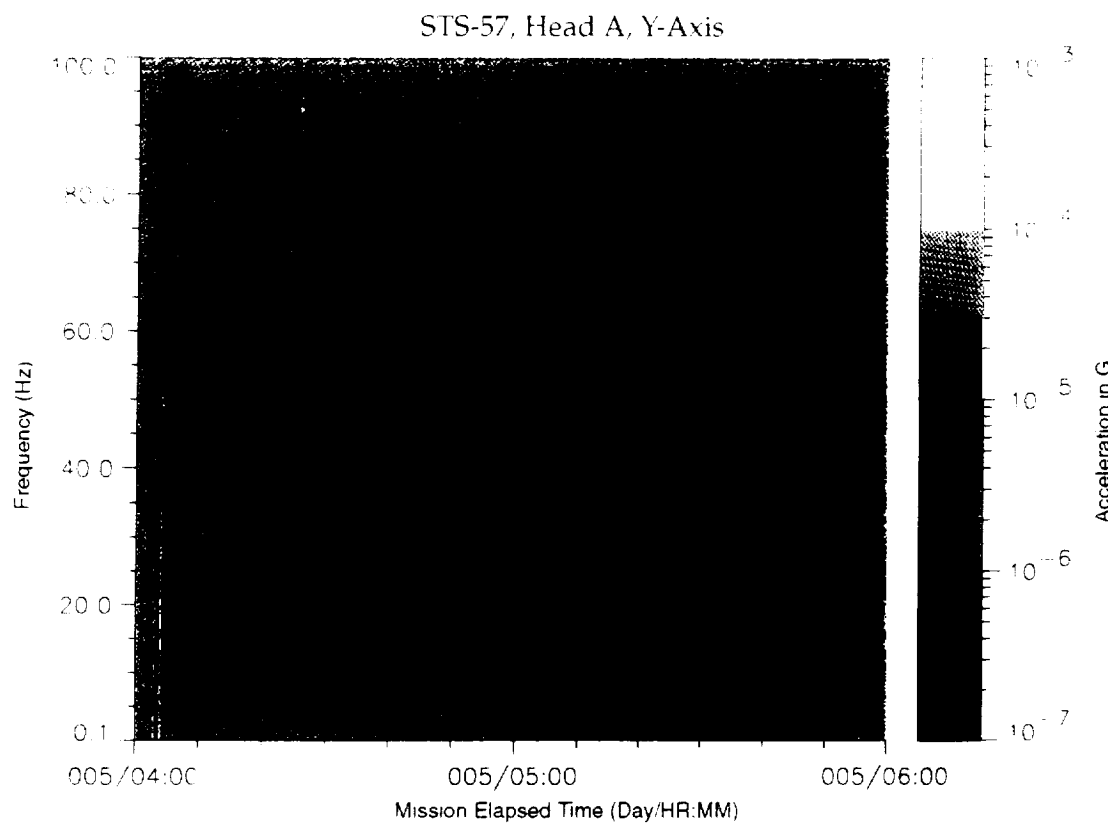


Figure B-207: SPACEHAB-1, Forward Bulkhead T-Beam

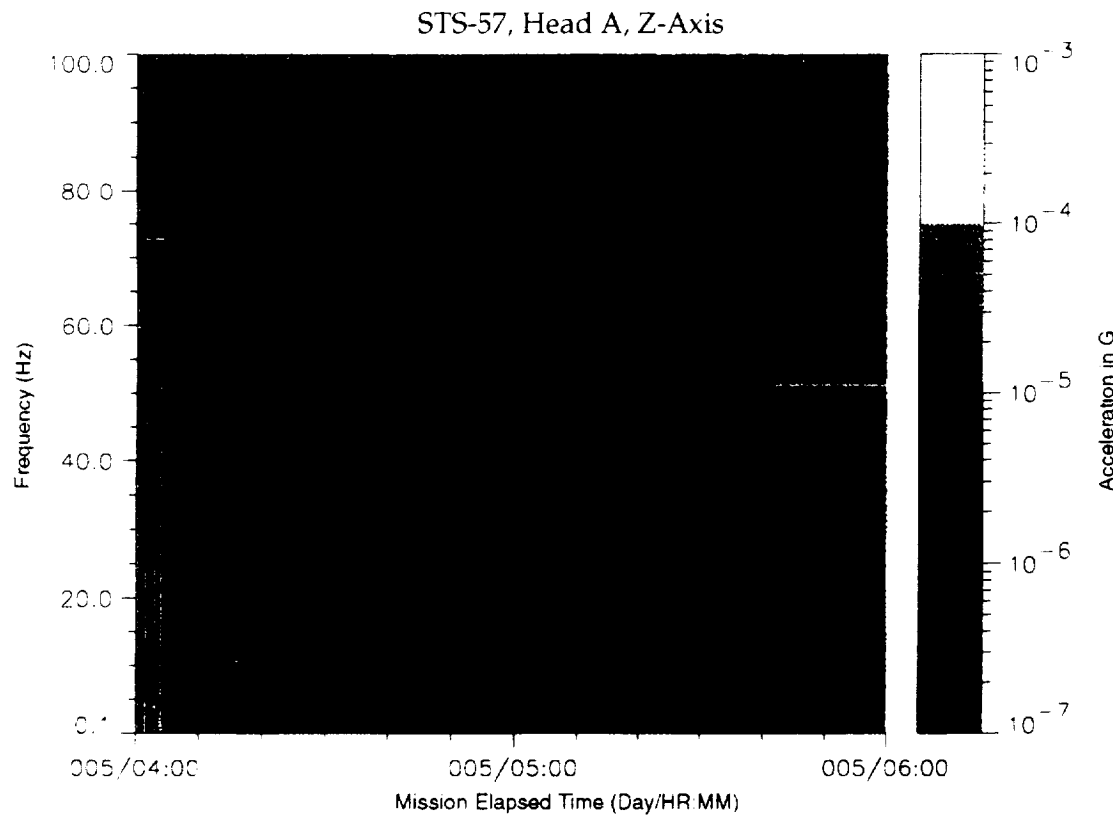


Figure B-208: SPACEHAB-1, Forward Bulkhead T-Beam

~~PROBLEMS, PAGE BLANK NOT FILMED~~

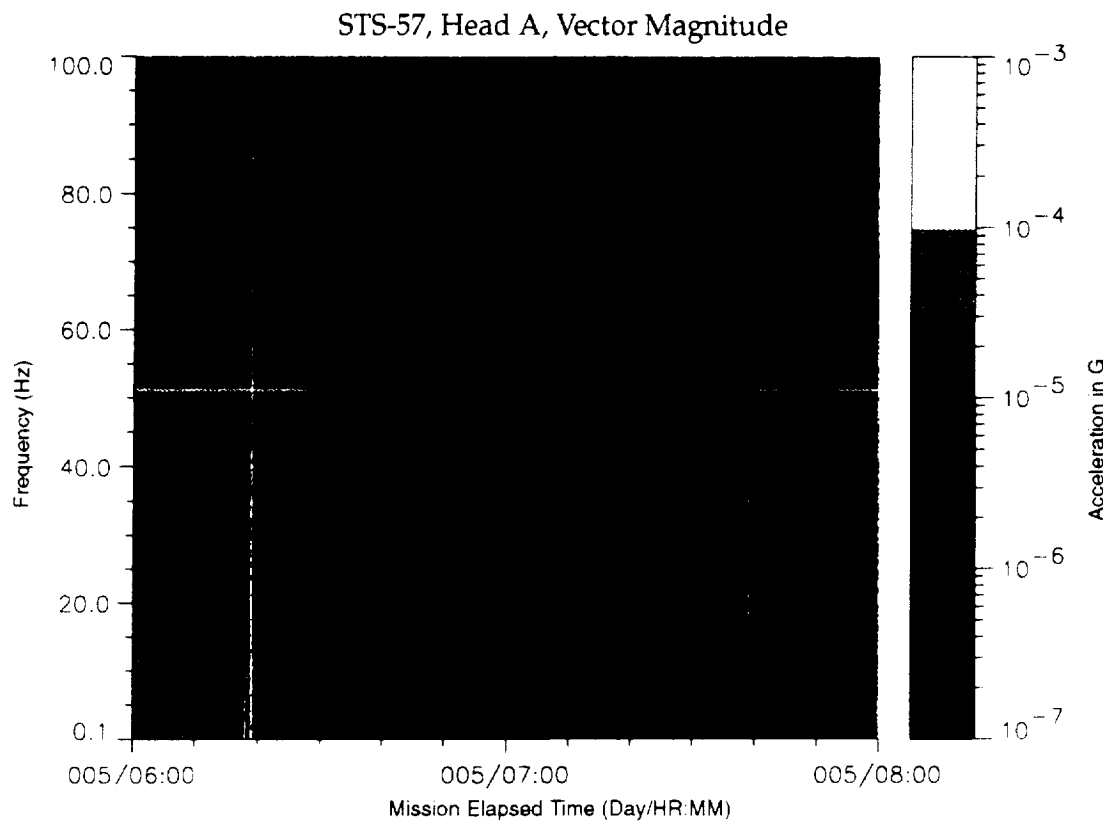


Figure B-209: SPACEHAB-1, Forward Bulkhead T-Beam

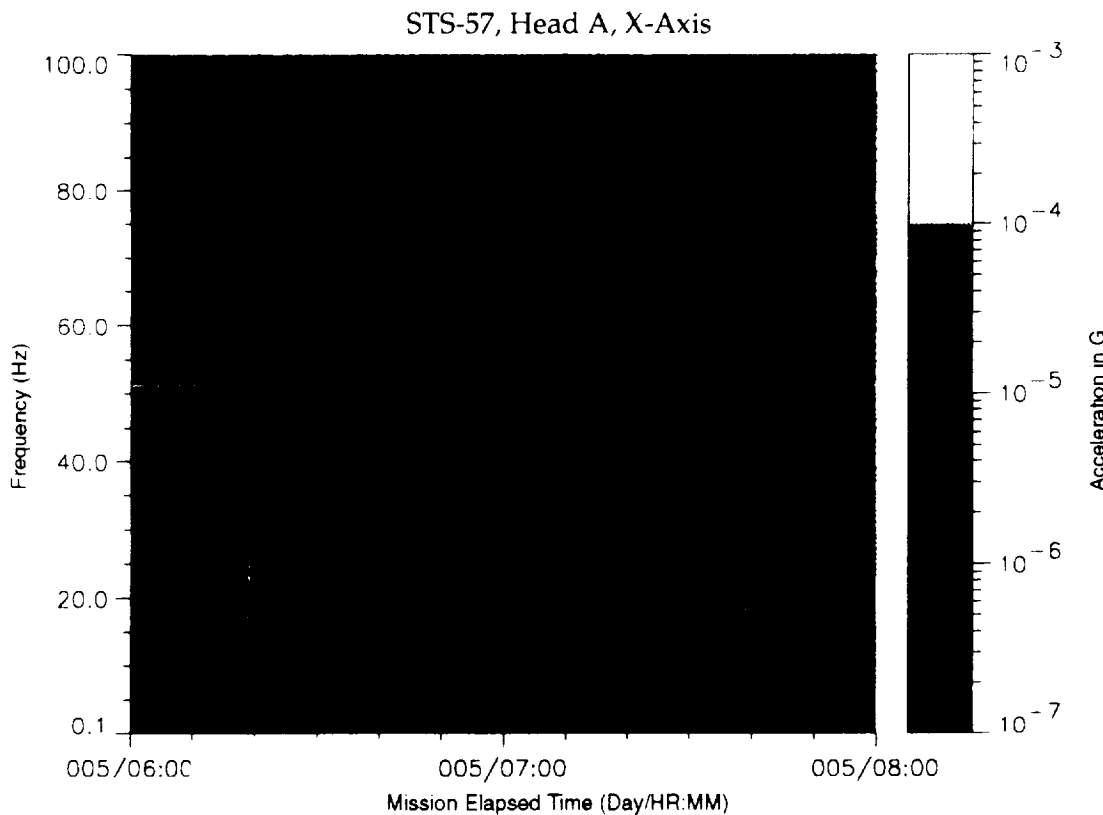


Figure B-210: SPACEHAB-1, Forward Bulkhead T-Beam

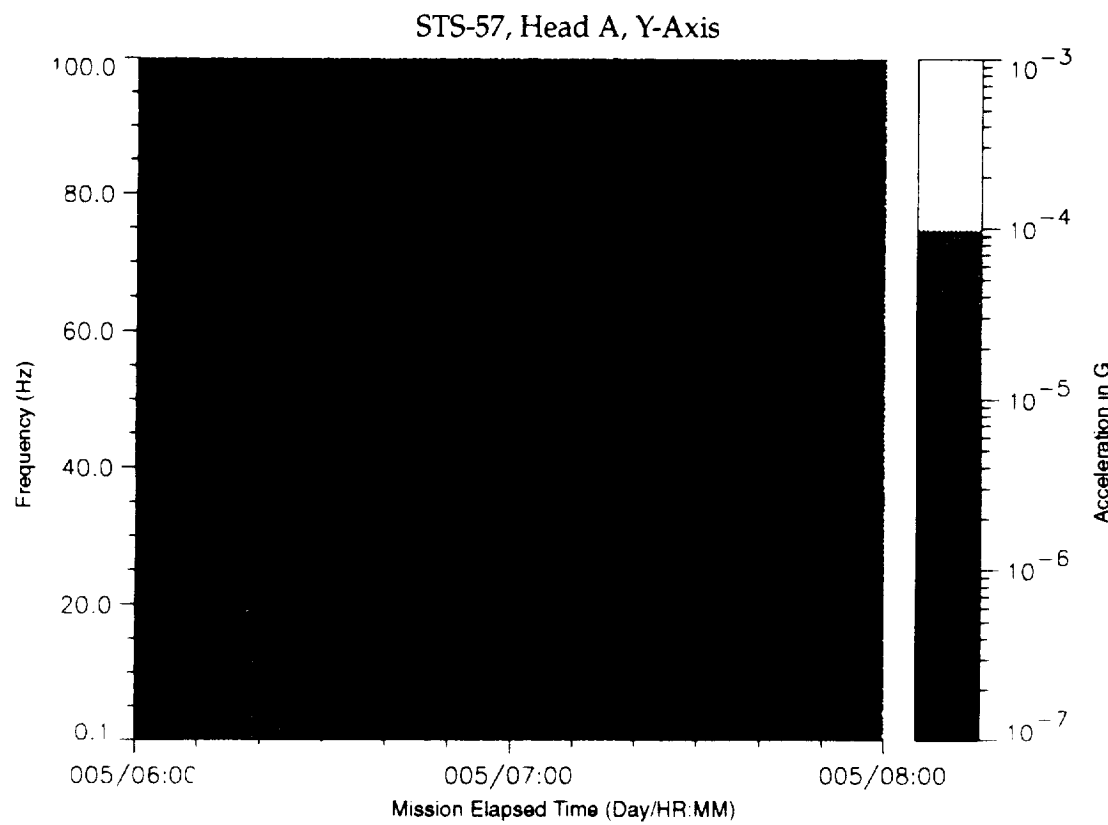


Figure B-211: SPACEHAB-1, Forward Bulkhead T-Beam

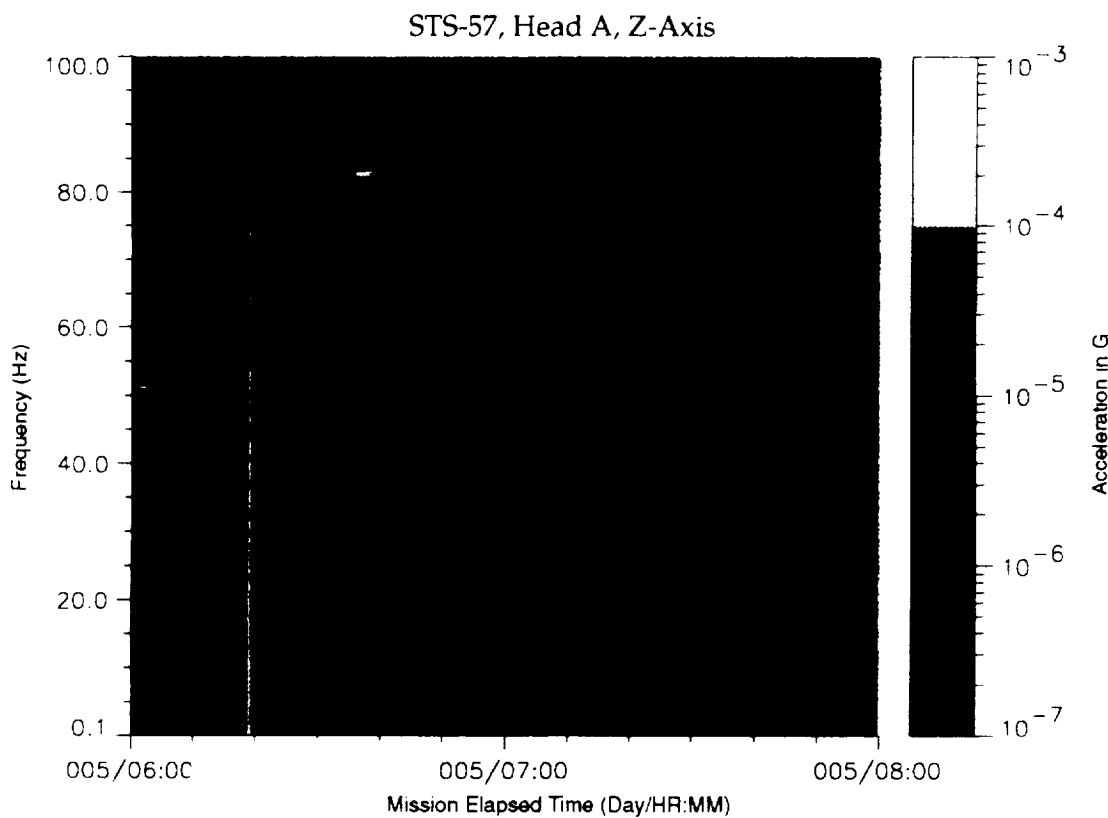


Figure B-212: SPACEHAB-1, Forward Bulkhead T-Beam

STS-57, Head A, Vector Magnitude

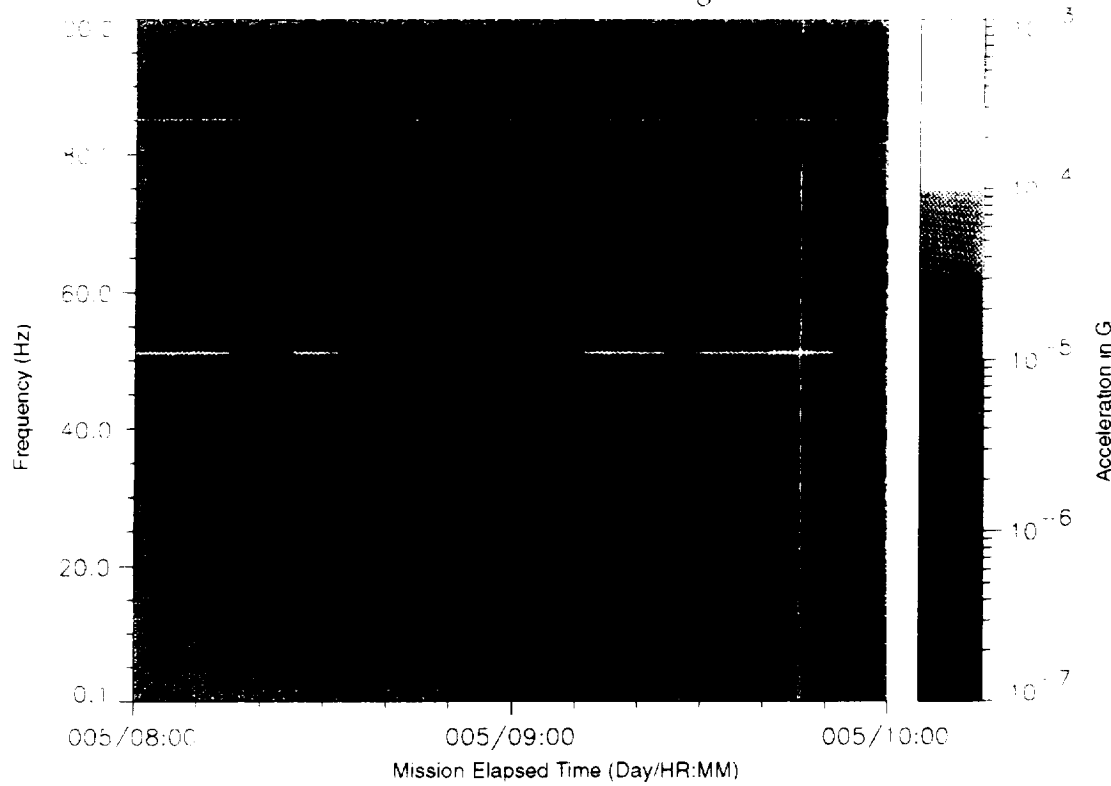


Figure B-213: SPACEHAB-1, Forward Bulkhead T-Beam

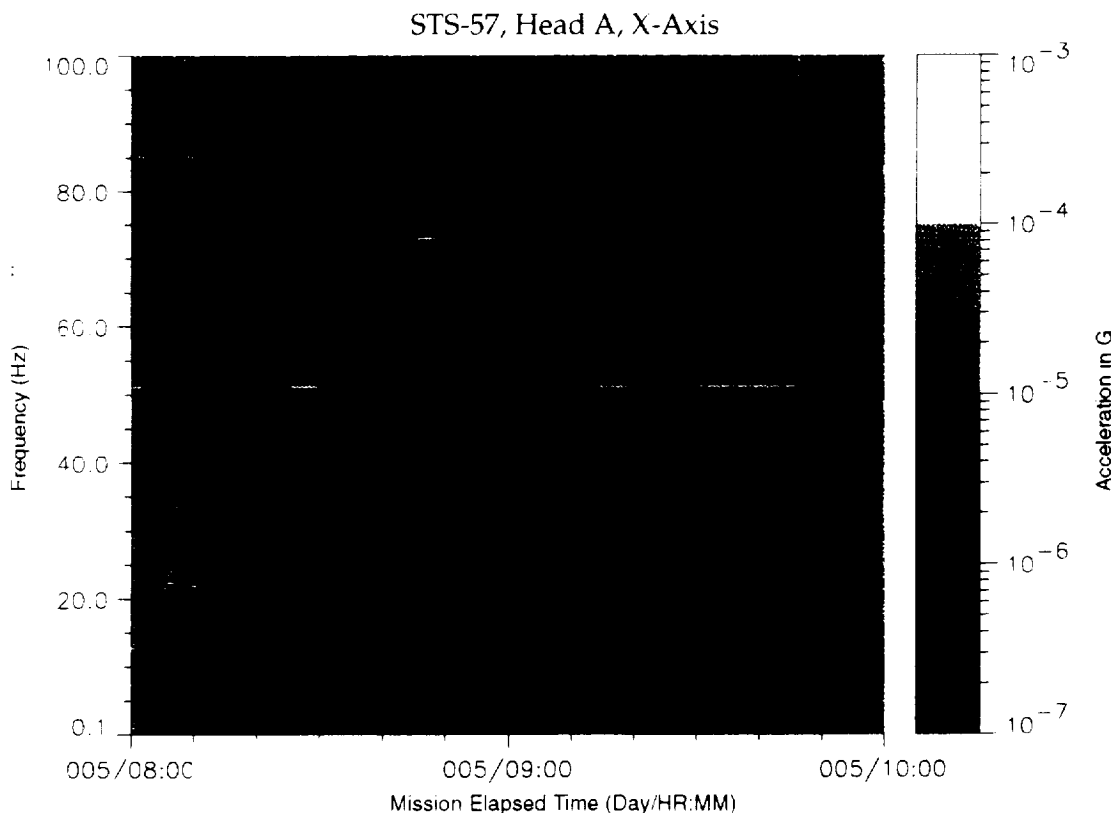


Figure B-214: SPACEHAB-1, Forward Bulkhead T-Beam

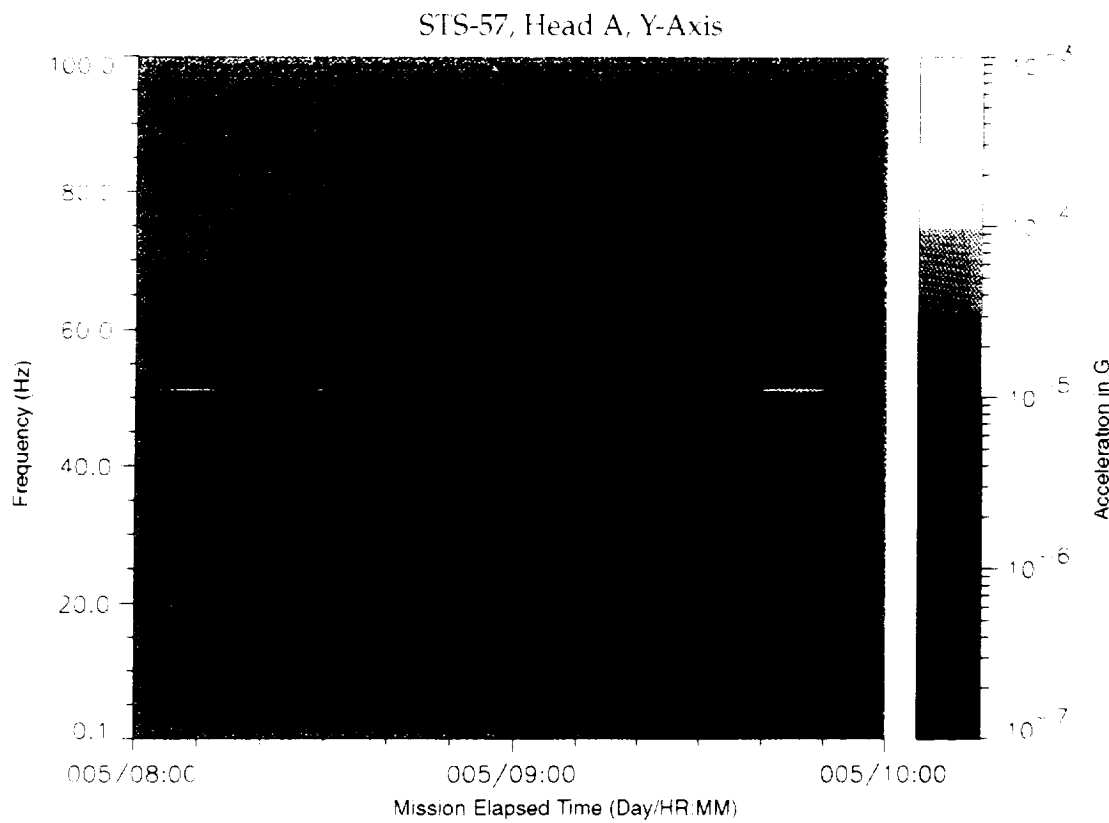


Figure B-215: SPACEHAB-1, Forward Bulkhead T-Beam

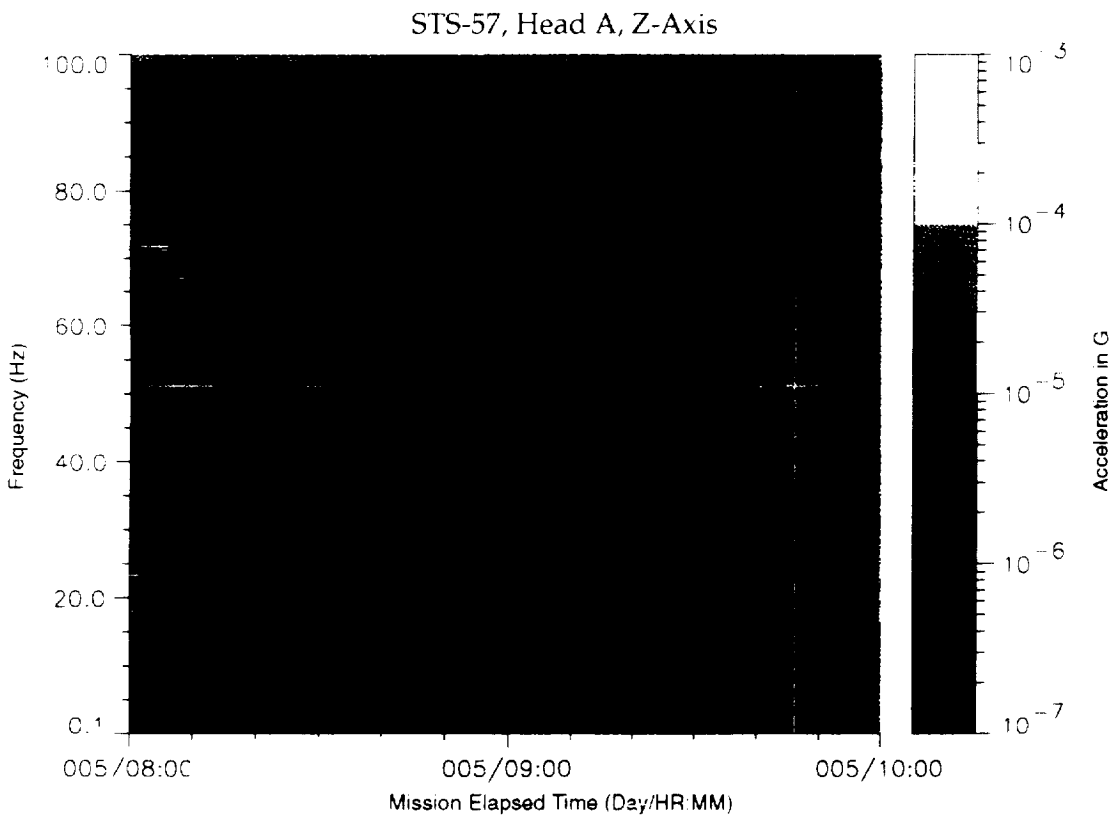


Figure B-216: SPACEHAB-1, Forward Bulkhead T-Beam

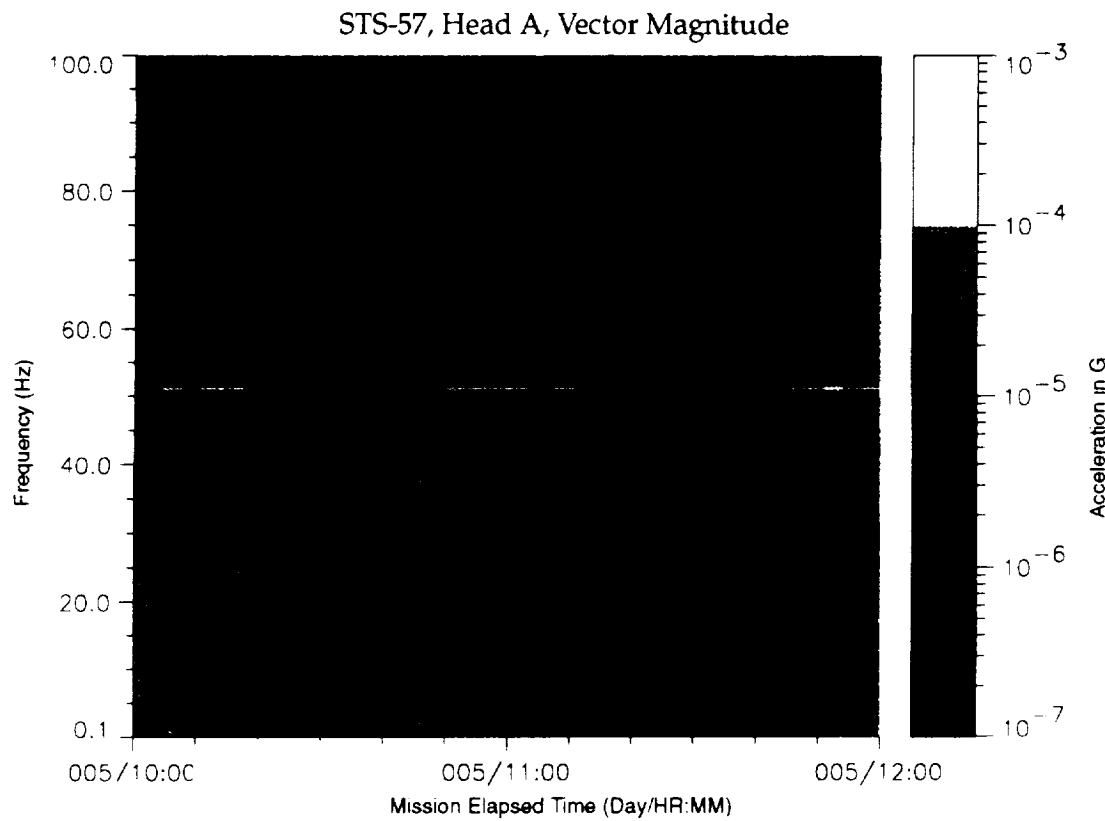


Figure B-217: SPACEHAB-1, Forward Bulkhead T-Beam

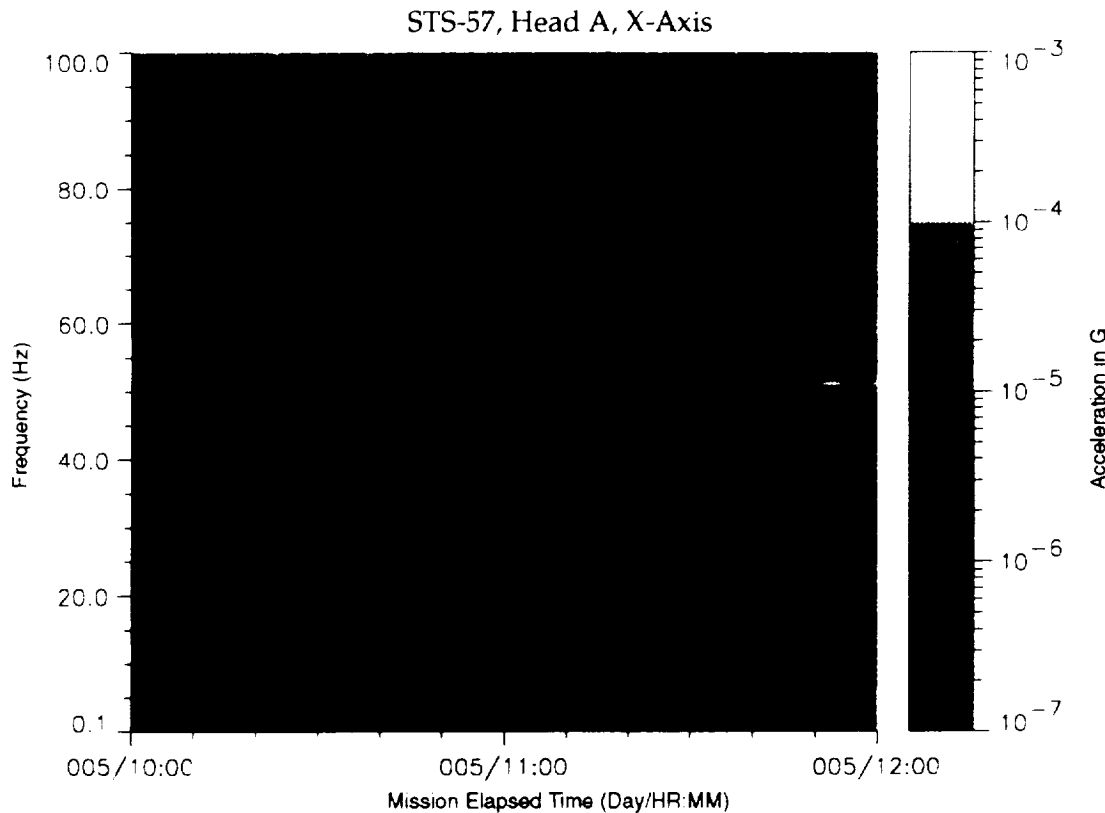


Figure B-218: SPACEHAB-1, Forward Bulkhead T-Beam

PRECEDING PAGE BLANK NOT FLOWED

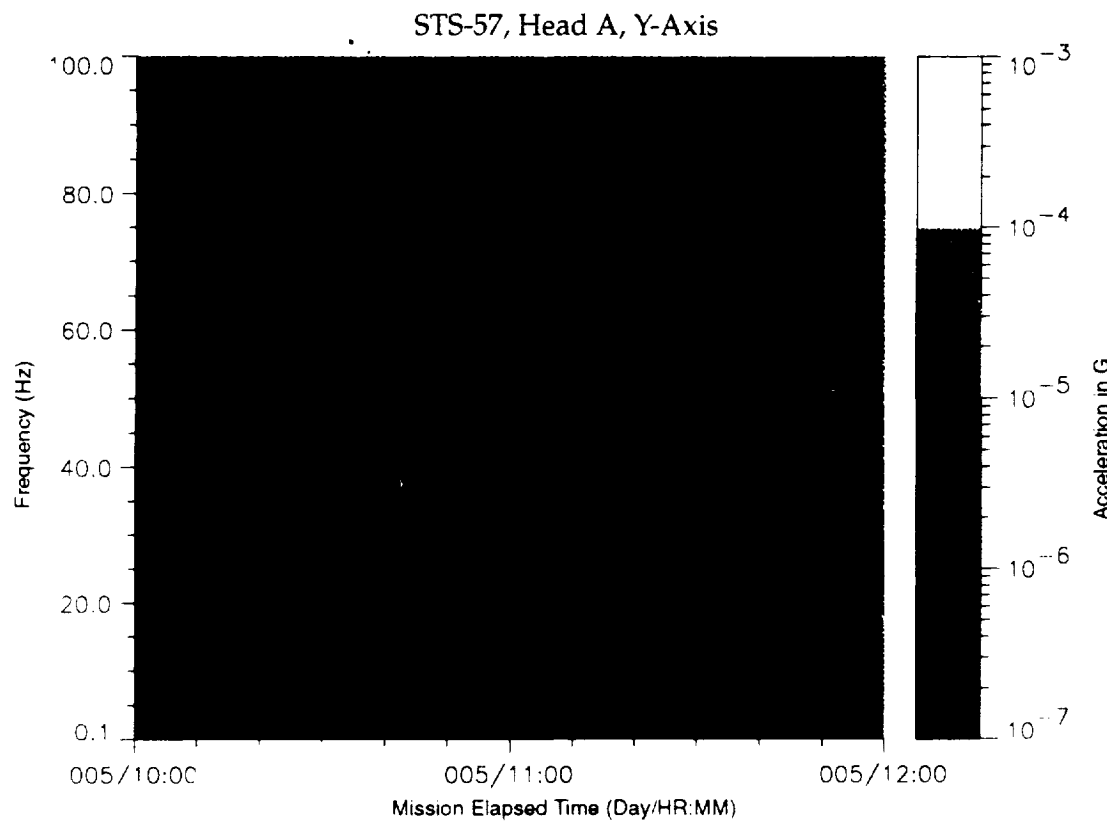


Figure B-219: SPACEHAB-1, Forward Bulkhead T-Beam

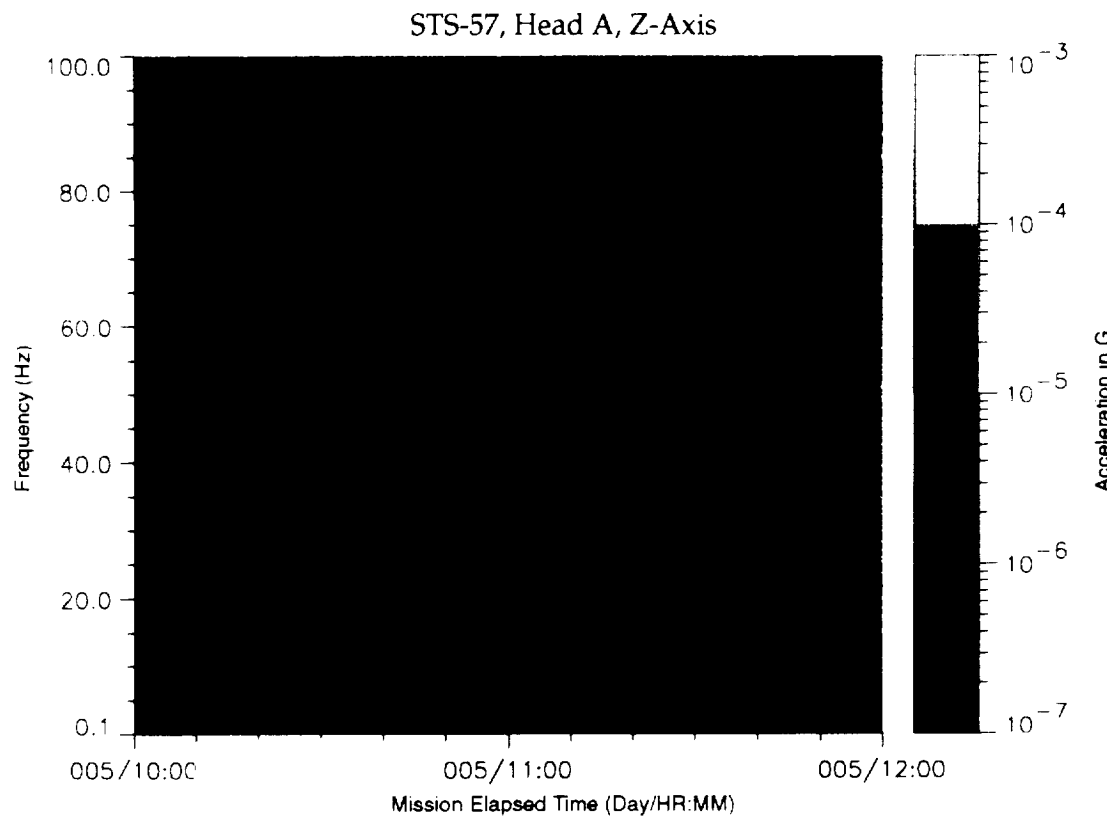


Figure B-220: SPACEHAB-1, Forward Bulkhead T-Beam

STS-57, Head A, Vector Magnitude

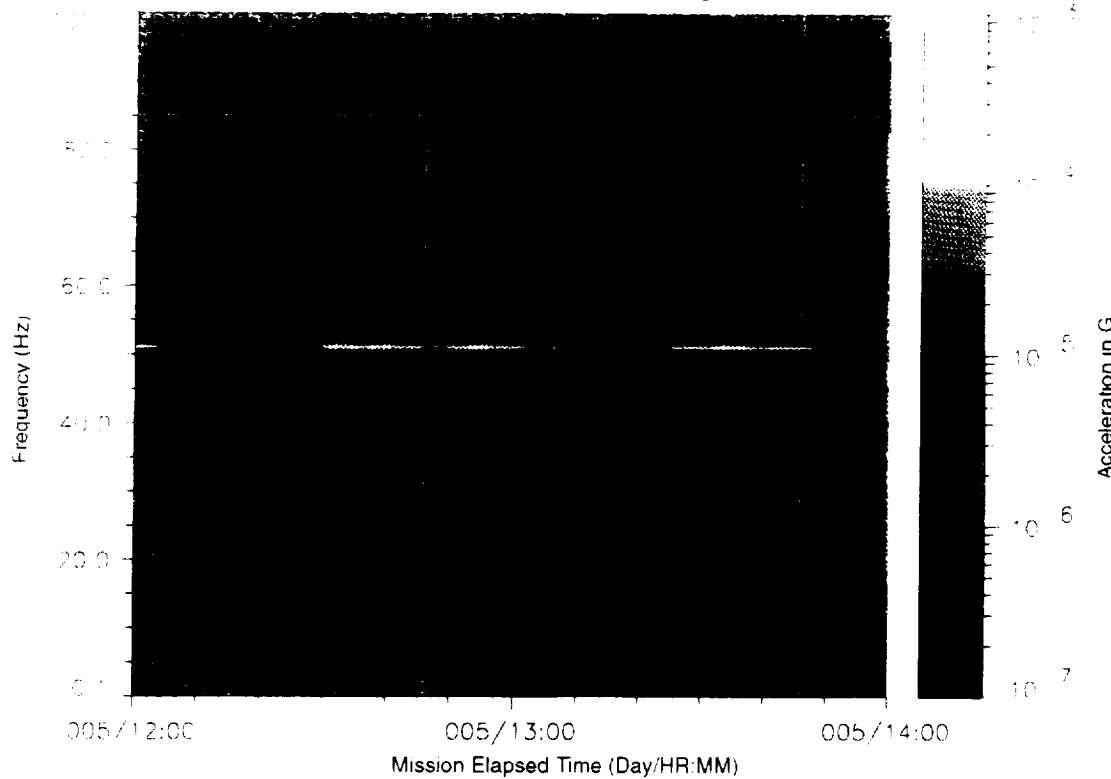


Figure B-221: SPACEHAB-1, Forward Bulkhead T-Beam

STS-57, Head A, X-Axis

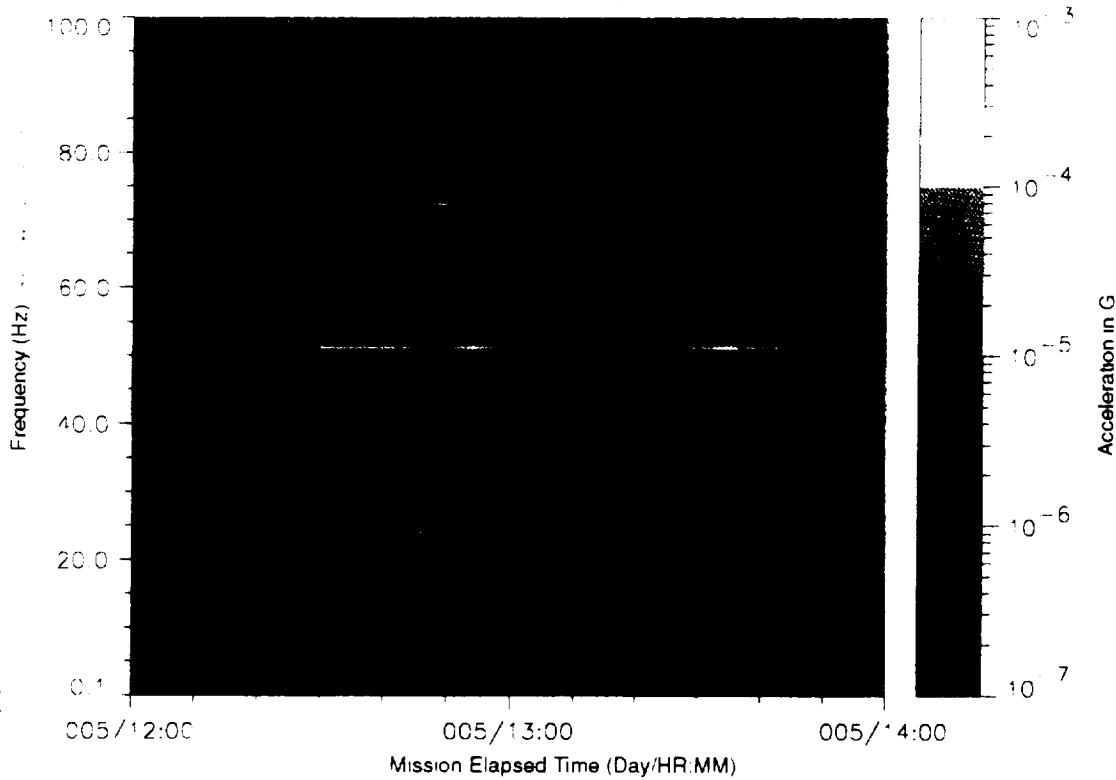


Figure B-222: SPACEHAB-1, Forward Bulkhead T-Beam

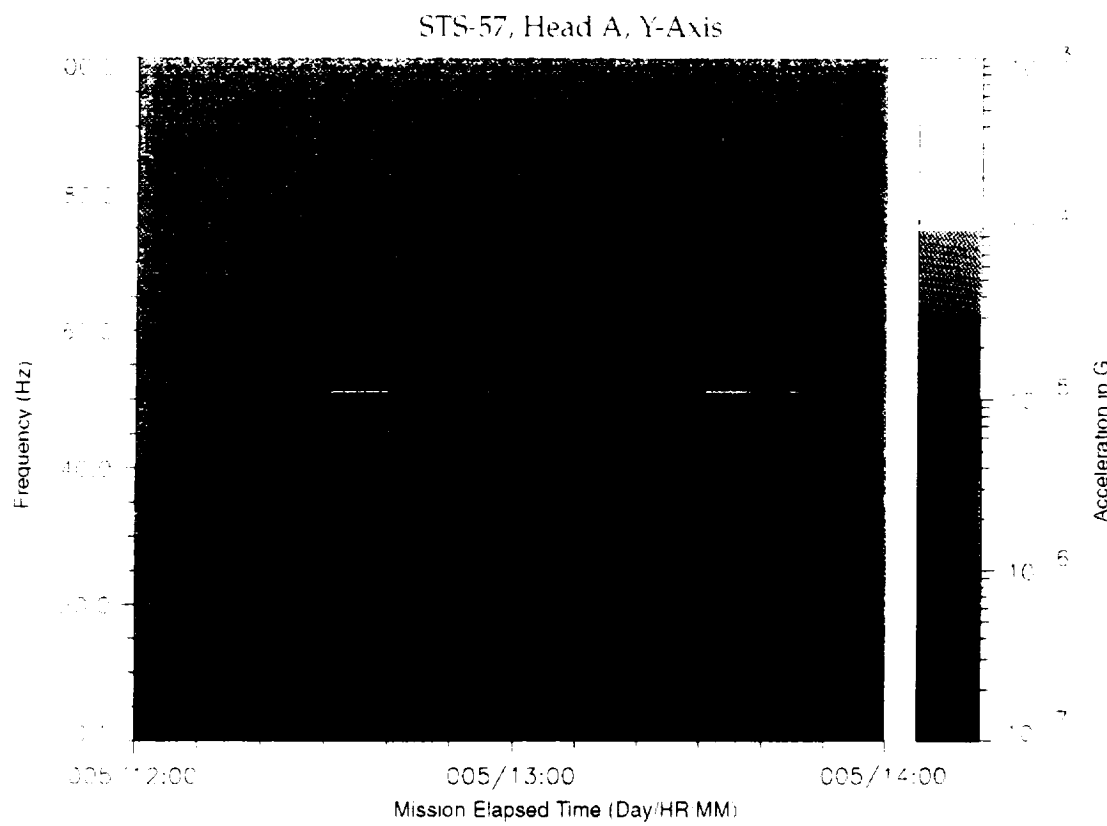


Figure B-223: SPACEHAB-1, Forward Bulkhead T-Beam

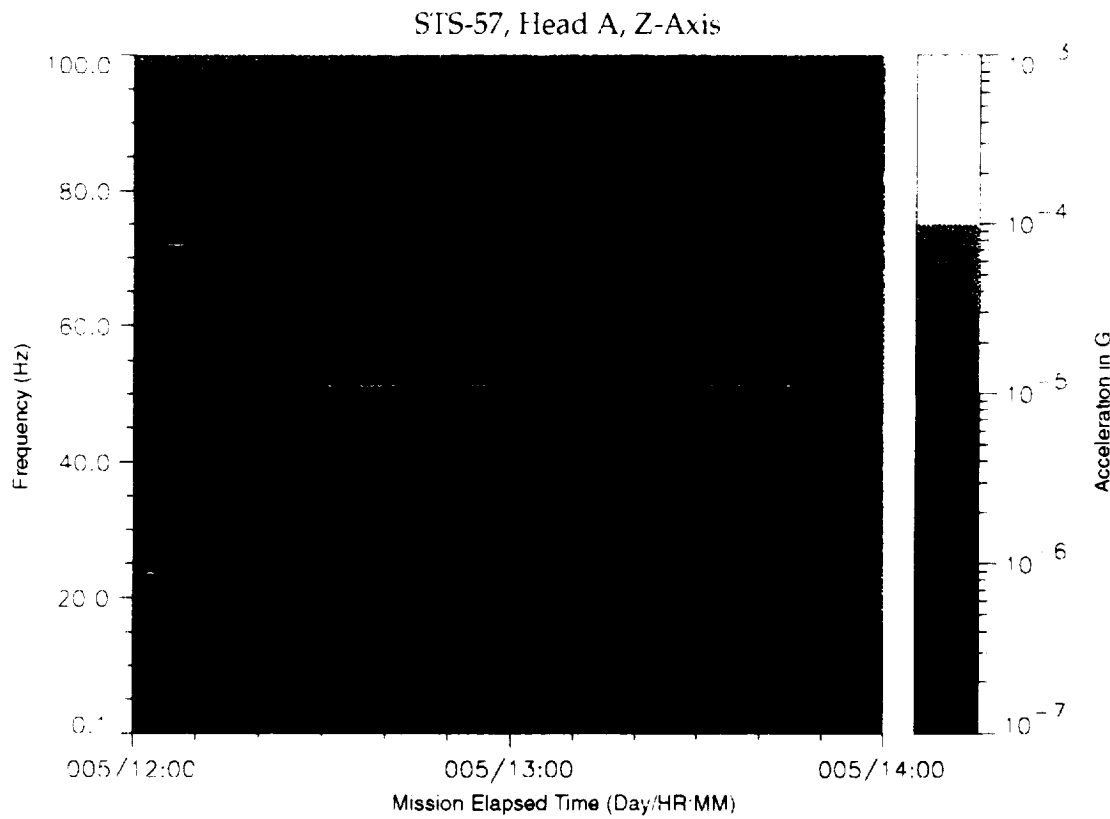


Figure B-224: SPACEHAB-1, Forward Bulkhead T-Beam

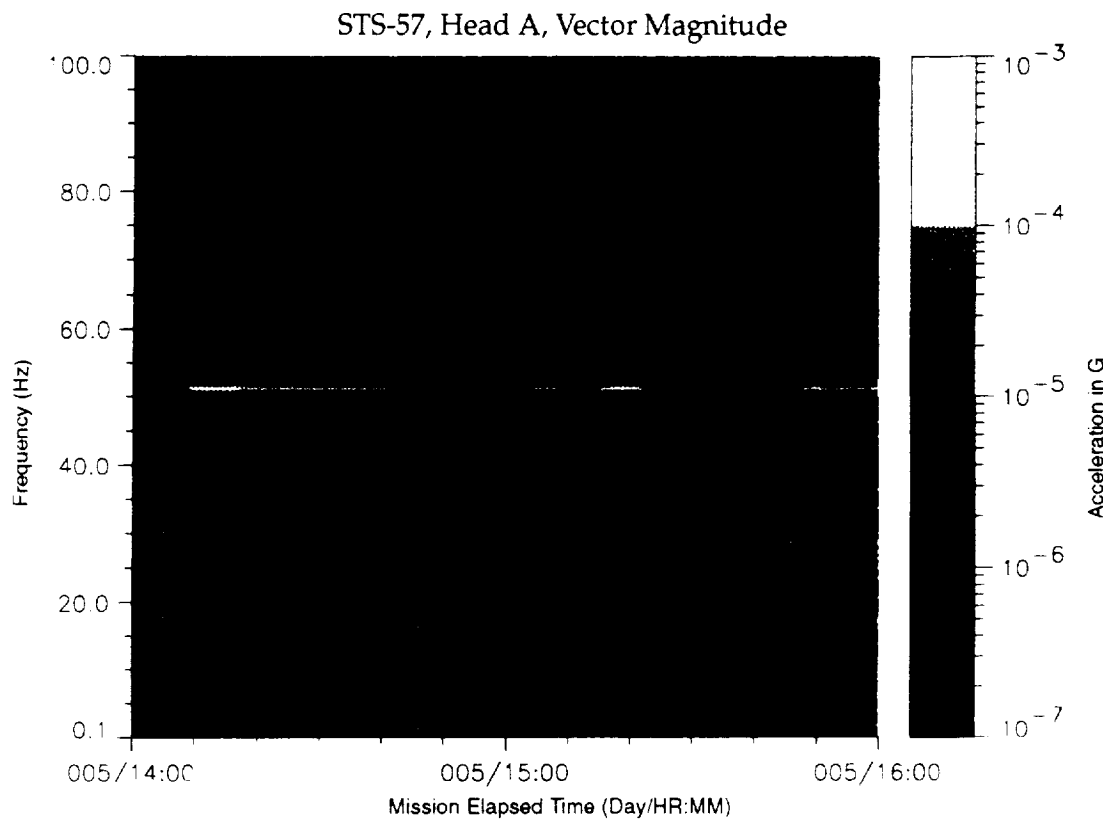


Figure B-225: SPACEHAB-1, Forward Bulkhead T-Beam

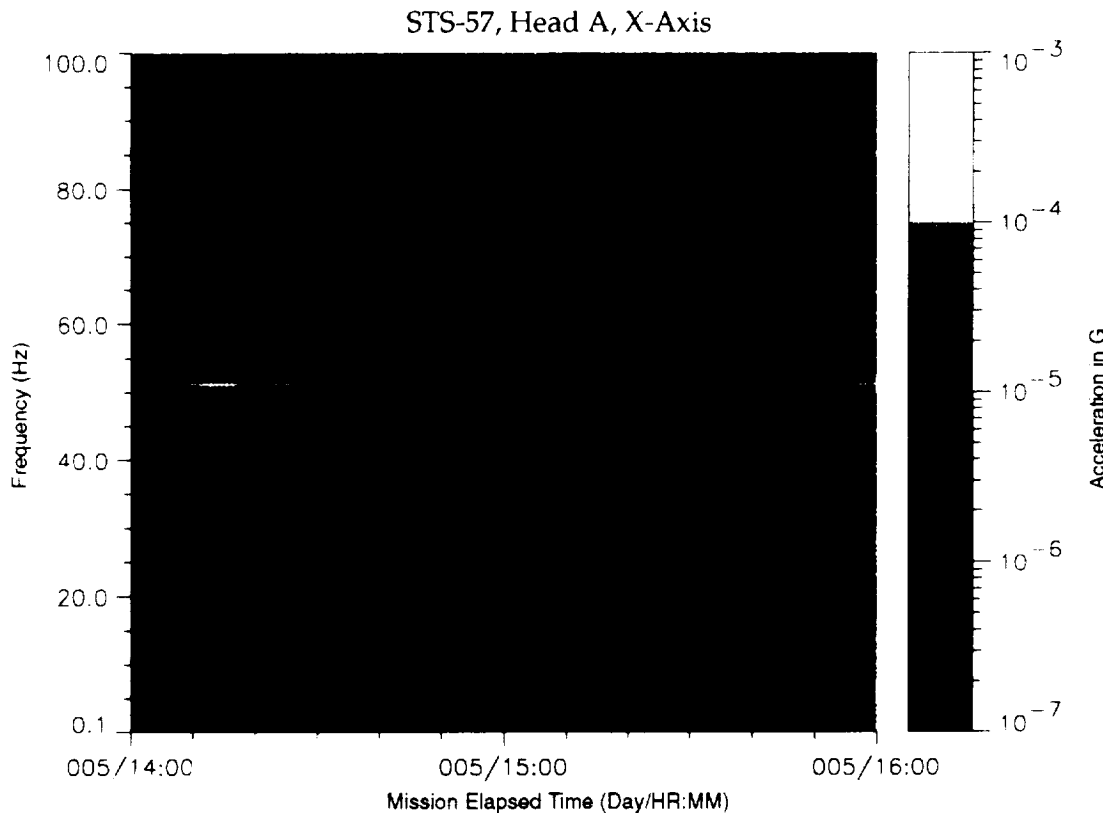


Figure B-226: SPACEHAB-1, Forward Bulkhead T-Beam

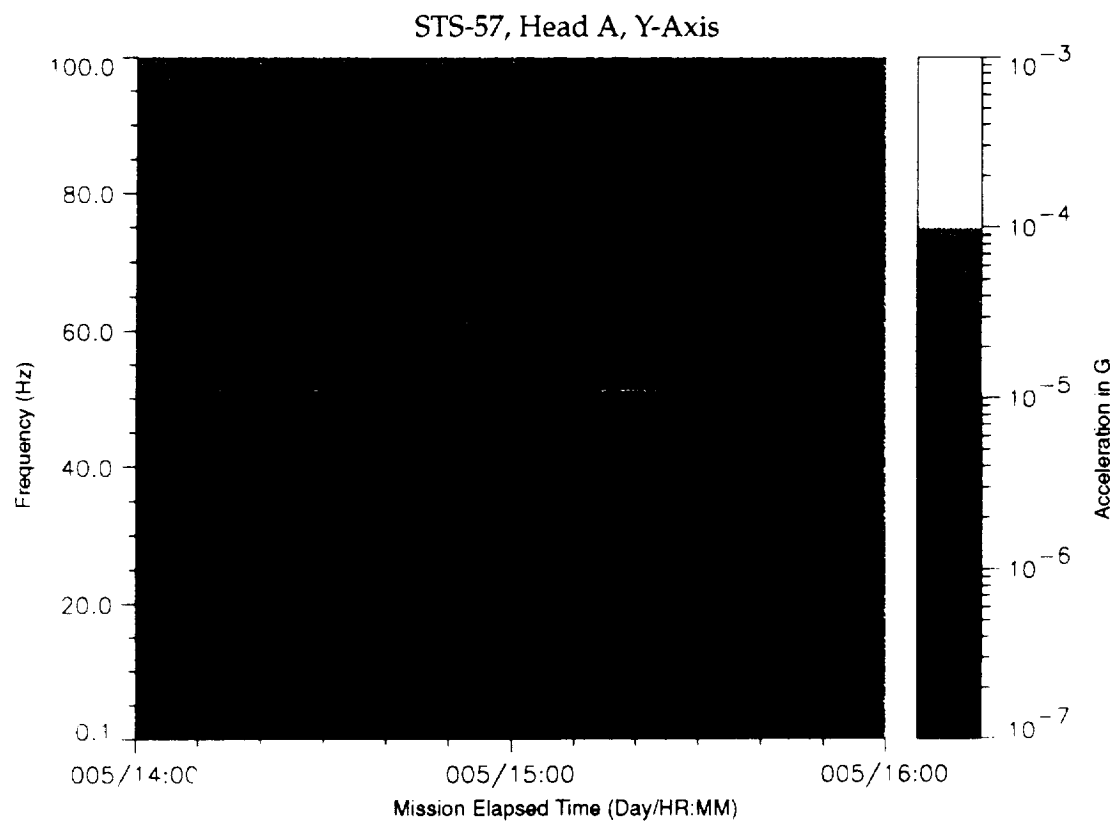


Figure B-227: SPACEHAB-1, Forward Bulkhead T-Beam

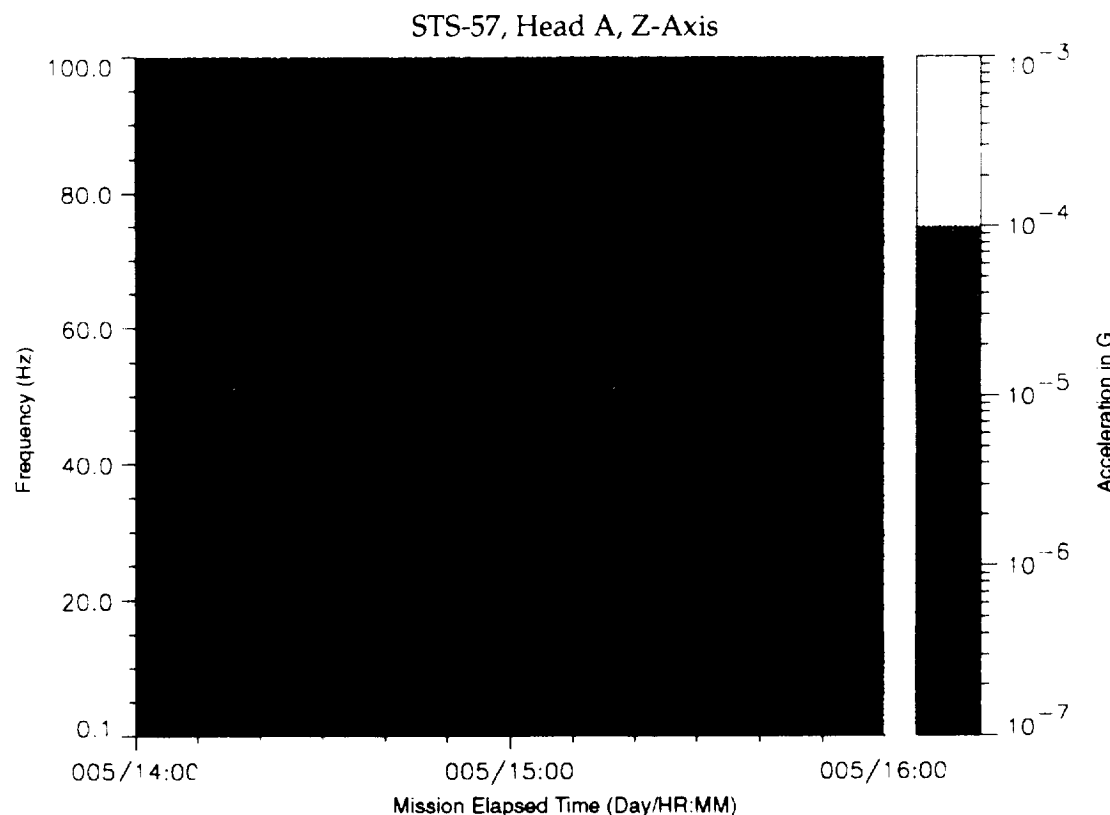


Figure B-228: SPACEHAB-1, Forward Bulkhead T-Beam

~~PRECEDING PAGE-blank NOT FILMED~~

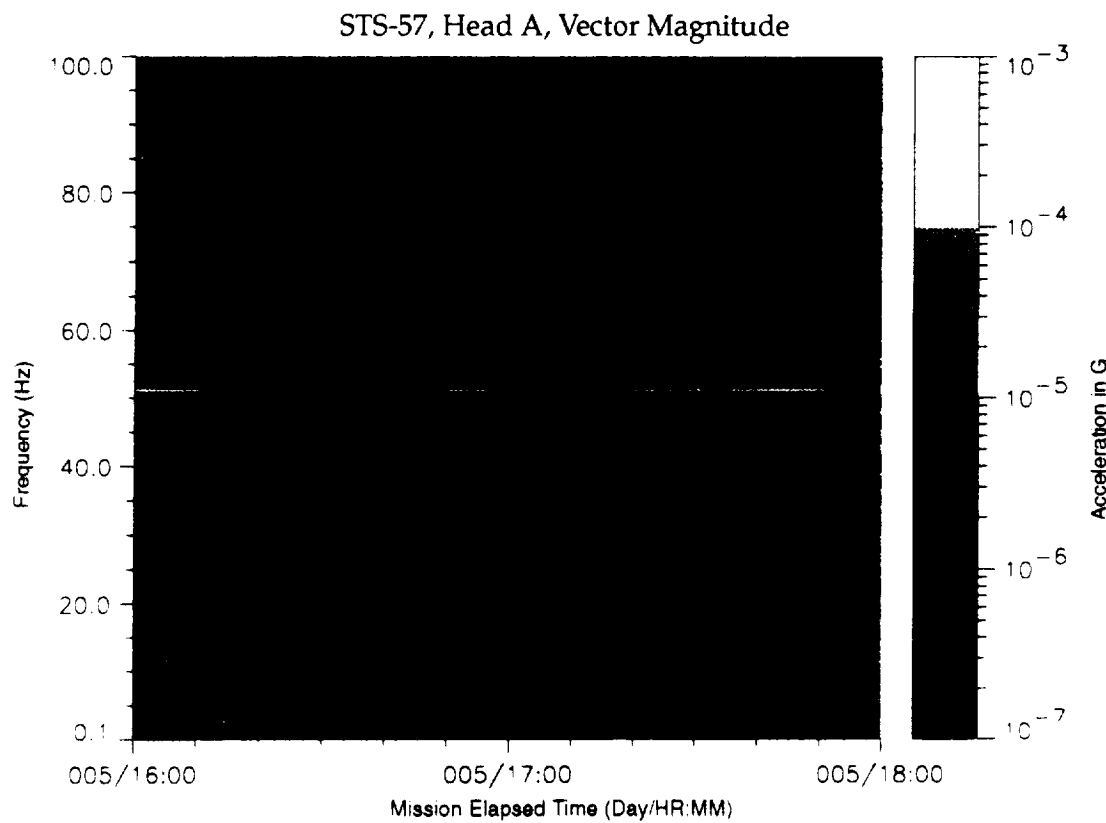


Figure B-229: SPACEHAB-1, Forward Bulkhead T-Beam

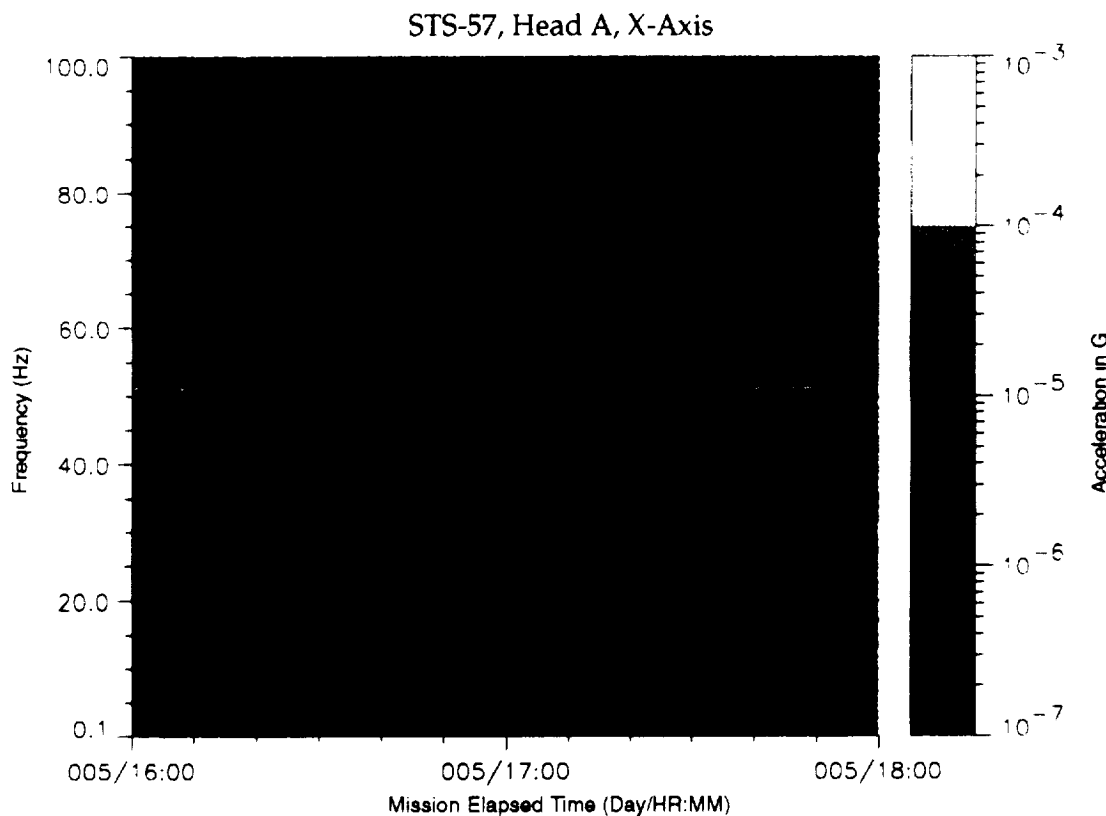


Figure B-230: SPACEHAB-1, Forward Bulkhead T-Beam

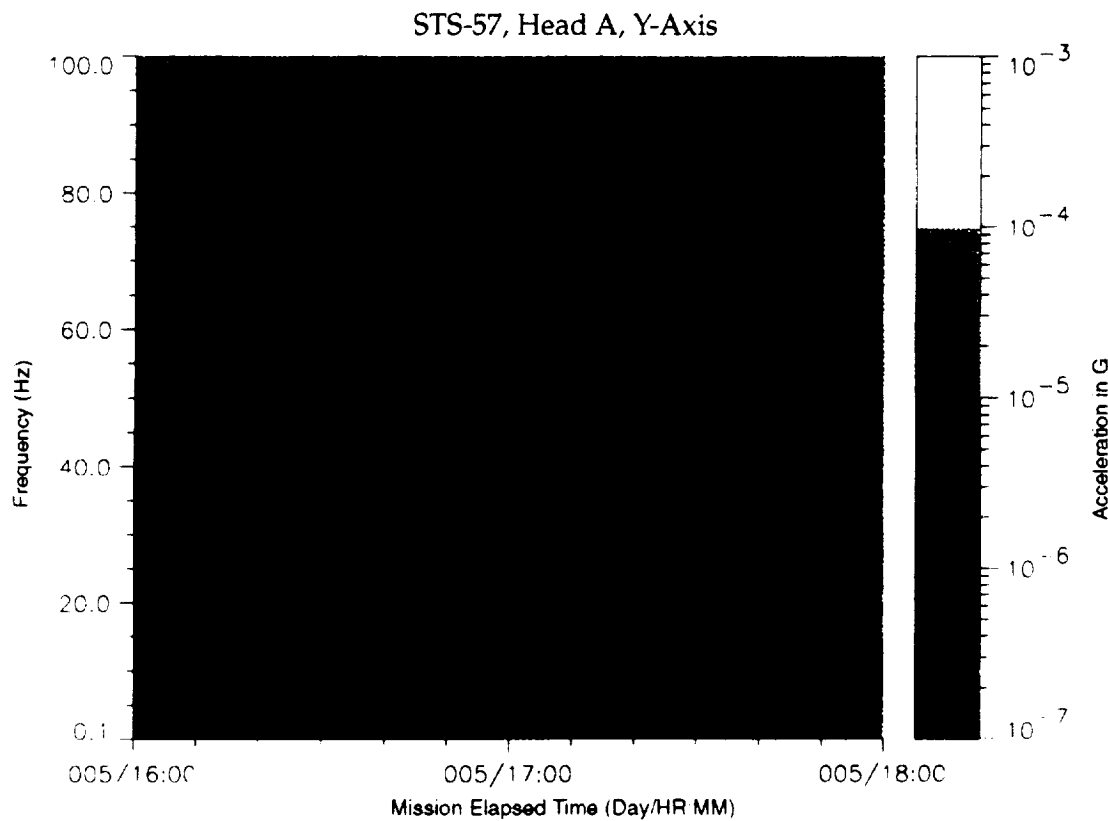


Figure B-231: SPACEHAB-1, Forward Bulkhead T-Beam

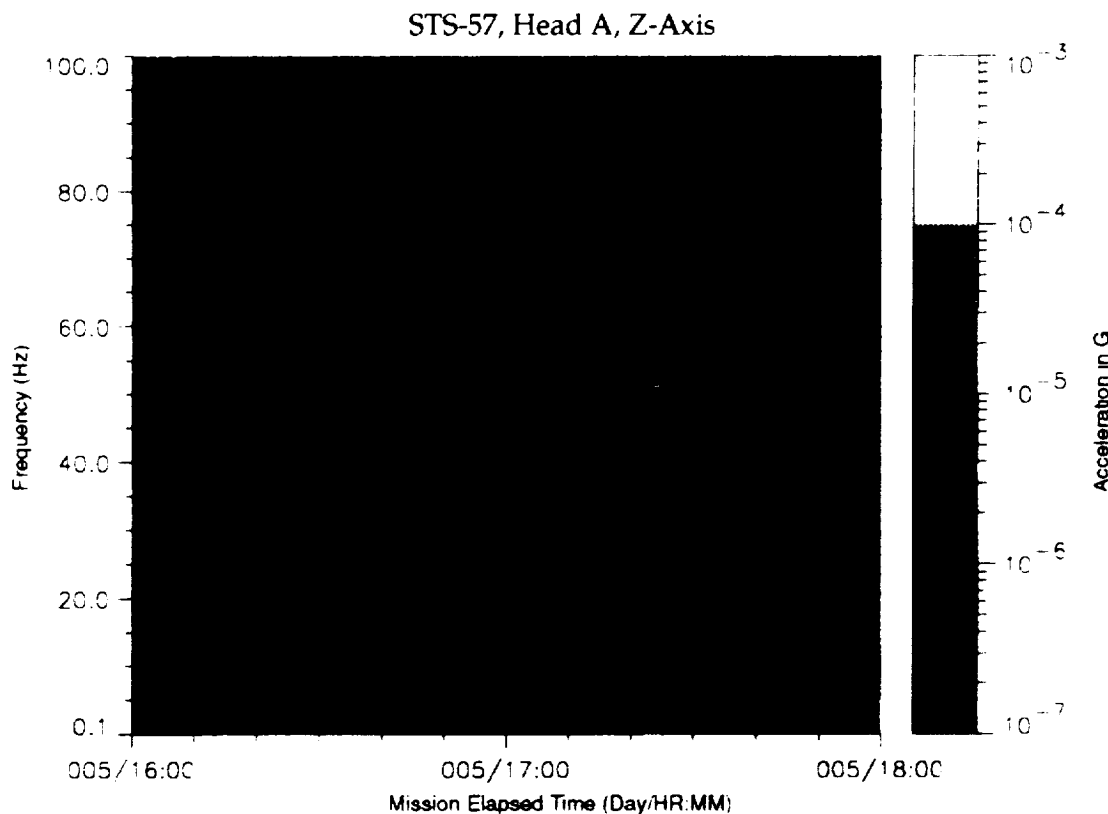


Figure B-232: SPACEHAB-1, Forward Bulkhead T-Beam

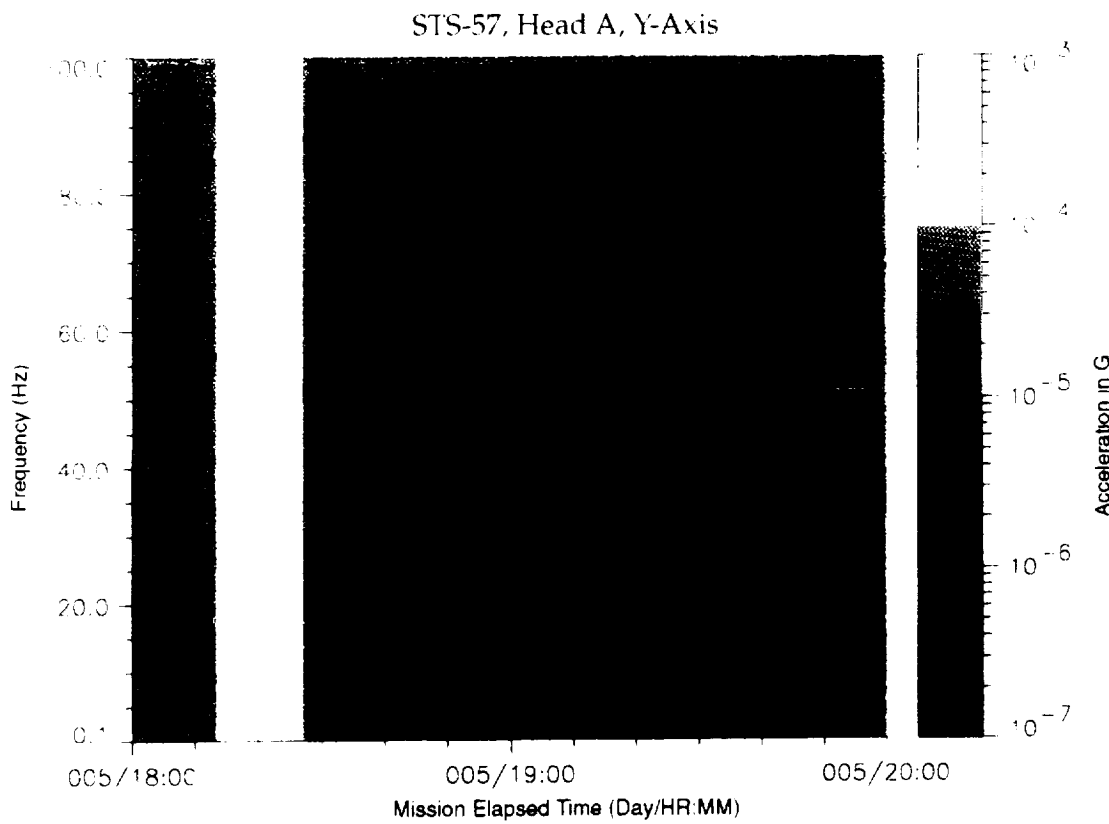


Figure B-235: SPACEHAB-1, Forward Bulkhead T-Beam

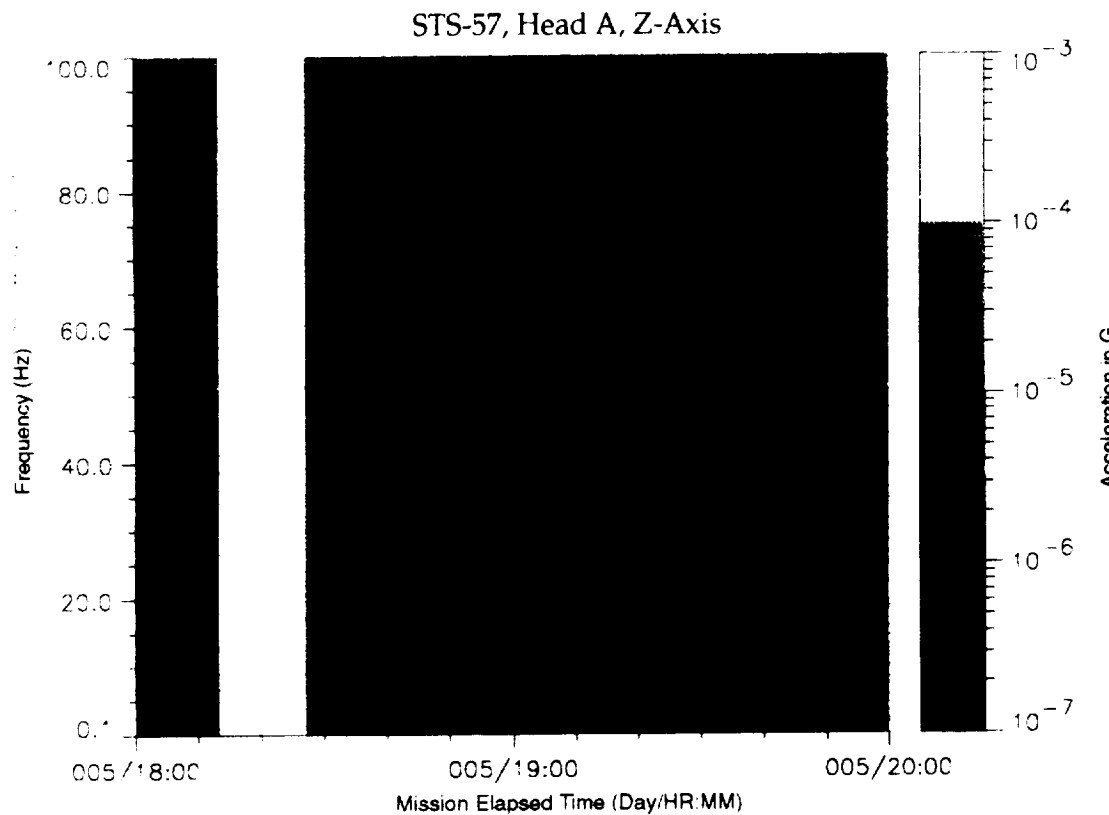


Figure B-236: SPACEHAB-1, Forward Bulkhead T-Beam

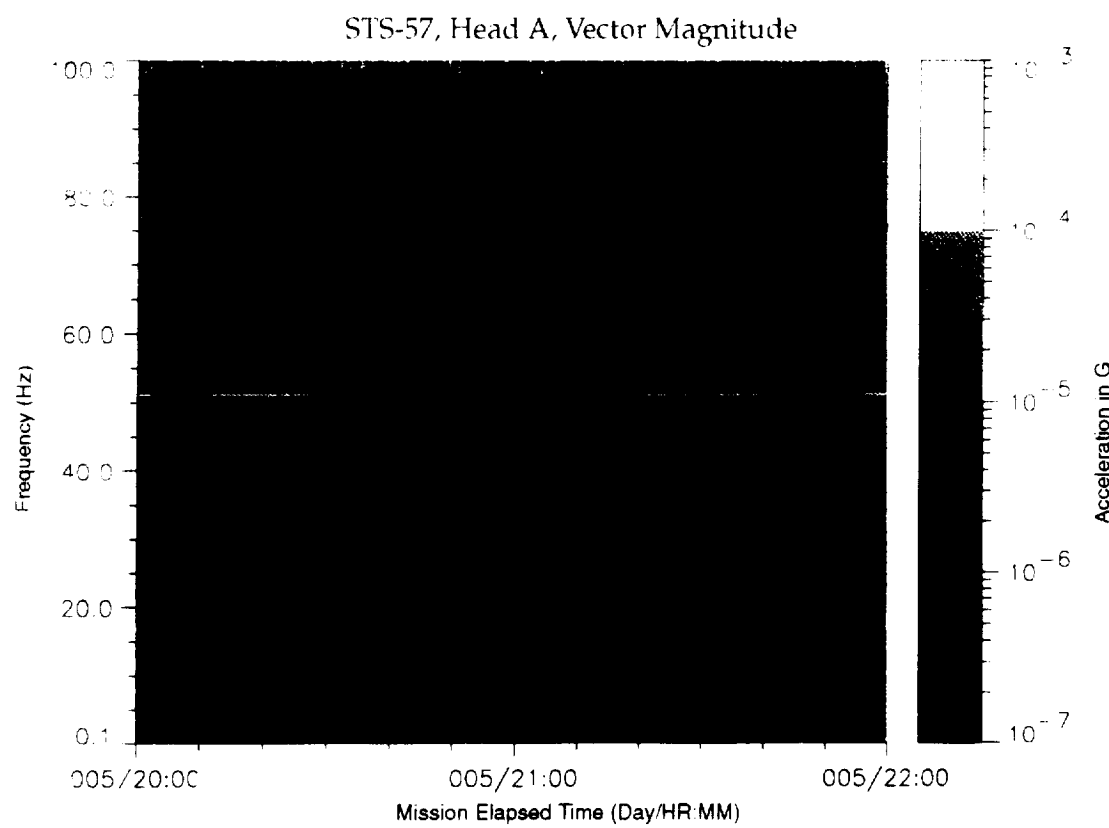


Figure B-237: SPACEHAB-1, Forward Bulkhead T-Beam

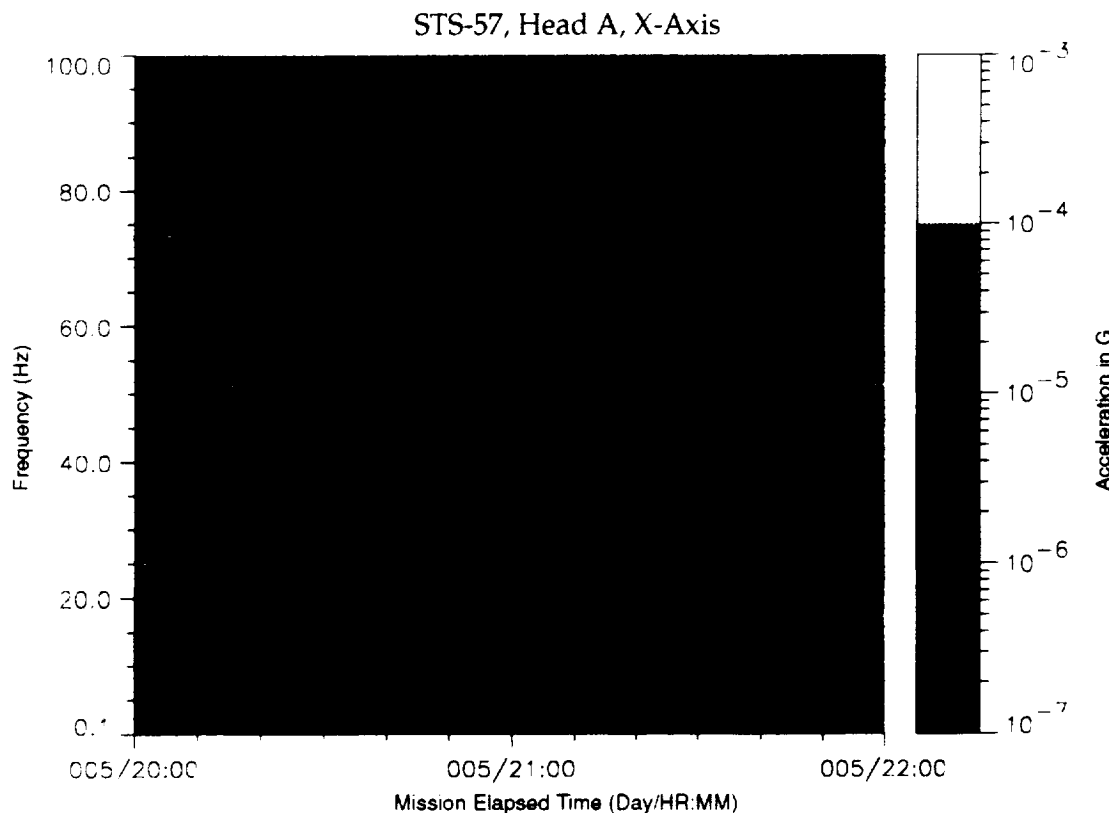


Figure B-238: SPACEHAB-1, Forward Bulkhead T-Beam

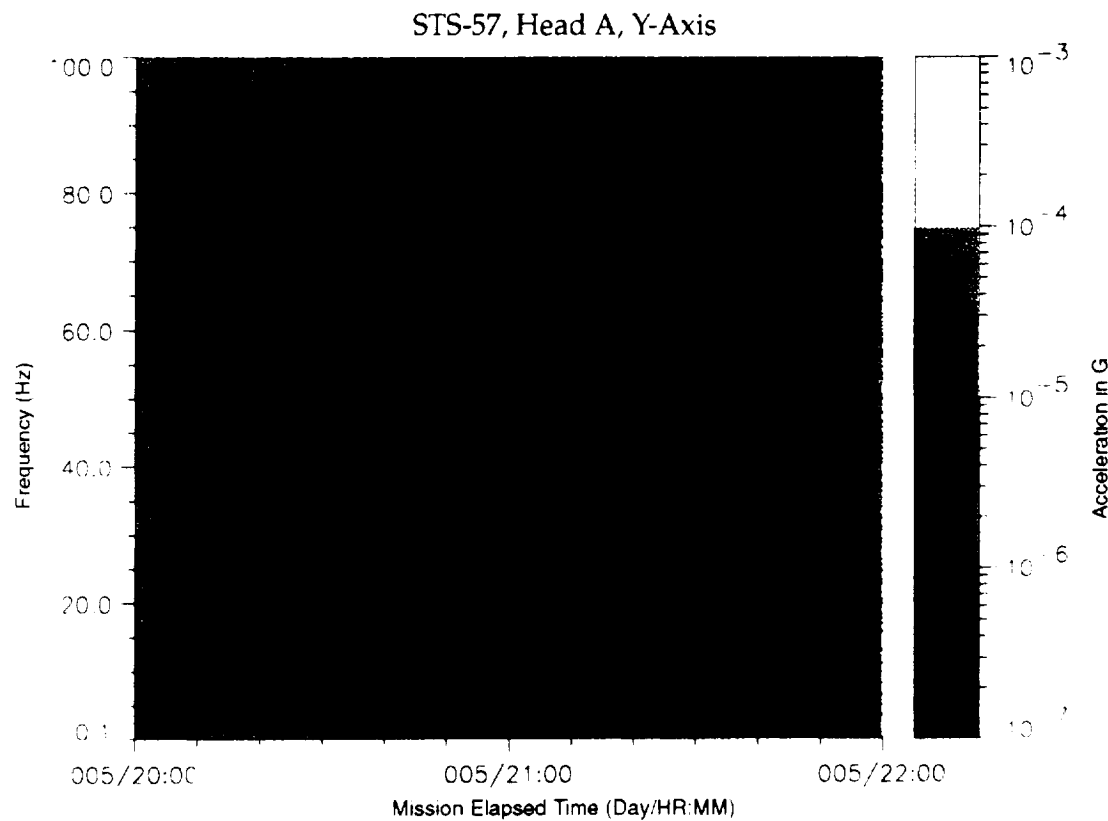


Figure B-239: SPACEHAB-1, Forward Bulkhead T-Beam

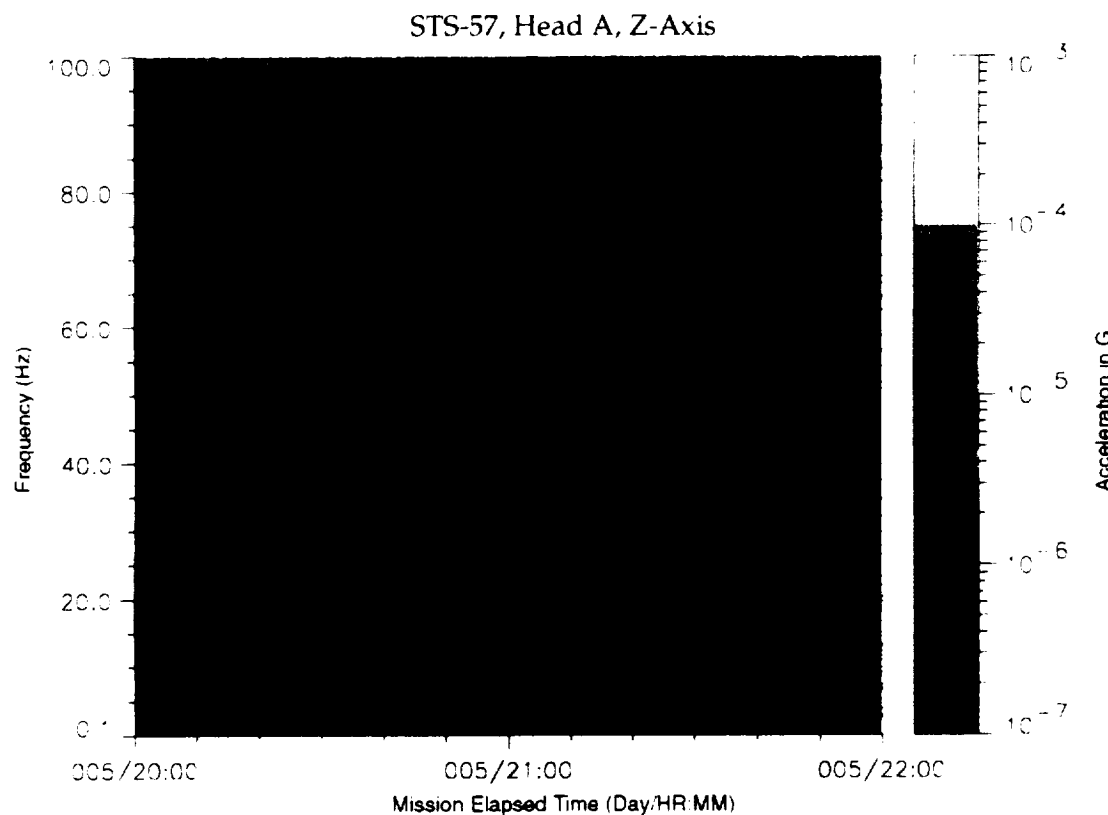


Figure B-240: SPACEHAB-1, Forward Bulkhead T-Beam

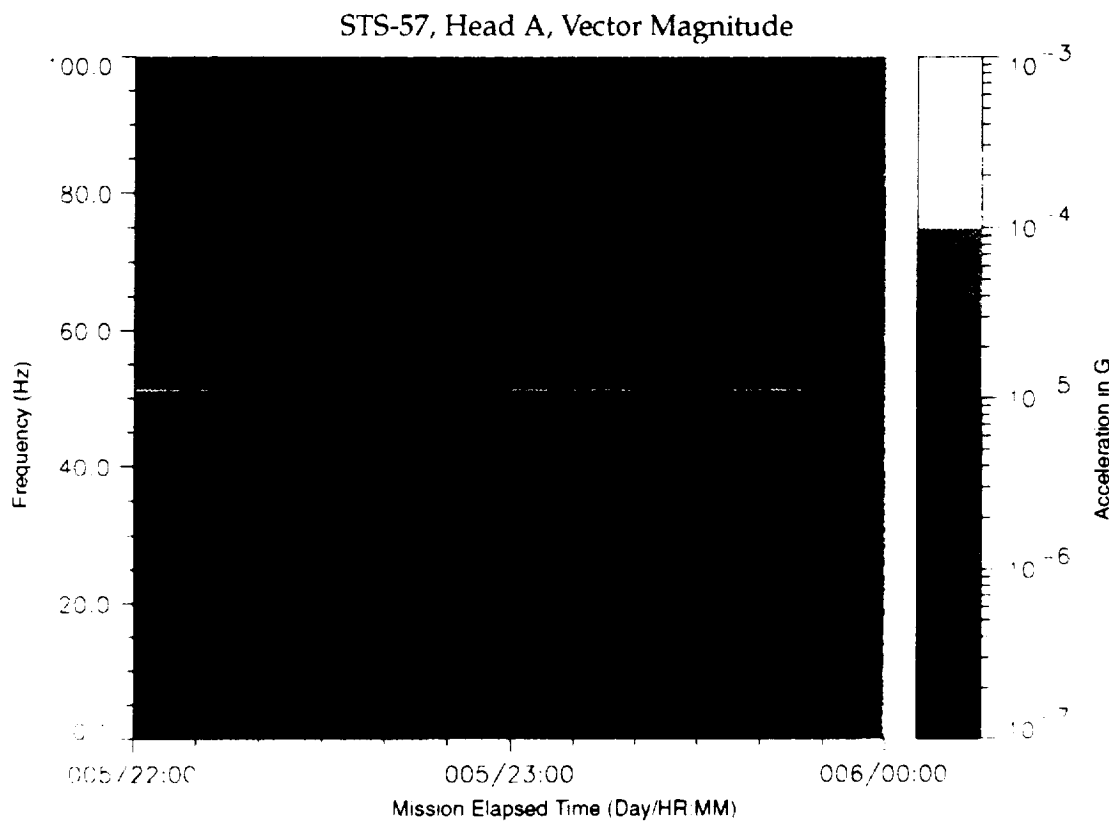


Figure B-241: SPACEHAB-1, Forward Bulkhead T-Beam

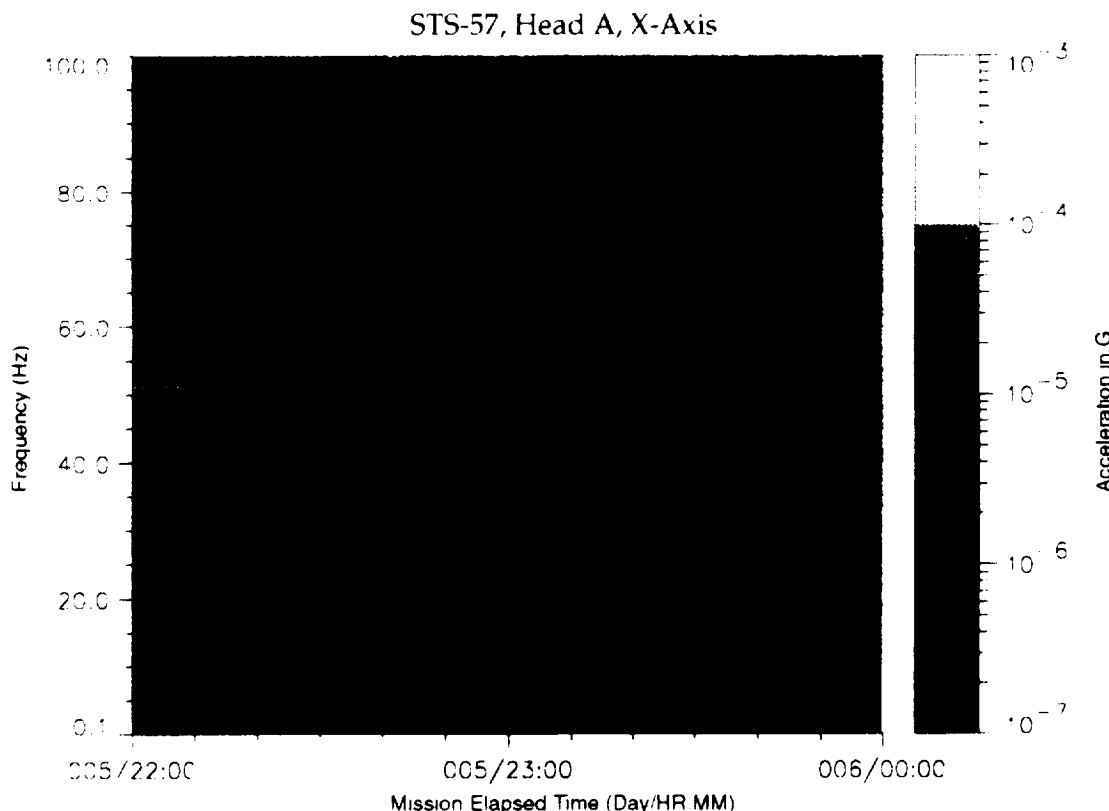


Figure B-242: SPACEHAB-1, Forward Bulkhead T-Beam

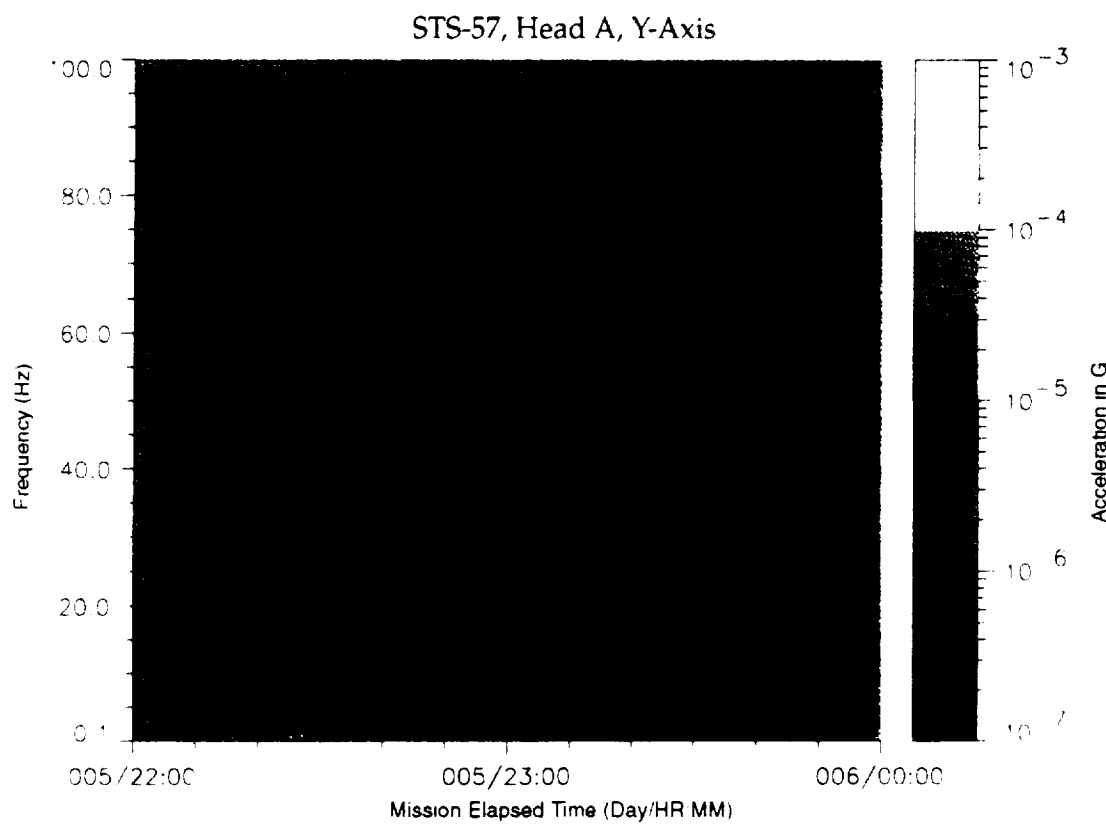


Figure B-243: SPACEHAB-1, Forward Bulkhead T-Beam

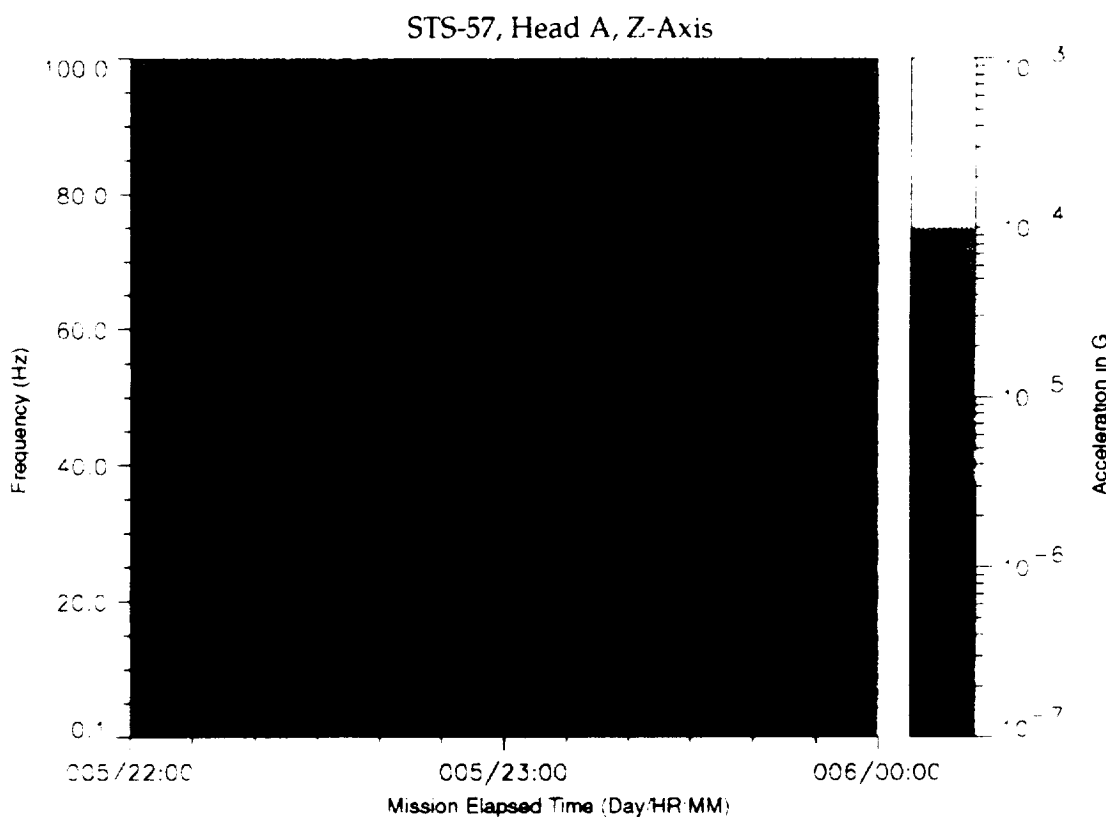


Figure B-244: SPACEHAB-1, Forward Bulkhead T-Beam

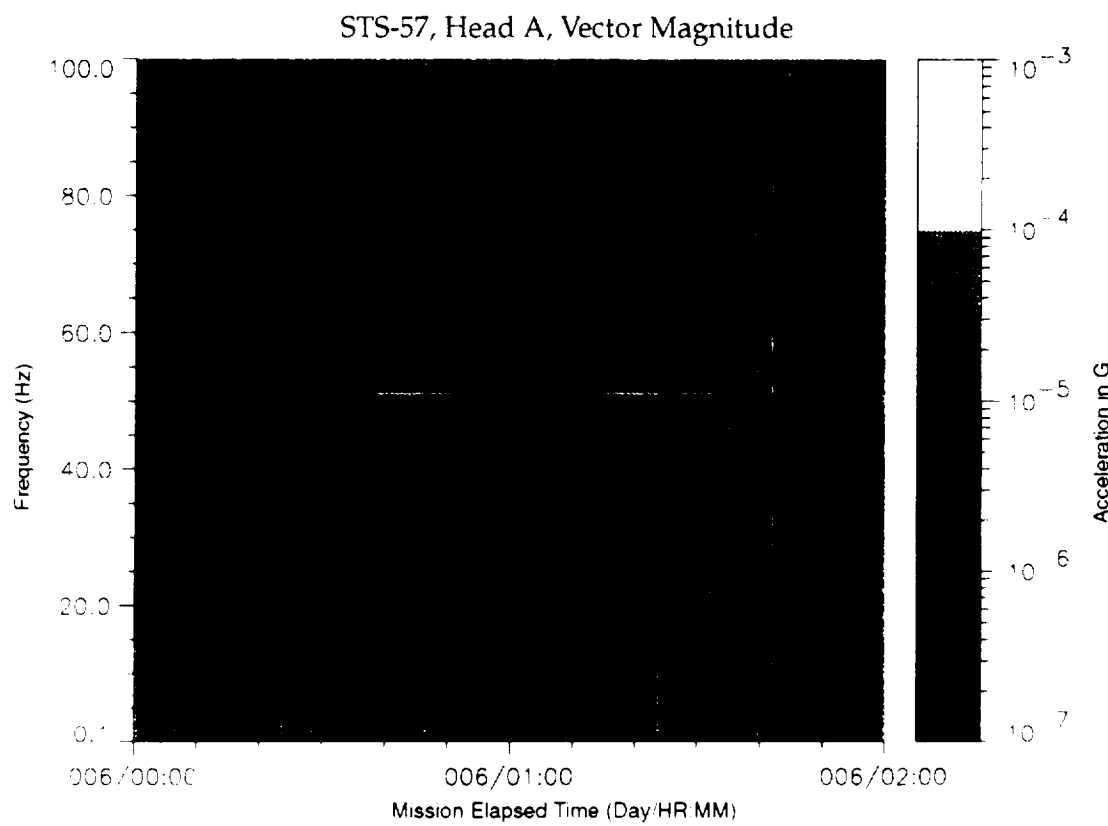


Figure B-245: SPACEHAB-1, Forward Bulkhead T-Beam

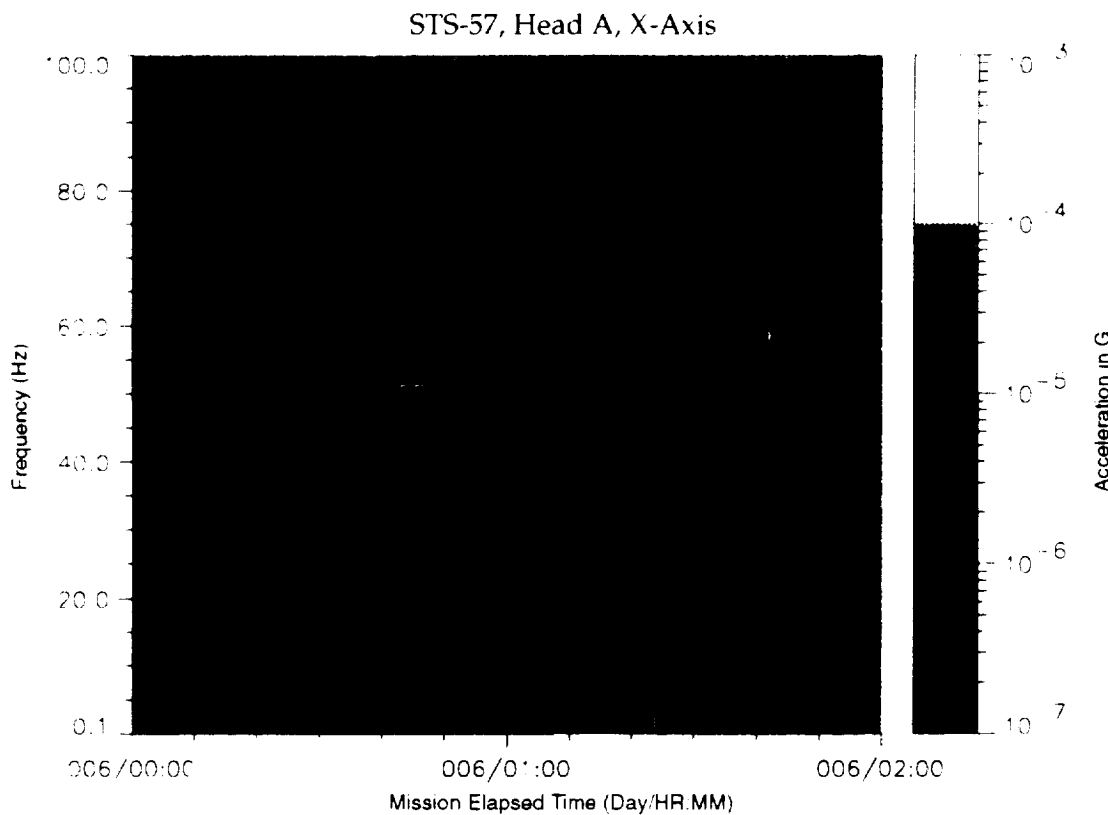


Figure B-246: SPACEHAB-1, Forward Bulkhead T-Beam

STS-57, Head A, Y-Axis

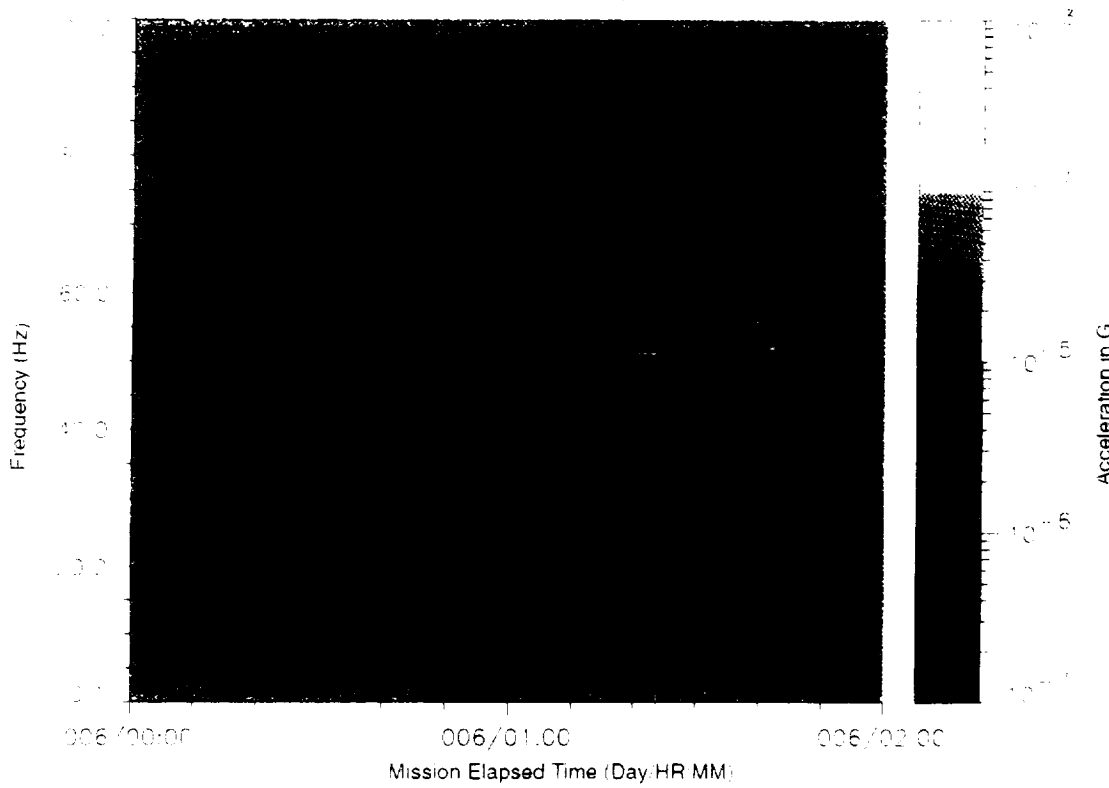


Figure B-247: SPACEHAB-1, Forward Bulkhead T-Beam

STS-57, Head A, Z-Axis

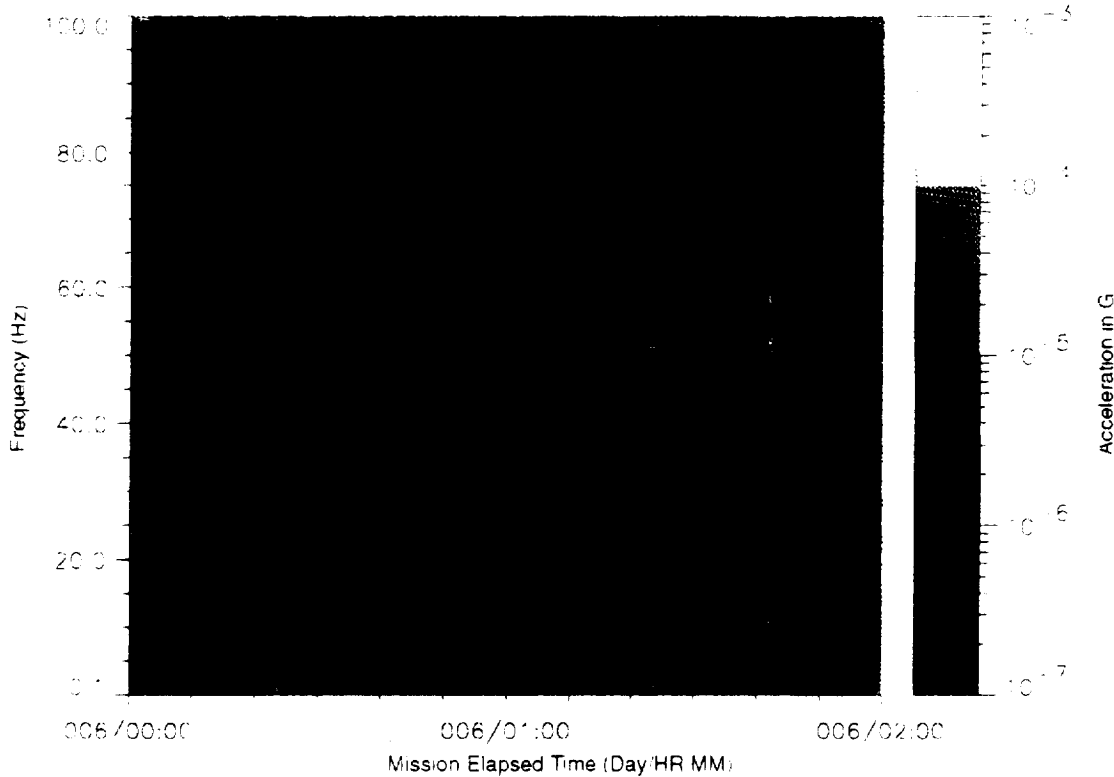


Figure B-248: SPACEHAB-1, Forward Bulkhead T-Beam

STS-57, Head A, Vector Magnitude

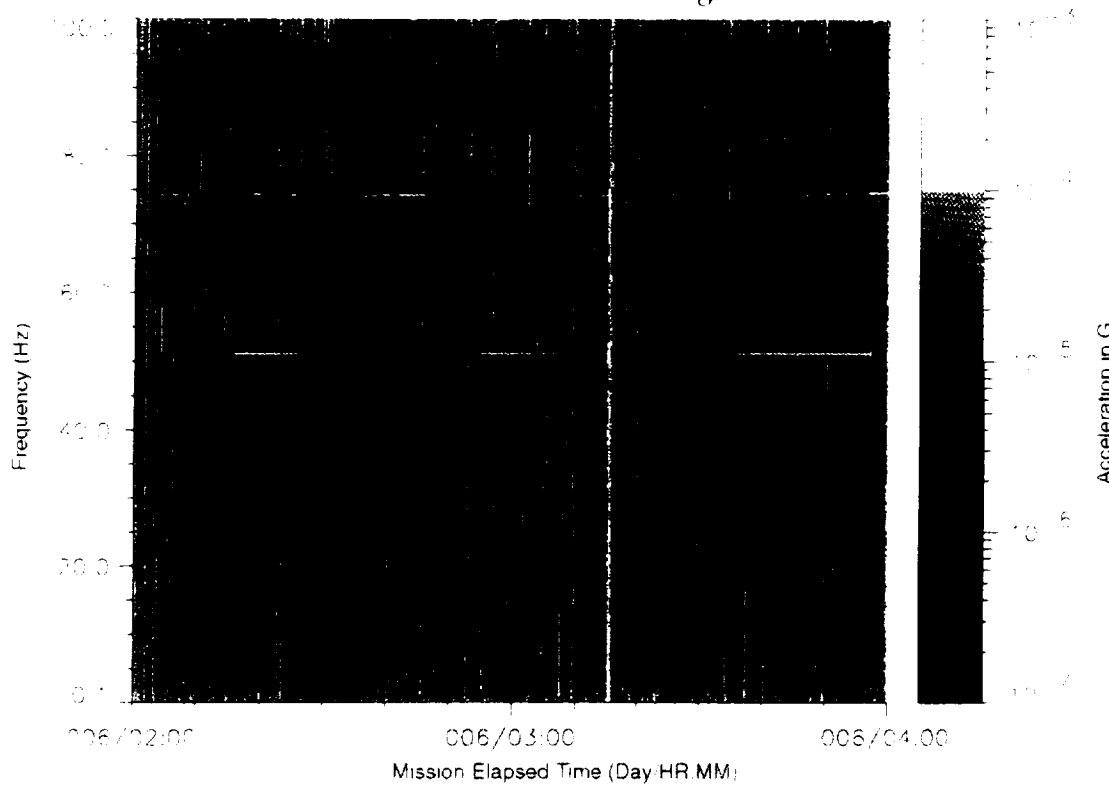


Figure B-249: SPACEHAB-1, Forward Bulkhead T-Beam

STS-57, Head A, X-Axis

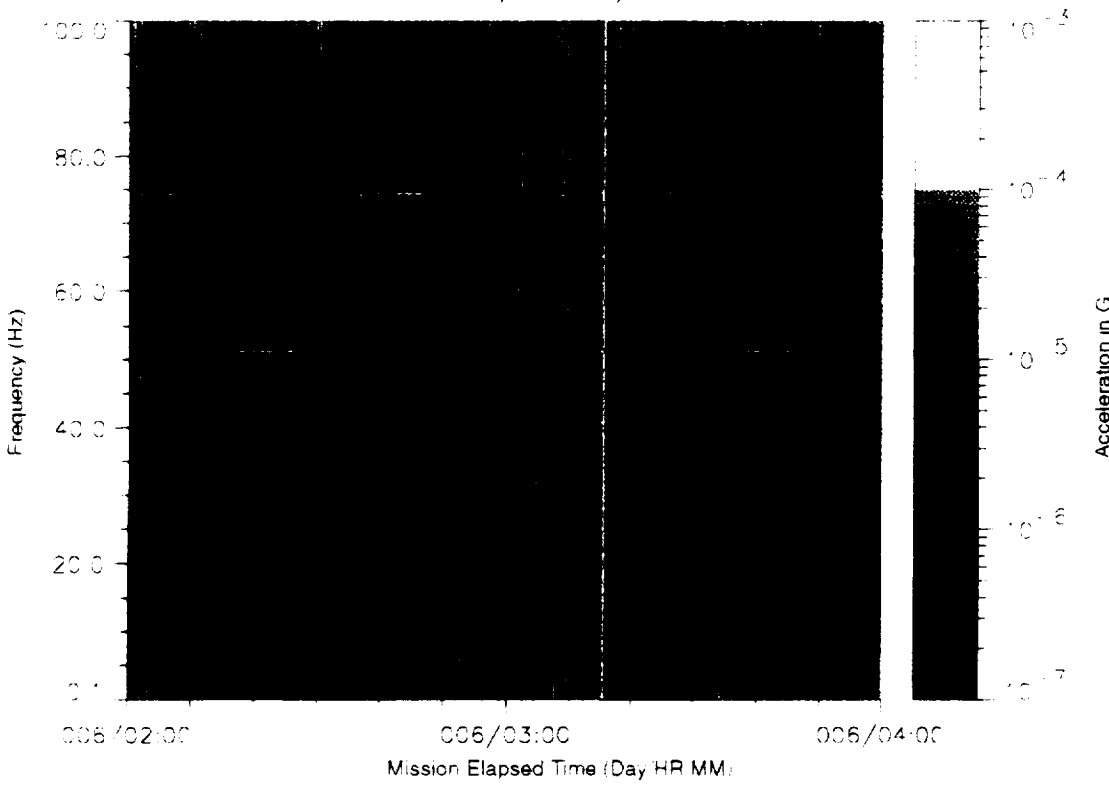


Figure B-250: SPACEHAB-1, Forward Bulkhead T-Beam

PRECEDING PAGE IS BLANK NOT FILMED

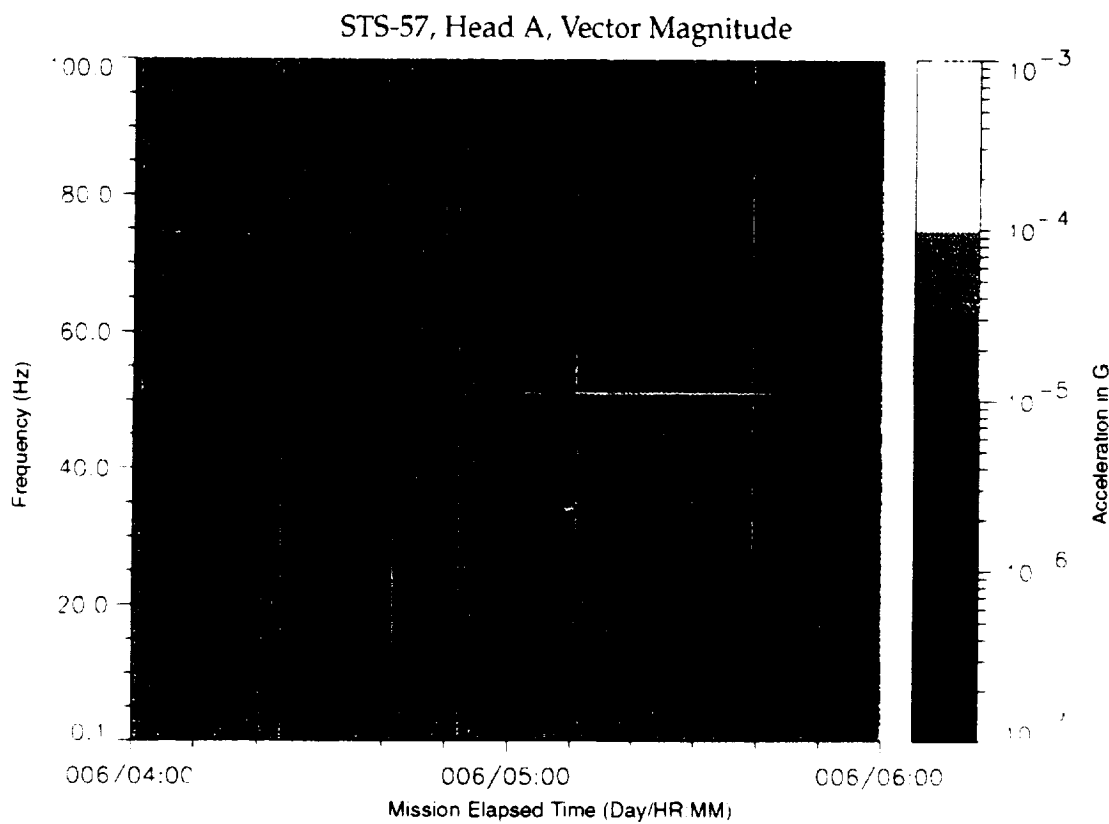
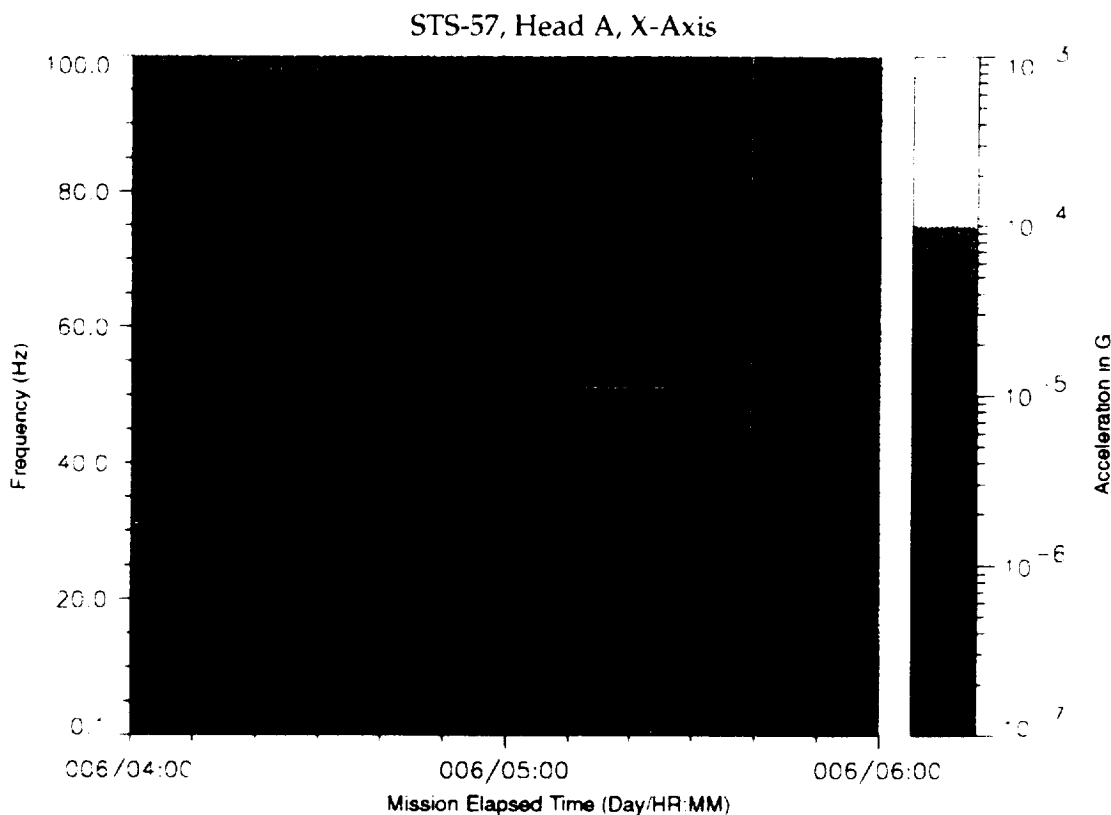


Figure B-253: SPACEHAB-1, Forward Bulkhead T-Beam

PROCEEDING PAGE ~~BLANK NOT FLOWN~~ Figure B-254: SPACEHAB-1, Forward Bulkhead T-Beam

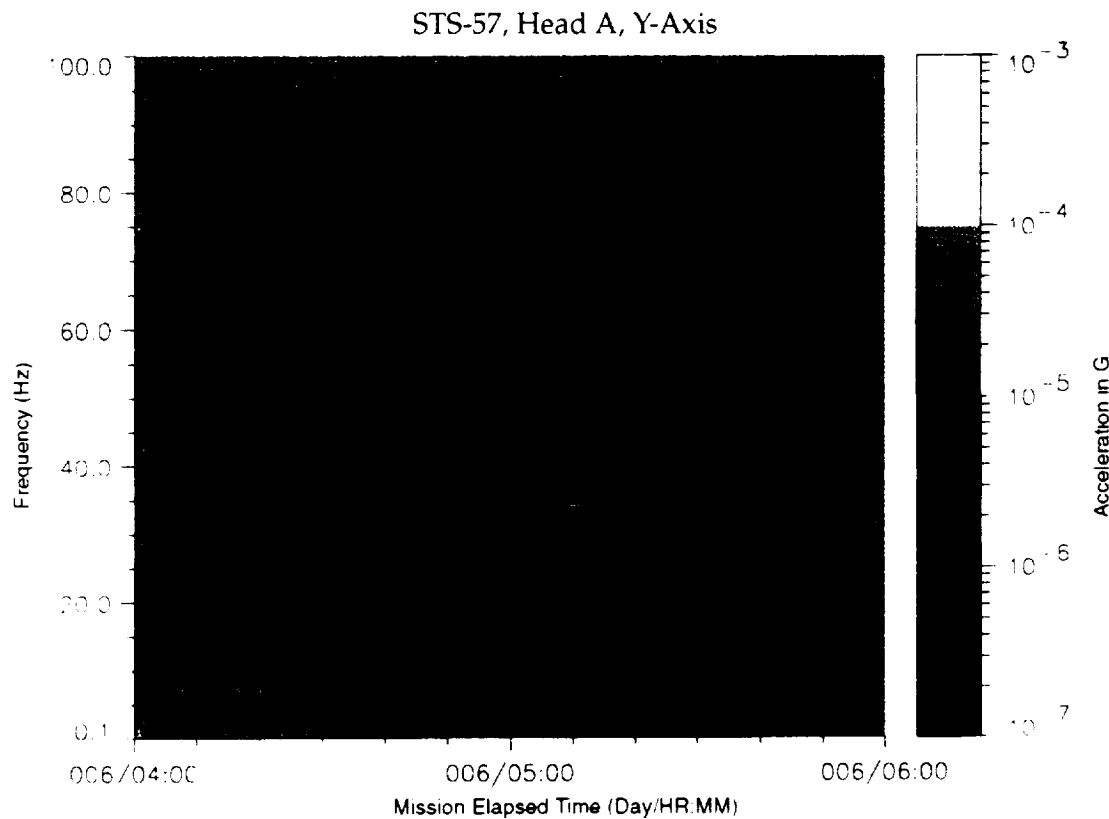


Figure B-255: SPACEHAB-1, Forward Bulkhead T-Beam

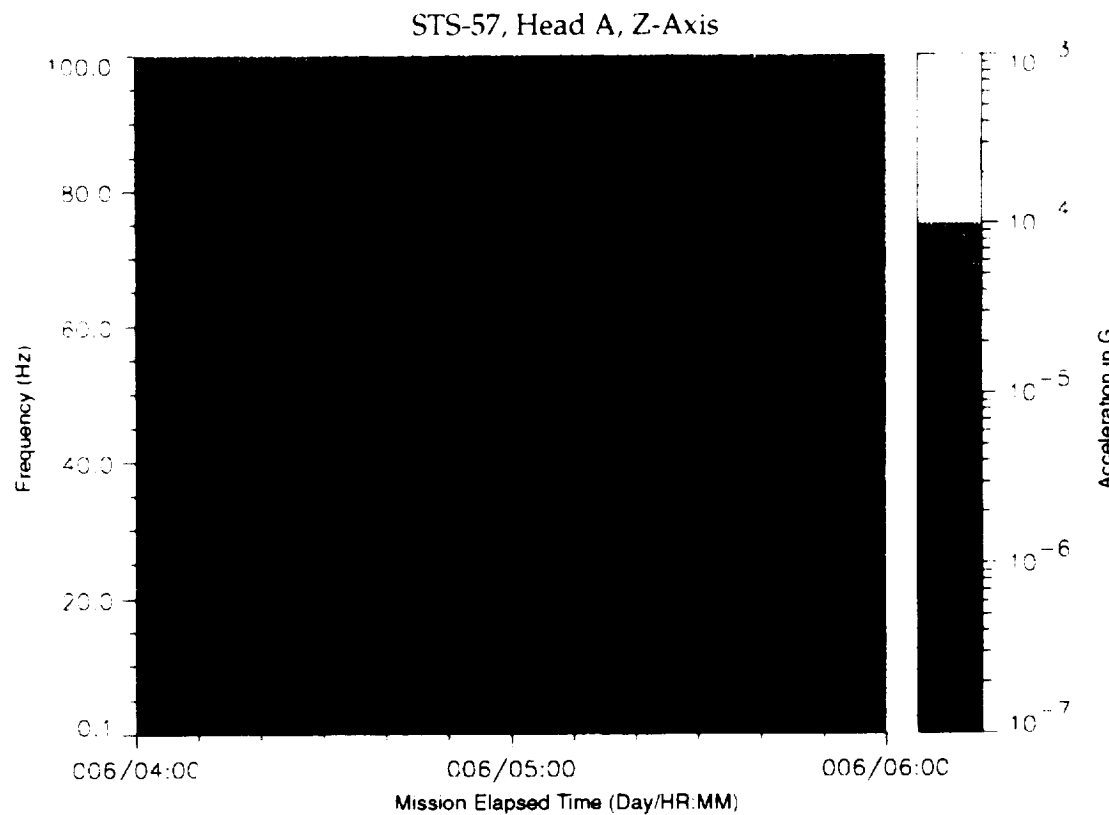


Figure B-256: SPACEHAB-1, Forward Bulkhead T-Beam

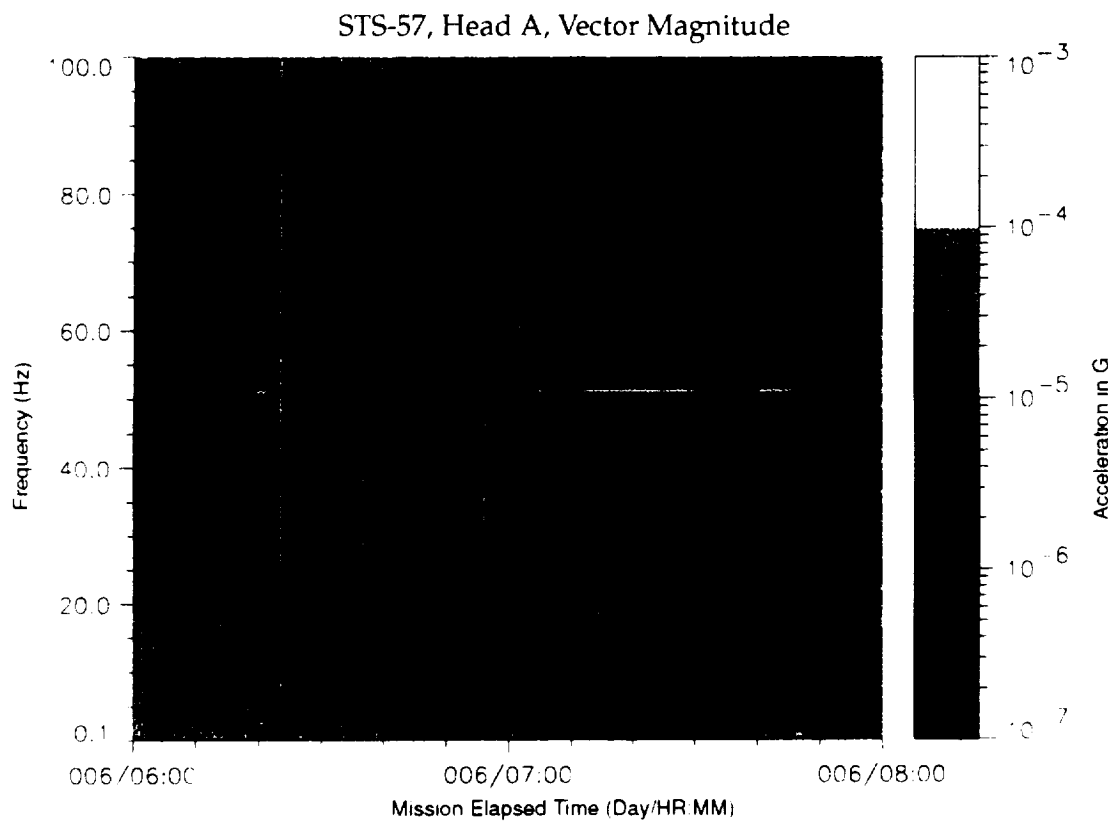


Figure B-257: SPACEHAB-1, Forward Bulkhead T-Beam

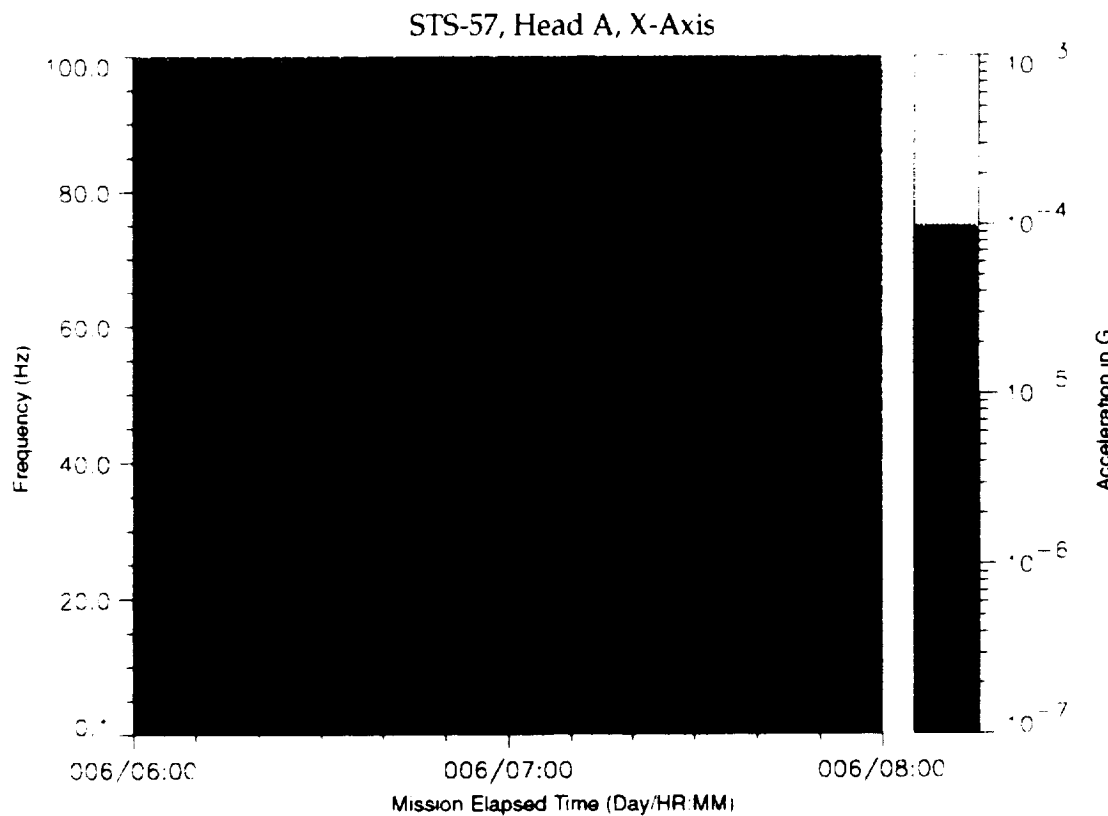


Figure B-258: SPACEHAB-1, Forward Bulkhead T-Beam

PRECEDING PAGE BLANK NOT FILMED

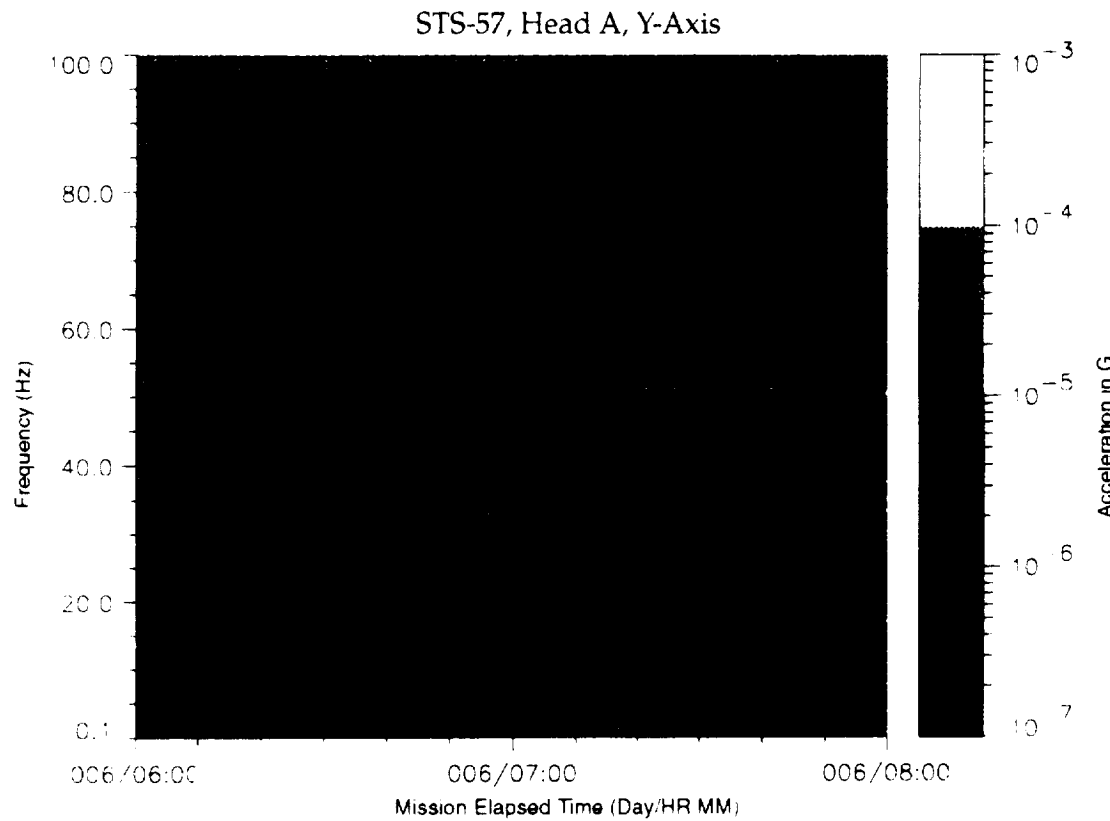


Figure B-259: SPACEHAB-1, Forward Bulkhead T-Beam

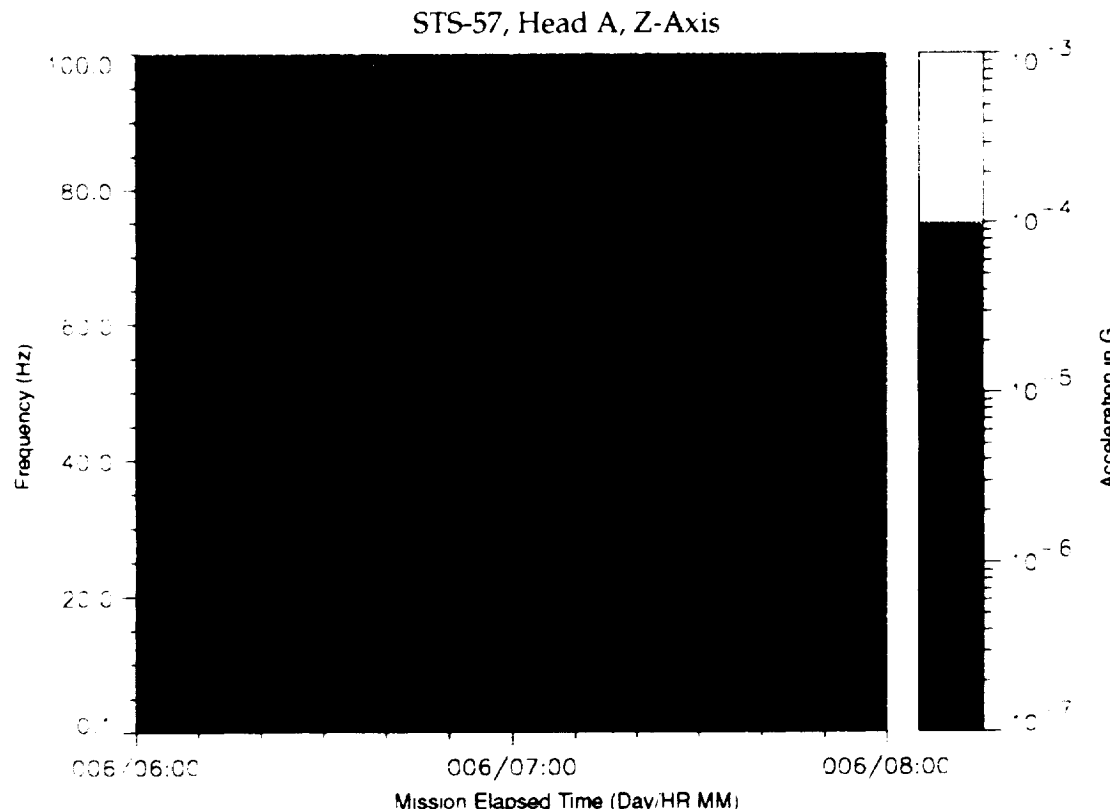


Figure B-260: SPACEHAB-1, Forward Bulkhead T-Beam

SIS-57, Head A, Vector Magnitude

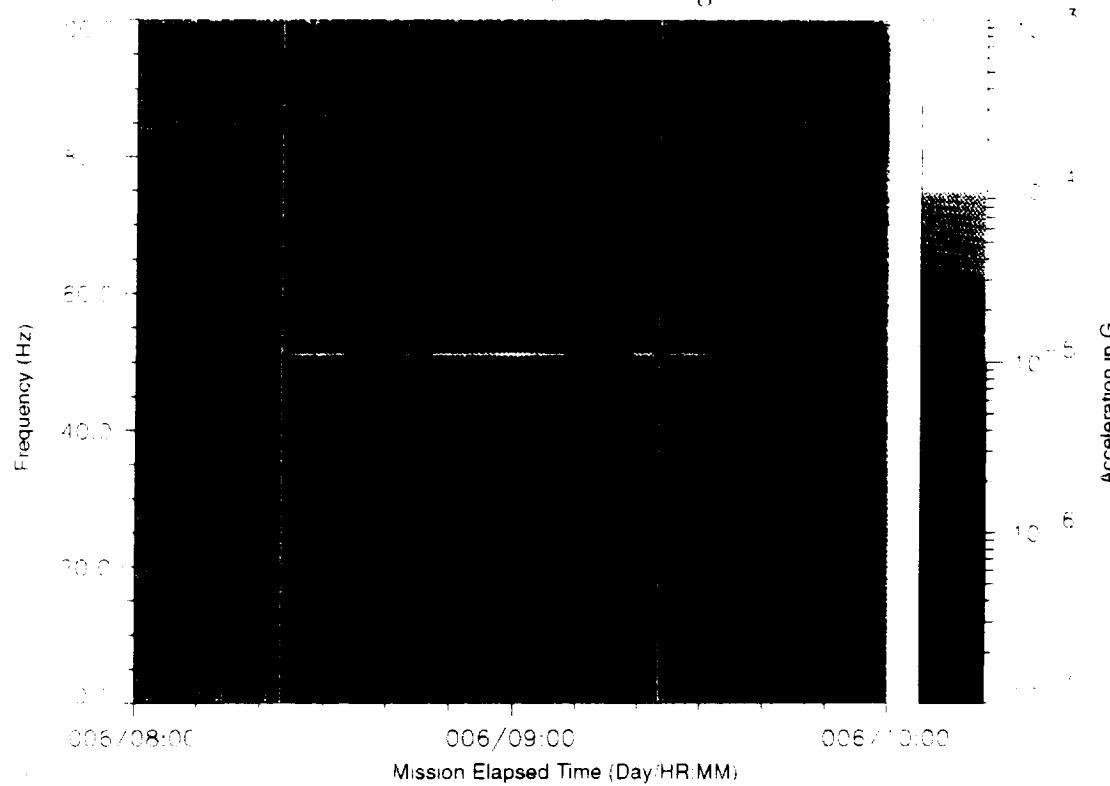


Figure B-261: SPACEHAB-1, Forward Bulkhead T-Beam

STS-57, Head A, X-Axis

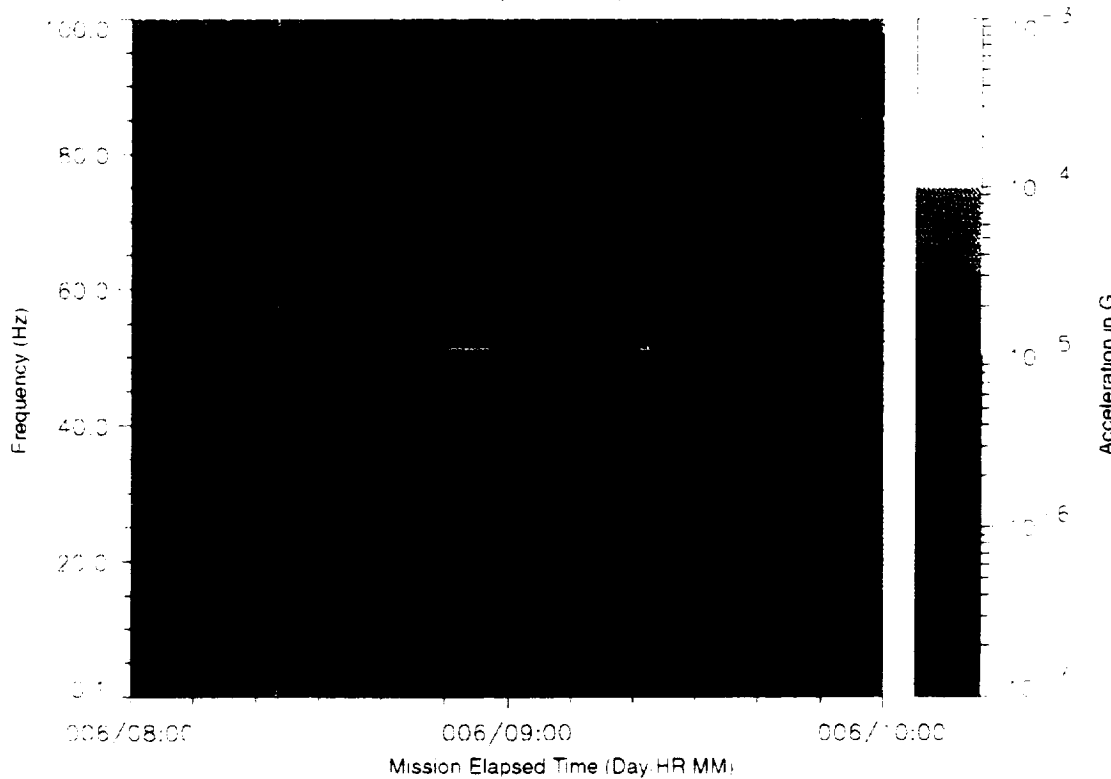


Figure B-262: SPACEHAB-1, Forward Bulkhead T-Beam

STS-57, Head A, Y-Axis

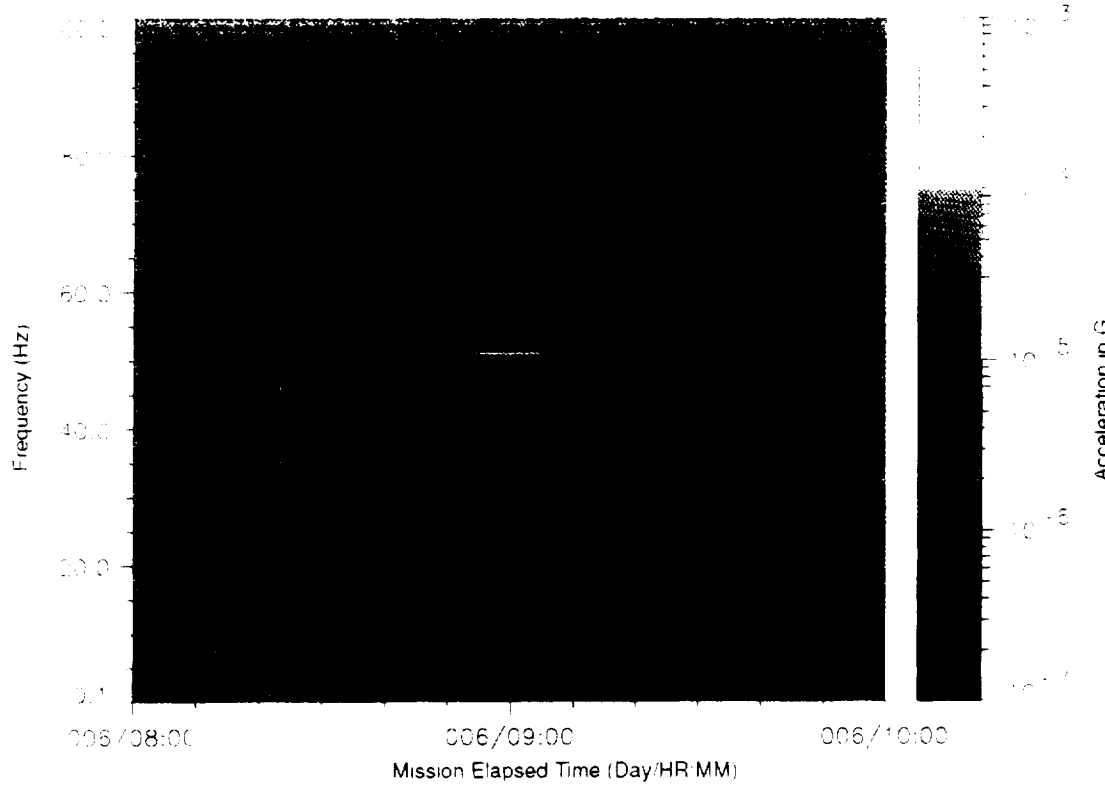


Figure B-263: SPACEHAB-1, Forward Bulkhead T-Beam

STS-57, Head A, Z-Axis

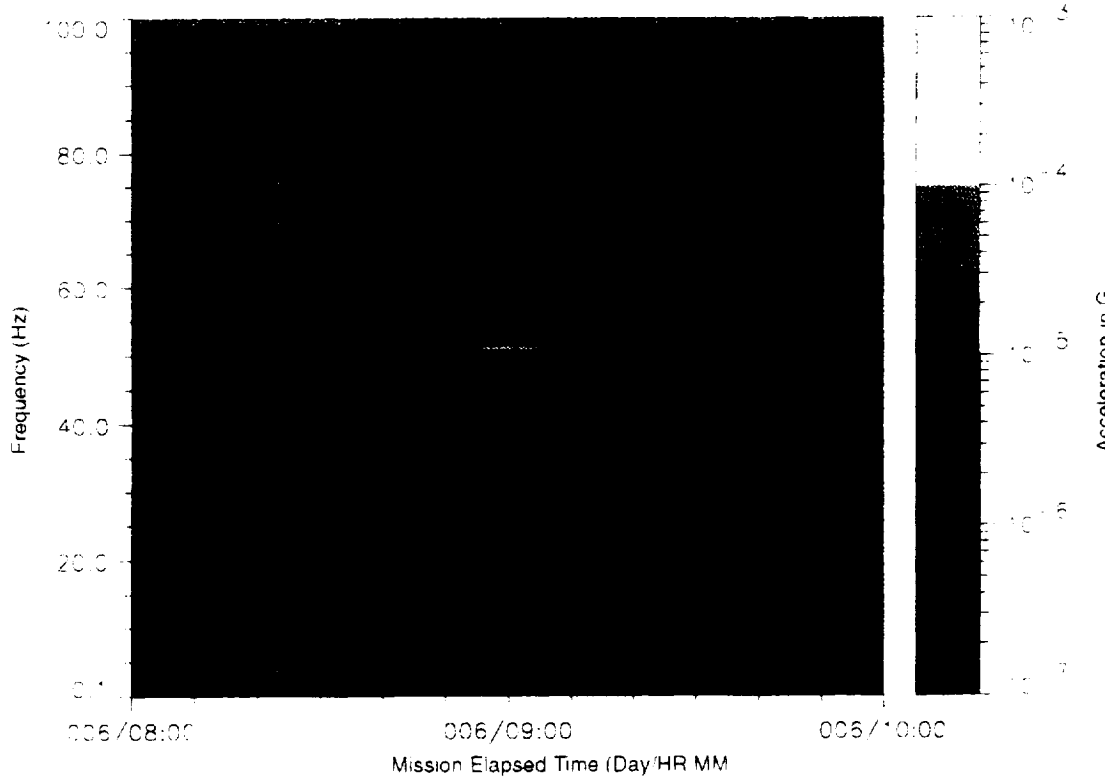


Figure B-264: SPACEHAB-1, Forward Bulkhead T-Beam

STS-57, Head A, Vector Magnitude

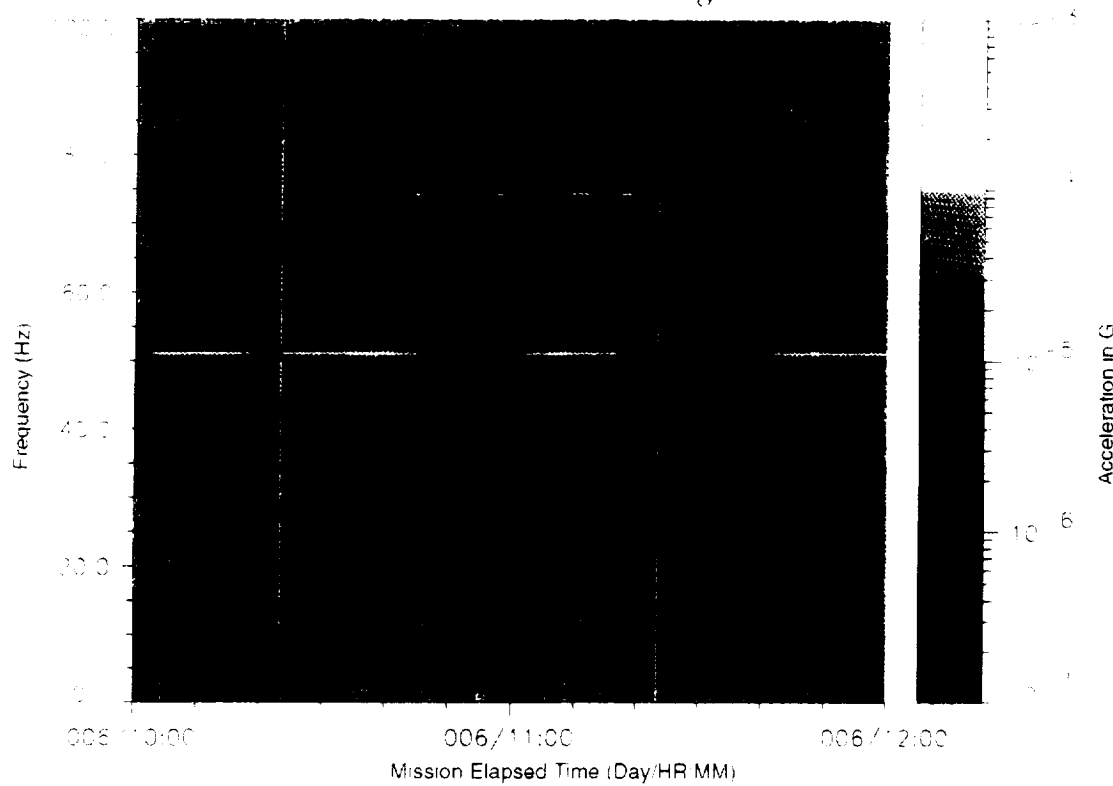


Figure B-265: SPACEHAB-1, Forward Bulkhead T-Beam

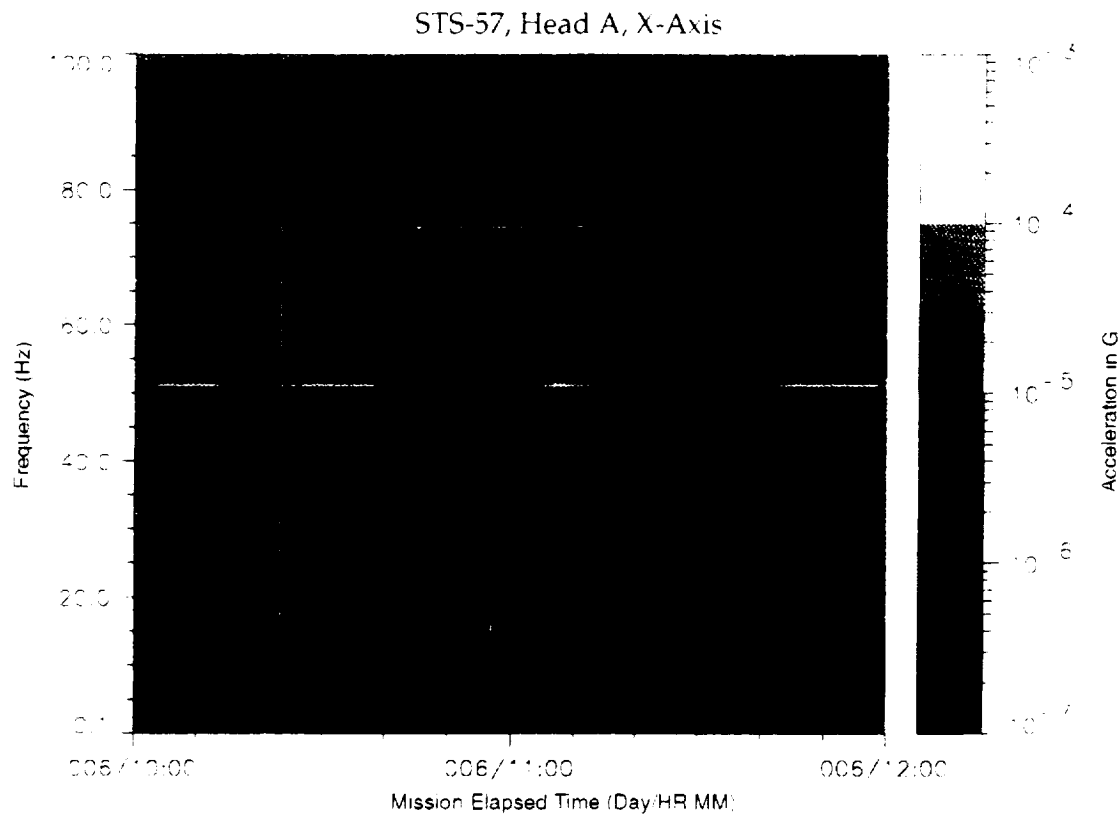


Figure B-266: SPACEHAB-1, Forward Bulkhead T-Beam

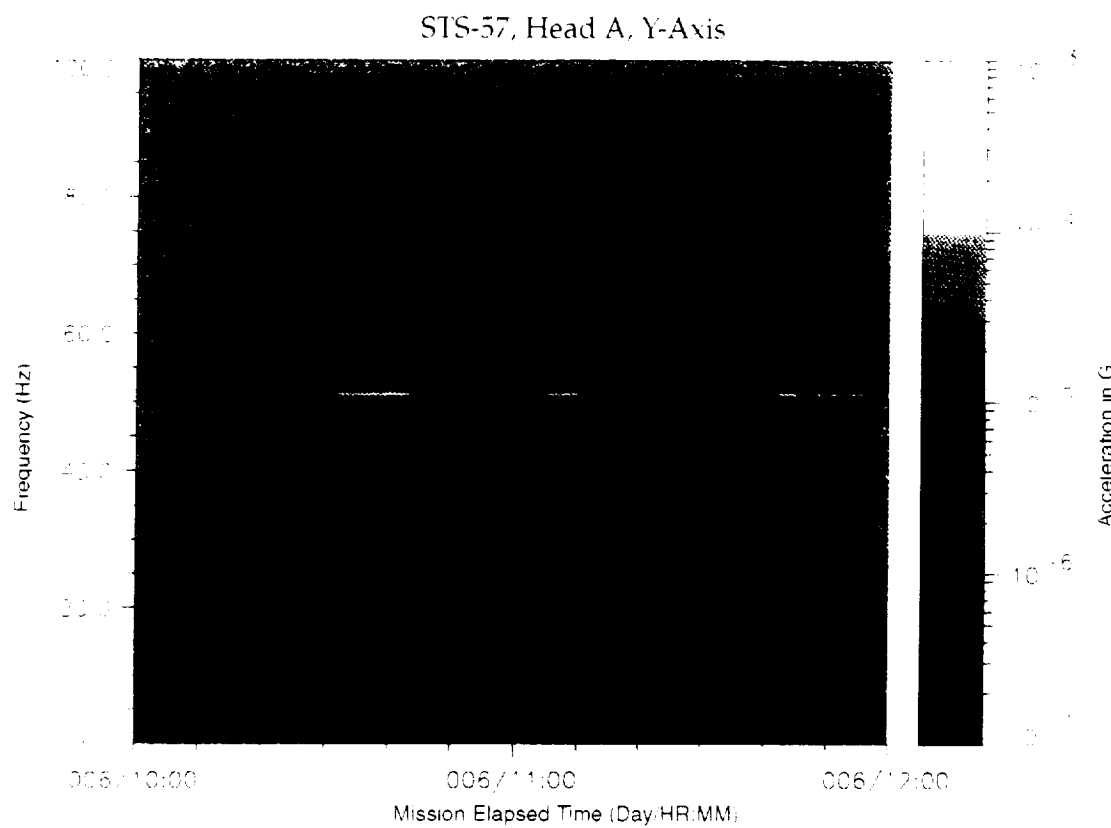


Figure B-267: SPACEHAB-1, Forward Bulkhead T-Beam

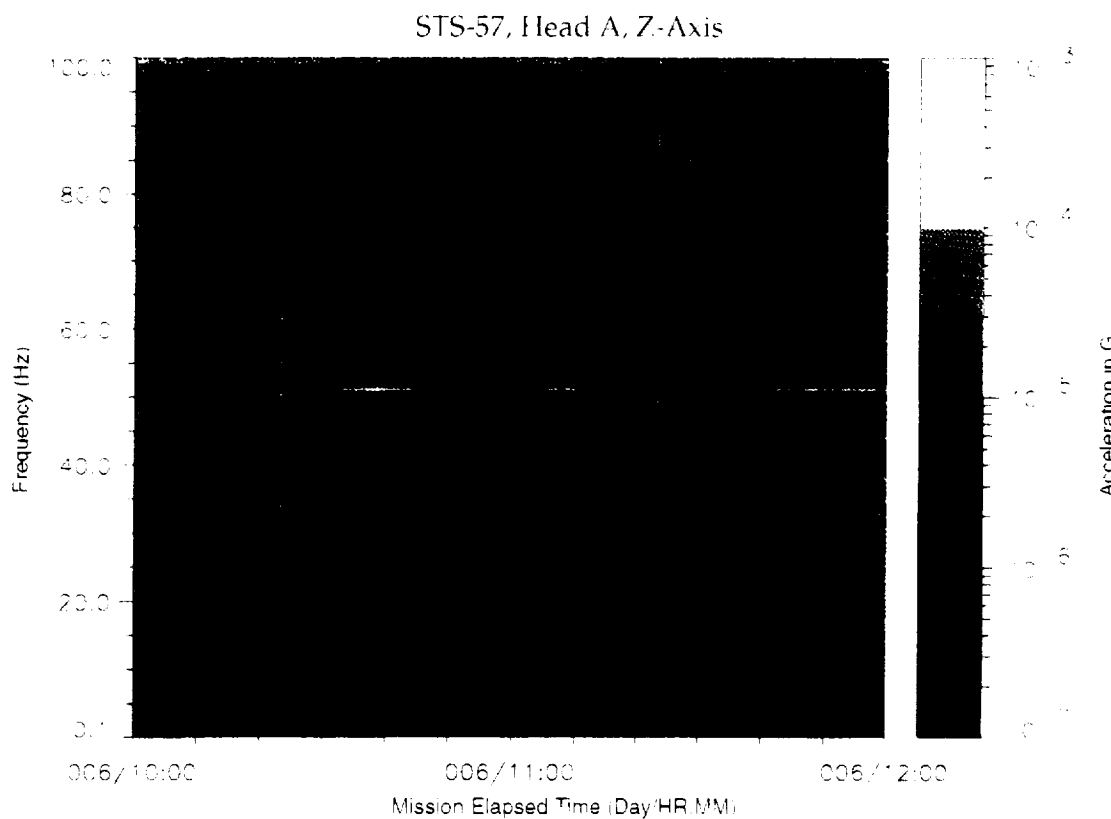


Figure B-268: SPACEHAB-1, Forward Bulkhead T-Beam

STS-57, Head A, Vector Magnitude

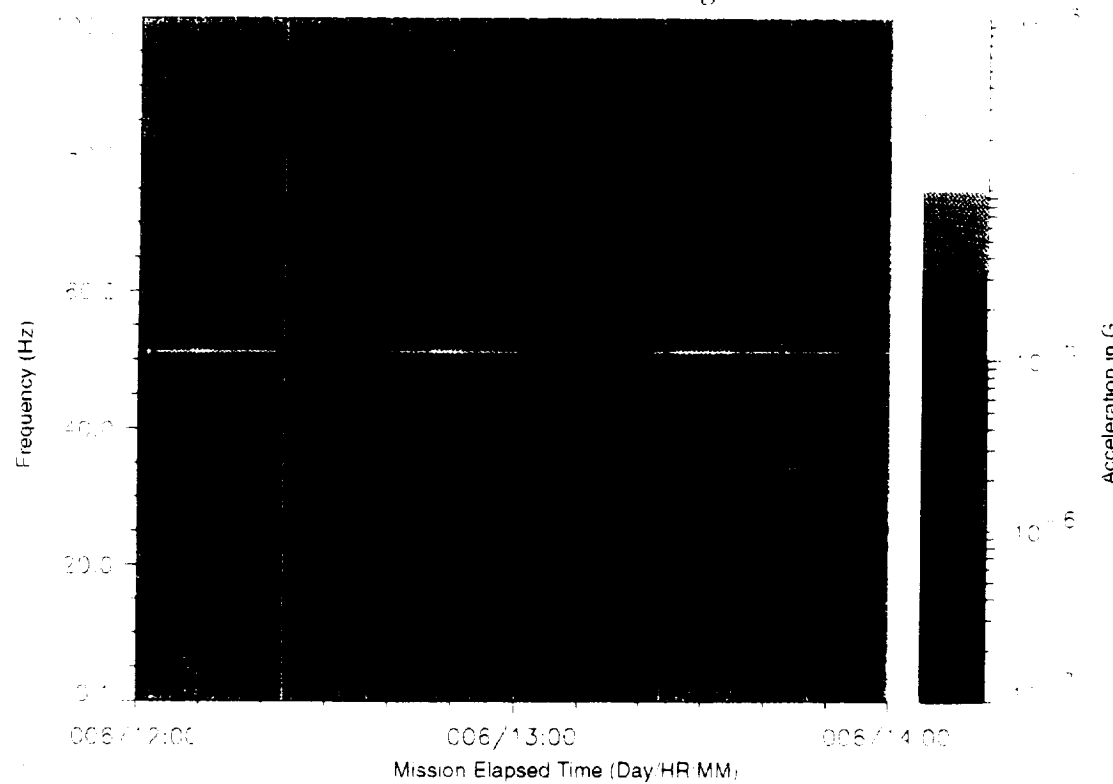


Figure B-269: SPACEHAB-1, Forward Bulkhead T-Beam

STS-57, Head A, X-Axis

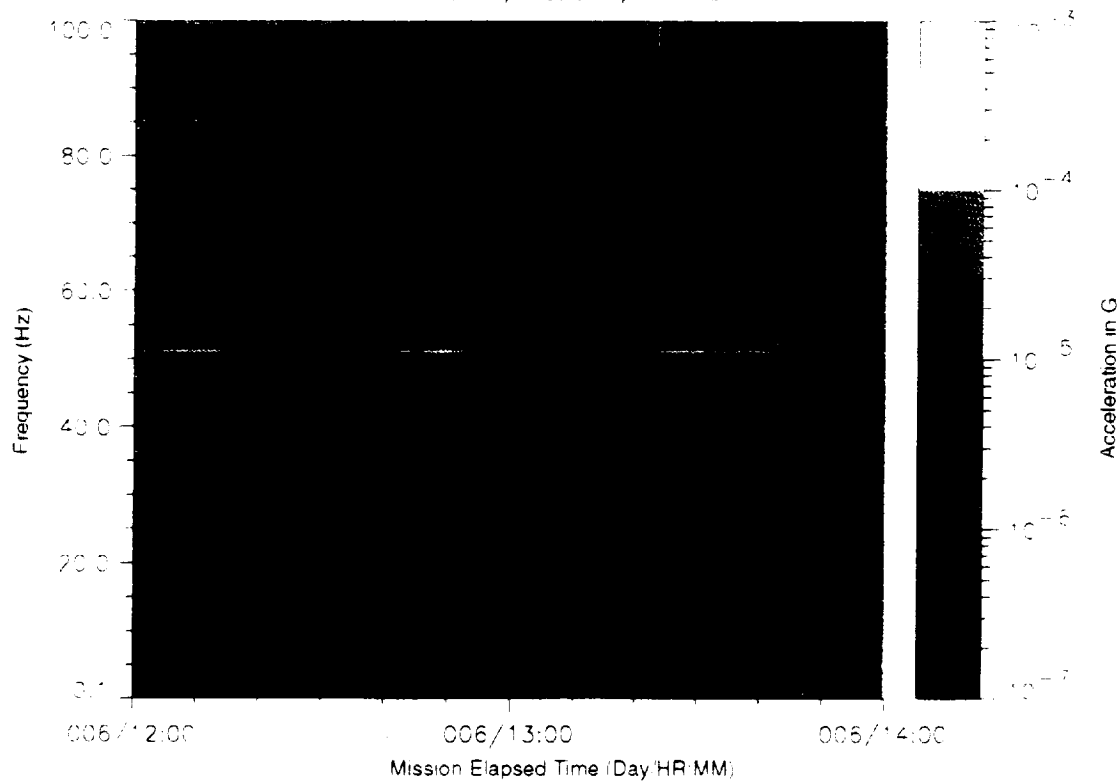


Figure B-270: SPACEHAB-1, Forward Bulkhead T-Beam

STS-57, Head A, Y-Axis

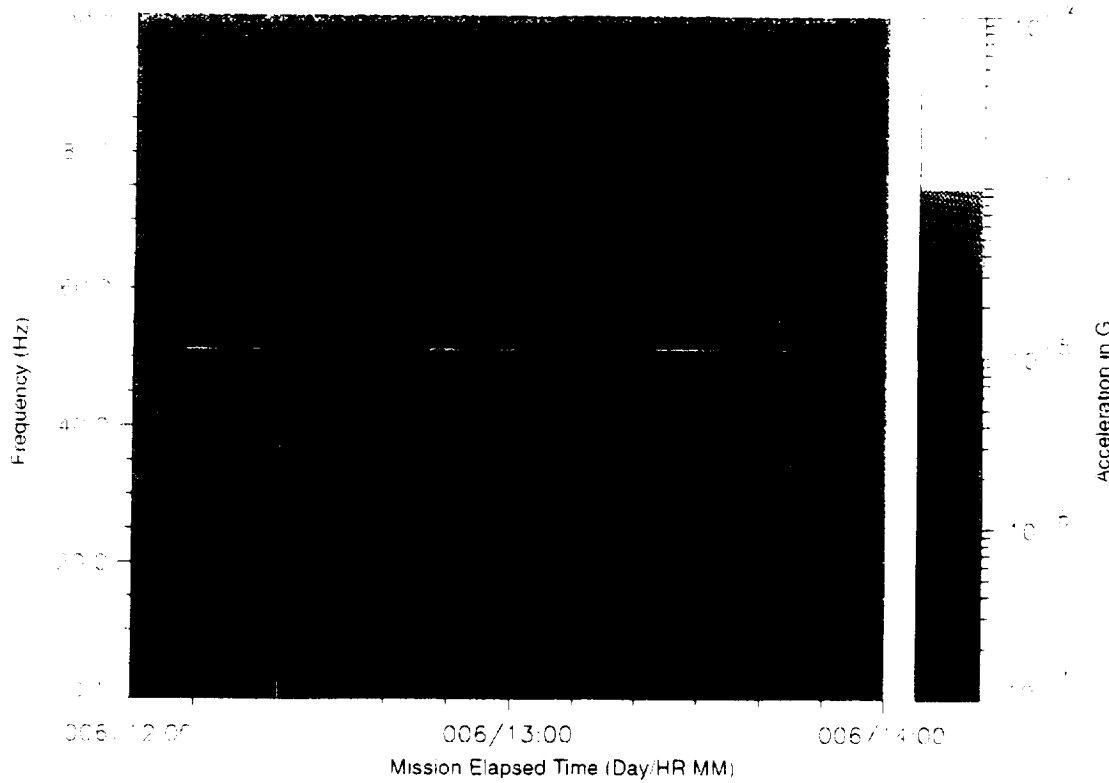


Figure B-271. SPACEHAB-1, Forward Bulkhead T-Beam

STS-57, Head A, Z-Axis

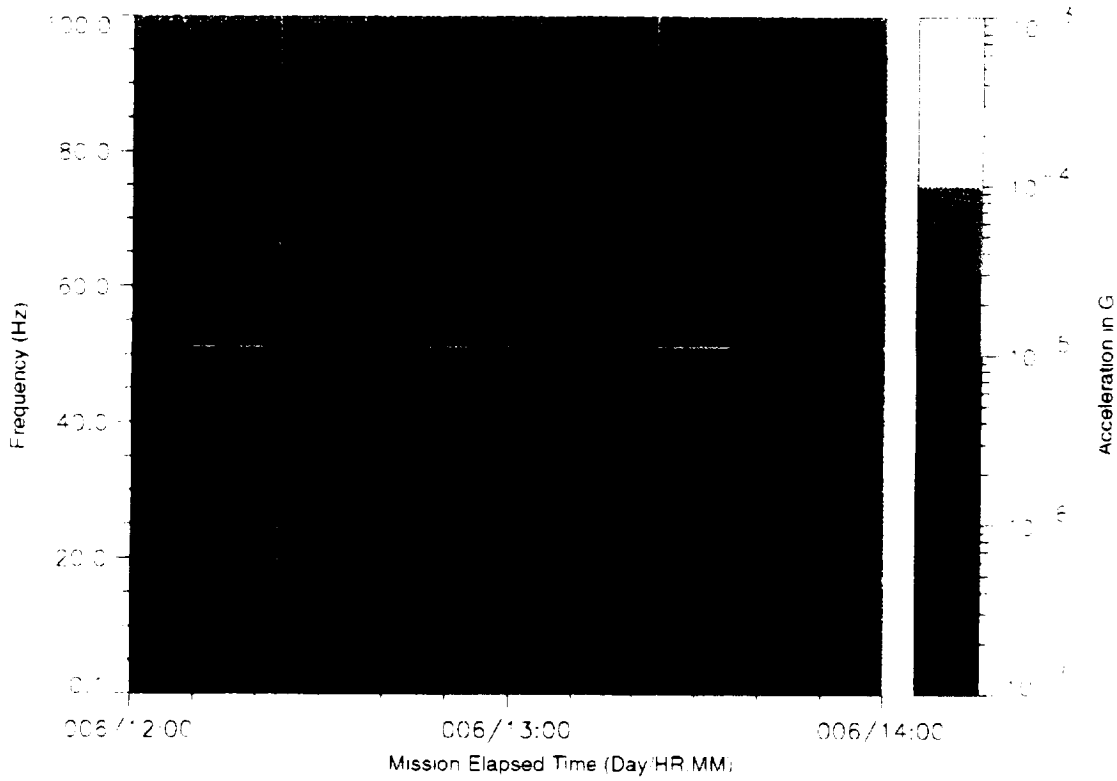


Figure B-272. SPACEHAB-1, Forward Bulkhead T-Beam

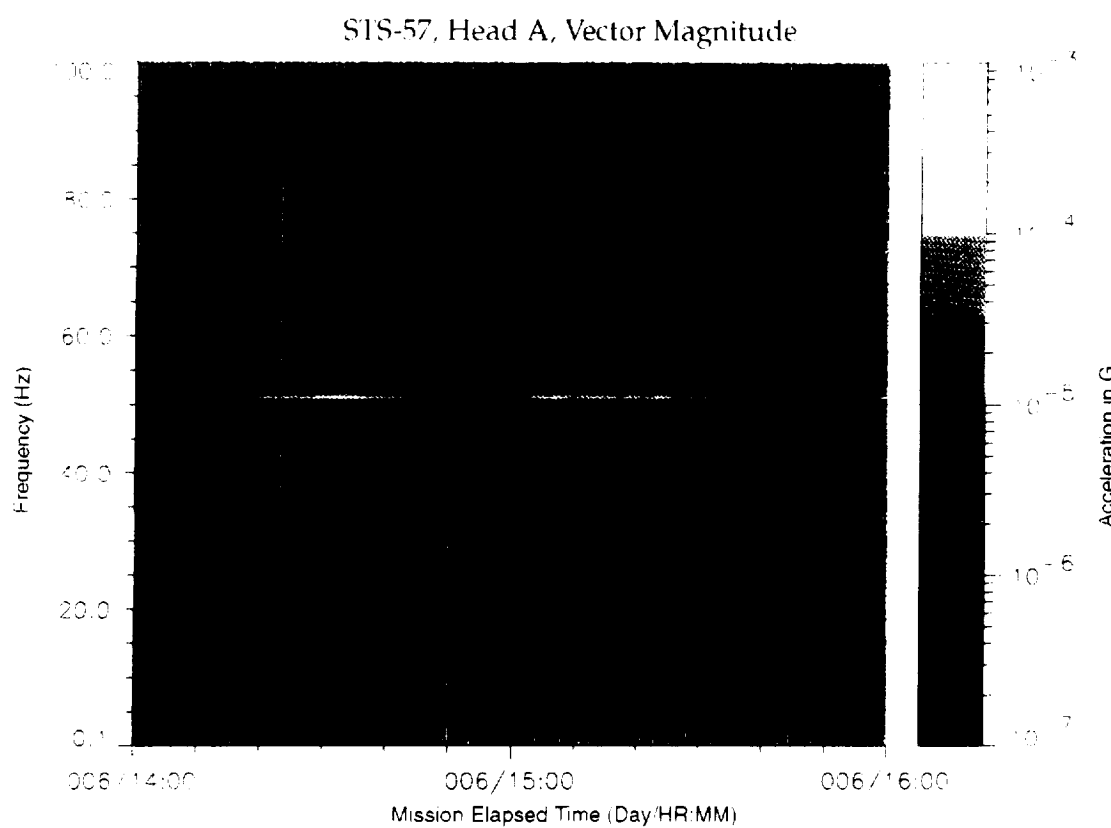


Figure B-273: SPACEHAB-1, Forward Bulkhead T-Beam

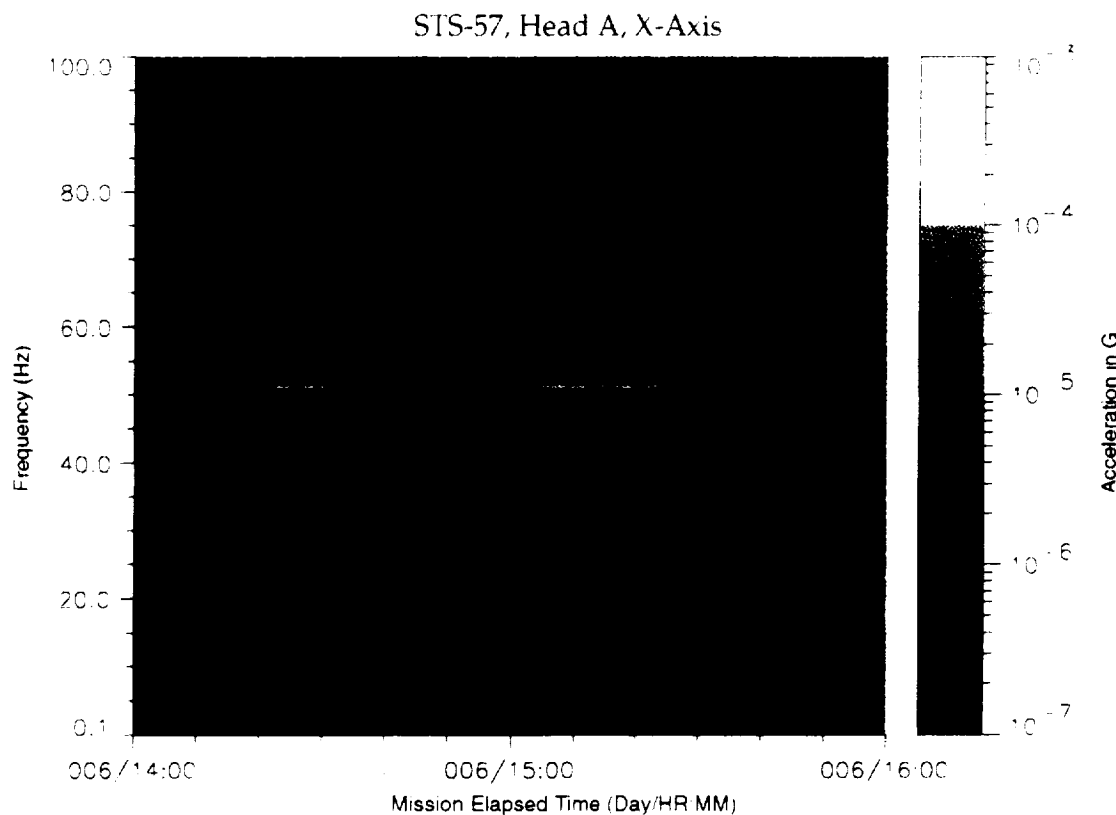


Figure B-274: SPACEHAB-1, Forward Bulkhead T-Beam

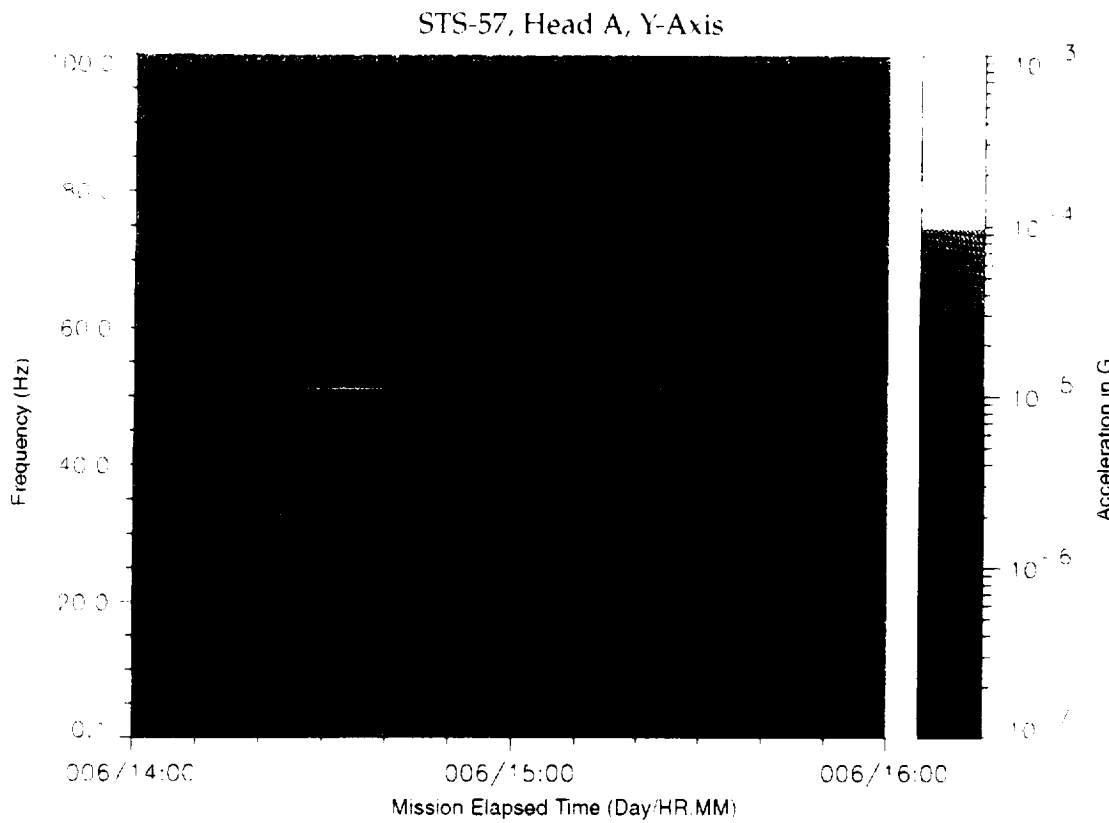


Figure B-275: SPACEHAB-1, Forward Bulkhead T-Beam

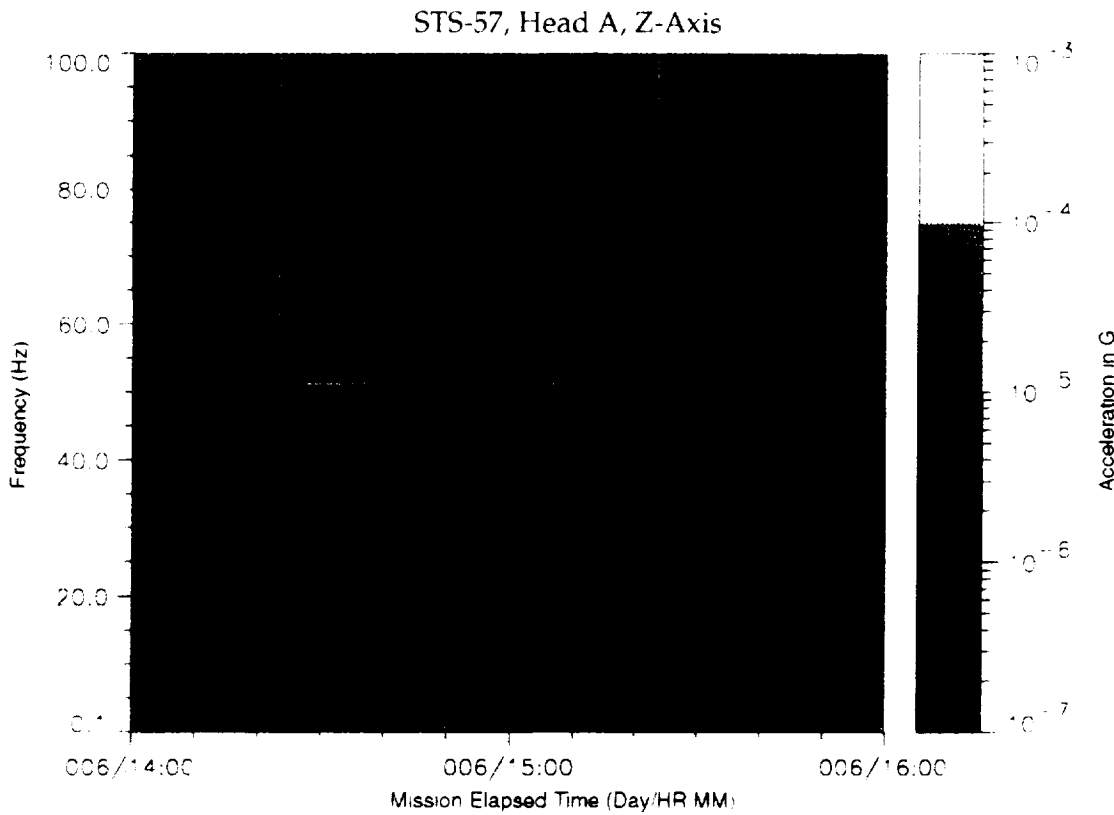


Figure B-276: SPACEHAB-1, Forward Bulkhead T-Beam

STS-57, Head A, Vector Magnitude

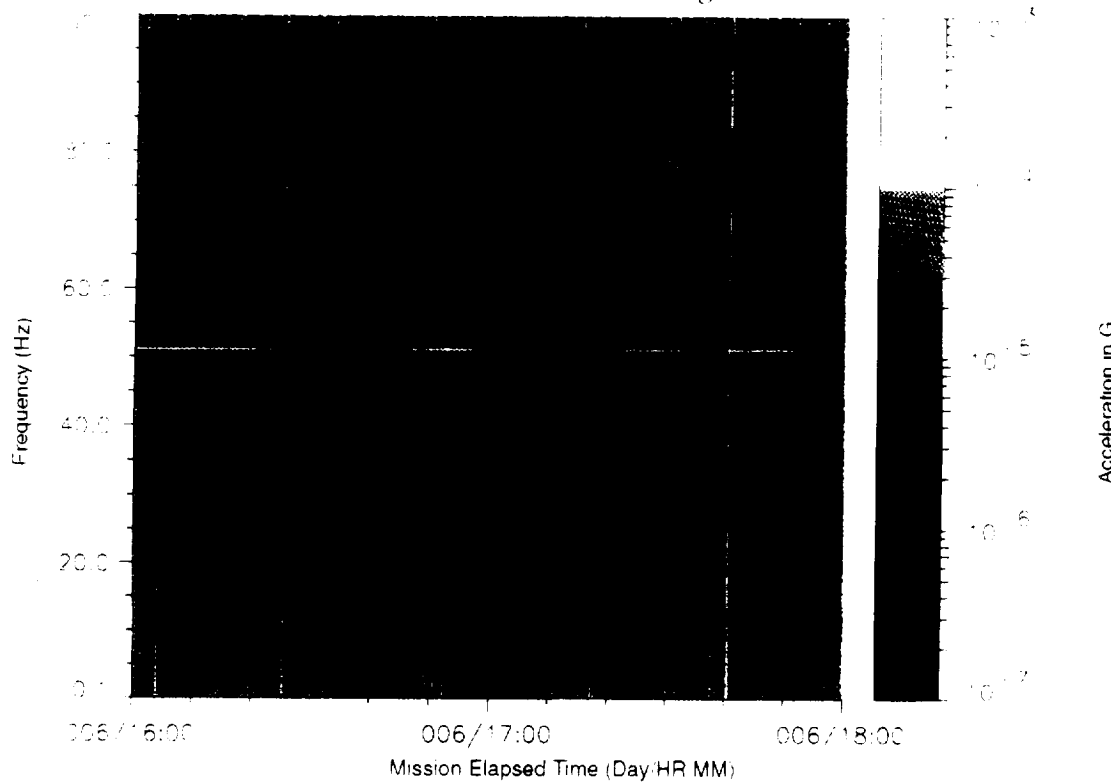


Figure B-277: SPACEHAB-1, Forward Bulkhead I-Beam

STS-57, Head A, X-Axis

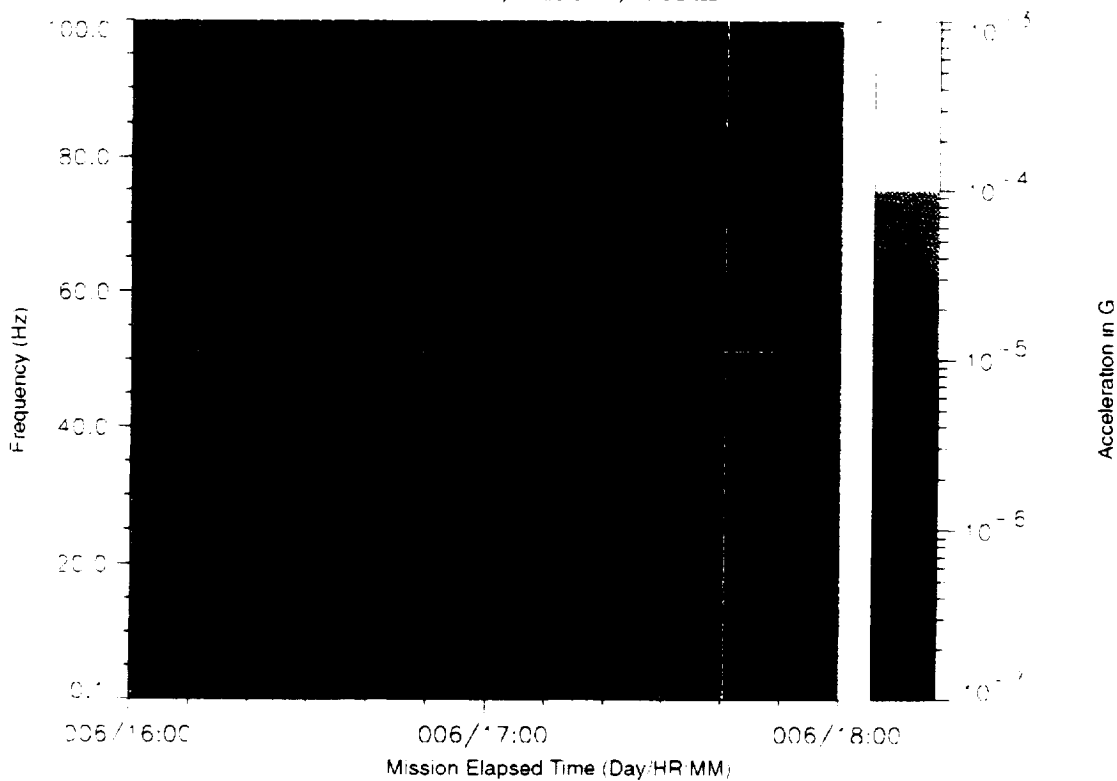


Figure B-278: SPACEHAB-1, Forward Bulkhead T-Beam

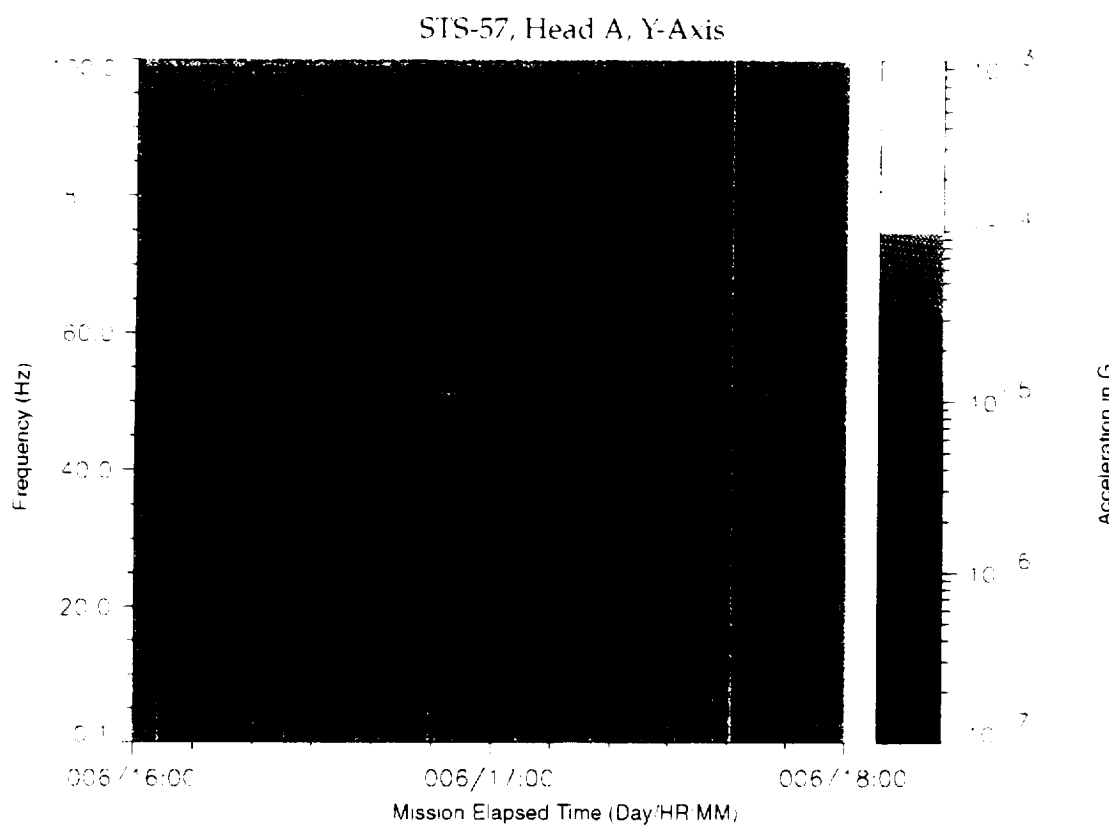


Figure B-279: SPACEHAB-1, Forward Bulkhead T-Beam

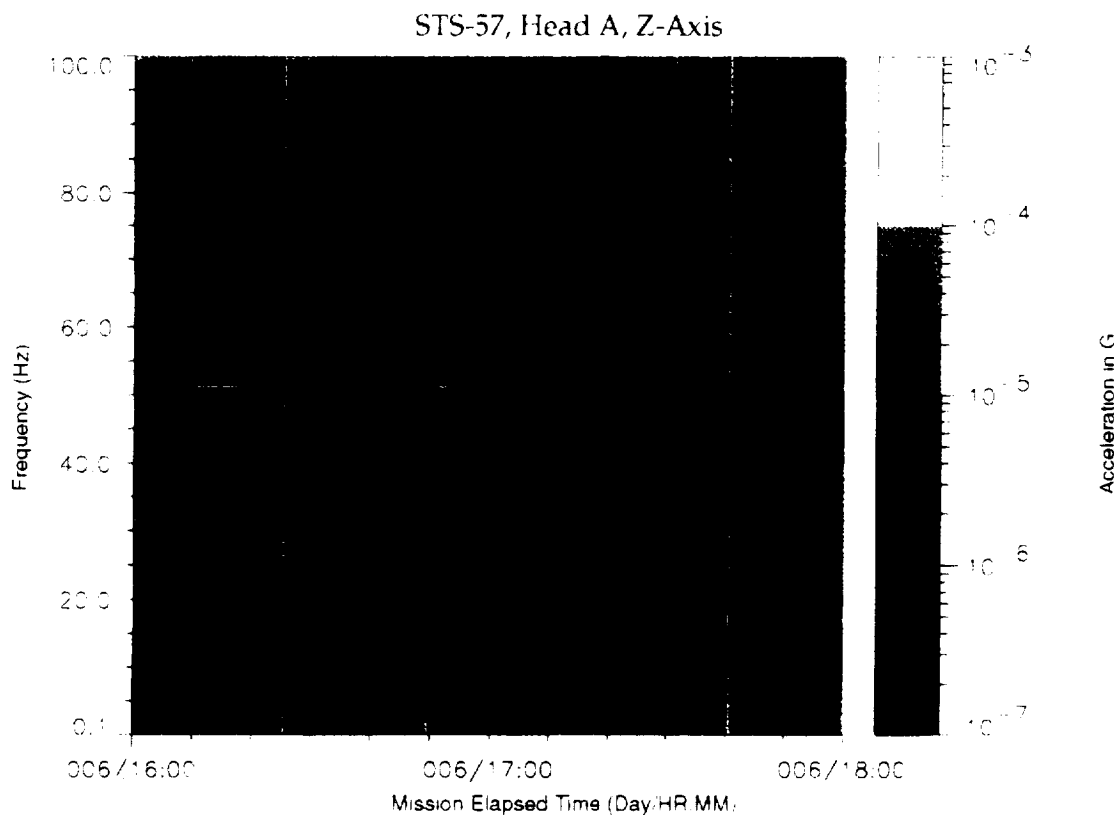


Figure B-280: SPACEHAB-1, Forward Bulkhead T-Beam

STS-57, Head A, Vector Magnitude

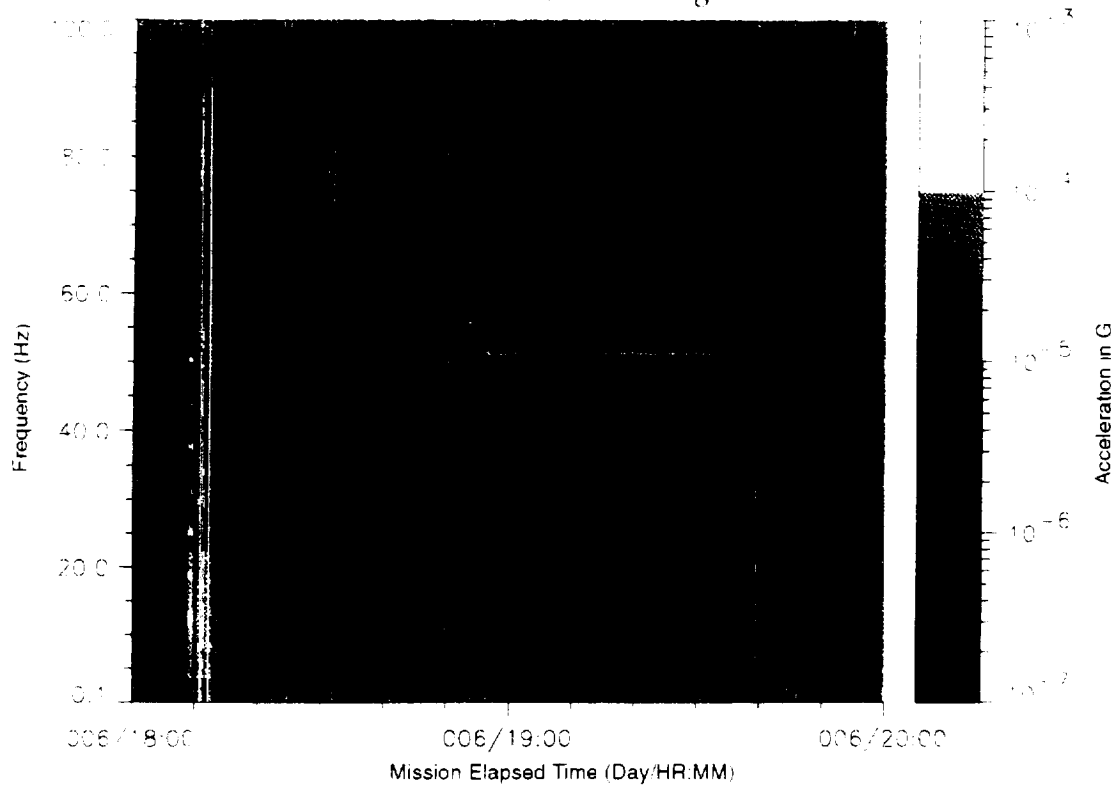


Figure B-281: SPACEHAB-1, Forward Bulkhead T-Beam

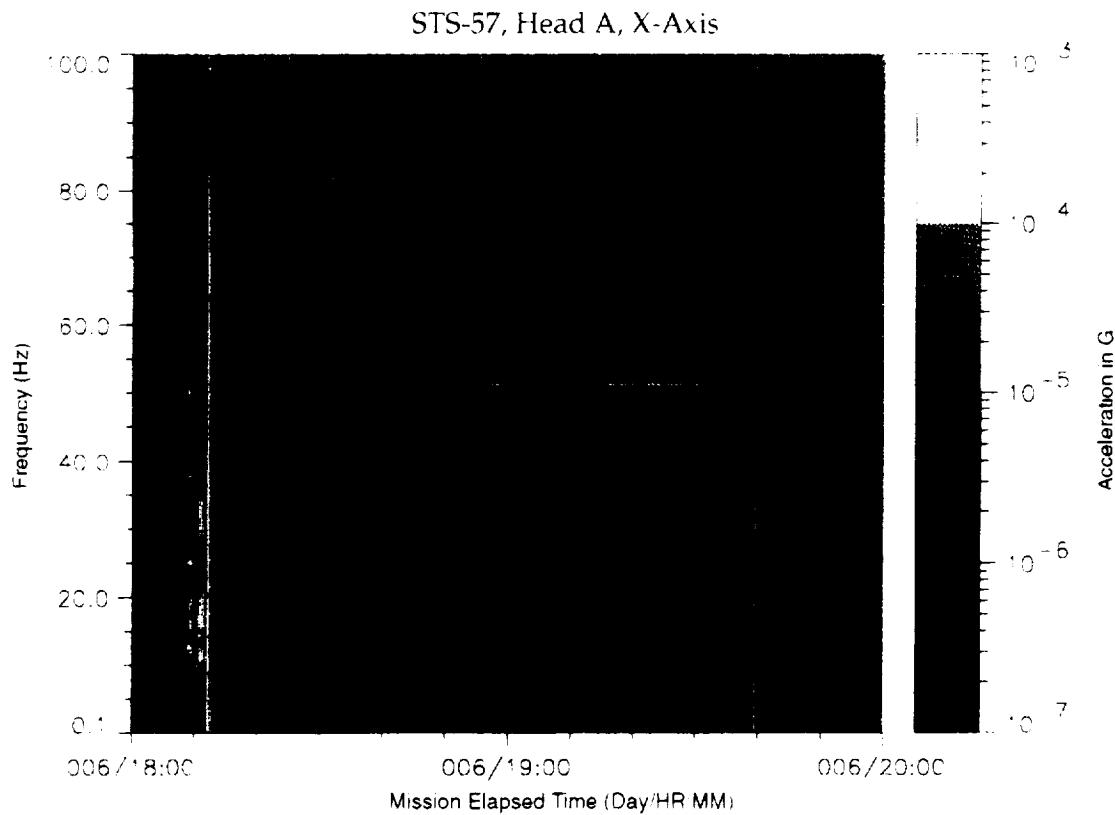


Figure B-282: SPACEHAB-1, Forward Bulkhead T-Beam

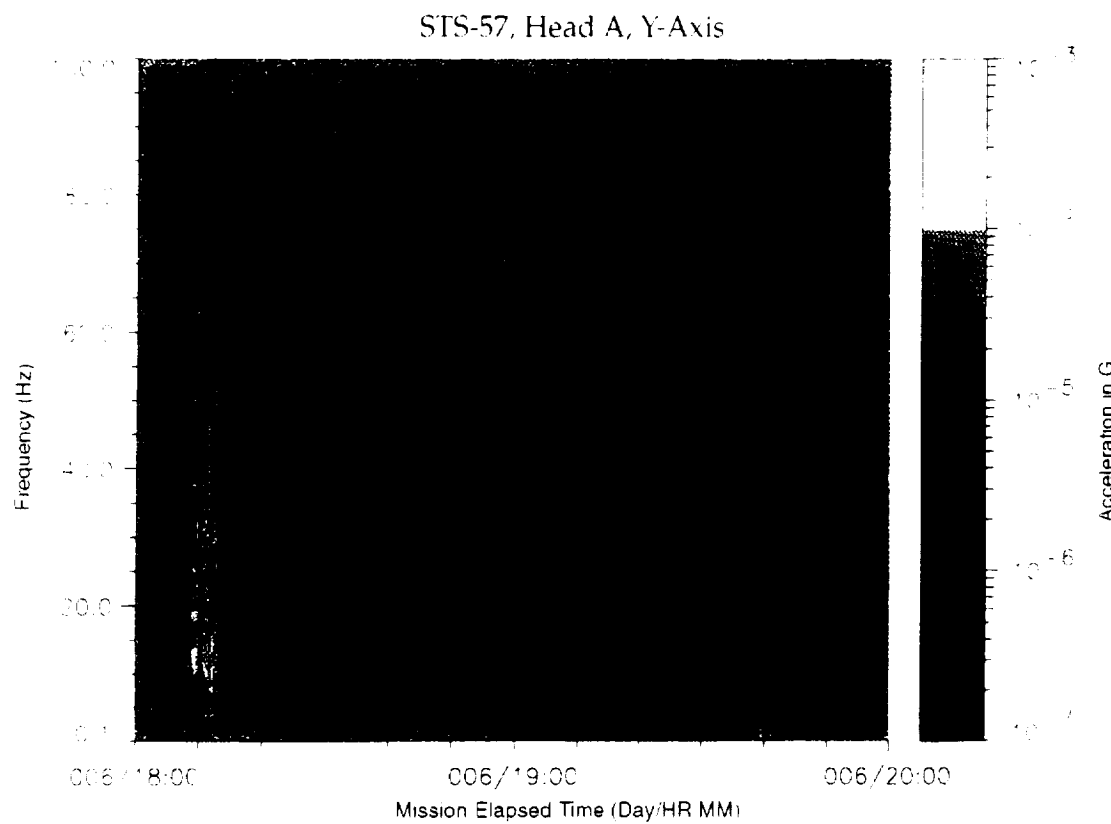


Figure B-283: SPACEHAB-1, Forward Bulkhead T-Beam

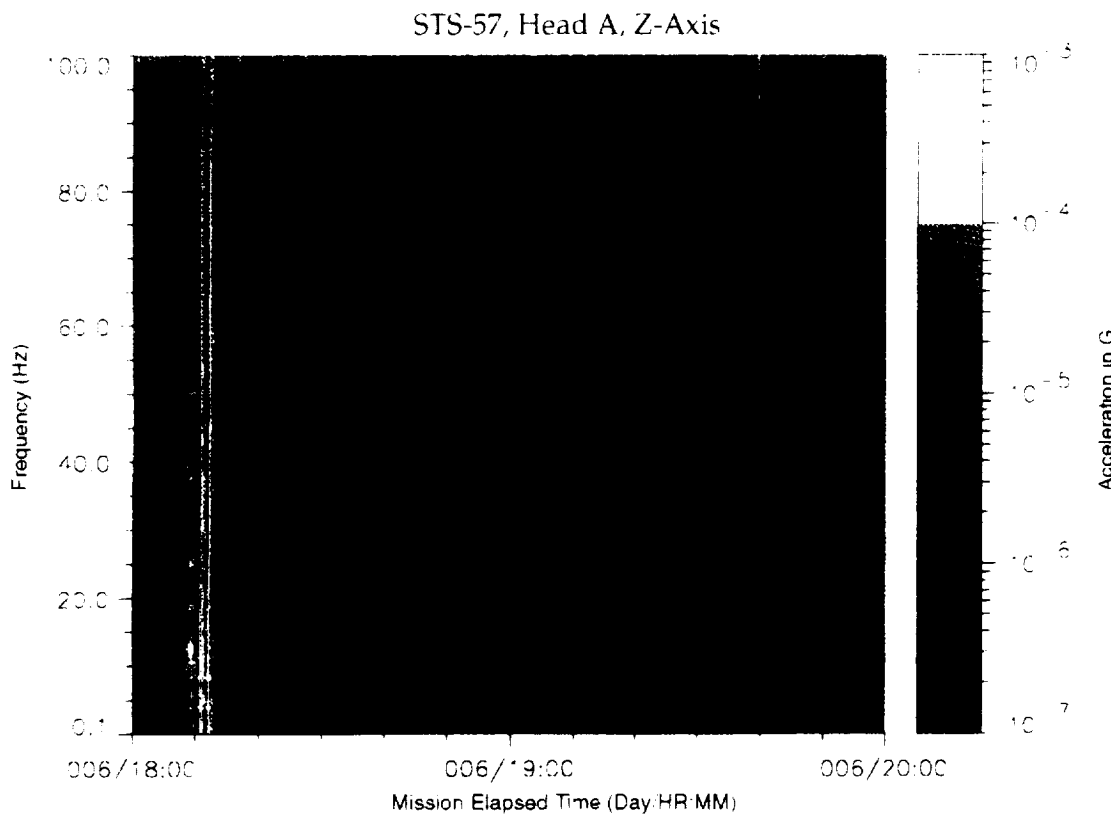


Figure B-284: SPACEHAB-1, Forward Bulkhead T-Beam

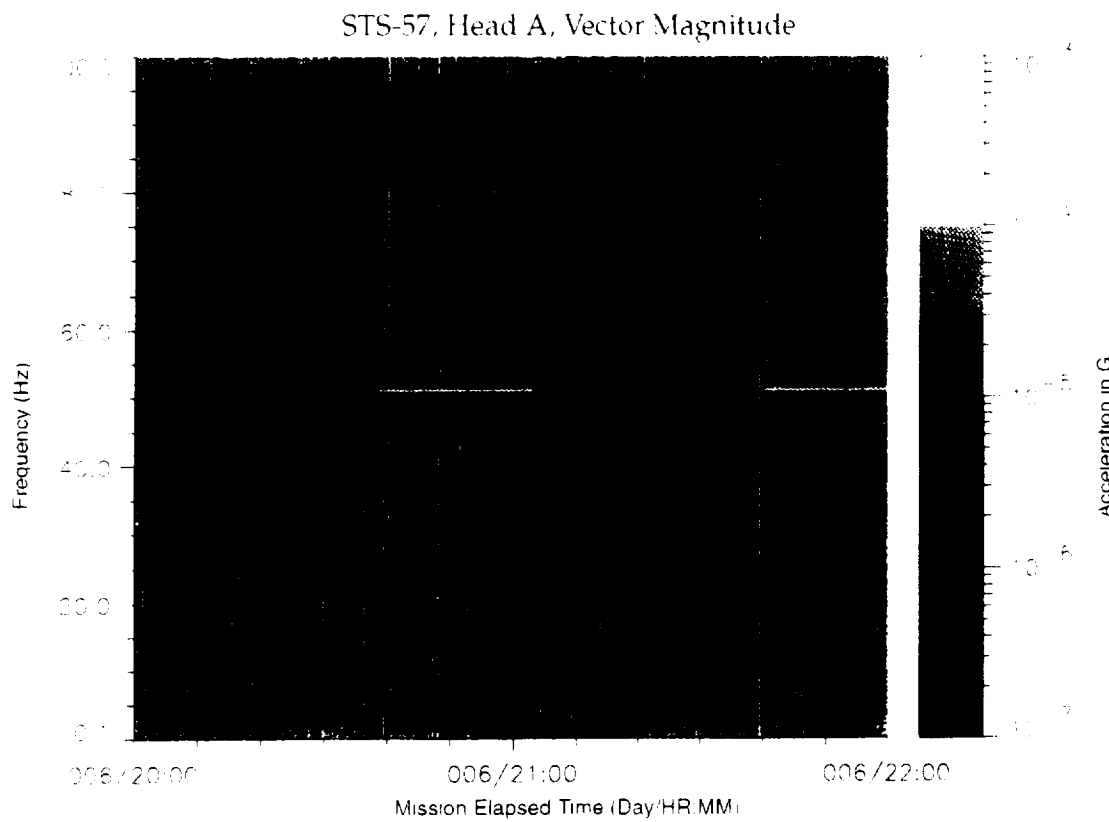


Figure B-285: SPACEHAB-1, Forward Bulkhead T-Beam

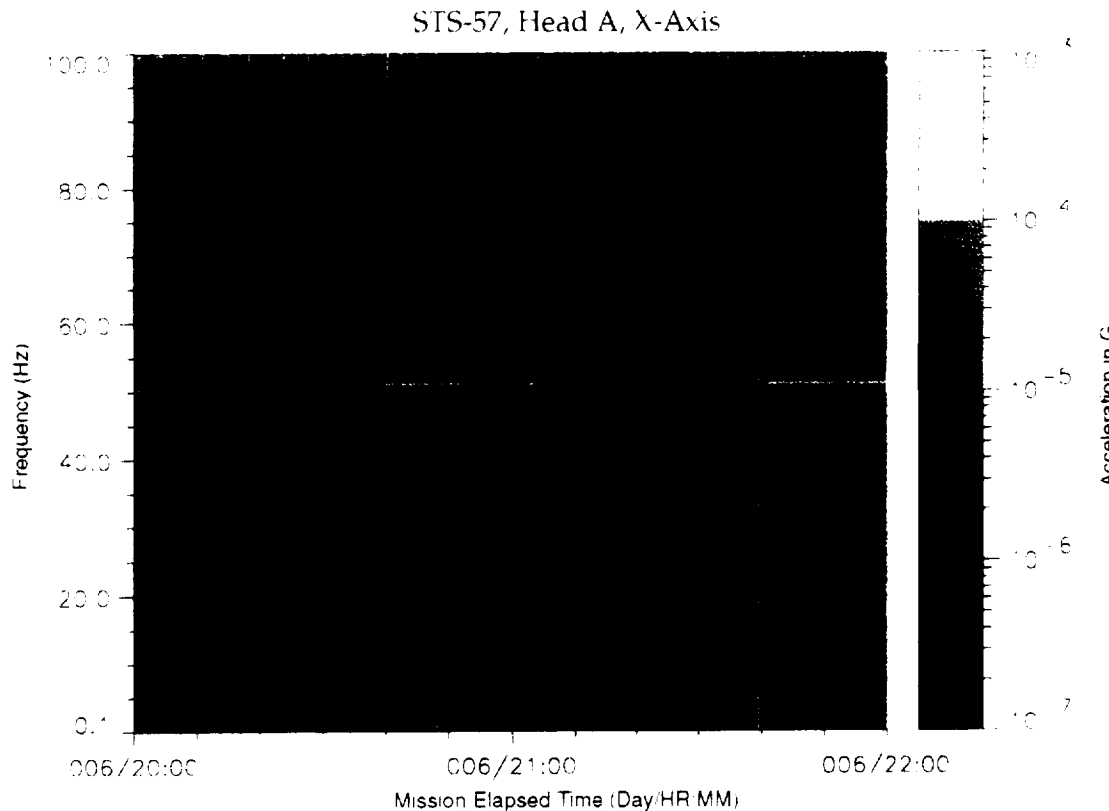


Figure B-286: SPACEHAB-1, Forward Bulkhead T-Beam

PROCESSED AND QUALITY CONTROLLED

STS-57, Head A, Y-Axis

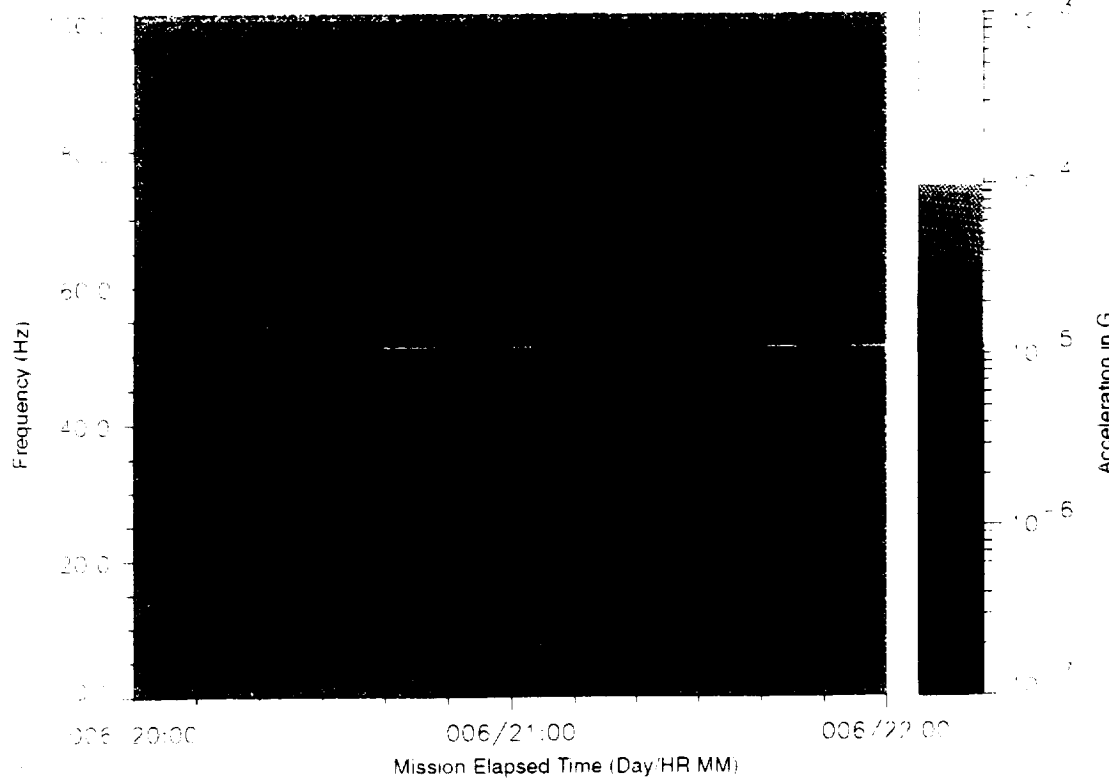


Figure B-287: SPACEHAB-1, Forward Bulkhead T-Beam

STS-57, Head A, Z-Axis

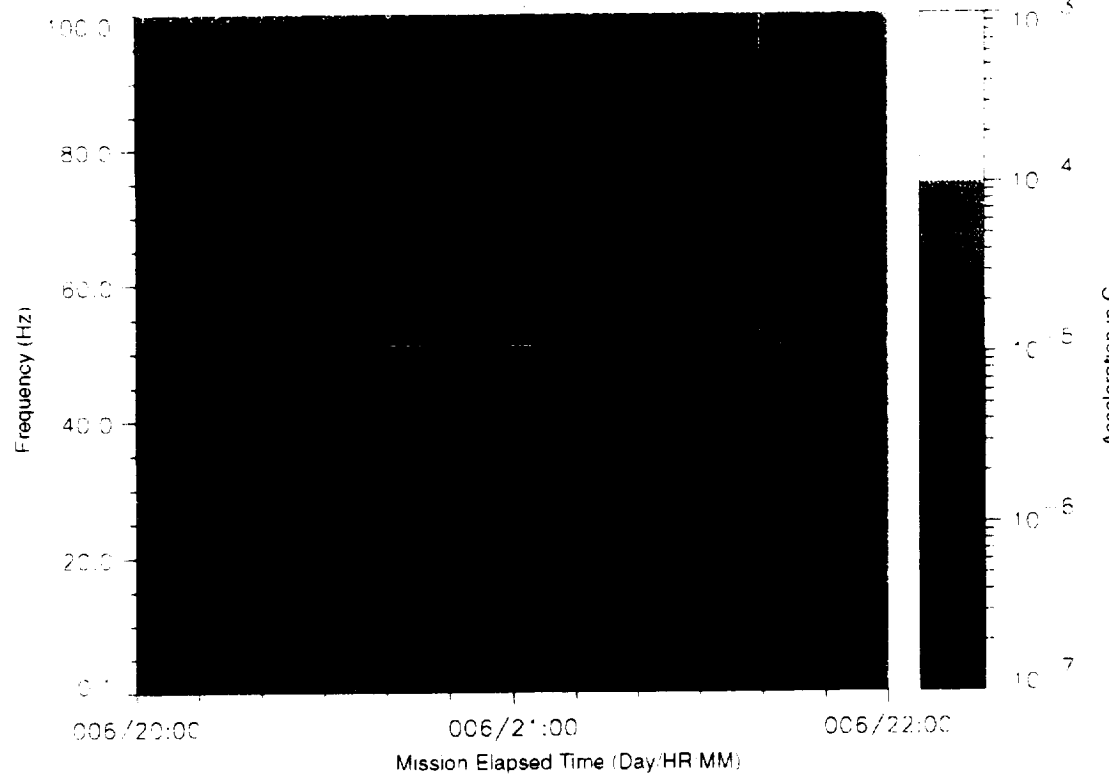


Figure B-288: SPACEHAB-1, Forward Bulkhead T-Beam

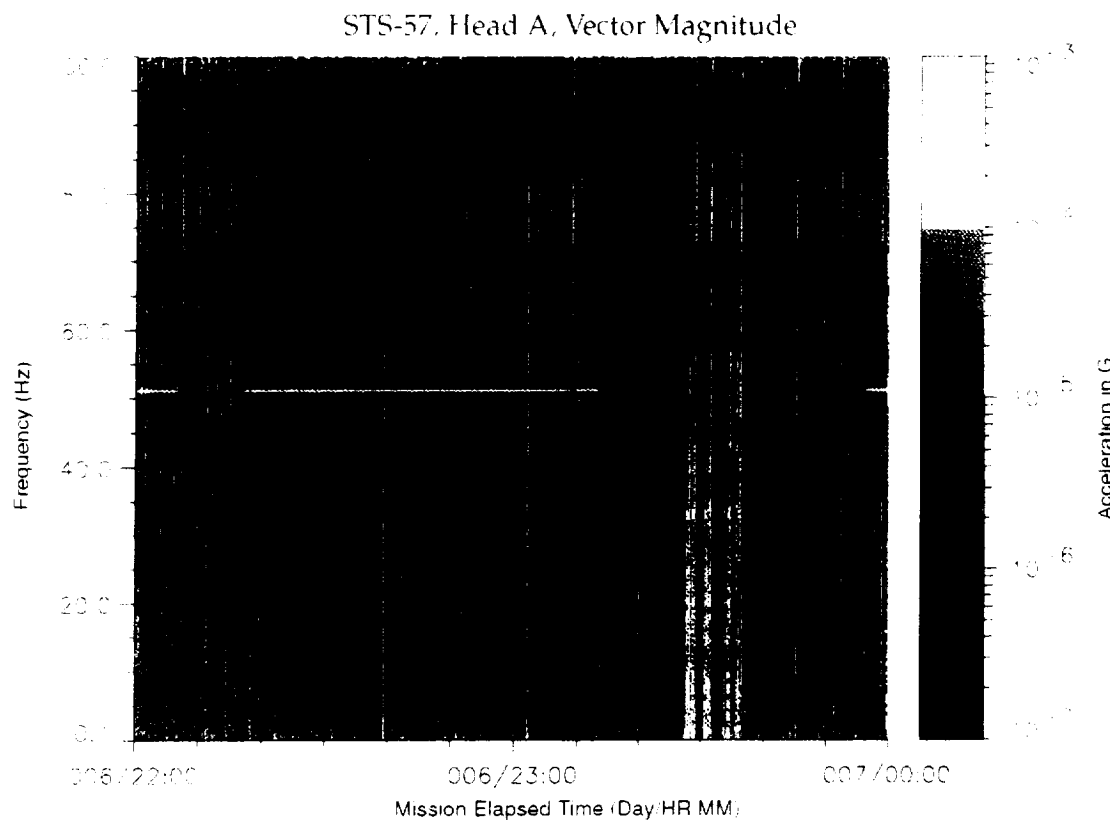


Figure B-289: SPACEHAB-1, Forward Bulkhead T-Beam

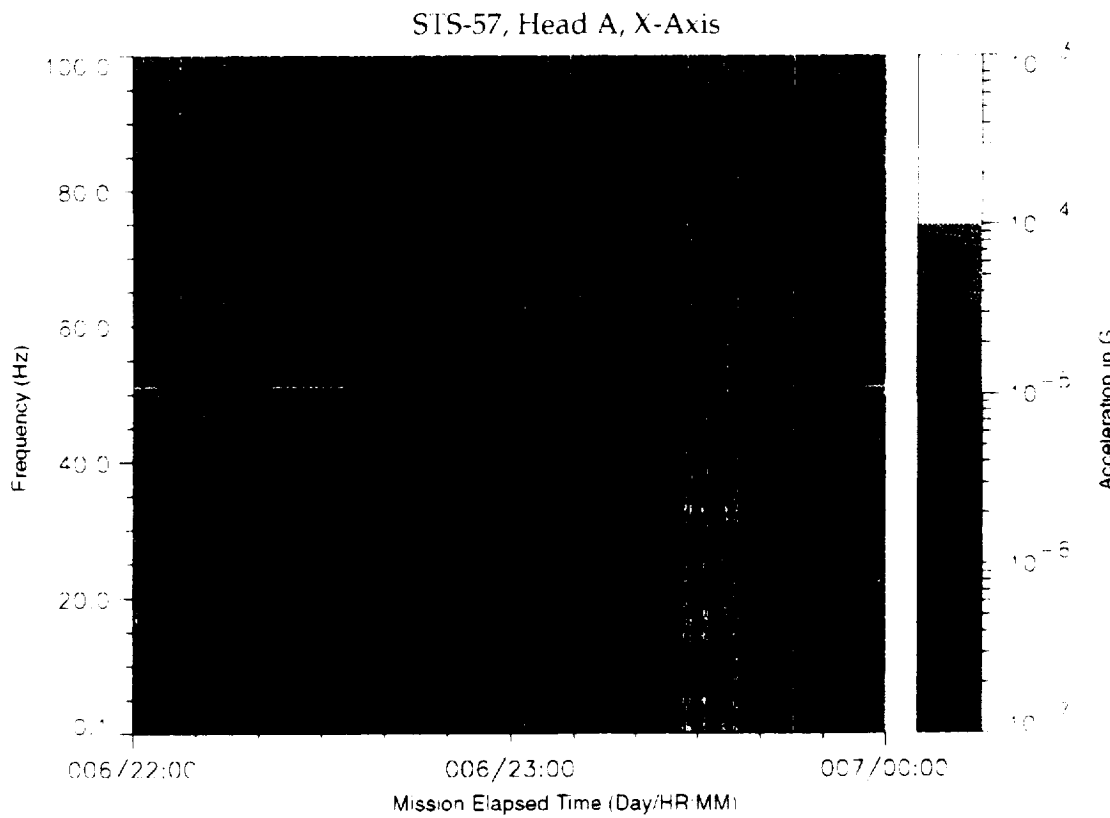


Figure B-290: SPACEHAB-1, Forward Bulkhead T-Beam

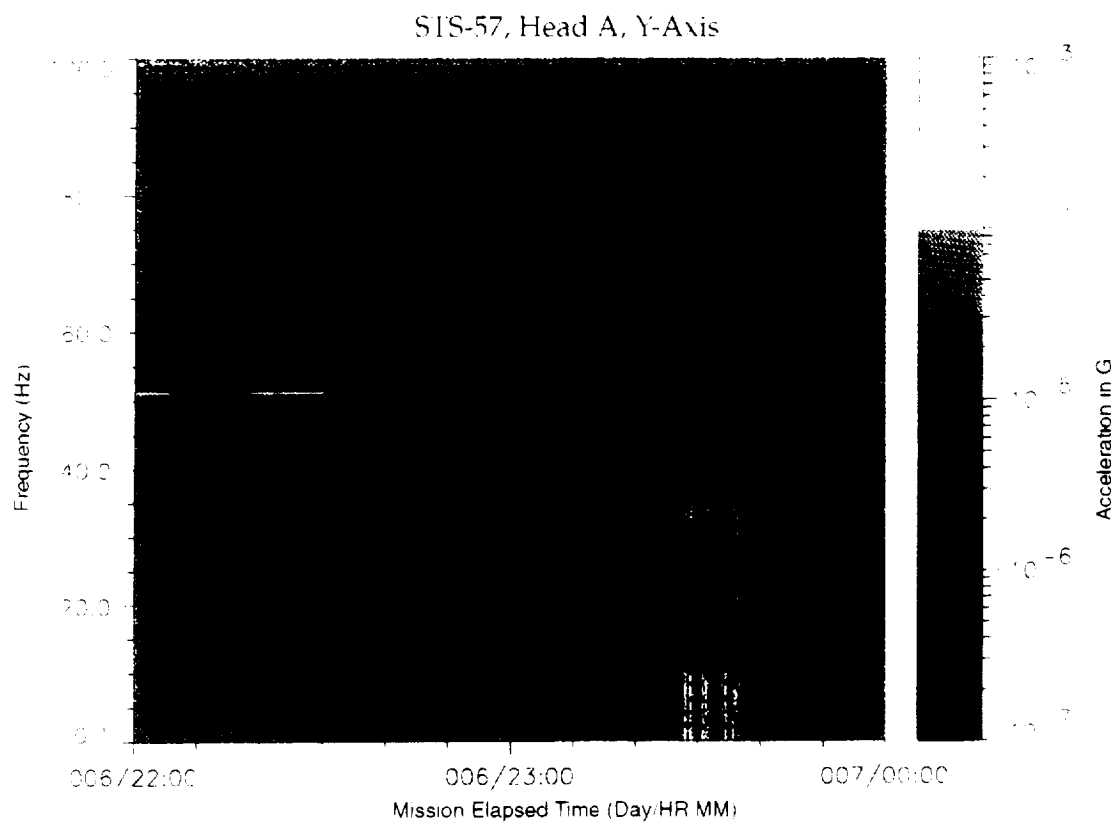


Figure B-291: SPACEHAB-1, Forward Bulkhead T-Beam

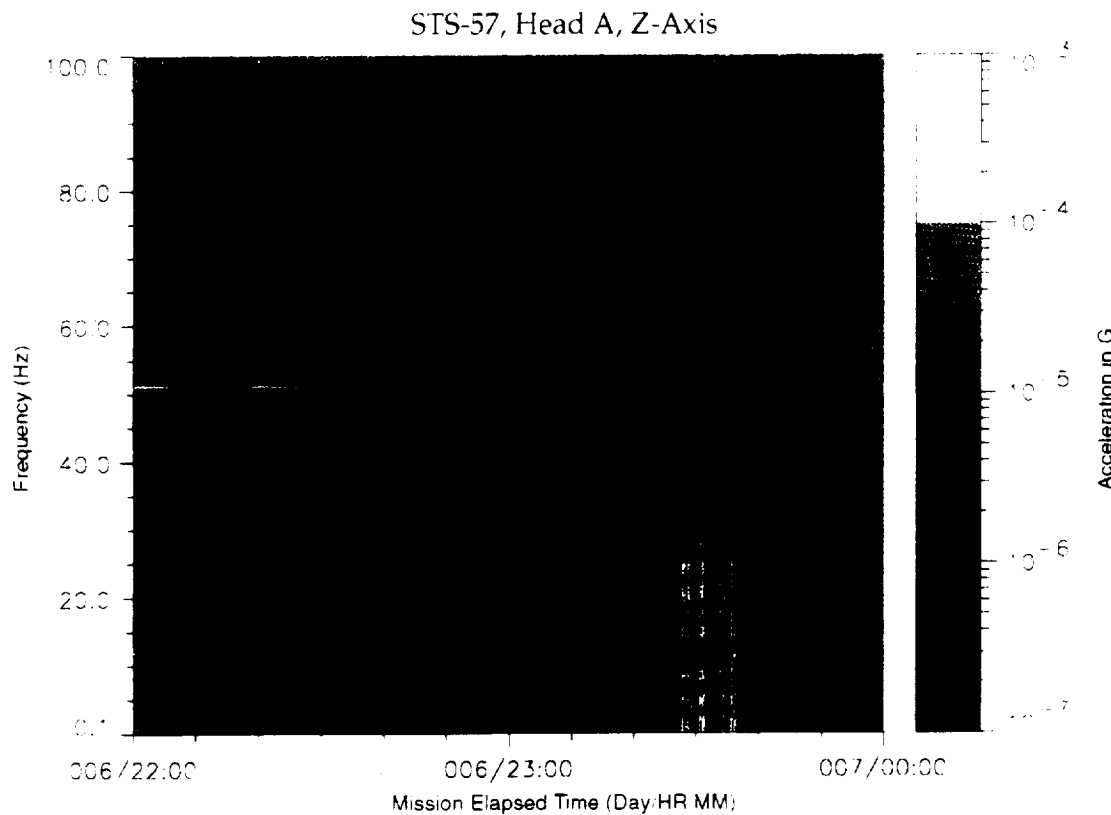


Figure B-292: SPACEHAB-1, Forward Bulkhead T-Beam

STS-57, Head A, Vector Magnitude

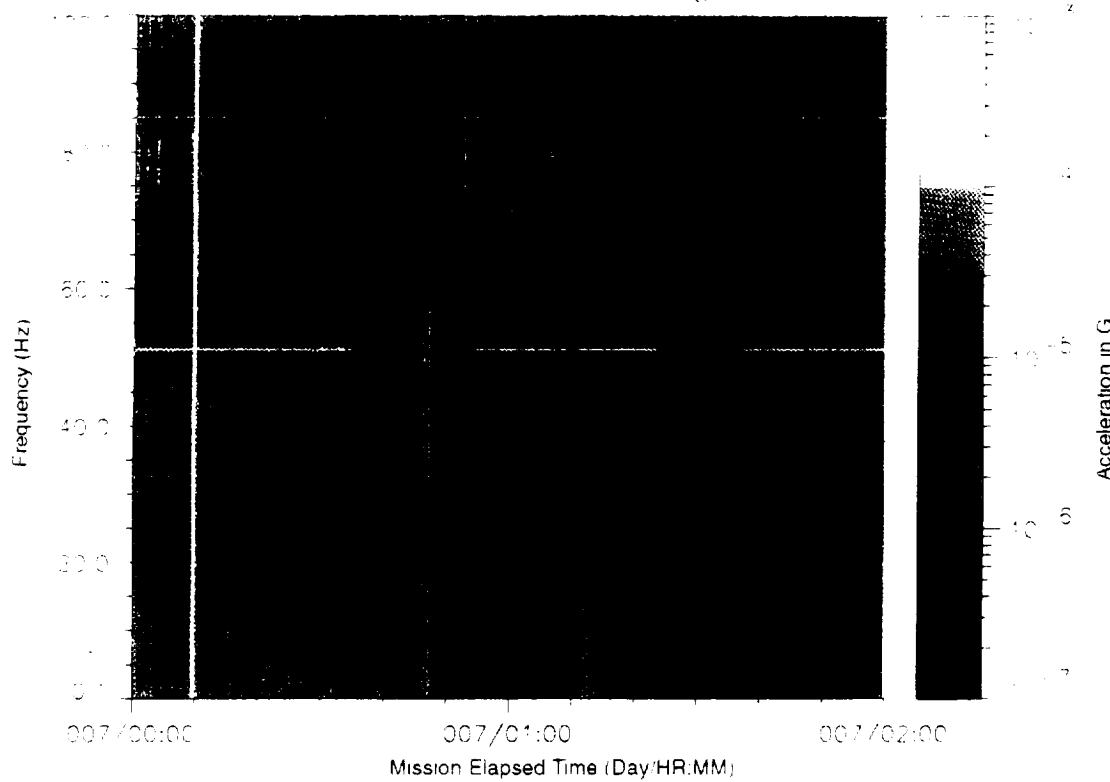


Figure B-293: SPACEHAB-1, Forward Bulkhead T-Beam

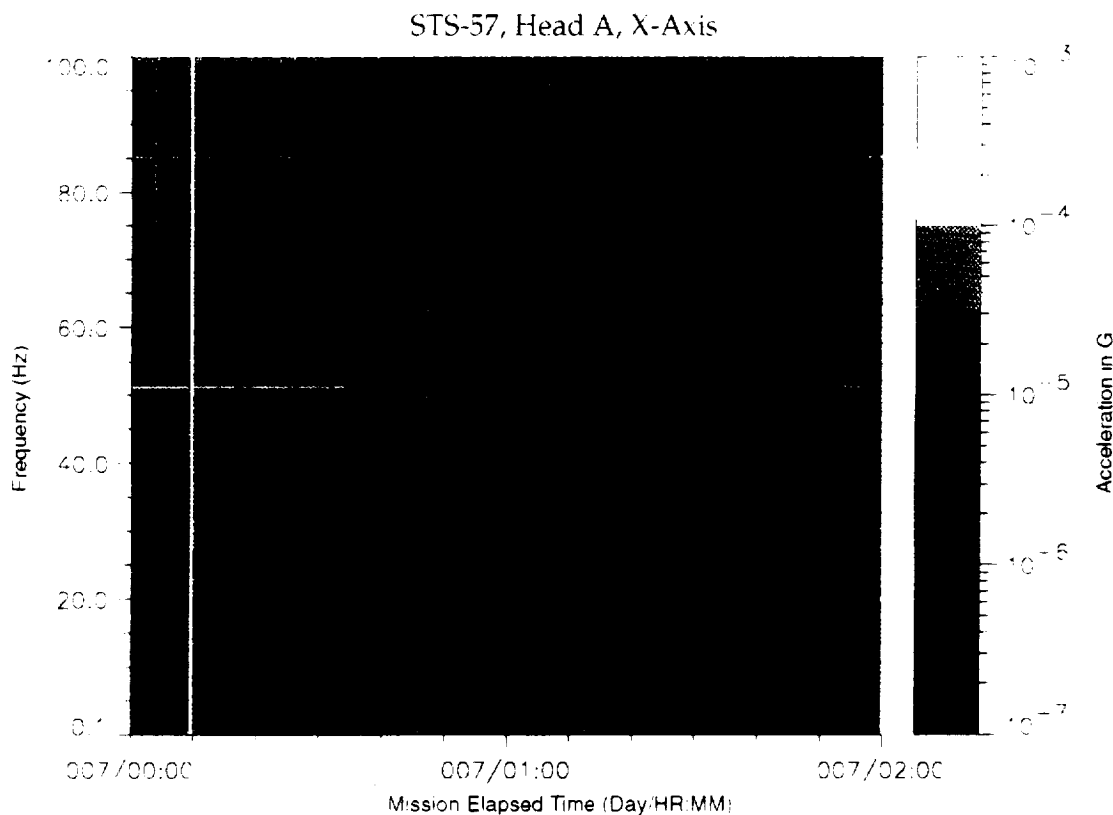


Figure B-294: SPACEHAB-1, Forward Bulkhead T-Beam

STS-57, Head A, Y-Axis

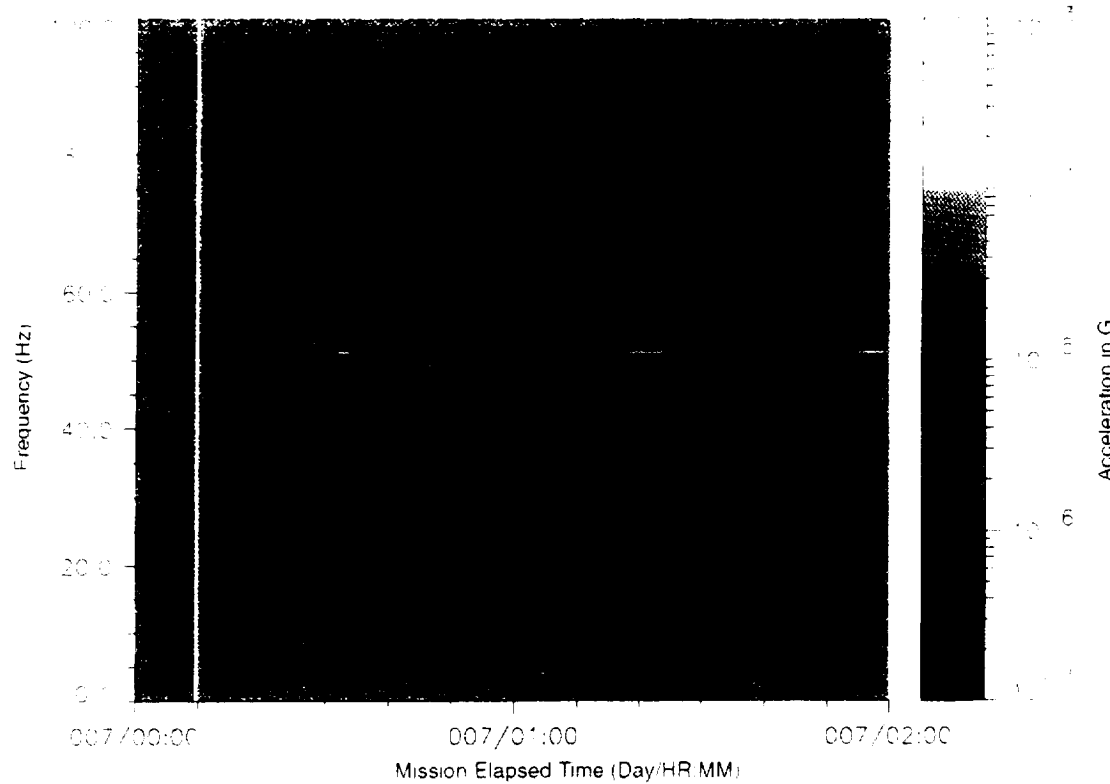


Figure B-295: SPACEHAB-1, Forward Bulkhead T-Beam

STS-57, Head A, Z-Axis

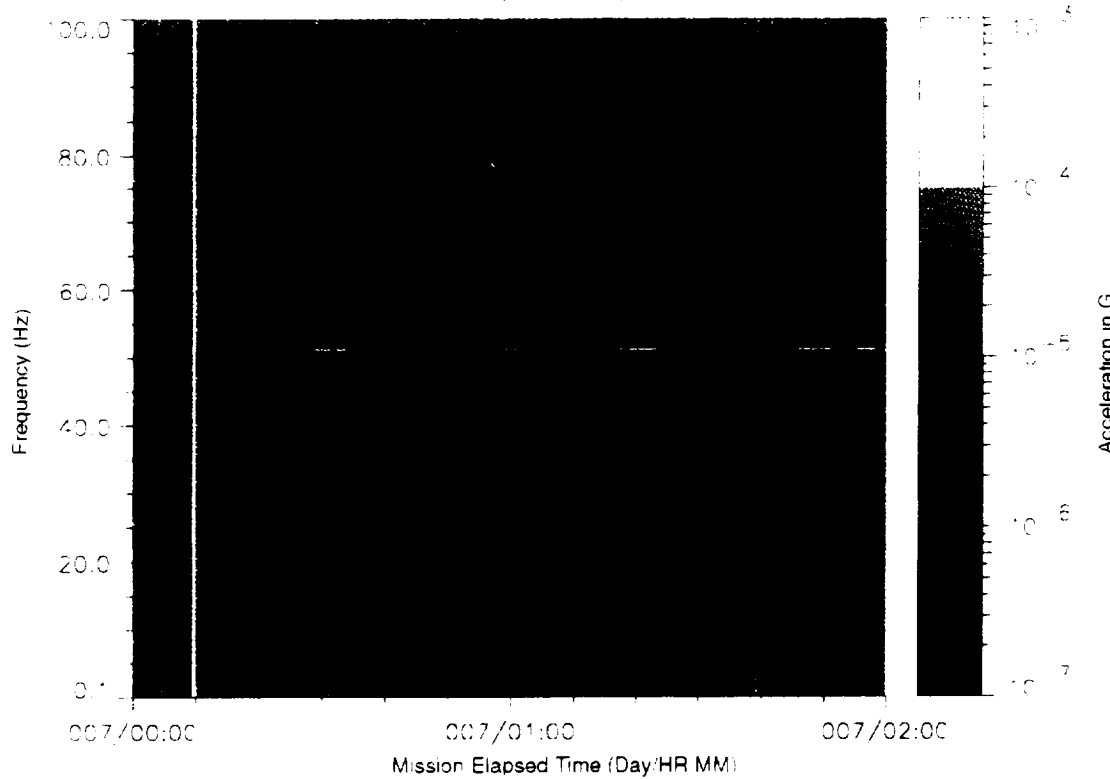


Figure B-296: SPACEHAB-1, Forward Bulkhead T-Beam

STS-57, Head A, Vector Magnitude

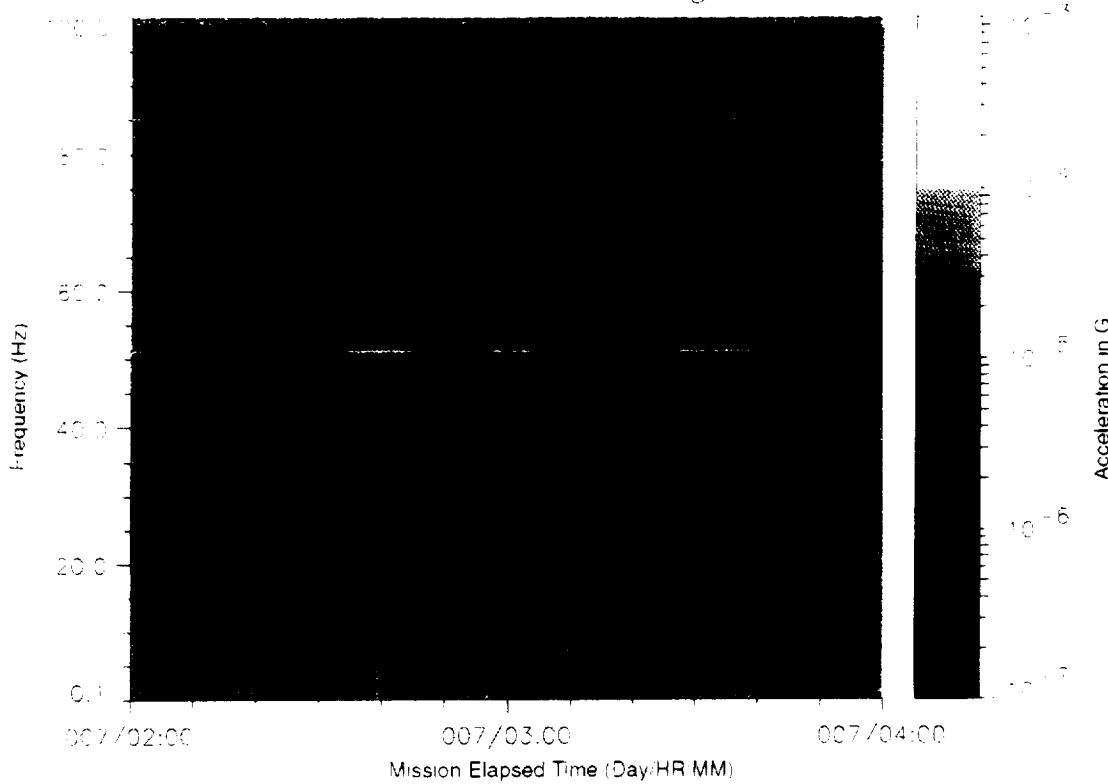


Figure B-297: SPACEHAB-1, Forward Bulkhead T-Beam

STS-57, Head A, X-Axis

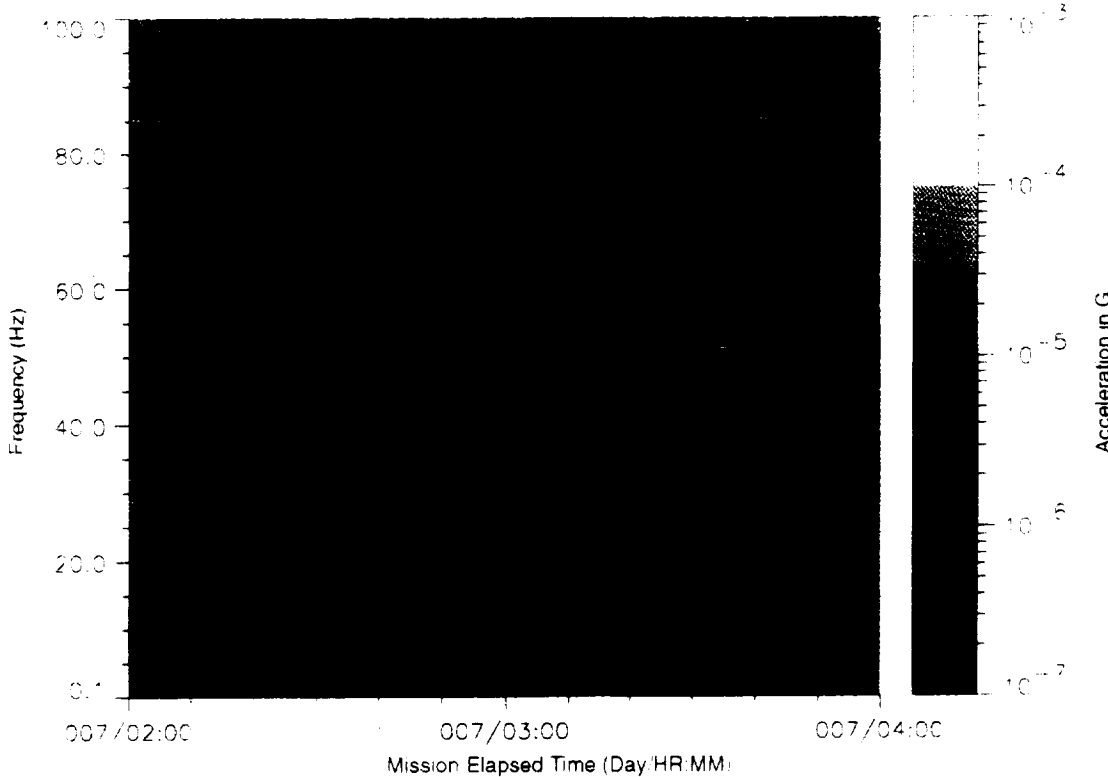


Figure B-298: SPACEHAB-1, Forward Bulkhead T-Beam

PRECEDING PAGE BLANK NOT FILMED

STS-57, Head A, Y-Axis

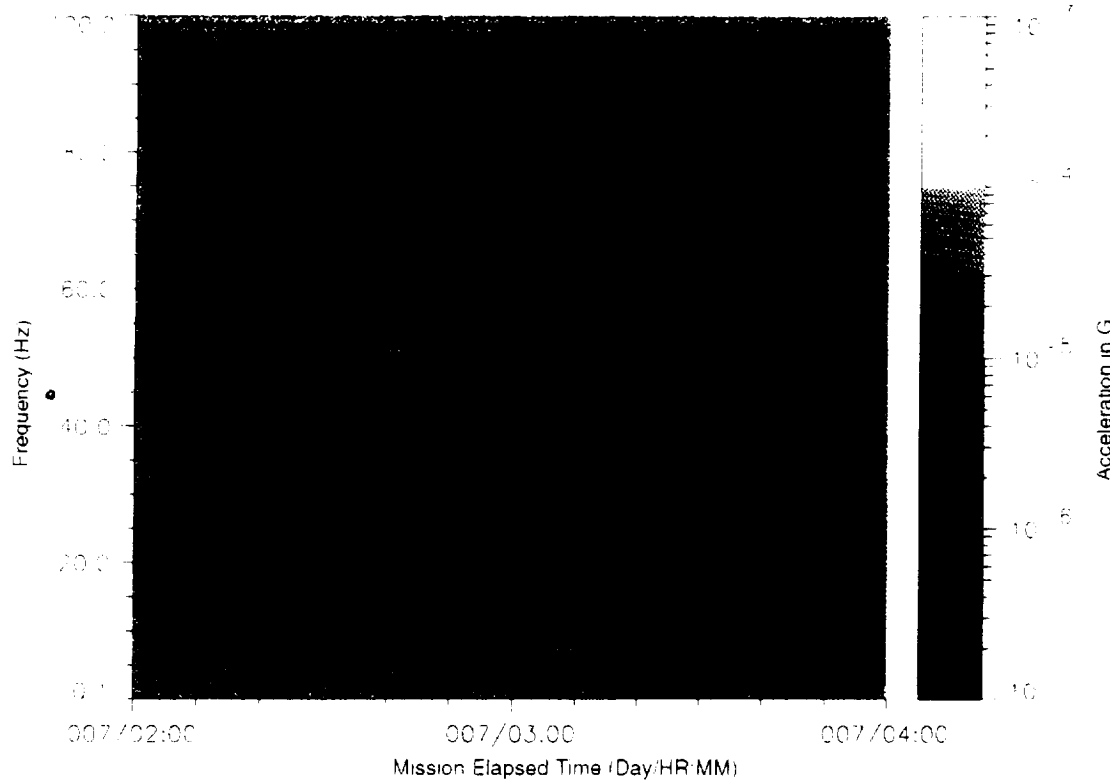


Figure B-299: SPACEHAB-1, Forward Bulkhead T-Beam

STS-57, Head A, Z-Axis

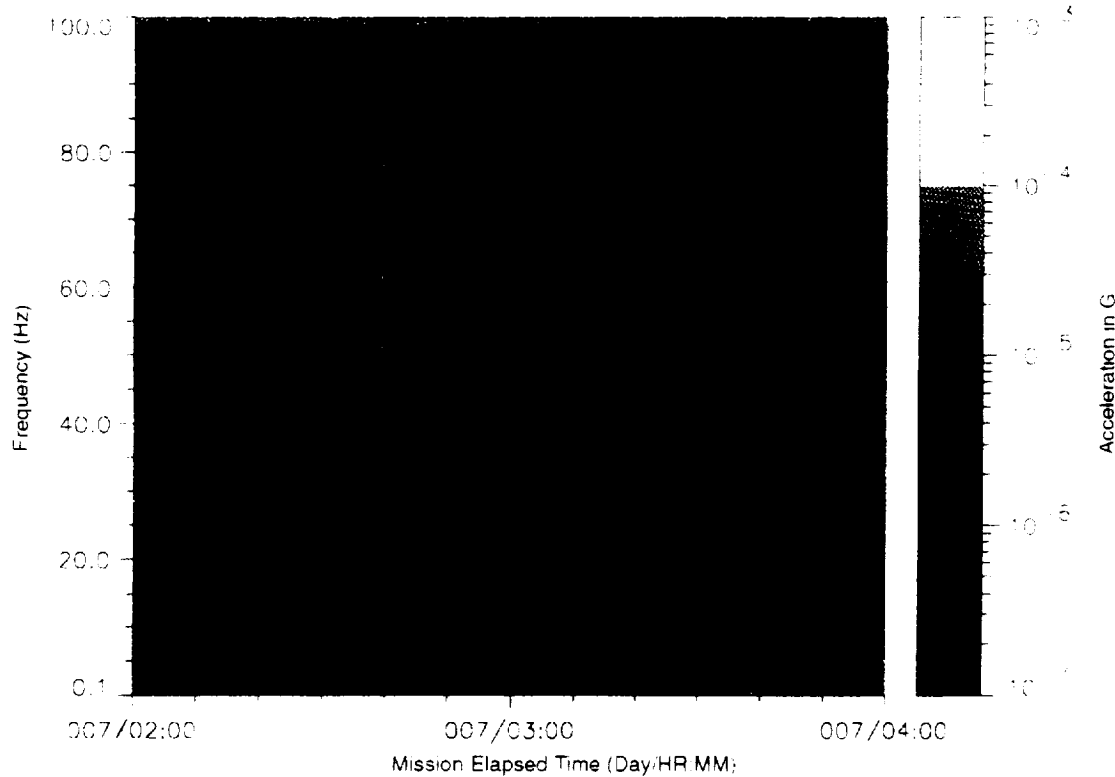


Figure B-300: SPACEHAB-1, Forward Bulkhead T-Beam

STS-57, Head A, Vector Magnitude

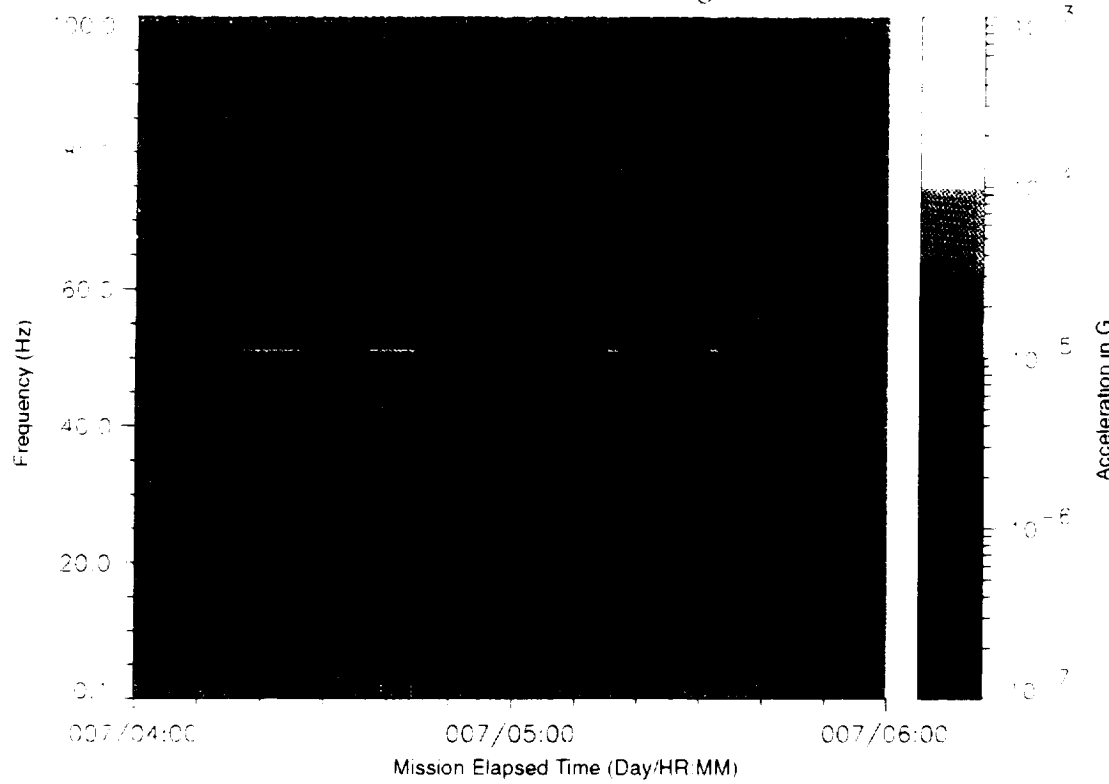


Figure B-301: SPACEHAB-1, Forward Bulkhead T-Beam

STS-57, Head A, X-Axis

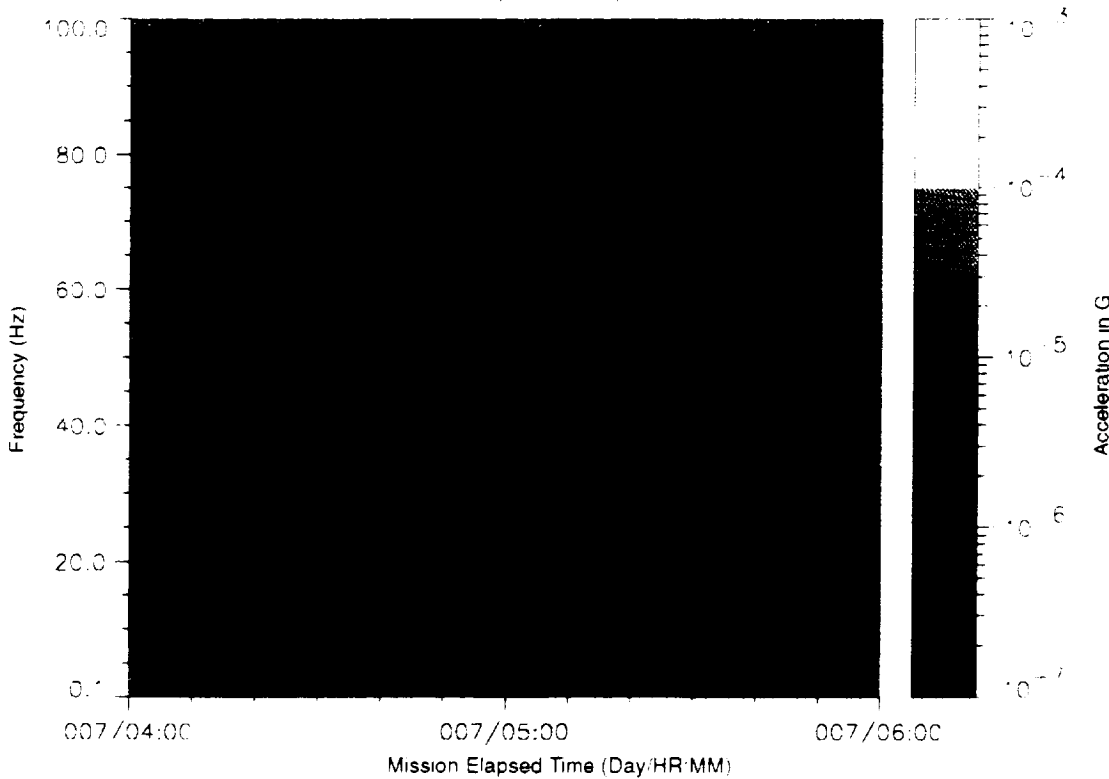


Figure B-302: SPACEHAB-1, Forward Bulkhead T-Beam

STS-57, Head A, Y-Axis

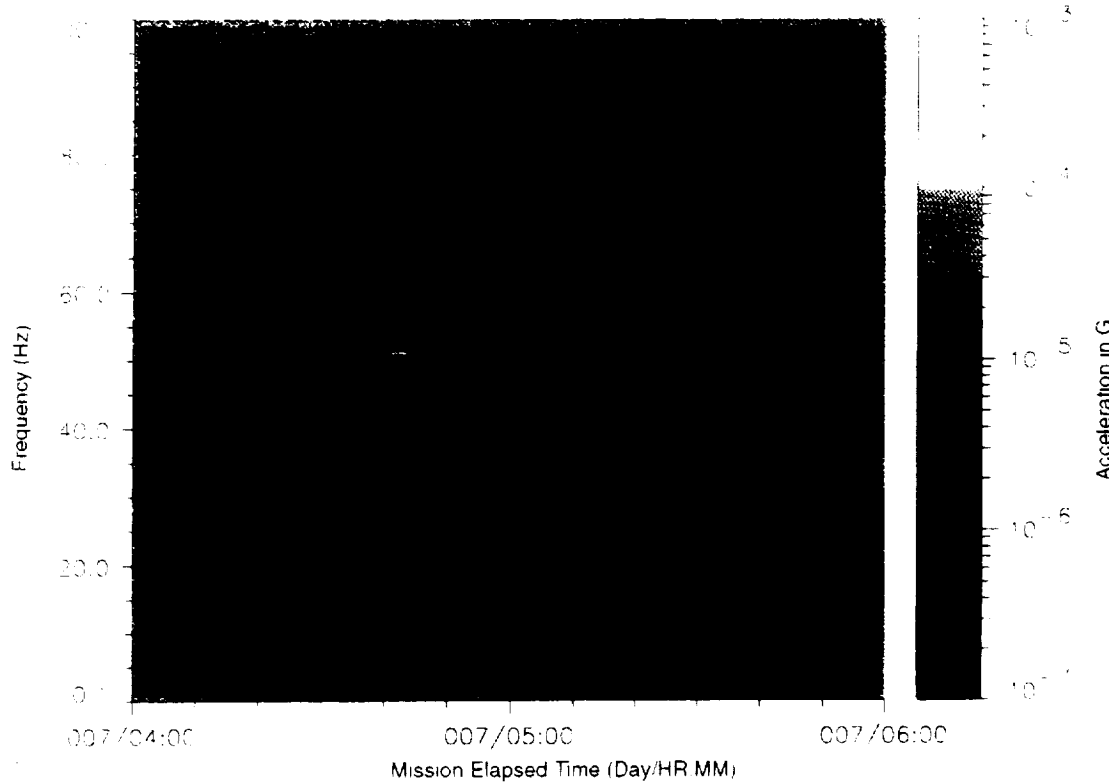


Figure B-303: SPACEHAB-1, Forward Bulkhead T-Beam

STS-57, Head A, Z-Axis

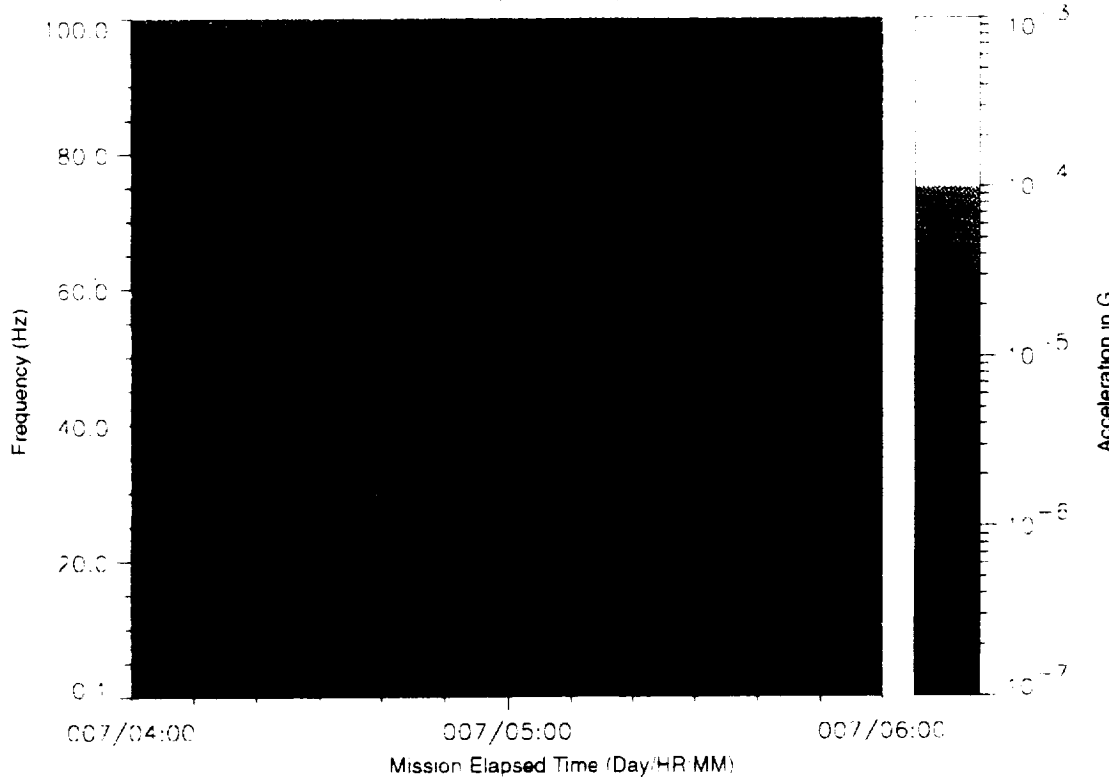


Figure B-304: SPACEHAB-1, Forward Bulkhead T-Beam

STS-57, Head A, Vector Magnitude

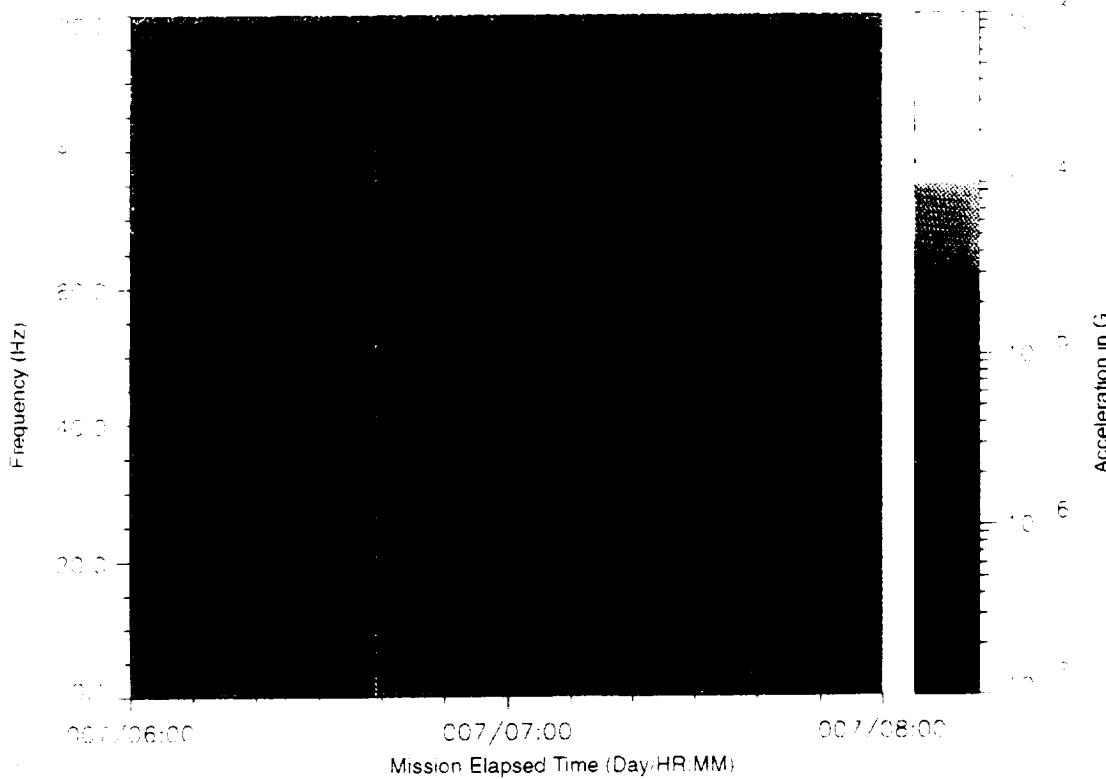


Figure B-305: SPACEHAB-1, Forward Bulkhead T-Beam

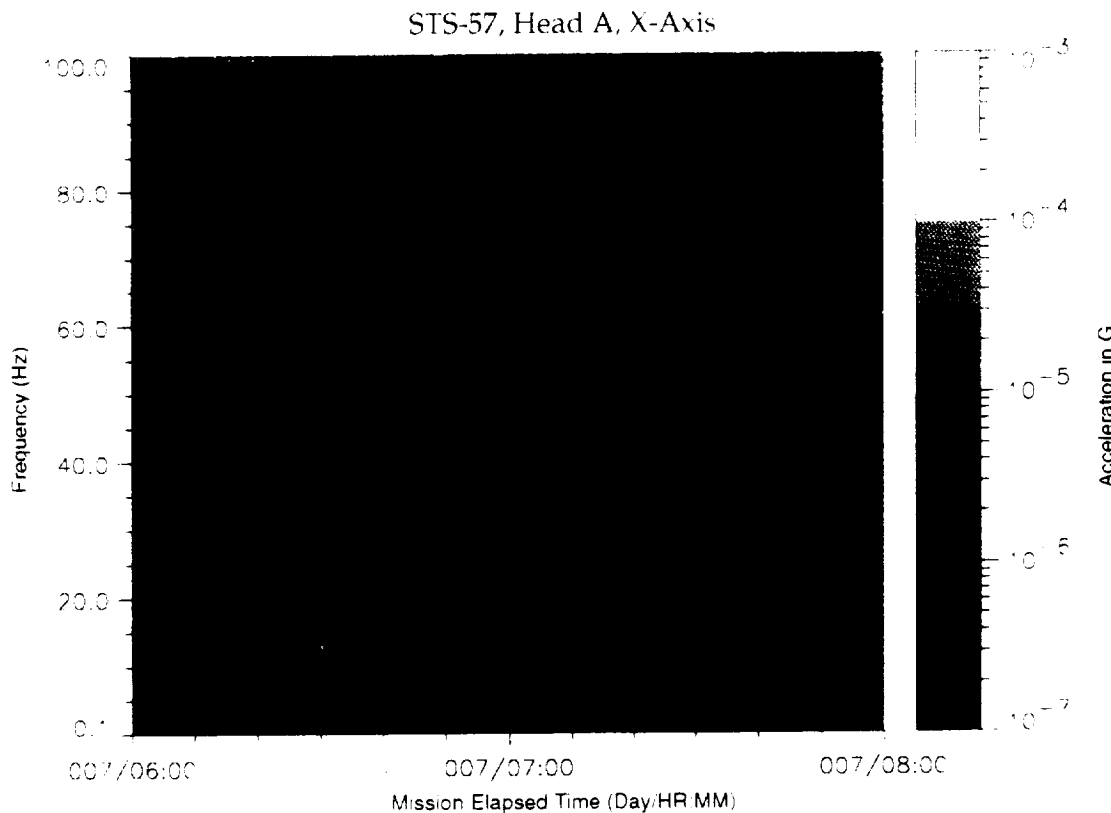


Figure B-306: SPACEHAB-1, Forward Bulkhead T-Beam

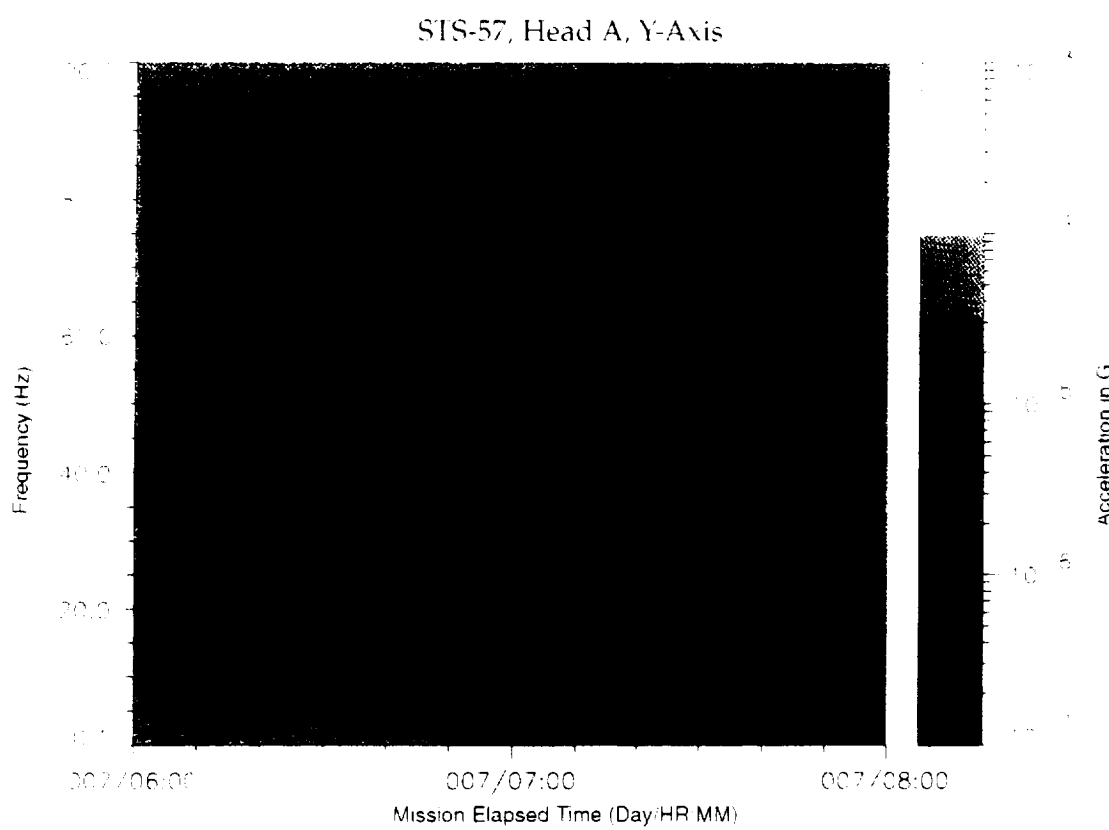


Figure B-307: SPACEHAB-1, Forward Bulkhead T-Beam

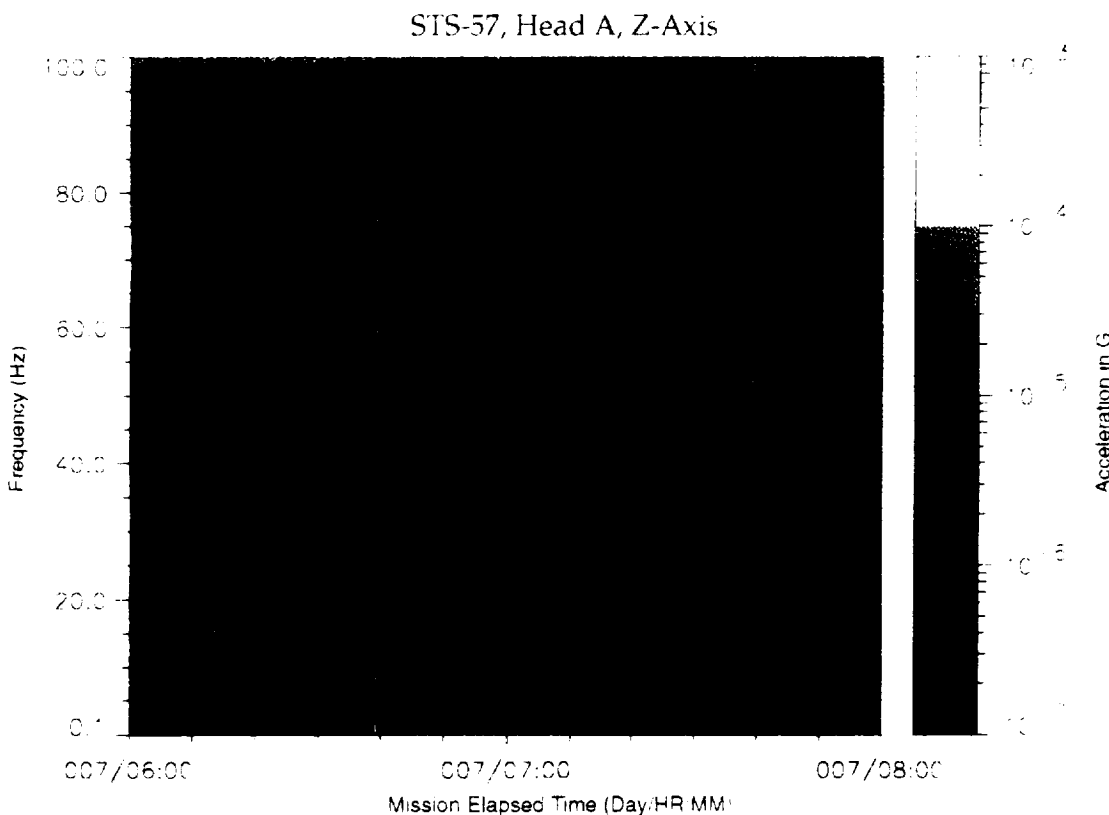


Figure B-308: SPACEHAB-1, Forward Bulkhead T-Beam

STS-57, Head A, Vector Magnitude

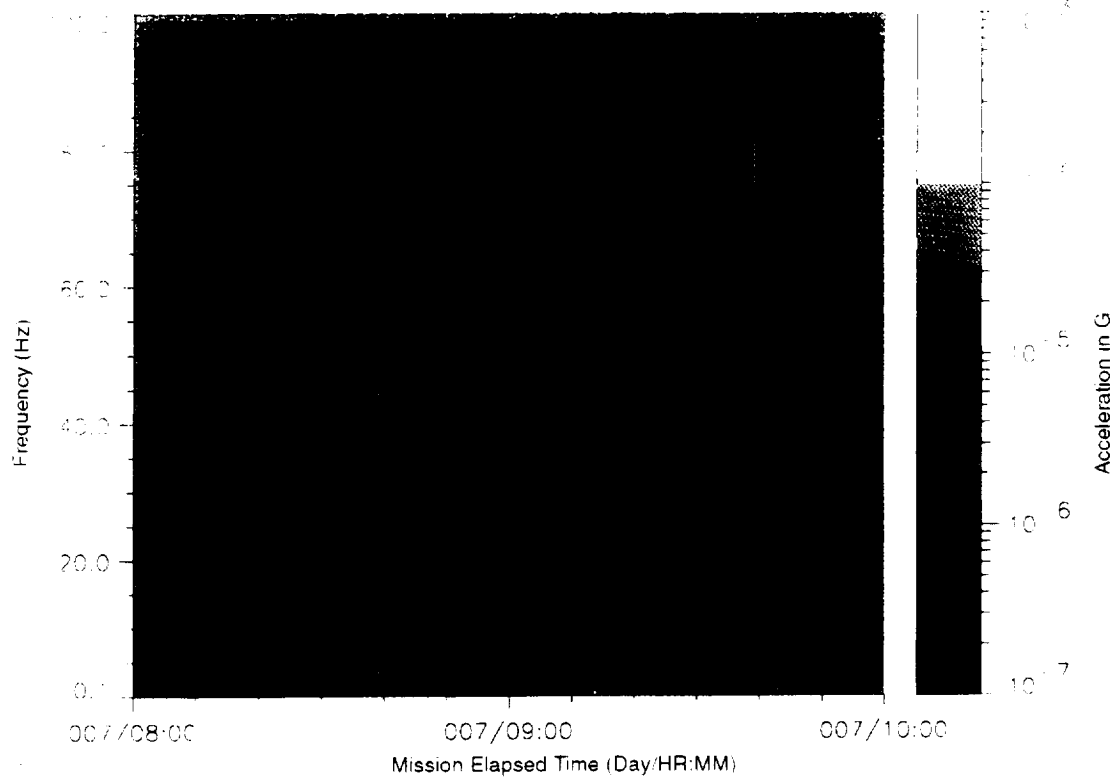


Figure B-309: SPACEHAB-1, Forward Bulkhead T-Beam

STS-57, Head A, X-Axis

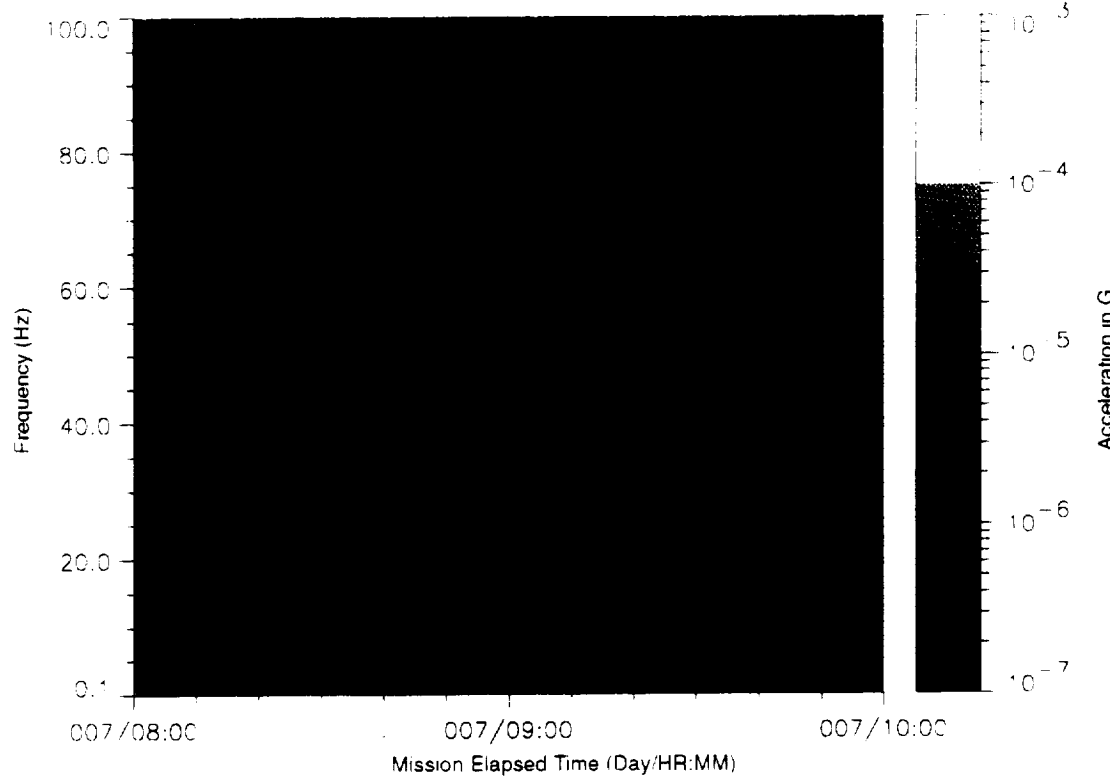


Figure B-310: SPACEHAB-1, Forward Bulkhead T-Beam

STS-57, Head A, Y-Axis

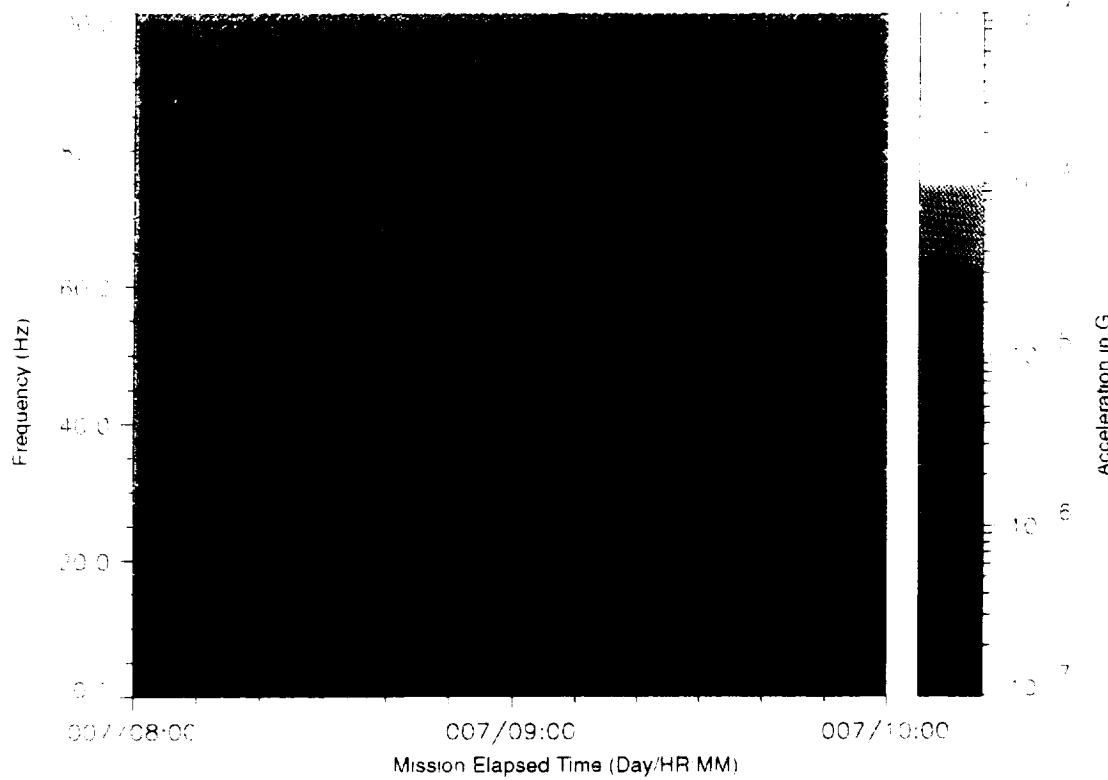


Figure B-311: SPACEHAB-1, Forward Bulkhead I-Beam

STS-57, Head A, Z-Axis

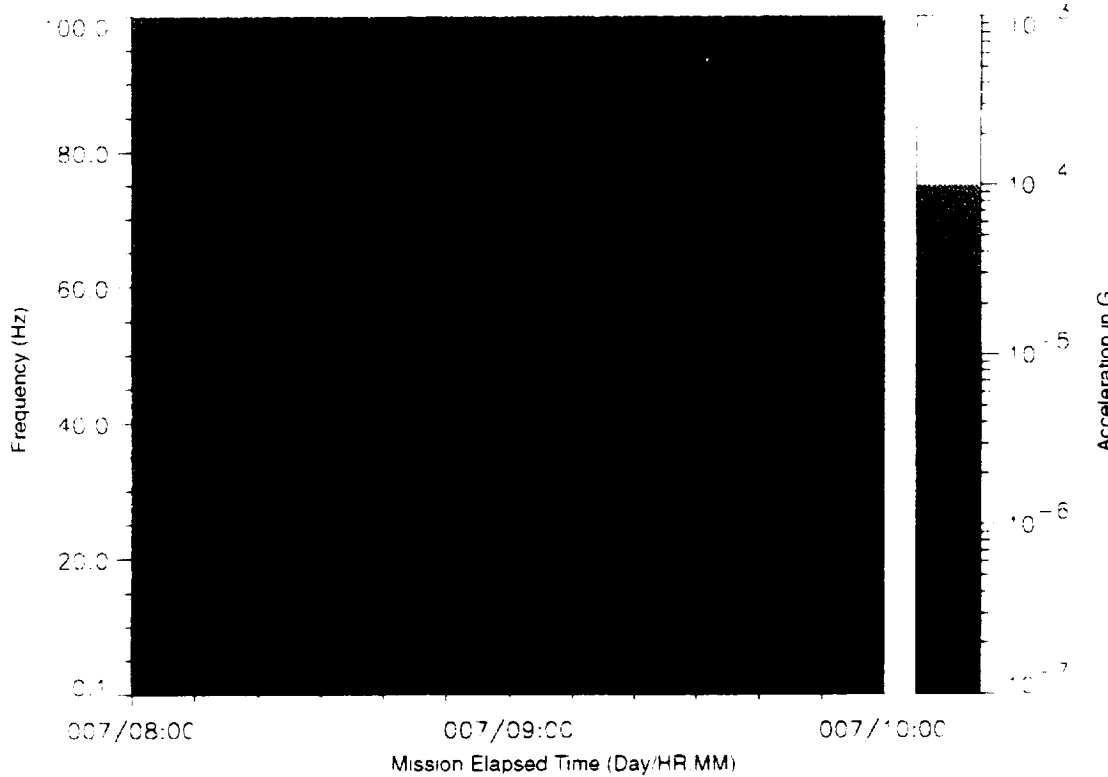


Figure B-312: SPACEHAB-1, Forward Bulkhead I-Beam

STS-57, Head A, Vector Magnitude

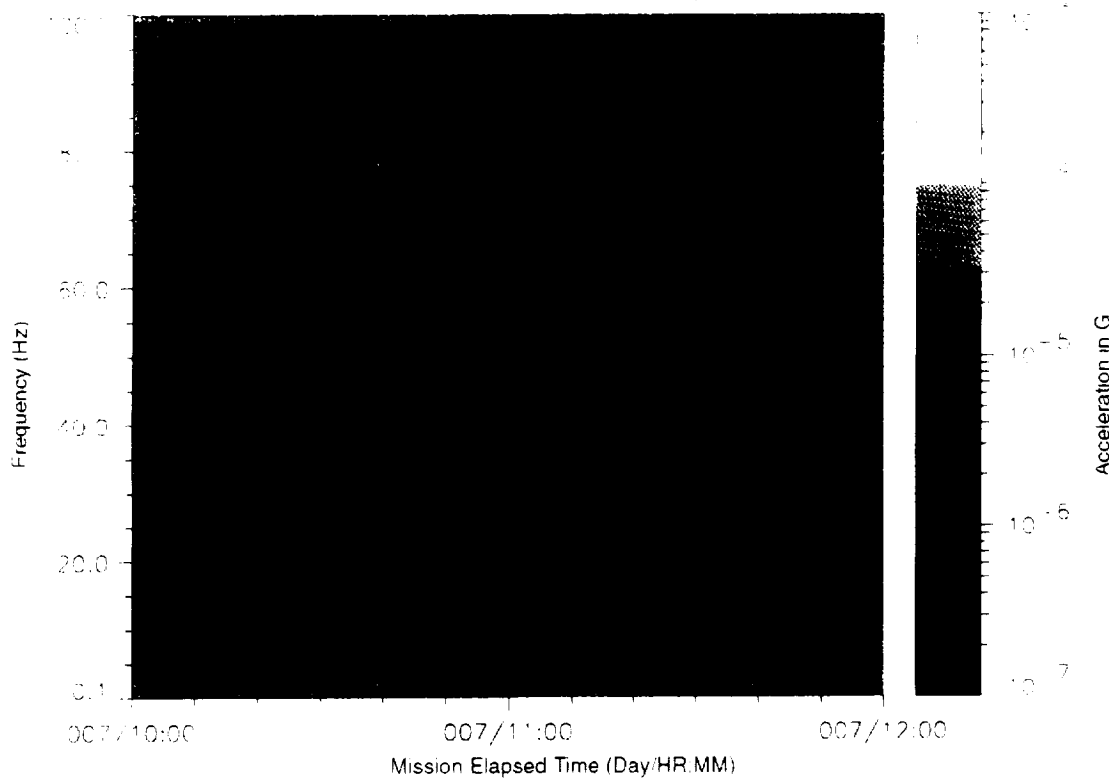


Figure B-313: SPACEHAB-1, Forward Bulkhead T-Beam

STS-57, Head A, X-Axis

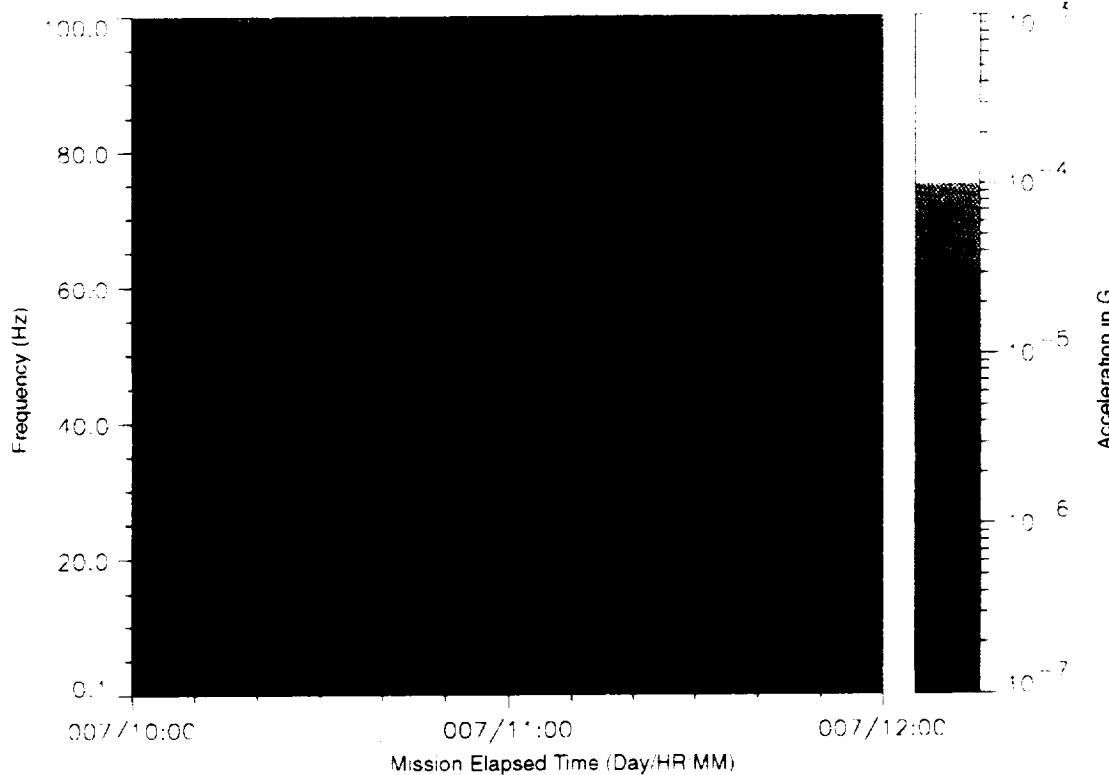


Figure B-314: SPACEHAB-1, Forward Bulkhead T-Beam

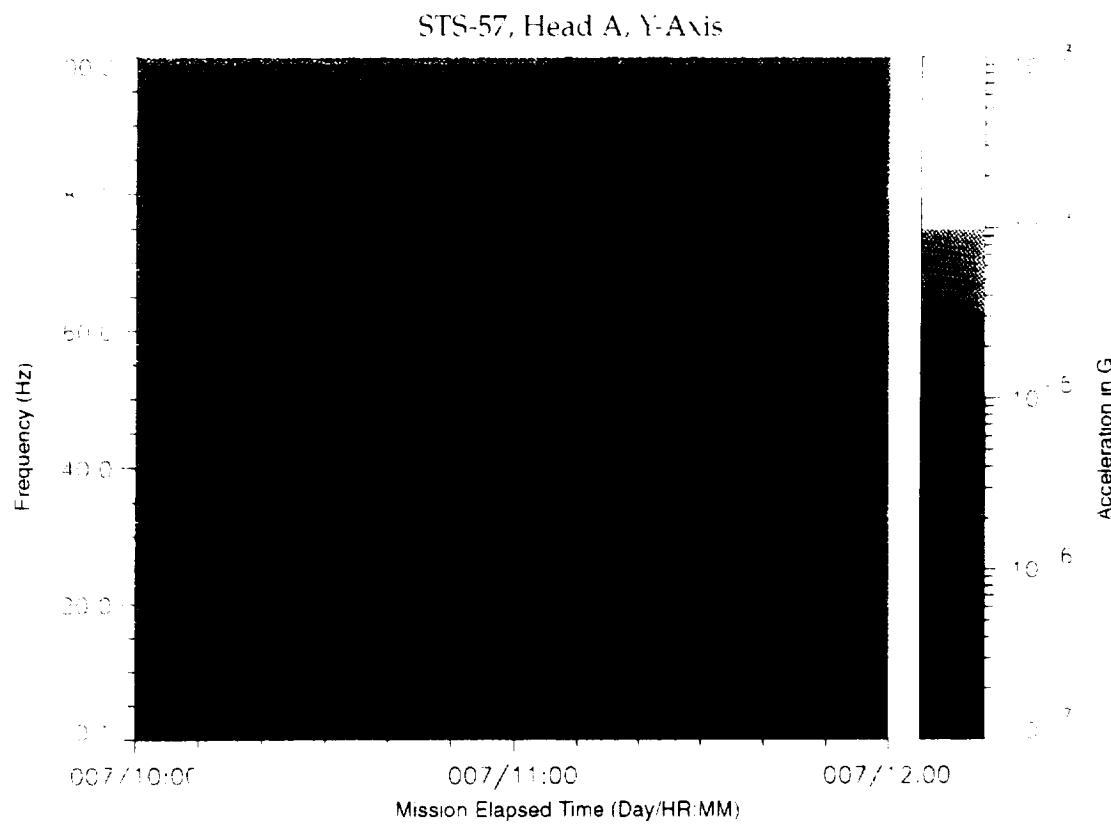


Figure B-315: SPACEHAB-1, Forward Bulkhead T-Beam

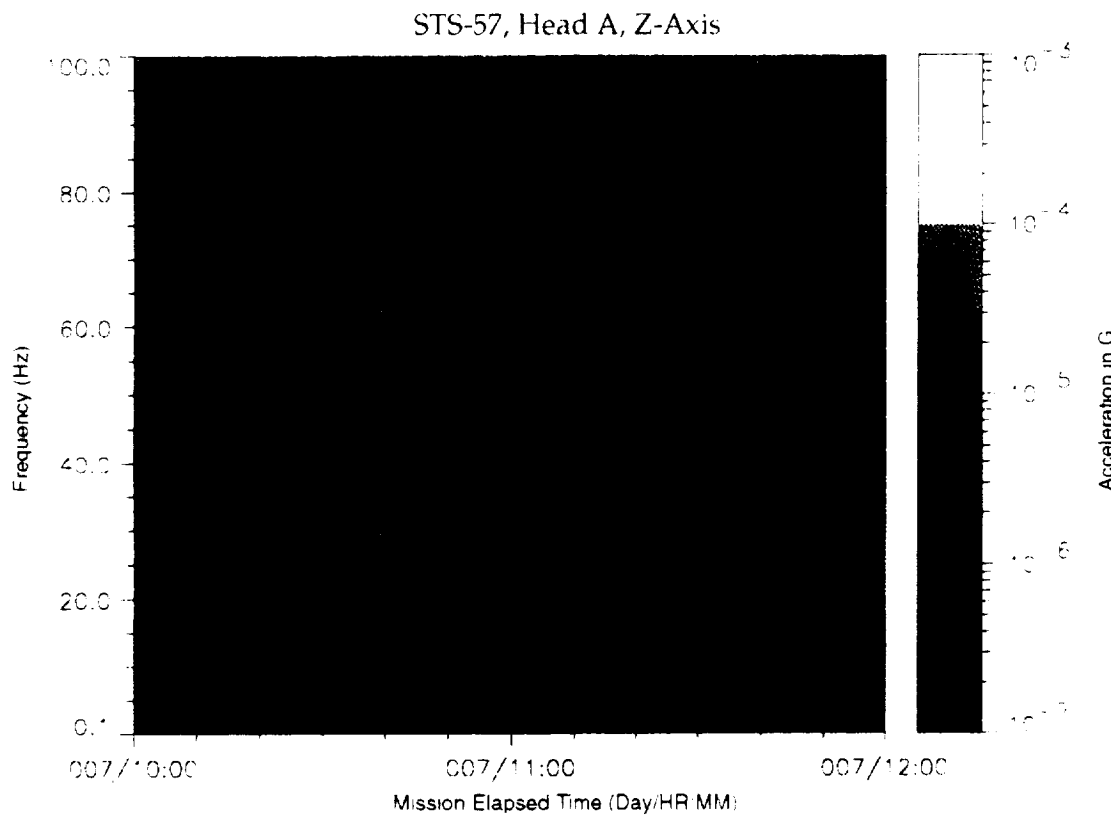


Figure B-316. SPACEHAB-1, Forward Bulkhead T-Beam

STS-57, Head A, Vector Magnitude

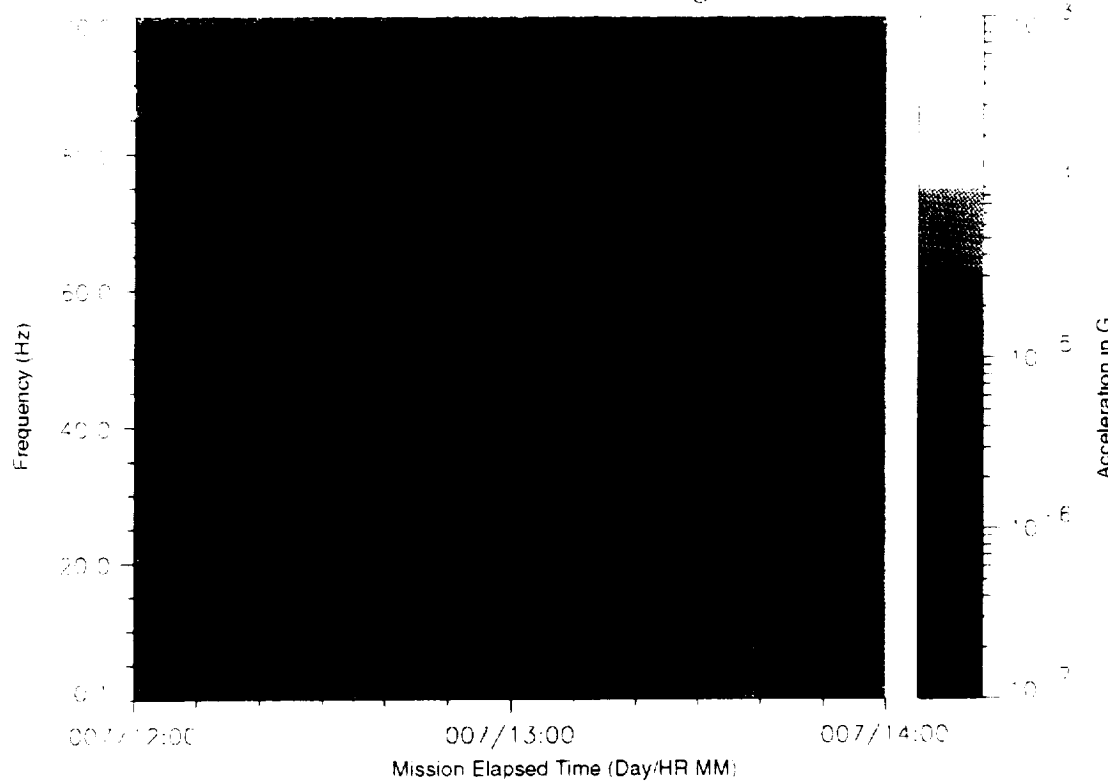


Figure B-317: SPACEHAB-1, Forward Bulkhead T-Beam

STS-57, Head A, X-Axis

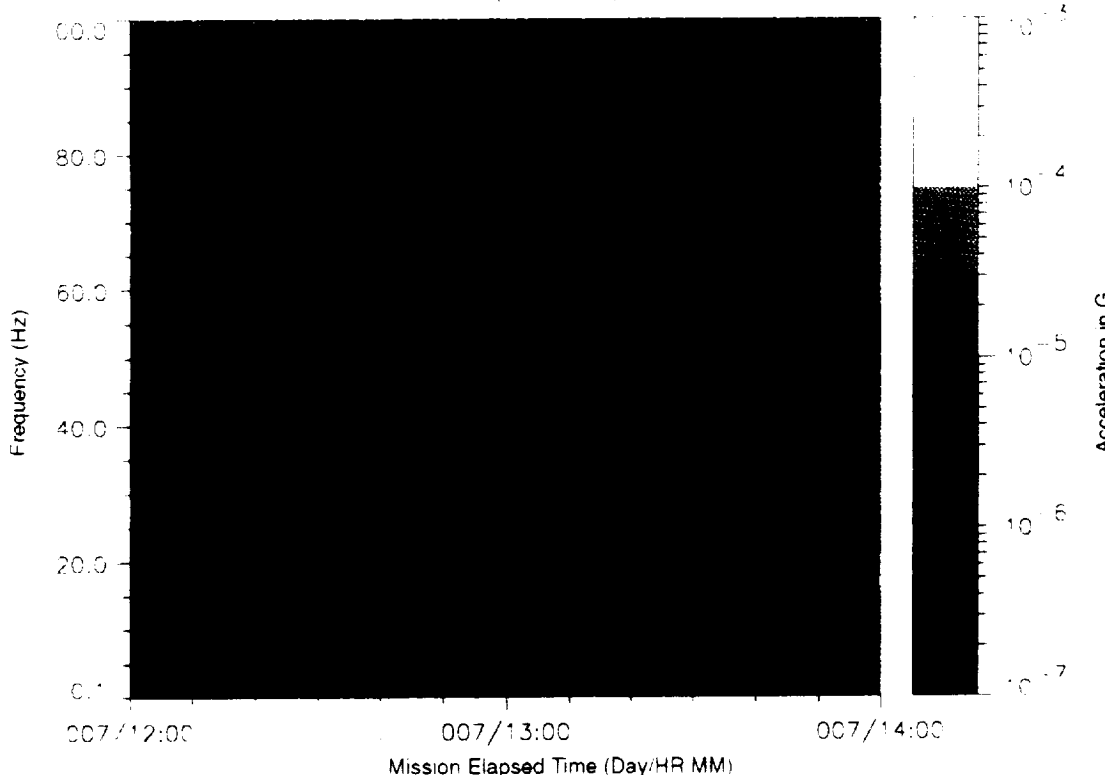


Figure B-318: SPACEHAB-1, Forward Bulkhead T-Beam

STS-57, Head A, Y-Axis

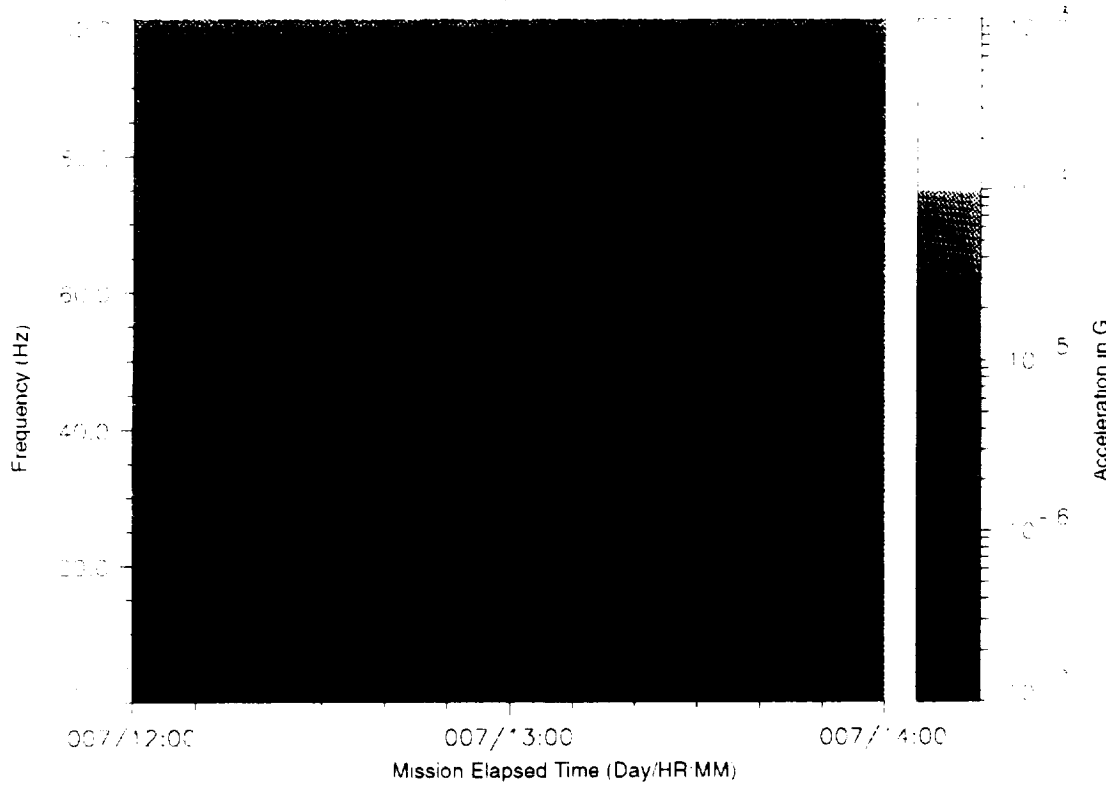


Figure B-319: SPACEHAB-1, Forward Bulkhead T-Beam

STS-57, Head A, Z-Axis

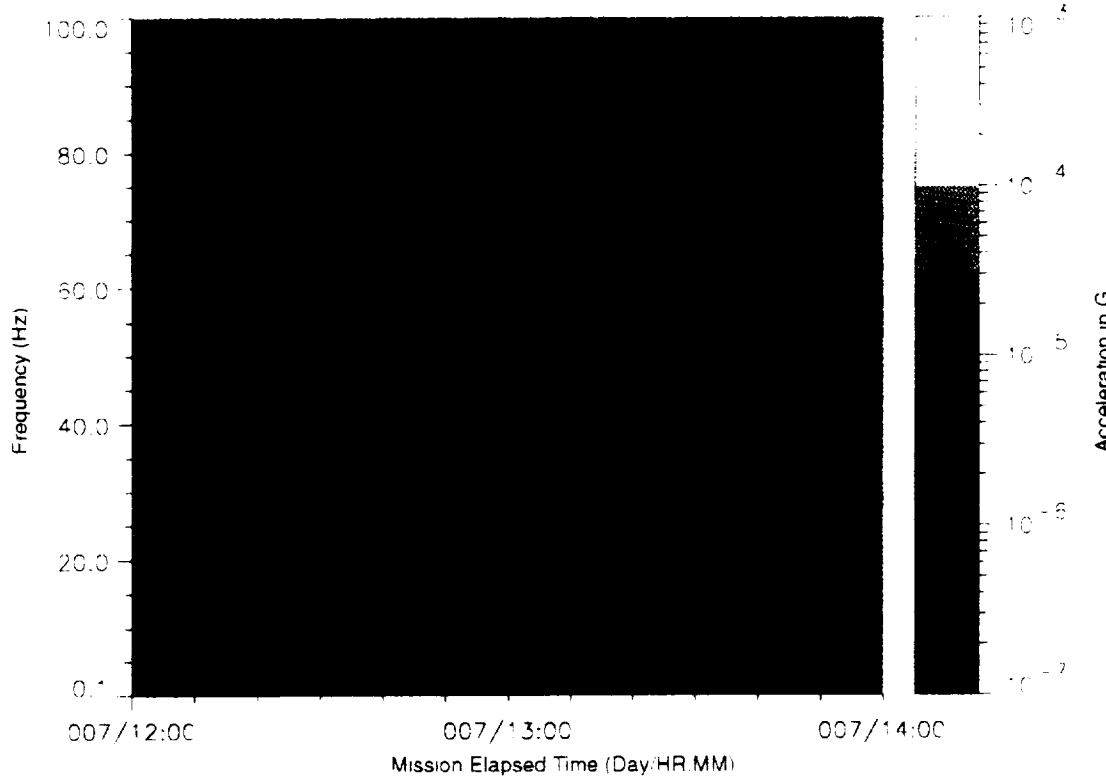


Figure B-320: SPACEHAB-1, Forward Bulkhead T-Beam

STS-57, Head A, Vector Magnitude

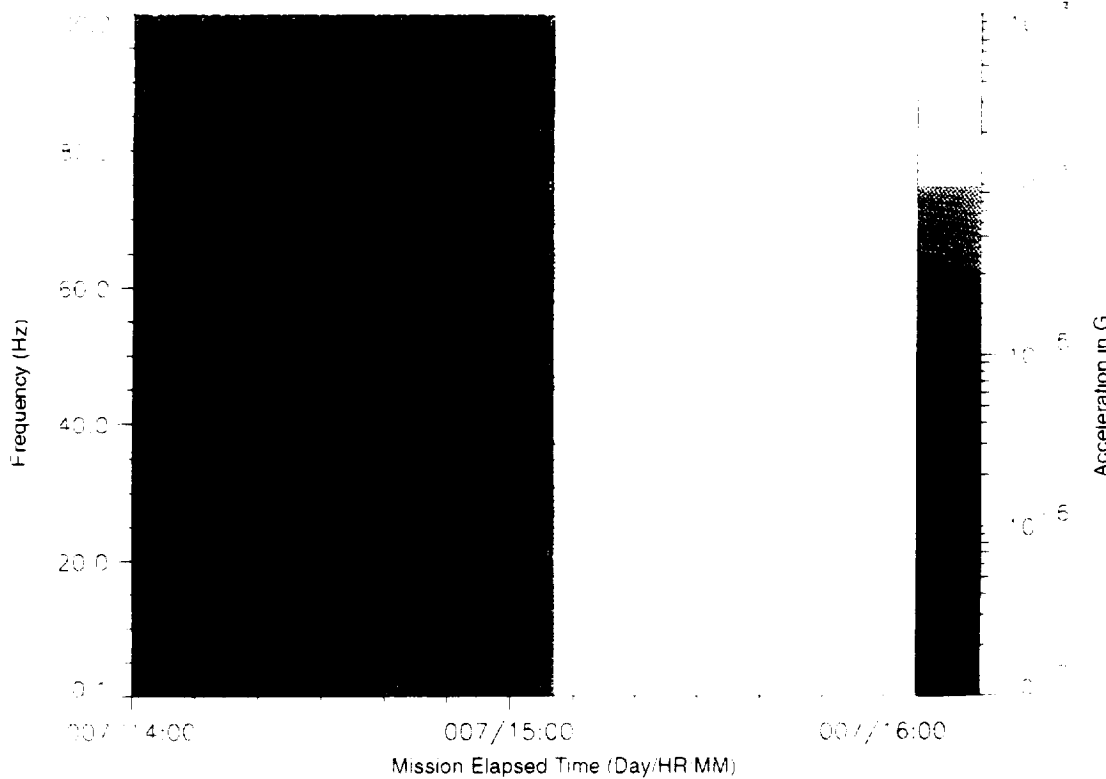


Figure B-321. SPACEHAB-1, Forward Bulkhead T-Beam

STS-57, Head A, X-Axis

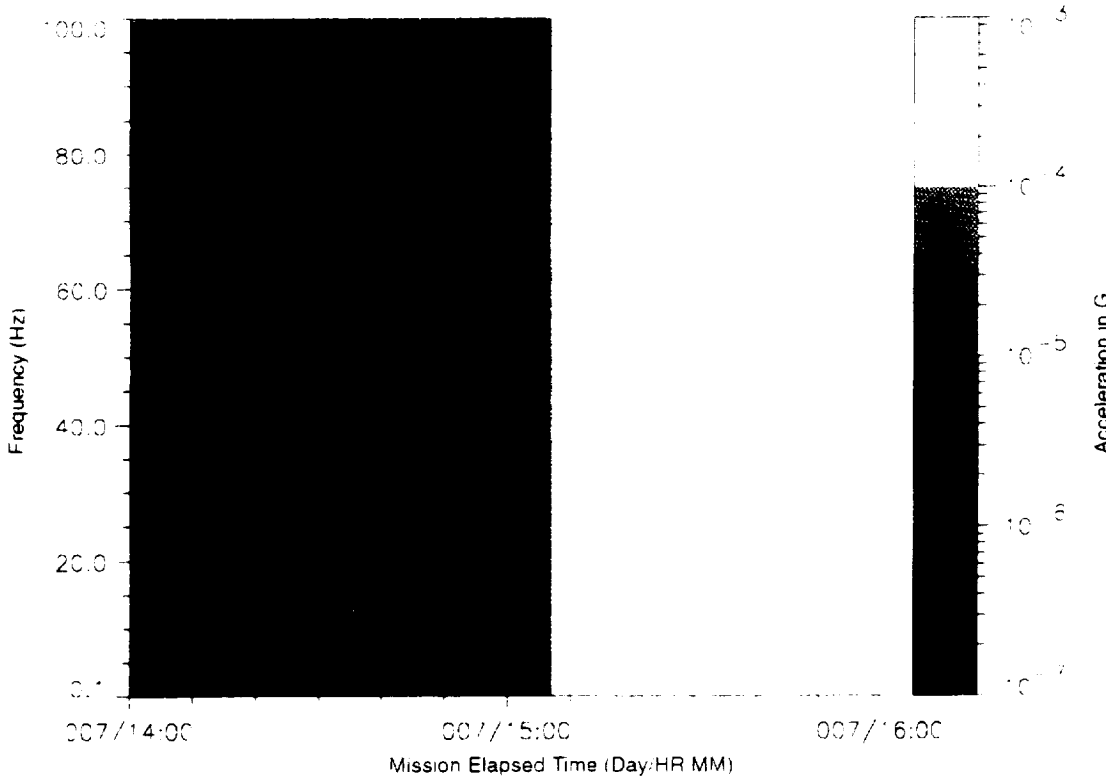


Figure B-322. SPACEHAB-1, Forward Bulkhead T-Beam

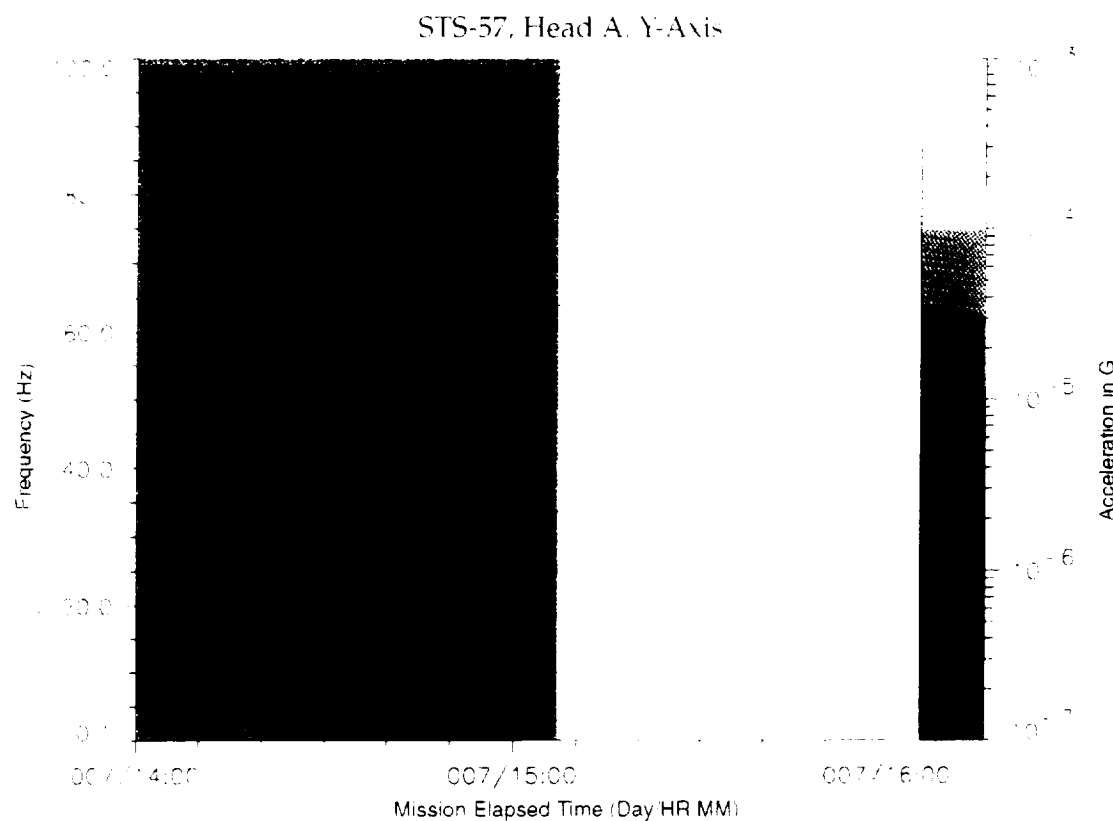


Figure B-323: SPACEHAB-1, Forward Bulkhead T-Beam

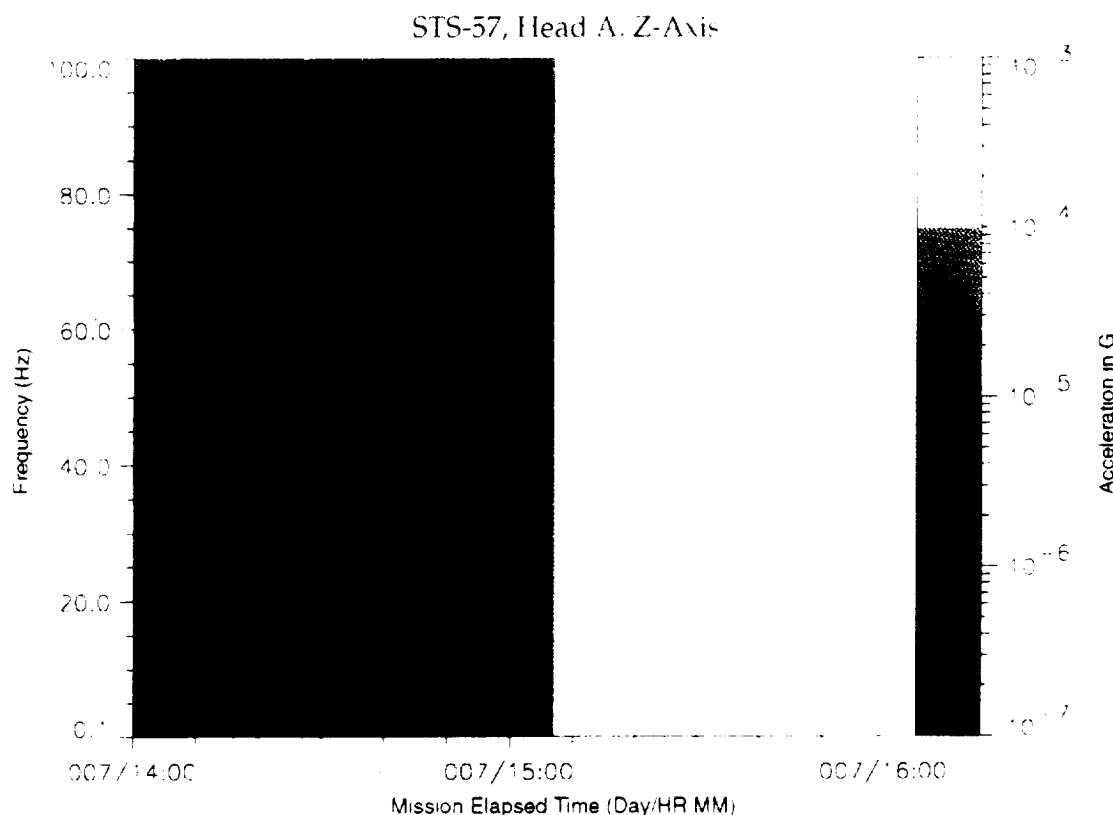
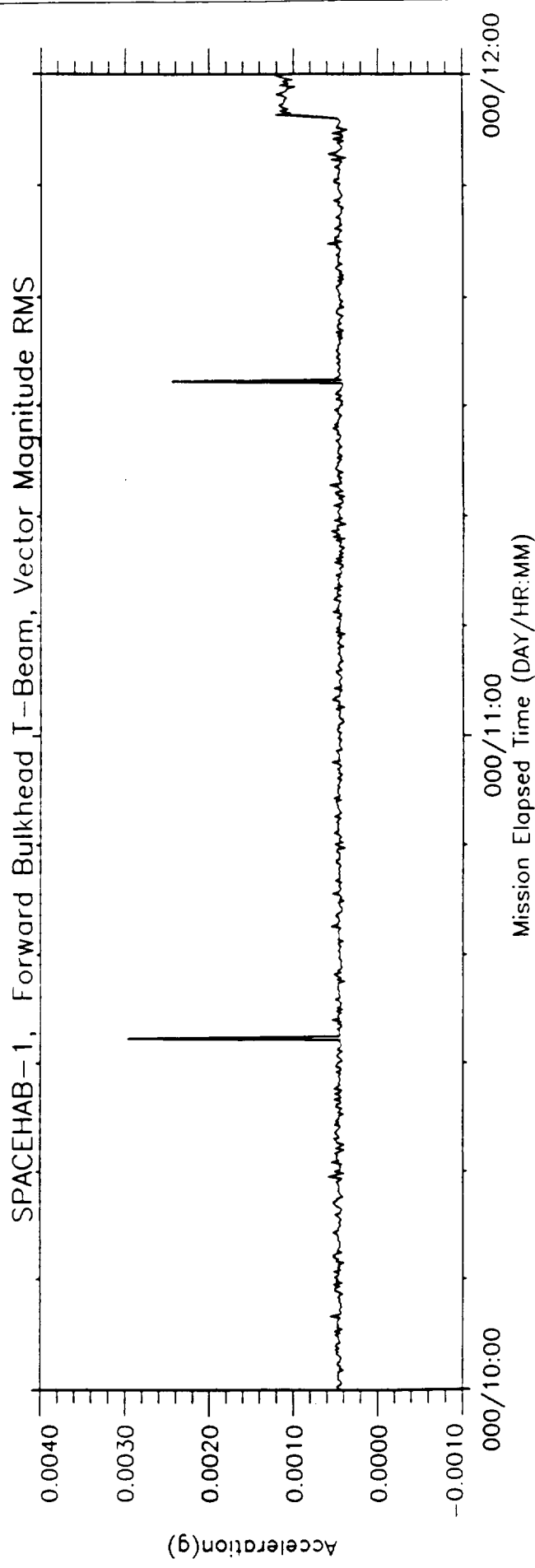
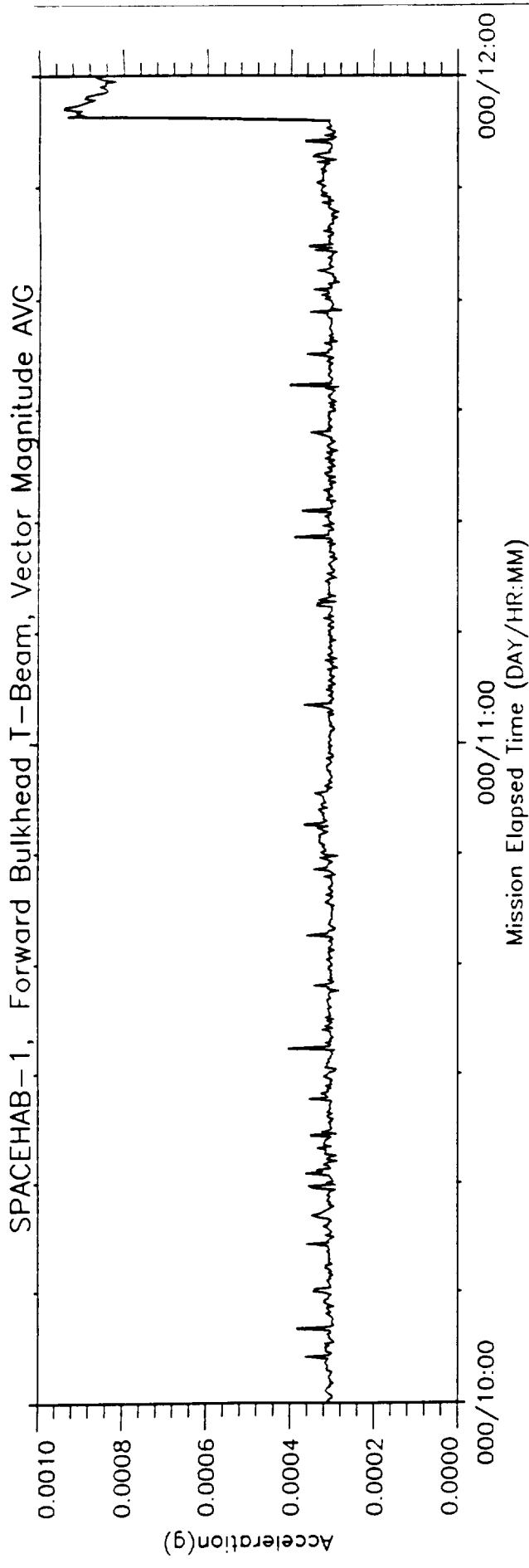


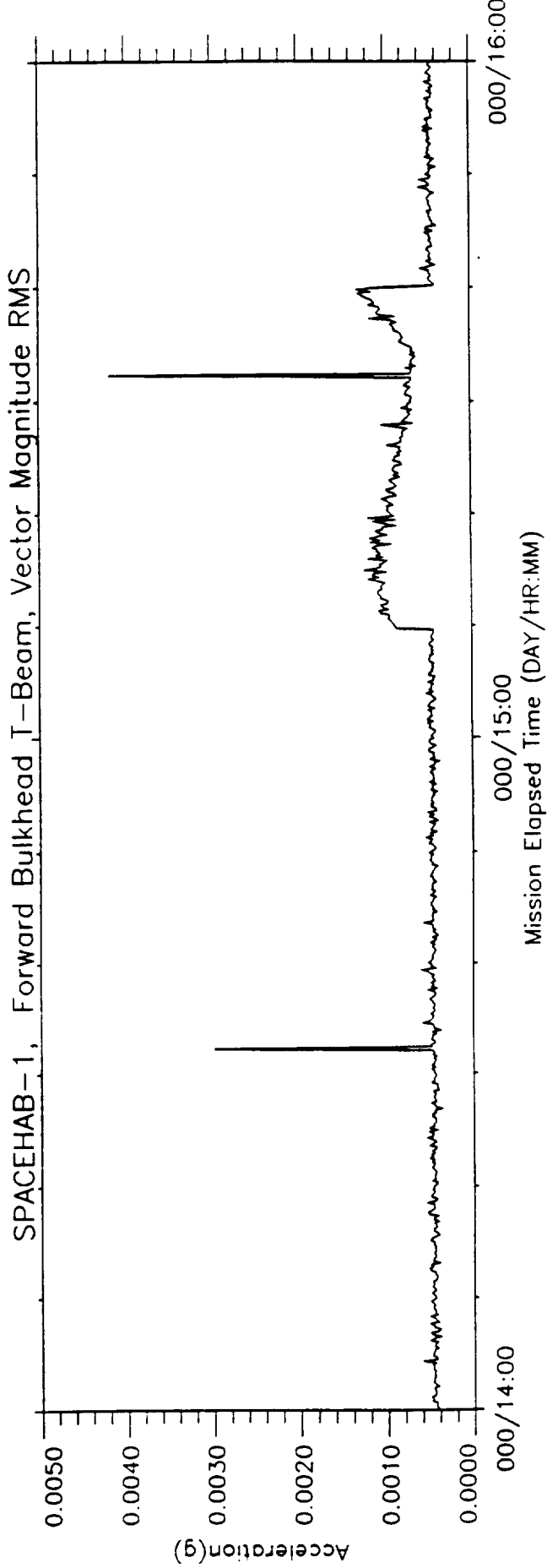
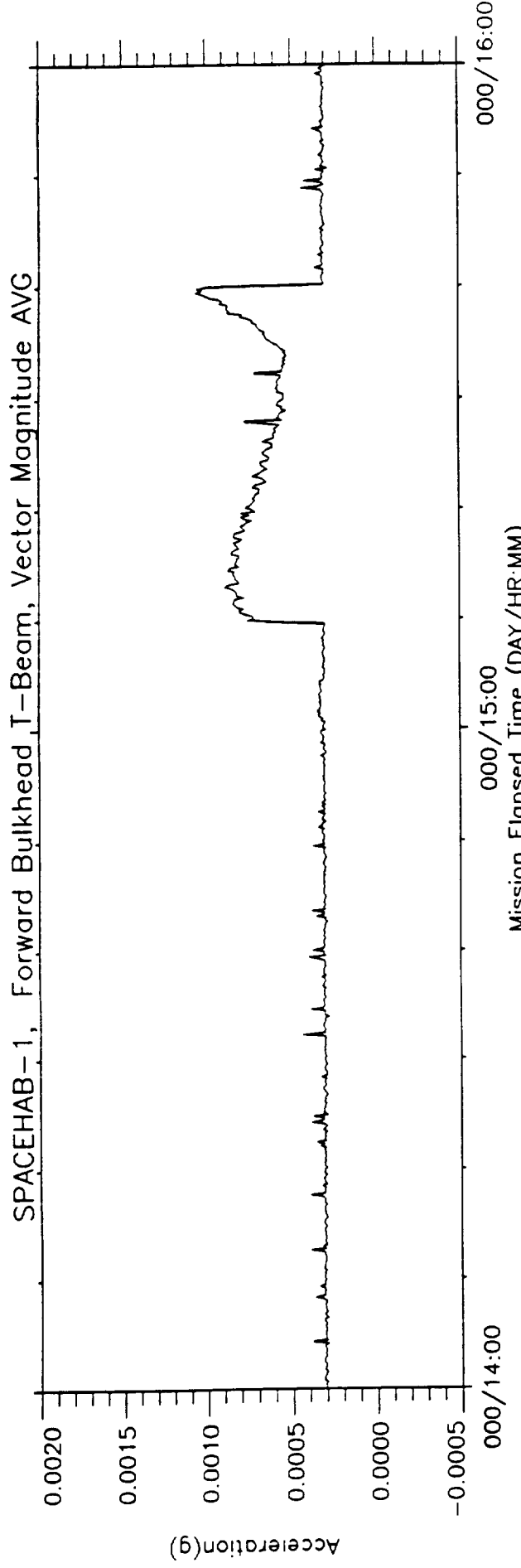
Figure B-324: SPACEHAB-1, Forward Bulkhead T-Beam

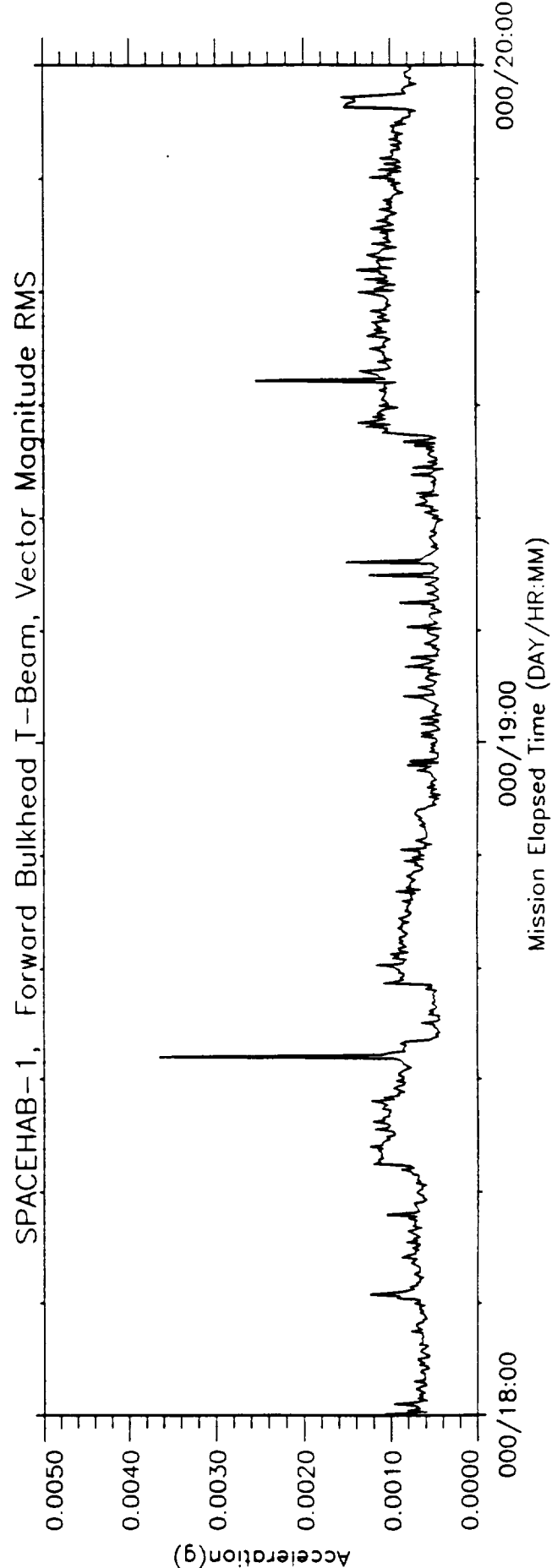
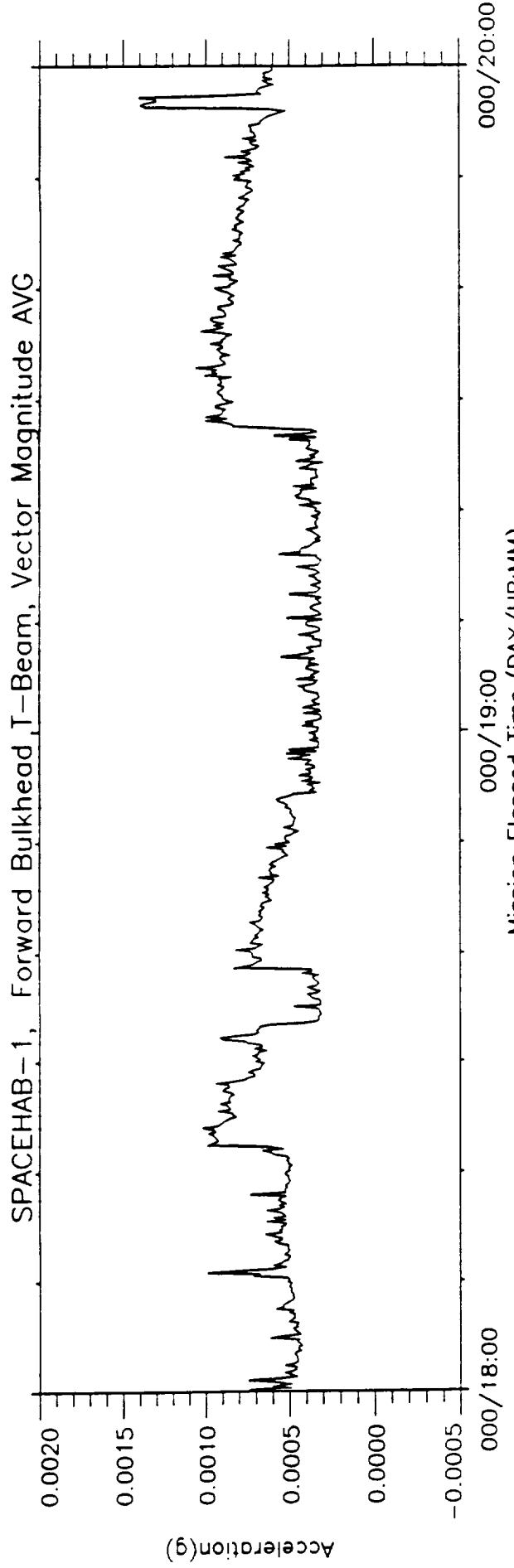
Appendix C: Average and RMS Plots

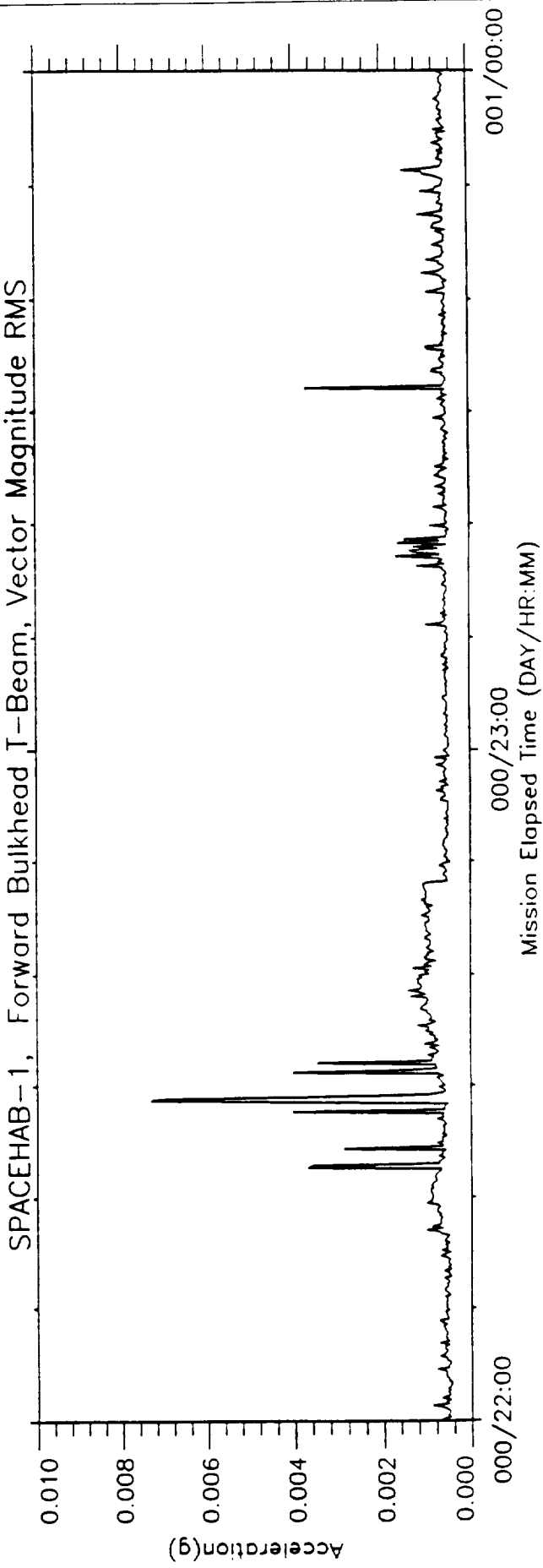
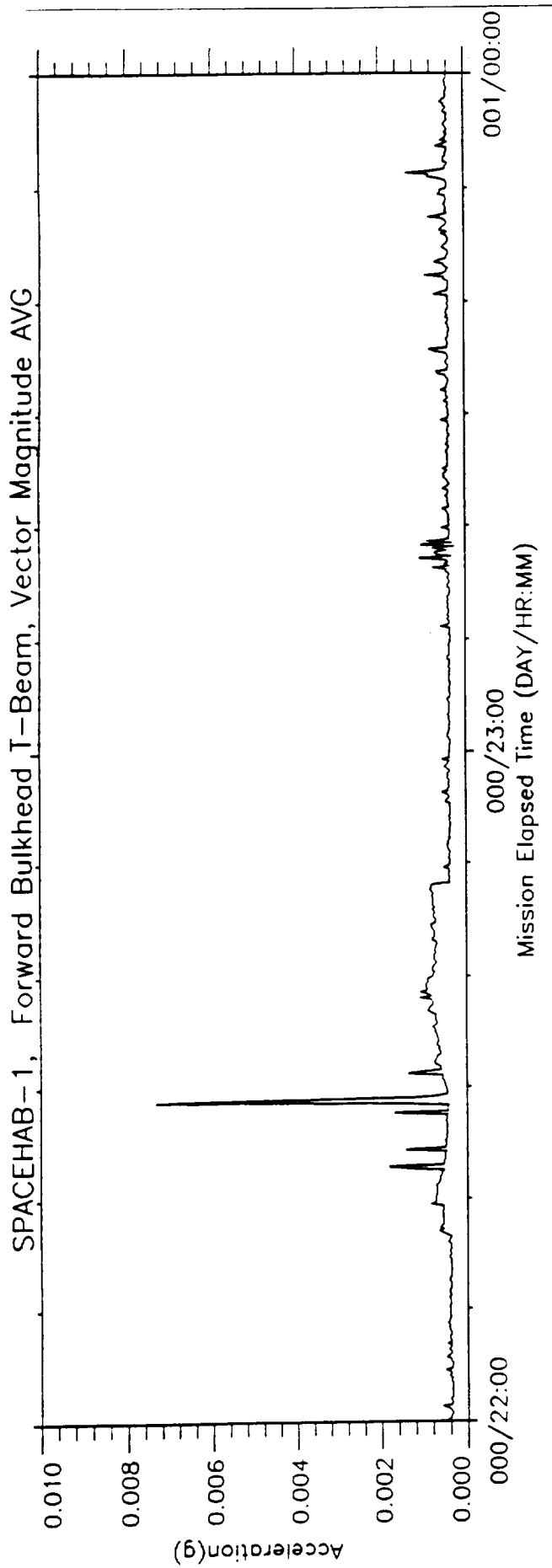
This appendix contains plots of the average and rms data from SAMS sensor head A. For comparison the average and rms results are plotted for two hour periods beginning at MET 000/08:00 and ending at 007/15:07.

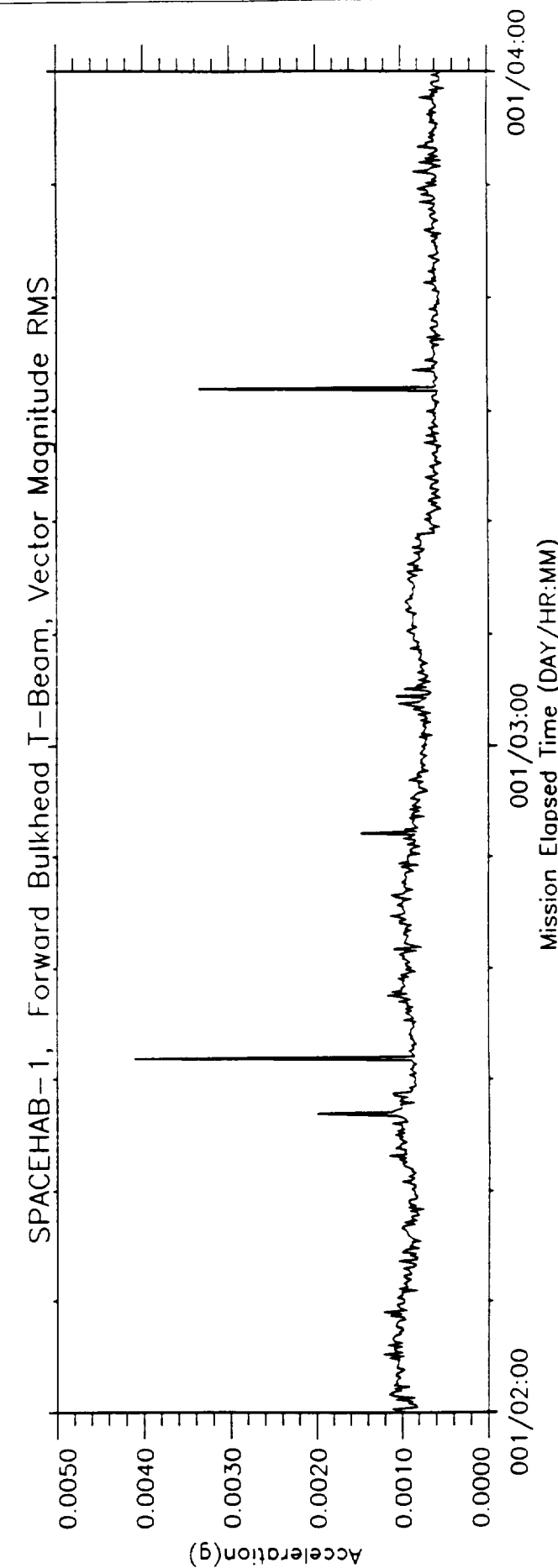
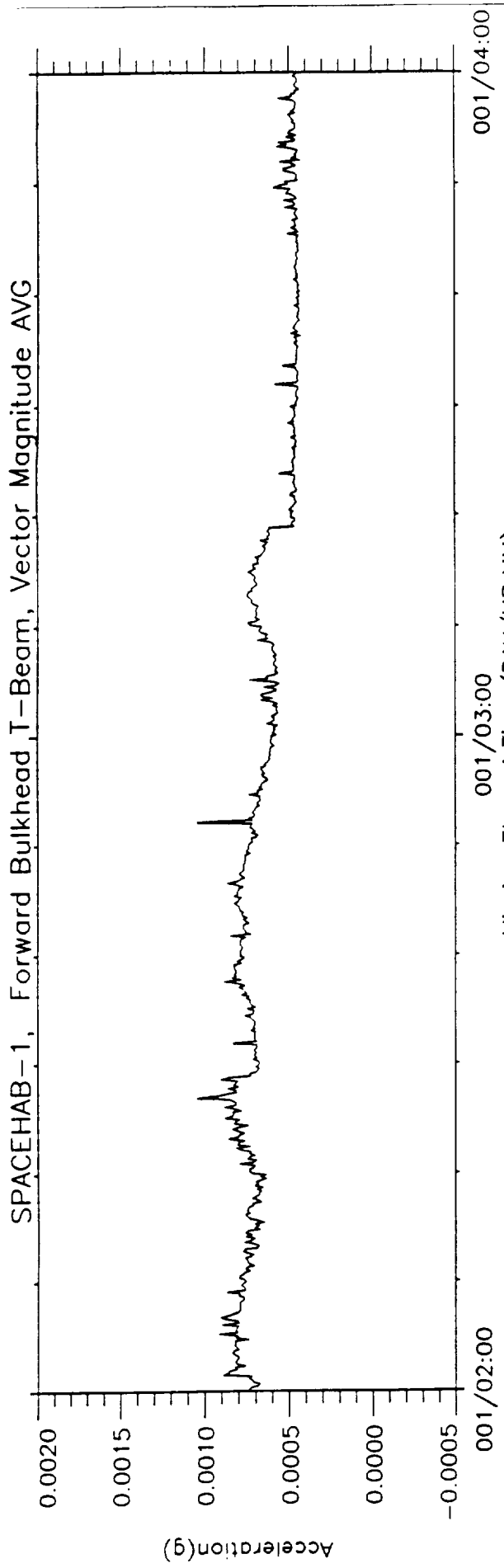
The bias acceleration magnitude levels represent the bias errors associated with each accelerometer axis. When taking the vector magnitude these bias errors are additive and thus, on the order of two to tree hundred micro-g's.

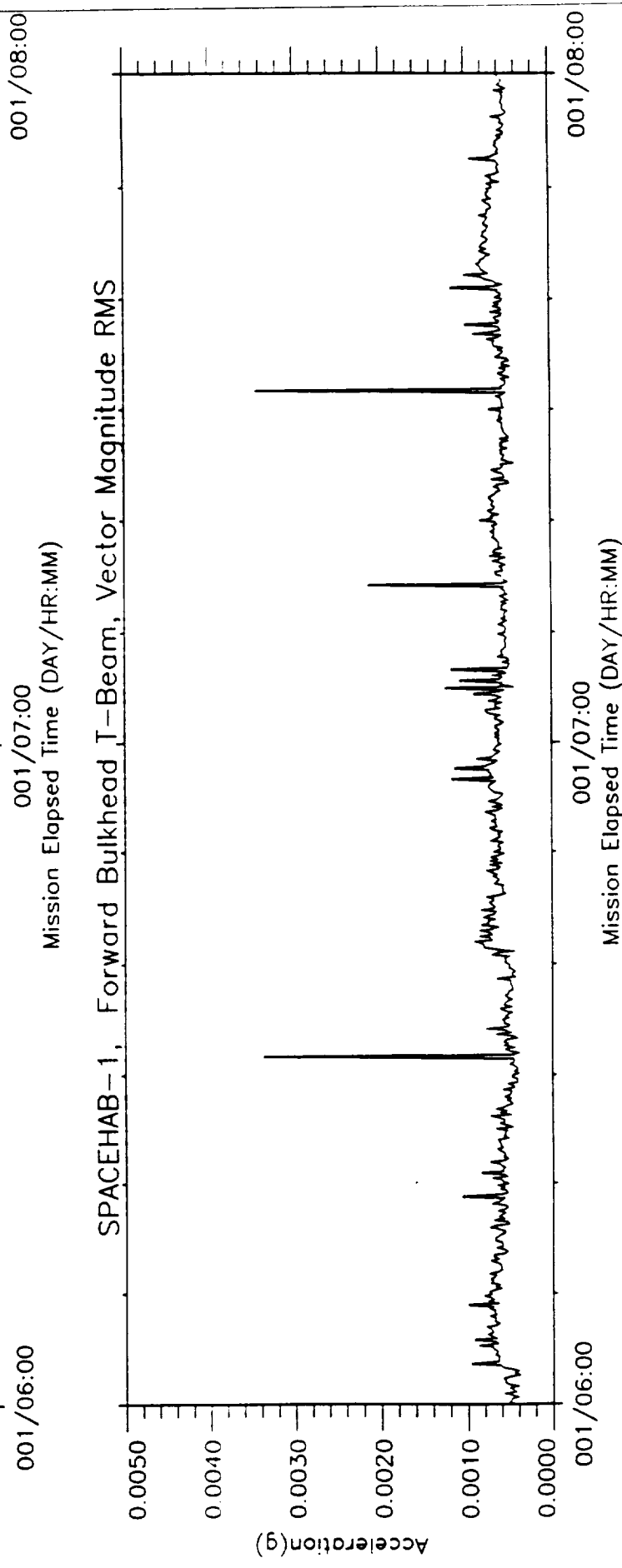
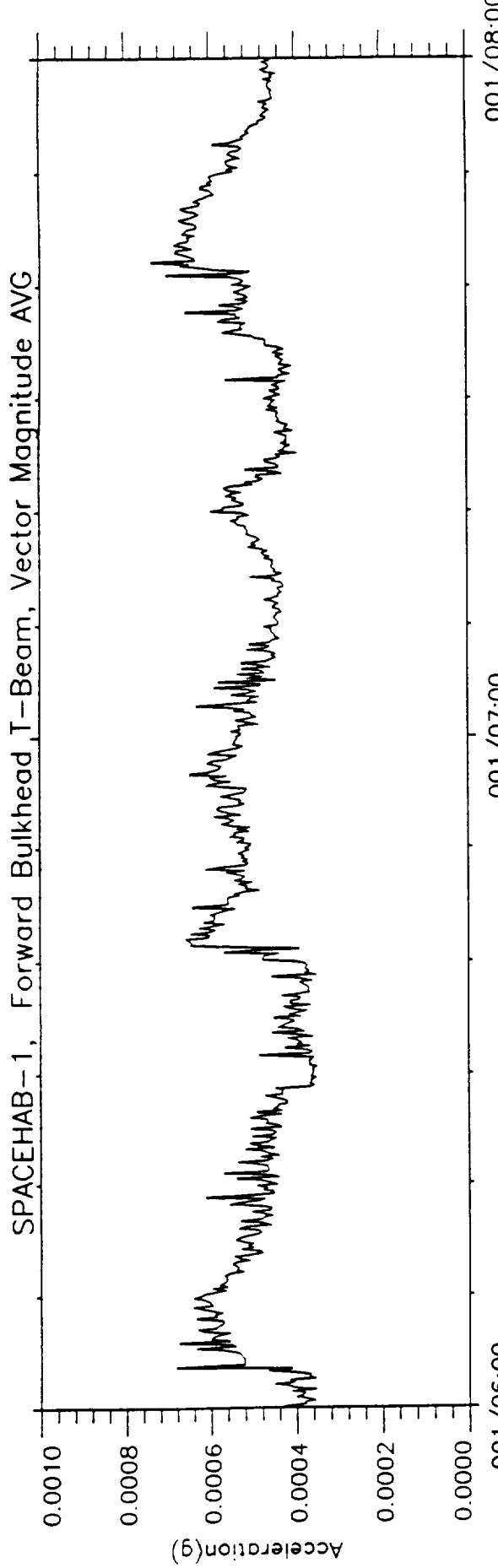


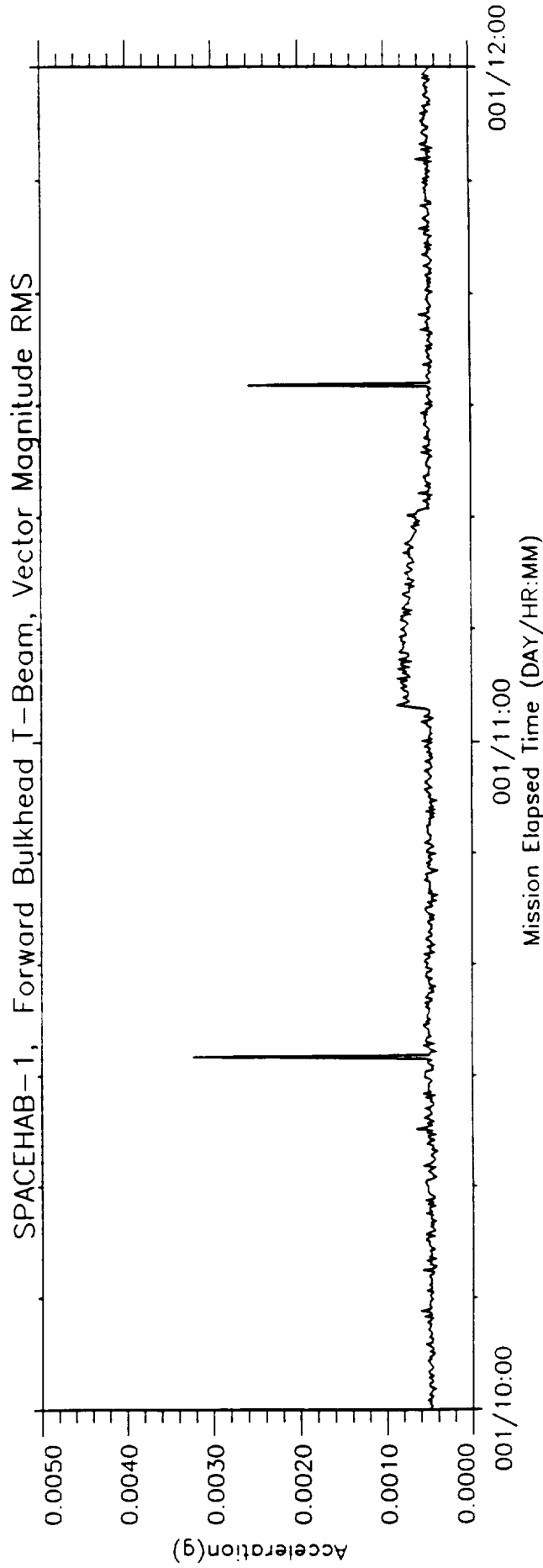
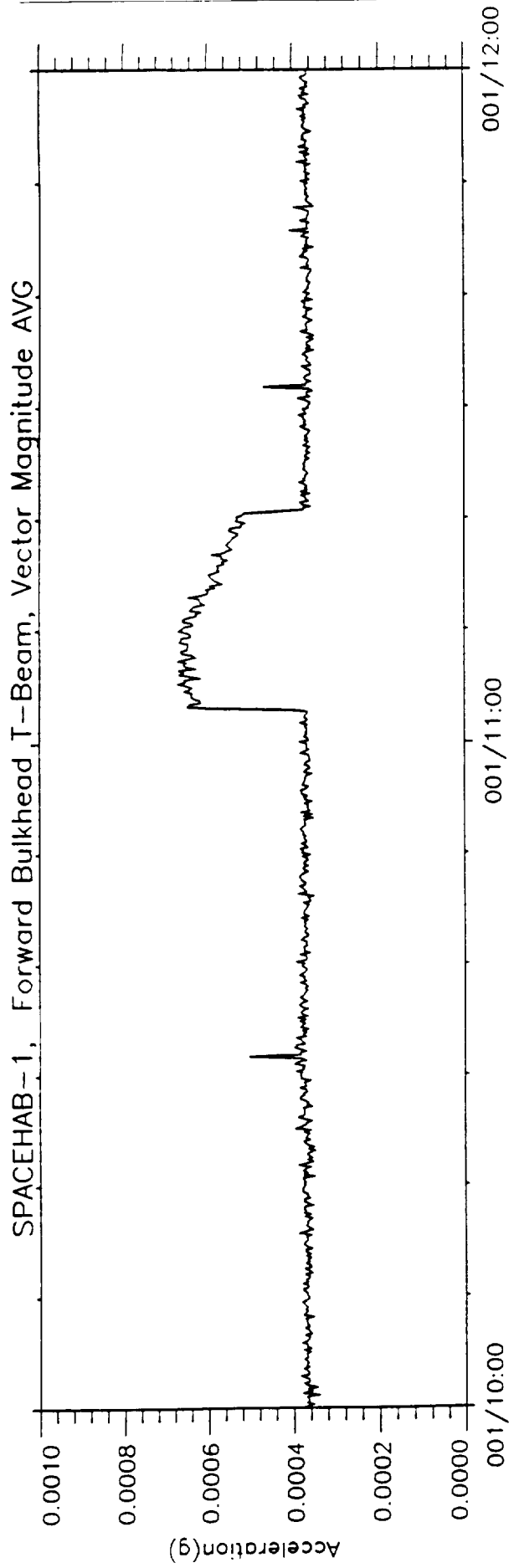


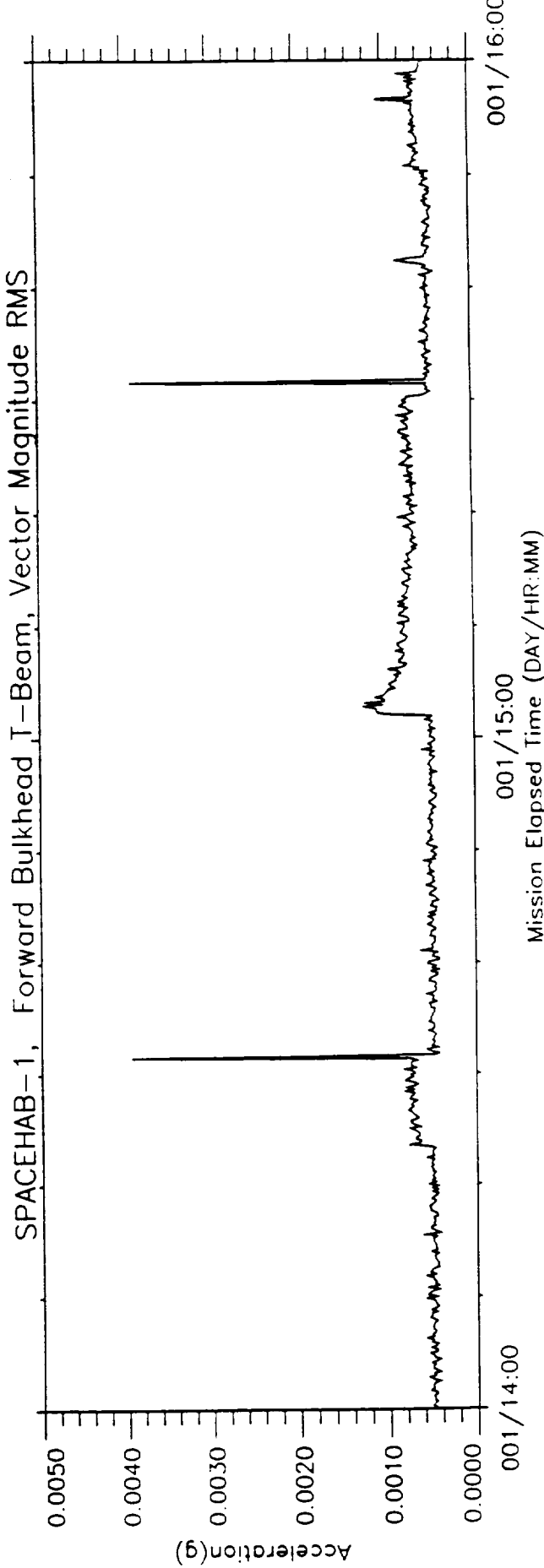
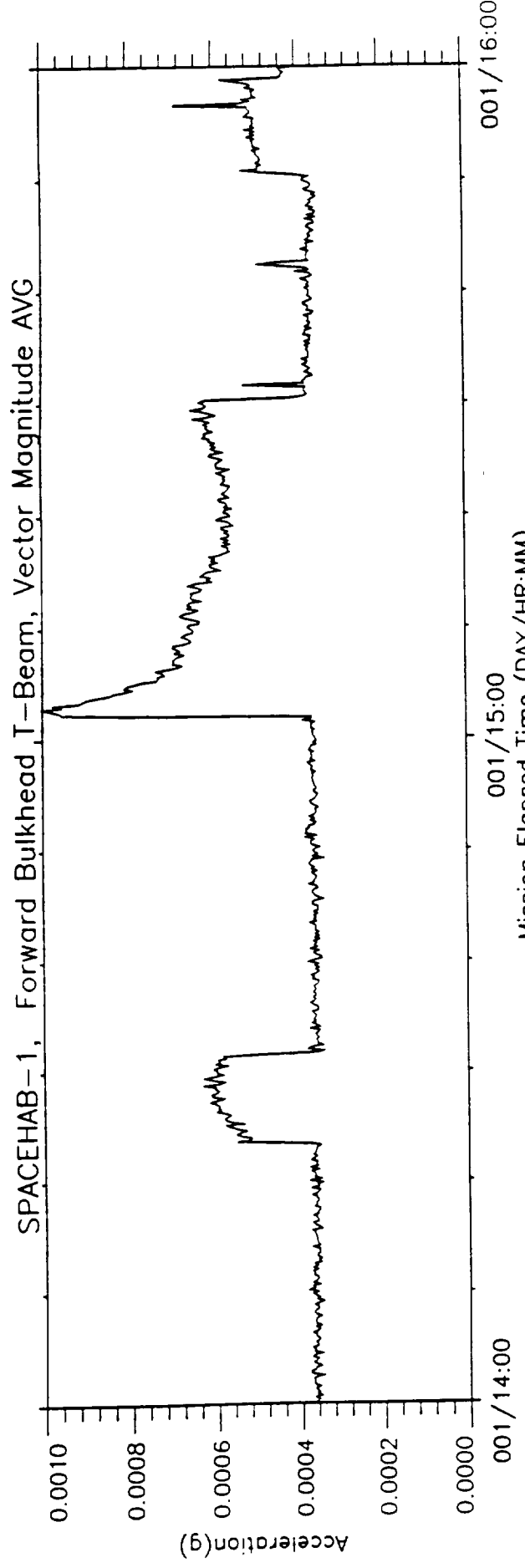


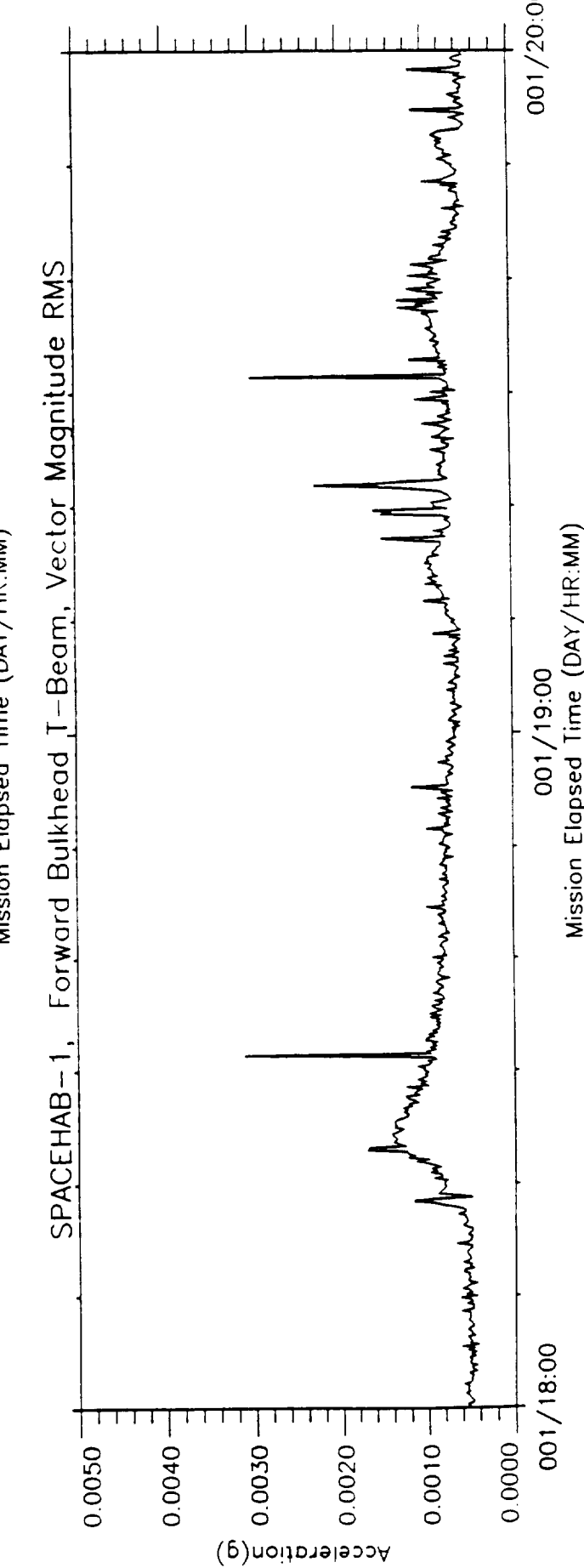
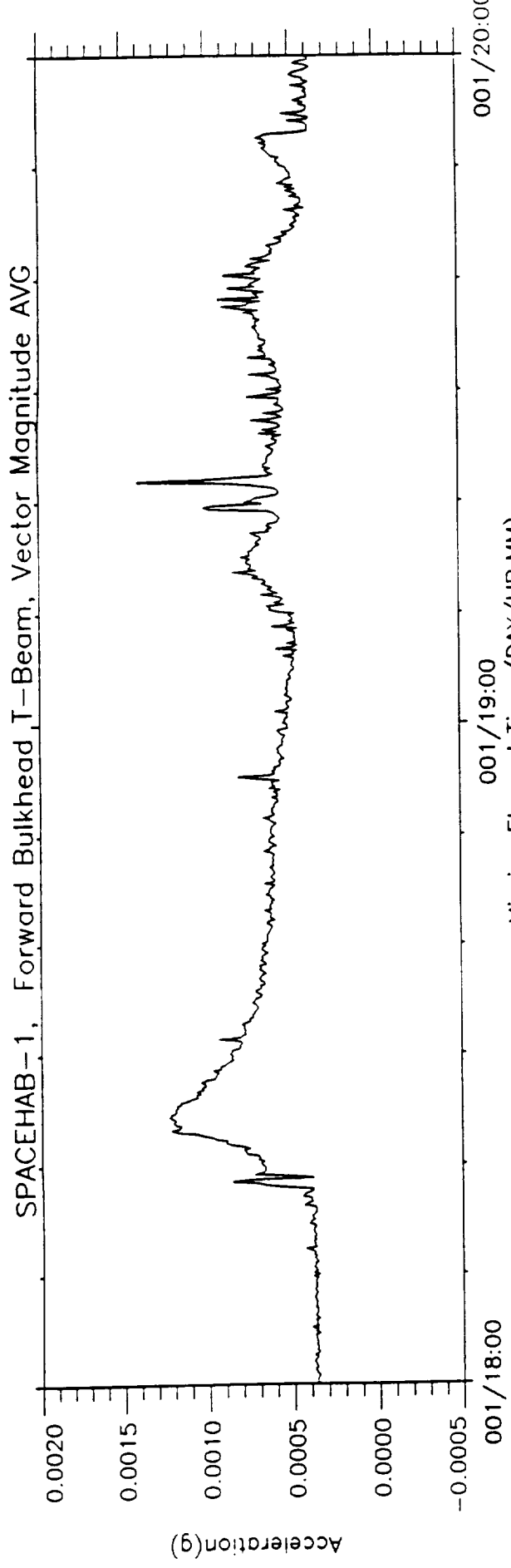


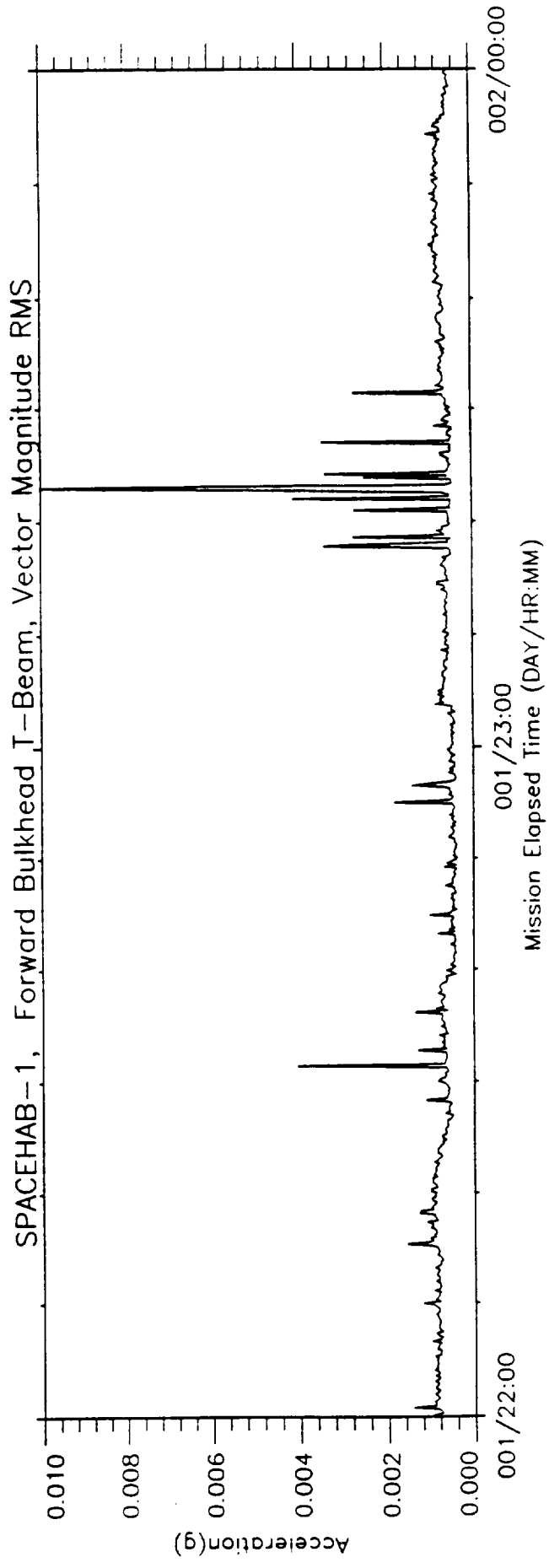
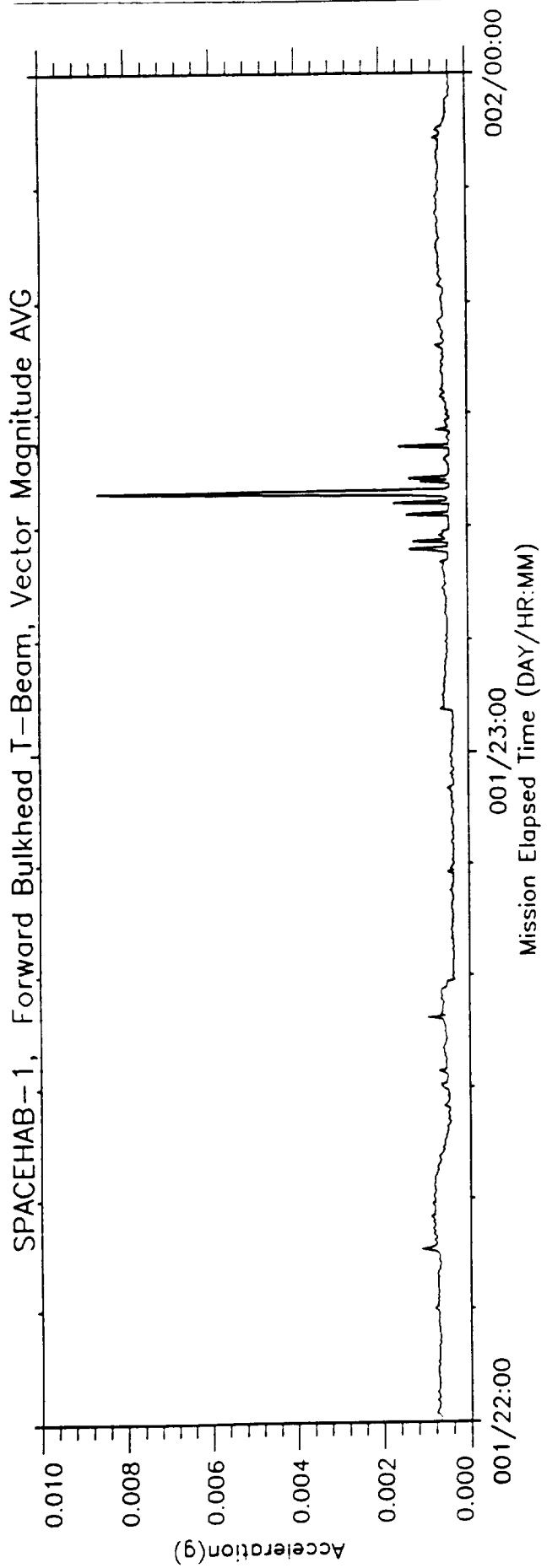


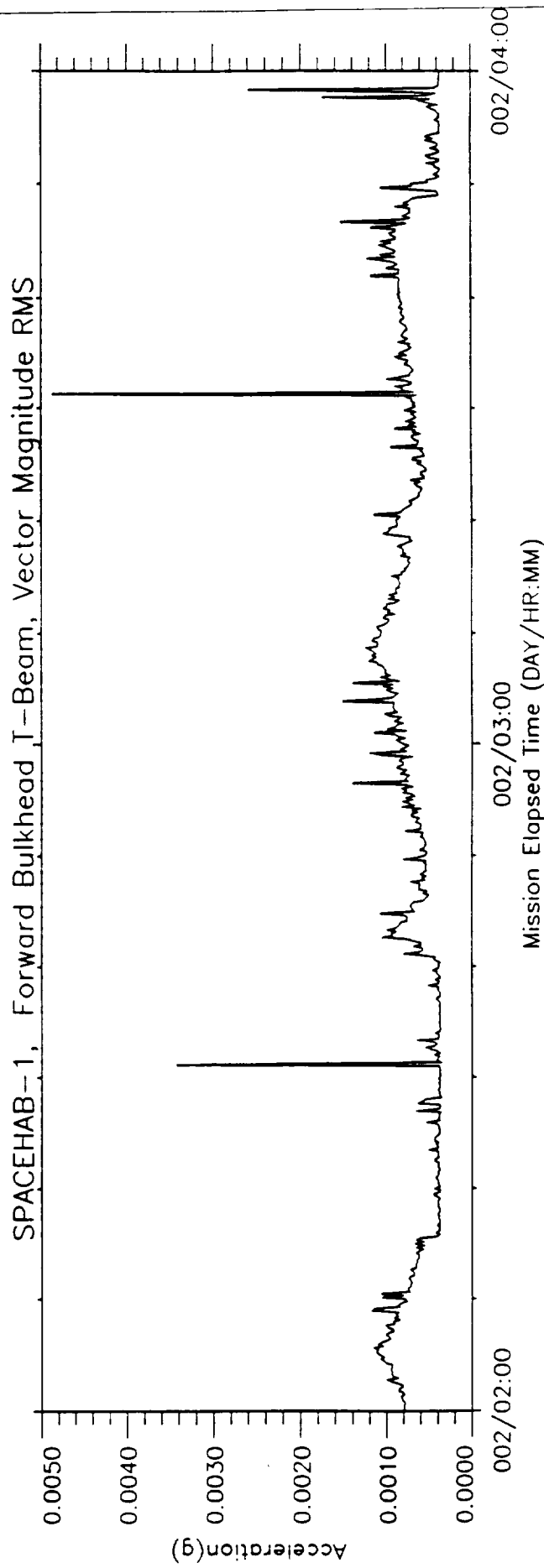
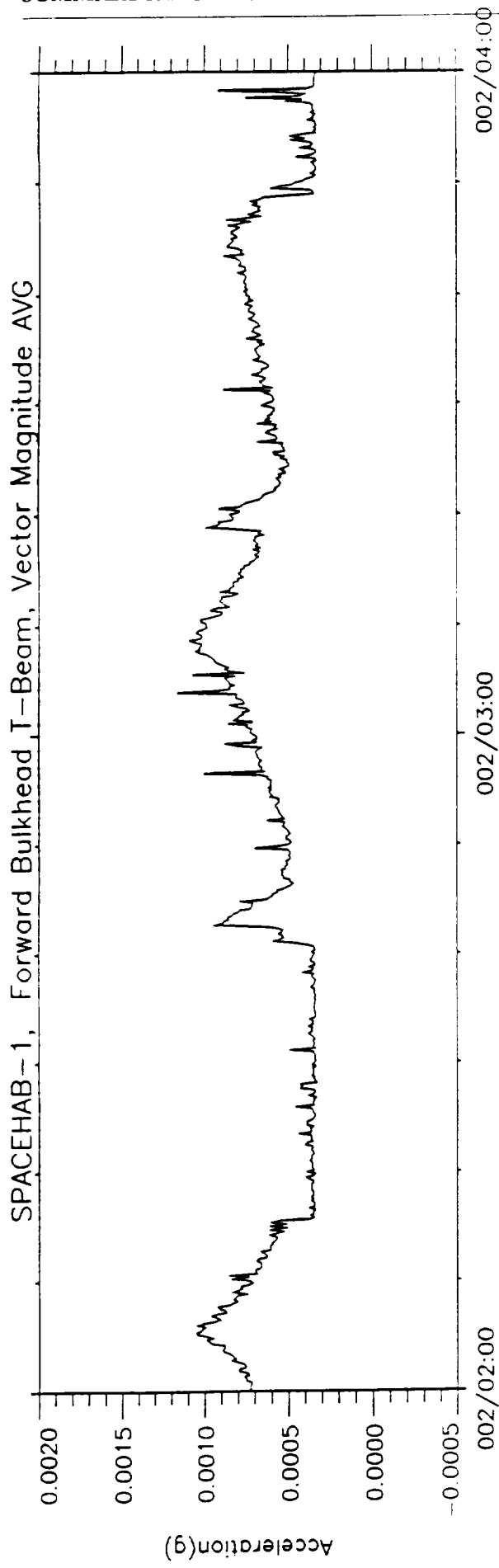


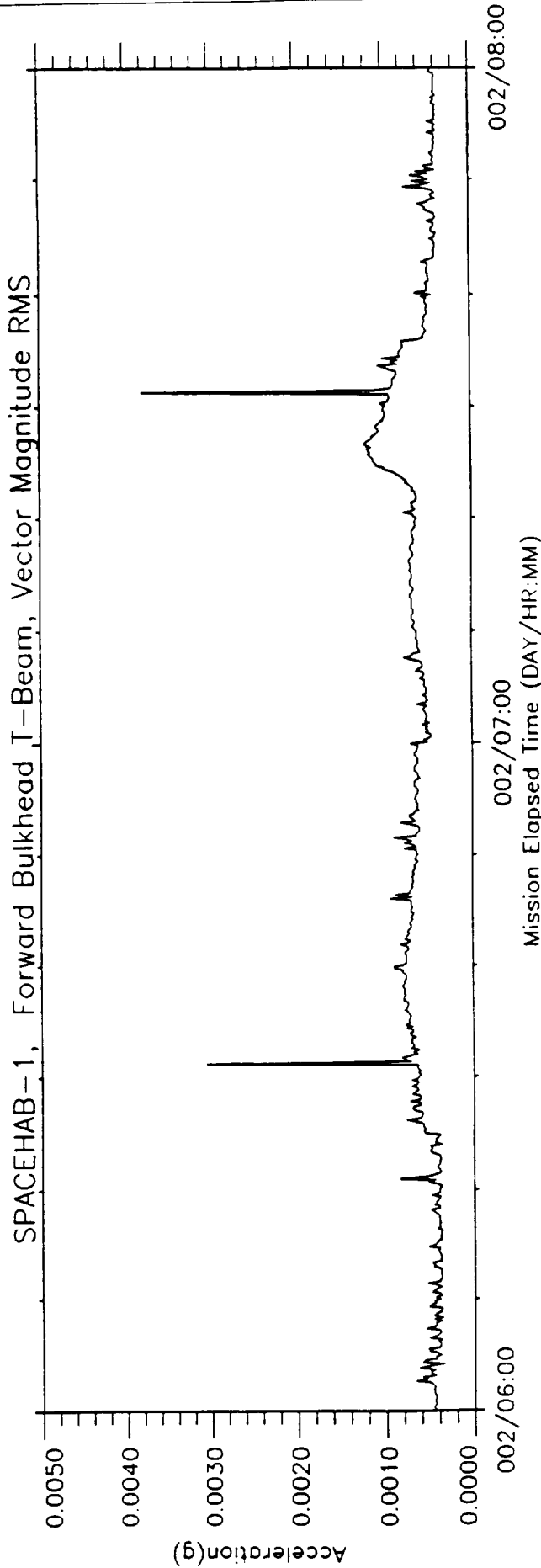
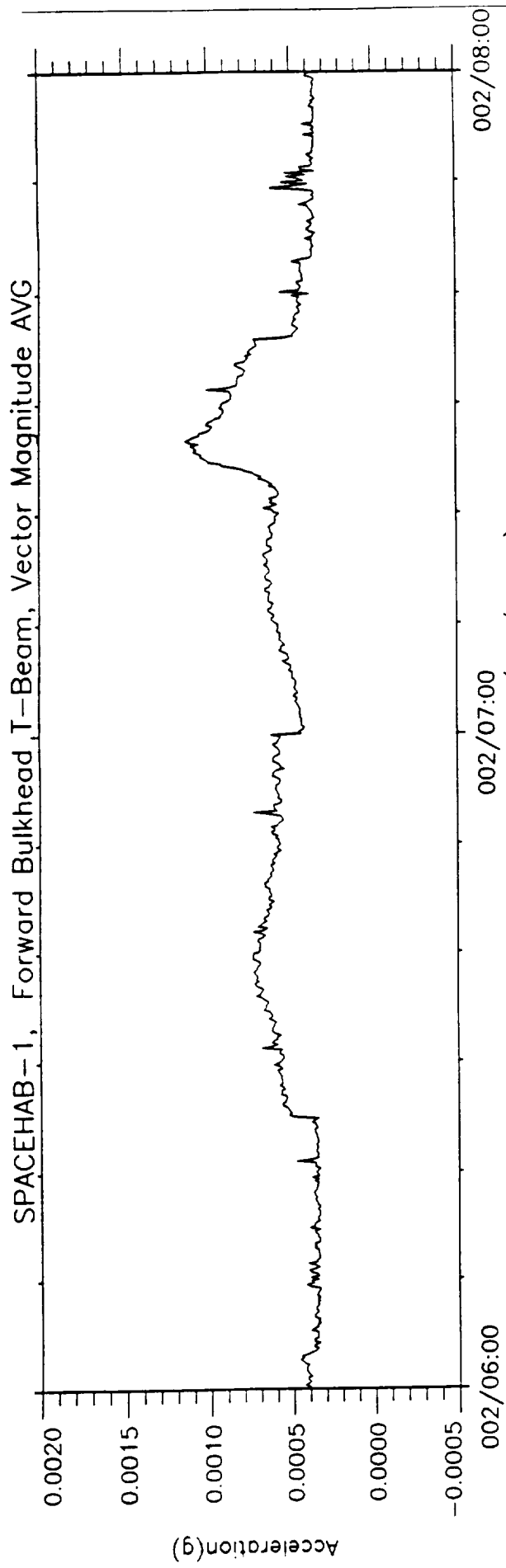


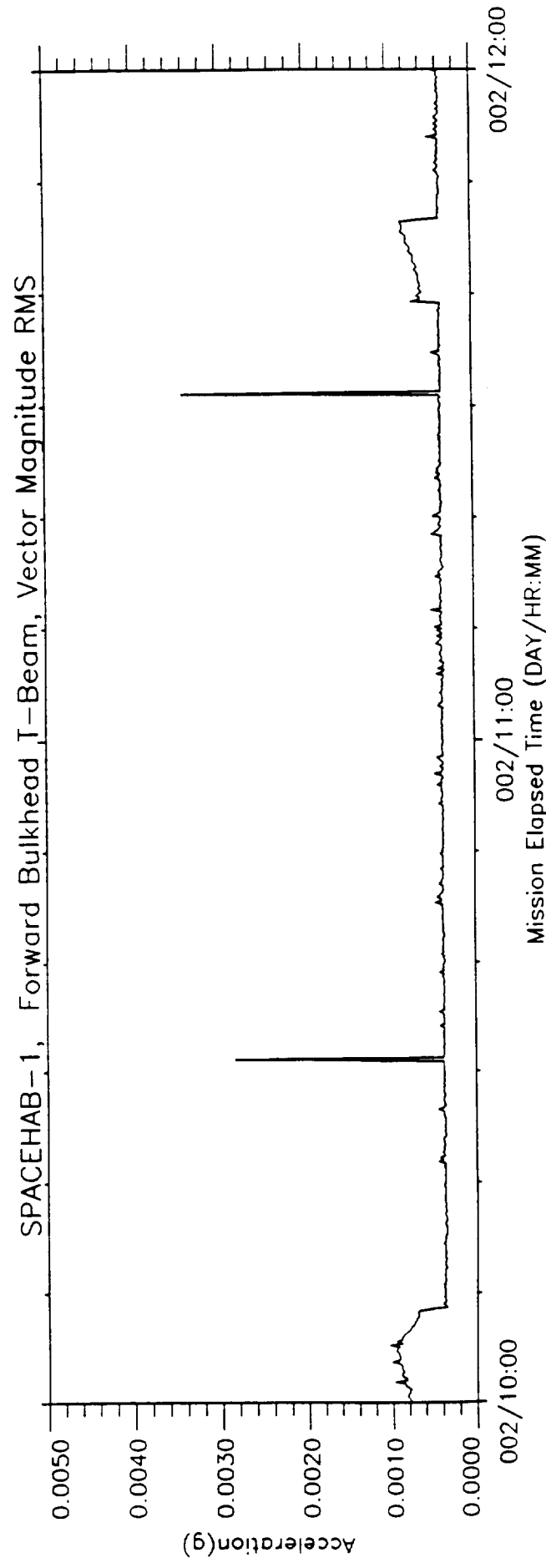
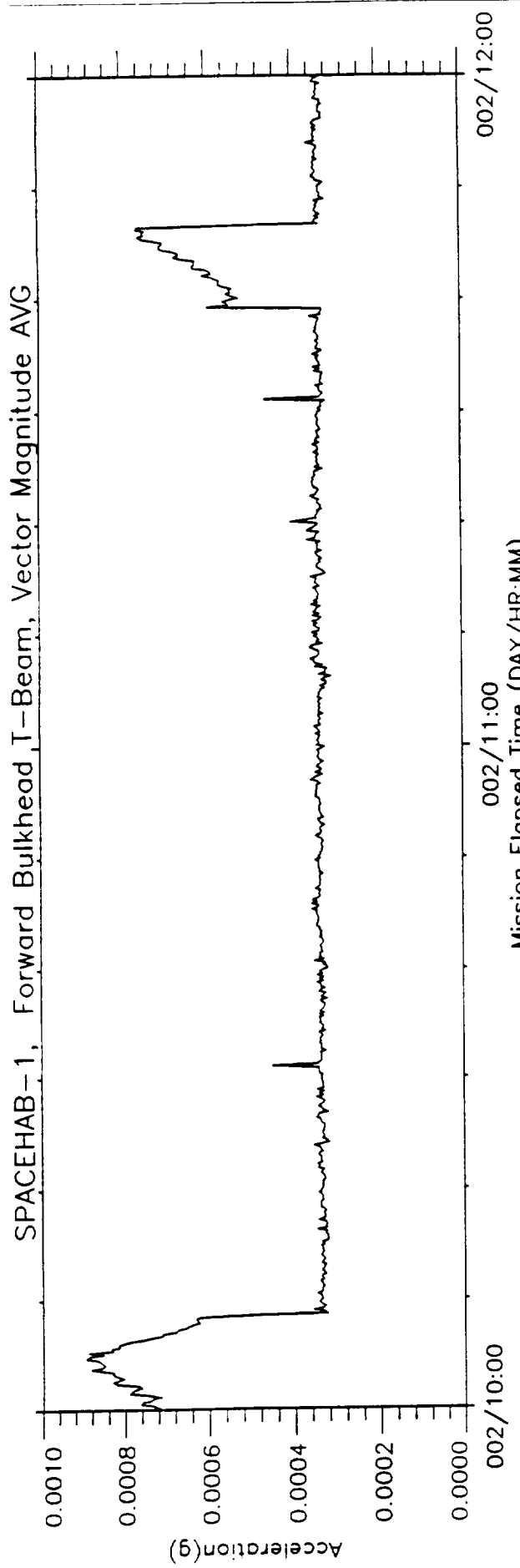


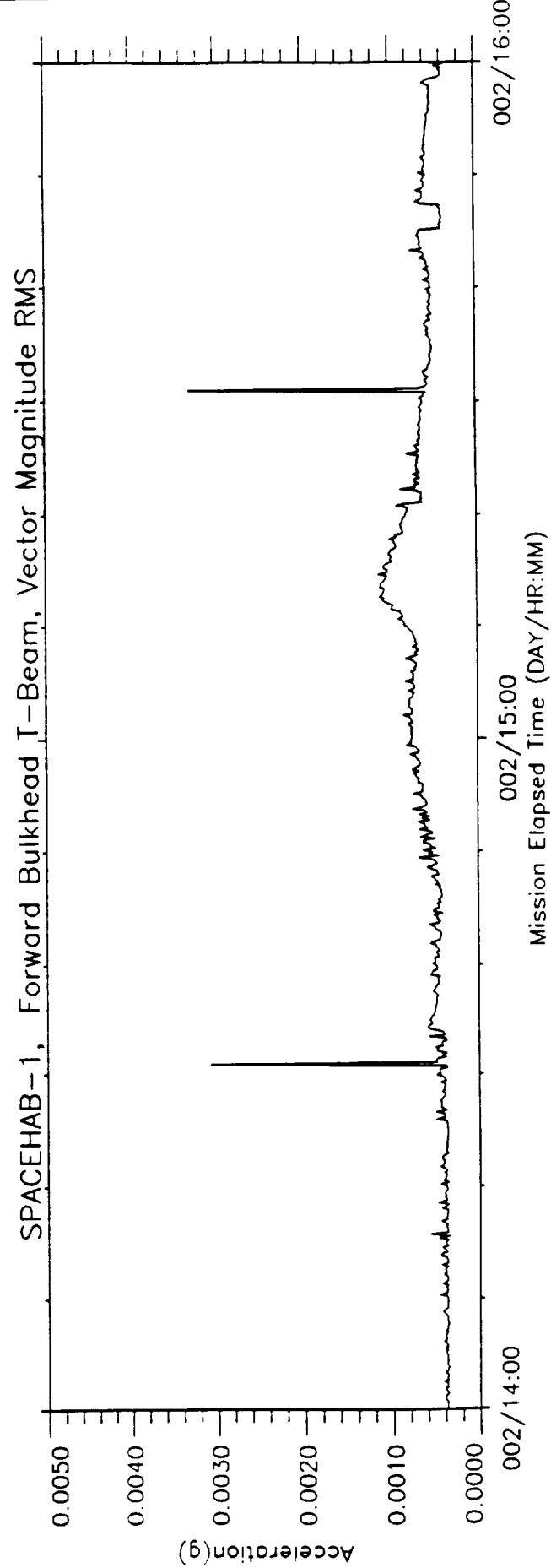
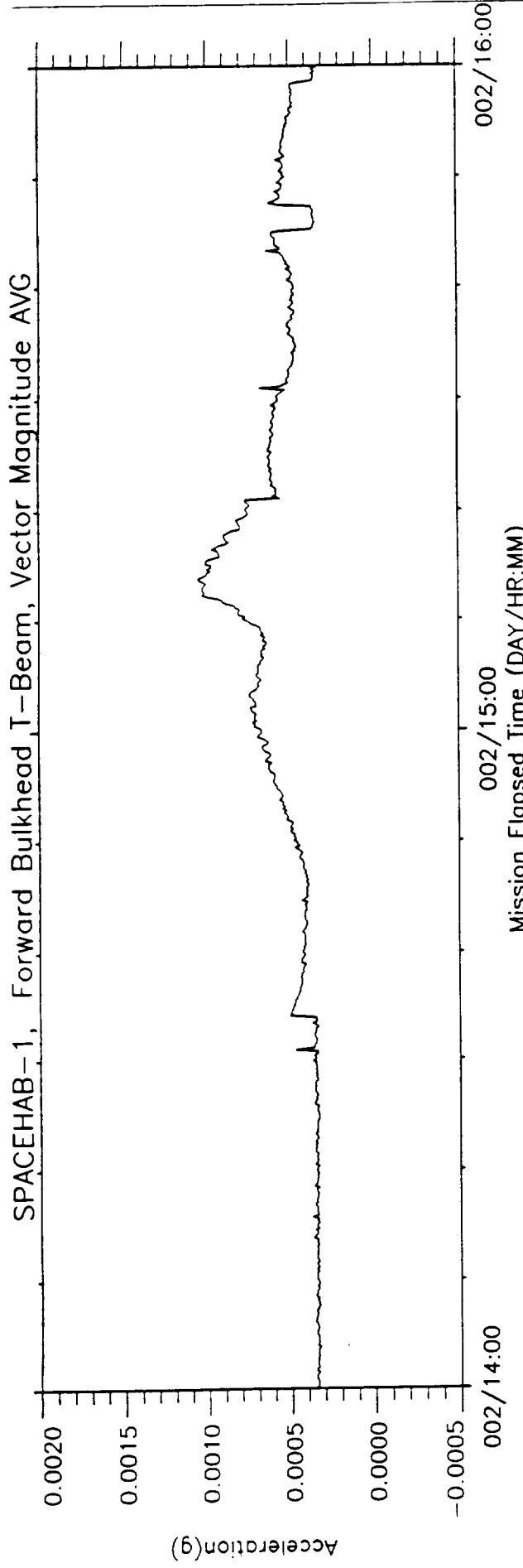


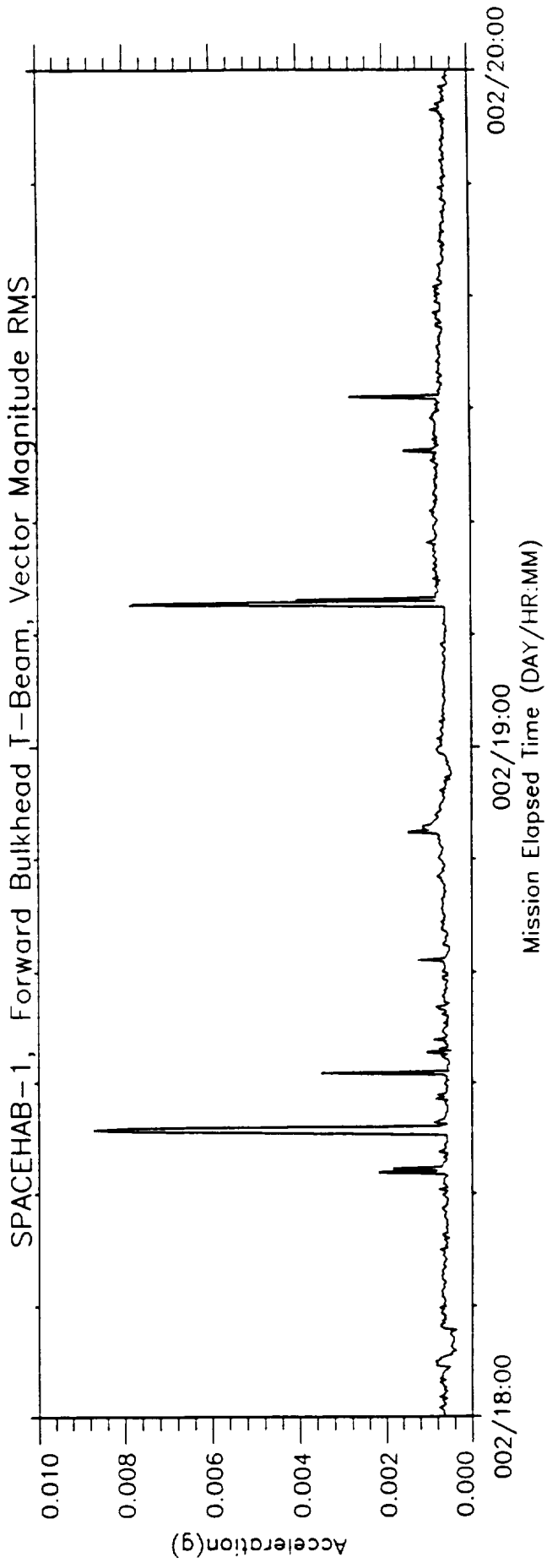
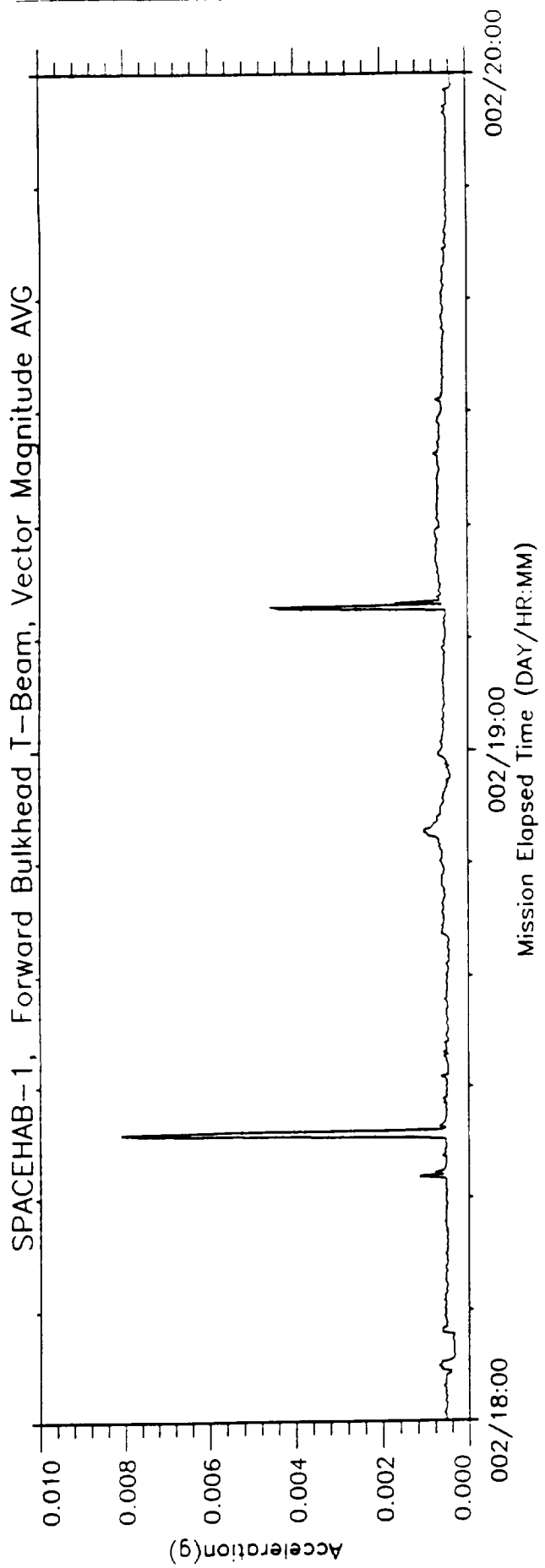


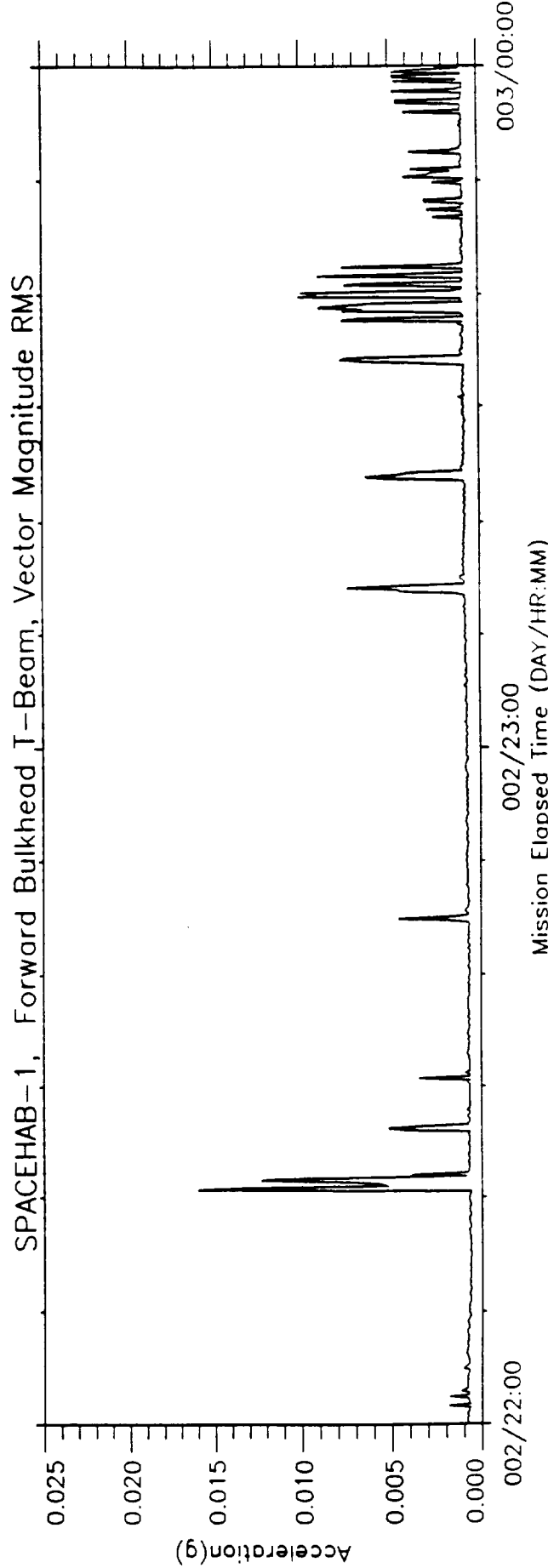
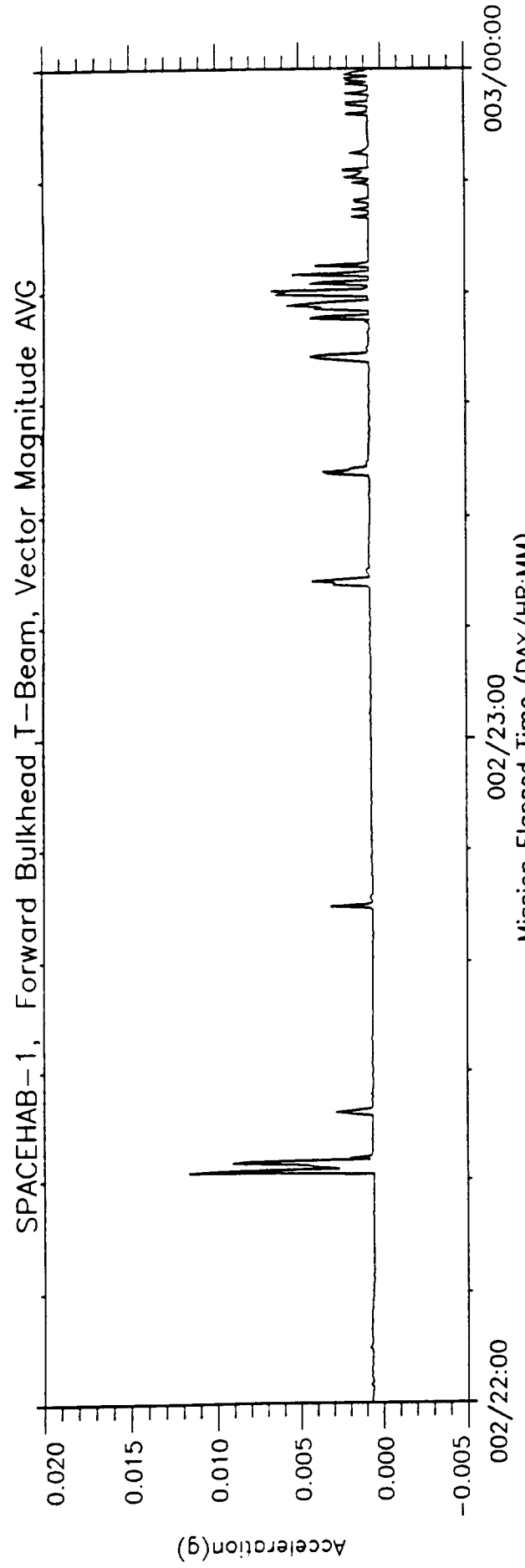


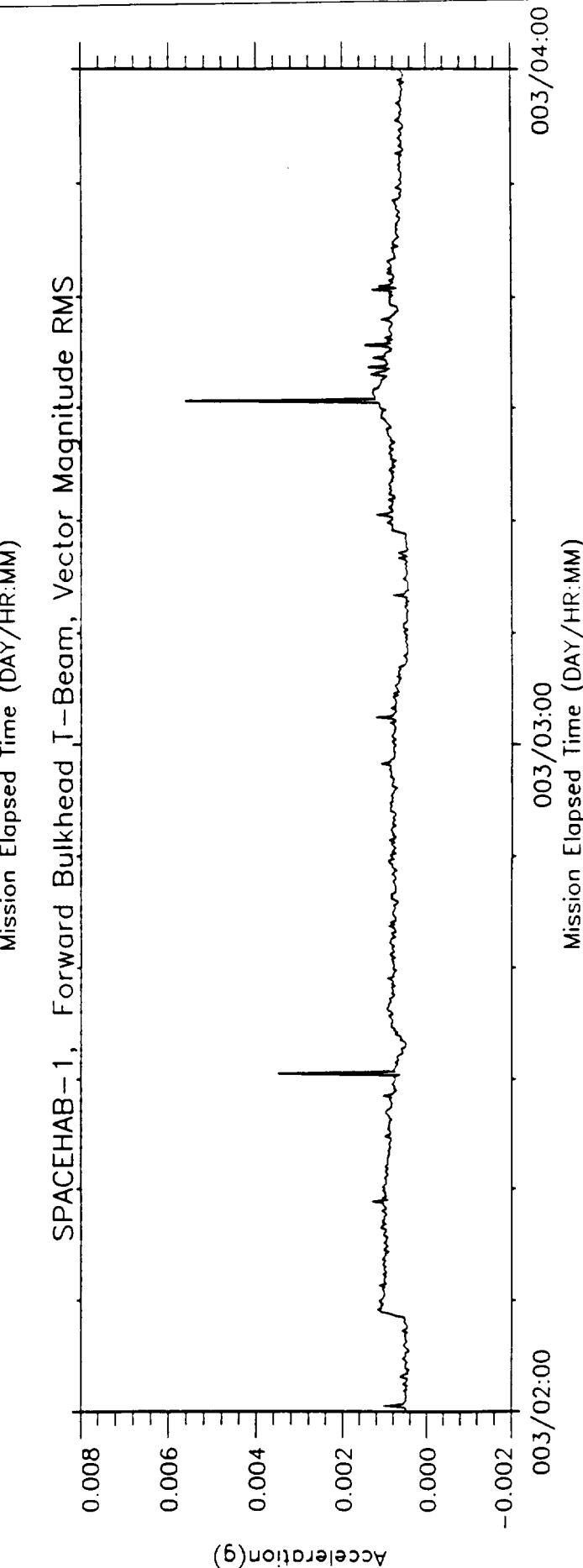
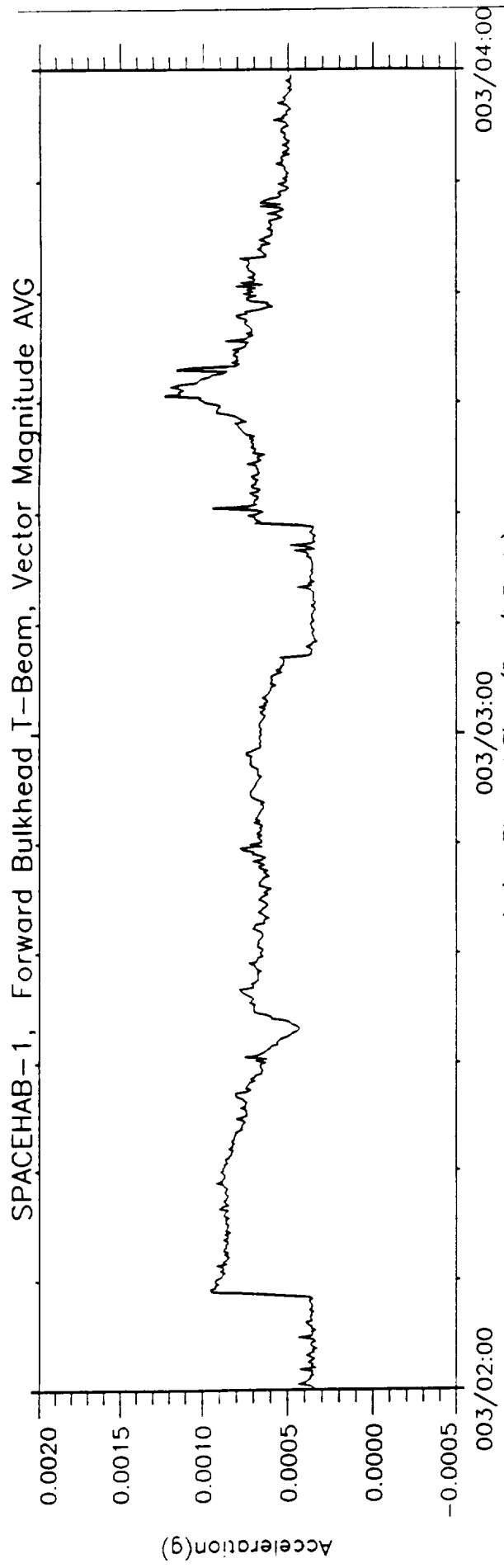


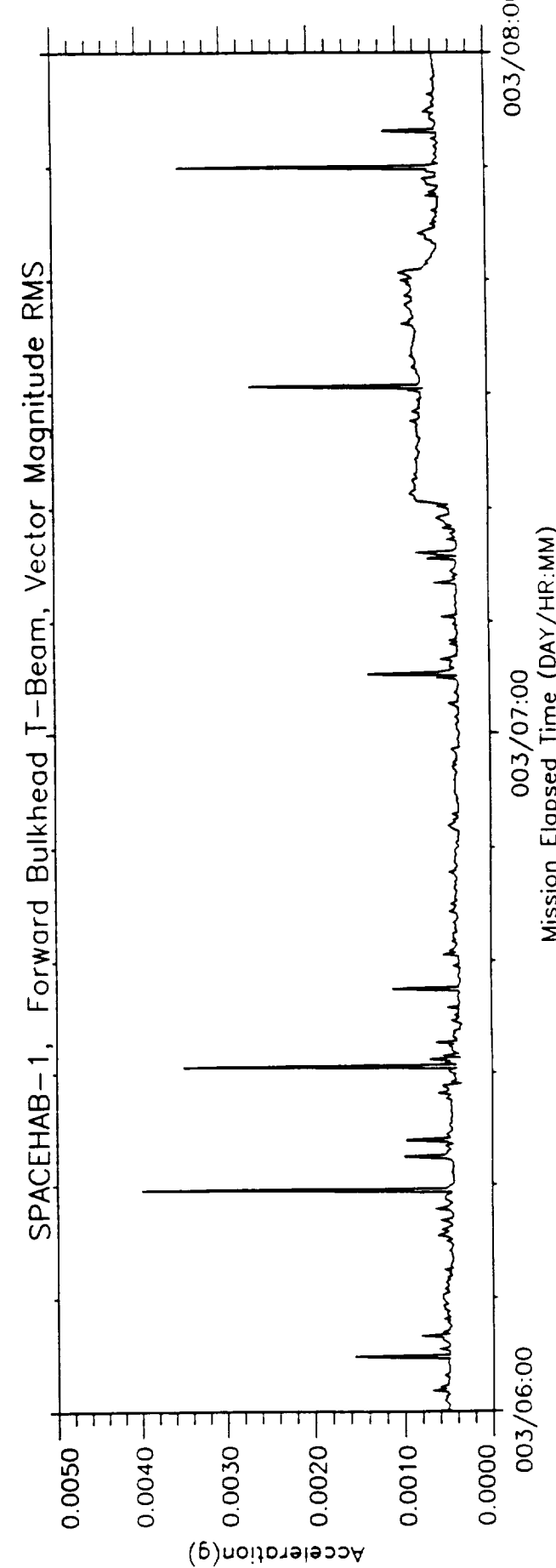
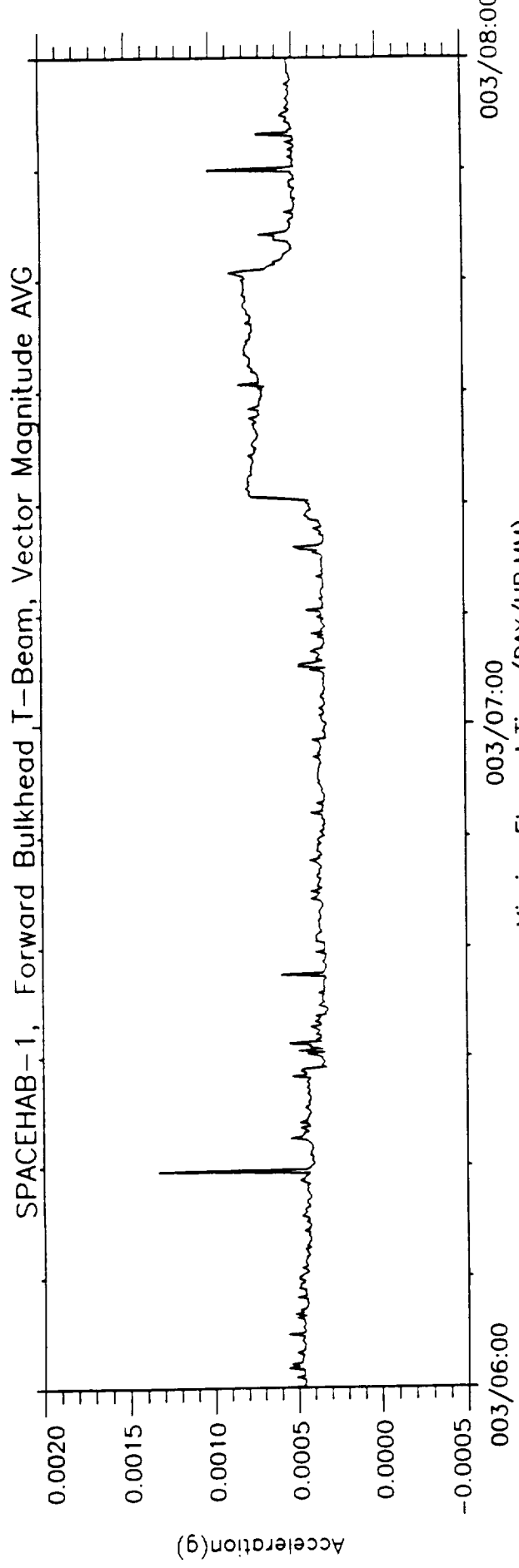


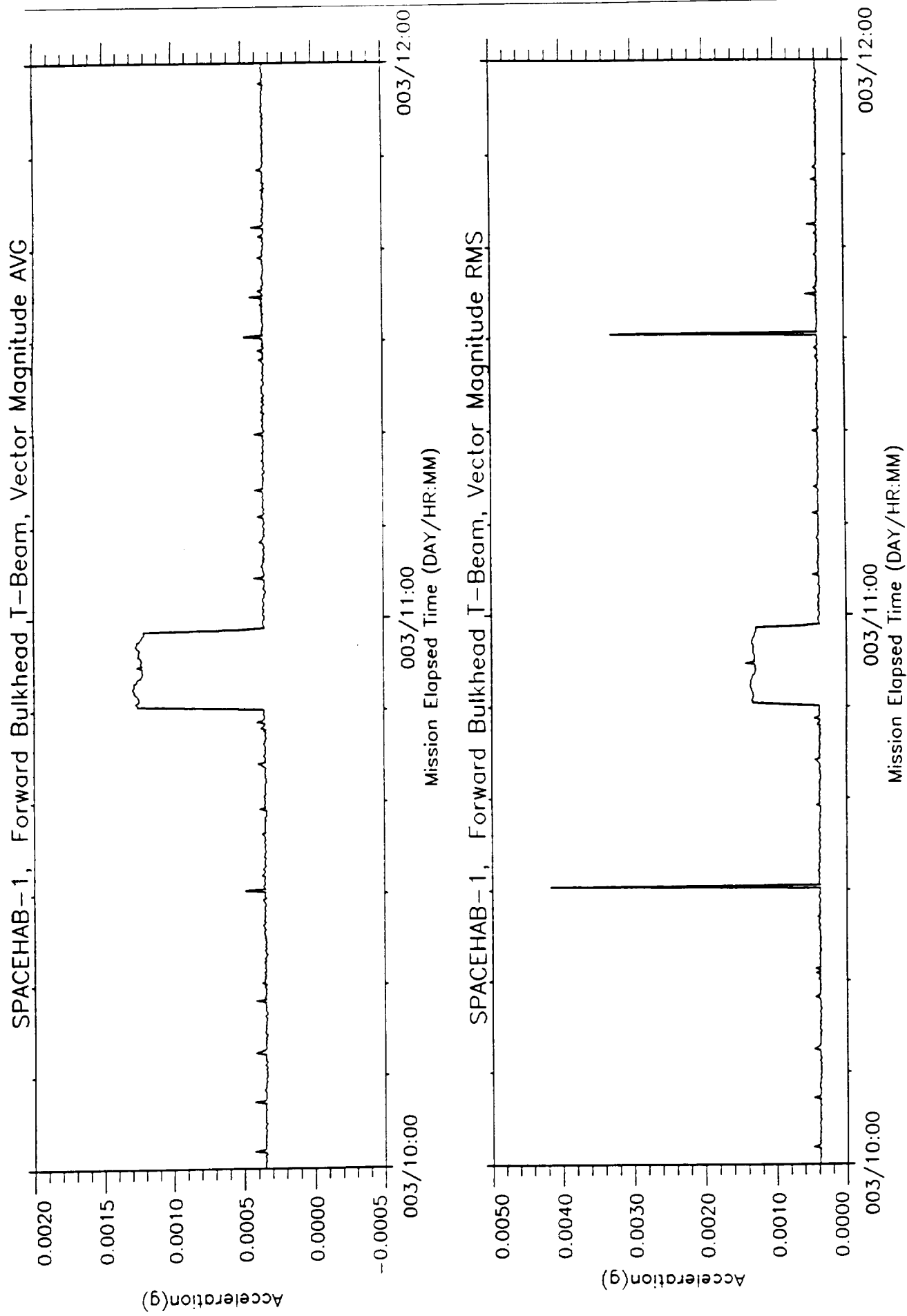


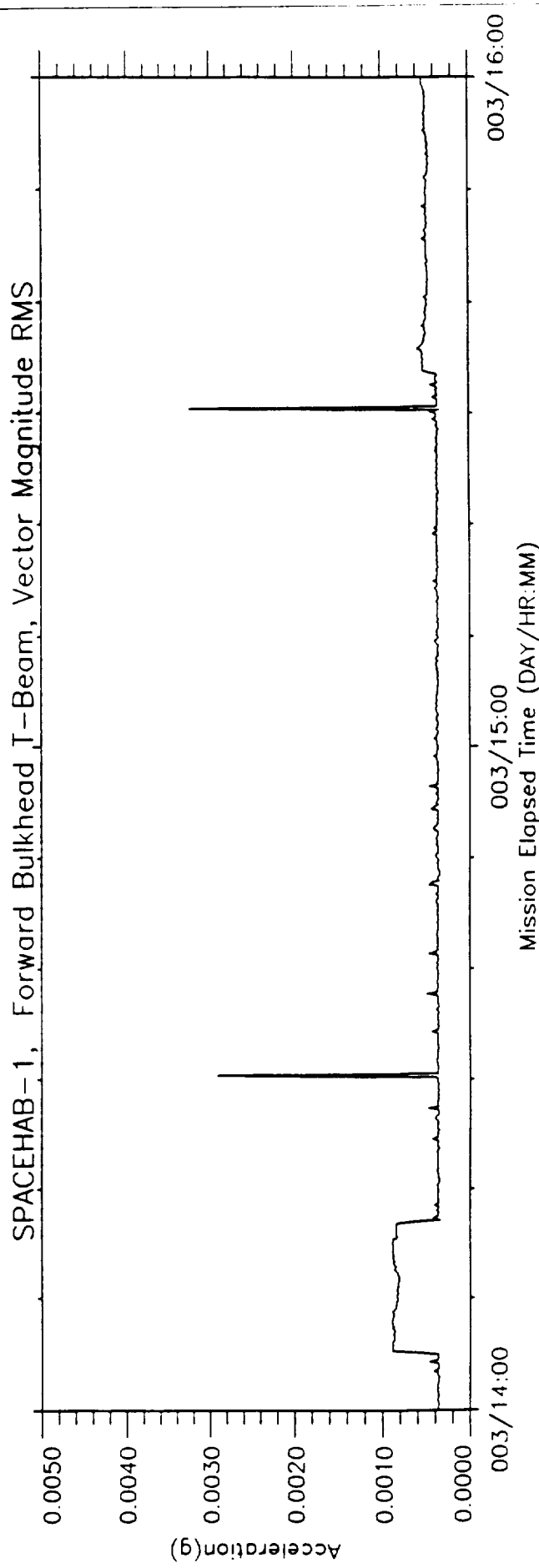
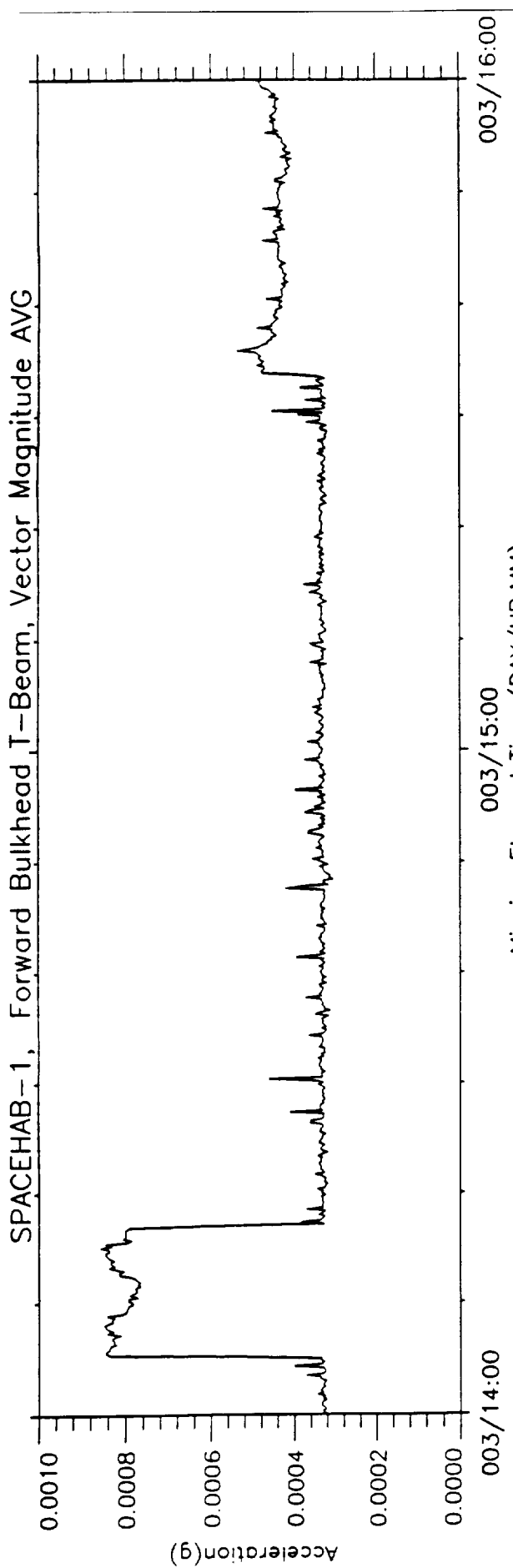


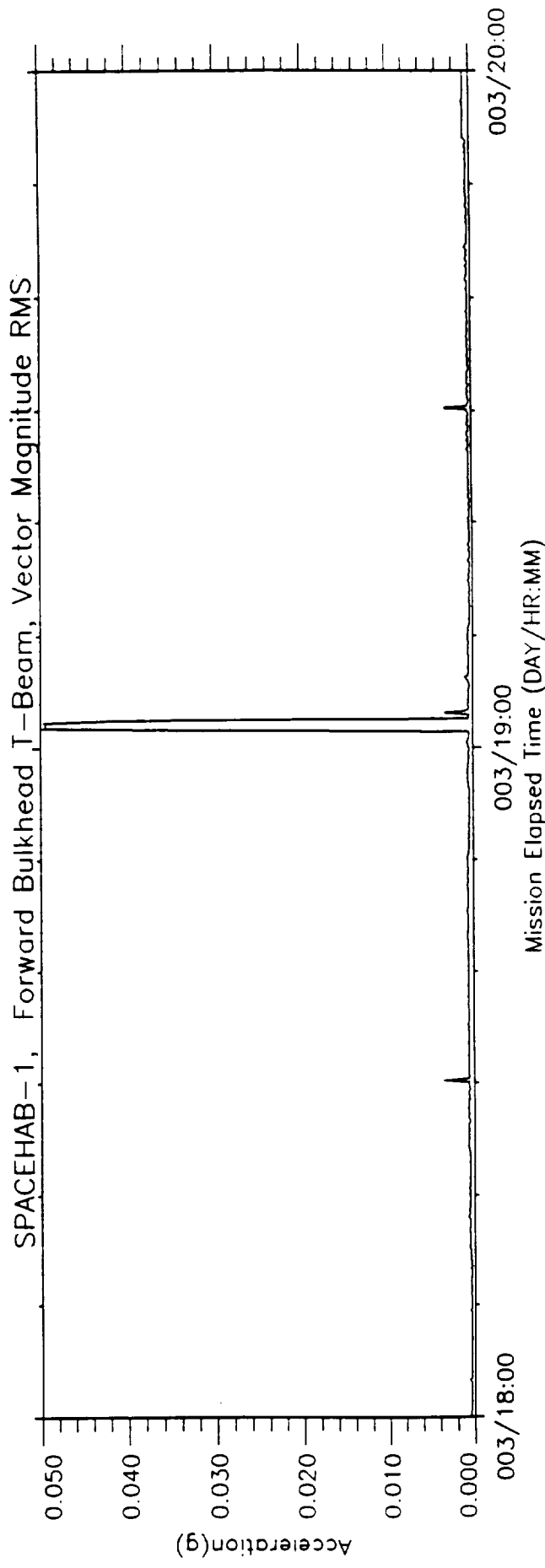
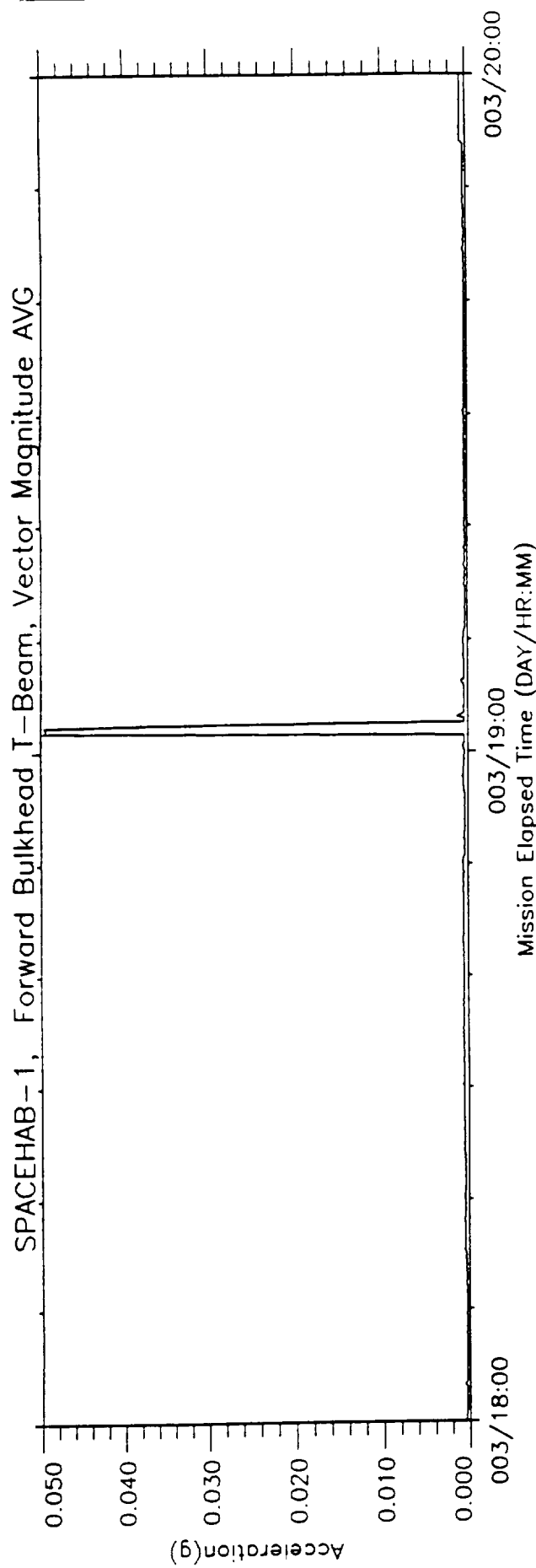


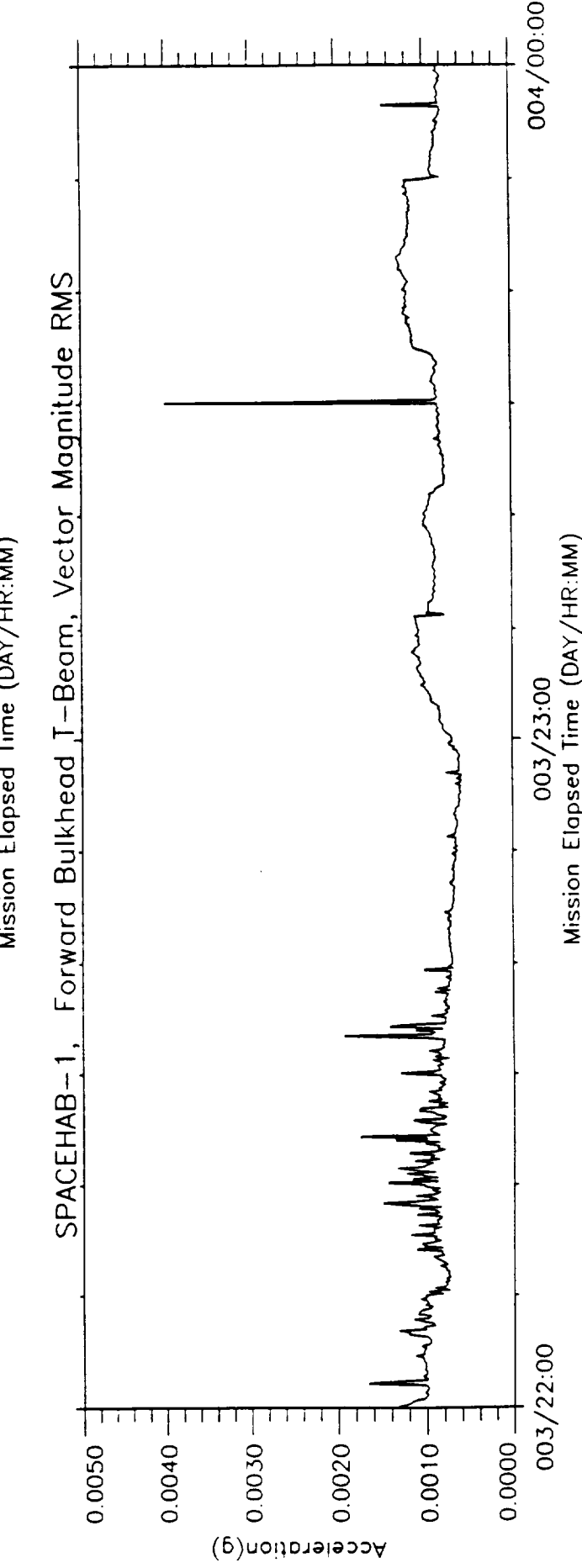
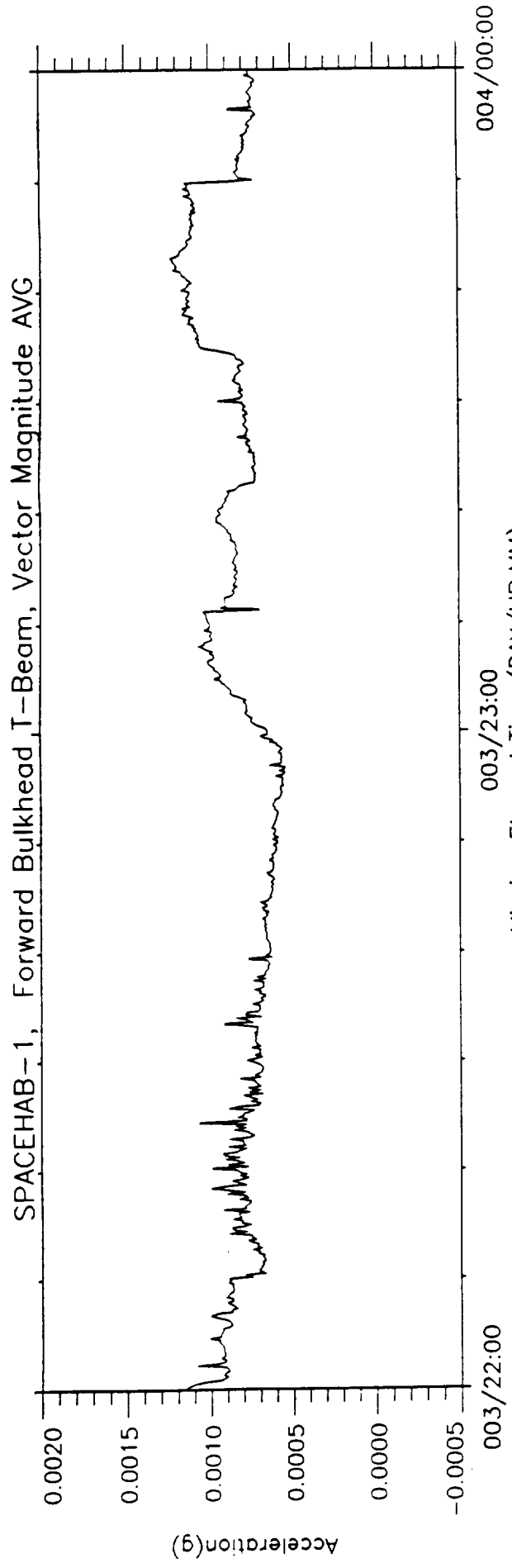


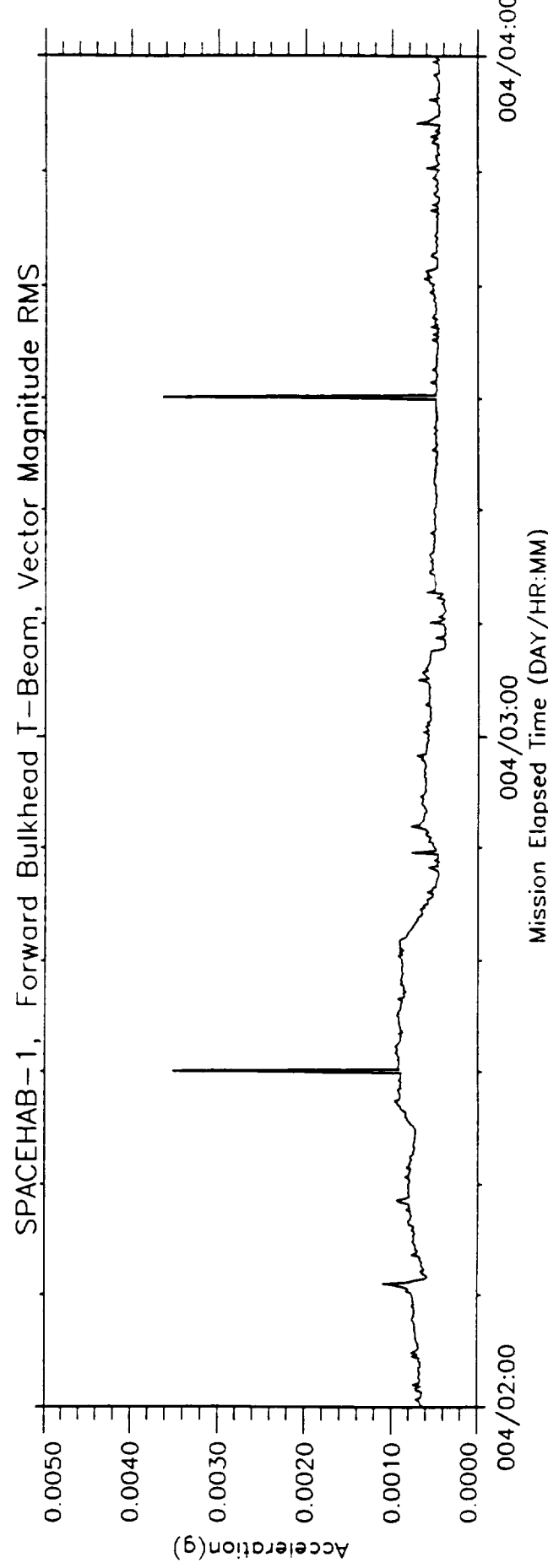
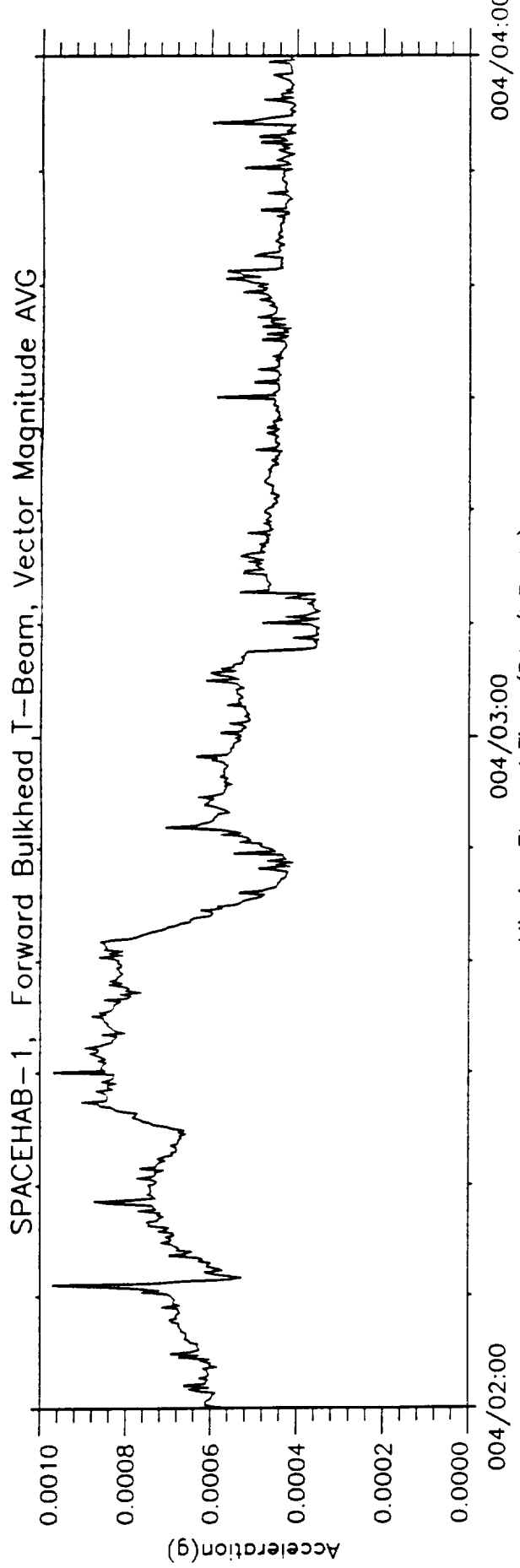












Data missing.

This page intentionally left blank.

Data missing.

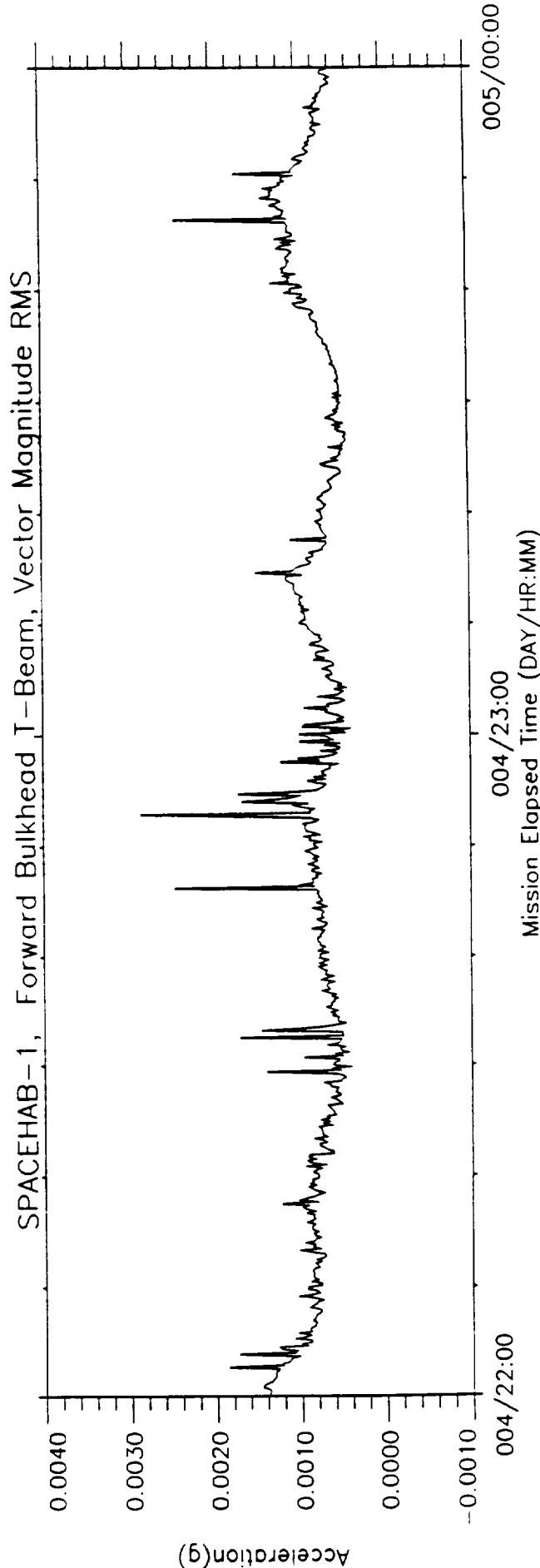
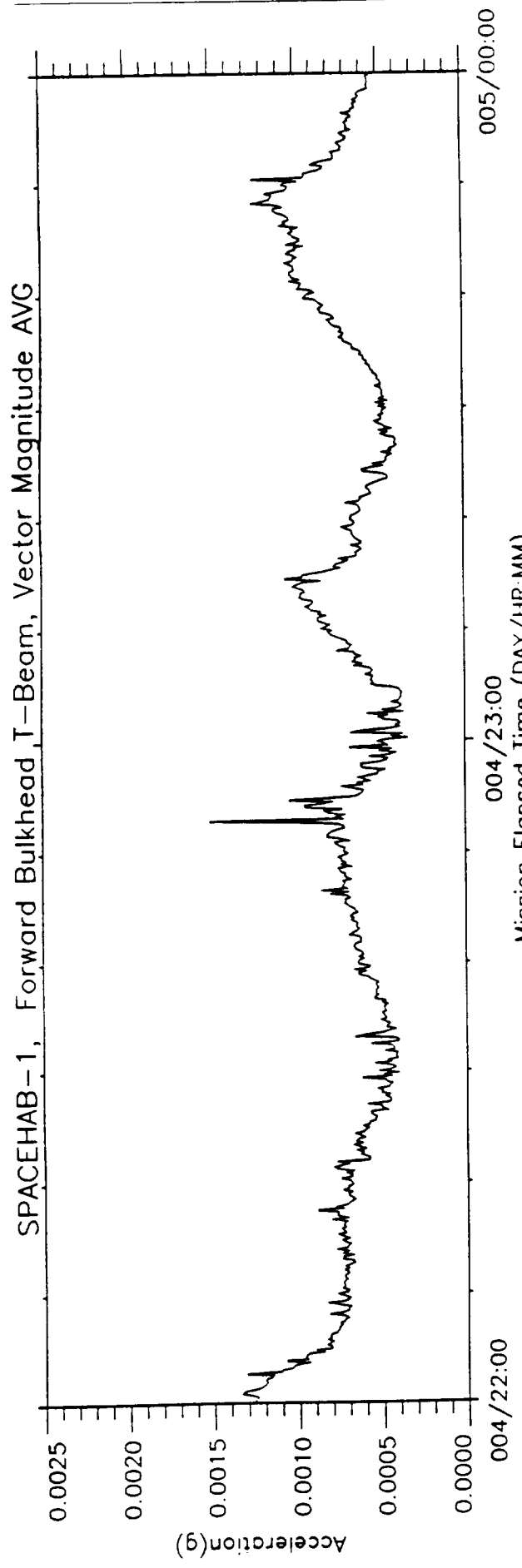
This page intentionally left blank.

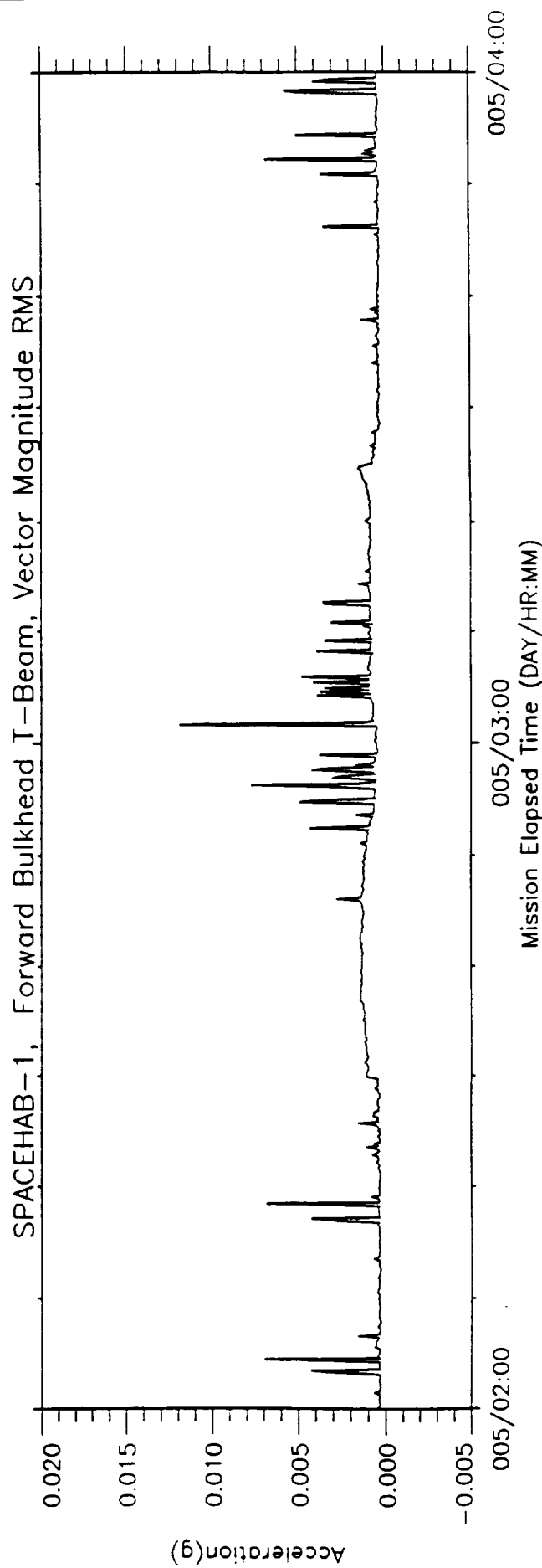
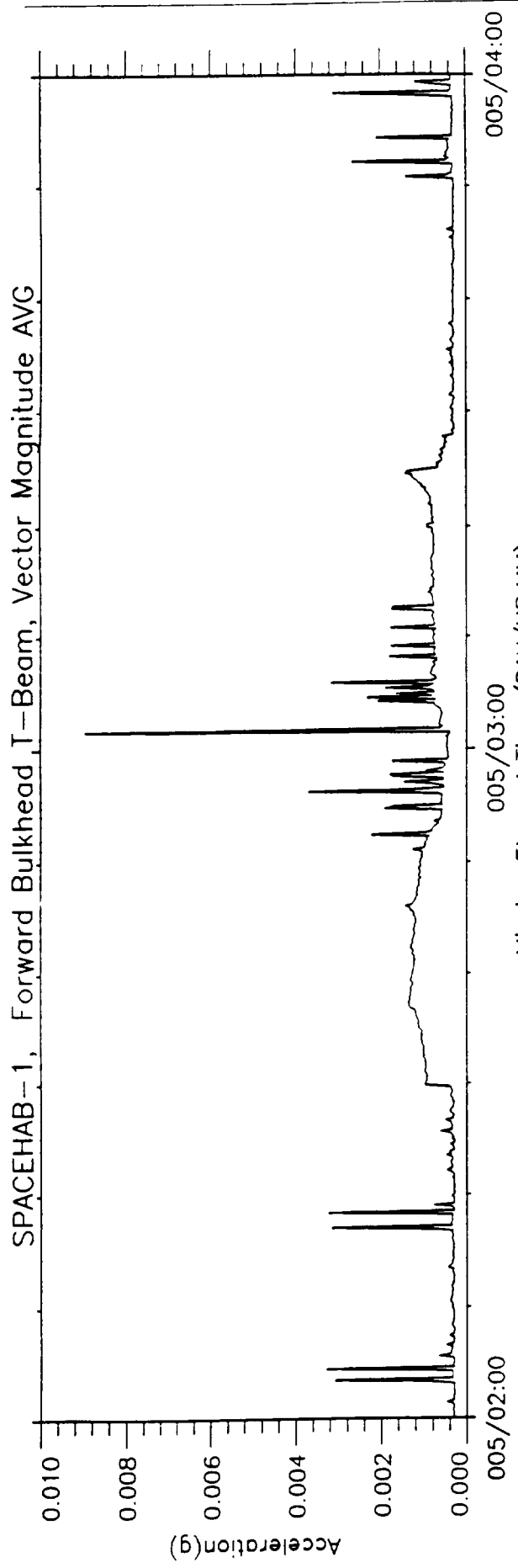
Data missing

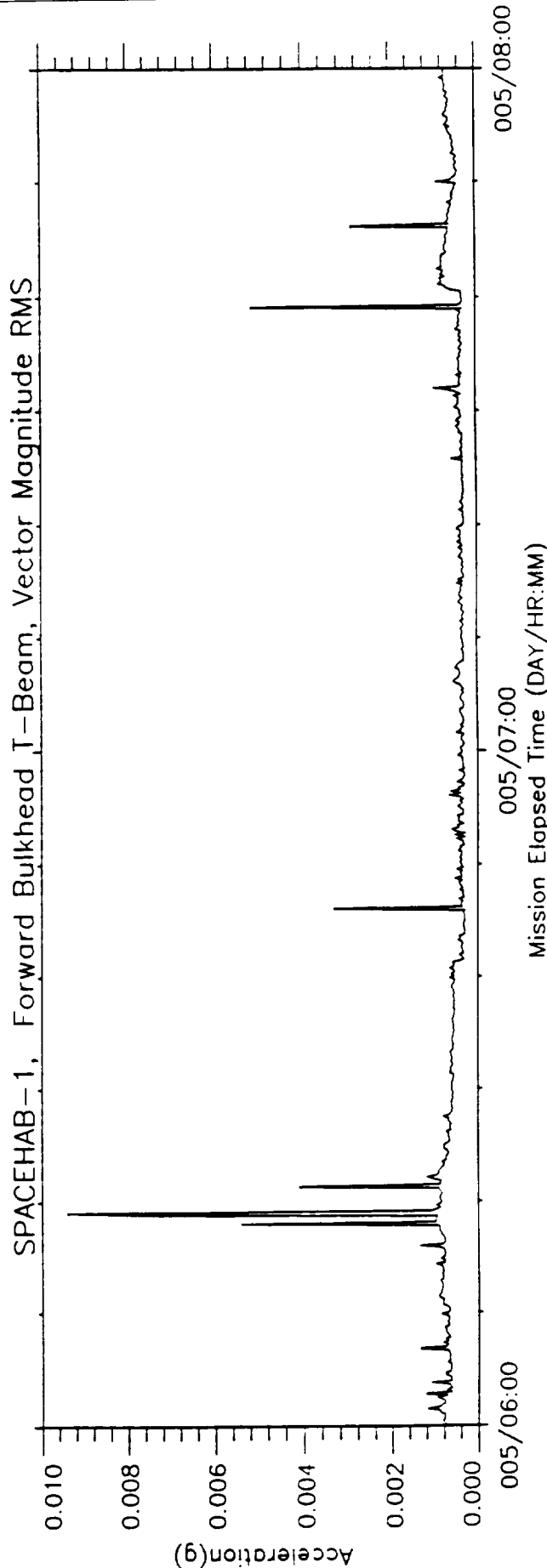
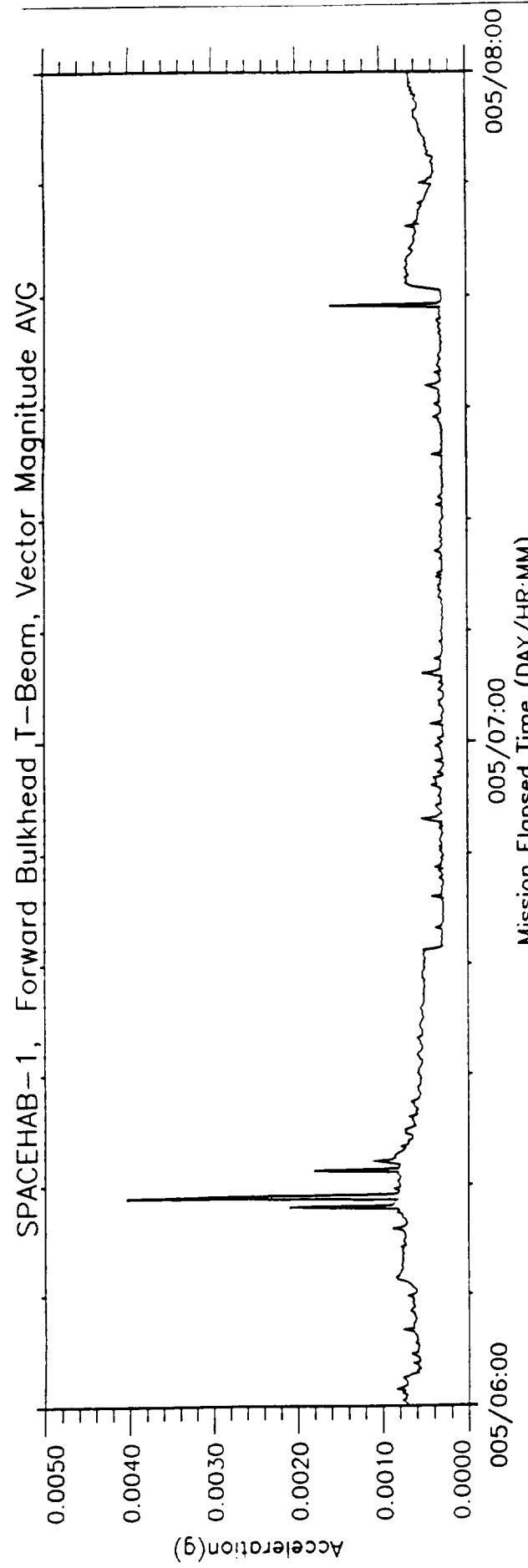
This page intentionally left blank.

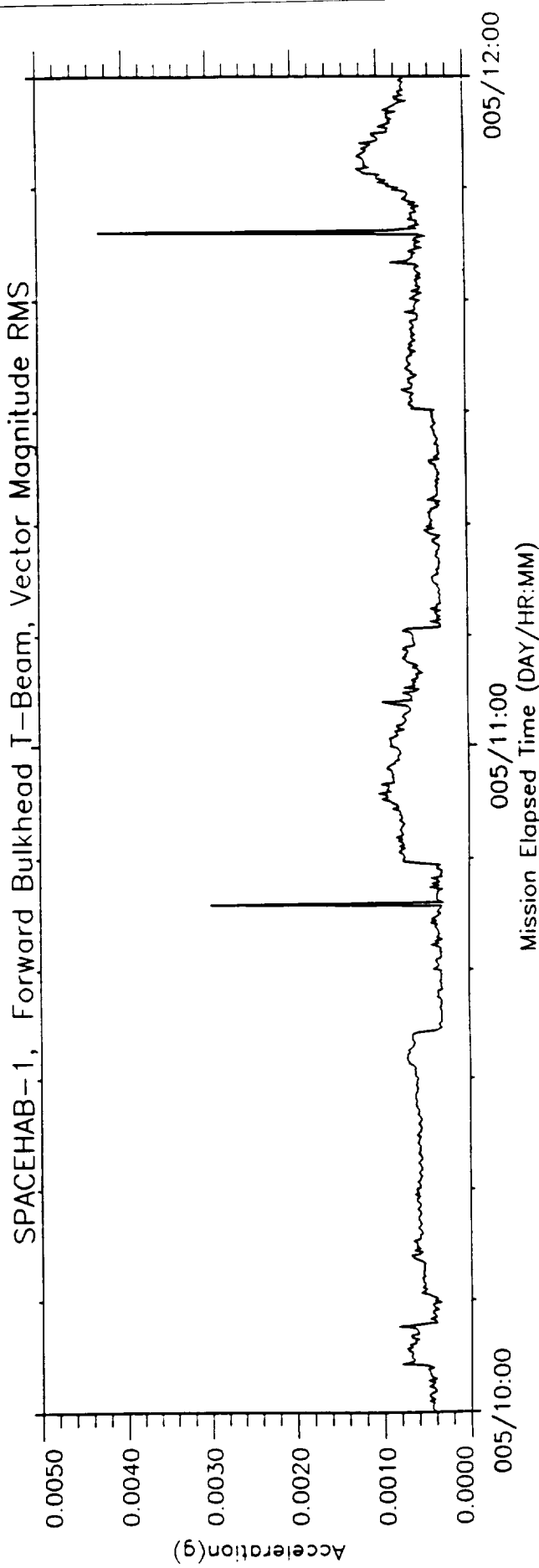
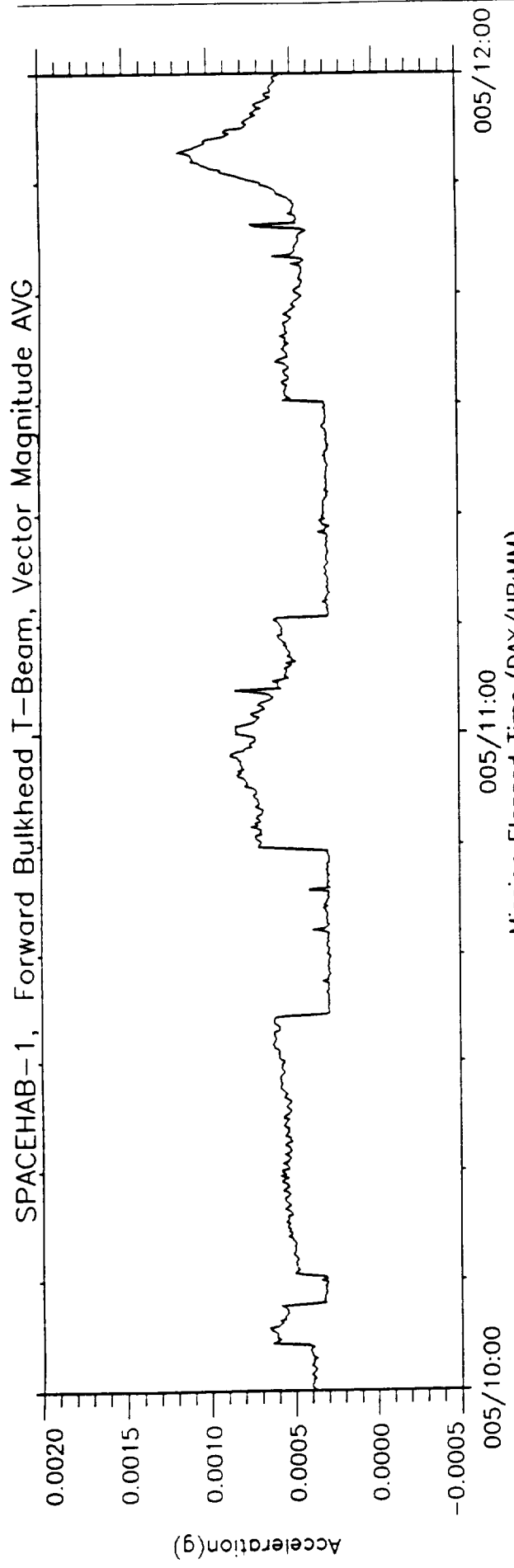
Data missing.

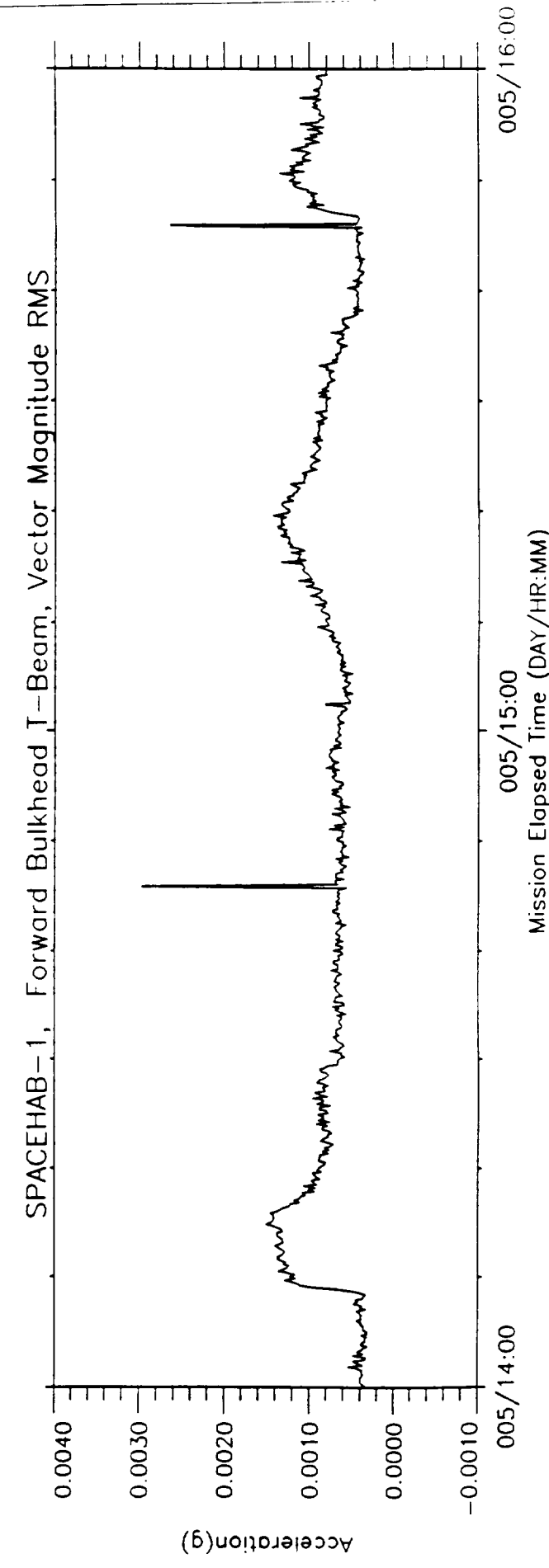
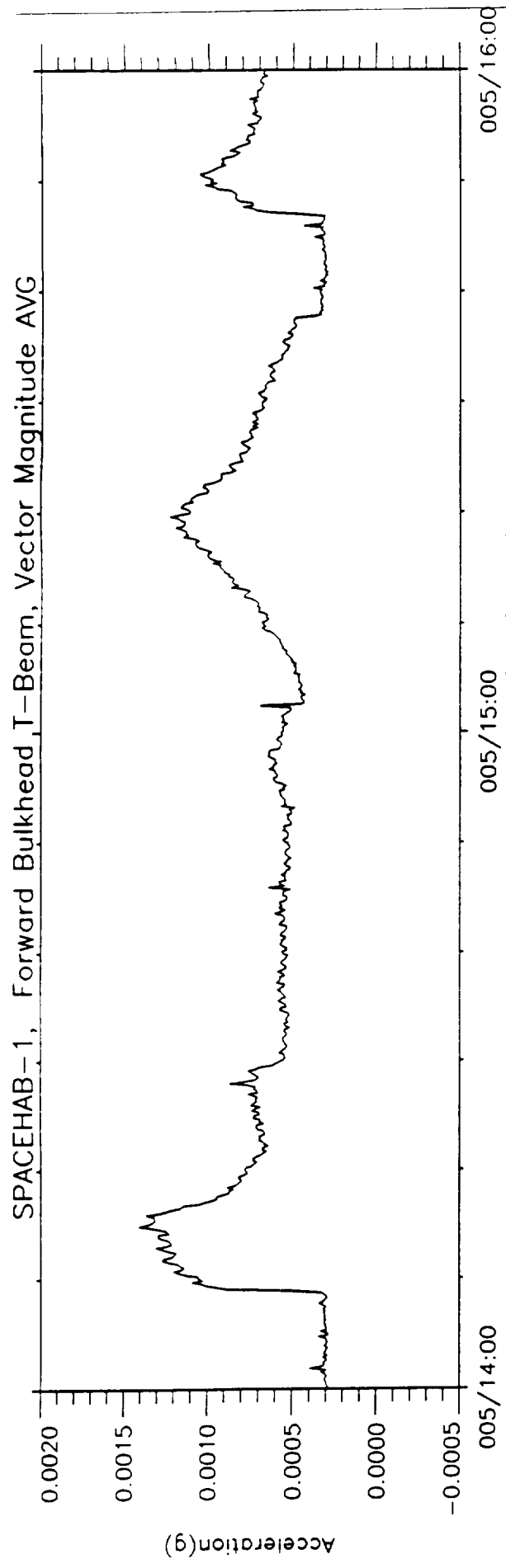
This page intentionally left blank.





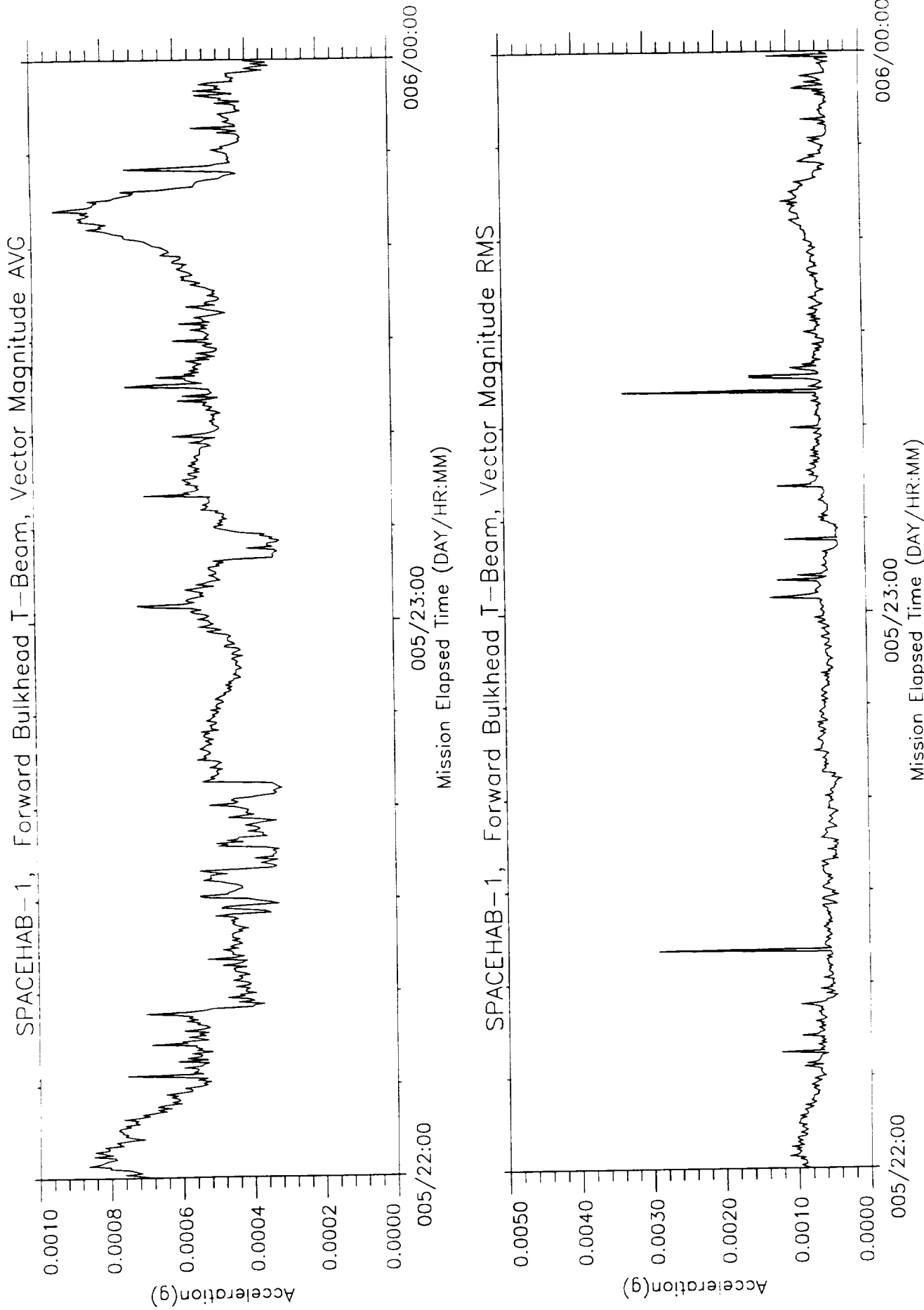


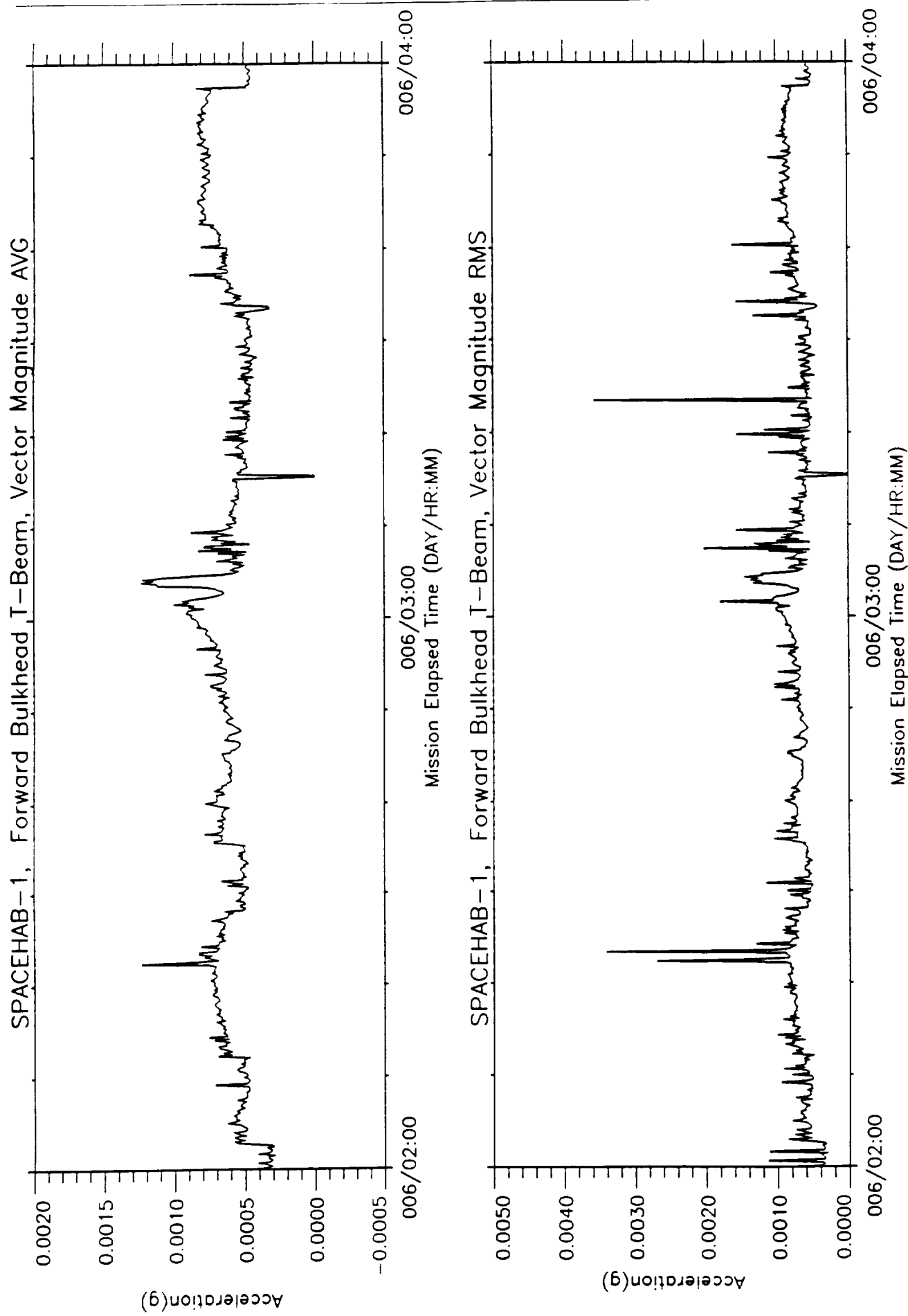


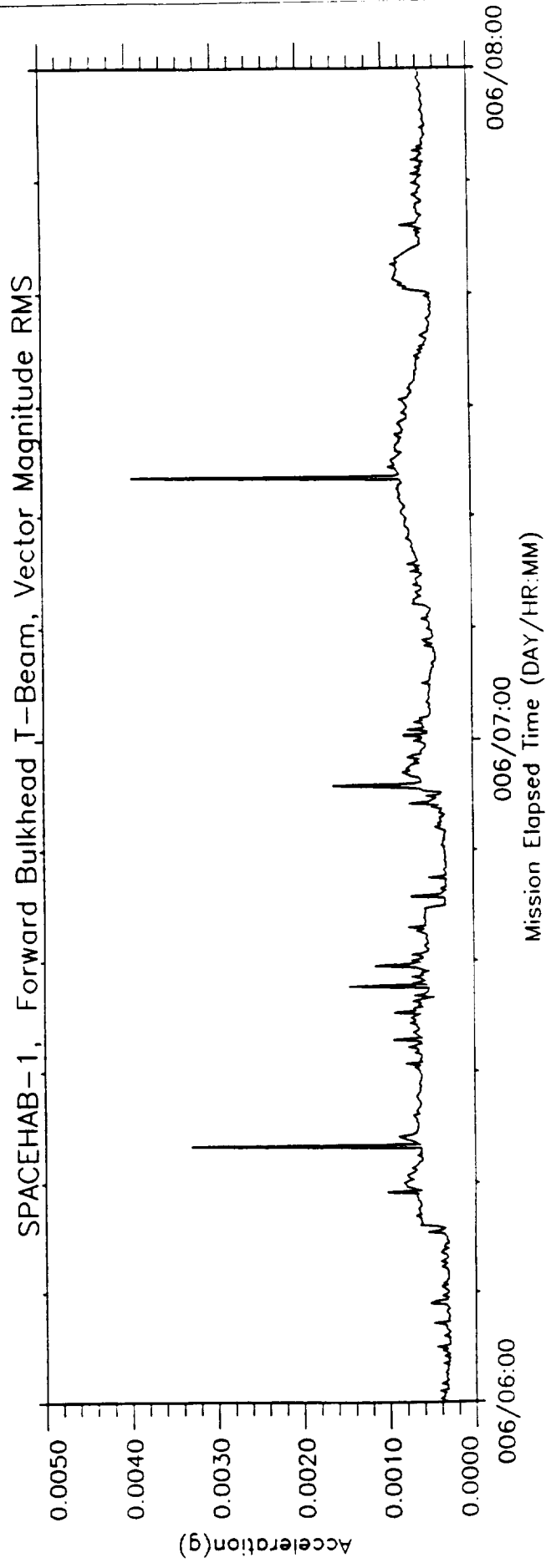
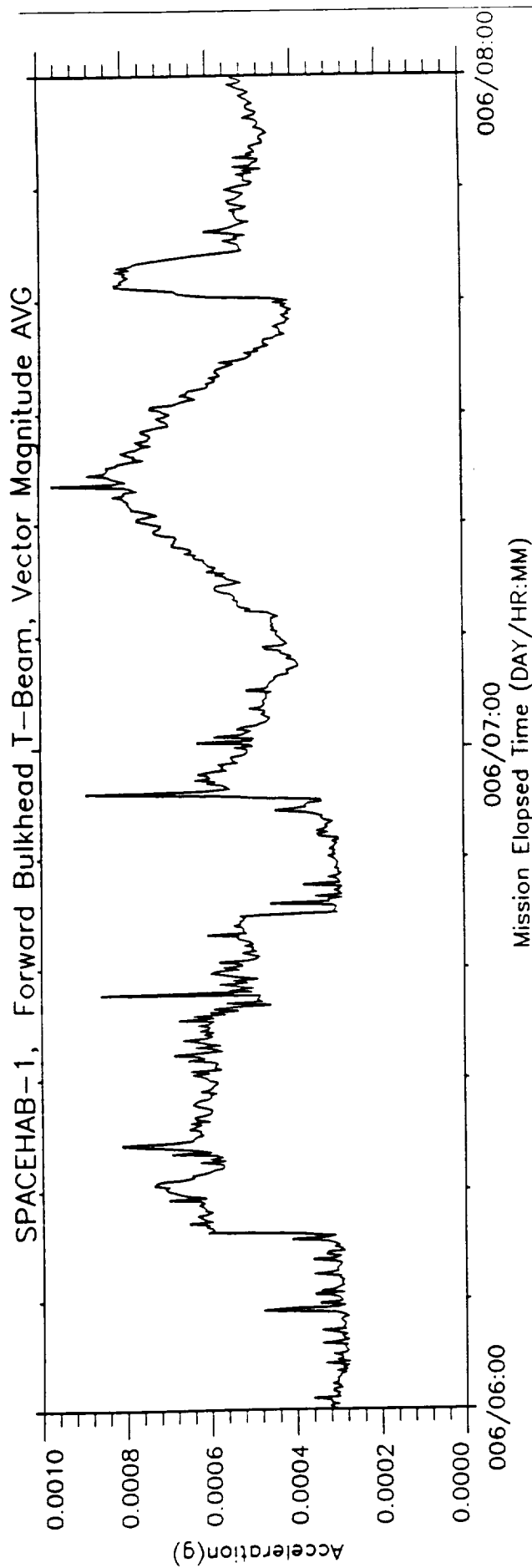


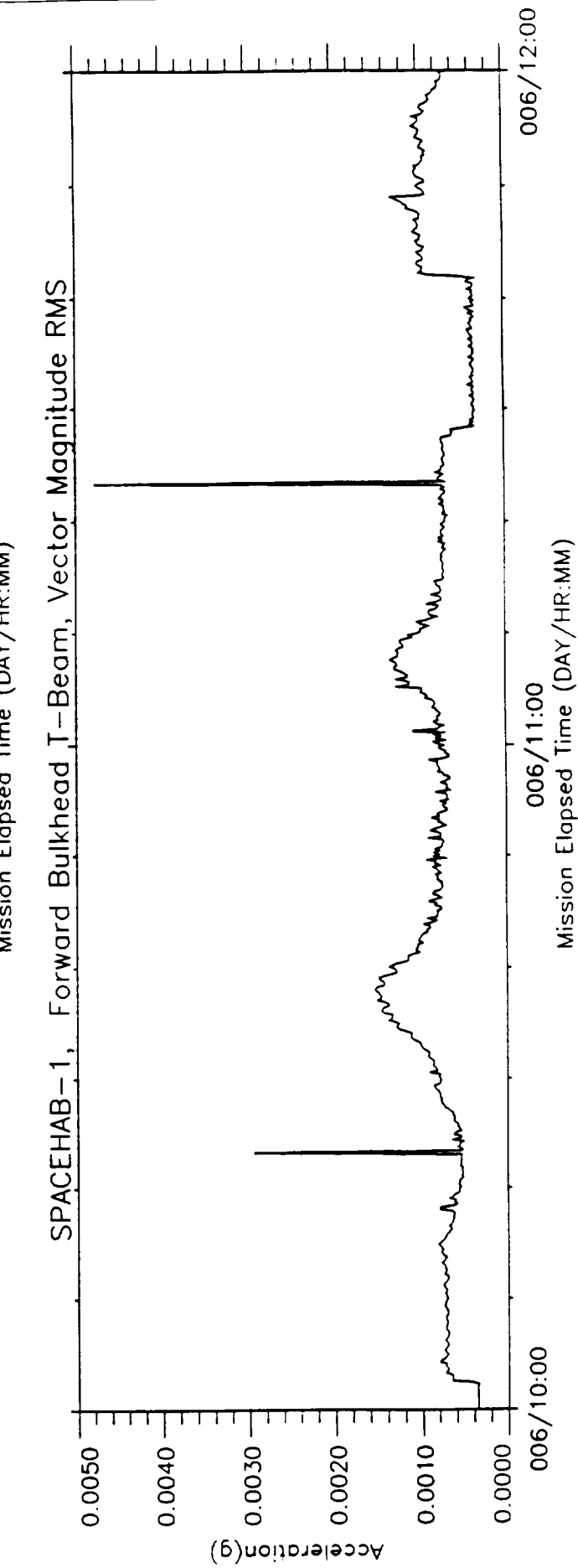
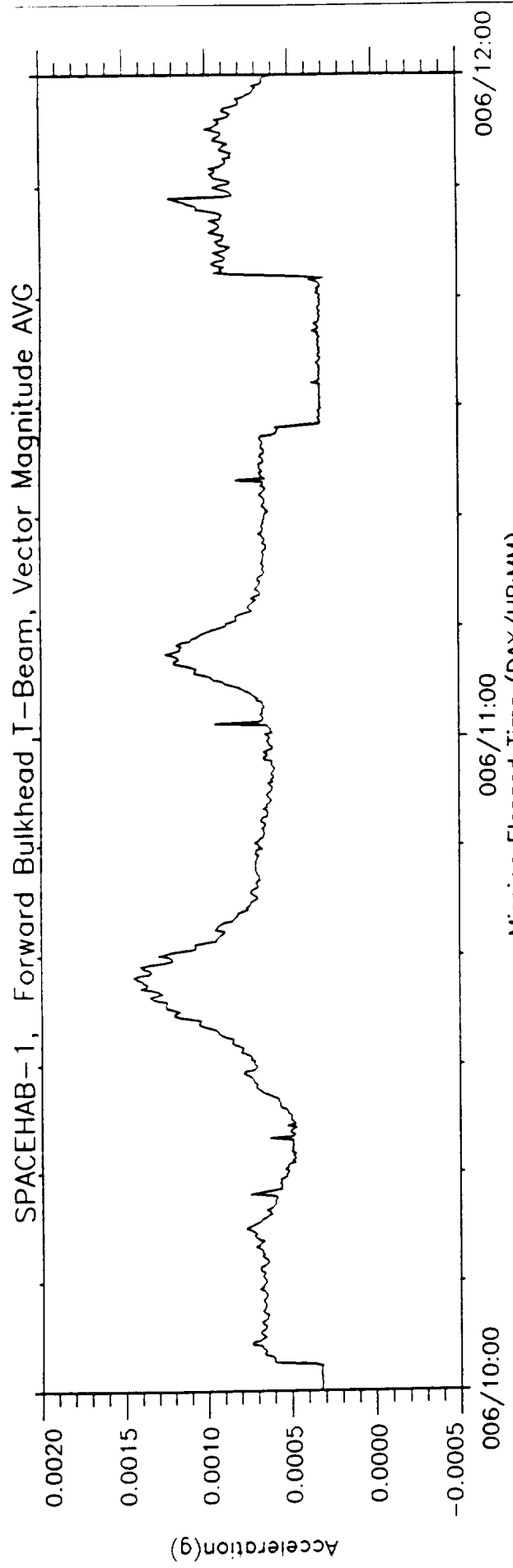
Data missing.

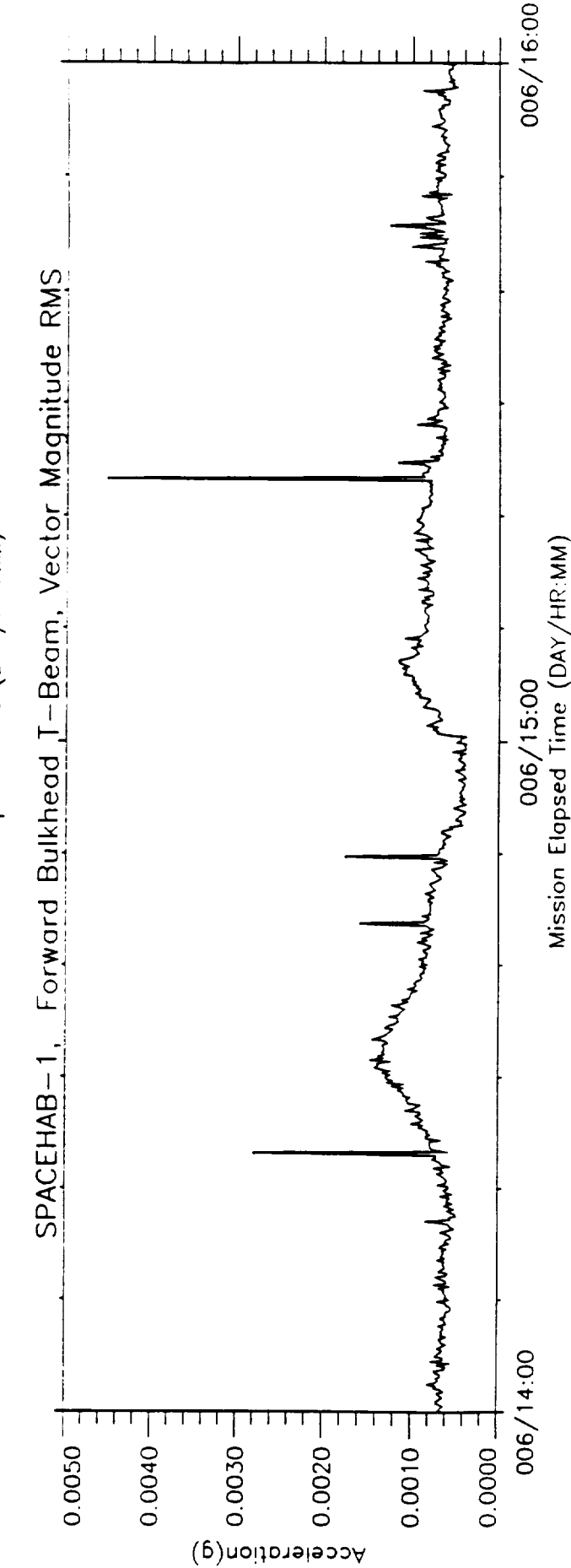
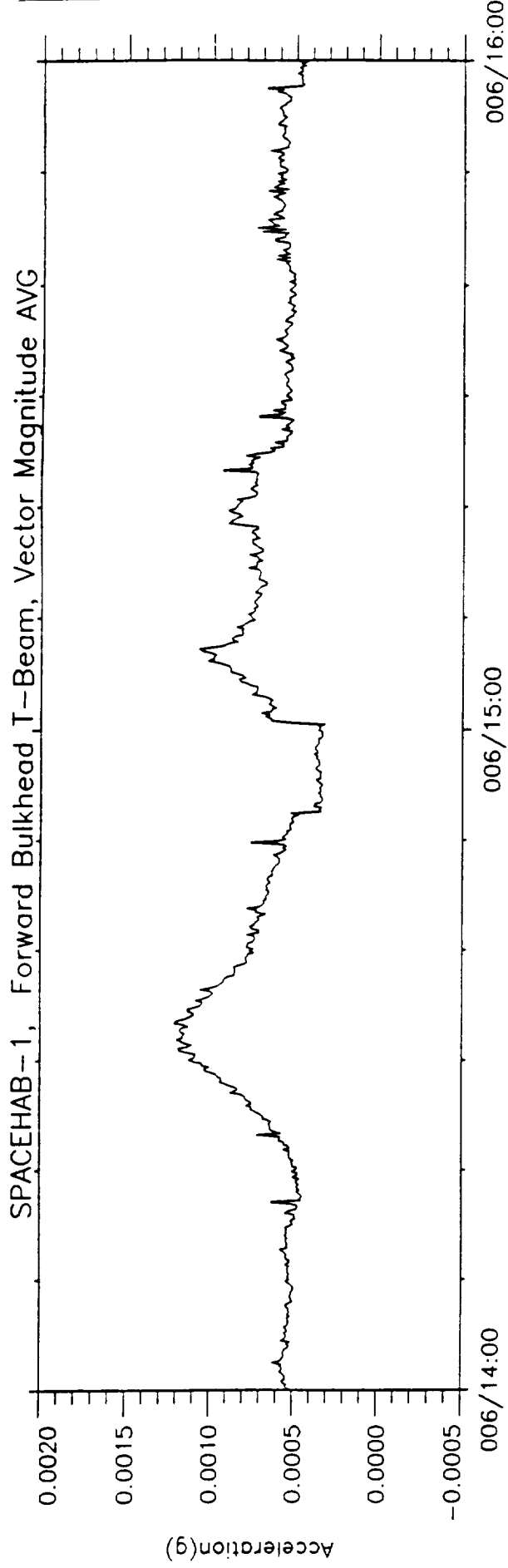
This page intentionally left blank.

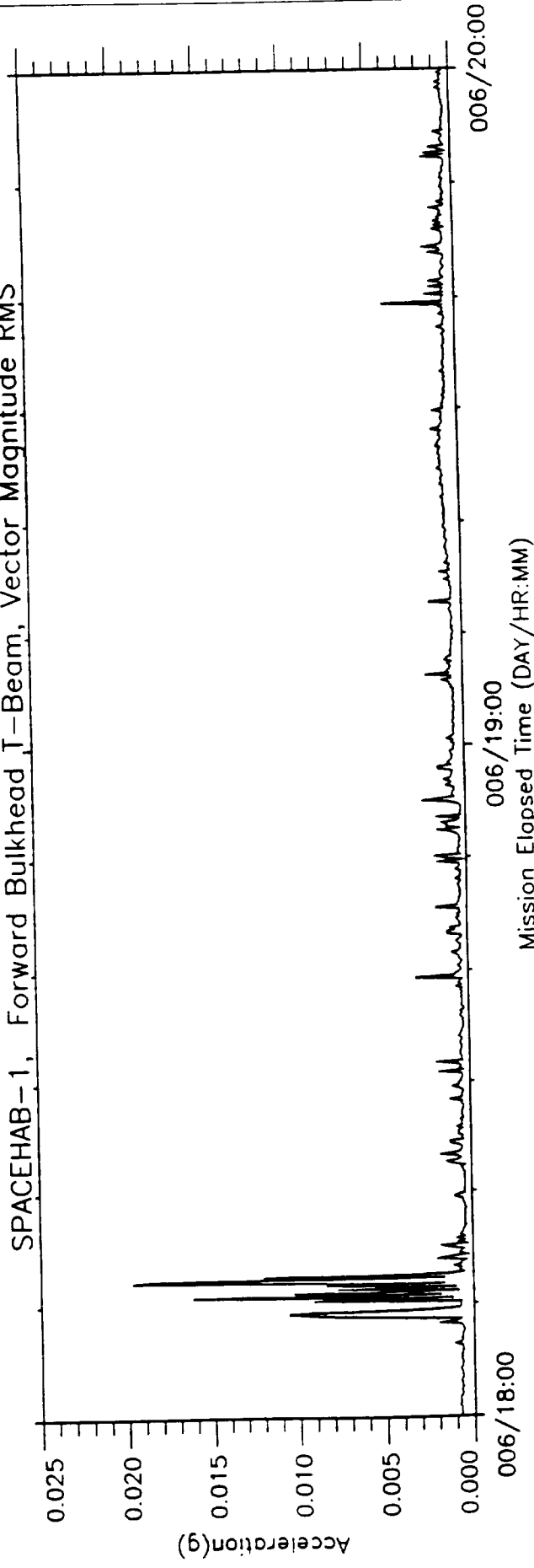
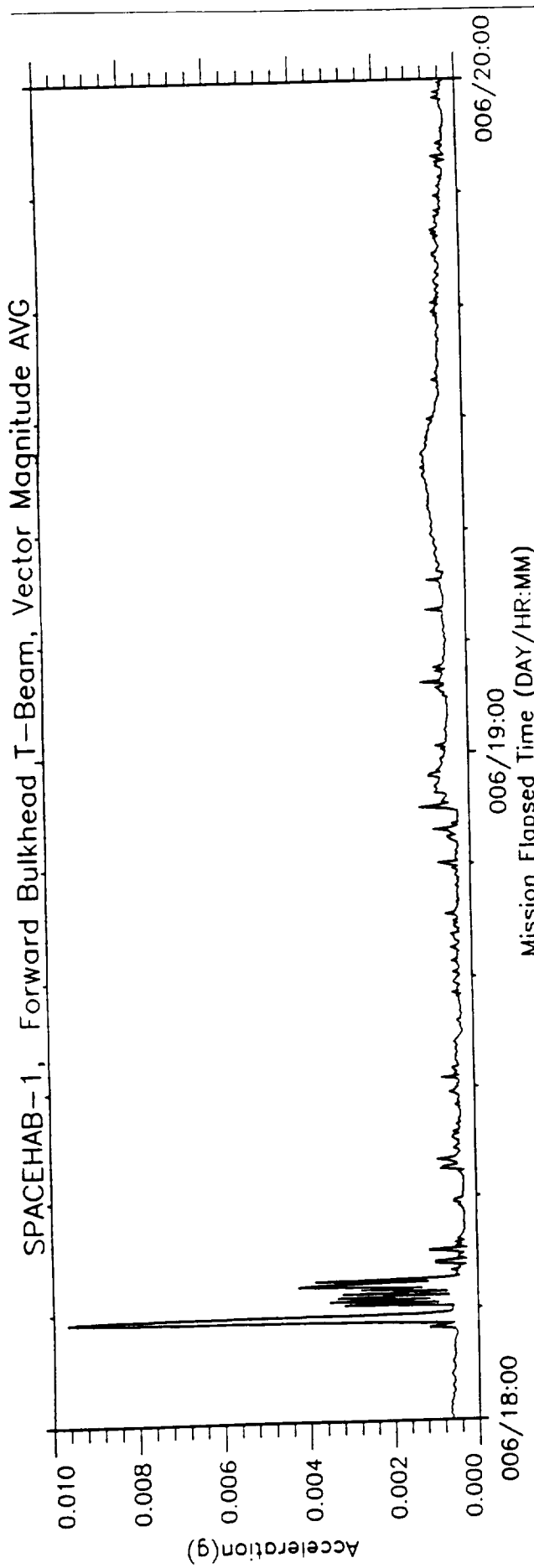


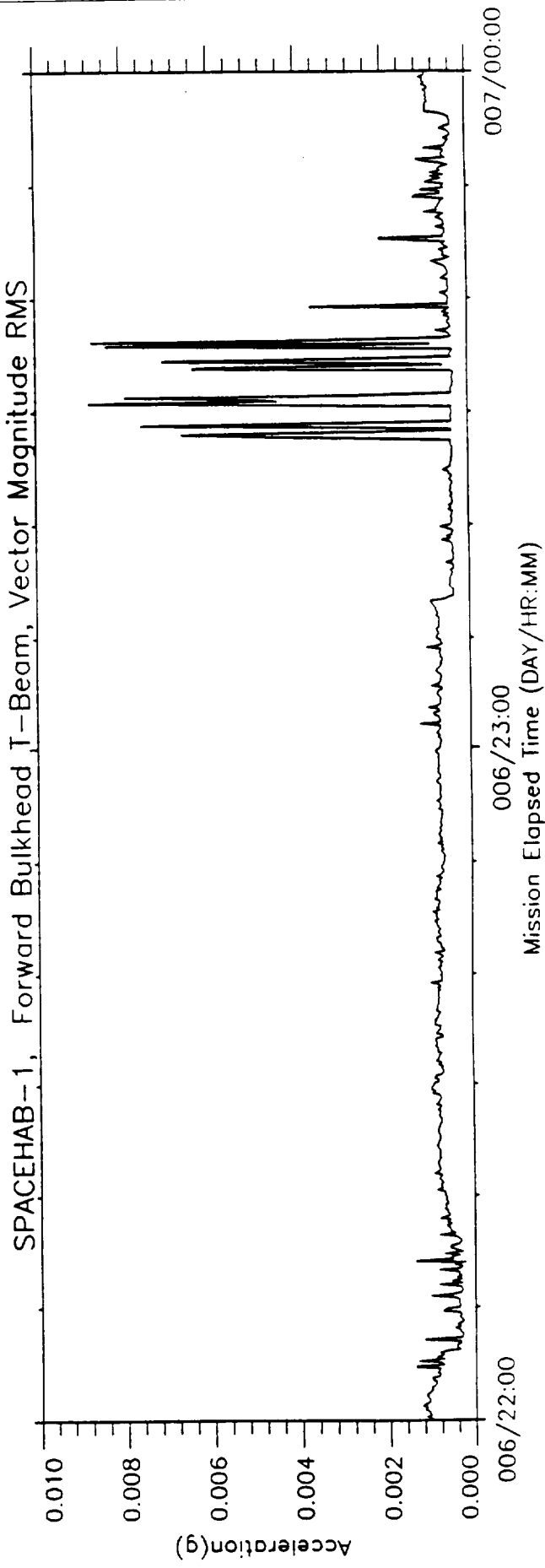
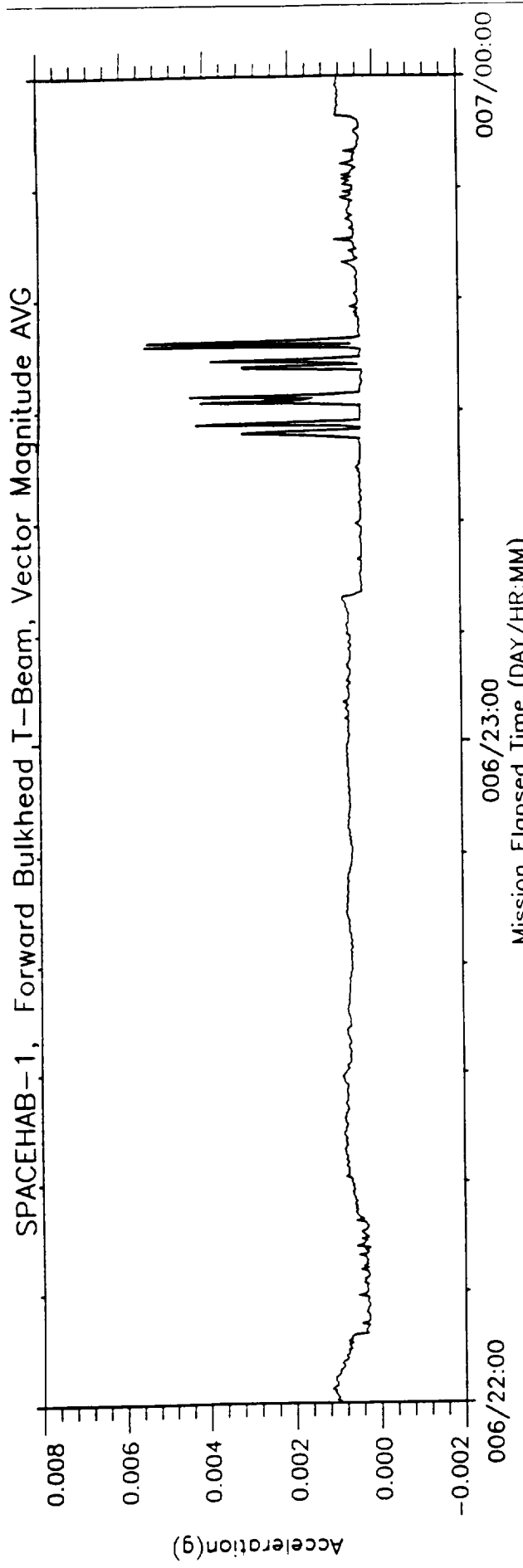


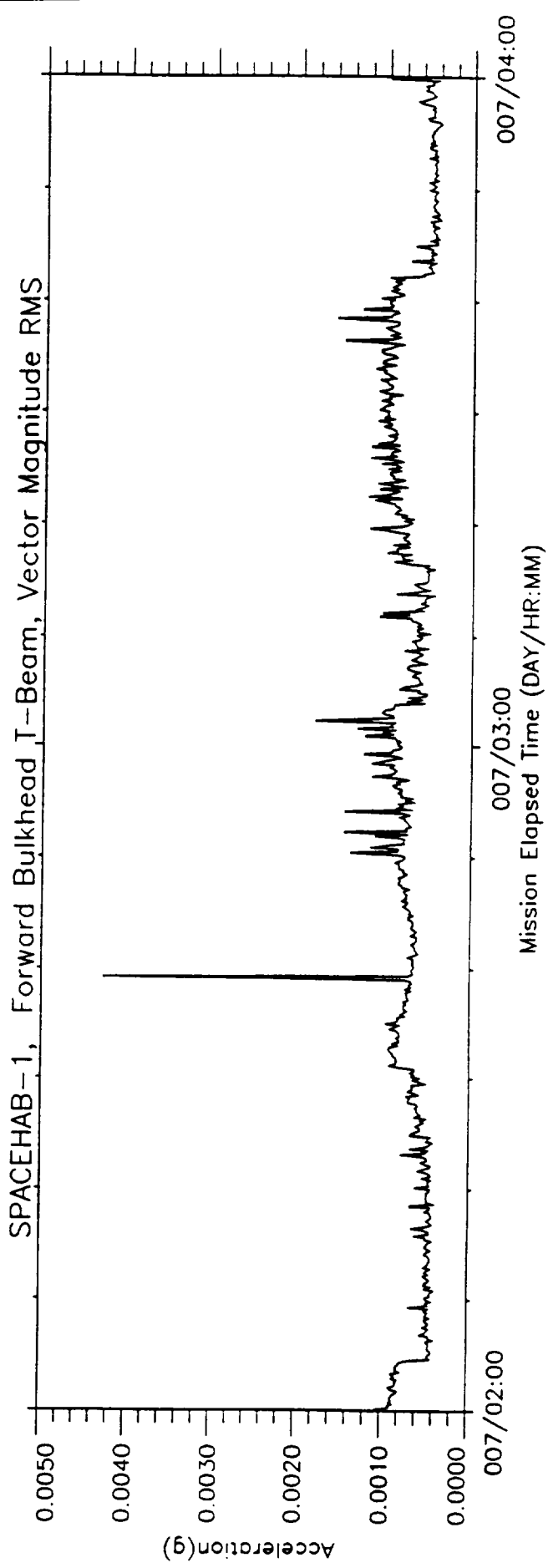
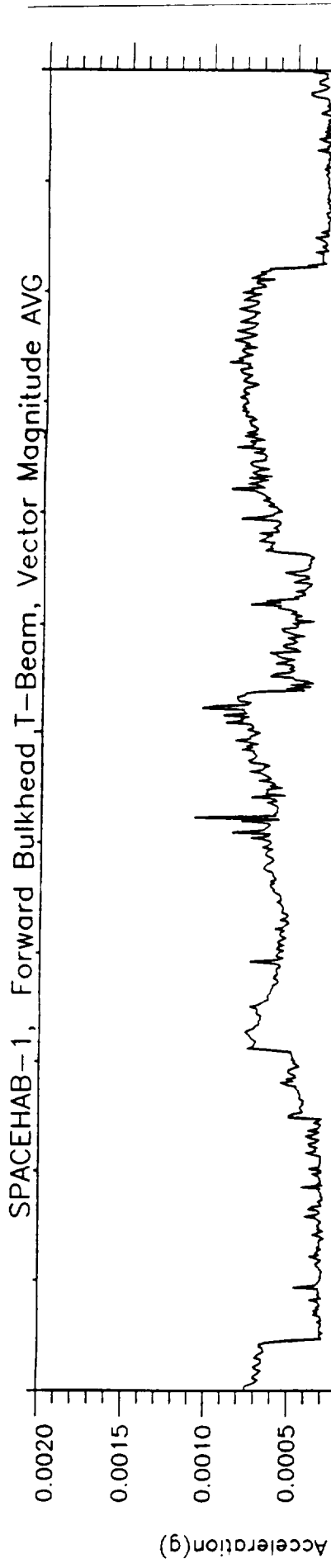


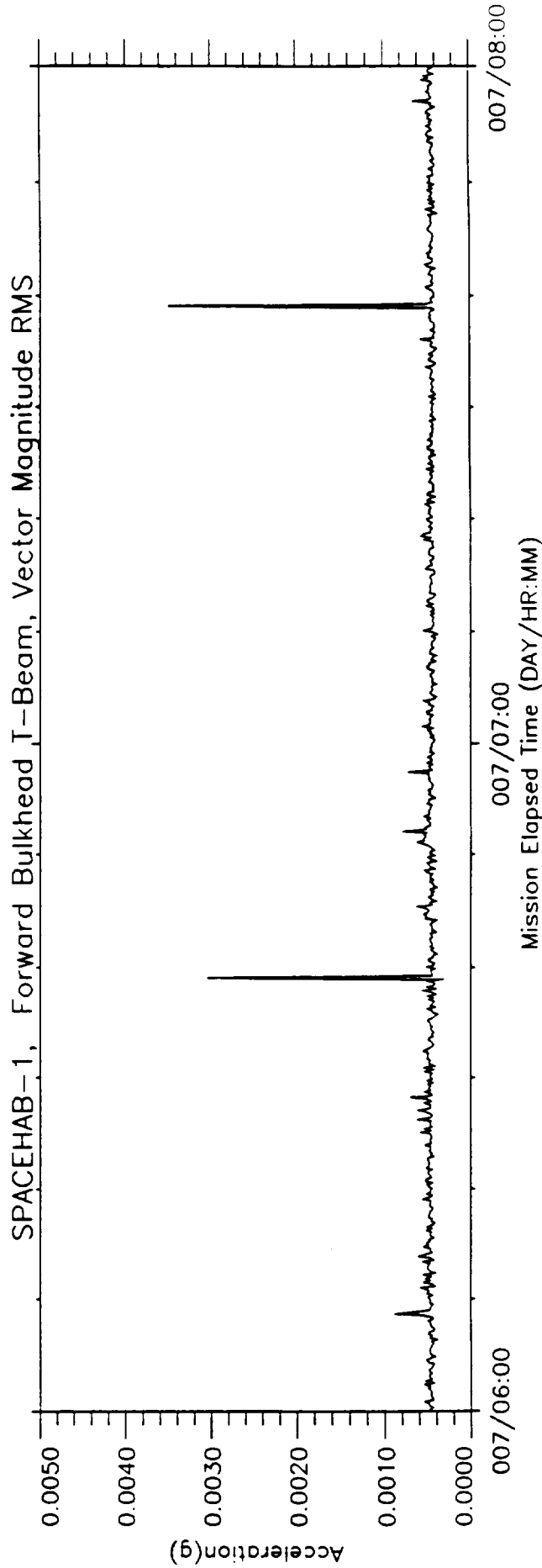
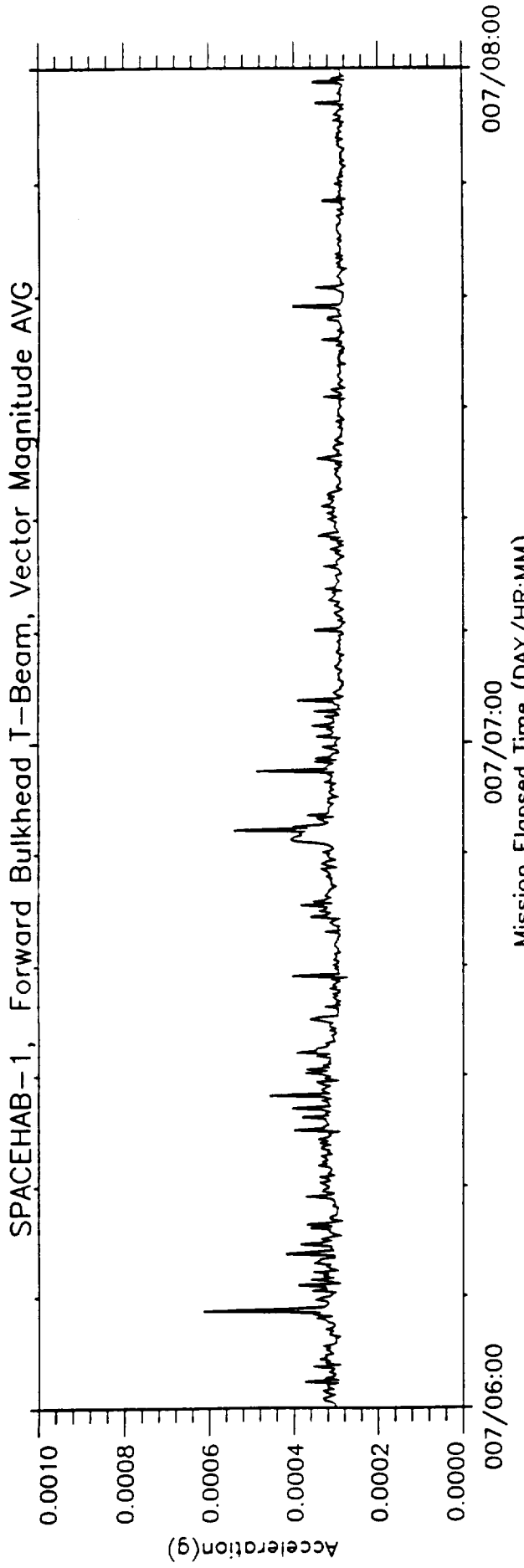


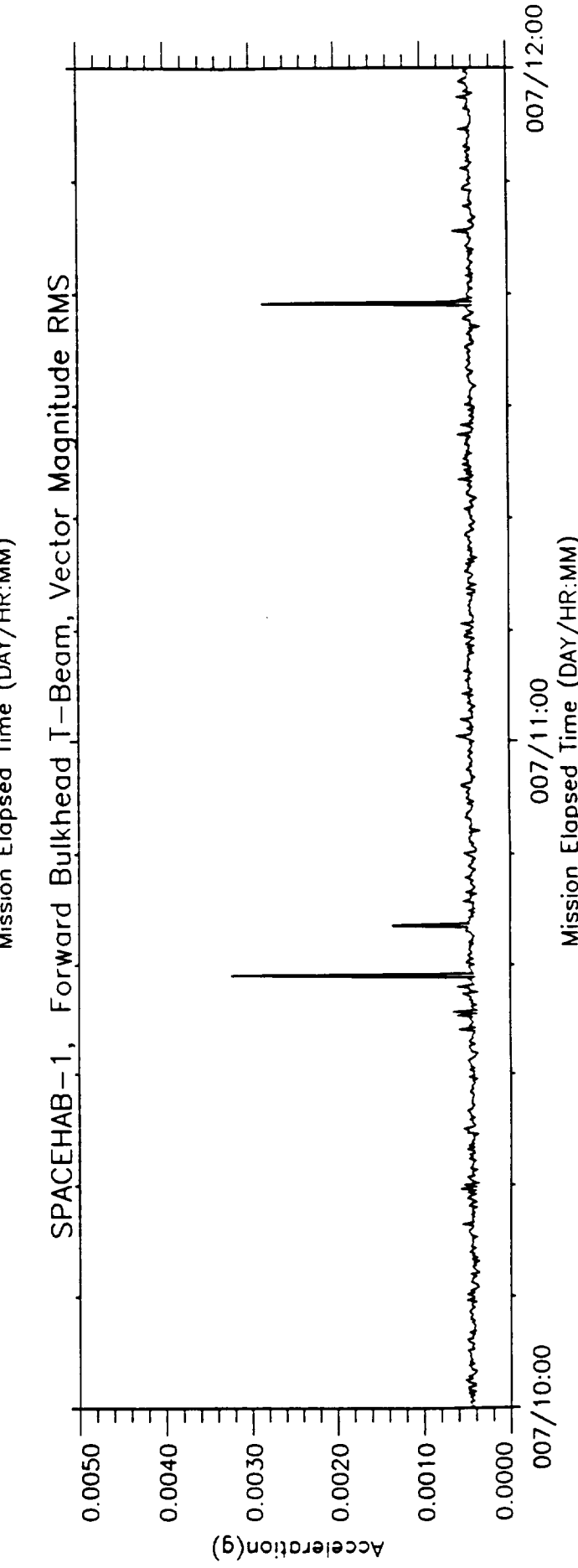
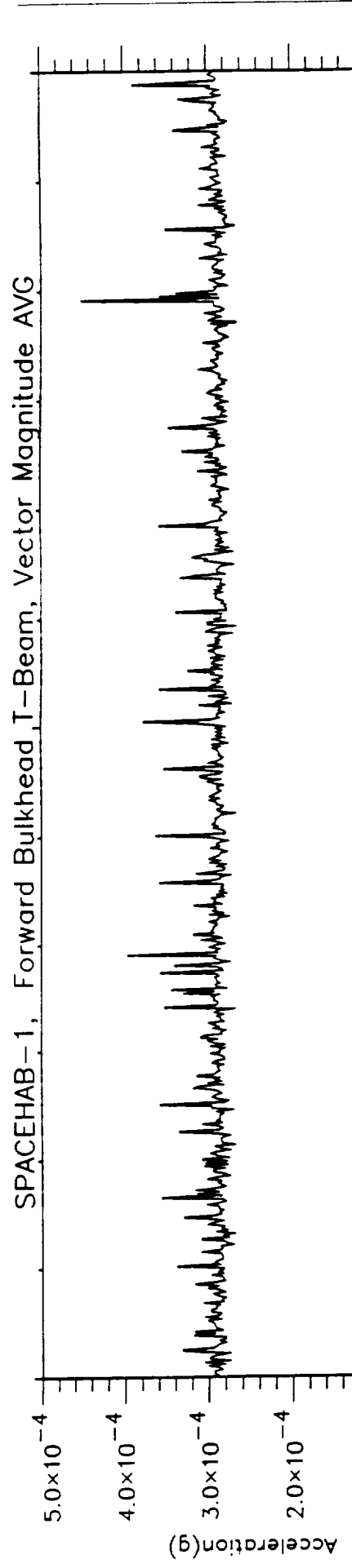


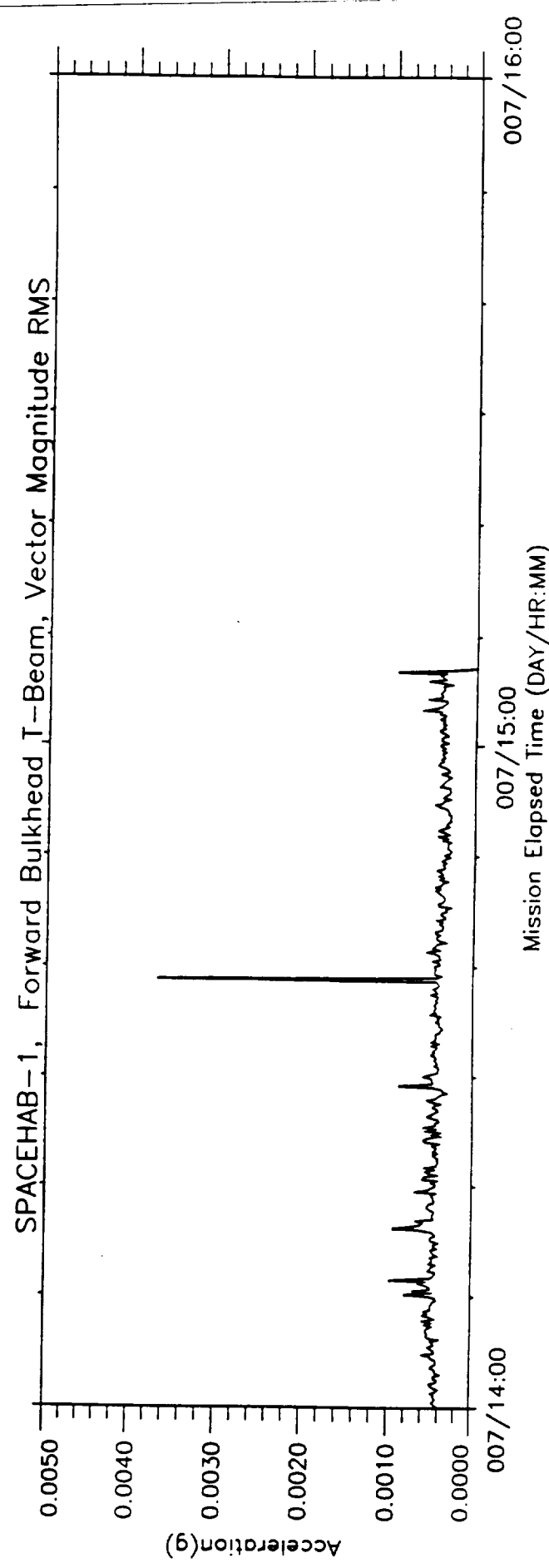
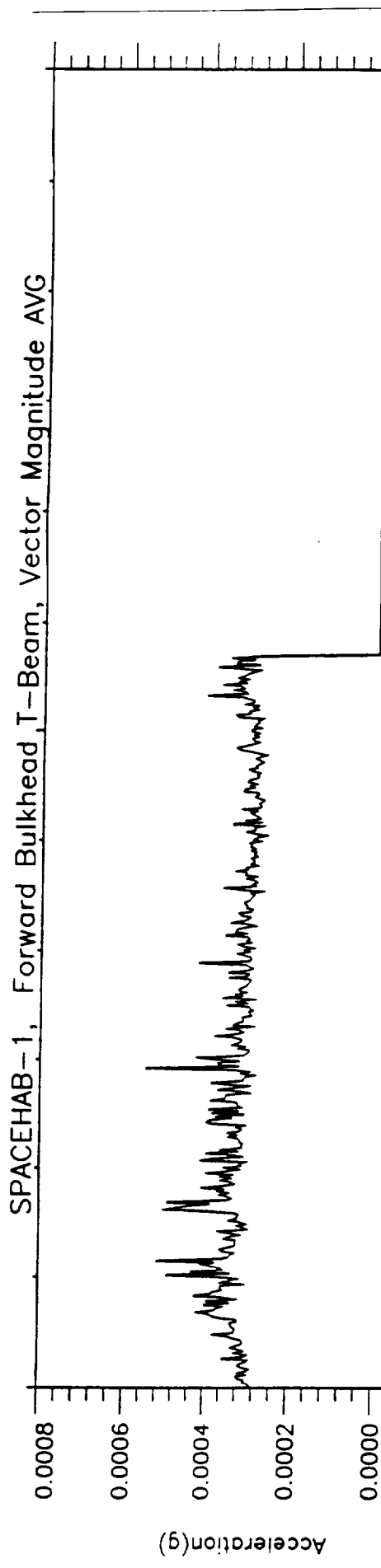












Appendix D: Shoot Rotational Maneuver Calculations

The SHOOT experiment required one of its four disturbance maneuvers to be a pitch rotation causing a centripetal acceleration on all locations of the shuttle as functions of the rotational rate and the distance from the center of mass of the shuttle, assuming this was the rotation point of the angular maneuver. According to an as flown attitude time line the pitch rate maneuver was performed with a 3 degree per second rotation having a deadband of nominally 0.2 degrees per second. The centripetal acceleration along a radial vector to each triaxial sensor head location can be calculated and therefore, the global structural coordinate components of this acceleration can be calculated and compared to the measured accelerations of the three triaxial accelerometers.

The centripetal acceleration of a point away from the center-of-mass, assuming only a pitch rotation about the x-axis, can be described by the following equation:

$$a_c = \omega^2 r$$

where a_c is the acceleration magnitude along a radial vector in the xz plane from the triaxial sensor to the center-of-mass of the shuttle, ω is the pitch angular rate of rotation and r is the distance from the sensor head location to the center-of-mass in the xz plane. Therefore, from Tables 2 and 3 each sensor heads' distance from the center-of-mass was calculated for the xz plane and the acceleration magnitude for an x and z sensor was calculated for all three sensor heads A, B, and C as follows:

$$a_{Axz} = \left(2\pi \frac{\dot{\theta}}{360^\circ}\right)^2 \frac{r_{Axz}}{386.4} [\cos(2.028^\circ) \hat{x} - \sin(2.028^\circ) \hat{z}]$$

$$a_{Bxz} = \left(2\pi \frac{\dot{\theta}}{360^\circ}\right)^2 \frac{r_{Bxz}}{386.4} [\cos(5.393^\circ) \hat{x} - \sin(5.393^\circ) \hat{z}]$$

$$a_{Cxz} = \left(2\pi \frac{\dot{\theta}}{360^\circ}\right)^2 \frac{r_{Cxz}}{386.4} [\cos(8.284^\circ) \hat{x} - \sin(8.284^\circ) \hat{z}]$$

where theta dot is the angular pitch velocity in degrees per second, and r_{Axz} , r_{Bxz} , and r_{Cxz} are the radial xz plane distances from the A, B, and C sensor head locations, respectively. Using the angular pitch rate from the as flown attitude time line of 3

$$\ddot{r}_{Cxz} = 2.75 \times 10^{-3} \hat{x} - 3.86 \times 10^{-4} \hat{z}$$

note: refer to section 6.2 for the magnitude versus time data plots for the four SHOOT maneuvers.

